Development of Improved Membranes For ROWPU Spiral-Wound Elements

Final Report

Period of Performance
November 13, 1998 Through March 1, 2001

Contract DAAD19-99-C-0003

Department of the Army
Army Research Office
P.O. Box 12211
Research Triangle Park, NC. 27709-2211

April 25, 2001

20010517 069

Separation Systems Technology, Inc.
4901 Morena Blvd., Bldg. 809
San Diego, CA. 92117

REPORT DOCUMENTATION PAGE

Public reporting burden for this collection of information is estimated to average 1 hour per response, including the time for reviewing instructions, searching existing data sources, gathering and maintaining the data needed, and completing and reviewing the collection of information. Send comment regarding this burden estimates or any other aspect of this collection of information, including suggestions for reducing this burden, to Washington Headquarters Services, Directorate for information Operations and Reports, 1215 Jefferson Davis Highway, Suite 1204, Arlington, VA 22202-4302, and to the Office of Management and Budget, Paperwork Reduction Project (0704-0188), Washington, DC 20503.

1. AGENCY USE ONLY (Leave blank)	2. REPORT DATE	3. REPORT TYPE AND DATES COVERED
	April 25, 2001	Final November 13, 1998 - March 1, 2001

4. TITLE AND SUBTITLE

Development of Improved Membranes for ROWPU Spiral-Wound Elements

5. FUNDING NUMBERS

Contract No. DAAD19-99-C0003

ACRNAA: 2192040 96U-6UO1
P665502.M4000-2552 S18129
9XM400/9SB39096/ $741,552

6. AUTHOR(S)

R. L. Riley, K.P. Ishida, S.W. Lin, A. Murphy, H. F. Ridgway

7. PERFORMING ORGANIZATION NAMES(S) AND ADDRESS(ES)

Separation Systems Technology, Inc.
4901 Morena Blvd., Suite 809
San Diego, CA 92117

8. PERFORMING ORGANIZATION REPORT NUMBER

2098-2

9. SPONSORING / MONITORING AGENCY NAME(S) AND ADDRESS(ES)

U.S. Army Research Office
P.O. Box 12211
Research Triangle Park,, NC 27709-2211

10. SPONSORING / MONITORING AGENCY REPORT NUMBER

ARO Proposal No.
39096-CH-SB2

11. SUPPLEMENTARY NOTES

The views, opinions and/or findings contained in this report are those of the author(s) and should not be construed as an official Department of the Army position, policy or decision, unless so designated by other documentation.

12a. DISTRIBUTION / AVAILABILITY STATEMENT

Approved for public release; distribution unlimited.

12 b. DISTRIBUTION CODE

13. ABSTRACT (Maximum 200 words)

Mobile reverse osmosis water purification units (ROWPU) have been used by the U. S. Armed Services for over a decade to produce potable water for field applications. Although advancements in the technology of operation and in the performance of the membrane elements have been significantly improved since that time, several major membrane deficiencies still exist. They are: poor lack of chemical stability to oxidants such as chlorine, high fouling rates due to membrane surface roughness and high bacterial attachment counts on the membrane surface leading to biofouling. The ROWPU membrane used today is the seawater polyamide (PA) thin-film composite membrane based on the interfacial reaction of m-phenylenediamine with trimesoyl acid chloride. This program pursues a new approach by utilizing molecular modeling to select new amines and acid chlorides combinations. Emphasis focused on synthesis and purification of the new acid chloride, PA membrane development and characterization studies utilizing infrared spectrometry, atomic force microscopy and electron dispersive X-ray to determine surface roughness. Bacterial attachment and mechanisms of the addition of chlorine to the membrane surface were studied extensively. RO field testing on chlorinated feed streams have demonstrated excellent transport properties and chlorine resistance on both brackish water and seawater.

14. SUBJECT TERMS

Reverse Osmosis, Polyamide Membranes, Chlorine Reaction Mechanisms, Chlorine Resistance, Molecular Modeling, Surface Roughness, Biofouling

15. NUMBER IF PAGES

324

16. PRICE CODE

17. SECURITY CLASSIFICATION OR REPORT	18. SECURITY CLASSIFICATION OF THIS PAGE	19. SECURITY CLASSIFICATION OF ABSTRACT	20. LIMITATION OF ABSTRACT
UNCLASSIFIED	UNCLASSIFIED	UNCLASSIFIED	UL

NSN 7540-01-280-5500

ACKNOWLEDGMENTS

GLOSSARY

In order to avoid lengthy descriptions of frequently repeated terms throughout this report, this glossary has been formed to serve as a guide to facilitate easy reading of the test.

Unless stated otherwise in the text of this document, the following terms will be used:

AFM	Atomic Force Microscopy
ATR/IR	Attenuated Total Reflectance/Fourier Transform-Infrared Spectrometry
BR	U.S. Bureau of Reclamation, Denver, CO
CA	Cellulose Acetate (as used in text)
CA	Contact Angle (as used in text)
C-AFM	Contact AFM
cccc	cis, cis, cis, cis isomer of cyclopentanetetracarboxylic acid
CPTC	Membranes prepared in this program from the cis, trans, cis, trans isomer of cyclopentanetetracarboxylic acid chloride interfacial reaction with MPD
CPTC-AC	CPTC acid chloride (particularly in reference to synthesis Lot No.)
C-13 NMR	Carbon-13 Nuclear Magnetic Resonance
CRADA	Cooperative Research and Development Agreement
ctct	cis, trans, cis, trans isomer of cyclopentanetetracarboxylic acid
DI	Deionized (in reference to DI water)
DMF	Dimethylformamide
DPM	Disintegrations per minute of radioactive isotopes
DU	Denver University
EDX	Electron Dispersive X-Ray
EDS	Electron Dispersive Spectroscopy

FT-IR	Fourier Transform-Infrared Spectrometry
GCMS	Gas Chromatograph Mass Spectrometry
H-NMR	Hydrogen Nuclear Magnetic Resonance
IC-AFM	Intermittent AFM
ICP	Ion Chromatography
ICP-MS	Inductively Conductive Plasma - Mass Spectrometry
IPA	Isopropanol
ITM	Instituto Tecnologico, Tijuana, Mexico
MBP	Membrane Biofouling Potential
MD	Molecular Dynamics
MPD	m-phenylenediamine
NC-AFM	Non-Contact AFM
NDMA	N-nitrosodimethylamine
NFESC	Naval Facility Engineering Service Center, Port Hueneme, CA
NMR	Nuclear Magnetic Resonance
OCWD	Orange County Water District, Fountain Valley, CA
PA	Polyamide
P-31 NMR	Phosphorous-31 Nuclear Magnetic Resonance
PMMA	Polymethylmethacrylate
PS	Polysulfone
RMS	Root Mean Square Roughness
RO	Reverse Osmosis
ROWPU	Reverse Osmosis Water Purification Unit
SDSU	San Diego State University

SPS	Sulfonated Polysulfone
SST	Separation Systems Technology, Inc., San Diego, CA
TCU	Test Cell Units
TEM	Transmission Electron Microscopy
TMC	Trimesoyl chloride. Also, membranes prepared by the interfacial reaction of TMC and MPD, i.e., TMC membranes, used as controls, prepared by the FilmTec method
TRC	Total Residual Chlorine
p-TSA	Para-toluenesulfonic Acid
WQIC	Water Quality Improvement Center, Yuma, AZ
UA	Uranyl Acetate
UC	Uranyl Cation
UCB	Uranyl Cation Binding

TABLE OF CONTENTS

7.0 SYNTHESIS AND PURIFICATION OF *CTCT*-1,2,3,4-CYCLOPENTANE- 65
TETRACARBOXYLIC ACID CHLORIDE

8.0 TECHNICAL APPROACH AND EXPERIMENTAL METHODS 80

1.0 INTRODUCTION

The first polyamide (PA) reverse osmosis (RO) membrane was commercialized in 1977 when it was placed in service in a large RO seawater desalination plant in Jeddah, Saudi Arabia.[1] At that time it was recognized that the membrane was not tolerant to chlorine and the pre-treatment for the plant had to be adjusted accordingly. Thus, the search for a chlorine-resistant membrane was begun more than twenty years ago.

Today, the RO membrane of choice worldwide is the PA thin-film composite membrane developed by Cadotte.[2] The PA membrane is made by forming a thin PA film on the finely porous surface of a polysulfone (PS) supporting membrane by an interfacial reaction between the reactant pair trimesoyl chloride (TMC) and *m*-phenylenediamine (MPD). Today, the membrane is commercially supplied by Dow/FilmTec, Koch/Fluid Systems, Osmonics/Desal, Tri-Sep, Nitto Denko/Hydranautics in the U. S., Toray Industries in Japan, Projectos in Spain and Saehan Industries in Korea. Although the membrane performance is excellent, major membrane deficiencies that contribute to fouling, reduced membrane life and higher operating costs remain. They are:

* Lack of chemical stability to oxidants such as chlorine
* High fouling rates due to surface roughness, and
* High bacteria attachment counts on the membrane surface leading to biofouling.

There is need to improve the stability of present state-of-the-art PA membranes to oxidizing agents. These improvements are critical for RO plants operating on wastewaters, surface waters and open seawater intakes where disinfection by chlorination is required to control growth of microorganisms (biofouling) on the surface of the membrane. These PA membranes are so susceptible to oxidation that dechlorination is required when chlorine is used as a disinfectant in the pretreatment. Dechlorination prior to the PA membrane creates added costs and effectively nullifies disinfection on the membrane surface where it is needed. Development of a chlorine-resistant PA membrane is a solution to control biofouling, thereby increasing membrane life.

A primary objective of this work was to develop a PA membrane for RO desalination that is resistant to chlorine-disinfected feedwaters that reduce biological fouling. The work of Ikeda and Tomaschke[3] reported PA membranes made from MPD and three stereoisomers of 1,2,3,4-cyclopentanetetracarboxylic acid chlorides, namely *cccc*-CPTC acid chloride, *ctcc*-CPTC acid chloride and *ctct*-CPTC acid chloride. The said paper revealed that PA membrane made from the *ctct*-CPTC isomer showed greater tolerance to 1 mg/L chlorine in a 1000-hr RO test than did the *cccc*-CPTC or the *ctcc*-CPTC isomers; chlorine tolerance of three to five years is the goal for a commercial membrane. Since the *ctct*-CPTC isomer must be isolated from a mixture of isomers, it could be expected that an isomeric purity of close to 100% would be required to attain maximum oxidation resistance. The methodology for selecting these acid chlorides, the percent conversion of the *cccc*-CPTC acid and finally the isomeric purity of the *ctct*-CPTC acid chlorides were not cited.

U.S. Patent 5,254,261 was issued to Tomaschke and Ary on the aforementioned PA membrane chemistry prior to the publication. This patent was not cited in the publication of Ikeda and Tomaschke, and there is no mention and/or claim in the patent of oxidation stability of the resultant PA membrane. However, Ikeda and Tomaschke cited in their publication that chlorine tolerance was the primary attribute of the membrane.

In recent years, membrane research at Separation Systems Technology (SST) focused on PA thin-film composite RO membranes. This work identified current membrane deficiencies, demonstrated cause and effect, developed methodologies for approaching the problems and determined pathways for solutions. One aspect of this work was to develop a methodology for the search for an oxidation-resistant PA membrane. Toward this end molecular modeling was selected as the methodology to determine the optimal combination of amine and acid chloride monomers to enhance oxidation resistance.

The 1,2,3,4-CPTC acid chloride with its six sterioisomers is an unique system for developing a methodology using molecular modeling, since each individual isomer from the six isomer mixture show differences in oxidation tolerance. As a result, six isomers formed from the conversion of *cccc*-1,2,3,4-cyclopentanetetracarboxylic acid to acid chlorides were modeled. It was found that the bond angles and steric energies of the isomers were quite different and that *ctct*-CPTC acid chloride bond angles were least strained. These results, of course, assume 100% isomeric purity. To confirm long-term oxidative stability, high purity isomers were produced, membrane processing optimized, and the membranes were evaluated in long-term RO tests on brackish water at the Water Quality Improvement Center (WQIC) Yuma, AZ, on municipal wastewater at the Orange County Water District (OCWD), Fountain Valley, CA and on seawater at the Naval Facility Engineering Service Center (NFESC) at Port Hueneme, CA for confirmation.

All membranes described in this report are polyamide (PA) membranes, whether commercial, SST membranes prepared from TMC/MPD or CPTC/MPD membranes. As a result, general reference to membranes imply polyamide membranes and the words polyamide or PA have been eliminated from most of this report. In addition, all membranes prepared from the *ctct*-CPTC isomer are referred to as CPTC membranes.

2.0 SUMMARY

This program possessed both depth and scope in pursuing a new approach to develop a new chlorine-resistant PA membrane. Molecular modeling was used to identify and select an acid chloride to react with *m*-phenylenediamine (MPD) for the interfacial formation of the PA desalination barrier. Based on steric differences, cis, trans, cis, trans-1,2,3,4-cyclopentanetetracarboxylic acid chloride (*ctct*-CPTC) was selected as the most promising of six stereoisomers of the same compound.

A major thrust of the program involved the synthesis, separation and purification of *ctct*-CPTC acid chloride from a mixture of six sterioisomers; analysis of the purified products were determined by C-13 NMR, H-NMR, P-31 NMR, GCMS, IR and ATR/IR spectrometry.

CPTC membranes were prepared and the RO transport properties were optimized for water flow, salt rejection and chlorine tolerance. The membranes were further characterized with respect to bacterial attachment (biofouling), surface charge, air bubble contact angle determinations (hydrophobicity), surface morphology (AFM and TEM) and chemical and structural analysis by EDX, IR and ATR/IR spectrometry. Chemical modification of the membrane surface was made to reduce biofouling. Finally, an RO field test program was carried out with the CPTC membranes using chlorinated feed waters at the WQIC on surface waters, at OCWD on municipal wastewater and at NFESC on seawater.

The success of this program can be attributed to the coordinated effort of six participating teams each of different disciplines. These included synthetic organic chemists, instrumental analysis specialists, microbiologists, membrane specialists and field test engineers.

2.1 Observations, Conclusions and Recommendations

* Molecular modeling techniques were utilized to explore the stability of six stereoisomers of CPTC, a cyclic multifunctional aliphatic acid chloride that can be reacted with the di-functional amine MPD in an interfacial condensation to produce a cross-linked thin-film composite membrane. Only the *ctct* isomer of CPTC is capable of producing a membrane that resists oxidative damage from free chlorine (sodium hypochlorite/sodium hypobromite).

* Custom software was designed to build and geometrically optimize (i.e. energy minimize) a model of the CPTC membrane. The CPTC membrane models may be constructed using any one of the six CPTC stereoisomers, thereby allowing comparisons to be made between the structural and energetic properties of the finished membranes. It is anticipated, in future work, that a detailed comparison of the structural and energetic features of the chlorine-resistant and the chlorine sensitive versions of the CPTC membranes could shed light on the mechanism of chlorine resistance in the membrane synthesized from the *ctct* isomer.

3

*   Molecular modeling techniques were employed to simulate the reaction of hypochlorous acid (HOCl) with model CPTC polymer fragments to identify reaction products of membrane chlorination. Preliminary reaction modeling clearly indicates that the chlorine atom from HOCl can add to the primary amine nitrogen that forms the backbone amide bond of the polymer chains. Chlorination of the aromatic MPD ring has also been observed in the preliminary modeling reactions that have were conducted. The role of bromide in membrane chlorination reactions should be explored.

*   Membrane models may be used as the starting point for molecular dynamics (MD) simulations of water and solute diffusion (i.e., mass transport) behaviors in the membranes. Water and solute diffusion coefficients computed from the results of MD simulations can be used to predict the flux and rejection of the six isomers of CPTC membranes.

*   Molecular modeling programs were developed to identify and select reactive acid chloride and amine pairs for interfacial formation of oxidation stable membranes. The criteria were based on bond angles, bond energies, steric considerations, etc. The success of this work provides a powerful tool for predicting membrane properties and will make future development of membranes less empirical. In the future, it is expected that molecular modeling will become common methodology in the search for new membrane materials.

*   A synthesis procedure was developed to produce high purity *ctct*-CPTC acid chloride in 5 gram quantities. High purity was required to attain optimum membrane transport properties and resistance to oxidation. *cccc*-CPTC membrane degrades very quickly relative to CPTC membrane when tested on chlorinated feed water in RO field tests. Thus, it was necessary to isolate and purify the *ctct*-CPTC acid chloride isomer from a mixture of six isomers to a very high purity, that is 99.9+%. Additional work is required to improve yield, synthesis time and the overall economics of the process. Future efforts to improve the overall synthesis process would lower the cost of the product.

*   CPTC acid chloride will not significantly increase the price of the PA membrane. One gram of *ctct*-CPTC acid chloride will make 254 ft^2 of membrane. Assuming that CPTC is 8 times more expensive than TMC, a worst case scenario, the cost of an 8- x 40-in. spiral-wound element would increase in price by only 1.8 percent.

*   In screening experiments, PA films were formed at the interface between an aqueous MPD solution and hydrocarbon solutions of TMC and CPTC. The formation, integrity and strength of the PA films formed were nominally the same for the aromatic-aromatic PA and the aliphatic-aromatic PA systems. Films of TMC and CPTC acid chloride systems could be continuously withdrawn at the interface and collected.

4

*   The transport properties of CPTC RO membrane improved with increasing purity of CPTC acid chloride. When the purity of CPTC acid chloride is 99.9+%, the transport properties of CPTC RO membranes are nominally the same as for TMC RO membranes. Typically, CPTC membrane exhibits 16 gfd and 99.5% rejection when tested at 225 psi applied pressure on a 2000 mg/L sodium chloride feed at pH 6.5.

*   RO membrane surface topography, as determined by AFM, is smooth for CA membranes and very rough for CPTC and TMC membranes. The following observations were made regarding the formation of surface roughness in CPTC and TMC membrane processing:

    a. Surface roughness is determined during the interfacial polymerization step at the amine (water phase)/acid chloride (hydrocarbon phase) interface and not during the membrane post treatment steps.

    b. Surface roughness is characteristic of both cross-linked and linear PA membranes made from MPD and di- and tri-functional aromatic acid chlorides. Thus, cross-linking *per se* is not the major factor in determining surface roughness.

    c. CPTC membrane surface roughness is nominally the same for membranes made with either hexane, Freon or Isopar as the solvent for the acid chloride.

    d. The surface roughness of CPTC and TMC membranes change with time, as do RO transport properties, when traces of MPD remain in the membrane after processing.

*   The surface roughness and area of CPTC membranes, determined by AFM, are similar to current FilmTec commercial membranes.

*   The desalination surface of the CPTC and TMC PA membrane barrier, as determined by AFM, appears as a dense concentration of pronounced peaks and valleys. A TEM study was conducted to determine the cross-sectional structure of the CPTC and TMC PA membrane barrier. Among the observations made were:

    a. The PA barrier of *cccc*-CPTC, *ctct*-CPTC, TMC and FilmTec membranes, have similar cross-sectional structures. The PA barrier of the membranes consists of two distinctive layers. The predominant feature, common to all PA membranes, is the large hollow closed cell structure that rests on a thin dense layer of PA. The hollow cells vary in shape, size, and packing density and range from a single to multiple layers, depending on the membrane processing parameters. These topography of the cellular structures appear as peaks on the AFM images taken "looking down" on the PA barrier.

b.   The cellular layer is relatively thick compared to the thin dense supporting PA layer which rests on the PS support membrane. The cellular structure represents the open or hollow area within the peaks shown by AFM. This structure explains the unusually high water productivity exhibited by PA membranes.

c.   The cellular layer of CPTC membranes is much thicker than the same layer of TMC membranes; the dense PA supporting layer of CPTC membranes is much thinner than the same layer of TMC membranes.

d.   The dense PA layer supporting the cellular layer is much thicker on FilmTec seawater membranes than on FilmTec brackish water membrane. This layer is thinner on the CPTC membrane than on either FilmTec commercial or TMC membranes.

e.   Relative to the TMC membrane, the PA barrier of the CPTC membrane shows a tendency to delaminate from the PS support membrane. Previous studies have shown that the aliphatic-aromatic PA membrane barrier of the CPTC membrane is not as well bonded to the PS supporting membrane surface as the aromatic-aromatic PA membrane barrier of the TMC membrane. Delamination may shorten CPTC membrane life, particularly with repeated RO system shutdowns.

f.   The thickness of the PA barrier on *ctct*-CPTC membranes is considerably thinner than on *cccc*-CPTC membranes; the cellular structure is also quite different between the two membranes.

*   Based on x-ray crystallographic analysis, the *ctct*- and *cccc*-CPTC membranes were non-crystalline with randomly oriented chains.

*   Generally, PA membranes are more susceptible to fouling than CA membranes. Bacterial attachment is greater for PA than for CA membranes by a factor of 2 or more. The surface roughness is also greater for the PA than for CA membranes by a factor of 2 or more.

*   Surface roughness as well as the transport properties of CPTC and TMC membranes can be beneficially modified by incorporating additives, such as isopropanol, acetone, phenol, etc., into the aqueous MPD phase, the hydrocarbon acid chloride phase or both during interfacial formation of the PA layer. The additive selected should exhibit some solubility in the opposing phase. The surface structure of the PA barrier is modified by altering the diffusion rates of reactant/reactants, MPD and/or CPTC or TMC, into the interfacial reactant zone. This approach for modifying the PA surface, to enhance transport properties and reduce fouling, has great potential and requires additional work.

*   ATR/IR spectroscopy analysis of the PA layer of CPTC and TMC membranes has shown that:

a. The PA film thickness of the CPTC membrane increases with increasing amine (MPD) concentration.

b. The relative carboxylate charge density of the CPTC membrane decreases with increasing MPD concentration.

c. The relative carboxylate charge density of TMC membrane was not altered by the acid chloride (TMC) concentrations. A similar conclusion would be likely for CPTC membranes

* The RO performance of CPTC and TMC membranes improve immediately after exposure to NaOCl over a broad range of pH.

* The CPTC membrane repeatedly exhibited less fouling in long-term field tests on surface water, municipal wastewater and seawater than either TMC control membranes and FilmTec commercial membranes.

* As a general rule, bacterial attachment and membrane fouling decrease with decreasing membrane hydrophobicity. The hydrophobicity of CPTC membranes was measured by captive air bubble contact angle for membranes made by differing process parameters. Membrane hydrophobicity increases with increasing contact angle. A summary of the results of this study follows:

a. CPTC membranes made with Freon solvent had lower contact angles (more hydrophilic) than other membranes made with hexane.

b. Membranes made from different synthesis lots of CPTC acid chloride exhibited similar contact angles.

c. Contact angles determined for CPTC and TMC membranes were very similar.

d. Varying TMC concentration and the method of MPD application during CPTC membrane processing had little or no effect on membrane contact angle or surface hydrophobicity.

e. The contact angle of CPTC membranes stored in water decreased with time over a 3-month period indicating that the membranes became more hydrophilic or more hydrated with time.

* The formation of HOBr is very fast in an RO feed water containing HOCl and a very small concentration of bromide ion which is present in most natural waters. Low concentrations of HOBr at pH 6.5 has a profound effect on the transport properties of CPTC and TMC membranes. HOCl at the same RO conditions has little, if any, effect on the transport properties of CPTC membrane.

* CPTC and TMC membranes are brominated very quickly by HOBr at very low concentrations. Although the data is not as conclusive, chlorination of CPTC and TMC membranes by HOCl appears likely. ATR/IR spectra suggest Cl or Br addition to the MPD ring. Elemental analysis by EDX of CPTC and TMC membrane surfaces after RO testing provided the following observations:

   a. Elemental bromine was not detected on any of the CPTC and TMC membrane samples that had not been exposed to HOBr.

   b. Elemental bromine was detected in increased percentages on all CPTC and TMC membrane samples exposed to NaOCl in the presence of NaBr The percentage of elemental bromine detected on CPTC membranes was greater than for TMC membranes. The data suggests that HOBr has brominated the PA structure making it an integral part of the membrane chemistry.

   c. Both CPTC and TMC membranes can be brominated in RO at low HOBr concentrations (< 3.5 mg/L free bromine) in DI water at pH 6.5.

   d. Elemental chlorine was detected on all CPTC and TMC membrane samples regardless of pre-treatment. The elemental weight percent of chlorine detected on CPTC membranes that had been exposed to HOCl are above baseline levels. It would appear that some chlorination of the membrane has occurred. Chlorination of TMC membranes is not pronounced.

* Free chlorine passage through the CPTC membrane is independent of the RO feed pH. Free chlorine passage is very low at pH 5.0 and increases with increasing feed pH.

* Synthesis of small quantities of ^{15}N-labeled MPD was completed and incorporated into the PA barrier of CPTC membranes. The ^{15}N-labeled membranes were prepared in an effort to better understand the interactions of chlorine/bromine with the PA barrier. Solid state NMR data collection on the membranes for the isotopes ^{15}N, ^{13}C, and ^{79}Br are underway. The interpretation of this data will result in valuable information that will make possible a more complete understanding of the mechanism(s) of membrane chlorination/bromination.

* Membrane surface charge, determined by uranyl cation binding, revealed that FilmTec commercial membrane is more negatively charged than CA membrane. CPTC membranes made with lower purity acid chloride exhibited the lowest relative surface charge. CPTC membrane made from the last and purest synthesis of acid chloride had a surface charge more negative than the new FilmTec membrane.

8

* CPTC membranes have demonstrated the ability to withstand high concentrations of NaOCl, without detrimental effects, in immersion tests where membranes were placed in full strength 3 wt-% (30,000 mg/L) NaOCl at pH 6.0 for 1 hr. The total membrane contact time with NaOCl was 30,000 mg/L-hr, or the equivalent of 6.8 years of membrane exposure at the level of 0.5 mg/L. After such exposure, CPTC membranes have operated for several thousand hours in long-term RO field tests on chlorinated feeds without degradation.

* Long-term RO field testing of *cccc*-CPTC and *ctct*-CPTC membrane samples in 1- x 3-in. test cells at WQIC on chlorinated brackish water demonstrated that:

    a. *cccc*-CPTC membranes deteriorated very rapidly, relative to CPTC and TMC membranes, in two field tests on different brackish water feeds at chlorine levels of 0.5 and 1.0 mg/L. A significant increase in salt passage was observed after 24 hr of operation. Pre-bromination of the cccc-CPTC membranes did not improve membrane life.

    b. CPTC and TMC membranes operated for several thousand hours in several test runs with no signs of chemical degradation. However, a quantum increase in salt passage was commonly observed for CPTC membranes after a system shutdown. Frequent system shutdowns limited the usefulness of the testing. Subsequent dyeing of the membranes showed physical damage at the O-ring/membrane interface. Physical delamination of the PA barrier from the PS support was observed in a parallel TEM study. Based on these observations, additional work is recommended to improve the physical durability of the PA barrier of the CPTC membrane.

    c. Future tests should be conducted in an O-ring free environment. It is recommended that CPTC membranes be incorporated into 2.5- x 14-in. spiral elements for future chlorine resistance testing. In the spiral configuration, there is no contact on the surface of the membrane as all seals are internal on the back side of the membrane

* Long term RO field testing of CPTC membrane samples in 1- x 3-in. test cells at OCWD were quite successful. CPTC membranes operated for more than 6 months in two independent RO tests on a chlorinated high-fouling municipal wastewater feed with little, if any, increase in salt passage. Because of the high nitrogen content of the wastewater, the chlorine was converted to chloramine. Under this condition, the CPTC membrane exhibited higher water flux, higher rejection and lower fouling than either TMC or FilmTec commercial membranes.

* Difficulties were encountered in the operation of the seawater field test system with numerous equipment failures and shutdowns. However, in a single test CPTC membrane operated equal with TMC and FilmTec for more than 1000 hr with no deterioration in performance. The system operated on natural seawater at 800 psi applied pressure, pH 5-5.6 with 0.6 mg/L free chlorine.

9

* 50 grams of high purity (99.9+%) *ctct*-CPTC acid chloride was produced near the end of the program for a large production run of CPTC membrane at a commercial membrane company. The membrane will be incorporated into 2.5- x 14-in. spiral-wound elements for field evaluation on chlorinated brackish, municipal and seawater feeds at WQIC, OCWD and at NFESC, respectively. Funding will be required to conduct long-term testing.

3.0 BACKGROUND AND TECHNICAL APPROACH

RO plants have been operating with spiral-wound thin-film composite membrane elements to desalinate brackish water and seawater since 1977. Presently, spiral-wound elements are supplied worldwide by eight major manufacturers. In the spiral configuration, the membrane dominates market share.

ATR/IR membrane surface analysis shows that all manufacturers use nominally the same aromatic membrane chemistry based on the interfacial reaction of MPD with TMC.[1] Thus, the propensity for fouling is similar for all membranes. The major membrane deficiencies that contribute to fouling, reduced membrane life and higher operating costs are:[5,6,7,8]

- Lack of chemical stability to oxidants such as chlorine,
- Enhanced fouling rates due to excessive surface roughness, and
- High bacterial attachment counts on the hydrophobic membrane surface.

There is great need to improve the stability of present state-of-the-art membranes to oxidizing agents. These improvements are critical for RO plants operating on wastewaters, surface waters and open seawater intakes where disinfection by chlorination is required to control growth of microorganisms on the membrane surface. These membranes are so susceptible to oxidation that dechlorination is required when chlorine is used as a disinfectant in the pretreatment. Dechlorination prior to the membrane creates added costs and effectively nullifies disinfection on the membrane surface where it is needed. Development of a chlorine-resistant membrane is a preferred solution to control membrane fouling, thereby increasing membrane life.

3.1 Membrane Oxidation Stability

Cadotte[1] originally demonstrated the utility of interfacial polymerization with TMC and MPD in preparing membranes with good desalination properties. Presently, this is the membrane of choice worldwide. Sundet et.al.[9] extended the aromatic/aromatic chemistry of Cadotte to aromatic/cycloaliphatic with 1,3,5-cyclohexanetricarbonyl chloride. Arthur et. al.[10] disclosed in U.S. Patent 4,749,488 (1988) the preparation of membranes by interfacial polycondensation of 1,2,3,4-cyclopentanetetracarbonyl acid chloride (CPTC) with MPD. More recently, Ikeda et. al.[2] reported results in the literature similar to that of Arthur using 1,2,3,4-CPTC acid chloride with MPD. In addition, it was reported that the chlorine tolerance of the membrane depended on which of the six stereospecific isomeric structures of 1,2,3,4-CPTC acid chloride was utilized.

Membranes prepared with cccc-CPTC and ctcc-CPTC acid chlorides reportedly deteriorated rapidly when operated in RO on a feed containing 1 mg/L chlorine for 50 and 150 hr, respectively. Membranes prepared with ctct-CPTC acid chloride, on the other hand, showed no deterioration after 1000 hr when operating at 214 psi applied pressure, 1500 mg/L NaCl, 1 mg/L chlorine and pH 6.5. This is a promising new approach to attaining a chlorine-resistant membrane. However, verification of this work is required since it is the only known reference on the subject.

The creation of a chlorine-resistant membrane has been under investigation by a number of researchers for more than twenty five years but without success. [8,9] During these studies many different acid chlorides and amines were evaluated including 1,2,3, 4-CPTC acid chloride. 1,2,3,4-CPTC has four reactive acid chloride groups that provide six possible geometric isomers. However, when the original studies were done, the steric configuration was not taken into consideration. Membranes had always been prepared from the isomer mixture of 1,2,3,4-CPTC acid chloride without isolation and purification of each isomer. For this reason, chlorine resistance may not have been observed.

To form a stable linkage between an amine and an acid chloride, the bond angles should be sterically optimized for maximum stability. Ridgway has determined the configuration for 1,2,3,4-CPTC using molecular modeling algorithms. [11] Each CPTC isomer shown was geometrically optimized (at 300°K, 1 atm, no water) to <0.001 kcal/mole-A using the Polak-Ribiere algorithm via classical mechanics (MM+, HyperChem). Molecular Dynamics (MD) simulations showed that a stable (low-energy) geometric conformer was attained after about 110 psec for the ctct isomer of CPTC acid chloride whereas, attainment of a similarly low-energy conformer for the cctt isomer of CPTC was observed out to 340 psec. This suggests the cctt-CPTC acid chloride isomer bond angle was generally more strained than the ctct-CPTC acid chloride isomer bond angle. In each case, potential energy declined as the system approached more stable geometric configurations. A somewhat higher final potential energy value for the cctt-CPTC acid chloride isomer was consistent with its comparative instability. Thus, it is hypothesized that the PA membrane bond angle created by the reaction of ctct-CPTC acid chloride with MPD has greater stability than those created by the other five isomers of 1,2,3,4-CPTC acid chloride, and this could be responsible for the reported chlorine resistance.

3.2 Membrane Surface Roughness

Collaborative work between SST and Ridgway et. al. [6,8] at the OCWD has shown that high levels of bacterial attachment occur on rough hydrophobic surfaces such as the fully aromatic membrane. Relatively low numbers of bacteria attach to smooth hydrophilic membranes such as cellulose acetate (CA). The PA membrane exhibits greater fouling rates than other types of membranes. The high level of surface roughness of membranes is partially responsible for fouling and has been well documented by SST and others by AFM. The low-fouling characteristics exhibited by CA membranes are, in part, attributed to the smooth surface of the membrane which does not trap or hold suspended solids in most RO feedwaters. [6] AFM photomicrographs

11

presented in Figures 3.0 and 3.1 show the smooth surface of a CA membrane, and the rough surface of a membrane made by the interfacial process with MPD and TMC. Previous work in this laboratory has shown that the mechanism responsible for surface roughness is not due to:

- Solvents - Membranes produced with acid chloride dissolved in hexane, isopar and Freon, have similar surface morphology.
- Cross-linking - both linear and cross-linked films show similar roughness.
- Post-treatment - processing following interfacial film formation.

It was shown in Phase I of this program that the surface roughness of the membrane can be modified without changing the RO transport properties.[27] This surface modification was achieved by increasing the transfer rate of MPD from the aqueous phase into the acid chloride hydrocarbon phase by altering the composition of the aqueous phase.

3.3 Membrane Surface Hydrophobicity

Biological fouling of membrane surfaces is a well-known phenomenon and a serious problem encountered in membrane plants. The PA membrane exhibits greater fouling than other types of RO membranes. Studies by Ridgway, in the U.S., and Flemming,[8] in Germany, have indicated that microorganisms exhibit very different affinities for surfaces of different membrane polymers. This suggests that membrane surface chemistry and structure play an important role in the bacterial adhesion process. Thus, membranes having special anti-fouling properties can be designed and manufactured. Ridgway et. al.[6,7,8] have shown that the attachment of bacteria to a membrane surface is dependent upon such variables as:

- The hydrophilic/hydrophobic nature of the membrane surface
- Membrane charge, surface roughness and available surface area
- The ionic composition and nutrient composition of the feedwater
- The nature of the bacterial cell surface

In these studies, it was shown that the Mycobacterium sp. strain are commonly present in pretreated municipal wastewaters used as RO feed. One isolated Mycobacterium strain BT2-4, exhibited high attachment to the more hydrophobic PA membrane and low attachment to the more hydrophilic CA membrane. Hydrophilic polymers exhibit greater water uptake than hydrophobic polymers. The highly cross-linked structure of the PA membrane has an intrinsic water content of ~5% while CA has an intrinsic water content of ~14%. Polysulfone (PS) membranes are very hydrophobic and foul very rapidly. However, when the PS membrane is made more hydrophilic by incorporating sulfonated polysulfone (SPS) into the membrane matrix, bacterial attachment is greatly reduced. During a parallel program, a procedure was devised to increase the hydrophilic nature of the PA membrane surface by covalently bonding a hydrophilic moiety to the PA surface immediately after interfacial film formation.
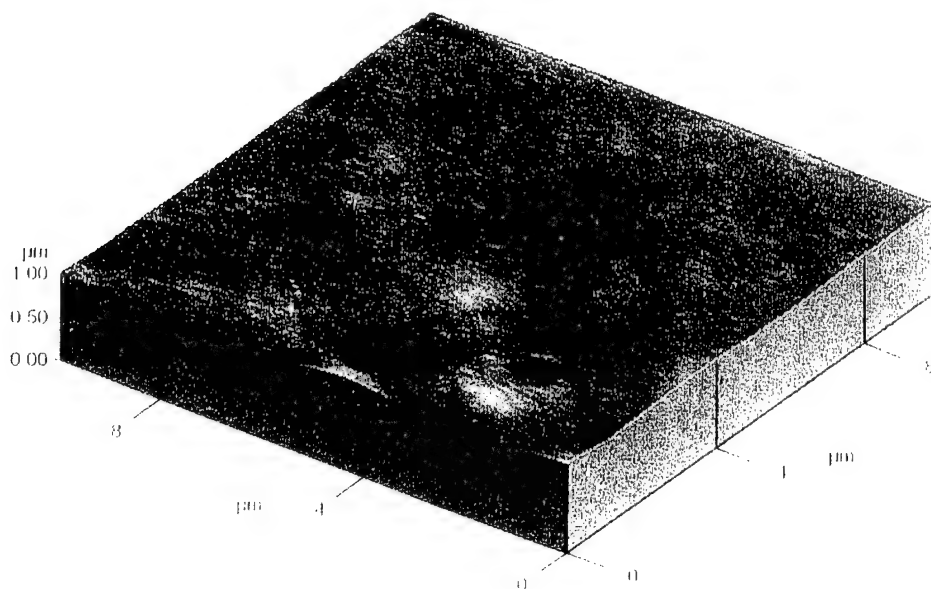
Figure 3.0 Three-D Atomic Force Topograph of the desalination surface of a
commercial CA membrane
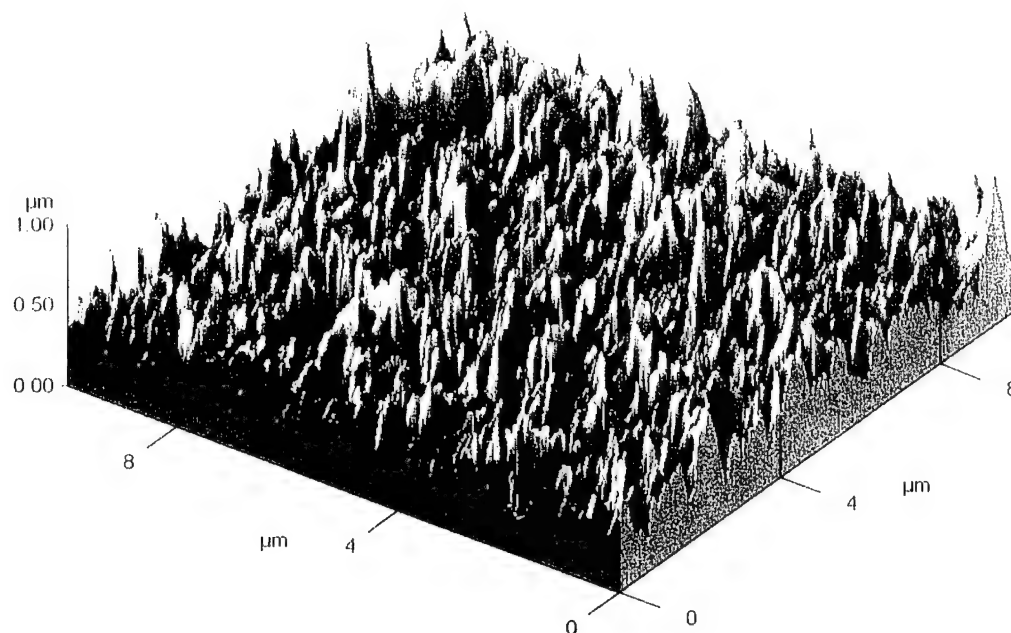
Figure 3.1 Three-D Atomic Force Topograph of the desalination surface of a
commercial TMC membrane

4.0 COST BENEFITS OF AN OXIDATION-RESISTANT MEMBRANE

The lifetime of RO elements is strongly influenced by membrane fouling and frequency of cleaning; that is, the greater the frequency of cleaning the shorter the membrane life. Leslie [16] at OCWD has estimated the annual savings that could be attained by reducing membrane fouling using the following assumptions: OCWD Water Factory 21 type RO plant, 6 mgd RO capacity, 5-yr membrane life and operation on secondary wastewater feed. For an improved low-fouling membrane, the annual savings ($/yr) attained by reducing membrane fouling to extend membrane life is as follows:

	5 Year Membrane Life Extended by (Hrs.)		
Membrane Fouling Reduction (%)	20 %	40%	100%
0	$36,000	$63,000	$108,000
25	$126,000	$153,000	$198,000
75	$306,000	$333,000	$378,000

The savings are quite apparent, emphasizing the benefit for a reduced fouling chlorine-resistant membrane.

5.0 POTENTIAL FOR COMMERCIAL APPLICABILITY

Membrane development at SST is conducted on a pilot level for rapid transfer to large-scale continuous processing. As a result, membrane improvements derived from this program can quickly move into production and the marketplace. These membrane improvements do not add significant costs to membrane processing or to the final product. Membrane manufacturers can use their current membrane processing equipment with little, if any, modification.

14

6.0 MOLECULAR MODELING OF AROMATIC CROSS-LINKED MEMBRANES PREPARED FROM CPTC AND MPD

6.1 Introduction

Molecular modeling was used to investigate the structure and energetics of polymeric cross-linked membranes built from alternating CPTC and MPD monomers. Comparison of the six isomers of the CPTC acid chloride molecule indicated that the *ctct*-CPTC isomer was the least strained sterically, having the lowest total steric energy and the lowest computed heat of formation. The *ctct*-CPTC isomer also exhibited the greatest ionization potential and, accordingly, the lowest energy for the highest occupied molecular (HOM) orbital. These observations are consistent with the enhanced chlorine resistance of the *ctct*-CPTC membranes compared to membranes prepared from the other five CPTC stereoisomers (e.g., *cccc*-CPTC membranes). Similarly, the calculated ionization potential of TMC was significantly lower than that of *ctct*-CPTC. This observation is consistent with the extreme sensitivity of standard RO membranes to oxidation by free chlorine (i.e., hypochlorous acid or the hypochlorite anion). Based on these observations, it is hypothesized that monomer stability and reactivity partially determine the stability and reactivity of the polymer membranes.

Using the Tool Command Language (Tcl/Tk), software was created for this project enabling automated construction and analysis of 3-D models of CPTC membranes that were either pseudo-randomly or randomly cross-linked. Whereas detailed experimental data on the molecular structure of the CPTC membranes is still largely lacking at this time, the membrane models currently provide the best approximation of the molecular structure of CPTC membranes.

In one modeling approach, membranes were built by linking together pre-formed polymer chains first into 2-D sheets and then into 3-D blocks. Cross-linking was pseudo-random in the sense that it could only occur between pre-determined bonding pairs in neighboring chains or sheets. The other modeling approach is based on a 'random walk' through a cubic block of alternating CPTC and MPD monomers to establish the pattern of bonding in the membrane matrix. This 'lattice' method is more flexible and allows all possible bonding arrangements to occur in a truly randomized manner. The lattice method also lends itself to the use of geometric constraints to control the degree of membrane cross-linking.

In *ctct*-CPTC membrane models that were geometry optimized to a local energy minimum of <0.1 kcal/mol-A, secondary structure (i.e., chain folding) was partially stabilized by formation of internal hydrogen bonds between protons on primary amines participating in backbone amide bonds and carbonyl groups on CPTC monomers. Bond bending, torsion bonds, and van der Waals interactions contributed most strongly to steric strain within the membrane models, and most steric strain was located toward the membrane interior.

Prior to energy minimization by molecular dynamics (MD), the density of a typical *ctct*-CPTC membrane model is ~0.72 g/cm^3, a value which is consistent with a somewhat open or porous molecular sieve-like structure that should facilitate high water transport rates. The models clearly indicate the presence of significant void spaces in the membrane interior that would likely be instrumental in water and solute transport processes. The membrane density could be increased significantly by performing MD simulations in the presence of positive ions to neutralize the repulsive effects of free carboxyl groups in the CPTC membrane models. Thus, it may be possible to use salt to control and reduce the membrane void space and increase the solute rejection properties of the membrane.

Comparison of *ctct*-CPTC and *cccc*-CPTC membrane models that were created using identical program setup parameters (e.g., torsion bond angles, cross-linking probabilities, etc.) has so far failed to reveal any structural features that might explain the greater chlorine resistance of the former membrane type. However, preliminary calculations indicate the *ctct*-CPTC membrane is more stable than the *cccc*-CPTC membrane, which is in agreement with the greater stability of the *ctct*-CPTC monomer. X-ray diffraction analyses indicated that the *ctct*-CPTC and *cccc*-CPTC membranes lacked any significant crystallinity, but their densities were identical.

Reaction modeling was also performed to help delineate the mechanism of chlorine resistance of the *ctct*-CPTC membranes. These efforts involved the application of MD methods to simulate the reaction of hypochlorous acid with *cccc*-CPTC or *ctct*-CPTC polymer fragments. Results from these modeling experiments indicated that HOCl is able to oxidize the primary amine nitrogen atom forming the backbone amide bond of the *cccc*-CPTC polymer chains. This oxidation reaction often results in deprotonation of the primary amine and subsequent addition of chlorine to the nitrogen atom (i.e., a primary amine chloramination reaction). The reaction is sometimes associated with migration of the chlorine atom to the MPD ring. Reaction products observed include water, hydrochloric acid, hydroxyl radicals, and free protons. The hydroxyl radicals may enter into additional reactions with the chlorinated amine nitrogens or other polymer centers, although this has not yet been explored. The amide bond in the *ctct*-CPTC model fragment was more resistant to this type of chloramination reaction than was the *cccc*-CPTC model fragment. The reaction modeling also suggested that the *ctct*-CPTC amide bond was more resistant to bond breakage than the corresponding *cccc*-CPTC bond.

6.2 Background

RO membranes remove (reject) virtually all microorganisms (including viral agents) and many inorganic and organic solutes from the feedwater. While water flux and solute rejection behavior can be modeled with considerable precision for RO membranes, the molecular mechanisms by which water and solute transport occurs in semi-permeable polymer membranes is still incompletely understood,[22] One of the barriers to understanding mass transport processes at the atomistic scale is the general lack of knowledge concerning the molecular structure of the membranes themselves. Information regarding membrane molecular structure may be obtained form X-ray crystallography, nuclear magnetic resonance spectrometry, high resolution atomic force microscopy, and other techniques. However, such analyses are costly and fail to provide information on the dynamical aspects of solute-membrane interactions (e.g., solute diffusion rates and mechanisms).

6.2.1 Application of Molecular Modeling

Another approach that can be used to help understand membrane molecular structure and dynamics is molecular modeling. Molecular modeling techniques have evolved extremely rapidly over the past decade and personal computers have gained sufficient central processor unit (CPU) speed and memory capacity to enable dynamic simulations of modestly sized polymer systems containing up to several thousand atoms.

Modern molecular modeling is built around the concept of the force field, which is a set of equations (encoded as computer algorithms) that describe the forces acting on each atom in the system. There are two broad categories of force fields, molecular mechanics force fields and quantum mechanical force fields. Molecular (classical) mechanics force fields describe atom forces and atom interactions in terms of Newtonian principles of motion.

Classical force fields are conceptually fairly simple and do not take into account the electronic structure of the atoms apart from a term that describes electrostatic (i.e., Coulomb type) interactions among charged atoms in the system (see Figure 6.0). Atoms are viewed more or less like solid billiard balls in molecular mechanics force fields, each having a fixed mass and diameter and attached to its neighbors by flexible spring-like bonds. Bond lengths and energies are effectively characterized in terms of 'spring constants' which are computed from equations that resemble Hook's Law.

Molecular mechanics force fields treat atoms as solid masses linked by bonds that behave more-or-less as elastic springs. As shown in the water molecule (Fig. 6.0, each bond possesses an ideal geometry consisting of a preferred bond length (stretch term), bond angle (bend term), etc. In addition, there are non-bonded interaction terms such as van der Waals and electrostatic forces. Summing all the energy terms results in the total steric energy of the molecule. Departure from the ideal geometry results in steric strain within the molecule and therefore greater instability (i.e., a steep steric energy

17

gradient). Geometry optimization of a molecule is performed by systematically changing the atom (nuclear) positions and re-computing the steric energy each time until the lowest energy state is found. Many versions of molecular mechanics force fields exist.

Molecular mechanics force fields must be calibrated (i.e., parameterized) for each bond type or atom type found in the system. For example, a carbon=carbon double bond must have a preferred or 'ideal' bond length (stretch mode) and angle (bend mode). A carbon-oxygen single bond would have a different ideal length, angle and overall energy. Deviations from these ideal bond conformations (e.g., in a non-optimized molecule) cause an increase in the steric energy of the system. Such bond parameters are usually determined from experimental data and they are somewhat generalizable between different molecular systems. A number of classical force fields have been devised over the past decade (e.g., MM3, MM+, AMBER, OPLS, etc.), each parameterized for certain sets of atom types.

Molecular Mechanics Force Fields:

Total Steric Energy $= E_{bend} + E_{stretch} + E_{torsion} + E_{vdw} + E_{elec} + E_{H\text{-}bond} + E_{cross\,terms}$

Geometry Optimization By Molecular Mechanics:

repeat until optimized

1. Assume initial atom positions
2. Calculate atom forces
3. Adjust atom positions
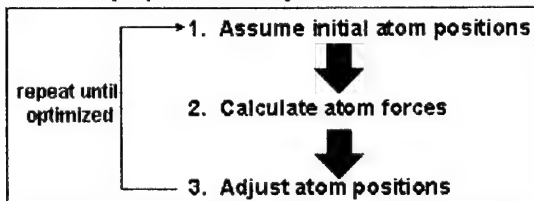
MM Force Field Examples:

- MM2, MM3, MM4 (organic molecules)
- MM+ (organic molecules, HyperChem)
- AMBER (proteins, nucleic acids)
- OPLS (like AMBER, explicit solvation)
- BIO+ (biological macromolecules)
- many proprietary versions

One Example of a Molecular Mechanics Force Field:

- $E_{stretch} = 1/2 k_s (l - l_0)^2$
- $E_{stretch} = 143.88 K_s/2 (l-l_0)^2 [1-2.00(l-l_0)]$
- $E_{bend} = 0.043828 k_b/2 (\theta-\theta_0)2 [1+7(10^{-8})(\theta-\theta_0)4]$
- $E_{torsion} = V_1/2(1+\cos\omega) + V_2/2(1-\cos2\omega) + V_3/2(1+\cos3\omega)$
- $E_{vdw} = \varepsilon[(r_0/r)^{12} - 2(r_0/r)^6]$
- $E_{vdw} = \varepsilon(-2.25(r_v/r)6 + 2.90(10\text{-}5)exp[-12.00(r/r_v)])$
- $V_{charge} = q_i q_j/D r_{ij}$
- $V_{dipole} = \mu_i \mu_j/D r_{ij}^3 (\cos\chi - 3\cos\alpha_i \cos\alpha_j)$
- $E_{cross terms} = $ stretch-stretch, stretch-bend, torsion-stretch, torsion-bend, bend-bend, etc.

Bend

Stretch
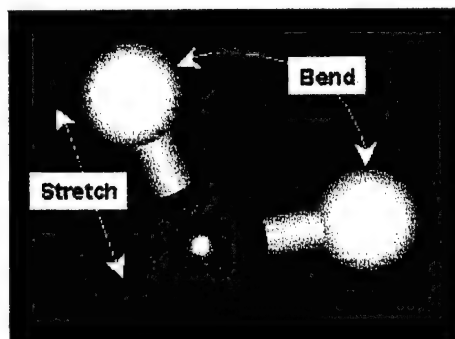
Figure 6.0 A generalized diagram of molecular mechanics force fields

Molecular mechanics force fields are generally used for polymer systems where large numbers of atoms are involved, not because they are more accurate (actually they are usually less accurate than quantum mechanical force fields), but rather because they require less CPU and memory resources since there are fewer computations involved.

Quantum mechanical force fields provide an approximate solution to the time independent Schoedinger wave function to arrive at the electron (orbital) energies and distributions around each atom comprising the molecular system (see Figure 6.1). The calculated atomic orbital shapes, degree of orbital overlap, and partial charges define how atoms interact to form the whole molecule. For example, the shape of the highest occupied molecular orbital of the OCl⁻ anion is shown. Deviation from the ideal (electronic or orbital) geometry results in steric strain within the molecule and therefore greater instability (i.e., a steeper steric energy gradient). Geometry optimization of a molecule is performed by systematically changing the nuclear positions and re-computing the new set of MOs each time until the lowest energy state corresponding to the least sterically strained conformation is found. Many versions of quantum mechanics force fields exist, each having parameters that are optimized for certain element or compound types.

Quantum mechanical force fields, which are CPU and memory intensive, are often employed prior to a molecular mechanics force field calculation to establish the partial charges on each atom of a molecular system. The sum of the partial atom charges yields the total molecular charge. In semi-empirical quantum force fields, some of the critical values for core electron and nuclear interactions are parameterized using experimentally derived data, but far fewer parameters are used in semi-empirical force fields than in classical force fields; thus, semi-empirical force fields can typically be applied to any molecular system regardless of atom types. Because solutions to the electronic wave functions require iterative computations for many complex integrals, such calculations are very CPU intensive and therefore take much longer to carry out. Therefore, they are not generally used for modeling intact polymer systems unless many simplifications are first made. However, quantum mechanical force fields are often employed to model the individual monomers (and set atom partial charges) which comprise the polymer membrane system. Classical force fields are then applied to compute polymer system properties (*e.g.*, total steric energy, surface free energy, *etc.*) or simulate dynamic processes such as water and solute diffusion within the polymer membrane.

6.2.2 Goals of Molecular Modeling in this Program

In the present investigation, molecular modeling techniques were utilized to explore the stability of the six stereoisomers of CPTC, a cyclic multifunctional aliphatic that can be reacted with the di-functional amine MPD in an interfacial condensation reaction to produce a cross-linked thin-film membrane. Only the *ctct* isomer of CPTC is capable of producing a membrane that resists oxidative damage from free chlorine (as hypochlorous acid). In addition to examining CPTC isomer stability, custom software was designed to build and geometrically optimize (i.e., energy minimize) a model of the CPTC membrane. The CPTC membrane models may be constructed using any one of the six CPTC stereoisomers, thereby allowing comparisons to be made between the structural and energetic properties of the finished membranes. It is anticipated that a detailed comparison of the structural and energetic features of the chlorine-resistant and the chlorine-sensitive versions of the CPTC membranes could shed light on the mechanism of chlorine resistance in the membrane built from the *ctct* isomer.

In addition, the membrane models may be used as the starting point for molecular dynamics (MD) simulations of water and solute diffusion (i.e., mass transport) behaviors in the membranes. Water and solute diffusion coefficients computed from the results of MD simulations can be used to predict the flux and rejection of the six isomers of CPTC membranes. Finally, molecular modeling techniques were employed to simulate the reaction of hypochlorous acid with model CPTC polymer fragments to identify potential reaction products of membrane chlorination.

Quantum Mechanical Force Fields:

Approximate solutions to the electronic Schrodinger wave equation describing the electron energy and orbital structure of atoms

Geometry Optimization By Quantum Mechanics:

Geometry Optimization By Quantum Mechanics:

repeat until optimized

1. Assume initial nuclear positions
2. Calculate molecular orbitals
3. Calculate nuclear forces
4. Adjust nuclear positions
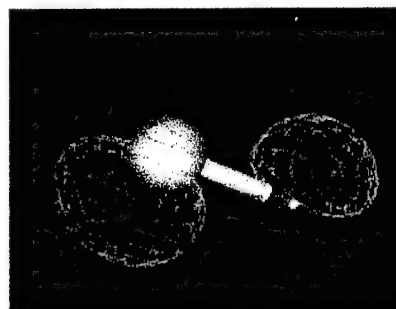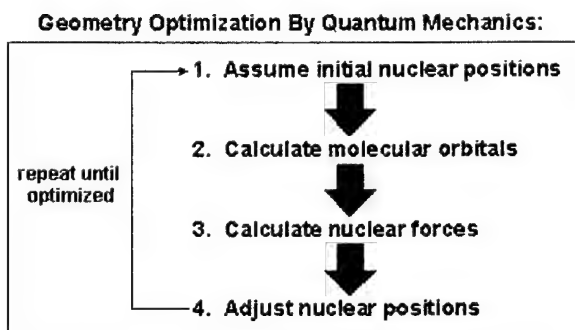
QM Force Field Examples:

- AM1 (very accurate, organics)
- PM3 (re-parameterization of AM1)
- Extended Huckel (any element)
- MINDO3 (large organics)
- ZINDO/1 (transition metals)

Figure 6.1   Semi-empirical quantum mechanical force fields

6.3 CPTC Monomer Structure and Energetics

The molecular structure of each CPTC stereoisomer is shown in Figure 6.2. In the all-cis isomer (e.g., cccc-CPTC), the four acid chloride groups all point in the same orientation (downward or upward) relative to the plane of the cyclopentane ring. In the ctct-CPTC isomer, the orientation of the acid chloride groups alternates relative to the ring.

ccccCPTC	ccctCPTC	ccttCPTC
ctccCPTC	ctctCPTC	cttcCPTC
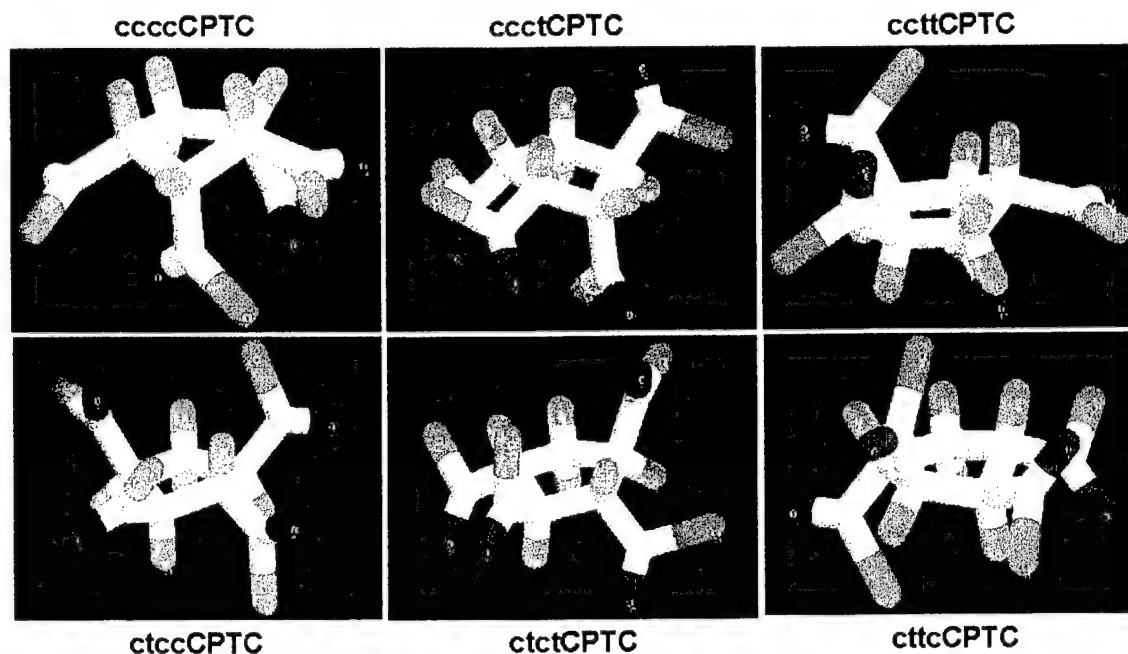
Figure 6.2 The six stereoisomers of the CPTC monomer. Carbon = white; Hydrogen = light blue; Oxygen = red; Chlorine = green. Torsion bonds in the structures shown have not been geometry optimized (i.e., energy minimized).

Only the *ctct*-CPTC stereoisomer is able to form a stable chlorine-resistant membrane when reacted with MPD. It seems reasonable that the enhanced stability and chlorine tolerance of this membrane may be related in part to the relative stabilities of the CPTC isomers. Therefore, the steric energies of the six isomers of CPTC were analyzed and compared. In order to compute the steric energies, each isomer was first geometry optimized using first the classical MM+ force field (Hypercube; see Figure 6.3), followed by the PM3 semi-empirical quantum mechanical force field (unrestricted Hartree-Fock method). All geometry optimizations were performed using the Polak-Ribiere conjugate-gradient method with a convergence limit of <0.1 kcal/mol-Å. The four acid chloride torsion bonds were rotated systematically at 10 degree increments to identify the conformer in each case having the lowest (global) energy minimum. A total of 1.67 million torsion bond conformations were examined for each of the six isomers. Once the global energy minimum was found, that conformer was further geometry optimized via the semi-empirical PM3 force field. The electronic structure and steric energies of each geometry optimized isomer was then computed using the PM3 force field.

The calculation results presented in Figure 6.4 indicate that the *ctct*-CPTC molecule is the most energetically stable of the six stereoisomers. The least stable molecules energetically were the *cccc* and *cttc* isomers. Apparently, when the acid chloride pendent groups point in the same orientation relative to the cyclopentane ring, they tend to interact sterically with one another more than when they are

MM+ Force Field

(Hypercube)

- Bond stretch (cubic, switiched function for >equilibrium bond lengths)

- Bond angle bending (simple harmonic and sextic term)

- Out-of-plane bending (quadratic term as above)

- Dihedral (torsion) angles (Fourier series term)

- Stretch-bend cross term (product of cubic/harmonic)

- Dipole interactions (specified dielectric)

- Electrostatic forces (explicit atom charges via QM methods)

- van der Waals (attractive + R^{-6} dispersion)

- MM2 parameters (1991 parameters via Allinger)

- Default Dreiding parameter scheme (Mayo et al., 1990)

  (hybridization; bond type; c-radii)

Figure 6.3   Hypercube's MM+ classical force field uses a default parameter scheme similar to that of Mayo *et al.* (1990). The estimated default parameters allow the MM+ force field to be used with almost any element or compound.

distributed more uniformly around the molecule (e.g., as in the *ctct* isomer). Such steric interference may not be surprising given the bulky nature of the chlorine atoms. This is perhaps most apparent when the *cccc* isomer is rendered as a space-filled model where all atoms are represented as CPK spheres using van der Waals radii (see Figure 6.5). Steric interferences between neighboring atoms can result from non-bonded interactions such as van der Waals forces and coulomb interactions.

The heats of formation of each of the CPTC isomers is also presented in Figure 6.4. The PM3 force field has been parameterized by fitting to experimentally derived heats (enthalpies) of formation for a set of molecules at 298°K. The heat of formation is calculated by subtracting the atomic heats of formation from the electron binding energies. As can be seen from an inspection of Figure 6.4, the *ctct*-CPTC isomer exhibits the lowest formation enthalpy, suggesting it is the most stable of the six stereoisomers.
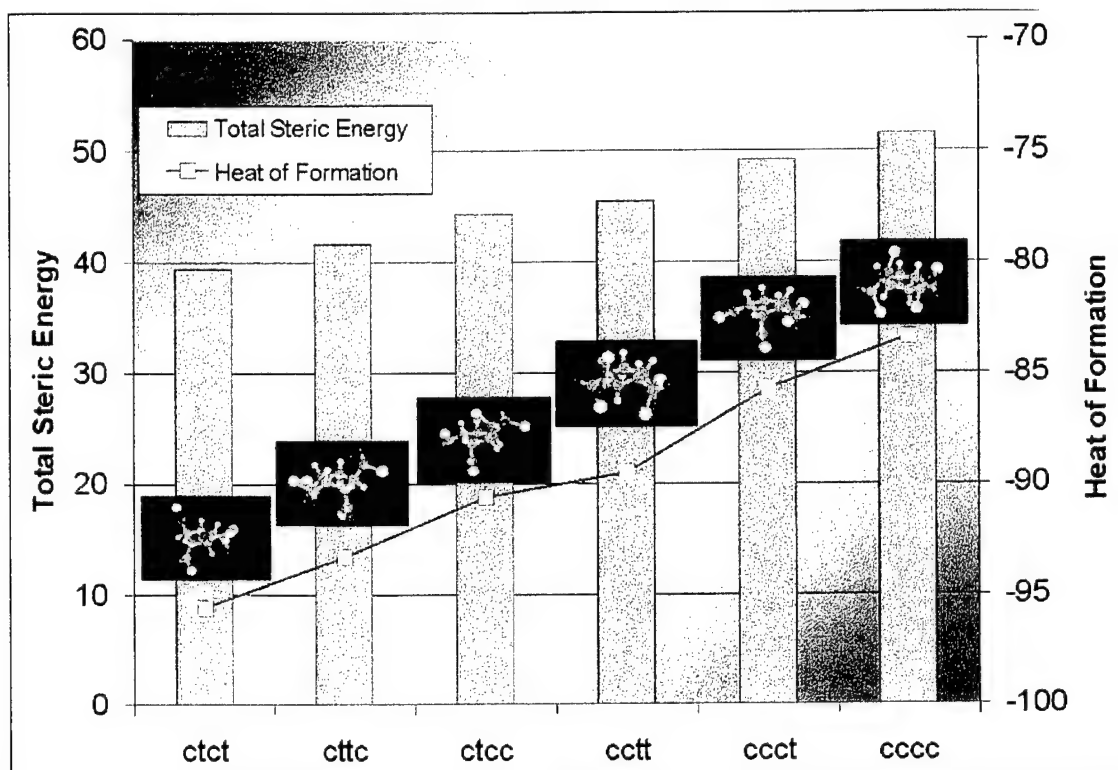
Figure 6.4   Total steric energies and heats of formation (in kcal/mol) for the six
CPTC stereoisomers. Energies were computed for the global minimum
conformation of each isomer using the semi-empirical PM3 force field
(see text for details). All energies are expressed in kcal/mol.

A higher degree of atom crowding and repulsive interactions was also suggested
by calculating the ovalities of each CTPC stereoisomer. The molecular ovality is defined
as the dimensionless ratio of the calculated surface area to the idealized surface area
assuming the molecule were a perfect sphere. Data presented in Figure 6.5 indicates
the *ctct*-CPTC isomer exhibited the greatest ovality, which is consistent with a lower
degree of atom crowding in this molecule. The *cccc*-CPTC isomer, on the other hand,
exhibited the lowest ovality suggesting a more compact structure with a higher degree of
atom crowding and interaction. The greater degree of atom interaction in the all-cis
isomer would tend to make this isomer less stable energetically.

The contributions of individual force field energy components to the total steric
energies for the six CPTC stereoisomers is given in Figure 6.6. All values are
expressed in kcal/mol. Torsion bond angles (for the acid chloride groups) and dipole-
dipole interactions contribute most to the total steric energies of the isomers. However,
it should be noted that bond bending energies increase significantly from left to right in
Figure 6.6. Thus, bond strain due to bending is disproportionately larger in the *cccc*-
CPTC isomer than in the *ctct*-CPTC isomer. These findings are in general agreement
with the net isomer dipole moments which are presented in Figure 6.7. The net
molecule dipole moment is computed by summing the X, Y, and Z dipole moments.

23

Since the dipole moment depends on atom position and partial charge, the isomer which exhibits the lowest dipole moment is likely to be the least strained due to internal coulomb interactions.
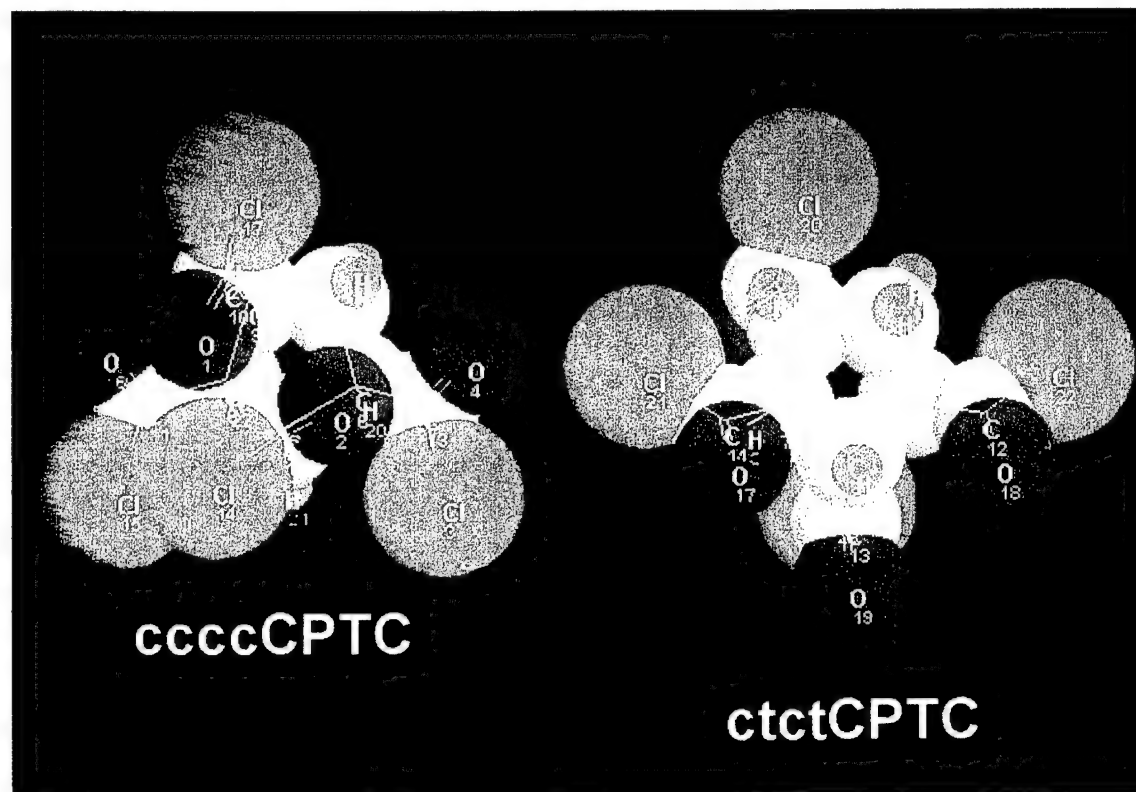
Figure 6.5   Space-filled molecular models comparing atom crowding in the *cccc*-CPTC and *ctct*-CPTC stereoisomers. Both isomers have been positioned in the same orientation to allow direct comparison of atom positions. Note that the chlorine atoms (green) are comparatively bulky and tend to interfere with one another in the *cccc*-CPTC isomer.

The electron binding energy of the *ctct*-CPTC isomer was larger than the other five isomers (data not shown). As a consequence, the computed ionization potential of the *ctct* isomer was also greater than the other isomers, although very high ionization potentials were also observed for the *cttc* and *cctt* isomers as well (see Figure 6.8). Accordingly, the *ctct* isomer also exhibited the lowest energy for the highest occupied molecular (HOM) orbital. Koopmans' theorem relates the ionization energy of a molecule directly to the inverse of the energy of the HOM orbital; thus, ionization potentials are computed directly from the HOM orbital energies gotten from quantum mechanical force field calculations.
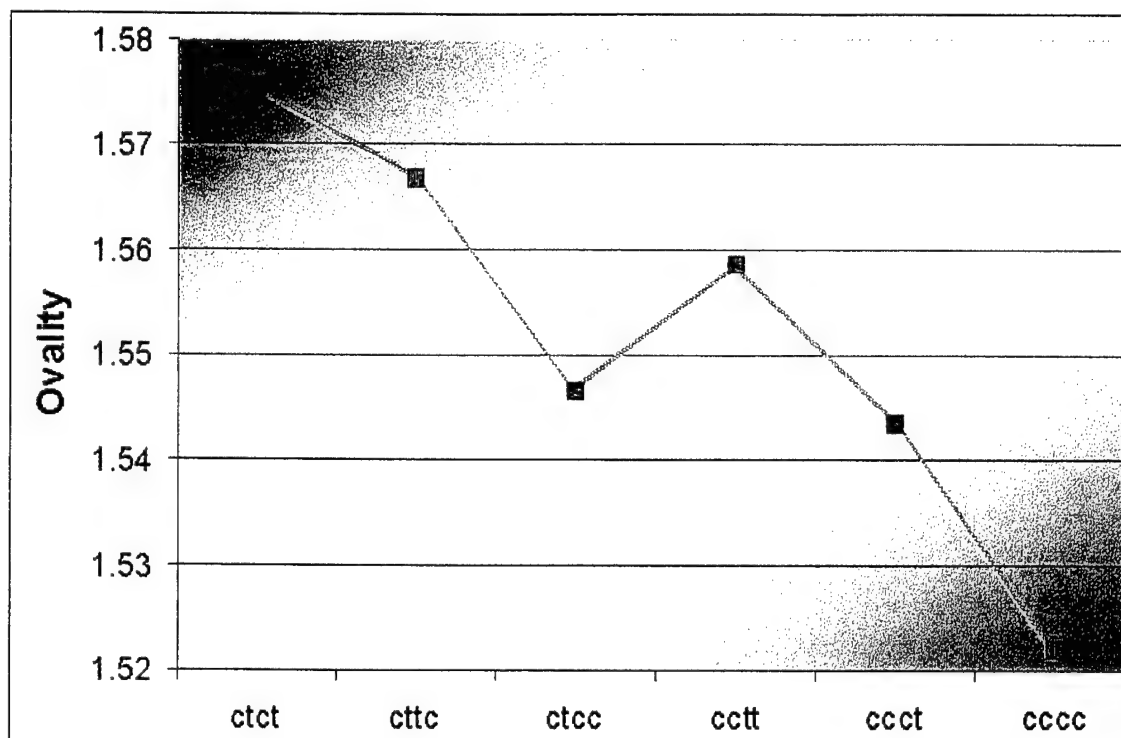
Figure 6.6   Calculated ovalities for the six CPTC stereoisomers
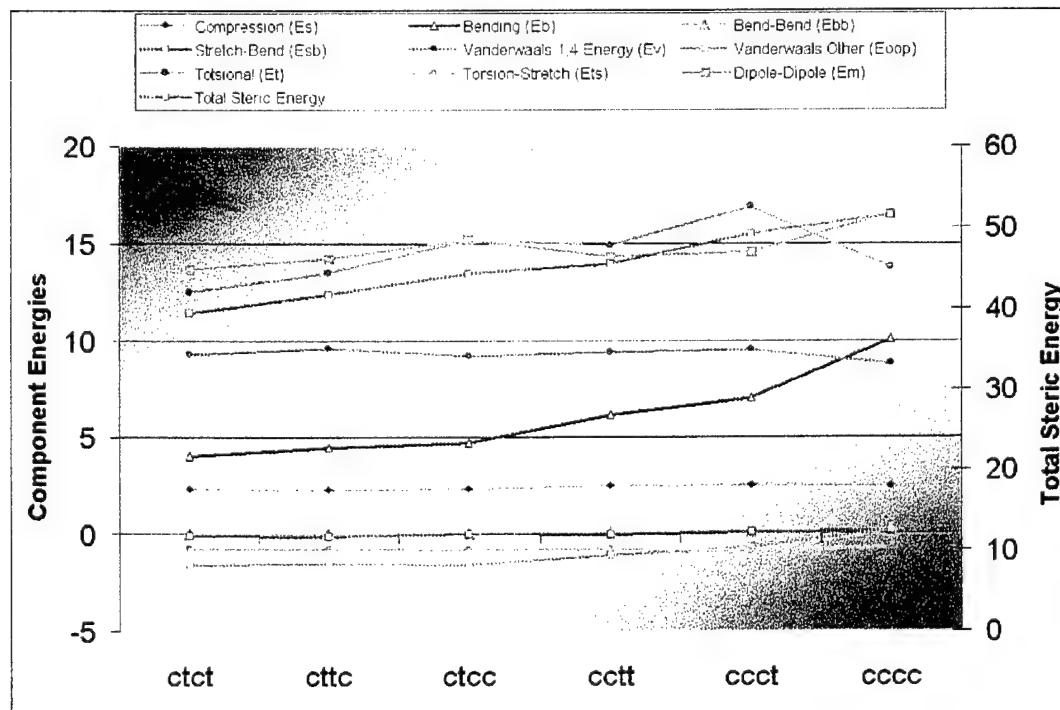
Figure 6.7   Contributions of component energies to the total steric energies for the six CPTC stereoisomers
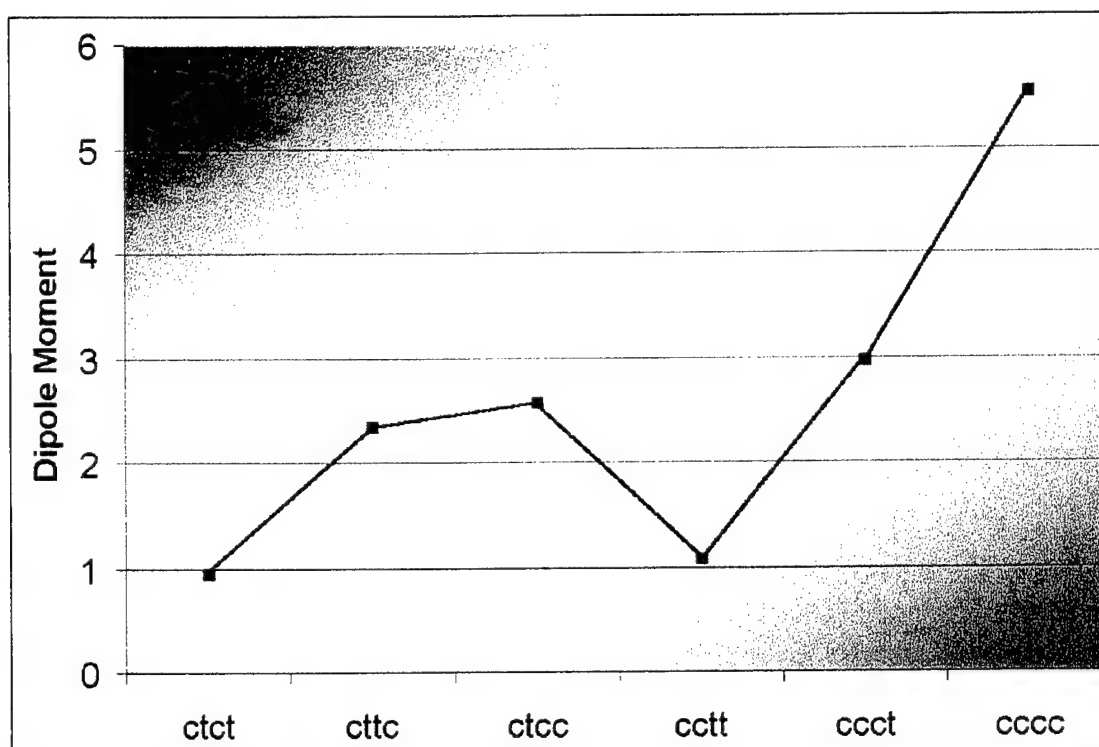
Figure 6.8   Dipole moments of the CPTC stereoisomers computed using the semi-empirical PM3 force field. Note that the *ctct*-CPTC molecule possesses the lowest dipole moment while *cccc*-CPTC exhibits the largest.

The *alpha* and *beta* electrons populating the HOM orbital were somewhat more symmetrically distributed over the atoms comprising the *ctct*-CPTC isomer compared to the situation for the *cccc*-CPTC isomer (see Figure 6.10). Because the molecular dipole moment results from atom locations and partial charges, the greater spatial asymmetry of the HOM orbital electrons in the *cccc*-CPTC molecule may have contributed significantly to the larger dipole moment observed for this all-cis isomer (see Figure 6.8). A larger dipole moment is sometimes correlated with greater compound instability and reactivity.

These calculations indicate that the *ctct*-CPTC stereoisomer is the least likely of the six isomers to donate an electron from its outermost (most reactive) molecular orbital during an electrophilic attack by an oxidizing agent. Thus, a chemical oxidizing agent such as chlorine (*i.e.*, hypochlorous acid) should be least effective against the *ctct*-CPTC isomer. In contrast, the *ctcc, ccct* and *cccc* isomers exhibited the lowest ionization potentials and the greatest HOM orbital energies, suggesting they would be the most reactive species and more susceptible to the effects of an oxidizing agent such as hypochlorous acid. The ionization potential of the aromatic acid chloride, TMC, was similar to those of the *ccct* and *cccc* isomers and would therefore suggest similarly enhanced susceptibility to chemical oxidation.
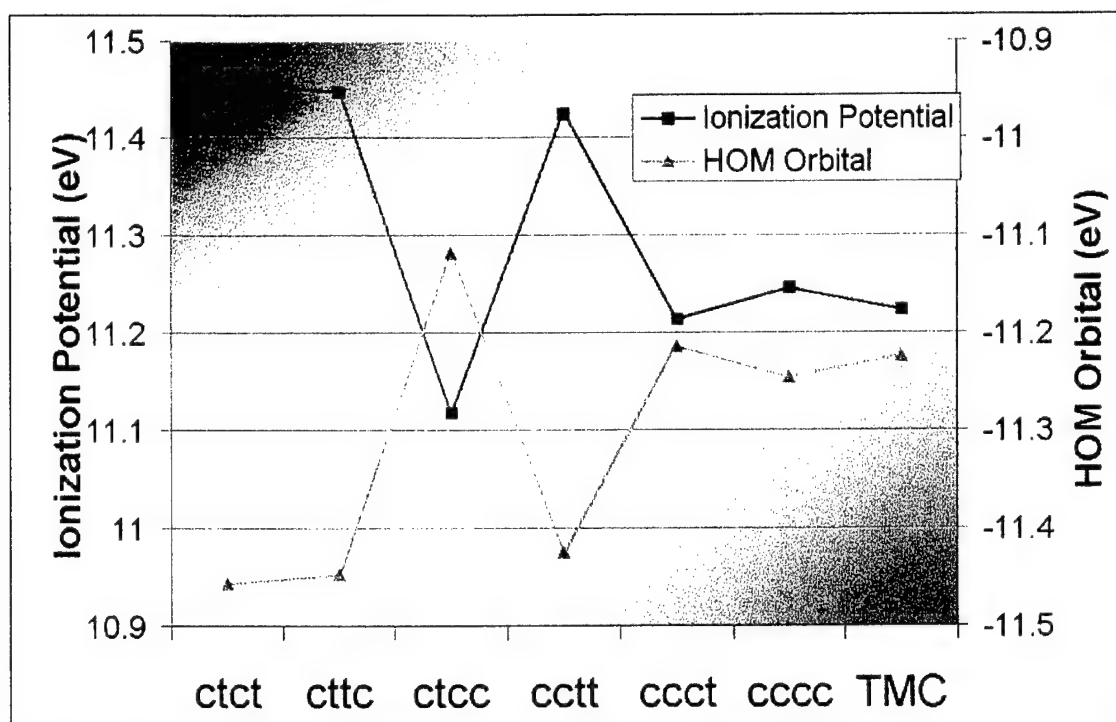
Figure 6.9   Ionization potentials and highest occupied molecular (HOM) orbitals for the six CPTC stereoisomers and TMC

It is uncertain how well the more favorable properties of the *ctct*-CPTC monomer will transfer to a polymeric system incorporating this isomer. However, it should be possible to answer this question by performing similar calculations on individual polymer chains comprised of the monomers or even small membrane models containing a few hundred to several thousand atoms (see Figure 10).

6.4 Building the *ctct*-CPTC Membrane Model

It was necessary to create generic software capable of building a molecular model of the *ctct*-CPTC membrane not only so that its 3D structure could be explored in detail, but also to use the model in future simulations of water and solute diffusion. Because of its generic nature (i.e., the ability to substitute other isomers as polymer building blocks), the model building software should permit a precise comparison to be made between membranes built using any of the six CPTC stereoisomers.

Two different strategies were employed to build model CPTC membranes. The first approach is referred to as the 'Layer Method'. The Layer Method involves synthesis of polymer chains followed by psuedo-random chain cross-linking to create 2-D membrane sheets. The sheets are then cross-linked pseudo-randomly to form the 3-D model. While this method works and gives structures that look reasonable, the cross-linking reactions are not entirely randomized, a factor which precludes certain conformations which would otherwise be permissible if bonding was truly random.

27
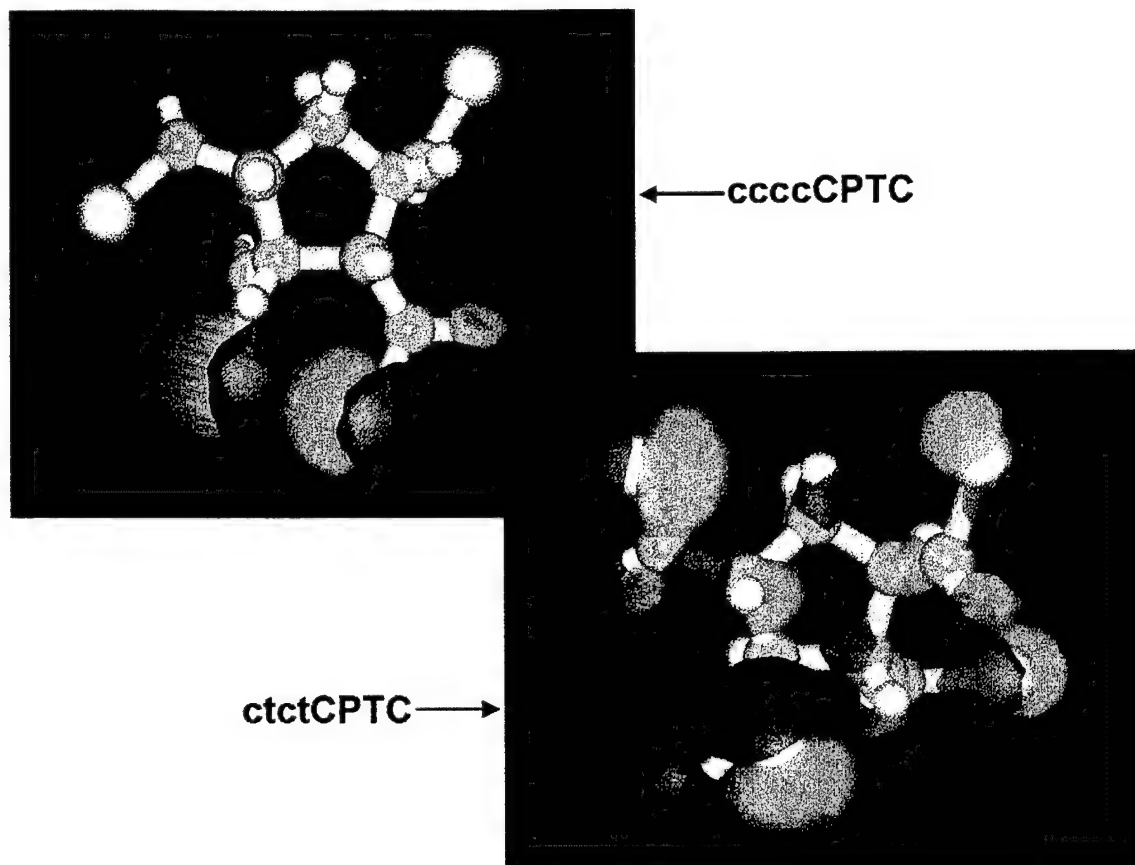
Figure 6.10 3-D plots of the HOM orbitals for the *cccc*-CPTC and *ctct*-CPTC
             stereoisomers. The two molecules are oriented similarly to facilitate
             direct visual comparison of atom locations.

The second approach was developed late in the project but is believed to be a
superior technique because it allows completely randomized bonding between
monomers (sometimes referred to as 'residues') comprising the membrane model. In
this approach, alternating CPTC and MPD residues are first laid down in the form of a
cubic lattice of $N \times N \times N$ dimensions. The residues are subsequently randomly
connected (bonded) to create the membrane model. One great advantage of this
'Lattice Method' is that geometry constraints can be invoked to control the likelihood of
the bonding (cross-linking) reactions. For example, if two residues lie beyond some
maximum allowable bonding distance, a bond will not be permitted to form.

Both the Layer Method and the Lattice Method are discussed in more detail below.

6.4.1 Use of the Layer Method to Build CPTC Membrane Models

Construction of a *ctct*-CPTC model by the Layer Method involves the following major steps. Custom software written in the Tool Command Language (Tcl/Tk) automates all steps of the membrane building process. The user has control of all major system (i.e., membrane structure) variables, such as polymer chain length, the degree and randomness of cross-linking, polymer backbone torsion angles, membrane charge, initial chain positioning, and the degree of geometry optimization (relaxation) to be applied at each step of the building process.

6.4.2 Monomer Construction

Modeling of the *ctct*-CPTC and MPD monomers was accomplished using HyperCube's classical MM+ force field (see Figure 6.3) to provide initial geometry optimizations (via the Polak-Ribiere method) followed by use of the semi-empirical (quantum chemical) PM3 force field to reach final (local) optimization and establish partial charges on all atoms in the system. The acid (non-chlorinated) form of the *ctct*-CPTC isomer was modeled to avoid the addition of chlorine atoms to the final membrane system. In reality, the acid chloride is rapidly hydrolyzed to its protonated acid form when it enters the aqueous phase during the interfacial condensation reaction.

6.4.3 Building the Individual Polymers

Individual polymers were modeled by alternately linking *ctct*-CPTC and MPD residues until the appropriate polymer chain length was reached. Each polymer chain has a unique conformation resulting from randomization of the backbone torsion bond angles. The software created for this project allows the user to specify a preferred torsion bond angle as well as the degree of random deviation about that angle (e.g., 125 degrees +/- 36 degrees). Following the chain elongation step, MPD residues are added to one of the two remaining carboxy acid bonding points on each of the *ctct*-CPTC monomers in the chain. These 'dangling' MPD residues serve as points for inter-chain and inter-sheet cross-linking (see below). Each polymer chain created in this manner is stored in a file and later retrieved to construct a 2-D membrane 'sheet' as described below. Each polymer chain built in this manner undergoes geometry optimization to a user specified degree (*e.g.*, <0.1 kcal/mol-A) before being stored. Due to the large size of the polymers, the MM+ molecular mechanics force field is used for this purpose (Polak-Ribiere method).

6.4.4 Building the 2-D Membrane Sheets

The individual polymers built under 6.4.3 are retrieved from file and positioned in one plane (perpendicular to the viewer) in a side-by-side fashion in the workspace in preparation for cross-linking to form a 2-D membrane sheet. The orientation and distance between the polymers is user selectable and can be randomized about a preferred position if so desired. Following positioning of the polymer chains in one plane, the polymer chains undergo 'pseudo-random' cross-linking reactions with

29

neighboring chains to form a cross-linked 2-D membrane sheet. The term pseudo-random is used here to indicate that cross-linking can occur only at prescribed points along the chains, but the probability of cross-linking occurring at each site is user selectable. Thus, a chosen probability of 0.5 would effectively randomize cross-linking events whereas a probability of 1.0 would always result in a cross-link being formed at every available point. Once the cross-linking reactions are complete, each 2-D membrane sheet is stored for later retrieval to create a membrane 'block', *i.e.*, a non-optimized 3-D membrane model comprised of a stack of 2-D membrane sheets that have undergone inter-sheet cross-linking.

6.4.5 Building the 3-D Membrane Block

A series of cross-linked 2-D membrane sheets are called back into the workspace and stacked one upon the other with a user selectable amount of separation between the sheets. The user may also specify how the sheets are to be oriented (rotated) relative to one another around the common axis which runs down the middle of the stack. Randomization of rotation about the common axis causes a greater degree of folding and a more globular appearing 3-D membrane. Once the 2-D sheets are vertically stacked, they undergo pseudo-random cross-linking reactions in much the same way the inter-sheet cross-linking took place (see previous step). At this point, a 3-D membrane block has been created that still must be geometry optimized.

6.4.6 Atom Charge Scaling

During the polymer construction, MPD additions, and cross-linking reactions described above, hydrogen atoms were deleted from potential bonding points. Each time a hydrogen atom is lost to create a bonding point for an MPD residue, for example, the total electron charge of the polymer system changes by an amount equal to the partial atom charge of the lost hydrogen atom. For a membrane model containing several thousand atoms, the net charge can change significantly. In fact values of 10-20 electron volts are not uncommon. Since the CPTC membranes are essentially charge neutral (in theory), the total membrane charge is set to zero by scaling the individual atom charges in the system by a small amount (typically <5% of the total partial atom charge). The algorithm created for the charge scaling takes into account the net charge of the nascent membrane, the number of atoms in the system, and the absolute magnitude of the partial atom charge on each atom. All atoms in the membrane system are then scaled by an equivalent proportion of their total charge. Thus, atoms with larger net partial charges are scaled by a larger amount and atoms carrying a low charge are scaled proportionately less. The user may select any final membrane charge including zero (neutral)

.

6.4.7 Geometry Optimization of the Membrane Model

The final step in the construction of the *ctct*-CPTC membrane model is geometry optimization. These steps are summarized in Figure 6.11.
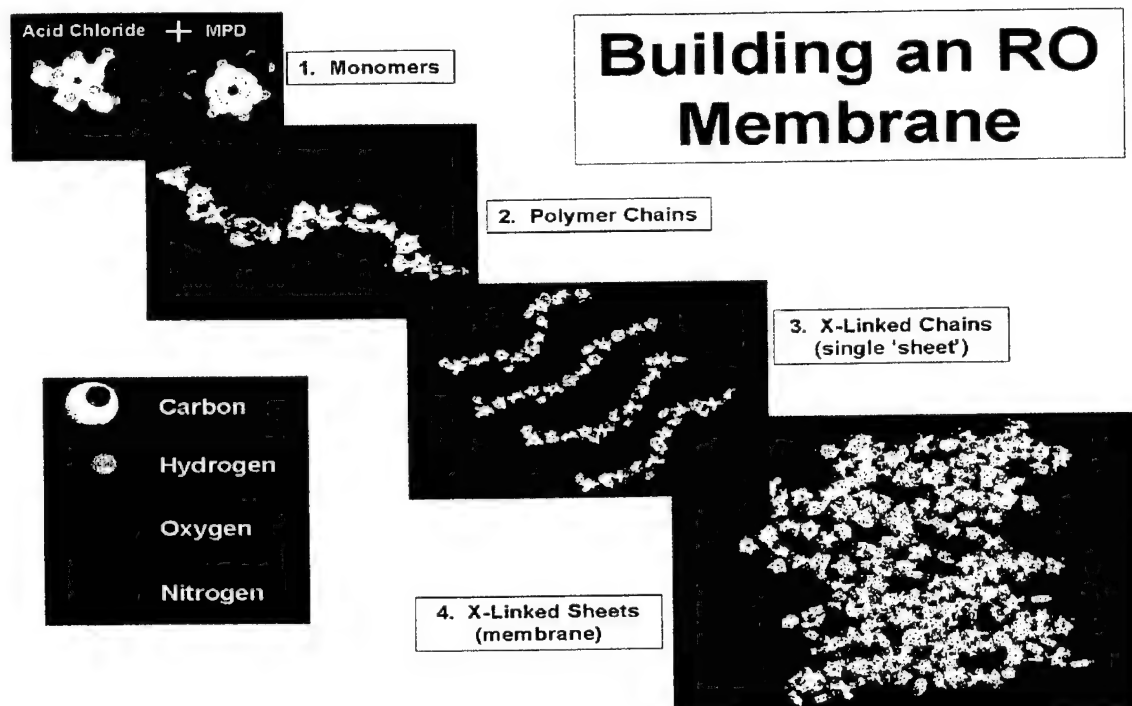
Figure 6.11   Outline of the major steps used to build the ctct-CPTC membrane models
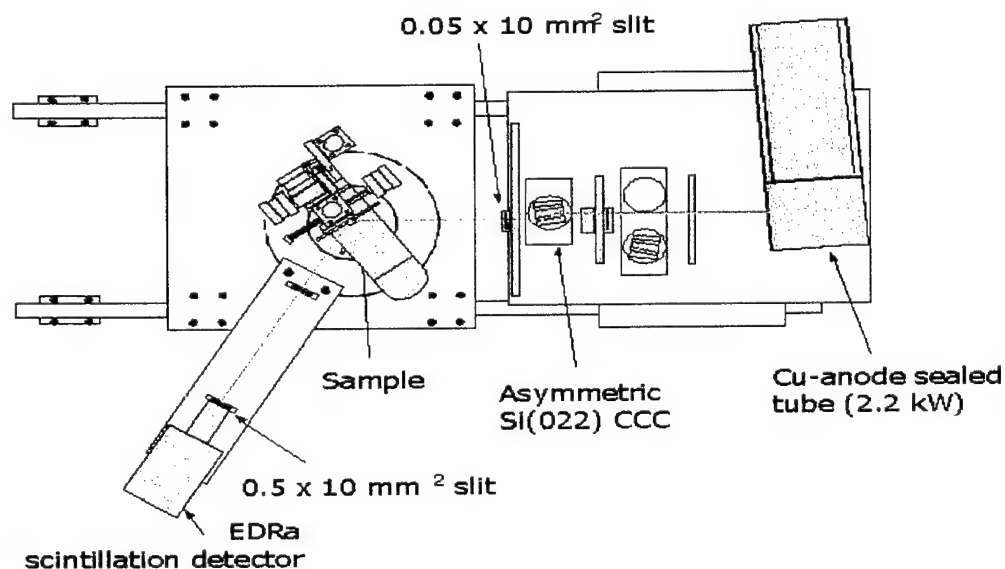
Figure 6.12   High-resolution X-ray diffraction measurements (004 Bragg reflection) performed on a FilmTec, *cccc*-CPTC, and a *ctct*-CPTC membrane

Because of the large size of the molecular system, geometry optimizations are performed using the MM+ force field via the Polak-Ribiere method. Two sequential optimization routines are performed, an initial optimization using united atoms (to provide a rapid first approximation) and a final optimization using all atoms. The finished membrane model is then stored in file.

6.5 X-Ray Diffraction Analysis of FilmTec and CPTC Membranes

Currently only limited experimental data are available concerning the molecular structure of cross-linked membranes. X-ray diffraction analyses were performed on the aromatic cross-linked FilmTec membrane and the *ctct-* and *cccc*-CPTC membranes. All x-ray measurements were taken on a *D1*-system outlined in Figure 6.12. Results for the FilmTec membrane indicated that the polymer structure was largely if not wholly non-crystalline in nature, i.e., the polymer chains were mostly randomly oriented as indicated in Figure 6.13.

Measurements were taken on a *D1*-system attached to a 2.2 kW sealed tube X-ray source fitted with a Cu anode and operated at 1.6 kW (40 kV and 40 mA). The Cu Ka_1 X-ray line was selected using a cut-channel crystal (CCC) and a precision slit. The angular acceptance of the detector was restricted using a narrow slit in order to reduce the diffuse contribution to the measured intensity. The measurements were performed by rotating the detector at twice the angular speed of the sample (θ/2θ-scan).
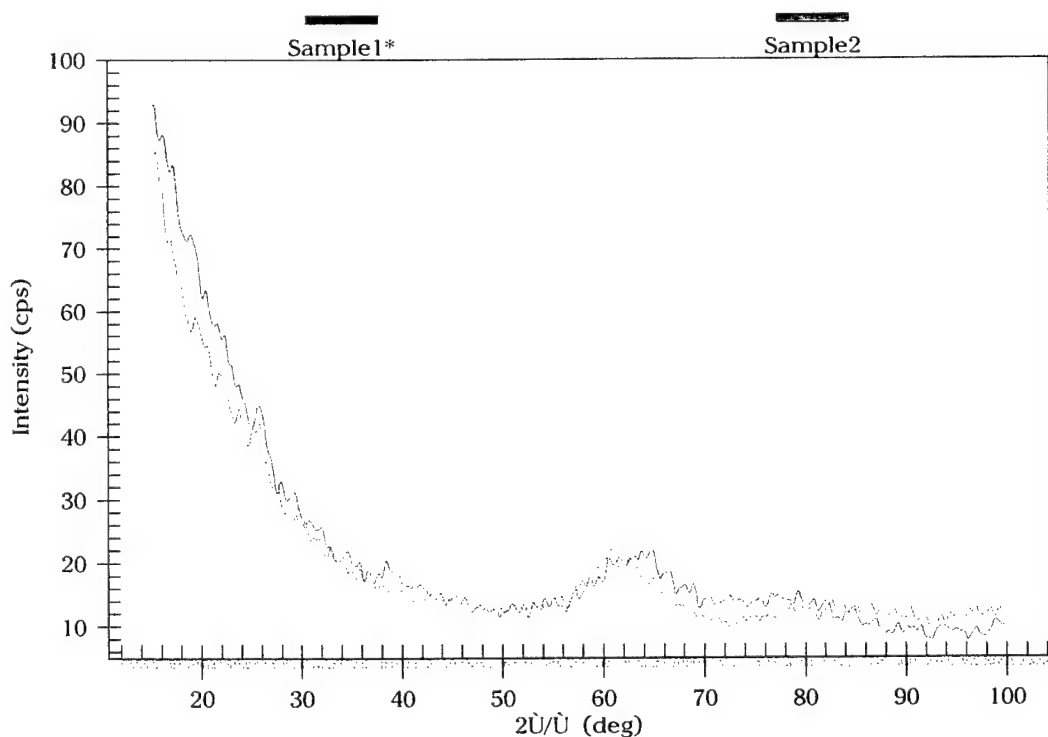
Figure 6.13   Powder Scans from two separate samples of a FilmTec membrane

32

A similar result was observed for the *ctct*-CPTC and *cccc*-CPTC membranes (Figure 6.14). Both membranes exhibited a prominent amorphous hump located around 17° in 2*Theta*. No diffraction peaks were observed from either membrane film that would have suggested crystallinity. Thus, it is concluded that both the *ctct*- and *cccc*-CPTC membranes were non-crystalline with randomly oriented chains. However, the amorphous scatter was somewhat different for the two membrane types with the *ctct*-CPTC sample showing a larger volume of scattering indicating it was somewhat 'less amorphous' than the *cccc*-CPTC sample. This was the only difference noticed between the two films. High resolution reflectivity measurements indicated the two films had identical densities. (See Figure 6.15) The low angle part of the curves(below 1000 arcseconds) is a measure of film density.

Based on the x-ray crystallographic analyses described above, it is concluded that the enhanced oxidation resistance of the *ctct*-CPTC membrane is probably not a result of special (non-random) polymer chain orientation or folding. Nor can differences in the density of polymer packing account for differential resistance to chlorine.

This conclusion has important practical ramifications because it suggests that nearly any randomly folded membrane model is likely to be a valid structure. If the membranes had exhibited significant crystallinity, the order and periodicity of the polymer unit cell would have to be understood before valid molecular models could be constructed and used in simulations.

6.6 Visualation and Analyses of the CPTC Membrane Models

Once constructed, the *ctct*-CPTC membrane model must be characterized to determine how well it matches experimental data. Experimental data may consist of either structural information about the membrane, such as X-ray crystallographic information, or functional data, such as water flux and solute rejection of the membrane. Structural properties may be analyzed by making detailed morphometric measurements on the static models, such as bond distances and angles, atom positions, membrane volume, membrane density, etc. Functional properties like water and solute transport, membrane swelling, or surface free energy determinations upon hydration may be made using molecular dynamics (MD) simulations which allow the system to evolve over time according to the laws of Newtonian mechanics. Since experimental water and solute flux data are available for the CPTC membranes, it should be possible to compare these data with theoretical flux values computed from MD simulations of of the membrane models (see below). Functional properties can also be predicted using a method known as quantitative structure property relationship (QSPR) analysis in which polymer membrane function or solution behavior (e.g., oxygen permeability) is estimated based on statistical correlations between fundamental structural features of the monomer units (e.g., monomer geometry, solubility, presence of functional groups, etc.) and experimental values for a range of known polymer types. The QSPR methods are much more rapid than MD simulations and results are reasonably accurate. However, MD simulations have the advantage of providing detailed information about the dynamics of molecular processes at the atomistic scale (e.g., water and solute transport mechanisms).

33
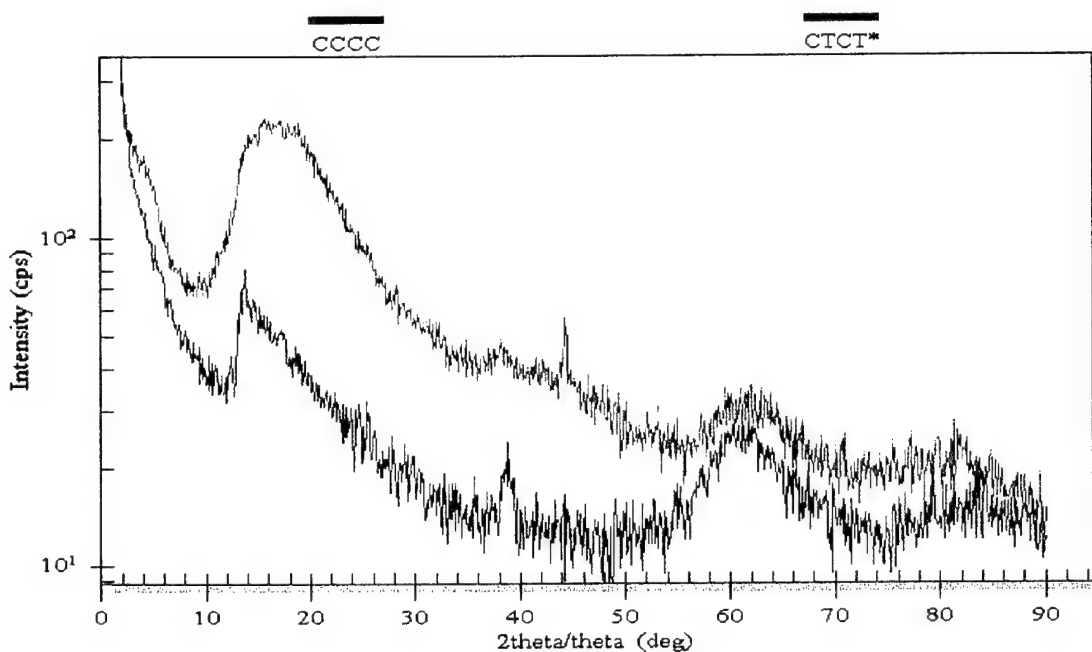
Figure 6.14   TH/2TH powder diffraction scans of the *cccc*-CPTC and *ctct*-CPTC membranes
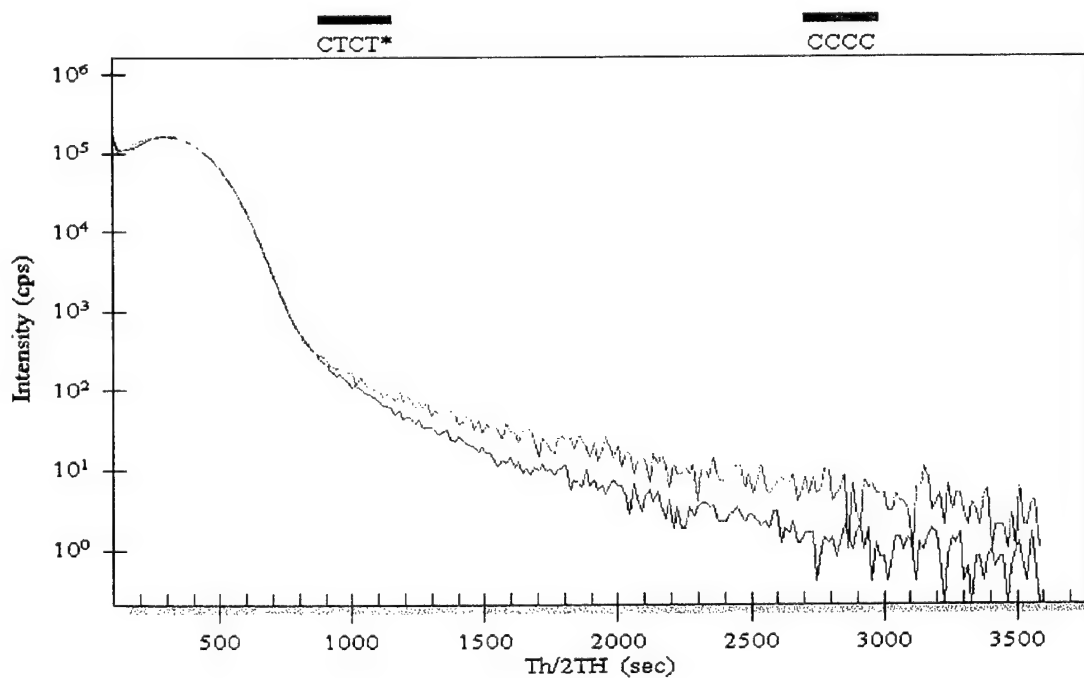
Figure 6.15 High resolution X-ray reflectivity curves for the two samples

An example of a geometry optimized *ctct*-CPTC membrane model constructed using the Layer Method of modeling strategy outlined above is shown in Figure 6.16. Covalent radii are used to represent the atoms depicted in the enlarged view (right). The membrane contains a total of 4634 atoms and was rotated about the vertical (Y) axis such that an image was captured at 30-degree increments for a total of twelve frames. Note (in the enlarged view) that the membrane contains many channels and pore-like structures (void spaces) that could influence how water and solutes diffuse through the polymer membrane matrix. For purposes of discussion in subsequent sections of this report, this particular membrane model will be referred to as the 'CPTC-mem/5' membrane. The specific features and software program (user) settings for constructing this membrane model are summarized in Table 6.0. Whereas the CPTC-mem/5 membrane model has undergone geometry optimization, it has not been subjected to MD simulation in an attempt to identify other meta-stable conformations having lower potential energies. Thus, the membrane conformation shown in Figure 6.16 represents only one of many possible local-energy-minimum structures and not the global minimum. A global energy minimum would correspond to the lowest possible energy state of a molecular system and typically can only be found for such complex atomic systems by performing Monte Carlo type MD simulations where many thousands or millions of possible conformations are examined.

The polymer chains comprising the membrane tend to lose their individual identity following cross-linking reactions and final geometry optimizations. However, when the polymer chains undergo folding during optimization, they often delineate open spaces (voids) within the membrane matrix. The size and distribution of the void spaces (which resemble pores) influence how water and solute diffusion processes occur within the membrane. The average size, shape, and distribution of the pores are likely to be important factors in determining the types of solutes that will be transported or rejected by the CPTC membrane. The pore structure could also influence how chlorine reacts with the membrane. Under dynamic conditions, the pore sizes and shapes will fluctuate to some degree, but their general shape and positions should remain relatively constant (*i.e.*, low membrane fluidity) due to the physical constraints imposed by the significant inter-chain cross-linking.

The total steric energy as well as the contributing bonded and non-bonded interaction energies were computed for the CPTC-mem/5 membrane model using the Hypercube molecular mechanics default (MM+) force field, although the membrane was not subjected to prior relaxation via MD, as mentioned above. As shown in Figure 6.17, bond bending and van der Waals attractive and repulsive forces and torsion bond strain contributed most significantly to the total steric energy of the membrane. Torsion angles and charge-charge interactions were less significant factors in membrane interior strain.

Table 6.0

Summary of Properties for *ctct*-CPTC Membrane Model #5.

Membrane Property	Value
Initial User Settings:	
Membrane ID No.	5
Model creation date	11 January 2000
Monomer number	5
Chain number	4
Sheet number	4
Chain X-link probability	0.25
Sheet X-link probability	1.0
A-Bond X-link probability	0.75
Backbone torsion angles	125+/-50 degrees
Rotate sheet Z-axis	22+/-90 degrees
Rotate chain Z-axis	-11+/-20 degrees
Initial membrane charge	-4.77 ev
Chain optimization	1.0 kcal/mol-Å
Membrane optimization (gradient)	0.097 kcal/mol-Å
Membrane Properties:	
Membrane atom count	4634
Final membrane charge	1.93×10^{-5} ev
Average density (from re-build model)	0.72 g/cm^3
Total volume (from re-build model)	110969 Å^3
Total volume (from atom summation)	82854 Å^3
Atomic volume (from re-build model)	8708 Å^3
Void volume (from re-build model)	102261 Å^3
Surface/Volume ratio (from re-build model)	0.128
Total membrane mass	37602 amu
Total steric energy	8669 kcal/mol

The theoretical surface free energy of the membrane can be computed from a knowledge of the membrane surface area and the total steric energy. However, this estimate cannot be made accurately until the system is first relaxed further via molecular dynamics (see below). An estimate of surface free energy for the un-relaxed CPTC-mem/5 is 167 erg/cm^2 which is judged to be higher than expected for a polymer of this type (typical values fall between 20 and 40 erg/cm^2).

CPTC-mem/5 Membrane Model
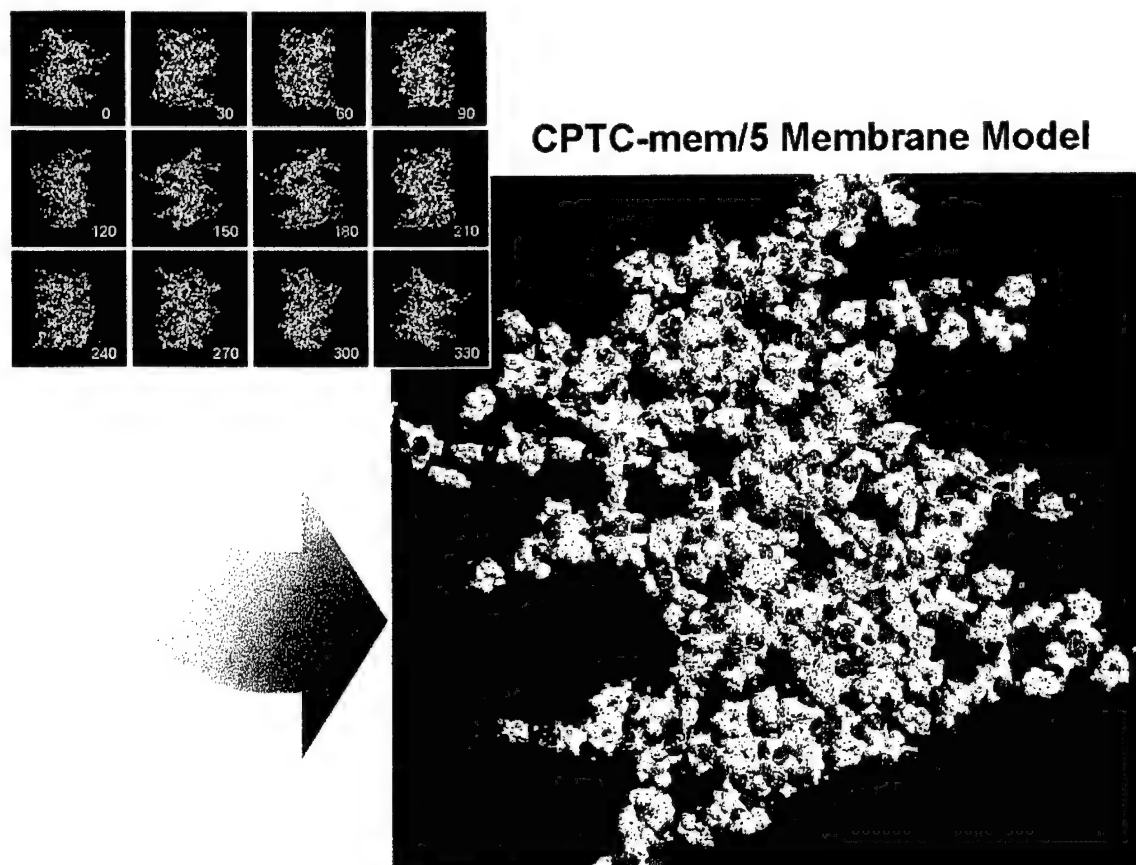
Figure 6.16   A geometry optimized (<0.1 kcal/mol-Å) *ctct*-CPTC membrane molecular
model (designated as CPTC-mem/5) rendered as CPK overlapping
spheres

Additional analytical software was created during this project that permits detailed
structural analysis of the CPTC membrane models that are prepared. For example,
special analytical software tools were created that allow virtual thin sectioning of the
membrane models so that potential relationships between various membrane internal
properties (e.g., atomic volume, void volume, atom charge distributions, etc.) may be
identified and explored. The sectioning software captures consecutive one Å-thick
slices along any specified axis of the membrane system. Using Image Pro Plus and
Voxblast software, the image slices can be reconstructed into a membrane volume
that may be freely rotated and examined from any geometric perspective. The volume
re-constructed CPTC-mem/5 model is shown in Figure 6.18. Inspection of this re-
construction reveals the general shape and contours of the outermost surface of the
membrane. Such reconstructions also provide qualitative visual information
concerning the relative amount of space occupied by atoms and voids.

37
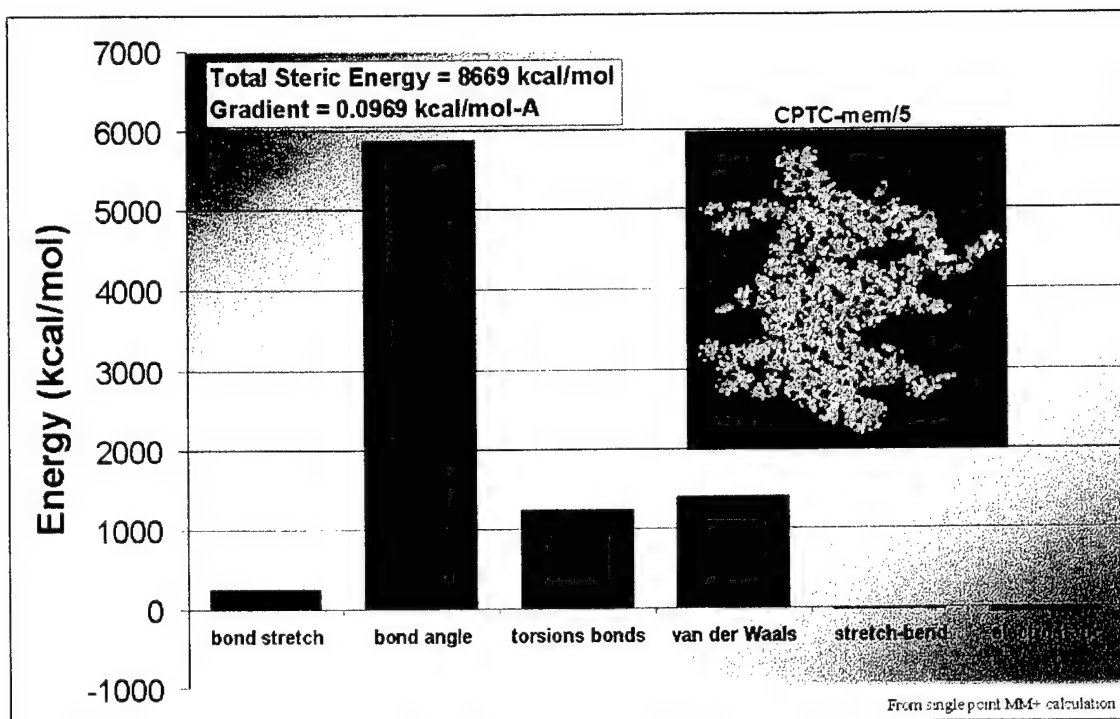
Figure 6.17   Contributions of individual force field energy components to the total steric energy of the CPTC-mem/5 membrane

The volume model was rotated about the vertical (Y) axis such that an image was captured at 24 degree increments for a total of fifteen frames. The model is post-lighted and false colored creating surface relief to better visualize the individual slices. Blue-green color represents the empty space (or void) volume of the membrane system whereas red-orange color denotes the locations and volumes of the individual atoms comprising the polymer membrane structure. Structural and energetic information about the membrane may be computed for each slice (see figures below).

Various molecular properties of each slice (e.g., the density or charge) may be evaluated thereby permitting 3-D dissection of the entire membrane model. The polymer membrane density and void space as a function of depth through the CPTC-mem/5 membrane model is presented in Figure 6.19. The 'top' of the membrane (as viewed in Figure 6.10) is to the left. Each slice is one Angstrom thick. A total of 89 slices were prepared, the first eight of which contained no atoms, i.e., these slices were still outside the membrane; thus, void volumes were zero for these slices and the densities were undefined (no value). The average density for the entire membrane is 0.72 g/cc; however, this value could change significantly if the membrane is permitted to undergo further relaxation via molecular dynamics. As expected, larger void volumes correspond to lower densities. The density of the polyamide FilmTec membrane has been reported as ~1.3 g/cm^3 (Kotelyanskii et al.). [22]

38

Volume Reconstruction of CPTC-mem/5 Membrane Model
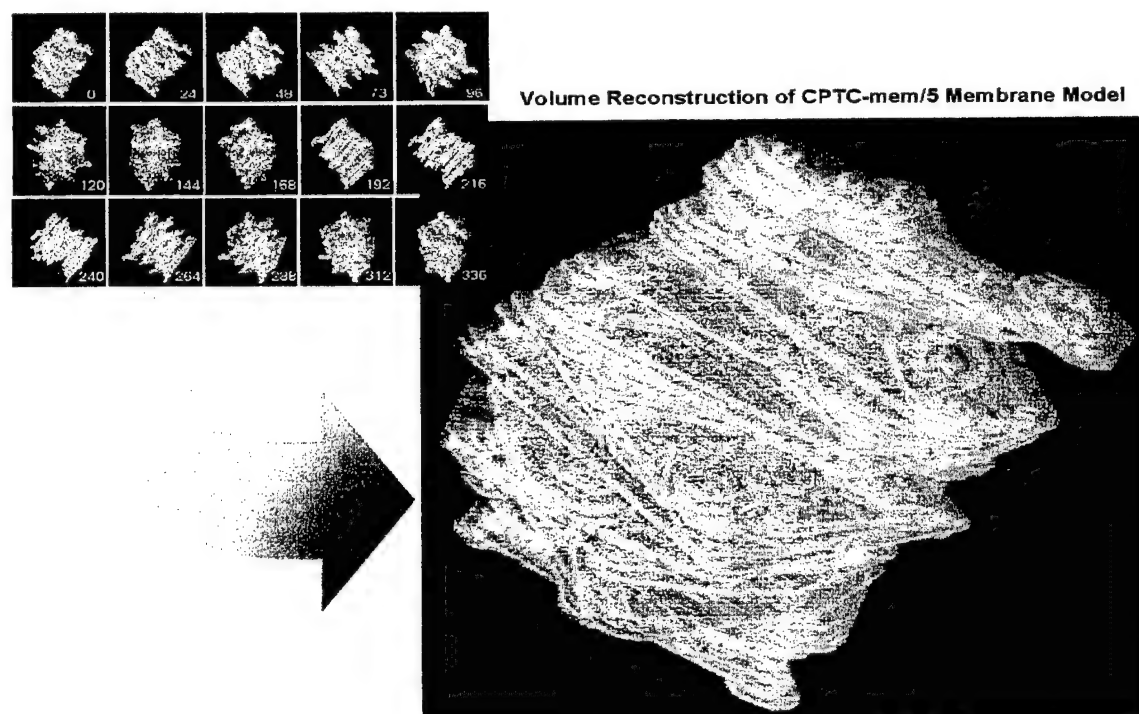
Figure 6.18   Volume reconstruction of the CPTC-mem/5 membrane shown in Figure 6.10 from 89 one-Angstrom thick slices

Data presented in Figure 6.20 indicates the membrane atomic volume, total volume, and void volume expressed as a function of depth through the CPTC-mem/5 membrane. The actual volume occupied by atoms in the membrane matrix is only about 5-10% of the total membrane volume. Thus, most of the membrane interior could be considered as empty space pores that would presumably be available for water and solute diffusion processes. The 'top' of the membrane (as viewed in Figure 6.9) is at the left (Y) axis. Each slice has a thickness of one Angstrom. A total of 89 slices were prepared, the first eight of which contained no atoms, *i.e.*, these slices were still outside the membrane; thus, all volumes fell to zero for these slices. Considerable variation in the void volume occurs through the membrane interior. Note that the actual volume occupied by atoms was relatively small compared to the total membrane volume. Using this analytical approach, changes in the total void volume could be monitored during simulations of diffusion processes or membrane swelling due to the addition of water to the system.

39
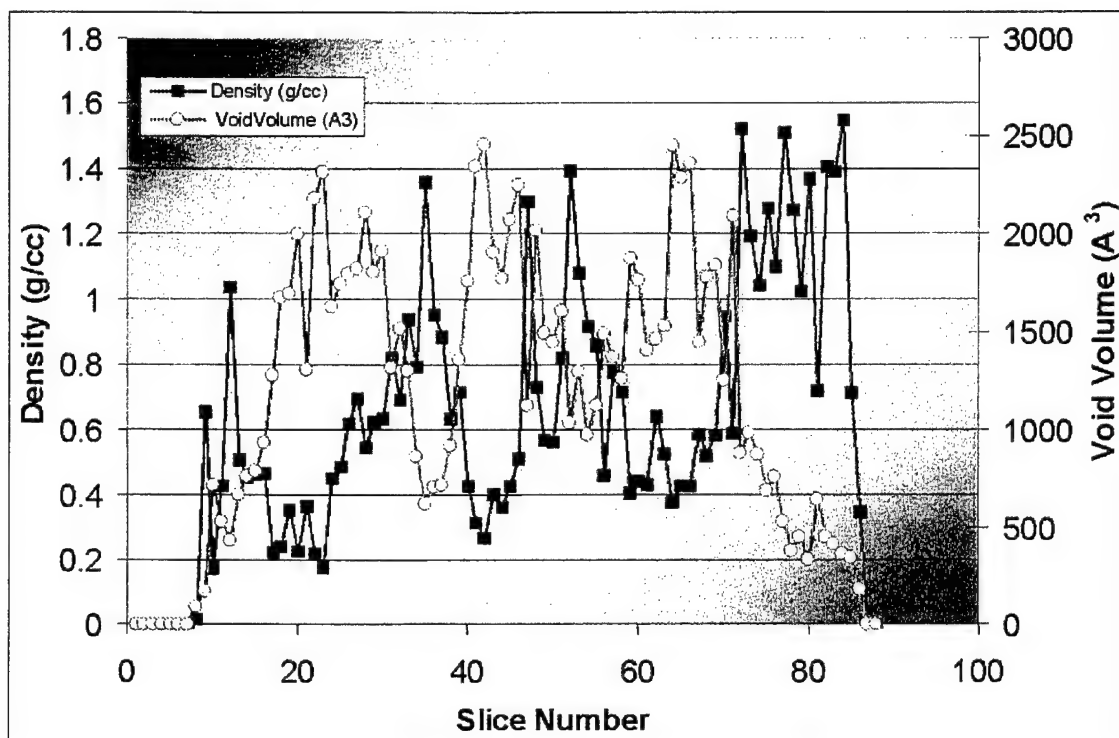
Figure 6.19   Polymer membrane density and void volume as a function of slice
number (depth) through the CPTC-mem/5 membrane

Figures 6.21-6.23 present the membrane energy gradient, bond bending energies,
and net atomic charge as a function of depth through the CPTC-mem/5 membane
model, respectively. The energy gradient data shown in Figure 6.20 suggests that the
membrane model is sterically strained toward its center and one of the largest
contributors to this strain are bond bending stresses (Figure 6.21; also see the energy
data presented in Figure 6.17 above). The energy gradient was computed for each slice
using the MM+ force field (Hypercube). Note that the gradient was steepest near the
center of the membrane system, i.e., the polymer chains were more strained sterically
in this region of the membrane. Portions of the membrane that faced the exterior of
the membrane would presumably have had more opportunity to relax energetically
due to more degrees of freedom of motion. Bond bending energies were the largest
contributor to the overall steric energy of the membrane.

Presumably those polymer chains that were located on the exterior of the
membrane surface would have had greater opportunity to relax energetically due to
more translational and rotational degrees of freedom. The net atomic charge in each
membrane slice varied between about +2 to –2 eV (Figure 6.22), but the average slice
charge was near zero since the membrane as a whole was charge neutral.

40
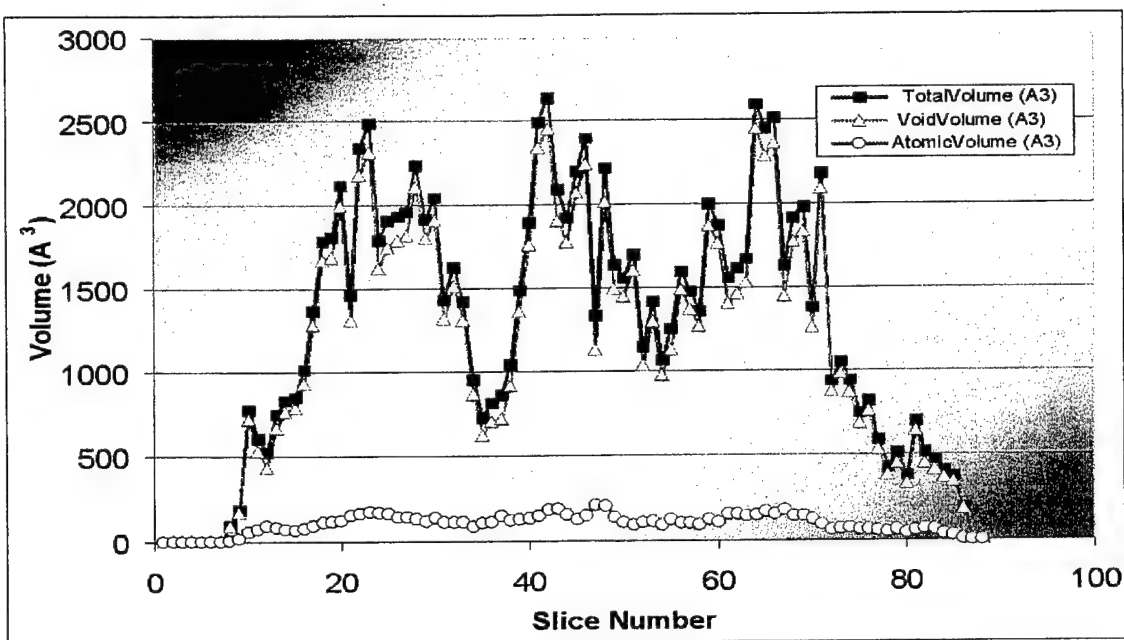
Figure 6.20   Membrane atomic volume, total volume, and void volume expressed as a function of the slice number (depth) through the CPTC-mem/5 membrane
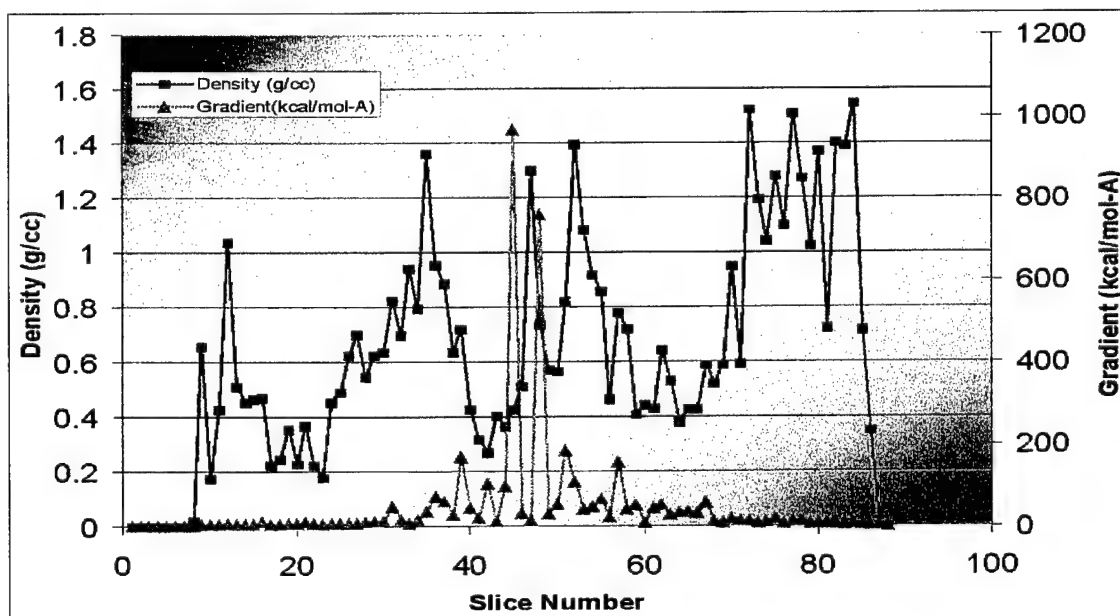
Figure 6.21   Polymer density and energy gradient plotted as a function of slice depth through the membrane
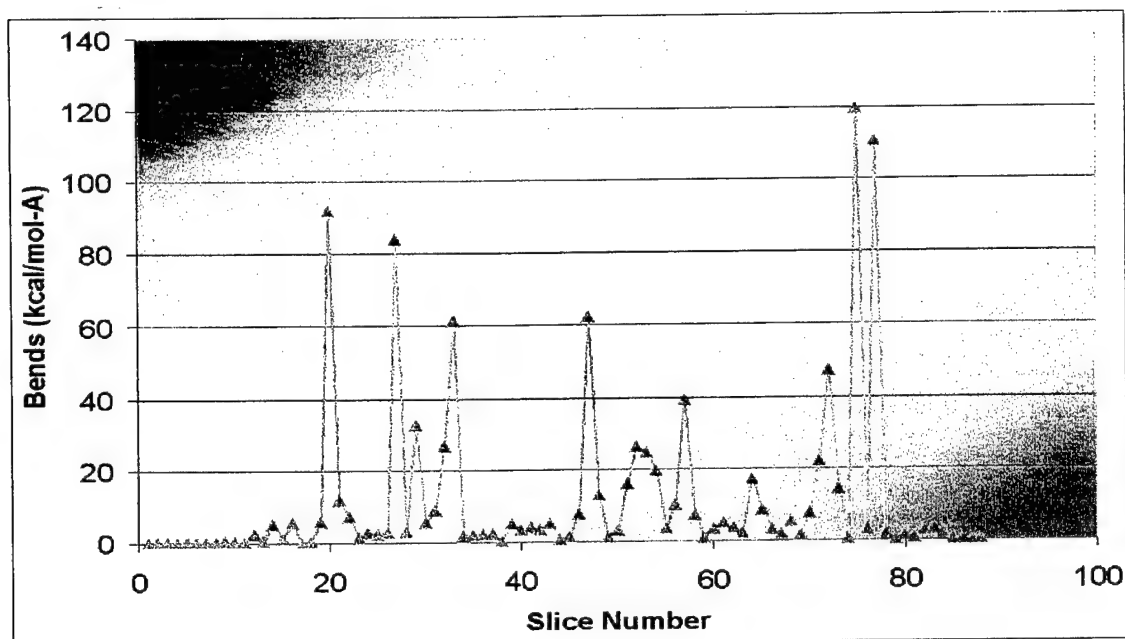
Figure 6.22   Bond bending energies as a function of membrane depth for the CPTC-mem/5 membrane model. Bend energies contributed strongly to the total steric energy of the membrane. Bend energies also appeared greatest at the Y-axis poles of the membrane.
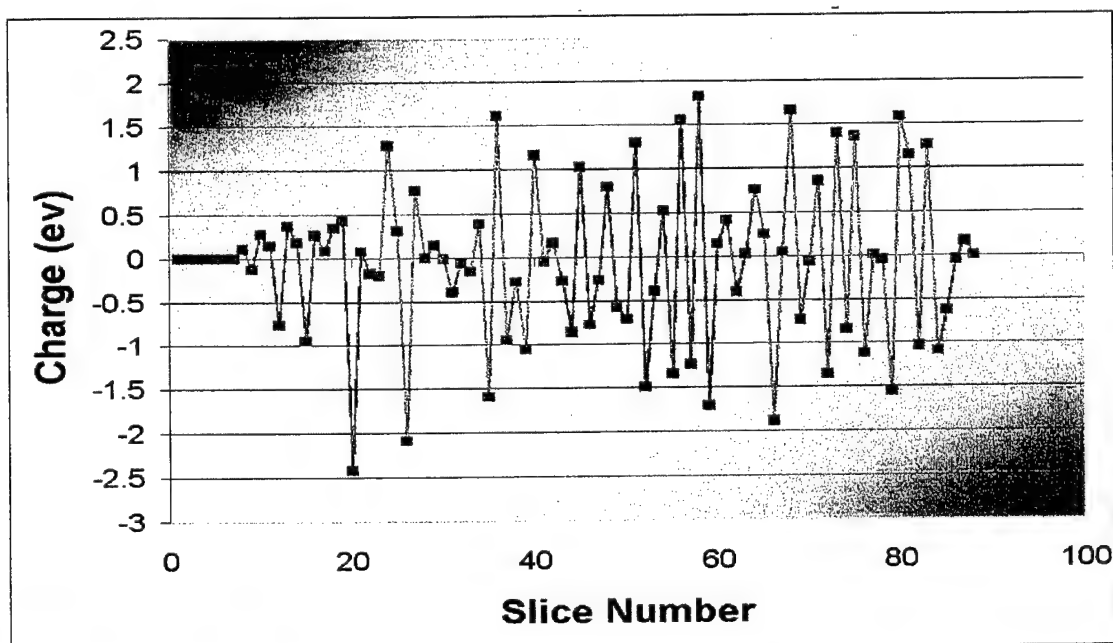
Figure 6.23   Net charge as a function of slice depth through the CPTC-mem/5 model membrane. Note that atomic charge per slice fluctuated more-or-less symmetrically about a zero value since the membrane was electrically neutral overall.

6.7 Comparison of CPTC Membranes Built using the *cccc*-CPTC and *ctct*-CPTC Stereoisomers

By substituting the *cccc*-CPTC stereoisomer for the *ctct*-CPTC isomer in the model building software described above, it should be possible to perform a detailed comparison of the structure and energetics of the two membrane types. Differences in the membrane conformations or steric energies could be related to the observed differences in resistance to chlorine oxidation for the two membranes.

Preliminary CPTC membrane models have been constructed using the *cccc*-CPTC and *ctct*-CPTC stereoisomers. The membrane models were created using identical set up parameters, *e.g.*, torsion bond angles, cross-linking probabilities, geometry optimization criteria, *etc.*, which are summarized in Table 6.1.

Table 6.1

Set up Parameters Used to Build the *cccc*-CPTC and *ctct*-CPTC Membrane Models

Parameter	Value
Monomer Number	4
Chain Number	4
Sheet Number	3
Chain XL Probability	0.25
Sheet XL Probability	1.0
A-Bond XL Probability	0.75
Torsion Angles (1 – 6)	125±50 degrees
Sheet Z-axis Rotation	6±90 degrees
Sheet Z-axis Initial & Offset	40 & 20 $Å^3$
Chain Z-axis Rotation	6±20 degrees
Chain Y-axis Initial & Offset	180 & 20 Å
Final Membrane Charge	-1.2×10^{-5} eV
Chain Optimization	1.0 kcal/mol-Å
Membrane Optimization	0.1 kcal/mol-Å

Based on an initial inspection of the model images presented in Figures 6.24 and 6.25, no obvious and consistent differences were observed in the molecular structures of the two membrane types. It must be emphasized that the models shown do not represent global energy minima, i.e., the most relaxed form of the membrane. Molecular dynamics simulations would have to be carried out to identify membrane conformations having lower energy minima. Both membrane types exhibited randomly distributed void spaces and channels. The polymer chains comprising both membrane types appeared to have folded by similar mechanisms. Thus, based on these preliminary results, we can propose no definitive structure-based mechanism for the observed differences in the chlorine susceptibilities of the two membranes.

43
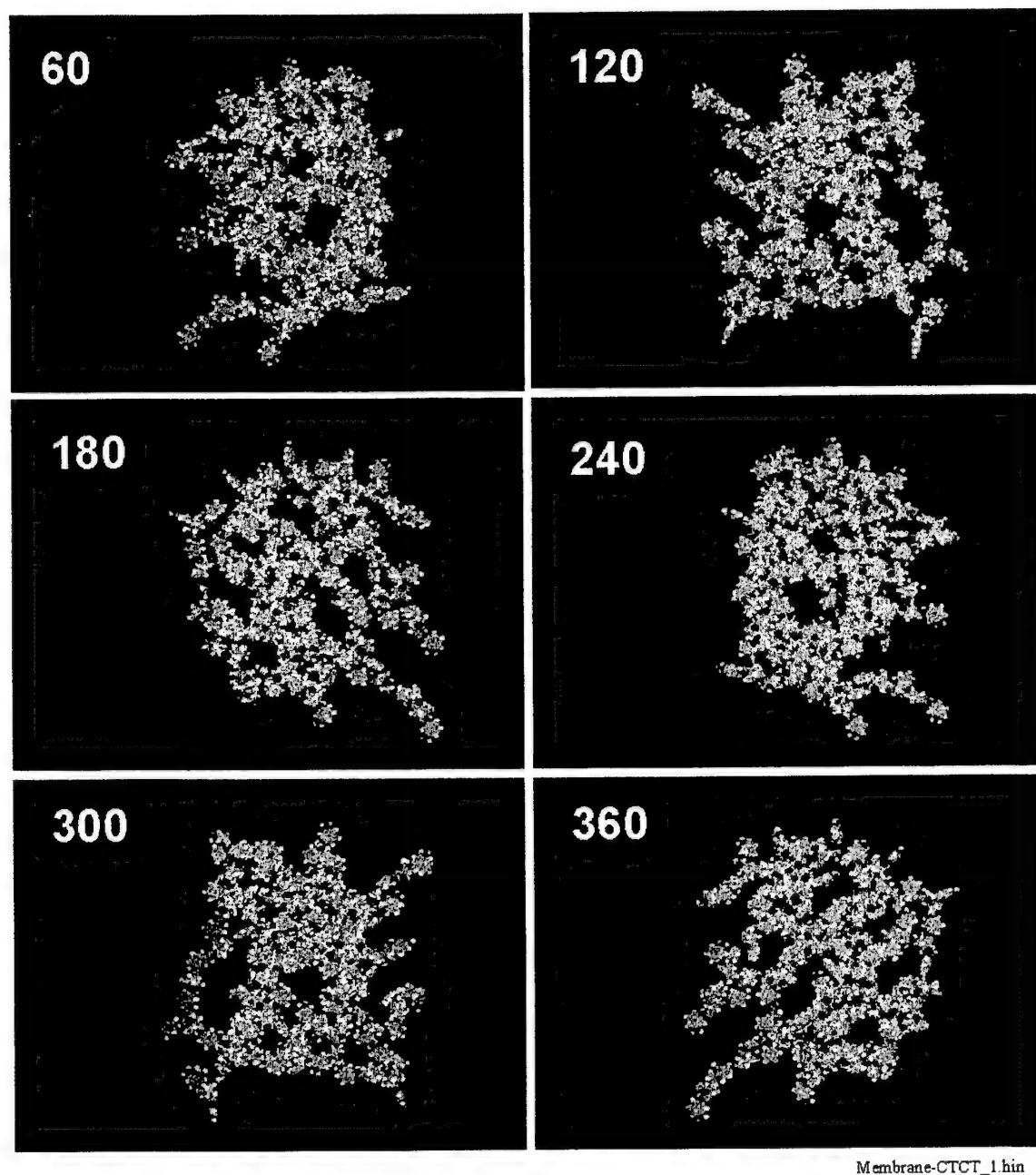
Figure 6.24 Rotational views of a *ctct*-CPTC membrane. Rotations were made about the inertial Y-axis. Note the many void spaces in the membrane interior.
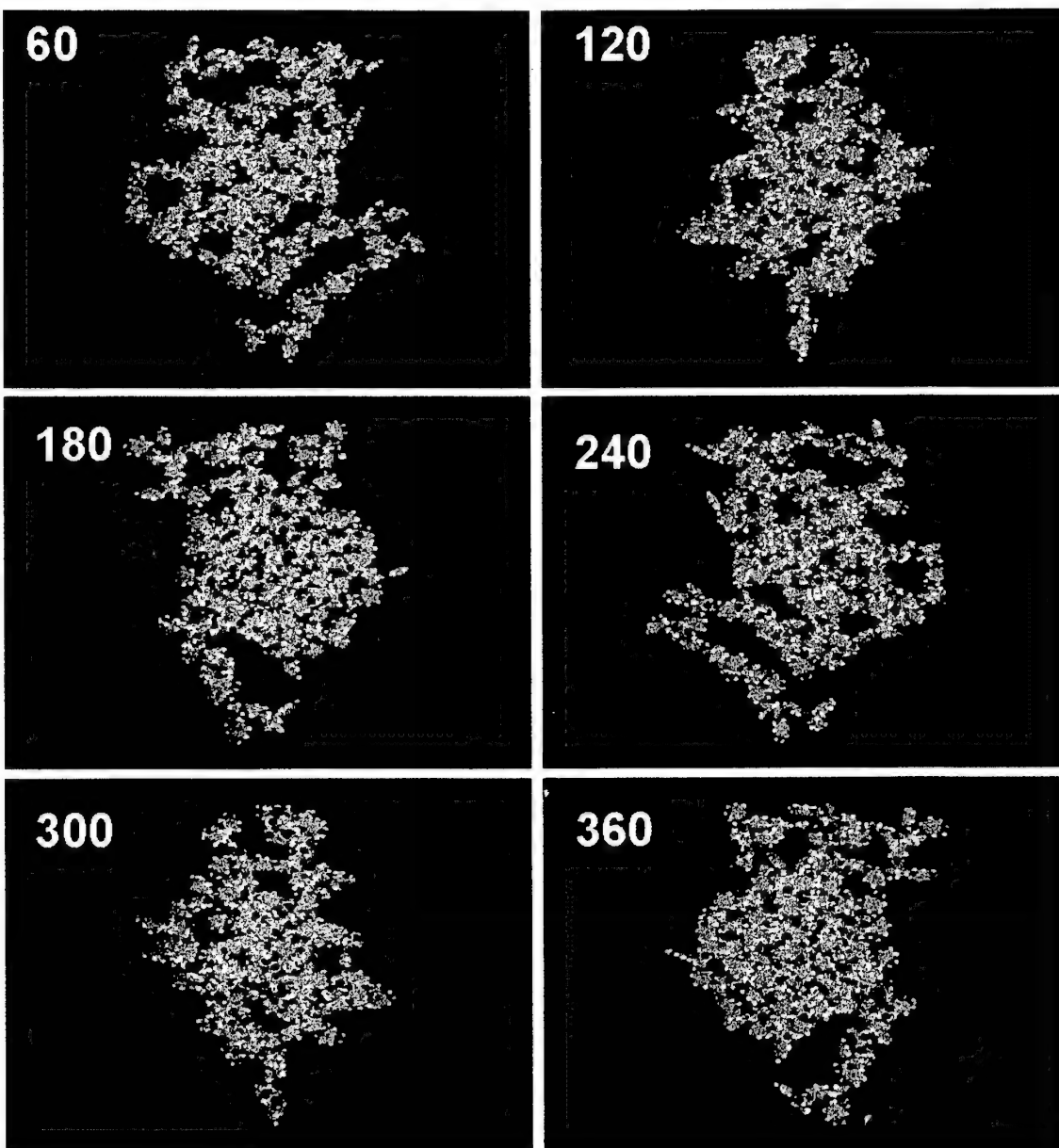
Figure 6.25 Rotational views of a *cccc*-CPTC membrane. Rotations were made about the inertial Y-axis. Note the many void spaces in the membrane interior. Whereas the morphology of this membrane differs in its details from the *ctct*-CPTC membrane depicted in Figure 6.24, the overall structural motif involving random chain folding and void space distribution appears identical.

45

Energetic data presented in Figure 6.26, however, does suggest that the *ctct*-CPTC membrane was sterically more stable than the *cccc*-CPTC membrane. This observation is consistent with the increased stability of the *ctct*-CPTC monomer compared to the other CPTC stereoisomers (see preceding sections). Thus, it is possible that the observed oxidation resistance of the *ctct*-CPTC membrane may be related to this enhanced steric stability.

To extend the above observations further, it will be necessary to run molecular dynamics (MD) simulations to seek membrane conformational states that are energetically more favorable than those depicted in Figures 6.24 and 6.25. It is possible that structural differences might become apparent as the two membrane types are permitted to undergo more extensive relaxation over time.
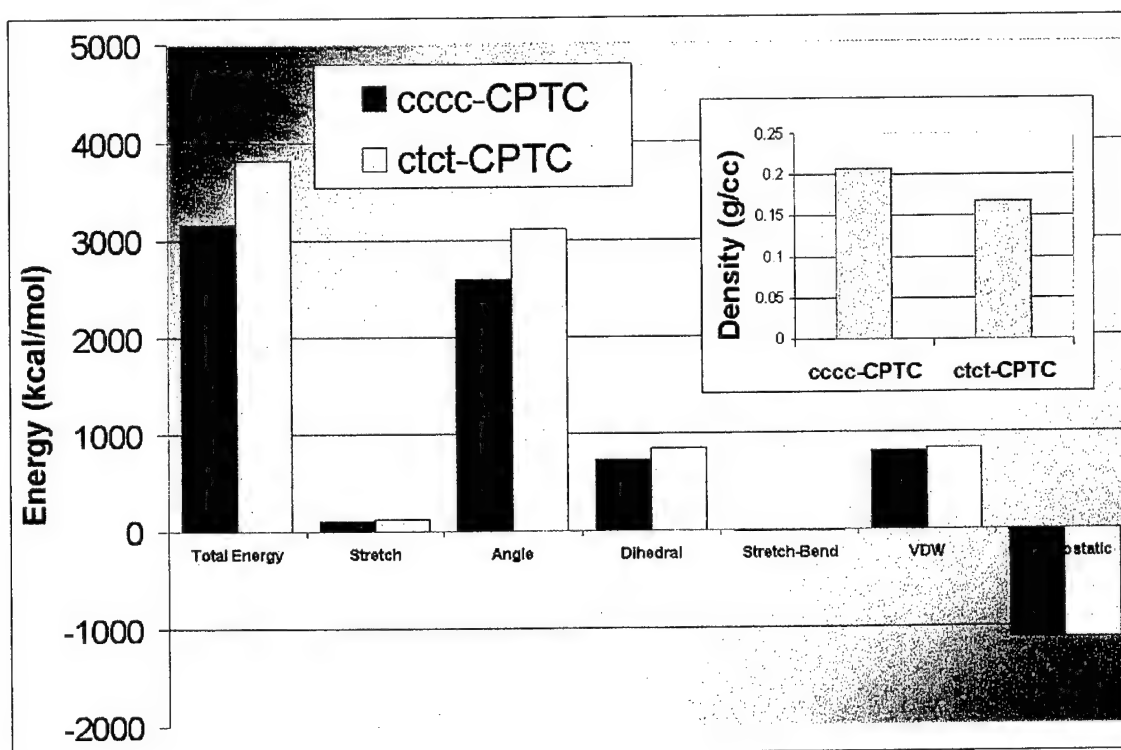
Figure 6.26   Comparison of the steric energies and densities (inset graph) of the *ctct*-CPTC and *cccc*-CPTC membrane models depicted in Figures 6.18 and 6.19, respectively. Note that the *ctct*-CPTC membrane was slightly less dense and sterically more stable than the *cccc*-CPTC membrane.

6.8 Addition of Water to the CPTC-mem/5 Membrane Model

Special software was created in this project (using the Tcl/Tk language) to randomly populate (i.e., solvate) the CPTC membrane models with water molecules. This was necessary to prepare the model membrane system for performing MD simulations of water and solute transport phenomena and also to investigate the influence of water on various structural properties of the membranes (e.g., swelling

response, etc.). The MD simulations are used to compute the diffusion coefficients of water and solute molecules in the membrane model. The diffusion coefficients can then be used to predict membrane water flux and solute rejection values for the membrane system. Using this approach, it should be possible to use molecular modeling tools to design new CPTC-based polymer membranes having improved water flux and solute rejection characteristics.

The image in Figure 6.27 shows the CPTC-mem/5 model following random hydration by 100 water molecules (the TIP/3P water model was used). The software allows the user to specify the number of water molecules to be added to the system as well as the minimum distance of the water oxygen atom to any atom in the membrane system. The software precluded placement of any water molecule closer than 2.0 Å from any membrane atom. The water molecules can be found occupying void spaces throughout the interior of the membrane system. Population of the molecular (membrane) system with water is based on an initial analysis of the overall dimensions and aspect ratio of the membrane. This analysis is followed by random placement of the water molecules within the boundaries defined by the maximum length and width of the molecular system. Any solute molecule or atom (*e.g.*, chloride or sodium ions) may be substituted for water in the solvation software.
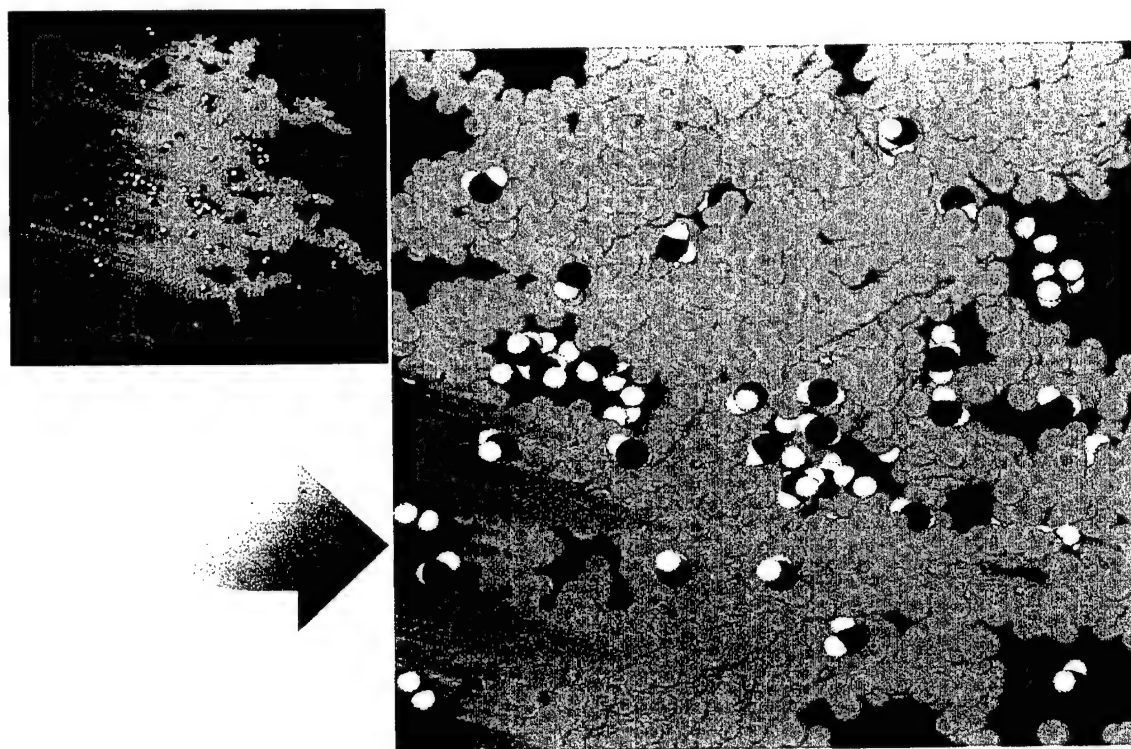
Figure 6.27   Image of the CPTC-mem/5 model membrane following random addition of one hundred TIP/3P water molecules (shown in blue/white) using custom software created for this project

47

6.9 Lattice Method for Modeling CPTC Membranes

While the Layer Method described above has certain convenient features, such as the ability to adjust torsion bond angles, there are also disadvantages. For example, the model assumes that polymer chains are created initially followed by random cross-linking. While it is true that cross-linking occurs according to a simple probability function ('coin toss'), the cross-linking process is not truly random since bonds are only permitted between certain predetermined loci along the polymer chains. This type of bonding mechanism may be more accurately described as 'pseudo-random cross-linking' and it tends to restrict the number of possible bonding arrangements (and hence conformations) that the membrane could potentially adopt. In addition, in the above modeling approach, the torsion bond angles initially specified by the user of the program are quickly altered during subsequent geometry optimization routines.

In order to avoid these issues, a new modeling program was written that allows truly random cross-linking between alternating CPTC and MPD monomers that are arranged in a 'crystal' lattice type structure. The basic steps for membrane model construction using this new Lattice Method program are as follows:

Step 1 A three-dimensional cubic crystal lattice structure consisting of alternating CPTC and MPD residues is built. The user has full control over lattice dimensions, monomer spacing in the lattice, and monomer orientation. Monomers are initially left non-bonded in the lattice structure.

Step 2 All of the nearest neighbors for each monomer in the lattice are identified. For example, each MPD monomer that is completely buried in the lattice (i.e., not on a corner or side of the lattice) possesses six CPTC nearest neighbors. An MPD monomer located at a corner of the lattice possesses three nearest CPTC neighbors and an MPD located on a side or the lattice possesses five nearest neighbors. All of the nearest neighbors for CPTC monomers are MPD monomers.

Step 3 Random bonding between nearest neighbors is allowed to occur. This is done by first randomly picking a 'parent' monomer (either MPD or CPTC) in the lattice. This parent residue then 'searches' through its list of nearest neighbors and finds those that have not already entered into a bond (i.e., 'available' neighbors). One of the available nearest neighbors is then randomly picked and a bond is made depending on whether certain geometric constraints are satisfied, such as bond distance and bond angle. After the parent residue has been bonded (or given the opportunity to undergo bonding), it is then eliminated from the neighborhood lists of all lattice members. At this point, another parent residue is randomly picked and the process is repeated until all possible lattice bonds have been made.

48

Step 4   Some monomers may fail to undergo bonding to any neighbor if geometric constraints are not satisfied or if all of their nearest neighbors have already entered into bonds with other members of the lattice. The user has the option of removing these non-bonded residues from the system at this point.

Step 5   Atom partial charges are adjusted to impart the proper overall charge to the membrane model.

Step 6   The model is then relaxed using an appropriate molecular mechanics force field such as Amber or MM+.

The scheme outlined above results in a truly randomly cross-linked membrane model. The various steps involved in lattice construction and bonding are outlined in the series of images shown in Figures 6.28 - 6.30.

Lattice Dimensions: 5 Residues x 5 Rows x 5 Layers
Bonding Probability: 1.0
Total Number of Residues in Lattice: 125
Number of Free MPD Groups: 0
Number of Free TMC Groups: 12
Total Unbound Residues in this Lattice: 12
Total Free Carboxyl Groups in Lattice: 122
Partial Free Carboxyl Groups in Lattice: 86
Number of Bonds in Lattice: 126
Total Lattice Mass: 135498.0
Total Carboxyl Group Mass: 5369.22
Partial Carboxyl Group Mass: 3784.86
Total -NH2 Groups in Lattice: 0
Total Dangling Amine (-NH2) Groups: 0
% Total -NH2 Group Mass: 0.0
% Dangling Amine (-NH2) Group Mass: 0.0
% Total Carboxyl Group Mass: 3.962582
% Partial Carboxyl Group Mass: 2.793296
Total Amide-II Groups: 126
Total Amide-II Mass: 1891.26
Molar Ratio Total-COO/AmideII: 0.968254
Mass Ratio Total-COO/AmideII: 2.838964
Molar Ratio Partial-COO/AmideII: 0.6825397
Mass Ratio Partial-COO/AmideII: 2.001237
Molar Ratio -COO/Dangling Amine: Undefined_Divide_By_Zero
Mass Ratio -COO/Dangling Amine: Undefined_Divide_By_Zero

Order of Residue Selections for Bonding: 0 2 90 60 10 78 109 73 22 77 104 5 29 35 56 71 58 66 118 52 65 97 87 32 34 43 28 54 85 51 62 83 84 41 23 57 45 102 4 91 95 6 74 68 107 61 106 121 76 44 92 111 86 120 46 11 98 112 33 38 119 31 69 24 37 75 81 94 55 20 96 9 48 49 1 25 113 100 99 89 17 19 64 79 7 115 67 39 116 30 26 18 60 27 36 108 101 14 72 122 105 123 53 8 70 103 110 50 3 42 40 16 114 47 117 13 124 59 15 88 63 33 12 21 82
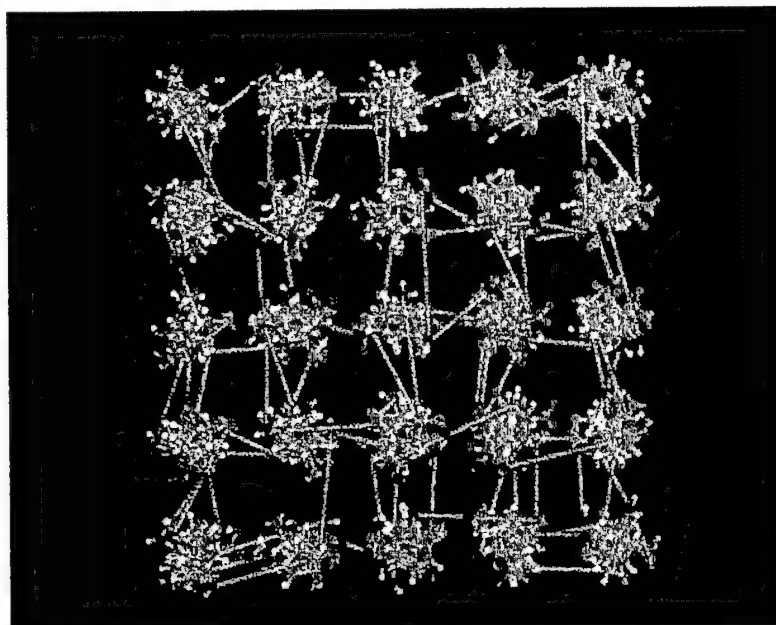
Figure 6.28   Lattice model of *ctct*-CPTC membrane prior to geometry optimization

49

The model in Figure 6.28 contains 125 residues and is seen looking at one side of the cubic system. The membrane is negatively charged because there are no positive counterions present to neutralize the carboxyl groups. Note that some CPTC residues (12 in all) failed to bond and remained free in the polymer matrix (green colored molecules). The bonds between residues are artificially extended since the membrane has not yet been energy minimized. No geometry constraints (such as a maximum allowable bonding distance) were placed on bonding; thus bonding opportunities were maximized in this particular model. The text table associated with the image displays various model properties such as molecular weight, number of free carboxyl and amino groups, and ratios of functional groups, such as the ratio of free carboxyl groups to free amine groups. The numbers listed at the bottom of the table give the order in which each member of the lattice was randomly picked for bonding operations.
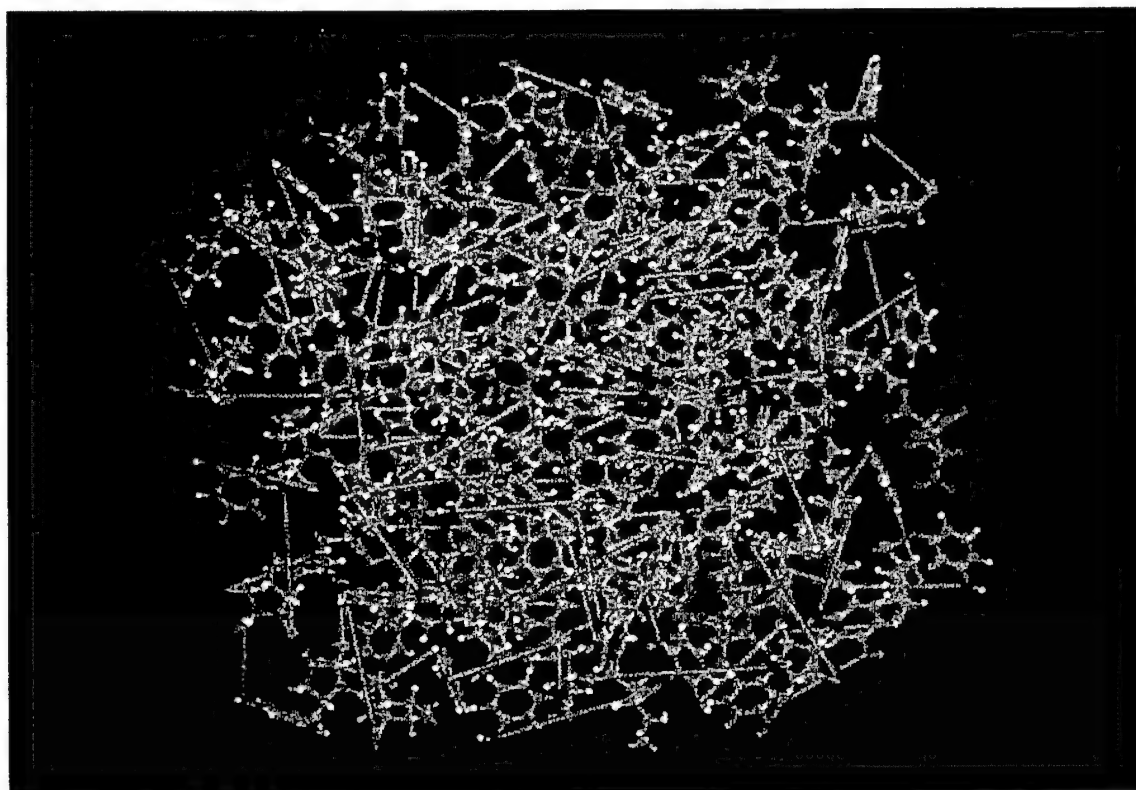
Figure 6.29   Same model as shown above in Figure 6.28, but displayed after rotating out of the lattice cubic symmetry plane

The geometry optimized lattice model is shown in Figure 6.30. Note that free (unbound) CPTC residues were ejected from the membrane matrix during the optimization process suggesting that membranes having buried acid chloride residues would be very unstable. This also indicates that free monomers would likely be rapidly lost from the membrane matrix just after polymer formation and cross-linking. Positive counter ions were not present in the model system shown in Figure 6.30. Thus,

considerable repulsion of acid side groups occurred with subsequent expansion (swelling) of the membrane polymer system. This swelling effect causes the appearance of large holes or molecular-scale bubbles in the membrane interior.

If we run MD simulations on these geometry optimized models, the lattice continues to expand even more until it completely unfolds. This effect is illustrated in the series of images shown in Figure 6.31. Interestingly, if positive ions such as sodium or calcium are placed at random in the starting molecular system, swelling is prevented in the MD simulations. In fact, the polymer system contracts dramatically into a much more dense membrane and the system potential energy declines accordingly (see Figure 6.32). These models suggest that it might be possible to control the final density of the CPTC membranes by using suitable concentrations of sodium ions during the interfacial condensation reactions.
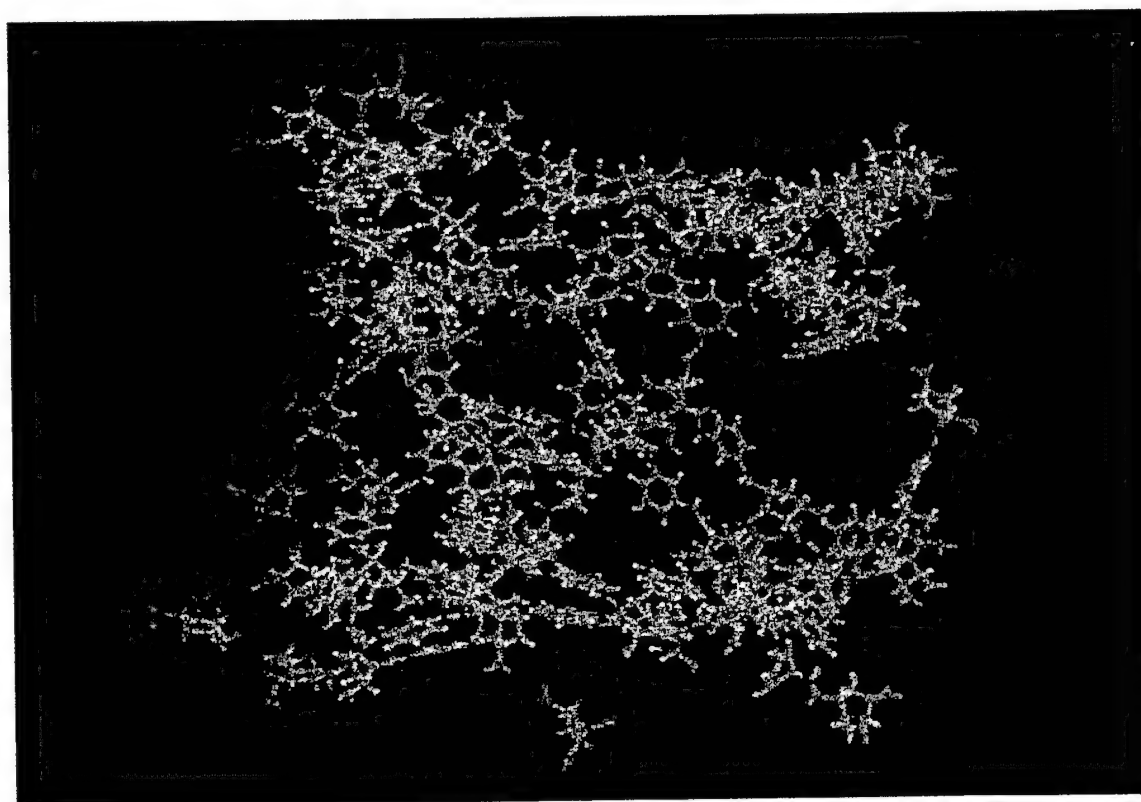
Figure 6.30   Same model as shown above in Figure 6.29, but after geometry optimization. Note the large bubble-like void spaces in the membrane model and the free (non-bonded) CPTC monomers (green molecules).
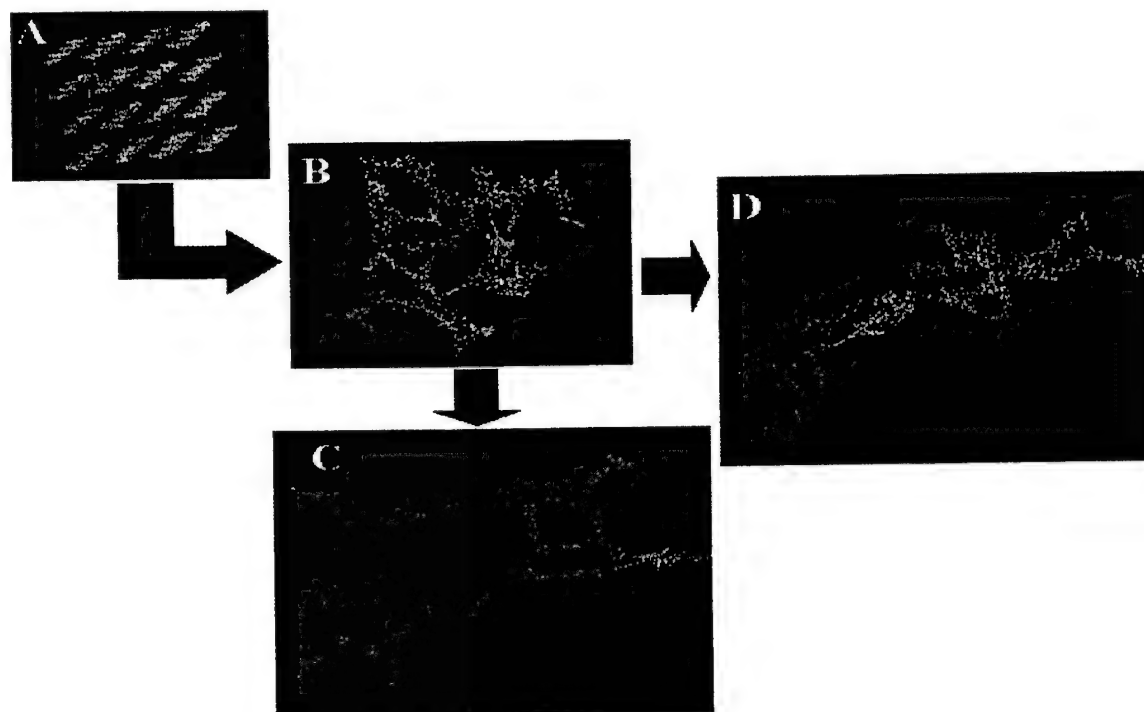
Figure 6.31 MD simulations of a *ctct*-CPTC lattice membrane model in the presence and absence of sodium ions. Image A = the 4x4x4 lattice prior to geometry optimization; image B = the lattice model following molecular mechanics geometry optimization to <0.1 kcal/mol; image C = result after ~100 psec of MD in the absence of sodium counter-ions; and image D = result after ~12 psec of MD in the presence of 20 sodium ions.

6.9.1 Assumptions Made in the Lattice Model Approach

Several assumptions were made in creating the lattice modeling technique described above. These assumptions are:

1. There are stoichmetric concentrations of the acid chloride and primary amine. This is not the case in practice since far more MPD is generally used to remove the H^+ produced in the process of amide bond formation. However, at the hexane/water interface, the concentrations of the acid chloride and MPD may be more stoichmetrically similar to one another than they are in the bulk phase, especially if there is a tendency for the monomers to become concentrated at the interface.

2. Mixing is 'ideal' such that each MPD residue is instantaneously surrounded by six nearest neighbor CPTC residues, and vice versa.

3. Monomer arrangement has cubic symmetry or is approximately cubic resulting in a six-neighbor cell.
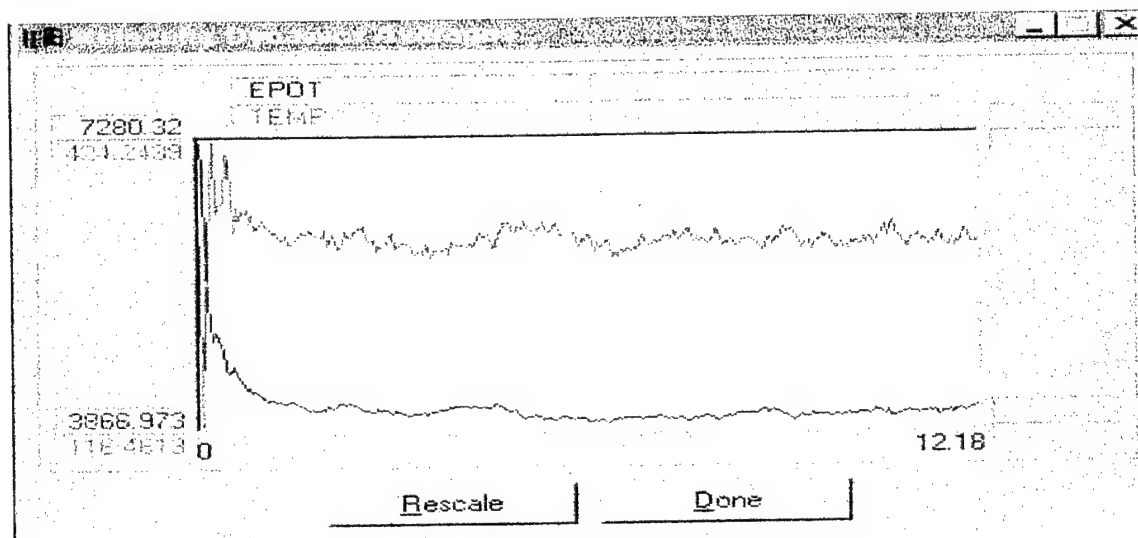
Figure 6.32   Temperature and potential energy curves for the MD simulation where
sodium ions were present as described in Figure 6.3.1. Note the rapid
decline in the membrane (system) potential energy indicating the
contracted state of the CPTC membrane was energetically more
favorable than an expanded state.

4. Bonding can only occur between nearest neighbors in the lattice. Thus, each
buried acid chloride monomer has six nearest MPD neighbors to which it can
potentially bond to, and vice versa. Monomers that are located on a face of the
cube have only five nearest neighbors and monomers located on corners of the
cube have just three nearest neighbors.

5. Bonding is essentially random, i.e., an MPD or CPTC monomer has equal
probability of bonding to any of its nearest neighbors. X-ray studies done as part
of this program were unable to identify any detectable crystallinity associated with
the CPTC membranes.

6. There is no diminishment (or increase) in the likelihood of bonding as the
bonding points on monomers become filled. In other words, an MPD residue
with one available (non-bonded) nitrogen atom has the same probability of
undergoing bonding to a CPTC residue as an MPD with two non-bonded
nitrogen atoms. This assumption is currently being examined by looking at the
structures of *ctct*-CPTC and *cccc*-CPTC each with three attached MPD residues.
The current hypothesis is that the *ctct*-CPTC isomer might remain somewhat
more open and available for bonding as MPD sites become filled (see below).

    Some of the key assumptions listed above lend themselves to experimental
verification. For example, if bonding is truly random, then we could expect a certain
statistical distribution of non-bonded CPTC residues to result. Using ATR-IR
spectrometry, it should be possible to obtain the ratio of free carboxylic groups to free
amine groups and compare this ratio with that predicted from models.

53

6.9.2 User Inputs to the Lattice Model

The user of the lattice model software can readily specify the following system variables:

1. Type of CPTC Isomer

    This feature facilitates qualitative and quantitative comparisons between membrane models constructed from the different isomers of CPTC.

2. Lattice Dimensions

    The lattice consists of rows and layers of monomers. The user must specify the number of monomers per row, the number of rows per layer, and the number of layers in the finished lattice.

3. Monomer Spacing

    The user can specify the spacing between monomers in Angstroms. A provision is included to make this distance 'fuzzy' so that monomers are positioned in the lattice at random distances from some mean monomer separation distance. The distance feature is important if geometric constraints are going to be used to control the likelihood of bond formation between neighboring monomers in the lattice. For example, the user can ask the question: "What will happen to cross-linking density, bonding arrangements, and overall membrane 3D structure if I apply a maximum allowable bond distance?"

4. Row and Layer Spacing

    Similar to the monomer spacing feature described above.

5. Monomer Orientation in Space

    The user can request that monomers be randomly or non-randomly oriented in space as they are added to the lattice structure. Orientation here refers to spinning of the monomer about its XYZ axes as it remains at a fixed location in space. The relative orientation of neighboring monomers affects the distance between their reactive side groups and therefore is useful in applying geometric constraints on the probability of bond formation.

6. Bond Probability

    The user may specify the overall likelihood of bond formation in the lattice model. There is no distinction made between bonding and cross-linking – they are considered to be equivalent to one another. The effect of reducing the bond probability would be equivalent to lowering the temperature of the reaction,

decreasing the reaction pH, or doing anything else that would generally inhibit bond formation between neighboring CPTC and MPD monomers.

7. Maximum Permissible Bond Distance

The user can request that bonds not be formed between neighboring monomers in the lattice if their separation distance exceeds some arbitrary amount that the user specifies.

6.9.3 User Selectable Variables Still to be Added

Two new factors will be added to the next version of the program. One will be the ability to select a bond angle window. Only if the reactive atoms in MPD and CPTC are oriented within this window will bonding be permitted. The other feature to be added to the program will be a steric hindrance factor which takes into account the fact that as more MPD molecules undergo bonding to a CPTC residue, it becomes increasingly difficult to add more MPD due to steric crowding. In other words, if the likelihood of MPD bonding decreases faster in the *cccc* isomer than in the *ctct* isomer as bonding sites become progressively filled, then a new factor can be programmed into our lattice model builder which takes this phenomenon into account. The result would be reduced bonding (cross-linking) in the *cccc*-CPTC membrane which could explain some of the observed instability of this membrane compared to the *ctct*-CPTC membrane. We suspect this effect is more pronounced for the *cccc*-CPTC isomer because all of the greater asymmetry of this compound compared to the *ctct*-CPTC isomer (see Figure 6.33). Reaction modeling experiments will be run to determine the relative magnitudes of the steric hindrance factors for these two isomers.

In Figure 6.33, in each case three MPD units were bonded to the acid chloride leaving one free acid chloride group for reaction. Note the more 'unfolded' state of the *ctct*-CPTC isomer compared to the *cccc*-CPTC isomer. The MD simulations were run for about 250 psec at 300°K.

6.9.4 Possible Applications of the Lattice Model

The lattice model described above has several potential applications. These are:

1. Water and Solute Diffusion Prediction

The lattice model should be useful for conducting molecular dynamic (MD) simulations of water and solute diffusion in the polymer matrix, similar to the work described by Kotelyanskii et al. [22] Water and solute diffusion coefficients computed from such MD simulations can be used to predict water flux and solute rejections. Changes to the membrane can then be made to see if water flux and rejection can be improved.

Figure 6.33 Views of the last frames of MD simulations for hydrated *cccc*-CPTC
(upper left) and *ctct*-CPTC (lower right)

2. Model Structural Comparisons

The lattice method should provide a convenient means to qualitatively and
quantitatively compare the structural features of membranes prepared with the
six different CPTC isomers. Properties such as overall shape, bond number (or
cross-link density, the ratio of free carboxyl to amide II groups, and buoyant
density could be readily compared between models.

3. Comparisons with Experiment

The lattice model as currently configured assumes equimolar concentrations of the
two reactants – CPTC and MPD. It also assumes random bonding (see above).
Given these two assumptions, there is a finite probability that some acid chloride
and primary amine residues may not be able to bond because all of their nearest
neighbors have already undergone complete bonding to other partners. This
likelihood increases if geometric constraints on bonding are applied by the
user. The program keeps records of how many non-bonded monomers remain in
the finished lattice model. Thus, it is possible to compute the ratio of free carboxyl
groups to amide-II groups in the membrane models, as shown in Figure 6.34. The
actual measured value for the carboxyl/amide-II ratio for the FilmTec type membrane
was about 0.4 – 0.5 (see ATR/IR data in this report). A value very close to this
(0.481) was obtained from the lattice models when the bond formation probability
was set at or close to 1.0. Thus, modeling suggests that cross-linking efficiencies

56

in the actual membranes must be quite high, perhaps approaching 100%, and that bonding is likely to be random between nearest neighbors. The models also suggest, as pointed out above, that there is almost always free unbound acid chloride remaining in the membranes. Invariably, the lattice models predicted that about 10-20% of the CPTC monomers remained unbound, even at a bond formation probability setting of unity.

The plotted equation is:

$$y = -1.0042 \ln(x) + 0.5043$$
$$R^2 = 0.9718$$
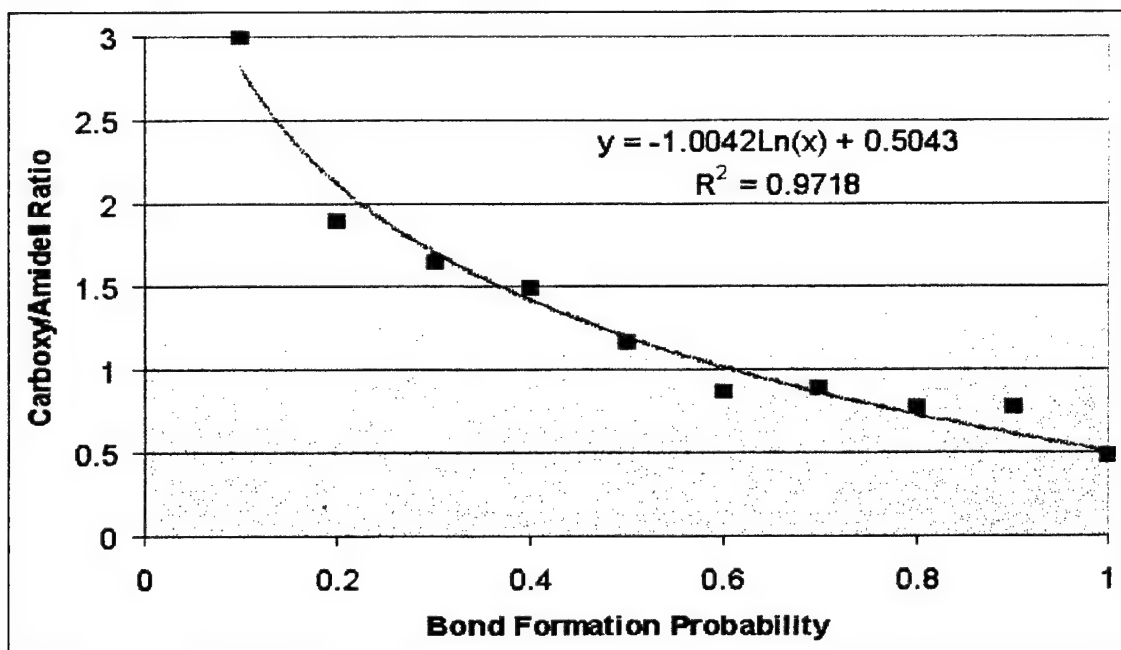
Figure 6.34   Carboxyl/Amide-II ratios predicted for ten lattice models. Each model contained a total of 216 monomers arranged in a 6 x 6 x 6 array. Bond (cross-linking) probabilities were varied from 0.1 to 1.0. No restrictions were placed on bonding distances; thus, monomers were free to bond to any available nearest neighbor.

6.10 Modeling N-Chlorination of the CPTC Backbone

Water flux and solute rejection data obtained during this study indicate that the CPTC membranes prepared using the *ctct*-CPTC stereoisomer are more stable and generally resistant to chlorine oxidation. However, changes in the performance of the *ctct*-CPTC membranes have been observed following chlorine exposure under certain conditions (e.g., at high ionic strengths). This observation suggests that chlorine may in fact react in some way with the polymer membrane. One likely site of chlorine attack is the nitrogen atom that forms the amide bond in the polymer backbone. Efforts were therefore made to model the reaction of free chlorine (hypochlorous acid) with the amide bond nitrogen to determine the susceptibility of the membrane to chloramination or other possible side reactions.

To accomplish this modeling task, a program was written in Tcl/Tk language to control the conditions and progress of an MD simulation of a reaction between hypochlorous acid (HOCl) and a target amide bond nitrogen atom in a small fragment of a membrane model. The model membrane fragments consisted of either MPD-*cccc*-MPD or MPD-*ctct*-MPD. This strategy allowed a comparison to be made of the relative susceptibilities of the two kinds of polymer fragments to chlorine attack, assuming initial starting reaction conditions were the same in each case.

The software allowed control over all reaction parameters including the temperature (i.e., the velocity or kinetic energy of the HOCl species), the initial spatial orientations of the reactants, the duration of each reaction in picoseconds, the number of reactions to be carried out in one series, as well as other properties. If so desired, parameters such as the reaction temperature and spatial orientations could be randomly varied from one reaction to the next in a series, although in the examples discussed below these parameters were held constant.

The software automatically sorted reactions into separate files depending on their outcome, e.g., whether the reaction 'successfully' resulted in N-chlorination or not. This approach greatly facilitated analysis of the many reactions (usually 100 or more) that were typically carried out in any one series. For example, if 200 reactions were run where reactant orientation was randomly varied each time, all those reactions resulting in chlorine addition to the target nitrogen atom would be sorted into one file, whereas all those reactions where chlorine failed to add would be filed elsewhere. The criterion for such file partitioning was the calculated straight-line distance of the chlorine atom to the targeted nitrogen atom at the end of the reaction. As an example, if chlorine was found to be greater than a certain distance (typically >4.0 Å) from the nitrogen atom at the end of the specified reaction time, then it was assumed that the reaction was unsuccessful and chlorine failed to oxidize the amide nitrogen atom. In this situation, the reaction would be stored separately in a file named 'unsuccessful reactions'.

Two N-chlorination reactions were modeled. In each reaction, the HOCl molecule was propelled at constant velocity (70 Å psec) toward one of the amide bond nitrogen atoms in the MPD-*cccc*-MPD or MPD-*ctct*-MPD polymer fragments. The system temperature (~1900°K) corresponded to the initial kinetic energy of the HOCl molecule since the target polymer's velocity was zero until the two molecules collided. Each reaction was run a minimum of 75 times to gather statistics on the types of reaction products produced while randomly varying the initial rotational orientation of the HOCl molecule relative to the target polymer fragment. The initial spatial orientation of the reactants and other reaction parameters are shown in Figure 6.35. Whereas the position of the chlorine atom in the HOCl molecule was held constant, the rotational orientation of the HOCl molecule was randomly varied between each reaction that was carried out. Different reaction products formed based on the random variations in the HOCl molecule at time = 0. The targeted amine nitrogen atom is indicated (tn).

The HOCl molecule was modeled using the semi-empirical PM3 force field as were the two polymer fragments. Each polymer fragment was geometry optimized to <0.1 kcal/mol-Å. The PM3 force field was also used to run the MD reaction simulations. This force field is able to model the breaking and formation of bonds. A successful reaction was defined as chlorine addition to the target nitrogen atom.
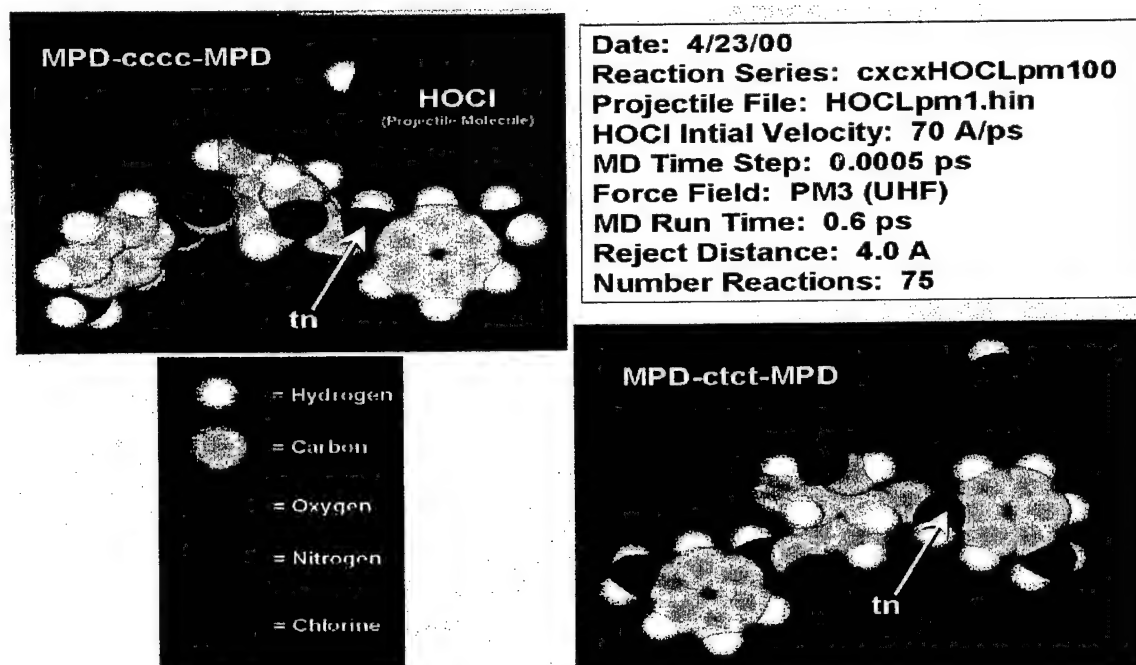
Figure 6.35   Reaction parameters used to model chlorination of MPD-*cccc*-MPD or MPD-*ctct*-MPD polymer fragments

Chlorine addition (*i.e.*, chloramination) was typically accompanied by deprotonation of the targeted amine nitrogen atom and substitution of chlorine for the proton. Often this resulted in the formation of water or a free proton and a hydroxyl radical. An example of one of the reactions (reaction #CNadd*cccc*HOCLpm101.hin) involving the MPD-*cccc*-MPD polymer fragment is shown in Figure 6.36. In this particular reaction, chlorine addition caused deprotonation of the amide nitrogen resulting in the formation and release of one water molecule.

Numbers shown are the elapsed picoseconds from the beginning of the reaction. The total reaction time was 0.6 psec. Note that one water molecule was formed as a product from the OH- group of HOCl and the proton originally associated with the target nitrogen. The initial velocity of the HOCl molecule was 70 Å/psec corresponding to a temperature of ~1900°K. The initial velocity of the target polymer was zero. The PM3 semi-empirical force field was used to model this and the other reactions discussed in this report.

The potential energy and the chlorine-to-nitrogen separation distance for reaction #CNadd*cccc*HOCLpm101.hin are plotted in Figure 6.37 as a function of the reaction time in picoseconds. There was a sharp increase in the system potential energy as the HOCl molecule began its approach toward the target nitrogen atom in the MPD-cccc-MPD polymer fragment. The highest inflection point for this potential energy curve corresponds to the activation energy for this reaction. Immediately following
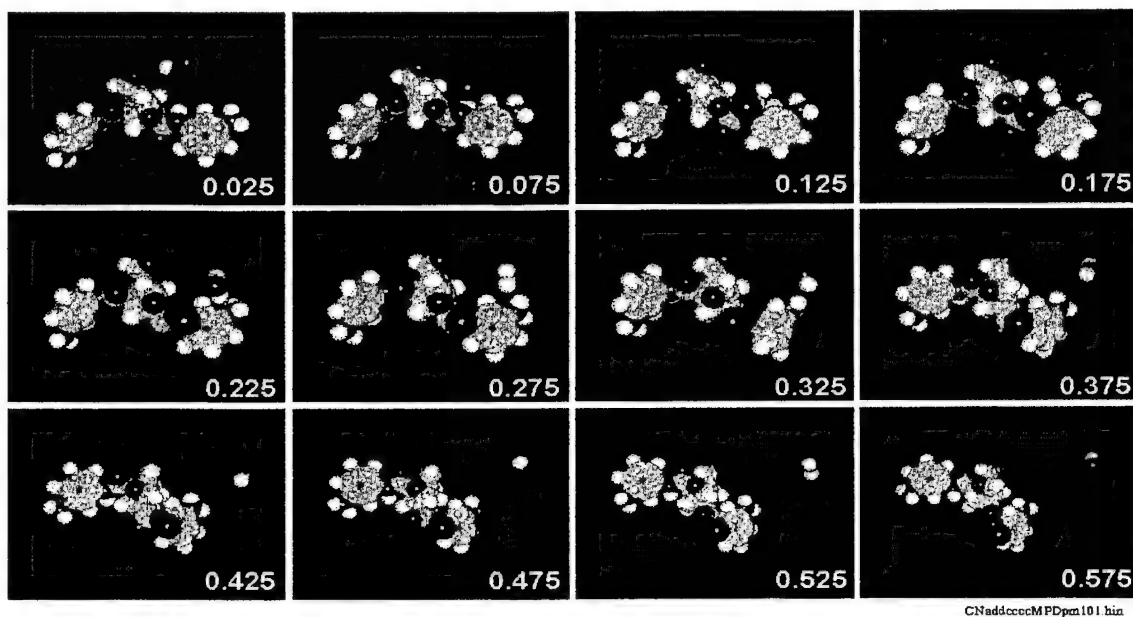
Figure 6.36 N-chlorination of the MPD*cccc*MPD polymer fragment
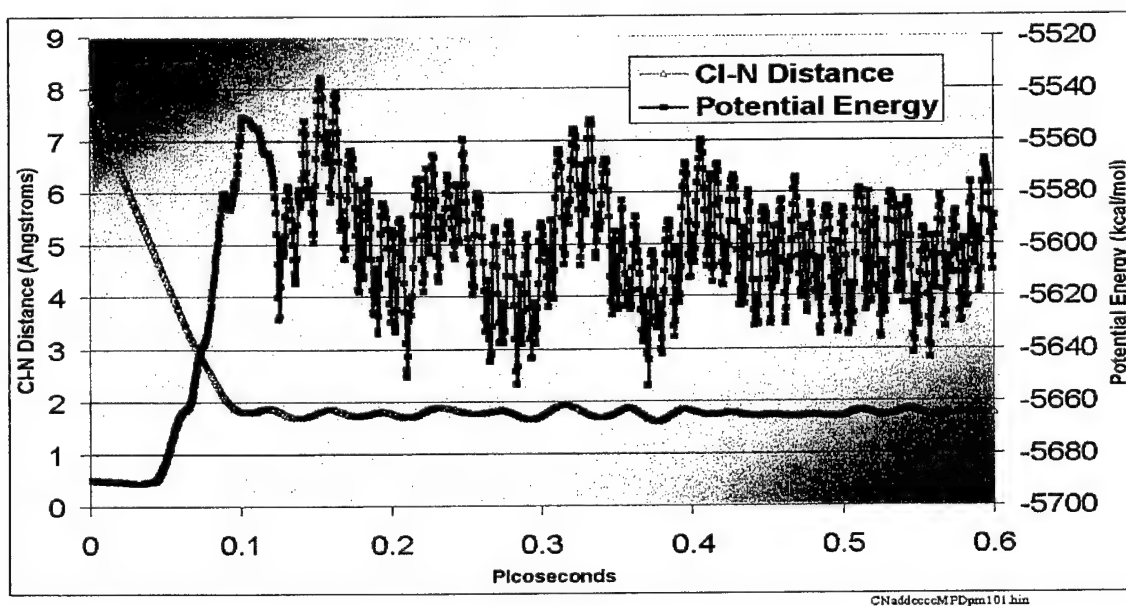
Figure 6.37 Potential energy and the chlorine-to-nitrogen separation distance for reaction CNadd*cccc*HOCLpm101.hin

deprotonation and chlorine oxidation of the amide nitrogen atom, the system potential energy rapidly declined suggesting a more stable system conformation. Subsequently, the potential energy of the molecular system fluctuated as the conformation of the polymer fragment (and that of the released water molecule) varied over the course of the reaction. These conformational changes resulted from transfer of the kinetic energy of the HOCl molecule to the target polymer and other reaction products.

The temperature of the above reaction and the chlorine-to-nitrogen separation distance are plotted in Figure 6.38. These data indicate that the system temperature remained constant for about 0.05 psec until the HOCl molecule began to slow in response to repulsive van der Waals and electrostatic forces encountered in the vicinity of the target molecule. Collision of two reactants (indicated by the Cl-N separation distance) transferred HOCl kinetic energy to both kinetic and potential energies in the MPD-*cccc*-MPD polymer fragment.

CNaddccccMPDpm101.hin
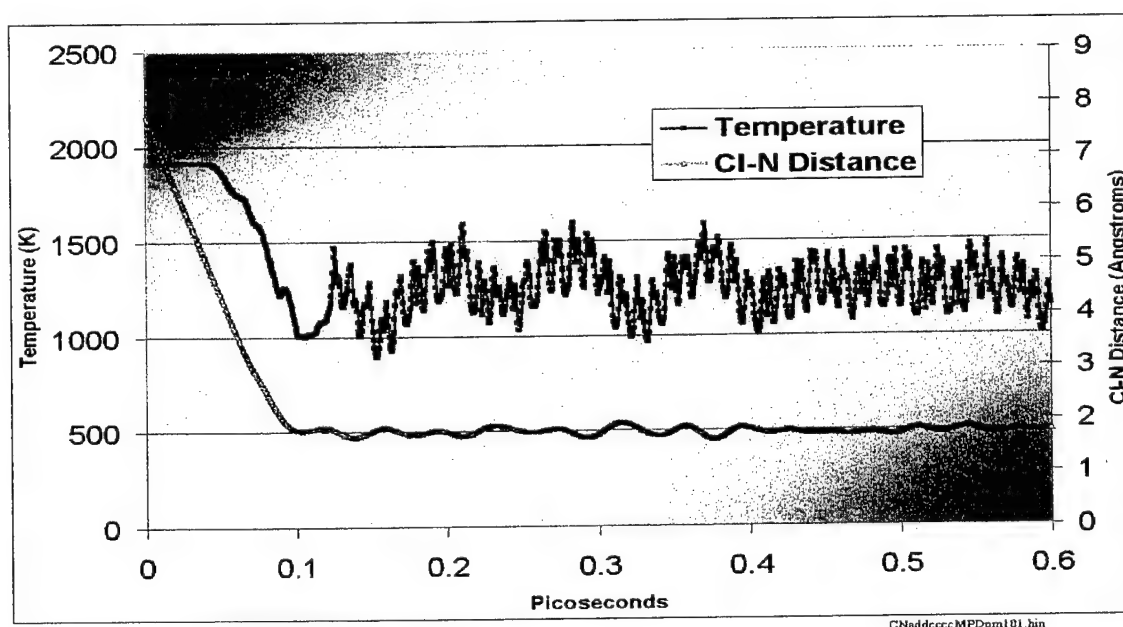
Figure 6.38   Reaction temperature and the chlorine-to-nitrogen (Cl-N) separation distance for reaction CNadd*cccc*HOCLpm101.hin

The results of a similar type of analysis are presented in Figure 6.39 and 6.40 for reaction BrkCl*cccc*HOCLpm128.hin which involved an initial chlorine addition to the amine nitrogen followed by rapid cleavage of the amide bond.

As shown in Figure 6.41, approximately 25% of the reactions involving the MPD-*cccc*-MPD polymer resulted in successful oxidation (i.e., chloramination) of the target amide nitrogen. In contrast, none of the reactions carried out using MPD-*ctct*-MPD as the target polymer resulted in a successful chloramination reaction. About 95% of the reactions involving the MPD-*ctct*-MPD polymer fragment resulted in no reaction of any kind, whereas approximately 60% of the reactions involving MPD-*cccc*-MPD resulted in

61

no reaction. These data are consistent with the notion that polymers formed from the *ctct*-CPTC stereoisomer are significantly more resistant to chlorine oxidation than those formed from the *cccc*-CPTC monomer.
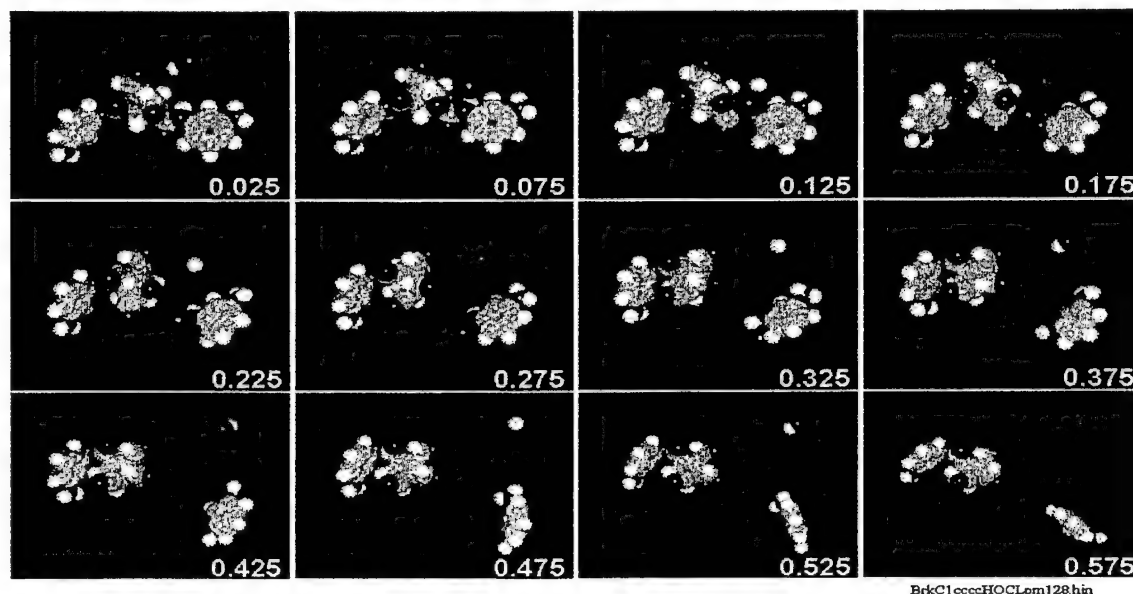
Figure 6.39   Chloramination of the amine nitrogen in MPD-*cccc*-MPD followed by amide bond cleavage for reaction BrkClccccHOCLpm128.hin. Numbers are picoseconds of simulated reaction time. Note formation of the -OH radical.
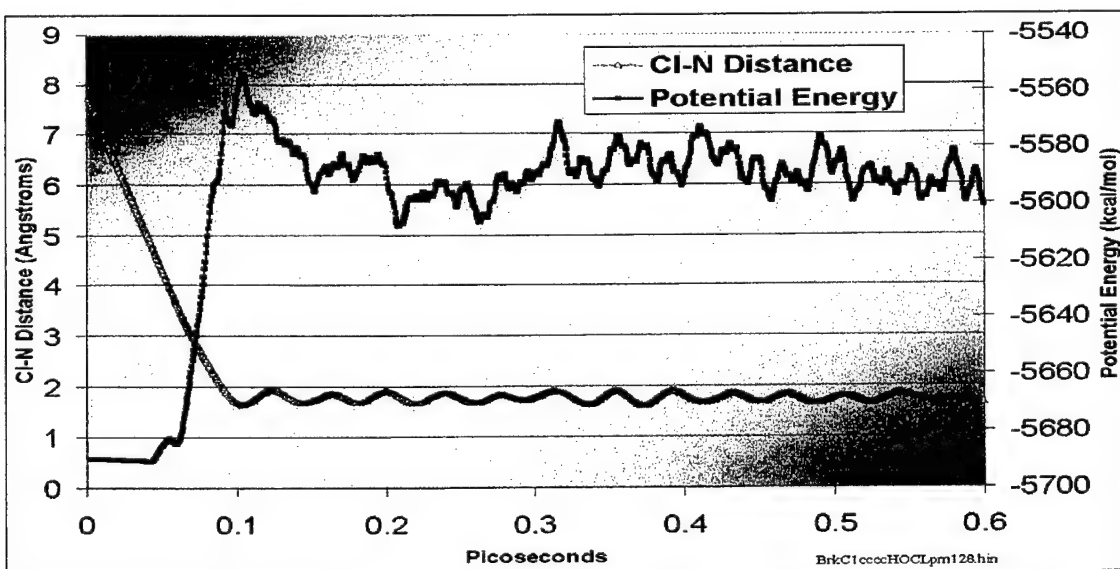
Figure 6.40   System potential energy and the chlorine-to-nitrogen (Cl-N) separation distance for reaction BrkClccccHOCLpm128.hin as shown in Figure 6.37

Each reaction was carried out 75 times. The rotational orientation of the HOCl molecule was randomly varied for each reaction. Note that the MPD-*cccc*-MPD polymer fragment was significantly more reactive than the MPD-*ctct*-MPD fragment. Brk+Cl = -C-N- bond breakage with chloramination; Brk-Cl = -C-N- bond breakage without chloramination; Cl+N = chloramination without bond breakage; NoRXN = no reaction observed; Other = other types of products formed. Chlorine addition to the amine nitrogen (Cl+N) was never observed for the MPD-*ctct*-MPD fragment. Reaction of HOCl with the targeted primary amine (i.e., either Brk+Cl, Brk-Cl, or Cl+N) typically resulted in the formation of water of hydroxyl ions.
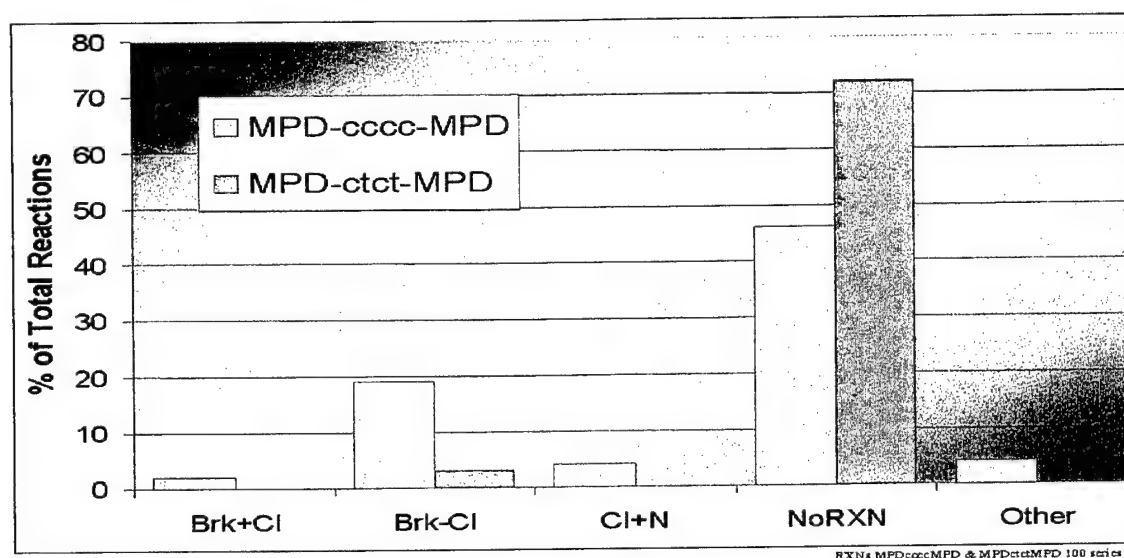
Figure 6.41 Summary of the reaction products formed from two chlorination reactions involving either MPD-*cccc*-MPD or MPD-*ctct*-MPD as the targeted primary amine

6.11 Recommendations

A number of molecular modeling (Tcl/Tk) software tools were designed and evaluated during this phase of the program. These software tools should continue to be refined and applied to explore and compare the molecular structures, energetics, and functions of membrane models prepared from the different CPTC stereoisomers. Specific recommendations for continued work in this area are as follows:

1. The conformational space of the CPTC membrane models must be explored in detail using MD or Monte Carlo type simulations. These molecular simulations will provide insight into the range of thermodynamically acceptable structures possible for these experimental membranes. Such simulations will also be required as a first step to obtain more accurate results of water and solute diffusion through these unique polymer membranes.

2. Water and solute diffusion in the different isomeric versions of the CPTC membranes should be modeled to delineate the mechanism of water and solute transport in these membranes. Chlorine (hypochlorous acid) penetration into the different membrane types (prepared from the different CPTC isomers) could also be explored in this manner.

3. The effect of ionic strength and water content on CPTC membrane molecular structure (e.g., the degree of swelling) should be determined using MD simulations. Experimental data indicates changes occur in the water flux and solute rejection of the CPTC membranes in response to ionic strength. This could be related to the type of salt-induced contractions that were described in this report.

4. The lattice software should be refined to include a feature that accounts for changes in steric hindrance during MPD bonding to CPTC. If this feature were available, it could shed light on possible structural differences in CPTC membranes prepared from the different CPTC isomers.

5. Preliminary reaction modeling clearly indicates that the chlorine atom from hypochlorous acid (HOCl) can oxidize (and add to) the primary amine nitrogen that forms the backbone amide bond of the polymer chains. Chlorination of the aromatic MPD ring has also been observed in the preliminary modeling reactions that have been conducted to date.

6. The role of bromide in membrane chlorination reactions should be explored.

7.0 SYNTHESIS AND PURIFICATION OF *ctct*-1,2,3,4-CYCLOPENTANE TETRACARBOXYLIC ACID CHLORIDE

7.1 Background

As previously indicated, PA membranes are made by interfacial polymerization of an acid chloride (TMC) and an amine (MPD). Reports in the literature[2,10] and molecular modeling show that membranes can be made using 1,2,3,4-cyclopentanetetracarboxylic acid chloride (CPTC-AC) in place of TMC. Because of four asymmetric carbons in the molecule, there are a total of six geometrical isomers possible (see Figure 3.0). Tests on the *ctct*-CPTC membrane indicated that this one isomer produced a superior membrane in terms of oxidative resistance, while the all cis membrane deteriorated rapidly in the presence of chlorine.[2] The explanation for these superior properties may be understood in terms of (1) the reduced bond strains, (2) higher degree of PA branching, (3) lower free ionic species on the polymer (minimizing transition metal catalyzed reactions) or (4) steric protection to the amide bonds.

Neither Arthur et. al.[10] nor Ikeda et. al.[2] reported the degree of isomeric purity of the *ctct*-CPTC-AC. All *ctct*-CPTC-AC was made from *ctct*-CPTC acid that had been synthesized from *cccc*-CPTC acid using a thermoconversion step. Based on our experience, and the chemical equilibrium, an isomeric purity of 85% was obtainable by this approach. The hypothesis of this research was that an increased isomeric purity would correlate with improved membrane performance in terms of salt rejection and chlorine resistance. Thus, the focus of the work was to increase the isomeric purity of the *ctct*-CPTC-AC, make membranes from this material and test our hypothesis.

Since neither author discussed a detailed preparative method, it was necessary to develop a synthetic route and procedures for purification and identification of the *ctct*-CPTC isomer. To improve the chances for success, scientists from four different institutions were involved in the synthesis and purification of the isomer.

7.2 Experimental Program

The synthetic development of high purity *ctct*-CPTC-AC was a coordinated effort among the BR, DU, ITM and SST. The *ctct*-CPTC acid used in the program was synthesized under the direction of SST. Subsequently, the material was transferred to DU for additional purification and conversion into *ctct*-CPTC-AC.

7.2.1 Thermal Conversion of *cccc*-CPTC Acid to *ctct*-CPTC Acid

Following published procedures on the thermoconversion of *cccc*-CPTC acid to *ctct*-CPTC acid, the 33.3 wt-% *cccc*-CPTC acid solution was transferred to a high pressure reactor at 200°C for 72 hr.[10] This reaction yielded approximately 80-85% of *ctct*-CPTC acid and other isomers. This step became the starting point for various studies yielding the final high purity CPTC-AC.

Another conversion method was studied that utilized an aluminophosphate catalyst. In this procedure, the *cccc*-CPTC acid was dissolved in water and reacted under atmospheric pressure, below 100°C for 12 hr. These reaction conditions are substantially milder and may be a useful method for producing the acid at a lower cost in the future. Because the thermoconversion process was already proven, documented in the literature, easy to transfer to another laboratory (ITM) and capable of delivering larger quantities of acid in a timely manner, the decision was made to stop the research on the catalytic conversion approach. The immediate goal was to prepare high purity *ctct*-CPTC-AC at greater than 99+% purity. Other tangential laboratory findings, such as above, were noted throughout the course of the investigation.

7.2.2 Conversion of CPTC Acid to CPTC-AC

Four chlorinating agents were investigated:

a. Phosphorus pentachloride
b. Phosphorus trichloride
c. Thionyl chloride
d. Oxalyl chloride

At first, phosphorous pentachloride gave poor yields and NMR data showed incomplete conversion of all acid functionalities to acid chloride. After adjusting reaction conditions, greater than 95% yield of acid chloride was obtained from the acid. Although there was no increase in isomeric purity using phosphorous pentachloride as the chlorinating agent there was no isomerization detected. This conclusive experimental result was very useful information. If the acid could be isomerically purified beforehand, then the use of this chlorinating agent might produce the desired high isomerically pure acid chloride.

Phosphorous trichloride was an unsuccessful reagent that led to incomplete conversion of the acid to the acid chloride. Perhaps reaction conditions could be modified to make this reagent work, but again the decision was to leave this for another time.

Thionyl chloride is often used industrially for chlorinating the carboxylic group and the by-products are the gases SO_2 and HCl. Thionyl chloride might have been the chlorinating agent for this synthesis except for incomplete conversion of the acid groups required the use of pyridine and DMF as catalysts. The final product was dark in color (possibly sulfur impurities) but the principal reason for abandoning $SOCl_2$ was that the acid chloride sample did not make a good membrane. With further work, this reagent might be found useful, although, it was also noted that this reagent did not increase the isomeric purity of the acid chloride.

The final reagent investigated was oxalyl chloride. Although an expensive reagent for scale-up production, its only by-products are the gases CO_2 and HCl which might yield a very pure acid chloride. The disadvantage of oxalyl chloride was incomplete

conversion to acid chloride. Also, there was no increase in the isomeric purity of the acid chloride.

The reaction conditions with phosphorous pentachloride reagent were 20 g of ~85% pure *ctct*-CPTC acid and 80 g of PCl_5 added to a 100 mL round bottom flask with 100 g of dry heptane. Heat at 80°C until a uniform yellow color is produced. Cool and filter through a 0.25 µM filter and remove the heptane by rotary evaporation followed by overnight vacuum.

7.2.3 Purification of CPTC-AC by Physical Separation Techniques

Physical separation techniques were considered to improve the isomeric purity of ~80-85% *ctct*-CPTC-AC synthesized. The purification technique employed in this work included:

a. Spinning band distillation
b. Zone refining
c. Falling film molecular distillation

Spinning band distillation (see Figure 7.2.0) is useful in separation of liquids with very close boiling points, such as the acid chloride isomers. Although other techniques such as chromatography might be used to separate extremely small quantities of chemicals for identification purposes, spinning band distillation remains one of the only technologies for separating larger quantities of liquids which have close boiling points. Another significant advantage is that acid chlorides are extremely reactive and corrosive and therefore most chemical systems cannot be used. The spinning band equipment, consisting of all glass and Teflon is ideally suited for such reaction environment.

The key to spinning band technology is the high number of theoretical plates which can be achieved in a very short column height. The principle behind this distillation technology is the helical band that spins at several thousand revolutions per minute in an open, insulated column. The action of the spinning helix on the ascending vapors and the descending condensate forces intimate contact between the two phases. This intimate contact of the phases, in turn, causes very good fractionation. At atmospheric pressure, and using a 36-in long Teflon band, such a system would have approximately 400 theoretical plates. This translates into separating liquids with boiling point differences as close as 0.3°C.

After many unsucessful attempts to distill the acid chloride, this technique had to be abandoned. Under vacuum and heat, the acid chloride would char before any sample could be collected.
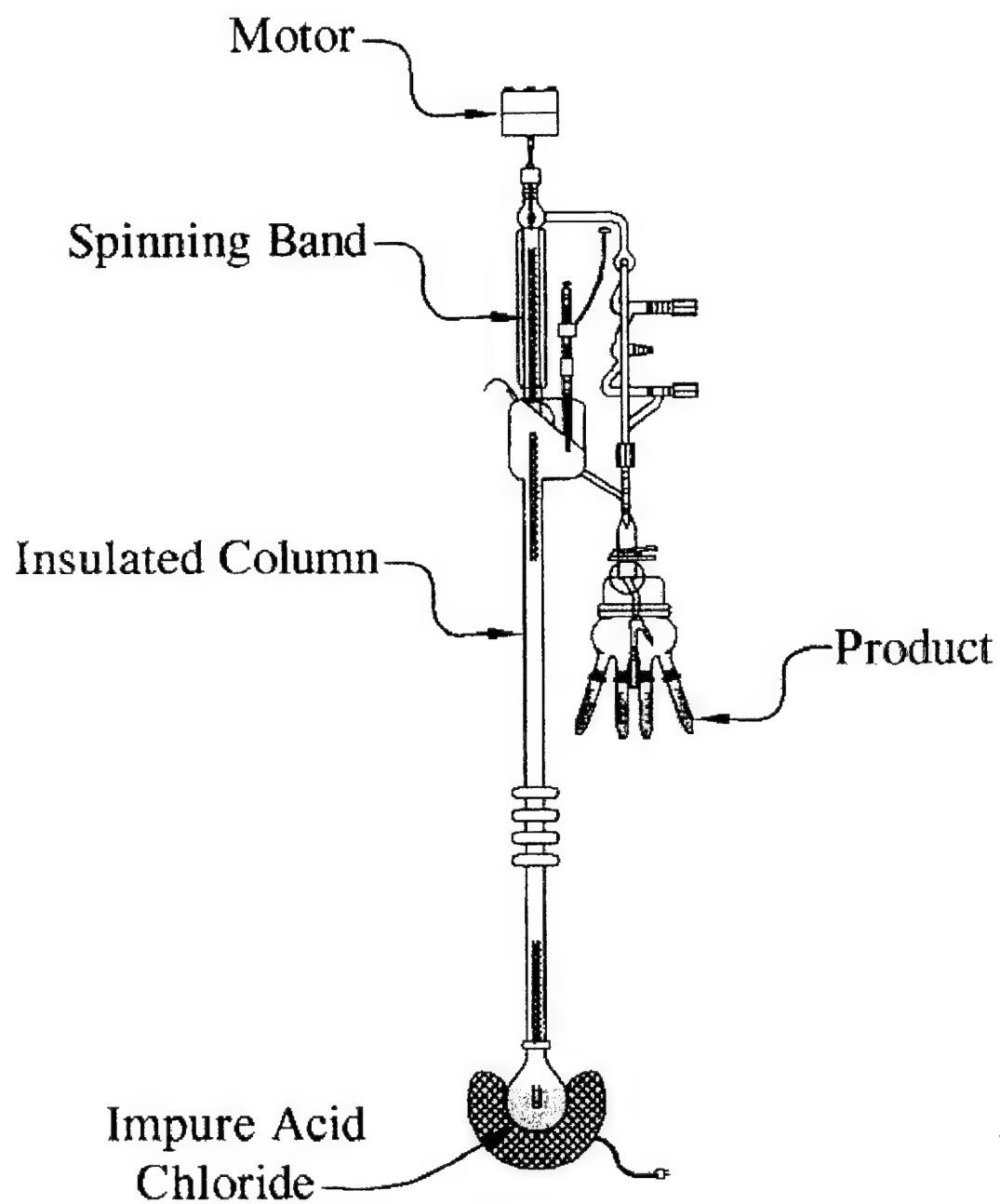
Figure 7.2.0   Spinning band distillation apparatus

Zone refining (see Figure 7.2.1) can be used to purify compounds using the phase transition of solid-liquid rather than liquid-vapor. This technology made the purification of silicon possible that is used in the semiconductor industry today. The sample travels through hot and cold zones at pre-set temperatures corresponding to melting and freezing points for the compound. As the sample melts and recrystallizes, the impurities tend to stay in the liquid phase. The crystalline phase is higher in purity than the liquid phase because the crystal structure tends to exclude molecules that do not readily fit in the crystalline lattice. The sample is passed through the molten zone many times, resulting in a purified product. The automated equipment runs unattended overnight, allowing many cycles. At completion, the impurities are at one end of the tray and are removed by cutting it off from the resulting final product.

At first, the acid chloride reacted with the solder at the corners of the tray and new trays were ordered to overcome this difficulty. The next problem was the low melting point of the acid chloride. Even using dry ice to aid in lowering the block temperature, it still was not possible to solidify the acid chloride. At this point, the technique was abandoned.

The first successful attempt at distilling the acid chloride was by falling film molecular distillation (see Figure 7.2.2). This technology uses short paths and large surface area for the distillation process. Because only a few theoretical plates are possible from this equipment and the boiling range of the isomers is narrow, the samples collected did not show any significant increase in isomeric purity. However, this technology was useful in purifying the acid chloride from other impurities.

7.2.4 Syntheses of CPTC Esters for Physical Separation Techniques

Two of the physical separation techniques, spinning band and zone refining, were attempted with the following esters of the ~80-85% *ctct*-CPTC acid:

a. Methyl
b. Propyl
c. Benzyl

Spinning band distillation of the methyl and propyl esters were not successful. Both compounds decomposed during the distillation and no product could be obtained. Zone refining of the methyl and propyl esters were attempted. The propyl ester did not have a favorable melting point, too low for the equipment. The methyl ester was suitable. Presumably, while the propyl ester has a higher molecular weight than the methyl ester, the methyl ester can "pack" while the n-propyl groups on the other ester get in the way. The methyl ester looked ideal for zone refining (mp ~75°C), with clearly distinct solid crystalline regions and melt regions. Unfortunately, after many run cycles, samples taken from various parts of the tray only showed marginal improvement in isomeric purity.
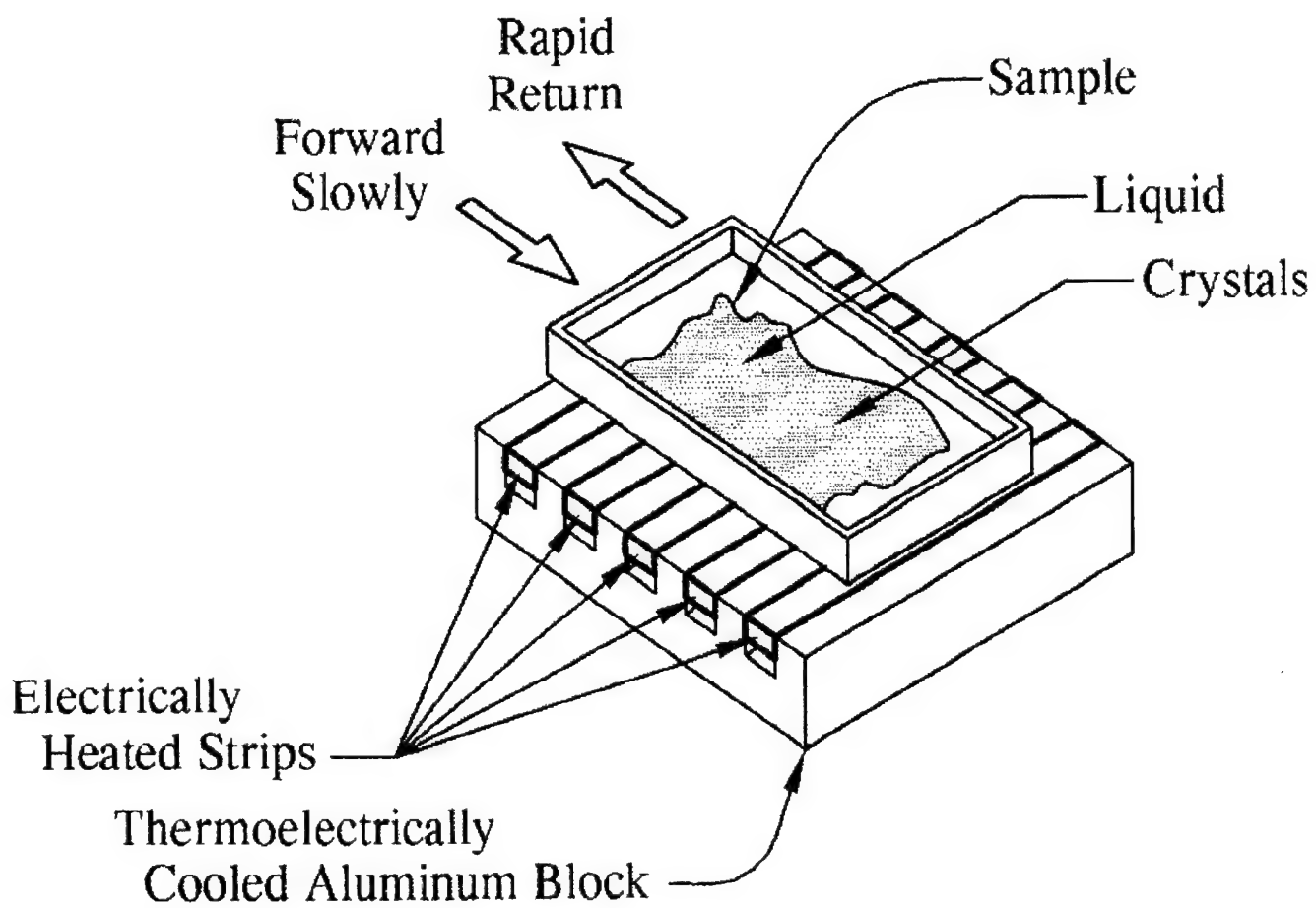
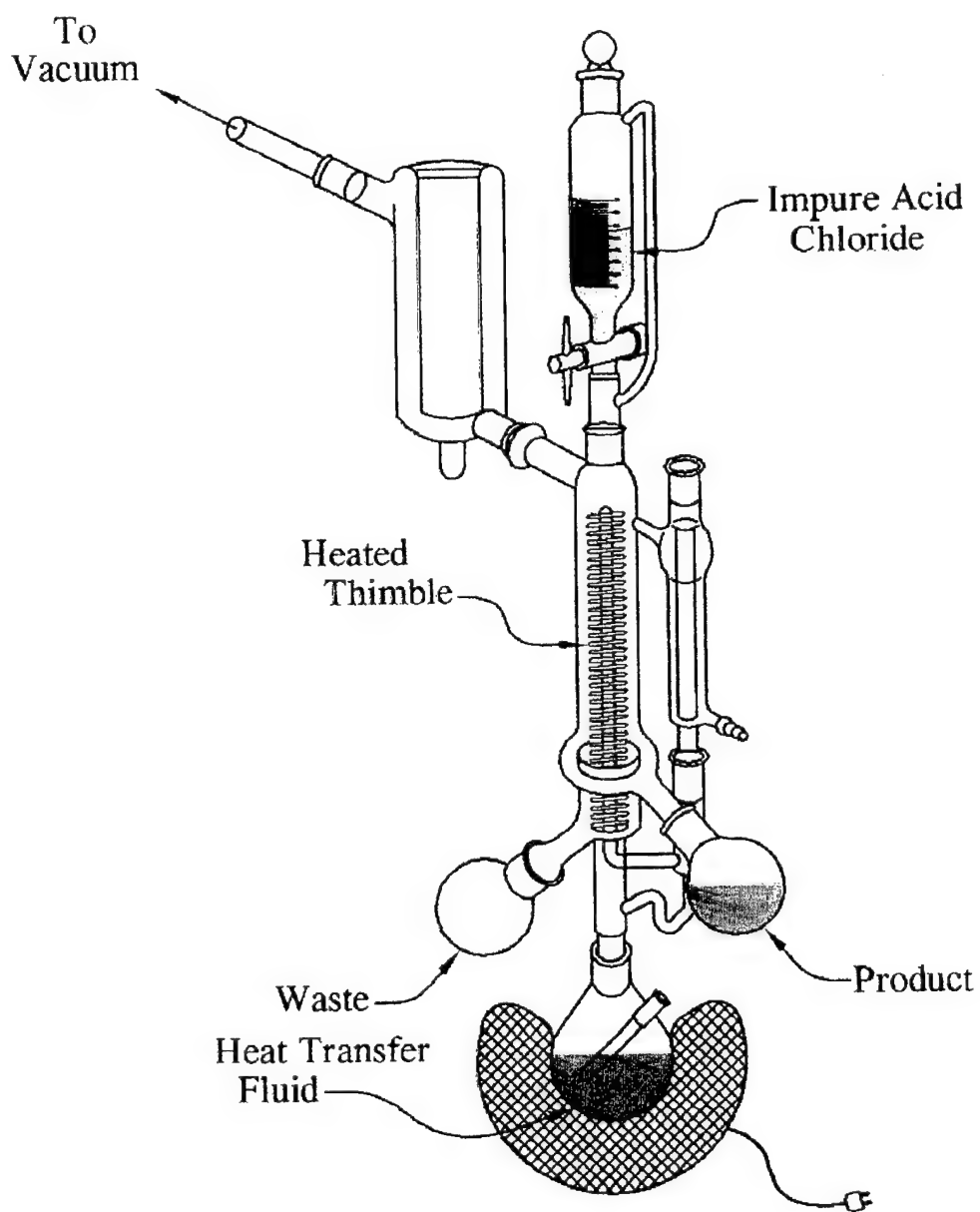Figure 7.2.1 Zone refining equipment

To
Vacuum

Impure Acid
Chloride

Heated
Thimble

Waste

Heat Transfer
Fluid

Product

Figure 7.2.2 Falling film molecular distillation apparatus

71

The benzyl ester had an unfavorable boiling point for distillation and the decision was made to abandon zone refining because, even if successful, distilling off the benzyl alcohol would make this approach unattractive.

7.2.5 Purification of the ctct-CPTC Acid by Wet Chemical Techniques

During the above investigations, various wet chemical approaches to the separation of the acid isomers were attempted. The hypothesis was that if the acid could be purified, PCl_5 would be used as the chlorinating agent and no significant isomerization would occur during the reaction to the acid chloride. This would produce the high purity *ctct*-CPTC-AC desired.

Although a rather lengthy procedure (see Figure 7.2.3), the final product was the isomerically pure >97% *ctct*-CPTC acid. Two variables interfered significantly with the crystallization process (and hence purity), moisture content of the starting acid material and an unknown colloidal material as a polymer. To overcome the moisture problem, the acid was dried by breaking it up into small pieces and placing it in a vacuum oven at 85°C overnight. The colloidal problem was not completely resolved but is believed to be responsible for the variability in the final acid. The final crystallized acid can vary from 97 to 99.9+%, making the delivery of very high purity acid time consuming.

7.2.6 Removal of Phosphorous from Synthesized *ctct*-CPTC-AC Using Falling Film Distillation

After synthesizing acid chloride, samples were analyzed for residual phosphorus using a phosphorus probe on a 400 Hz NMR. Phosphorus could be removed to below detection levels by processing the acid chloride with falling film molecular distillation. Improvements were made to the filtration process and the vacuum system, that resulted in a product free of residual phosphorus, as determined by elemental analysis, thus saving an entire distillation step.

7.2.7 Synthesis of High Purity *ctct*-CPTC-AC and Analytical Methods for Characterization

The acid chloride was synthesized using the procedure described at the end of Section 7.2.2. Improvements in the acid crystallization procedure led to higher purity acid chloride.

The acid samples were characterized using ^1H and ^{13}C NMR. Samples were contracted out for elemental analysis to confirm that the ratios of elements were in agreement with the stoichiometry and no anhydride had formed. An example of the ^1H and ^{13}C NMR on the *ctct*-CPTC acid is shown in Figures 7.2.4 and 7.2.5, respectively. The data indicate the samples are of high purity. The isomeric purity of the *ctct*-CPTC acid and the *ctct*-CPTC-AC were determined by comparing the integrated triplet peaks relative to the others as can be seen in Figures 7.2.6 - 7.2.8.

PROCESS OF SEPARATING ctct-CPTC ACID
FROM OTHER ISOMERS
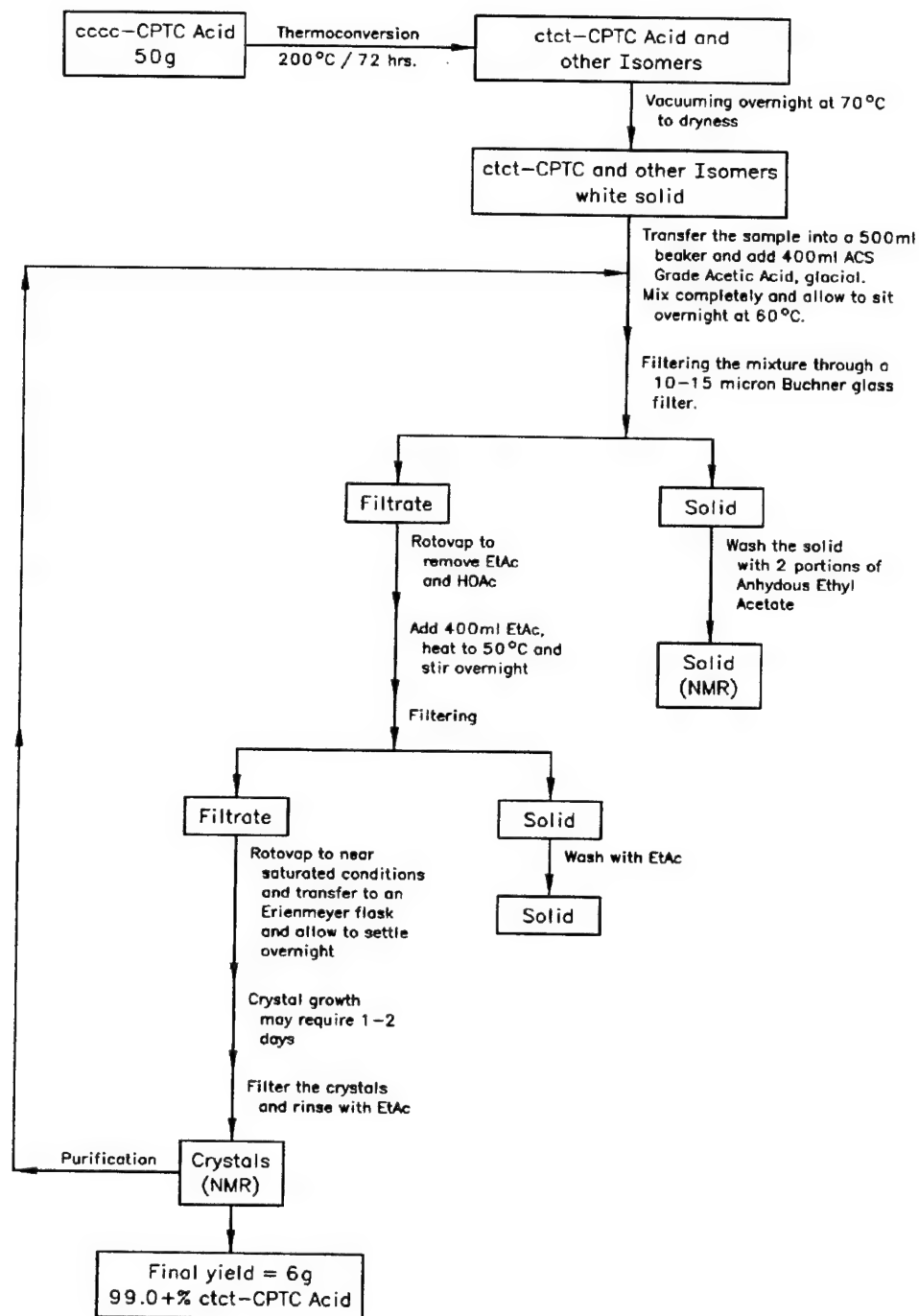
Figure 7.2.3 Flow diagram for acid purification
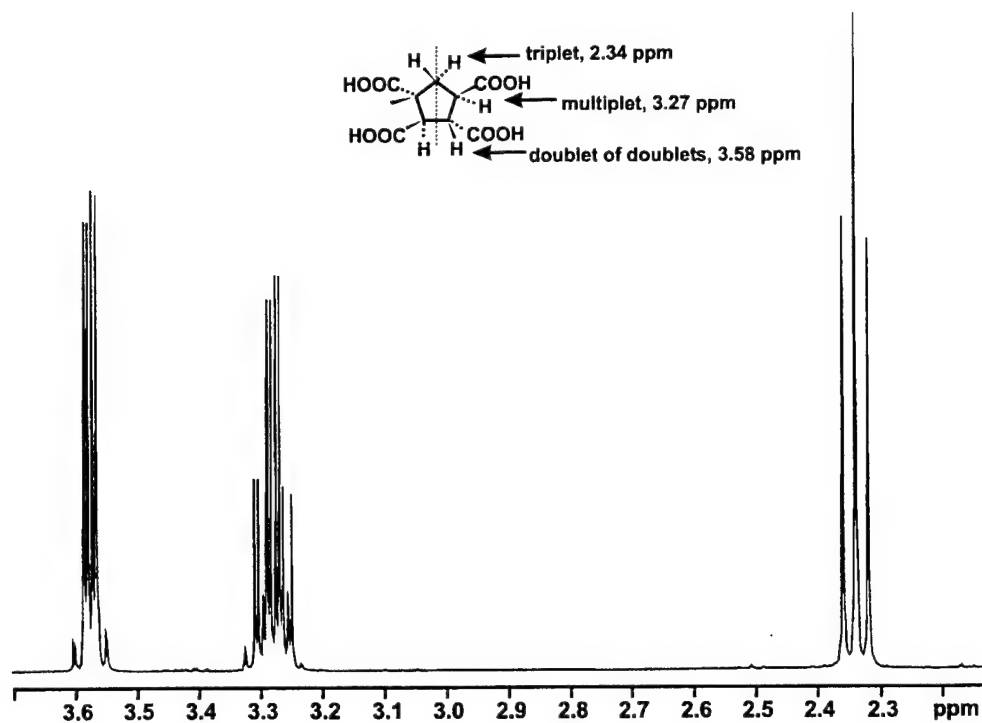
Figure 7.2.4 ^{1}H NMR of high purity CPTC acid
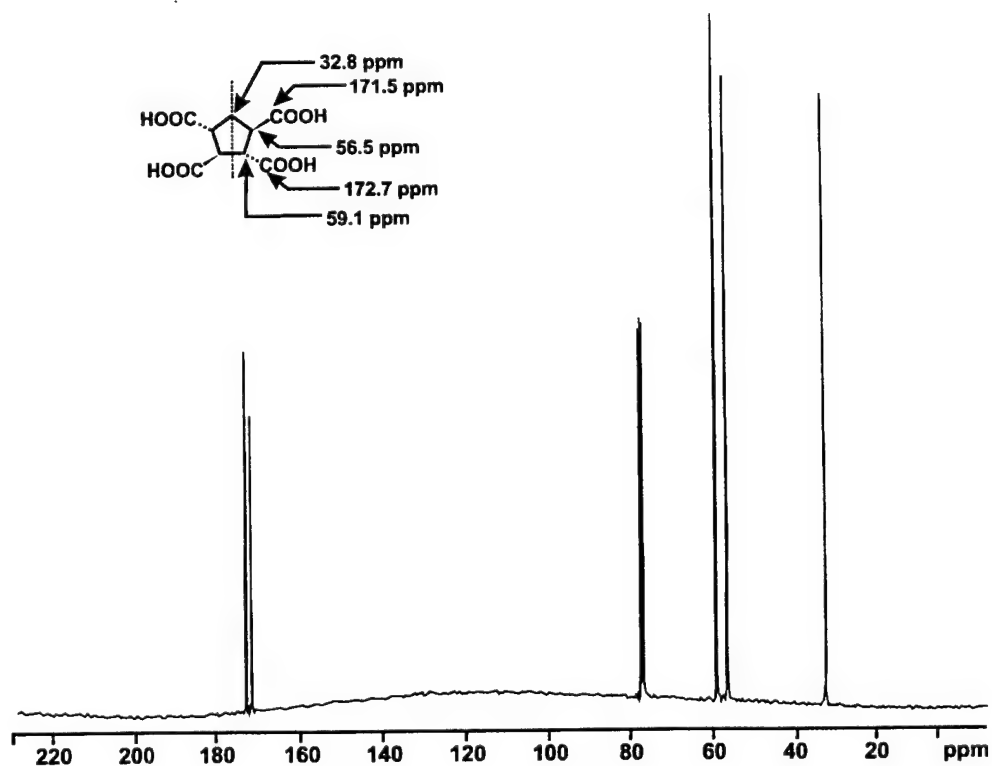
Figure 7.2.5 ^{13}C NMR of high purity CPTC acid

74
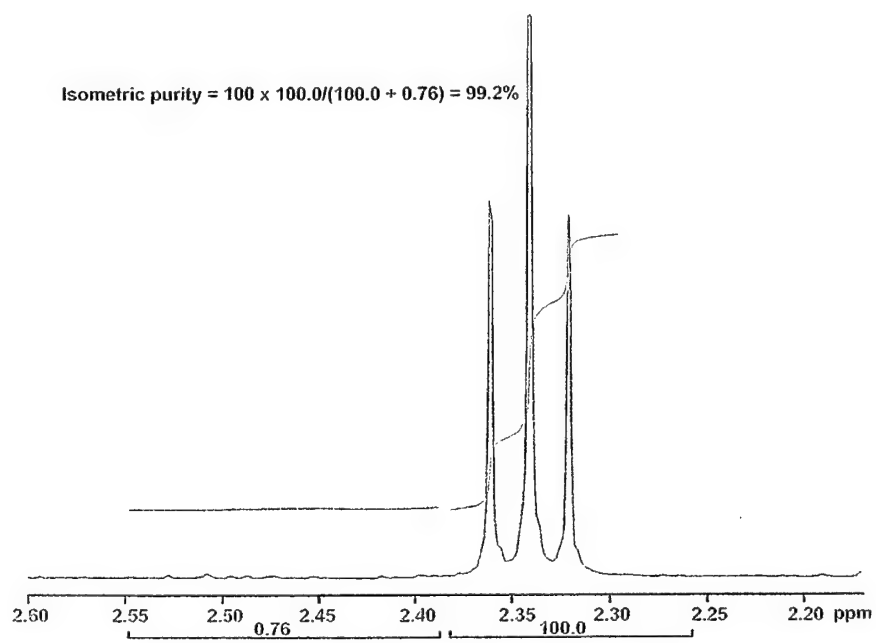
Figure 7.2.6 85.6% isometrically pure CPTC-AC
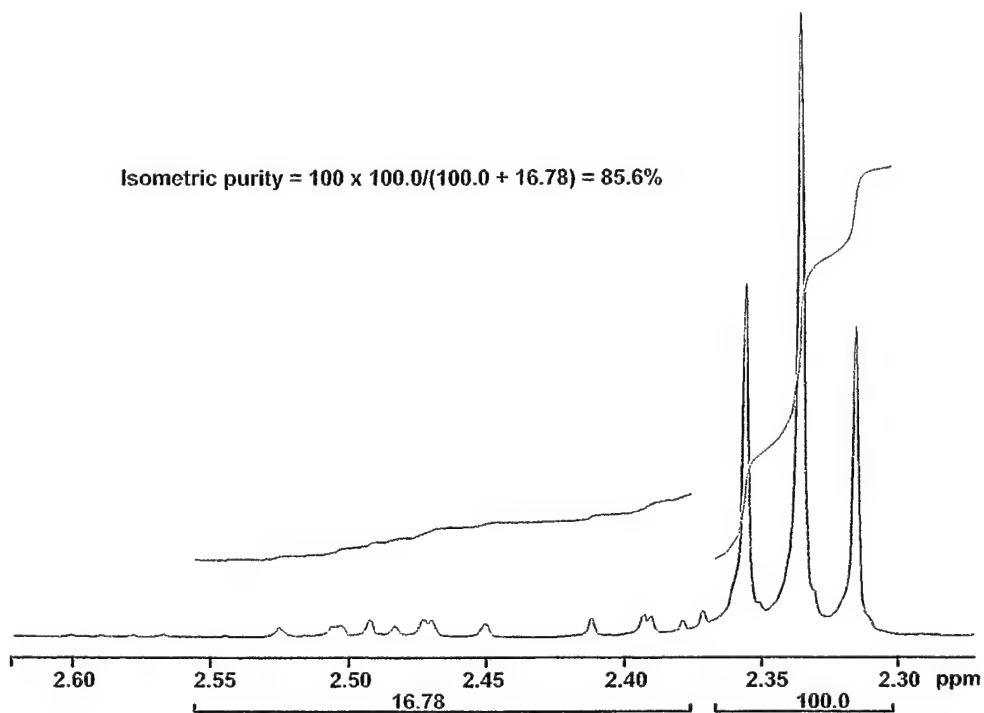
Figure 7.2.7 99.2% isomerically pure CPTC-AC

The acid chloride samples were characterized using ^{1}H, ^{13}C, and ^{32}P NMR. Elemental analysis confirmed the stoichiometry of the acid chloride and that phosphorus concentrations were in agreement with ^{32}P NMR and acceptable for membrane processing. Conformation that all four carboxylic acid groups were successfully converted to acid chlorides required infrared spectroscopy and GC/MS analyses on the corresponding esters. An example of the conversion of acid to acid chloride with no isomerzation is evident by comparison of the ^{1}H NMR in Figures 7.2.9 and 7.2.10.

After a great deal of effort, the synthesis and purification of *ctct*-CPTC-AC at >97% purity were successful. It was anticipated, however, that even higher purity material would be required to produce a chlorine-resistant membrane. By recrystallization of the acid and repeating various steps in the extraction, samples of *ctct*-CPTC acid with purity at >99.9+% were obtained and the corresponding acid chloride (same purity) synthesized for membrane fabrication.

7.2.8 Salt Rejection and CPTC-AC Purity

The purity of the CPTC-AC used to fabricate membranes had a significant effect on performance, as salt rejection improved with increasing acid purity as shown in Table 7.0.

Table 7.0

CPTC-AC and Improved Membrane Performance

Date	Acid Chloride Isomeric Purity (%)	Rejection (%)
11/98	~70	98.6
11/98	~98	98.8
2/99	~99	99.2
9/99	99+	99.3
7/00	99.9+	99.5

Isometric purity = 100 x 100.0/(100.0 + 0) = 100.0%
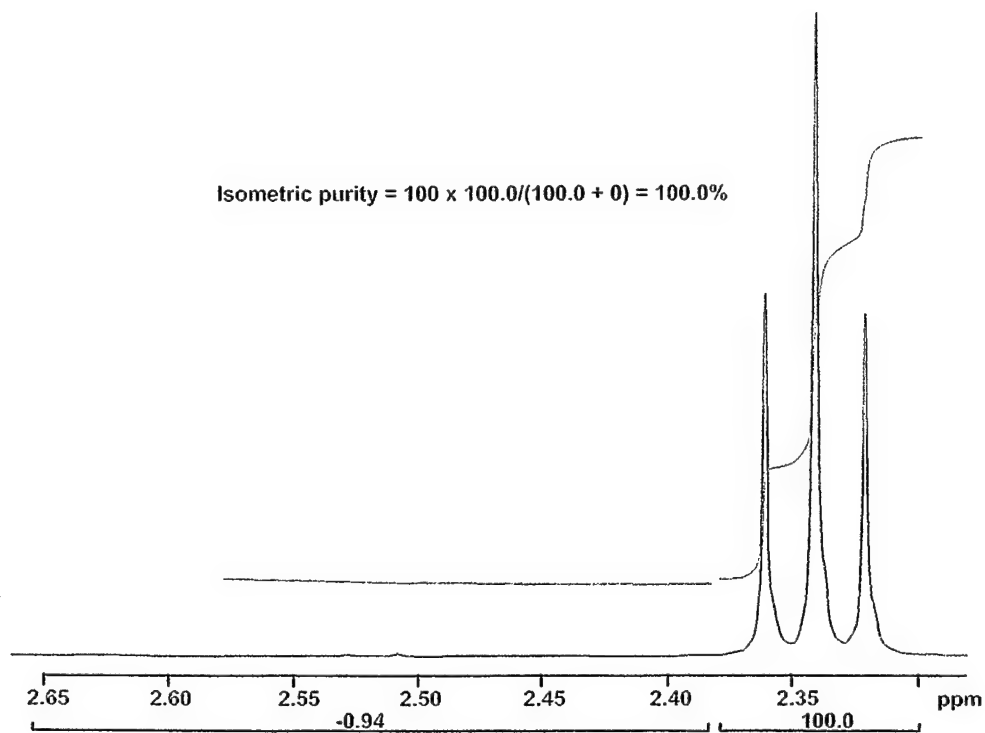
Figure 7.2.8 100% isomerically pure CPTC-AC
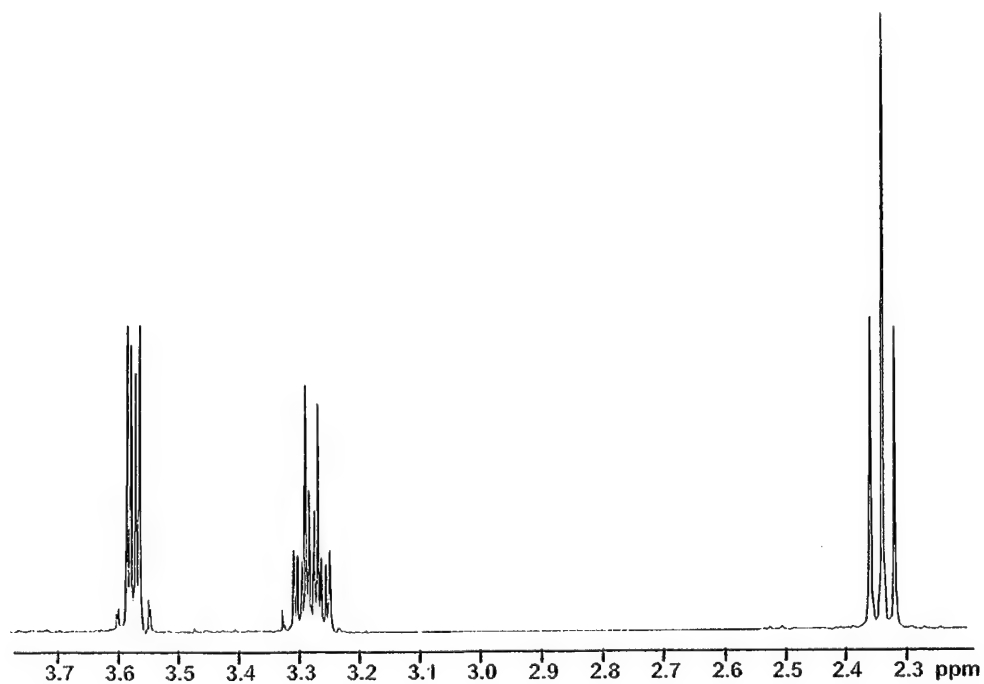
Figure 7.2.9 NMR spectra of high purity CPTC acid
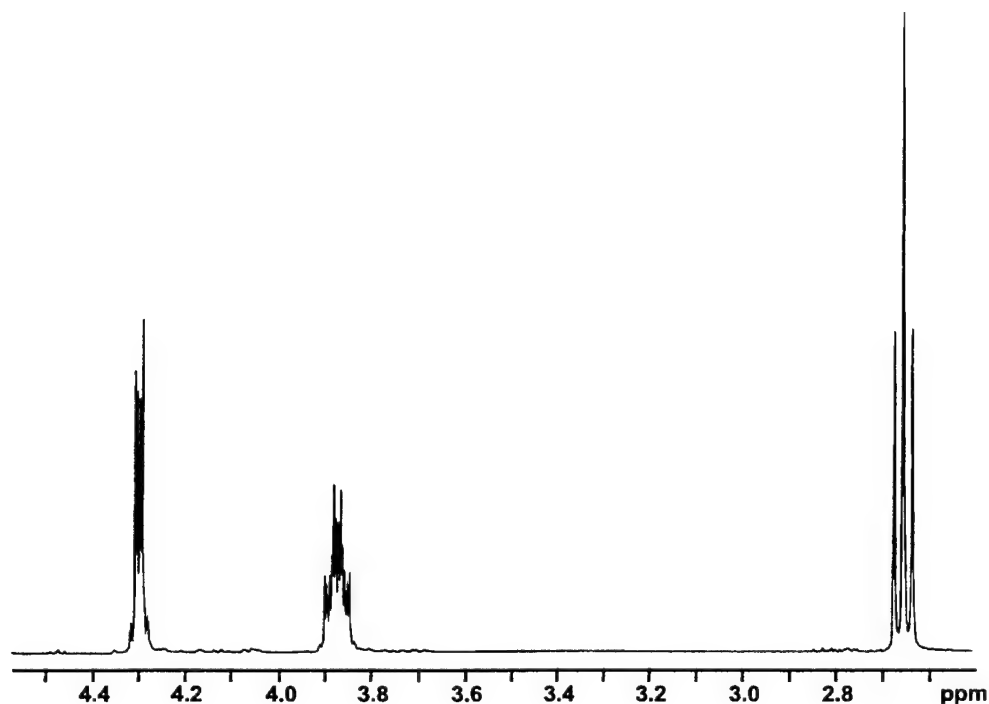
Figure 7.2.10   NMR spectra of acid chloride synthesized from acid in Figure 7.2.9

7.2.9 Membrane Costs with CPTC Acid

The starting compounds are trimesic acid ($0.33/g) and CPTC ($0.69/g) - the acid chloride precursors for TMC and CPTC-AC,[18] respectively. Using this information, a cost comparison in Table 7.1 shows:

Table 7.1

Membrane Costs Using TMC vs CPTC-AC for Manufacture of
8- X 40-in Spiral-Wound Element

Acid	Comment	$/g of Acid	g of Acid Element	$ Acid/ Element	Cost % of Element ($600 ea.)*
TMC		0.84 [18]	1.59	1.34	0.2%
CPTC	2 x TMC	1.68	1.60	2.69	0.4%
CPTC	4 x TMC	3.36	1.60	5.38	0.9%
CPTC	8 x TMC (worst case)	6.72	1.60	10.75	1.8%

- Estimated retail price of an 8- x 40-in element

2 mg PA film covers ~60 in^2; CPTC = 45.6 wt-% of film; 1 g CPTC-AC makes 254.4 ft^2 of membrane; 1 g TMC makes 252.7 ft^2 of membrane

These data show that the new acid chloride would not significantly increase the cost to manufacture these elements.

7.2.10 Conclusions and Recommendations

The fact that no isomerization occured and the isomeric purity was maintained during the synthesis of the acid chloride is remarkable and confirms the hypothesis, that the way to synthesize high purity acid chloride is to purify the acid first, and then synthesize the acid chloride using PCl$_5$.

Additional efforts are required to improve the yield, synthesis time and the overall economics of the process. The work performed was driven primarily to get a high purity acid chloride for membrane manufacturing and testing. Future efforts to improve the overall synthesis process would lower the cost of the final acid chloride product.

8.0 TECHNICAL APPROACH AND EXPERIMENTAL METHODS

8.1 Evaluation of Experimental Membranes in Field Tests

8.1.1 Water Quality Improvement Center, Yuma, AZ

Field testing of CPTC membranes at the WQIC was initiated during the first quarter of the program with two test cell units (TCUs), each operating on a different feedwater. Initially, each TCU operated with three PVC test cells connected in series, with a membrane area of 19.4 cm^2/cell. Throughout the program the test cells were upgraded, and the number of cells was increased to nine in each TCU. TCU-1 operated on a clearwell feed with a feed conductivity of ~3,800 μS/cm, and TCU-2 operated on a potable water feed with a feed conductivity ranging from ~350 - 1,000 μS/cm. Midway through the first year, an acid injection-pH control system was installed so that both systems could be pH controlled. A 5 mg/L EDTA concentration was maintained in the feedwater to prevent iron fouling.

Each of the TCU operated with three test cell sets, such that each set could be isolated to allow membrane replacement without shutting down the entire train. TCU-1 operated in a single-pass mode with a reservoir located ahead of the test cell train to allow switching to a recirculation mode when a shutdown was planned. TCU-2 operated in a similar fashion except in a partial recycle mode, where freshwater was added as the overflow goes to drain.

Operating on two WQIC water sources enabled the evaluation of the effects of different pH, various chlorine levels and different feed compositions. The approximate compositions of the two waters are:

Test Unit	Water Source	TDS (mg/L)	pH	Cl_2 (mg/L)
TCU-1	PSI Clearwell	3,000	4.0	1.5
TCU-2	Potable water	350	8.0-8.5	0.5

The frequency of the manual data collection was 3 times per 24 hr shift. The raw data was telefaxed to SST daily where it was entered into an Excel spreadsheet program, standardized, evaluated and plotted. Data collection included: Date and Time, Pressure (kPa), Temperature (°C), pH, Free Chlorine (mg/L), Conductivity (μS/cm) and Permeate Flow (g/min).

8.1.2 Naval Facility Engineering Service Center, Port Hueneme, CA

Membrane testing on seawater was conducted at NFESC using three (6.614 in.^{2}) membrane disks in stainless steel test cells connected in series and operated with a feed flow of 1 gal/min. Initial testing was carried out using a 1500 gal seawater reservoir connected to the three-cell system. All components were constructed from Type 316 stainless steel.

Following the initial test period, the Seawater Test Facility was moved to a new location and was completed in late February 2000. The membrane test system continued to operate in a closed loop mode, except the 1500 gal feed reservoir (previously located outdoors) was replaced with a 500 gal feed reservoir located inside of the building. This was done to provide a more steady level of chlorine in the feed and control of the feed pH should be easier. In addition, the seawater feed was passed through a Xenon ultrafiltration system before entering the reservoir. Thus, fouling of the membranes was minimized. A 5 mg/L EDTA concentration was maintained to prevent iron fouling from the stainless steel components in the test system.

The frequency of manual data collection was somewhat random, as compared to WQIC, due to the lack of available personnel. Data might be collected once daily for several days then, generally, only 2 or 3 times each week. Data collection included: Date and Time, Pressure (psi), Temperature (°C), pH, Free Chlorine (mg/L), Conductivity (µS/cm) and Permeate Flow (mL/min).

8.1.3 Orange County Water District, Fountain Valley, CA

Membrane swatches were fed with conventionally pretreated secondary effluent from Water Factory 21. The pretreatment process included chemical (lime) clarification, multimedia sand filtration, antiscalent, sulfuric acid and approximately 5 mg/L chlorine addition before water was passed through the RO pressure cells. The wastewater feed was high in nitrogenous materials. Thus, chlorine combines with these materials to form chloramines; the combined chlorine contacting the membrane ranged from 2 to 5 mg/L. The chemical composition of the feedwater in terms of total organic carbon (TOC), total dissolved solids (TDS), alkalinity and pH are shown in Table 8.0.

Membranes were evaluated in PVC flat sheet test cells (the same design as used at WQIC) with a membrane area of 19.4 cm^2/cell operated at 225 psi (155 kPa) applied pressure at a feed flow rate of 0.9 gal/min. Operating conditions were such that that there were only two supervised shutdowns throughout the entire 5,000 hr run.

Permeate flow and conductivity measurements were taken daily (Monday through Friday). Feedwater pH and total residual chlorine (TRC) concentrations were monitored on a regular basis; pH measurements were taken daily while TRC values were taken via an on-line meter every 15 sec and the daily averages plotted. A more thorough ion rejection analysis was carried out after 1000 hr of operation.

Table 8.0

Chemical Analysis of Water Factory-21 RO Feedwater (Q-22A)

Chemical Assay	Concentration (mg/L)
Total Organic Carbon (TOC)	10.5
Total Dissolved Solids (TDS)	1130
Total Alkalinity	110
pH	6.8

Membrane samples were also run on product water from a different source (Green Acres Project). Water was processed by flocculation with alum and sand filtration, followed by contact with chlorine at 3.5 mg/L. The chemical characteristics of this water is shown in Table 8.1.

Table 8.1

Chemical Analysis of Green Acres Project Product Water

Chemical Analysis	Concentration (mg/L)
Chloride	161
Calcium	62.8
Magnesium	9.9
Potassium	12.2
Sodium	181
Total Dissolved Solids (TDS)	932
Total Alkalinity	189
pH	7.0

8.2 Chemical Characterization of PA Membranes - ATR/IR Spectrometry

8.2.1 ATR/IR Spectroscopic Analysis

In the mid-infrared (4000 cm^{-1} - 400 cm^{-1}), absorptions are related to the fundamental vibrations of component chemical bonds from functional groups, the background structures and molecular fragments. Information about particular functional groups or bonds in the molecule can be found between 4000 cm^{-1} and 1400 cm^{-1}. Below 1400 cm^{-1}, absorption bands provide more information about skeletal vibrations. Band assignments derived from group frequency charts reveal correlations between structure and band frequencies.

ATR/IR spectroscopy provides a non-destructive method for characterizing membrane surface chemistries. The technique works by focusing radiation on the end of an infrared-transmitting crystal of high refractive index (n) at near normal angle of incidence. When the IR radiation is transmitted into the crystal, light striking the interface between the optically dense (e.g., zinc selenide, $n_1 = 2.4$) and the optically rare medium

82

(e.g., air, n_2= 1.0) is totally internally reflected provided that the angle of incidence of the radiation is greater than the critical angle (Figure 8.0). At each internal reflection, the IR radiation penetrates a short distance into the adjoining medium. The energy intensity of this radiation decays exponentially as a function of distance normal to the interface; thus, it is referred to as an "evanescent wave" (Figure 8.1). The depth of penetration of the evanescent wave is the distance at which the electric field intensity drops to 1/e of its magnitude at the interface. For the most common IREs, germanium and zinc selenide, the depth of penetration varies from ~300 to 1000 nm at an angle of incidence of 45°. Any chemical species within the depth of penetration of the evanescent wave can be detected provided it absorbs light in the mid-infrared region of the spectrum. When the sample absorbs light the beam is attenuated and thus the given name 'attenuated total reflectance' spectrometry.

Mid-infrared ATR/IR spectrometry was used to chemically characterize the experimental CPTC membranes. These spectra were also used to determine the relative film thickness, relative degree of cross-linking or the relative carboxylate density. Carboxylate density was used to assess the extent to which the acid chloride reacted to form amide bonds. In theory, the more complete the reaction between acid chloride and MPD, the greater degree of cross-linking and lesser free carboxylate charge.

8.2.2 Relative Film Thickness

ATR/IR spectroscopy was used to determine relative PA film thickness. The absolute band intensities of the PA or PS layers was not used to assess the thickness of the film layer from membrane to membrane, as the size of the swatch affects the magnitude of the vibrational band intensities. The greater the membrane surface area in contact with the IRE, the greater are the intensities of the absorption bands. It is very difficult to place the same amount of membrane in contact with the IRE each time a sample is analyzed. Another factor that affects band intensities is membrane surface morphology or roughness. In general, rougher samples tend to produce ATR spectra with lower band intensities, as good surface contact is more difficult to achieve. Therefore, use of absolute band intensities was not considered a valid method for measuring PA film thickness.

The thin-film composition of the membrane can actually be used to an advantage to assess relative PA thickness. At each internal reflection, infrared radiation passes through the PA film into the PS layer. The thicker the PA film the greater the band intensities and the weaker the PS band intensities. Therefore, ratios of the PA and PS band intensities can be used to assess film thickness more specifically, ratios of the amide II (~1550 cm^{-1}, N-H bending) band of PA and the 874 cm^{-1} (C-H wagging) band of PS. As the film thickness increases, the ratio between PA and PS bands will increase, i.e., PA band intensities will increase and PS band intensities will decrease. There is, one drawback to this method. PA density can throw off this measurement. Two membranes, one with a thin dense nonporous PA layer and the other with a thick porous or lacy PA layer, could have similar PA/PS band intensity ratios. However, all membranes used in this study had lacy foam-like structure. (See Section 12.0)
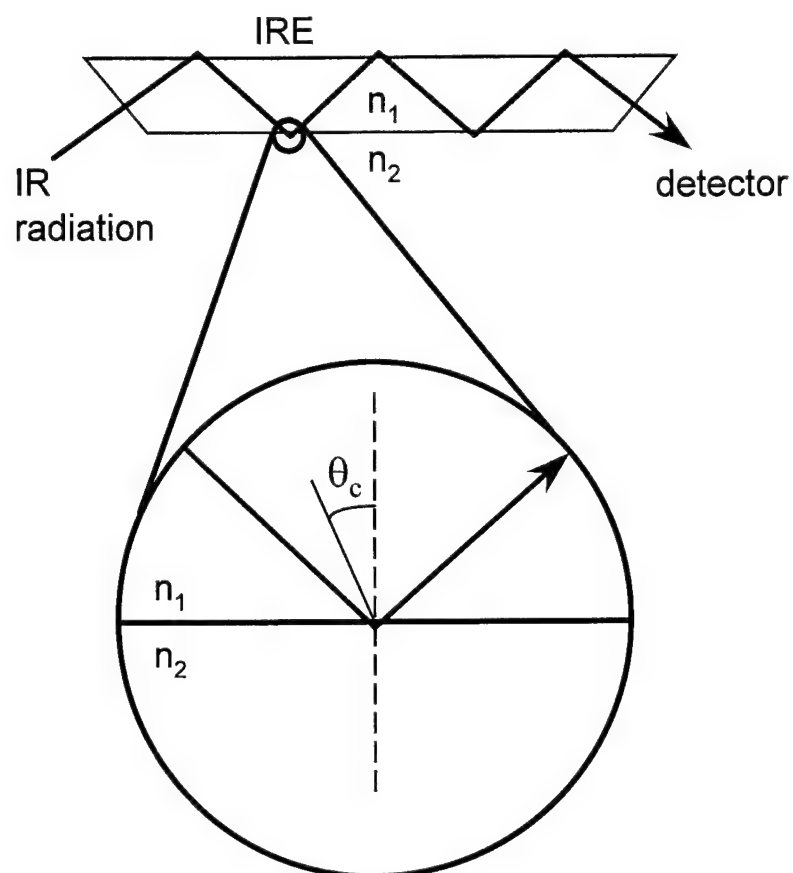
Figure 8.0   Internal reflection of light at an interface where n_1 and n_2 are the refractive indices of the IRE and optically rare medium and θ_c is the critical angle.

evanescent wave

n_2

n_1 ~ 1 μm   IRE

z

e^{-z/d_p}

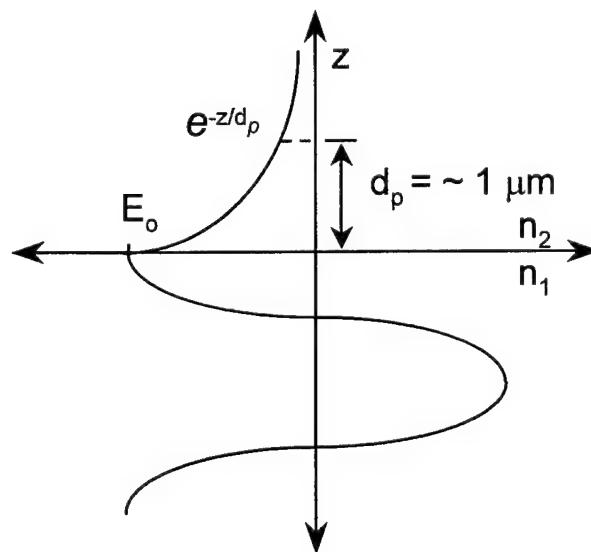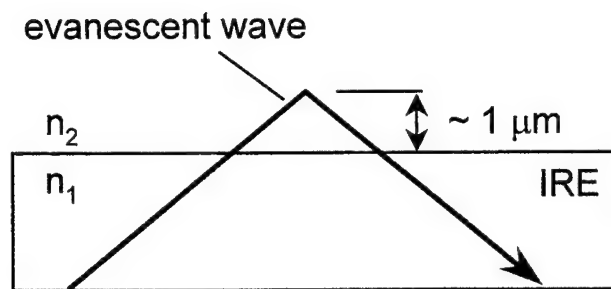E_o $d_p = ~ 1$ μm

n_2

n_1

Figure 8.1   Internal reflection at a totally reflecting interface (top) and electric field diagram of standing wave formed at the interface (bottom).

8.2.3 Relative Carboxylate (Cross-Link) Density

The relative carboxylate density or cross-link density can be assessed from the ratio of carboxylate (symmetric or asymmetric) stretching band intensities and the amide (I or II) band intensities. The more complete the interfacial reaction between amine groups of MPD and the acid chloride groups of TMC or CPTC, the fewer the number of free carboxylate groups. Thus, the lower the carboxylate/amide band intensity ratio is the lower the charge density. Typically, the ratio of the symmetric carboxylate (~ 1414 cm^{-1}) and amide II (~ 1544 cm^{-1}) bands is used, as there is less overlap with vibrational bands of the PS support. Since the IR radiation passes through the entire PA layer, the carboxylate density provides a measure of the bulk chemical properties of the membrane.

The carboxylate/amide II band intensity ratio can also be thought of as a measure of the cross-link density in the film layer. The cross-link density and carboxylate density are inversely related membrane properties. TMC has three acid chloride groups, and CPTC-AC has four groups. As more acid chloride reacts, more cross-linking occurs, and less free carboxylate groups remain. At the same time, the number of amide bonds increases. Therefore, membranes with low carboxylate band intensities should be cross-linked to a greater extent than membranes with more intense carboxylate bands.

8.2.4 ATR/IR Experimental Method

Small strips of membrane ($\sim 1 \times 4$ cm) were cut from sheets supplied to OCWD from SST. These membrane "swatches" were washed in 18 Mohm-cm E-pure deionized water (Barnstead/Thermolyne, Dubuque, IA) for 30 min and then dried overnight in a glove box purged with dry air (Balston, Haverhill, MA). Membrane swatches were pressed against each side of a 45°, $50 \times 10 \times 2$ mm zinc selenide (ZnSe) internal reflection element (IRE). Each sample consisted of 256 scans collected at 4 cm^{-1} resolution with a Magna 550 Fourier transform infrared spectrometer (Thermo Nicolet Instrument Corp., Madison, WI). The single-beam spectra were (1) ratioed against a bare IRE background spectrum, (2) converted to absorbance, (3) corrected for the wavelength dependence of internal reflection and (4) baseline corrected utilizing GRAMS/32, software Version 5.1, (Galactic Industries, Salem, NH).

8.3 Membrane Surface Morphology - AFM

8.3.1 AFM Analysis

Microscale surface features can influence performance of the separations membrane. AFM can be used to map microscale topography and pore geometries of air-dried as well as fully hydrated polymer membranes. Images are acquired utilizing silicon ultralevers, which are gold-coated cantilevers with integrated high-aspect ratio silicon nitride conical tips. These cantilevers are designed for maximum penetration into pores and other surface irregularities that are frequently encountered on the surface of polymer membranes. Tapping-mode AFM is employed to minimize translational forces between the AFM tip and the membrane surface. The root mean square (RMS)

roughness and mean surface height can be calculated for each membrane. Image analysis of the polymer surface can be applied to determine pore geometries.

8.3.2 AFM Experimental Method

The surface morphologies of the membranes were characterized by tapping mode AFM using Park Scientific Instruments (Sunnyvale, CA) Model CP Auto Probe equipped with a non-contact/contact head and a 100-μm scanner, operated in a constant force mode. Small membrane pieces were attached to a stainless steel sample holder using 12-mm carbon conductive tabs and mounted on the piezo scanner of the AFM. Images were acquired utilizing silicon "ultralevers" (force constant = 0.24 N/m). AFM images were acquired at a scan rate of 1.0-1.5 kHz with an information density of 256 x 256 pixels. The RMS roughness and mean surface height were calculated for each membrane using Park Scientific software provided with the CP AutoProbe. For a transect containing N data points, the RMS roughness is given by the standard deviation of the individual height measurements. The mean height is given by the average of the individual height determinations within the selected height profile.

8.4 Membrane Structural Analysis - TEM

8.4.1 TEM Analysis

TEM was used to obtain high-resolution images of the cross section of the TFC membranes. TEM provides information about the thickness and internal structure of the thin film separations layer of membrane that is not provided by AFM measurements. The TEM analysis was performed at the Central Facility for Advanced Microscopy and Microanalysis on the campus of University of California-Riverside.

8.4.2 TEM Experimental Method

Membrane samples were stained with 1% aqueous OsO_4 for 1 hr. The samples were then dehydrated in a graded ethanol series of 30%, 50%, 70%, 90% and 100% for 10 min each, followed by 3 changes of 100% ethanol for 10 min each. Samples were placed in 1/3 Spurr resin and 2/3 ethanol for 2 hr, 2/3 Spurr and 1/3 ethanol for 2 hr and two treatments of 100% Spurr for 2 hr each. Samples were placed in flat embedding molds in fresh resin and polymerized overnight at 70° C. Sections were taken on an RMC-MT-X ultramicrotome and then viewed on a Philips CM 300 transmission electron microscope.

8.5 Membrane Surface Hydrophobicity - Contact Angle (CA)

8.5.1 CA Analysis

The hydrophobicity of the polymer surface influences molecular water transport through a membrane. Therefore, the relative hydrophobicities of polymer membranes can be an important surface parameter in these studies. The surface hydrophobicities of polymer membranes can be determined by captive (air) bubble contact angle

measurements. The captive bubble method was used instead of the conventional water drop method since many polymer membranes could not be air-dried without introducing artifacts, such as shrinkage and cracking. In addition, a dry membrane swells when water is applied to the surface. Since the membranes are normally operated in a fully hydrated state, captive bubble determinations on wet membranes are more relevant for actual operating conditions.

Departure of an air bubble from a sphere with height to diameter (H/D) ratio of 1.0 is related to the degree of spreading of the bubble over the membrane surface. An H/D ratio less than 1.0 corresponds to bubble spreading and a more hydrophobic surface (larger contact angle) as the water is excluded from the surface. The following formulas were used to convert the H/D bubble ratio values to contact angles.

contact angle = 2 arctan (2h/d) for angles ,<90∞
contact angle = 2 arctan [(2d/h) − 1)] for angles >90∞

where h = the bubble height and d = the bubble diameter.

8.5.2 CA Experimental Method

The relative surface hydrophobicities of CPTC-AC membranes were compared by captive (air) bubble contact angle measurements. The determinations were made by introducing a 10-µL air bubble under the surface of a membrane submerged in 18 Mohm-cm deionized water with the membrane surface facing down. The bubble trapped under the surface of the membrane was imaged with a CCD camera. The digitized image was analyzed using CUE2 Series Image Analysis software (Olympus America) to measure the bubble height, diameter and the tangent contact angle. Each sample was run five times, and the mean was reported.

8.6 Membrane Surface Charge - UCB

8.6.1 UCB Analysis

Most polymer separations membranes possess some degree of surface charge due to trace quantities of free carboxylate, sulfonate or amino groups. Relative membrane surface charge (due to the presence of free carboxylate groups in the membrane) can be determined by uranyl cation binding (UCB). Depending on the nature of the polymer system under investigation, the contact time can be varied. Brief contact times (few minutes) may provide a more accurate indication of the true polymer surface binding capacity. Longer contact times probably result in a greater proportion of the counts originating from uranyl ions bound deeper within the polymer matrix. Surface binding capacity can be estimated by back extrapolation of UCB kinetics through the y-axis (at T = 0), thereby yielding a theoretical uranyl binding activity at an infinitely short contact time.

8.6.2 UCB Experimental Method

Relative membrane surface charge (due to free carboxylate groups) was determined by uranyl cation adsorption. Membrane coupons were secured in 15- x 125-mm plastic tubes with screw caps as the "reaction vessel" in the binding assay. The bottom third of the tubes was cut off and a 1-in. diameter coupon of test membrane was placed over the threaded end of the tube with the active surface facing the tube interior. Five mL of a 10 mM solution of uranyl acetate in buffer were added to reaction tubes to initiate the adsorption assay. After set intervals, the membrane coupons were removed and rinsed 10 times with deionized water. The amount of bound uranyl cation was then determined by liquid scintillation counter.

8.7 Membrane Biofouling Potential (MBP)

8.7.1 MBP Analysis

Bacterial adherence to polymer membrane was tested rapidly by allowing radiolabeled bacteria to contact a membrane surface for several hours. Loosely adherent bacteria were removed by rinsing the membranes and irreversibly bound bacteria quantified by liquid scintillation counting. It was therefore possible to rapidly evaluate the potential of polymer membranes to undergo biofouling, i.e., the membrane biofouling potential (MBP). Test bacteria included a hydrophobic *Mycobacterium* and hydrophilic *Flavobacterium* species previously isolated from membranes at OCWD.

8.7.2 MBP Experimental Method

In the standard assay, sterile 16- x 125-mm plastic tubes with screw caps served as the "reaction vessels" in the adhesion assay. The bottom third of tubes was cut off and a 1-in. diameter coupon of membrane was placed over the threaded end of the tube and oriented with the active (semipermeable) surface facing the tube interior. Membranes were washed 10 times in 18 Mohm-cm ultrapure water prior to use in adhesion assays. Washed radiolabeled cell suspension (100 μL) was immediately added to each tube at T = 0 to initiate the adhesion assay. Reaction vessels were incubated on a rotary shaker at 200 rpm for 5 hr at 28°C. Following incubation, vessel contents were decanted and membrane surfaces rinsed by two consecutive 5-mL volumes of MS buffer to remove unbound cells. Rinsed membranes were removed from reaction vessels, placed in scintillation vials with 10 mL of cocktail (OptiFluor, Packrd, Meriden, CT) and analyzed for radioactivity using an LKB Rackbet 1219 liquid scintillation counter (Wallac, Gaithersburg, MD) with external (226Ra) quench correction. The quantity of membrane-bound radioactive bacteria was reported in disintegrations per minute (DPM) and compared with the amount of free (unbound) radiolabeled bacteria at T = 0. The degree of bacterial attachment to membrane coupons was expressed as the ratio of bound:free cells (B:F). The specific activity of mycobacteria (DPM/cell) was determined by dividing total radioactivity (DPM/mL) of the initial (T = 0) cell suspension by cell concentration (determined by epifluorescent microscopy). The number of membrane-bound bacteria were estimated from: DPM/coupon x cell/DPM.

8.8 Inorganic Anion and Cation Analysis

The concentration of anions (chloride and bromide) was determined by ion chromatography. Sodium ion concentration was determined by inductively coupled plasma. Procedures for these assays are outlined in *Standard Methods for the Examination of Water and Wastewater*, 17th Edition, 1989. The Main Laboratory of The Orange County Water District performed this analysis.

9.0 FULLY AROMATIC COMPOSITE MEMBRANE FORMATION

9.1 Porous PS Membrane Substrate Process

The porous PS membrane support is the foundation upon which the interfacial thin-film is formed. The properties of the surface of the PS support are critical, since the thin semipermeable desalination barrier is formed in-situ upon this surface by interfacial polymerization. Thus, the formation of the support membrane must be closely monitored and controlled to produce optimal surface properties.

The porous PS support membrane is formed by a phase inversion process on a continuous casting machine using the process shown in Figure 9.0.
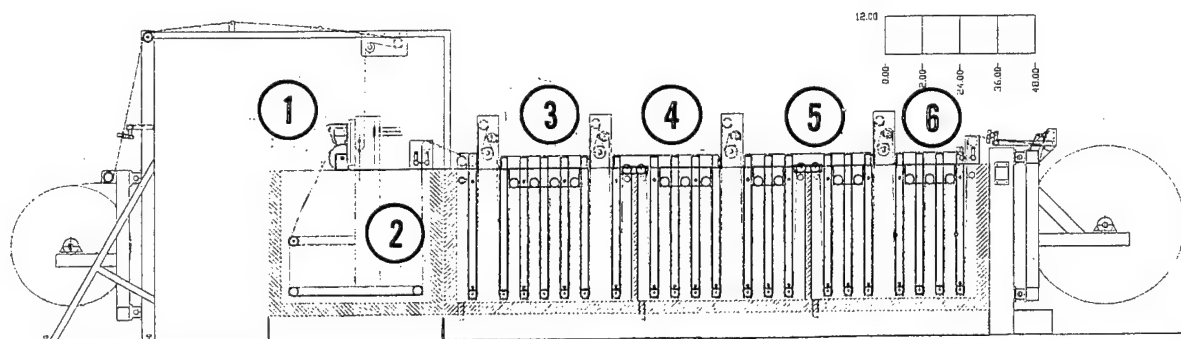

Figure 9.0 Process schematic of continuous casting machine for producing porous PS membrane by phase inversion for PA composite membrane development. (1) Knife over roll casting assembly above non-woven casting fabric, (2) Aqueous phase inversion gelation tank, and (3), (4) and (5) Water rinse tanks for solvent removal.

The PS casting solution consisted of a 15 wt-% solution of 35,000 MW PS dissolved in dimethyl formamide (DMF) which exhibited a viscosity of ~ 270 cps. The solution was filtered through a 5 μm filter and vacuum degassed before casting to minimize membrane imperfections. Subsequently, the solution was placed in the casting trough of the casting machine and deposited onto the surface of a polyester non-woven fabric. The thickness of the wet PS film was varied and controlled to close tolerances by an adjustable metering blade. The more important casting variables in producing defect-free porous PS membrane are:

90

- Composition and viscosity of the PS casting solution
- Uniformity, thickness and permeability of polyester non-woven substrate
- Casting speed, i.e., web speed
- Degree of penetration of casting solution into the non-woven web
- Thickness of casting solution on web
- Web tension
- Composition and temperature of gelation bath

Porous PS support membrane produced commercially for the production of the Army's ROWPU RO membranes often have imperfections which are created by the introduction of air into the casting solution as it is being cast onto the non-woven fabric. To minimize imperfections, a major redesign and upgrade of the knife-over-roll casting assembly of the polysulfone casting machine used in this work was implemented that eliminated the introduction of air into the casting solution during casting.

Photographs of the casting assembly are shown below in Figure 9.1
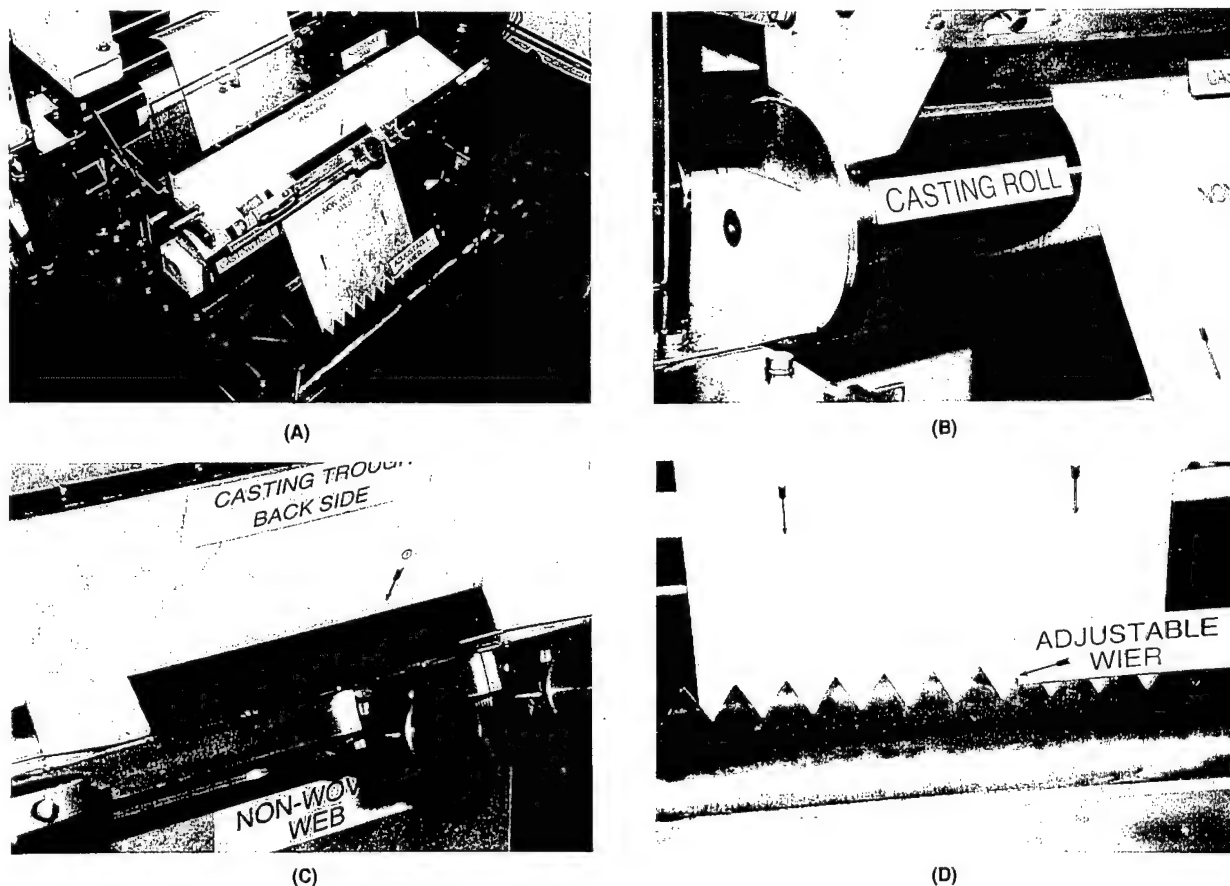

(A)

(B)

(C)

(D)

Figure 9.1   Photographs of PS membrane casting machine

Photograph 9.1.A shows an overview of the knife-over-roll casting assembly located on a casting roll above the gelation bath. Photograph 9.1.B shows the tilted casting trough, metering knife and non-woven fabric resting on the fixed casting roll. The assembly is designed so the casting trough can be rotated on the surface of the casting roll. Photograph 9.1.C shows the inside of the casting trough in a tilted forward position on the casting roll. The nonwoven web that passes under the casting trough during casting is shown in red. In most machines, the PS casting solution is metered into the casting trough until the solution reaches a height of about 3 in. above the non-woven web. Thus, the solution is in contact with the nonwoven web that is in contact with the casting roll for a distance of 1-3/8 in. The penetration of the solution into the web is controlled mainly by:

- The permeability of the non-woven web
- Viscosity of the PS solution
- Height of the solution in the casting trough
- Web tension
- Speed of the web, and
- Time of casting solution contact with web in casting trough

The difficulty with this mode of operation, however, is the introduction of air into the casting solution at the back side of the casting trough where the non-woven web enters the trough. At this location, air is drawn into the casting solution by the web. The entrapped air results in tiny membrane voids in the final PS support membrane which creates imperfections in the thin film during the interfacial polymerization. To avoid this phenomenon, the tilted redesign of the casting trough allows the solution to avoid contact with the back surface of the casting trough. The casting solution is metered into the casting trough at a controlled rate so that the solution covers only ~1 in. of the non-woven fabric. Numerous runs were made in this mode with excellent results.

An adjustable weir is located at the point where the newly cast membrane (on the surface of the non-woven web) enters into the gelation water (Photograph 9.1.D). Water, carrying a high concentration of DMF, is removed by the weir at the rate of 4 gpm. The sawtooth weir, precision cut by laser, allows for uniform removal of solvent laden water. The concentration of solvent in the gelation water at this location strongly influences the surface porosity of the PS membrane. In addition, the distance between the weir and the membrane can be varied to eliminate vibration on the surface of the water which introduces quench lines on the surface of the membrane. PS membrane processed on this casting machine produced excellent defect-free membrane. Samples of the membrane surface were analyzed by AFM and ATR/IR. All PS porous support membrane used during this program for the production of RO membranes was made in this manner.

9.2 Porous PS Support Membrane Characterization

The porous PS membrane is the foundation upon which the interfacial thin-film is formed. Thus, the formation of the support must be closely monitored and controlled to produce a uniform support with optimal surface properties upon which to conduct the interfacial polymerization to form the thin semipermeable barrier. Characterization of the

wet porous PS membrane, prior to the formation of the thin desalination barrier by the interfacial polymerization, consisted of the following:

- Determine the total thickness the PS membrane plus the thickness of the non-woven casting web. Typically, this total thickness is approximately 175 µm (7 mils). The PS is peeled from the surface of the non-woven casting web to determine both the adhesion and the thickness of the peeled PS membrane. The adhesion of the PS membrane to the substrate, determined by the penetration of the casting solution into the non-woven web, must be adequate to withstand subsequent thin-film processing and long-term operation in an RO plant with high-velocity feedwater passing over its surface. Ideally, the thickness of the peeled PS membrane should be on the order of 60 - 65 µm.

- Determine the pure water permeability through the wet PS support membrane in a cross-flow cell at 40 psi applied pressure. The water permeability is expressed in terms of a membrane constant commonly referred to as the A-value, (g/cm^2-sec-atm). Typically, the membrane constant required to produce a high performing composite membrane is in the range of 400 - 2000 x 10^{-5} g/cm^2-sec-atm.

- The porous surface of the PS membrane was dyed with a methyl violet solution to determine uniformity and to locate and identify defects. The membrane was dried in an oven and subsequently the porous surface was examined with an optical microscope for surface defects. Many known surface defects are not visible when the membrane is wet.

- SEMs and molecular weight cut-off determinations were conducted on a periodic basis. However, a correlation of those findings with composite membrane performance was not always direct.

* AFMs were used to evaluate the porous surface of the PS membrane.

* ATR/IR spectroscopic analysis was performed to determine consistency of chemical structure

Typically, PS support membranes were cast in 100 ft lengths on the continuous machine for composite membrane processing. A summary of the casting solution compositions and relevant membrane properties are shown in Table 9.0

Eleven different PS support membranes were manufactured for use in the two-year study. A list of these support membranes is shown in Table 9.0. Each membrane was analyzed by AFM to determine membrane surface morphology. Topographical images (10 µm) of these membranes are shown in Figure 9.2 and 9.3. The surface morphology of these membranes varied from one preparation to the other. Occasional defects or depressions appear on the surface of the membrane. These holes increase the statistical range of the reported mean height. The surface morphology is expressed in terms of the mean height and RMS roughness and is displayed in Figures 9.4 and 9.5.
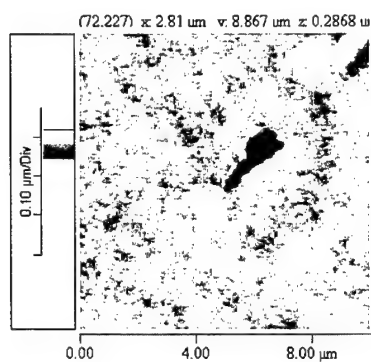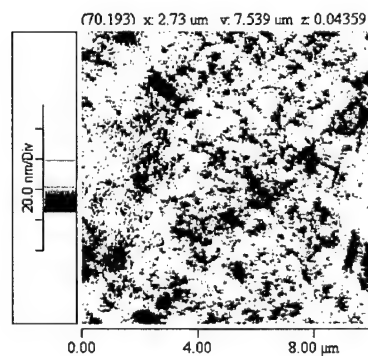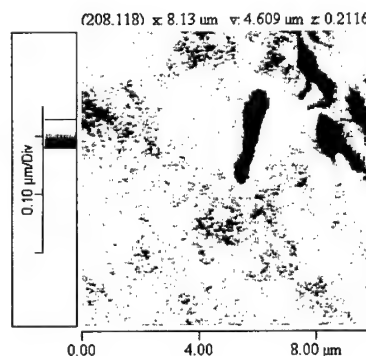
FilmTec
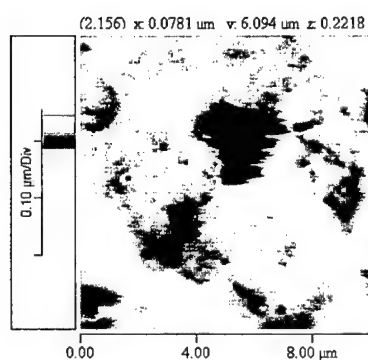
PS-197

**No
Image
Obtained
By AFM**
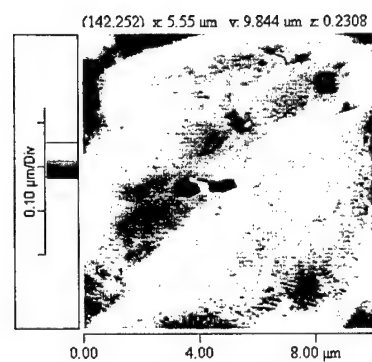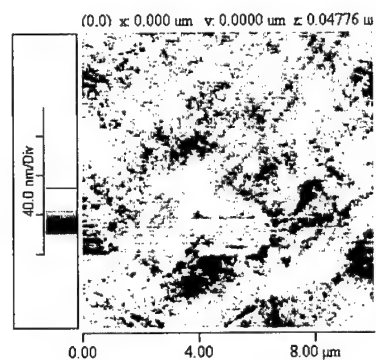
PS-198

PS-201

PS-202

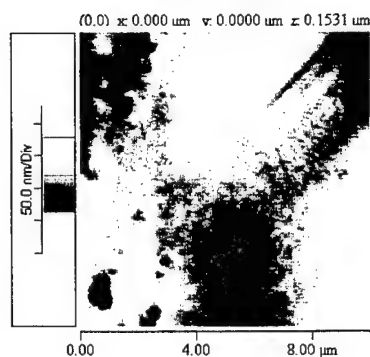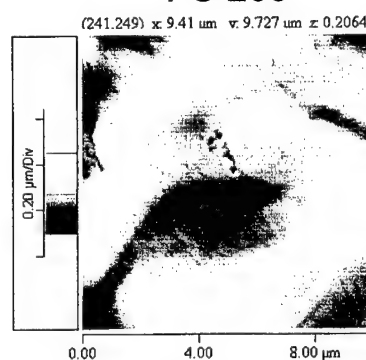Figure 9.2   AFM images of PS support membranes (10 µm).

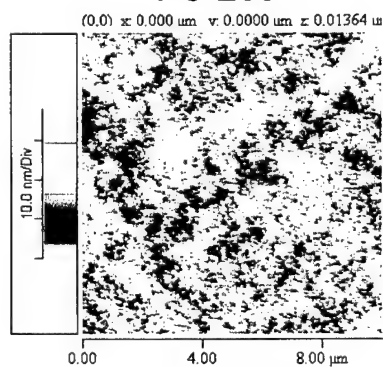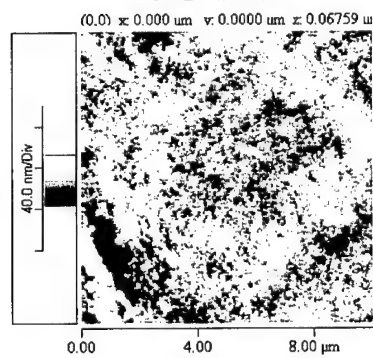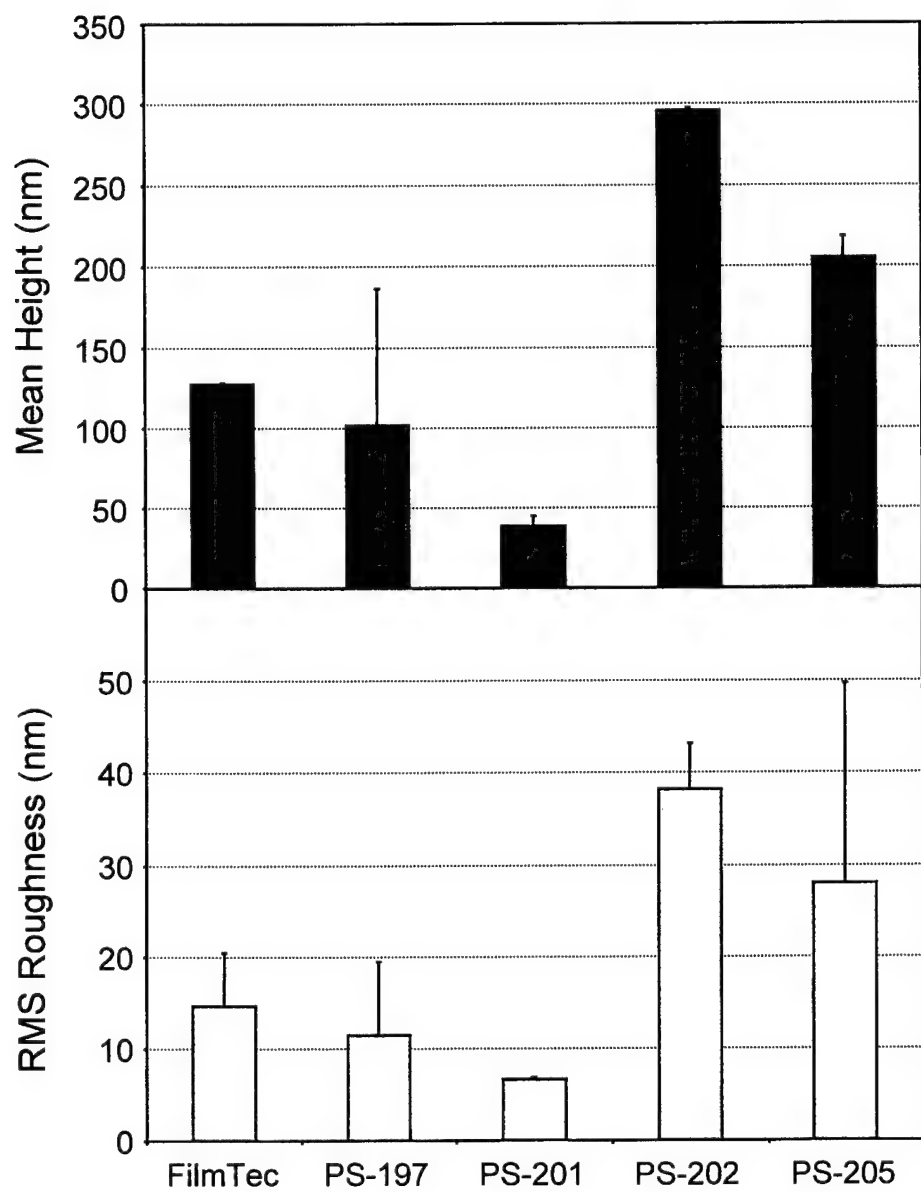Figure 9.3   AFM images of PS support membranes (10 μm).

Figure 9.4   Surface morphology of PS support membranes, mean height (□) and
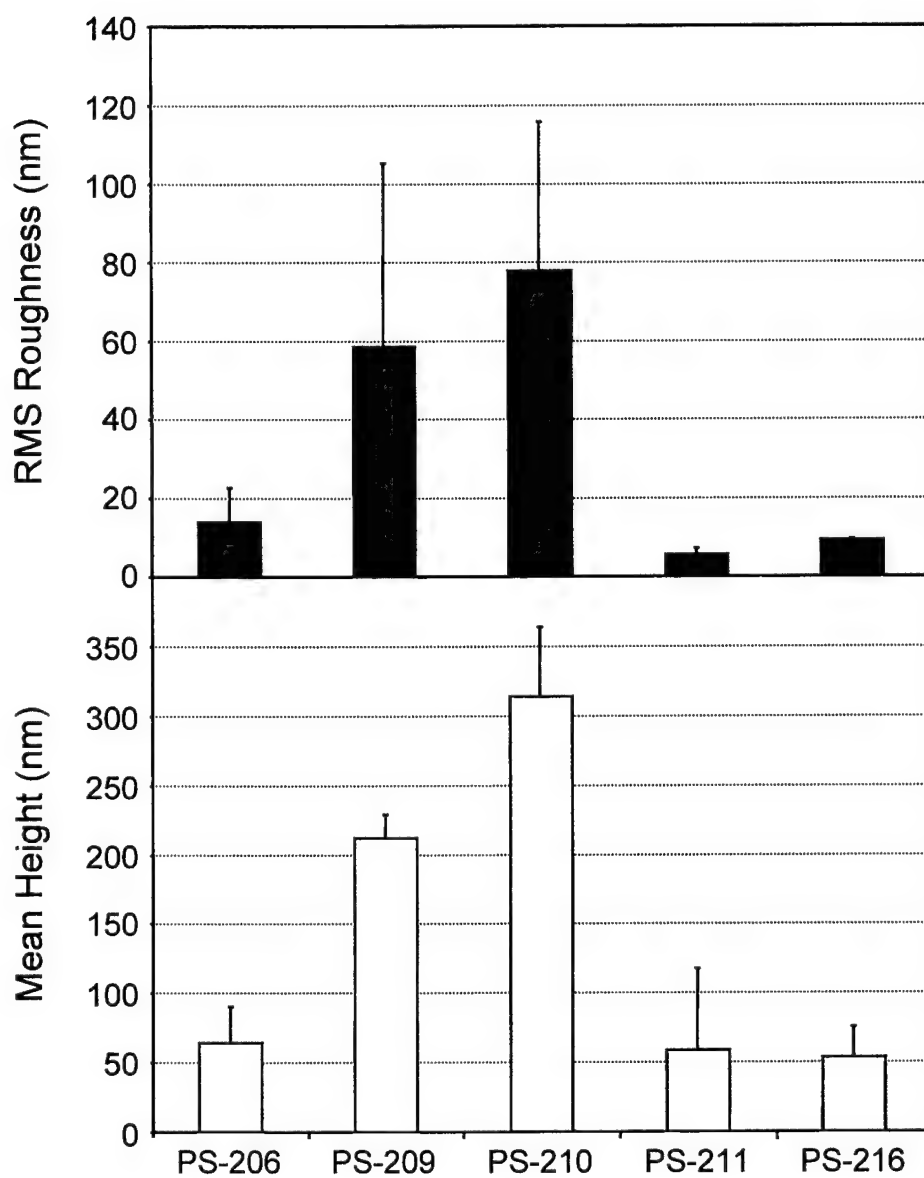RMS roughness (■).

Figure 9.5   Surface morphology of PS support membranes, mean height (■) and RMS roughness (□).

ATR/IR spectra of each of PS support membrane were collected, and a representative spectrum of each is displayed in Figures 9.6 through 9.11. The 1414 / 874 cm^{-1} and 1416 / 874 cm^{-1} band intensity ratios were determined. These ratios were used to calculate relative carboxylate density that was used to correct for the PS contribution to the symmetric carboxylate 1414 cm^{-1} (or 1416 cm^{-1}) band intensity of the PA component of the membrane spectrum (see discussion below). Ratios of the 1416 / 874 cm^{-1} bands and 1414 / 874 cm^{-1} bands are shown in Table 9.1.

Table 9.0

Polysulfone Support Membrane

Support No.	Fabric	Casting Solution	Solvent	Knife Gap (mil)	Casting Speed (ft/min)	A-Value (x 10^{-5} g/cm^2-sec-atm)
PS-197	AWA 51	18 wt-% PS+ 1wt-% LiBr	DMF	8	25	1141 X
PS-198	AWA 51	18 wt-% PS+ 1 wt-% LiBr	DMF	8	25	NA X
PS-201	Hollytex 3329	18 wt-% PS+ 1 wt-% LiBr	DMF	8	25	453 X
PS-202	AWA 620	18 wt-% PS+ 1 wt-% LiBr	DMF	8	30	1037 X
PS-205	AWA 620	18 wt-% PS+ 1 wt-% LiBr	DMF	8	50	677 X
PS-206	AWA 620	18 wt-% PS+ 1 wt-% LiBr	DMF	7	25	1192 X
PS-209	Hollytex 3329	16.5 wt-% PS	NMP	9	20	3513 X
PS-210	Hollytex 3329	16.5 wt-% PS	NMP	9	20	2770 X
PS-211	Hollytex 3329	16.5 wt-% PS	NMP 1:1 Molar Ratio	9	20	2928 X
PS-216	Hollytex 3329	16 wt-% PS+ 1 wt-% LiCl	DMF	8	25	1946 X

NA - Not available

Figure 9.6   ATR/IR spectra of PS support membranes between 4000 cm^{-1} and 600 cm^{-1}.

Figure 9.7   ATR/IR spectra of PS support membranes between 2000 cm^{-1} and 600 cm^{-1}.

Figure 9.8   ATR/IR spectra of PS support membranes between 4000 cm^{-1} and 600 cm^{-1}.

Figure 9.9   ATR/IR spectra of PS support membranes between 2000 cm^{-1} and 600 cm^{-1}.
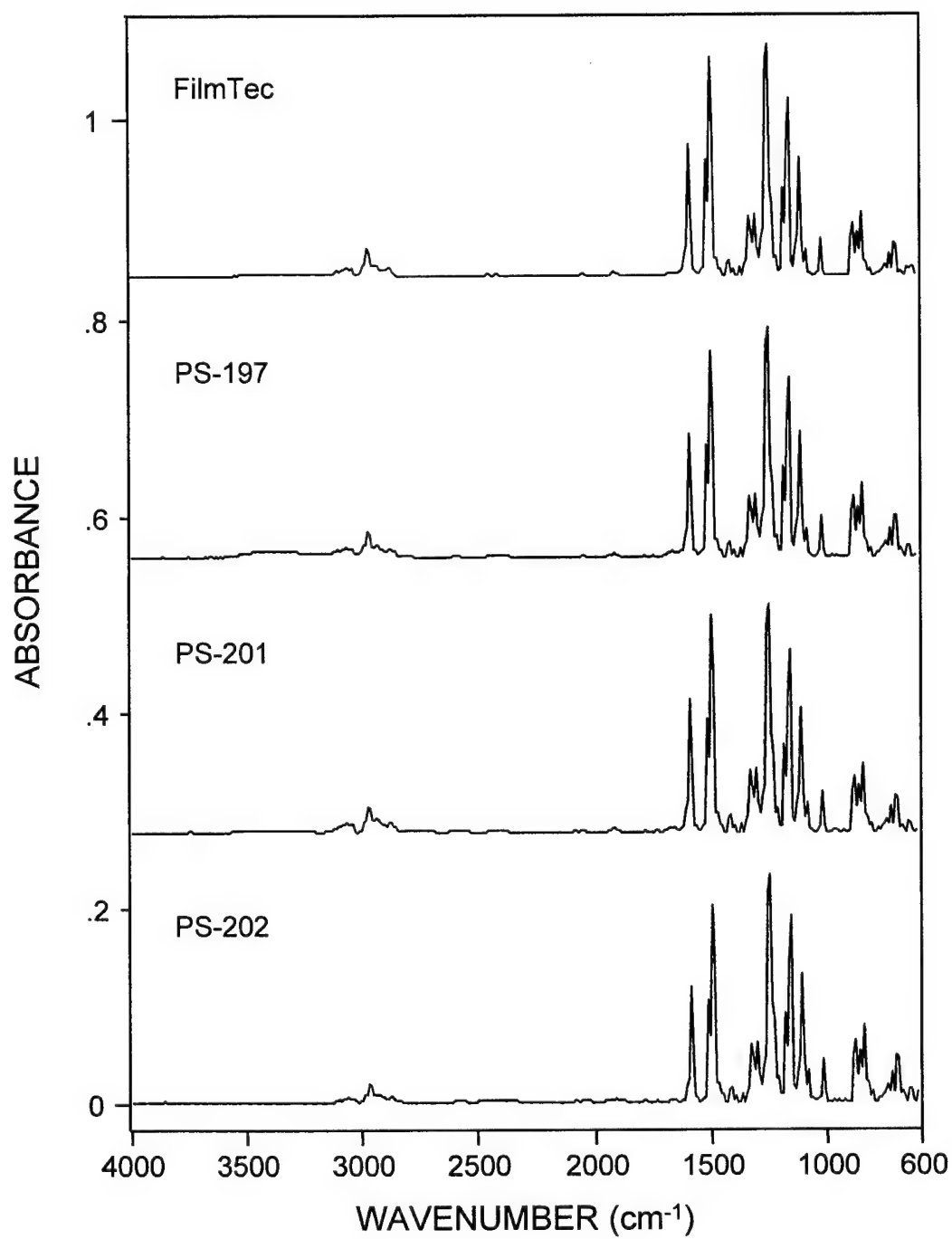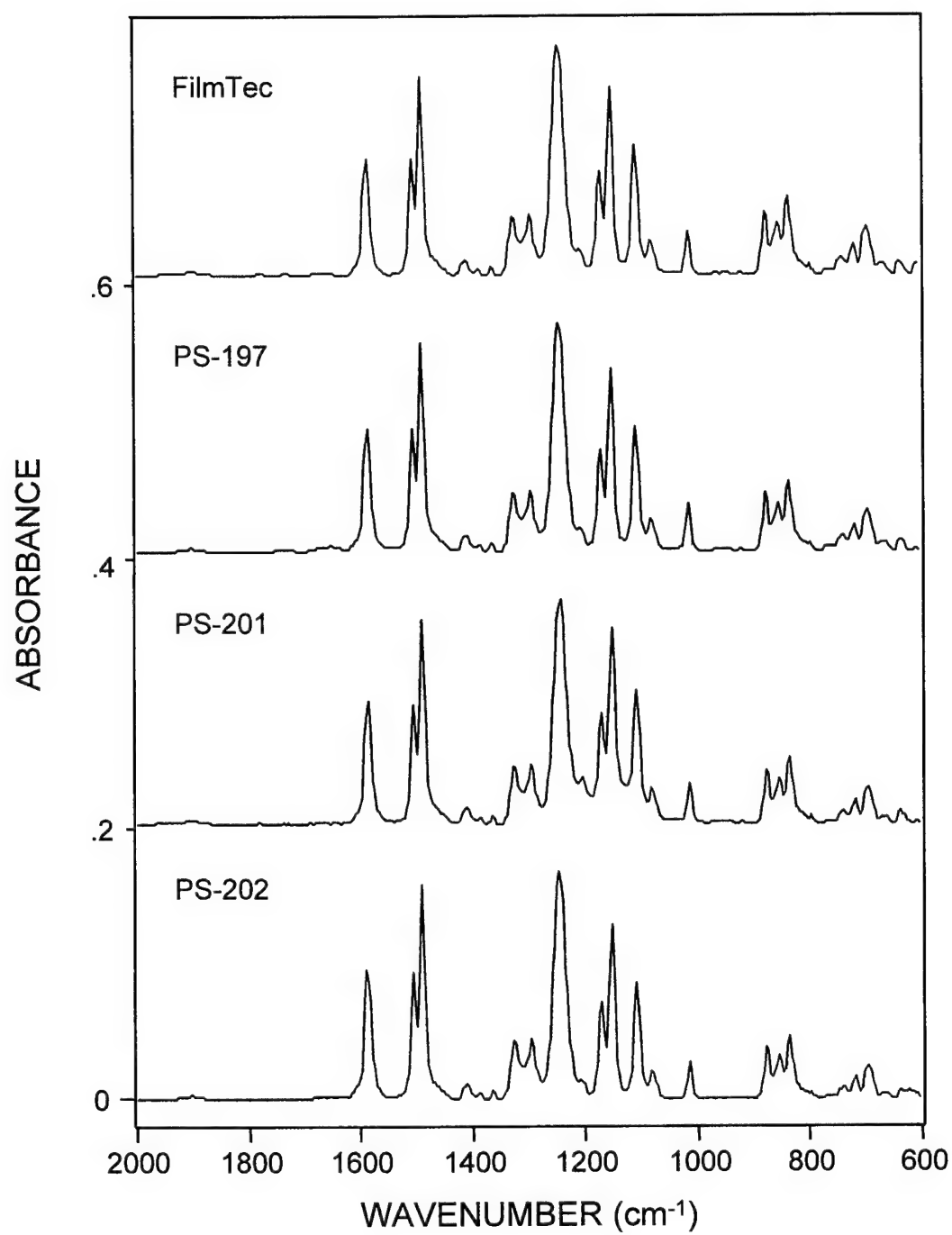
Figure 9.10   ATR/IR spectra of PS support membranes between 4000 cm^{-1} and 600 cm^{-1}.

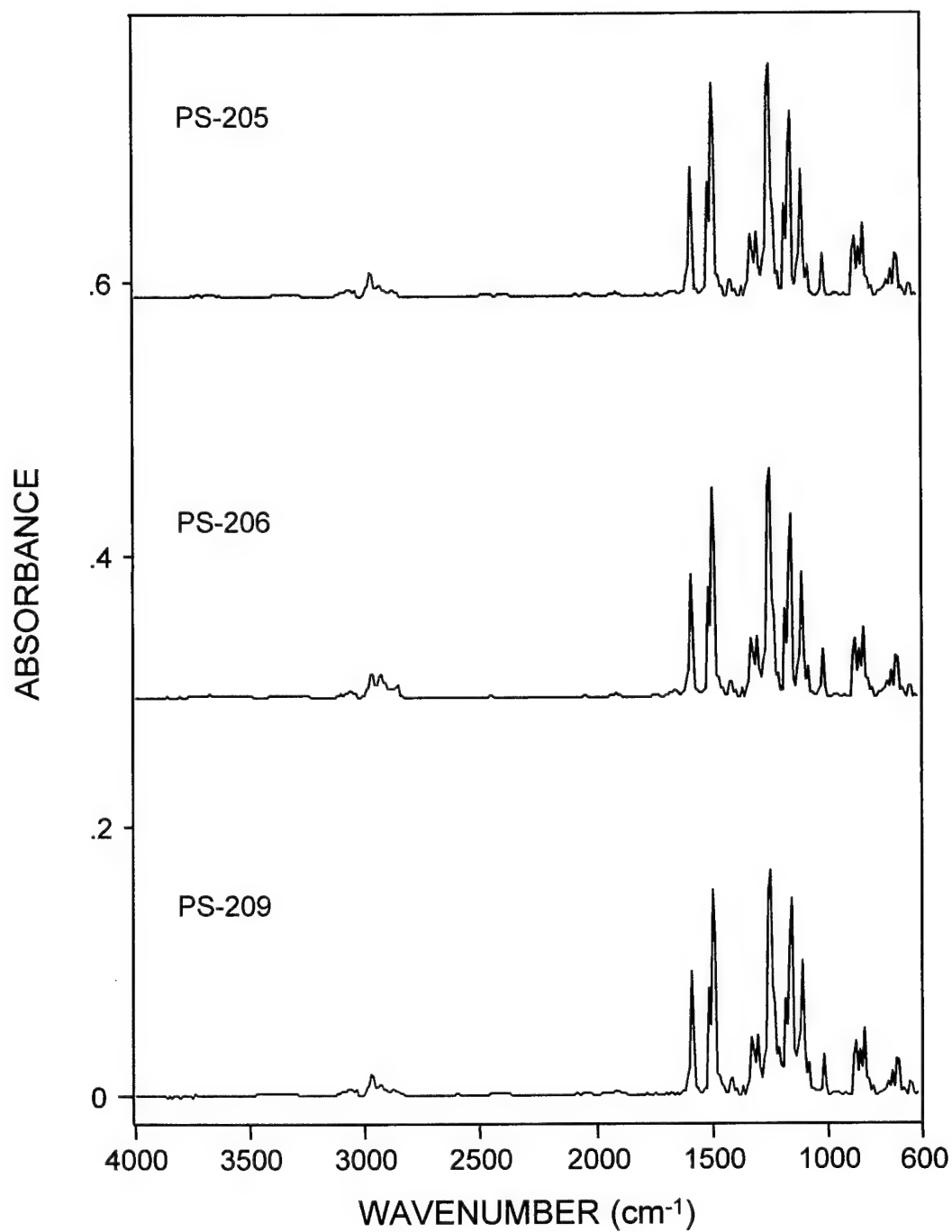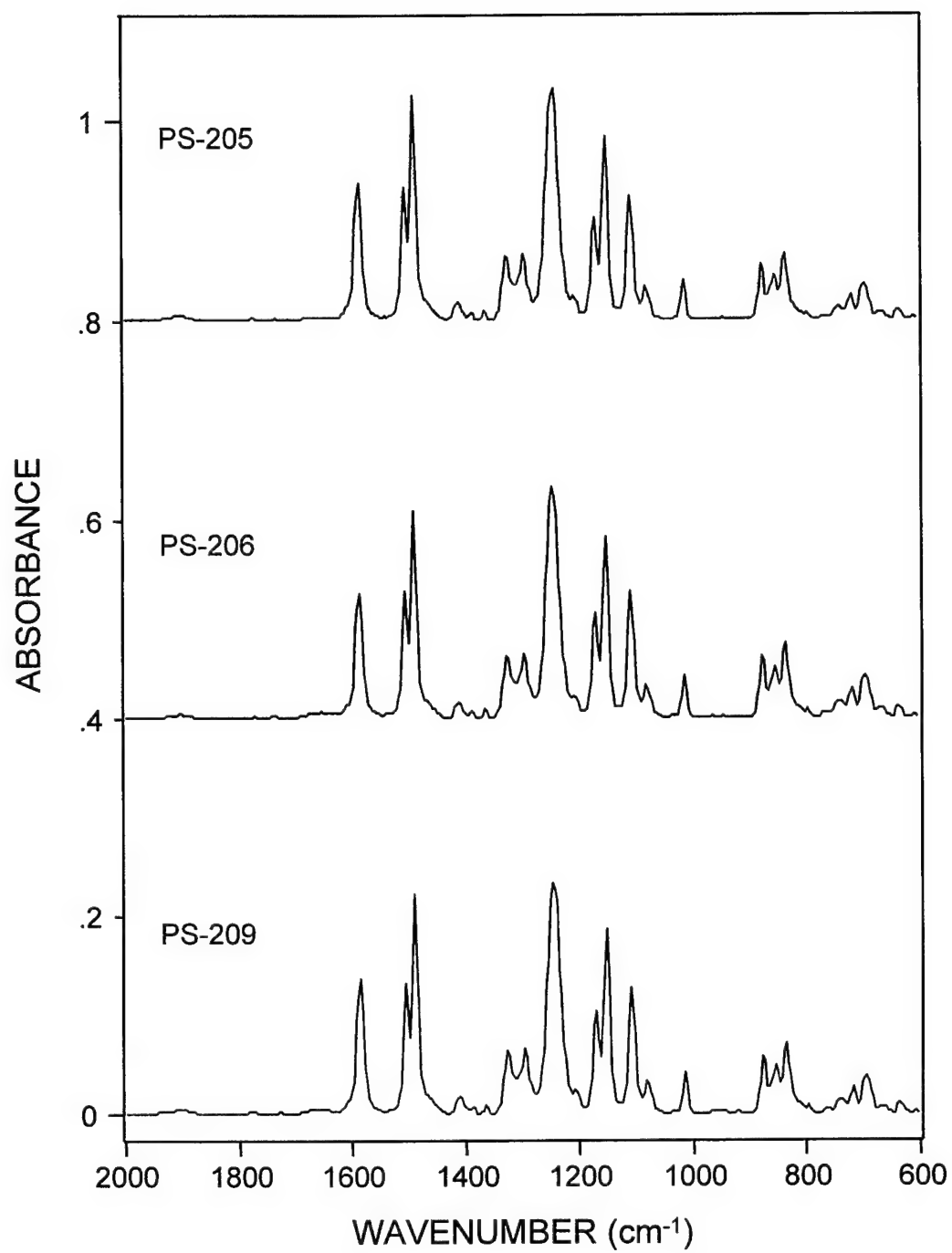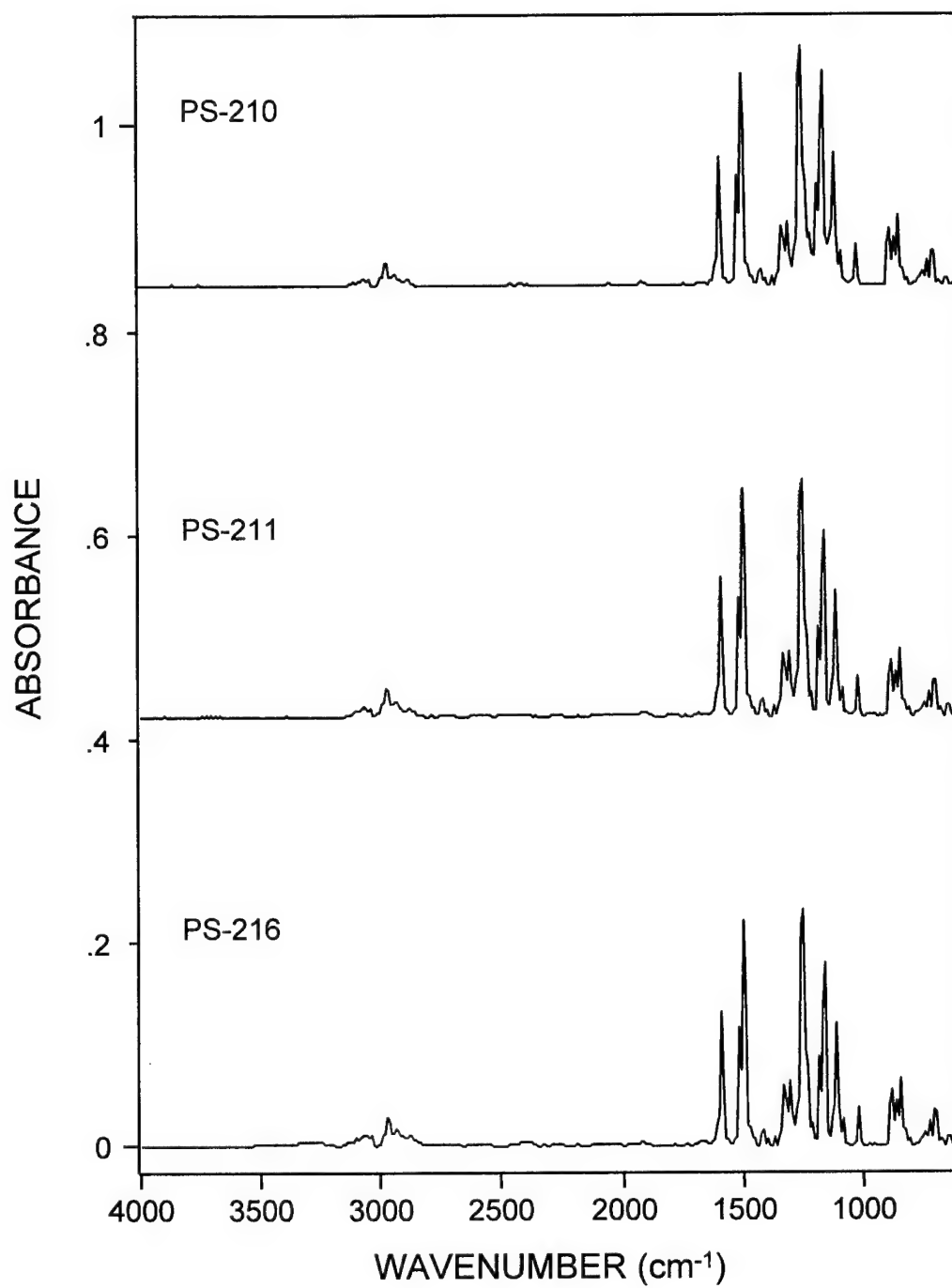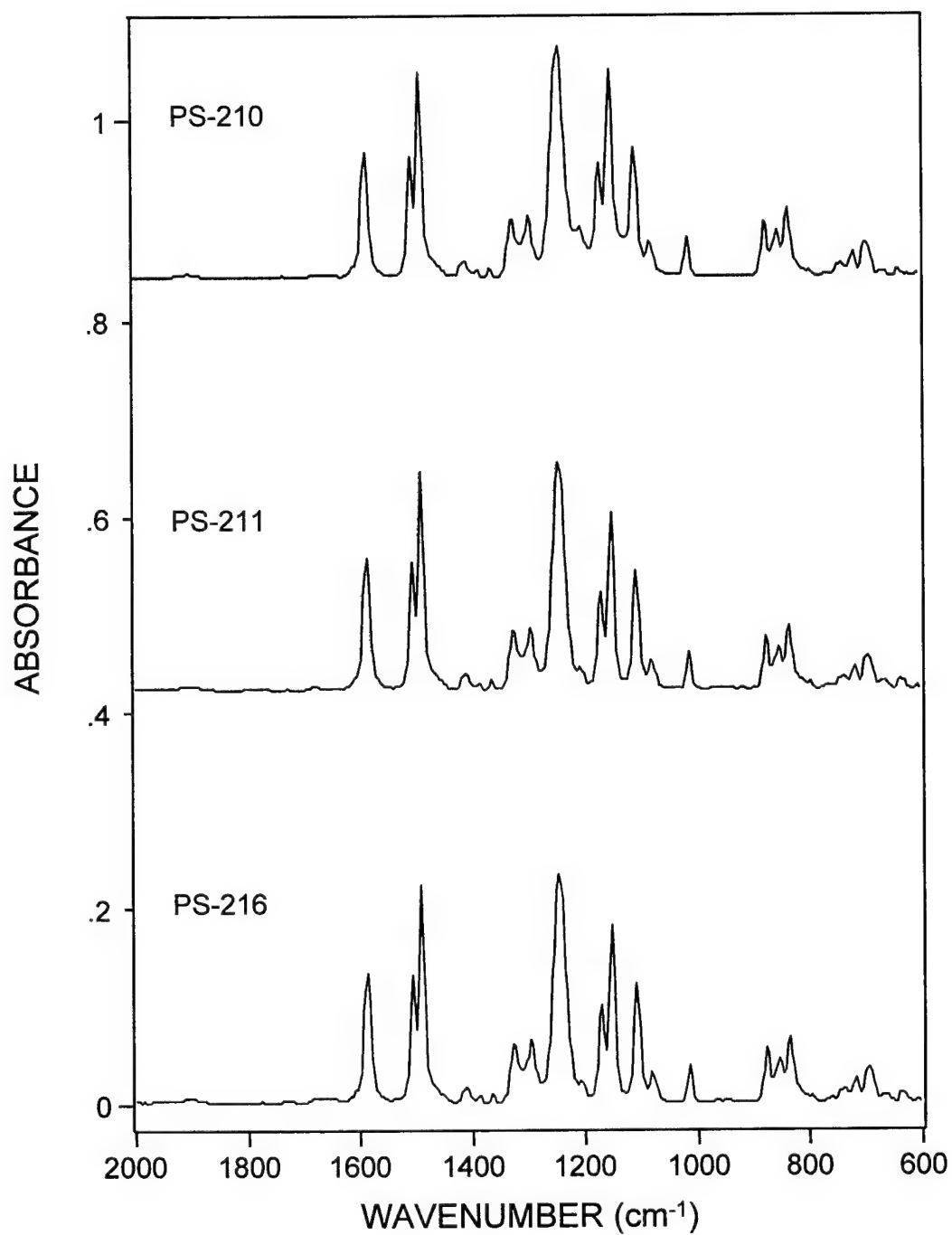Figure 9.11 ATR/IR spectra of PS support membranes between 2000 cm⁻¹ and 600 cm⁻¹.

104

Table 9.1

Polysulfone Support Membrane

$1416 / 874 \text{ cm}^{-1}$ and $1414 / 874 \text{ cm}^{-1}$ Band Intensity Ratios

Support No.	$1416 \text{ cm}^{-1} / 874 \text{ cm}^{-1}$	$1414 \text{ cm}^{-1} / 874 \text{ cm}^{-1}$
FilmTec	0.20484 ± 0.00145	0.26036 ± 0.00167
PS-197	0.17390 ± 0.00814	0.22337 ± 0.01048
PS-198	NA	NA
PS-201	0.20348 ± 0.00186	0.25921 ± 0.00209
PS-202	0.19015 ± 0.01456	0.24151 ± 0.01780
PS-205	0.20604 ± 0.01604	0.25948 ± 0.01633
PS-206	0.20701 ± 0.01553	0.26143 ± 0.01832
PS-209	0.20704 ± 0.00911	0.23024 ± 0.08000
PS-210	0.22185 ± 0.02647	0.26816 ± 0.00880
PS-211	0.21572 ± 0.00179	0.27325 ± 0.00183
PS-216	0.20202 ± 0.00193	0.25694 ± 0.00147

NA - Not available

9.3 Interfacial TMC/MPD RO Membrane Formation

The predominant RO membrane used by the desalination industry is a thin-film composite PA membrane. This membrane consists of three different polymer layers - a polyester backing material, a PS support layer and a thin PA barrier. Membranes are fabricated in a two-step process.[1] First, the porous PS membrane support, is prepared on a non-woven polyester fabric by a knife-over-roll phase inversion process as described in Section 9.1. Briefly, in review, after applying the PS-DMF solution onto the fabric (30 ft/min or greater), the membrane is immersed in water to remove the solvent and precipitate the PS, thereby forming the porous PS membrane structure.

Subsequently, the finished PS membrane roll is transferred to a second machine where a desalination barrier is formed on the porous surface by an *in-situ* interfacial reaction. Thus, the porous PS membrane becomes the foundation upon which the interfacial membrane is formed. The membrane is processed by first applying an aqueous MPD solution onto the finely porous surface of the PS membrane. Later, the MPD-coated PS membrane is passed through a hydrocarbon solution containing TMC. At the immisible interface between the two solutions, a very thin PA film is formed. The chemistry of the standard commercial membrane is shown in Figure 9.12.

Approximate Polyamide Thin Film Chemistry

m-Phenylenediamine
in Water

Trimesoyl Chloride
in Hydrocarbon
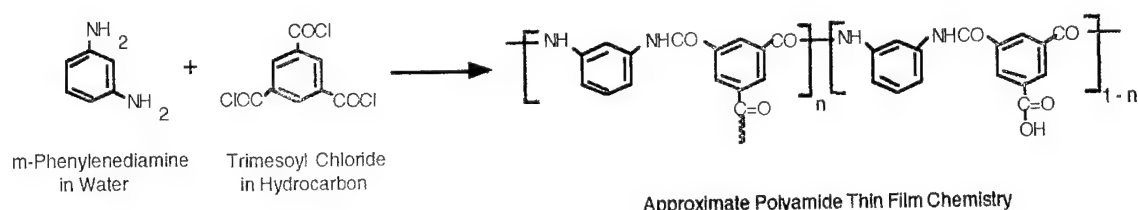
Figure 9.12   Aromatic/Aromatic TMC Membrane

It should be noted that both the TMC and the MPD are aromatic, thereby creating a fully aromatic desalination barrier.

After the interfacial film is formed, the membrane passes through a series of leaching tanks to remove residual monomers before final drying. The MPD, entrained in the solid membrane phase, is particularly difficult to remove and if any residual remains it will oxidize, thereby discoloring the membrane. More importantly, the transport properties of the MPD-laden membrane deteriorate with time and the membrane exhibits greater biofouling. Thus, it is imperative to utilize effective methods of removing MPD. All TMC membranes prepared during this program were made by this general process. The specific process for making these membranes used in this study are shown in Figures 9.13 and 9.14.

Nominally the same processing methods were used in the development of the aliphatic/aromatic CPTC membrane. The major difference is the replacement of TMC by CPTC-AC. This work is described in Section 10.0.

Figure 9.13   Process flow diagram for the interfacial formation of TMC membranes

Figure 9.14   Process steps in the preparation of TMC membranes

10.0 ALIPHATIC/AROMATIC CPTC MEMBRANE FORMATION

10.1 Interfacial CPTC/MPD RO Membrane Formation

Unlike the fully aromatic TMC membrane which is made from an aromatic acid chloride and an aromatic amine, the CPTC membrane is made with an aliphatic acid chloride and an aromatic amine. The chemistry of formation of the thin film on the CPTC is shown in Figure 10.0.

m-Phenylenediamine
in Water

ctct-1,2,3,4-Cyclopentanetetracarboxylic
Acid Chloride in Hydrocarbon

Approximate Polyamide Thin Film Chemistry
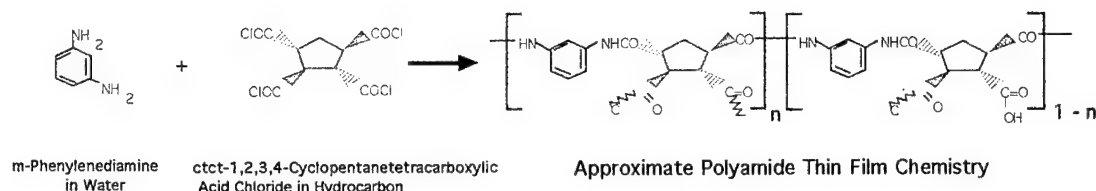
Figure 10.0   Aliphatic/Aromatic CPTC Membrane

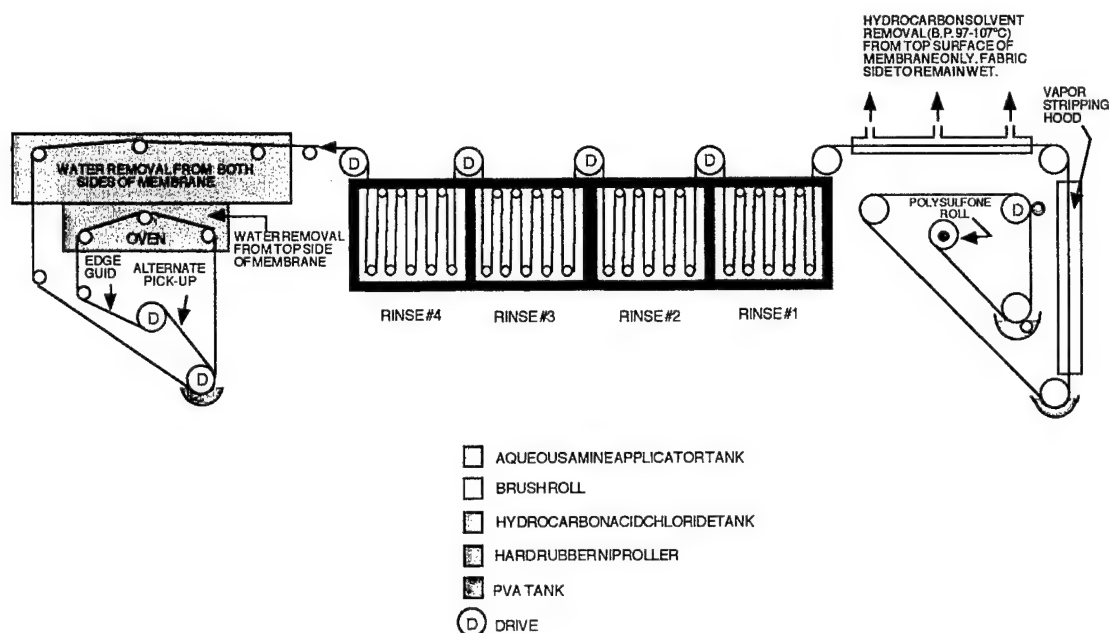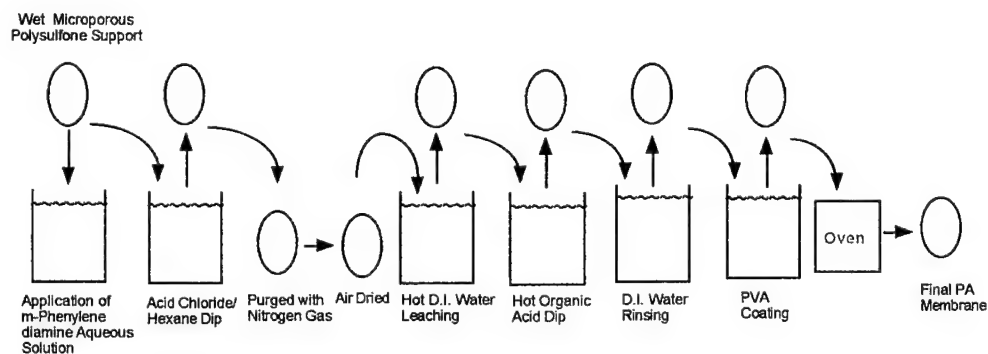Considerable effort was devoted to evaluating the acid chloride samples received from Denver University for CPTC membrane preparation. Seventeen synthesis lots were received throughout the program at regular intervals with each lot containing approximately six grams of material. About seventy (8- x 10-in) membrane sheets were prepared from each sample lot. Throughout the program, more than 1000 membrane sheets were made from the seventeen acid chloride synthesis lots.

TMC control membranes were made with each set of CPTC membranes using the same preparative conditions. During the developmental acid chloride synthesis phase, the purity and reactivity of CPTC-AC varied between lots. Thus, it was necessary to vary, control and optimize the CPTC membrane preparative parameters for each individual synthesis lot of acid chloride in order to attain comparative RO transport data.

All membranes prepared from each lot of acid chloride along with TMC membrane control membranes were evaluated side by side in laboratory RO tests at 225 psi applied pressure, pH 6.5, 25°C with a 2,000 mg/L sodium chloride feed solution. The transport properties of the CPTC membranes were determined and compared with the controls. This information provided feedback required for optimizing membrane preparative parameters.

The transport properties of CPTC membranes were optimized to equal or surpass those of the commercial TMC control. To achieve this objective it was necessary to make significant changes in the preparative parameters. A summary of the acid chloride synthesis lots, purity and the RO performance of CPTC membranes made therefrom is given in Table 10.0. (These results were based on unchloronated feed solutions.)

Table 10.0

RO Performance of CPTC Membranes

Test Conditions: 225 psi applied pressure, 2,000 mg/L sodium chloride feed (4,000 µmhos-cm^2), 25°C, pH 6.9, 0.9 gal/min feed flow

Date	Acid Chloride Synthesis Lot	Acid Chloride		Reverse Osmosis Performance	
		Purity (%)	Color	Water Flux (gfd)	Rejection (%)
Nov 98	DU-1	~70	Dark purple/brown	15.6	98.6
Nov 98	DU-2	~70	Dark purple/brown	-	-
Nov 98	ITM All Cis	~98	Dark purple/brown	16.9	96.8
	021599 SE-FF	~98	Clear pink	15.4	98.8
Feb 99	021799 SE	~98	Dark purple/brown	19.2	98.6
Feb 99	030399	~99	Dark purple/brown	20.3	99.2
Mar 99	041299**	99+*	Clear - amber	13.9	98.1
June 99	061099	99+*	Dark purple/brown	22.3	99.20
June 99	062199	99+*	Not soluble in solvent required to make membrane		
(1,4 cis 2,3 trans isomer)					
July 99	070899	99+*	Light color	13.0	99.0
Aug 99	081399	99+*	Dark purple/brown	14.0	99.2
Sept 99	092099S1	99+*	Clear amber	11.0	99.30
Oct 99	100199S1	99+*	Dark purple/brown	15.6	99.0
Nov 99	110899S1	99.9	Light purple/brown	18.4	99.20
Feb 00	02200051	99.9	Light purple/brown	15.8	99.20
July 00	070700	99.9+	Clear - slightly pink	16.0	99.54
Oct 00	102600-40	99.9+	Clear - No insolubles	10.1	99.30
	TMC Control Membrane			14.8	99.70
	FilmTec Control Membrane			25.4	99.53

- Determined by GC/MS-SE = Selective Extraction
FF = Falling film molecular distillation
DU = Denver University, ITM = Institute of Technology, Mexico
** Sample was stored in polypropylene vials which may have contaminated sample.

Optimized CPTC membranes were characterized as follows: (1) surface topography by AFM, TEM, (2) surface hydrophilicity by air bubble contact angle determinations, (3) fouling potential by bacterial adhesion assay, (4) chemical and structural integrity by surface charge analysis and (5) IR and ATR/IR spectroscopic analysis by uranyl cation binding assay. In addition, membranes were placed on long-term RO testing on a chlorinated surface water feed at WQIC, Yuma, AZ, a chlorinated municipal wastewater feed at OCWD, Fountain Valley, CA and a chlorinated seawater feed at NFESC, Port Hueneme, CA. The results of these studies with CPTC membranes are reported in the following sections of this report.

10.2 Basic Chemical Characteristics of the TMC and CPTC Membranes - ATR/IR Spectroscopic Analysis

It is important to point out some of the basic chemical features of the CPTC and TMC membranes before the results of the optimization experiments are discussed in the following sections. ATR/IR spectra of thin-film composite membranes measured with a 45° ZnSe IRE are composed of both PA and PS vibrational bands, as the IR radiation passes through the PA film into the PS support layer at each internal reflection (Figure 10.1). ATR/IR spectra of a pure PA film, a PS membrane and the commercial FilmTec membrane are shown in Figures 10.2 and 10.3. Major PS vibrational bands include the 1586, 1504 and 1489 cm^{-1} C=C ring stretching bands, 1245 cm^{-1} and 1106 cm^{-1} asymmetric and symmetric C-O-C stretching bands, and 874, 853 and 834 cm^{-1} out-of-plane C-H wagging bands of the aromatic ring. These vibrational bands are labeled on the spectrum shown in Figure 10.4. Some of the major vibrational bands of PA include the 1744 cm^{-1} carbonyl, 1665 cm^{-1} and 1540 cm^{-1} amide I and amide II bands, and the 1611 cm^{-1} and 1416 cm^{-1} asymmetric and symmetric stretching carboxylate bands. C=C ring vibrations overlap the 1608 cm^{-1} asymmetric carboxylate, but also appear near 1490 cm^{-1} and 1446 cm^{-1}. The 1244 cm^{-1} band is a combination of C-N stretch and N-H bend associated with the amide band of PA (see Figure 10.5).

TMC membranes were made along with experimental CPTC membranes throughout the duration of the two-year program. These membranes served as a control along with the commercial FilmTec brackish water membrane. ATR/IR spectra representative of these membranes are shown in Figure 10.6 and 10.7. The TMC and CPTC membranes made by SST are similar in appearance. All have a distinctive ~1720 cm^{-1} vibrational band. This absorption band is indicative of a carbonyl (C=O) functional group and is likely from a carboxylic acid. This band is most evident in the spectra of membranes made with TMC and to a lesser extent in the spectra of the membranes made from a batch of 99+% CPTC. This 1720 cm^{-1} carbonyl band is not visible in any of the FilmTec ATR/IR spectra. The FilmTec IR spectra all have an intense ~3300 cm^{-1} band that is virtually nonexistent in the spectra of the TMC and CPTC PA membranes (Figure 10.7). The band is an O-H stretching vibration that could originate from a carboxylic acid. However, if this O-H stretch originates from a carboxylic acid, there should be a carbonyl in the FilmTec IR spectrum near 1720 cm^{-1}, and none is present. Therefore, the O-H stretching band in the FilmTec spectrum may originate from an alcohol functional group. This would seem to imply that the FilmTec membrane has been modified in some way. At this time, the details of any surface modification performed by FilmTec are not known.

The vibrational bands described in this section were used to access how different modifications to the purification process and chemical and physical treatments affected CPTC and TMC polymer chemistry, structure and performance.

110
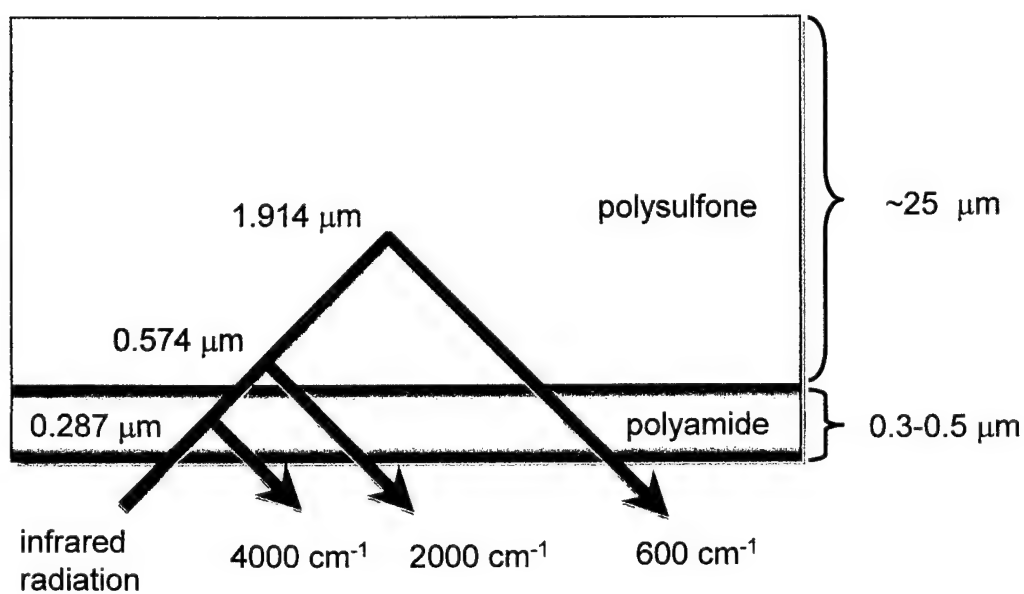
Figure 10.1 Cross section of a thin-film composite polyamide reverse osmosis
membrane including polyester backing, polysulfone support and
polyamide separations layer.
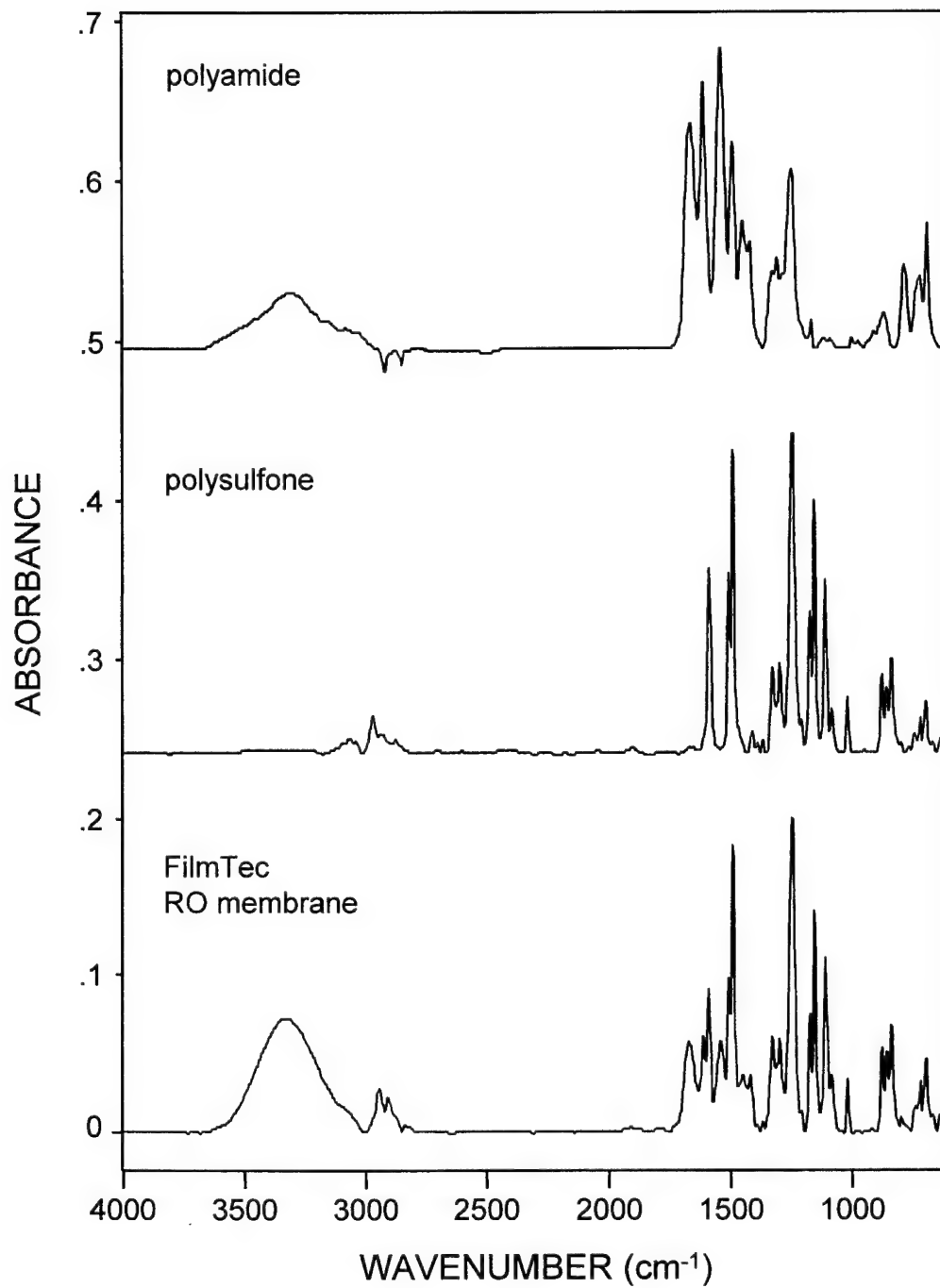
Figure 10.2   ATR/IR spectra of polyamide, polysulfone and a typical thin-film composite
polyamide reverse osmosis membrane.
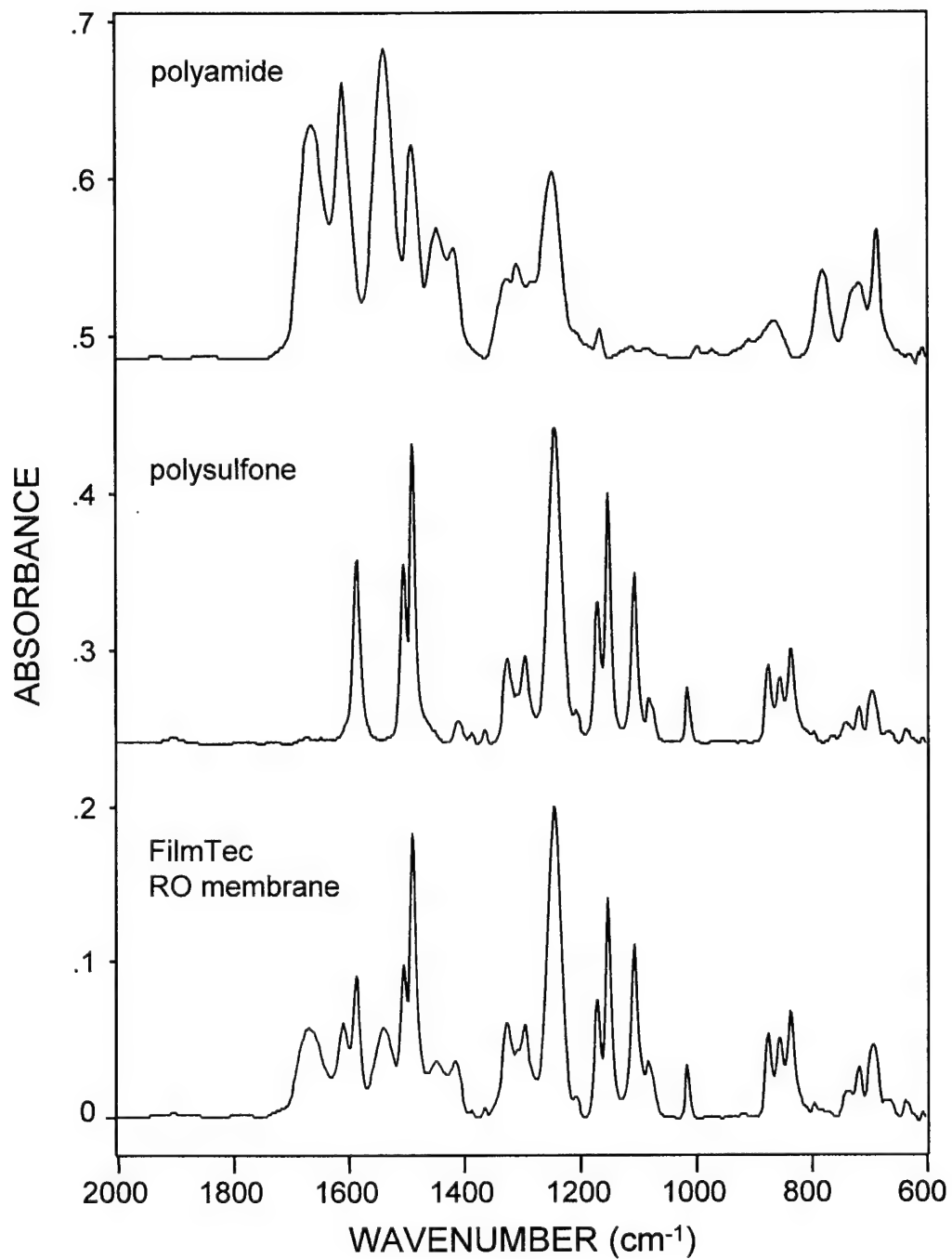
Figure 10.3   ATR/IR spectra of polyamide, polysulfone and a typical thin-film composite polyamide reverse osmosis membrane.
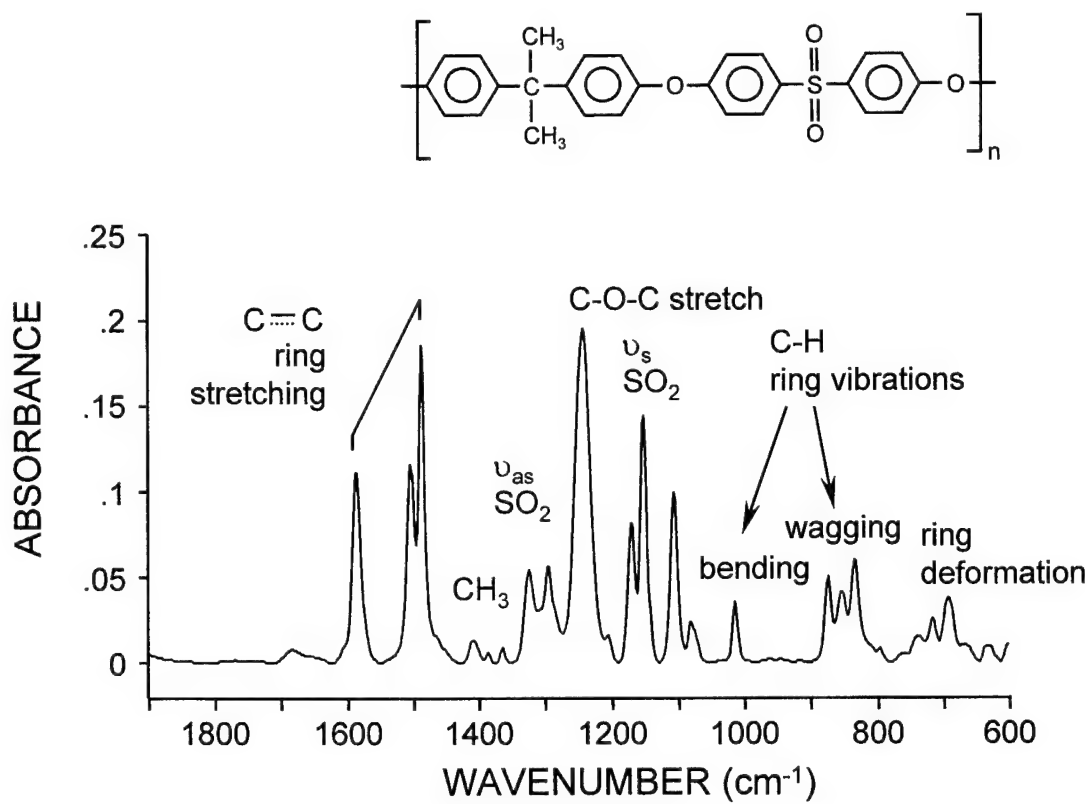
Figure 10.4   Assignments for some of the major mid-IR vibrational bands of PS.

114
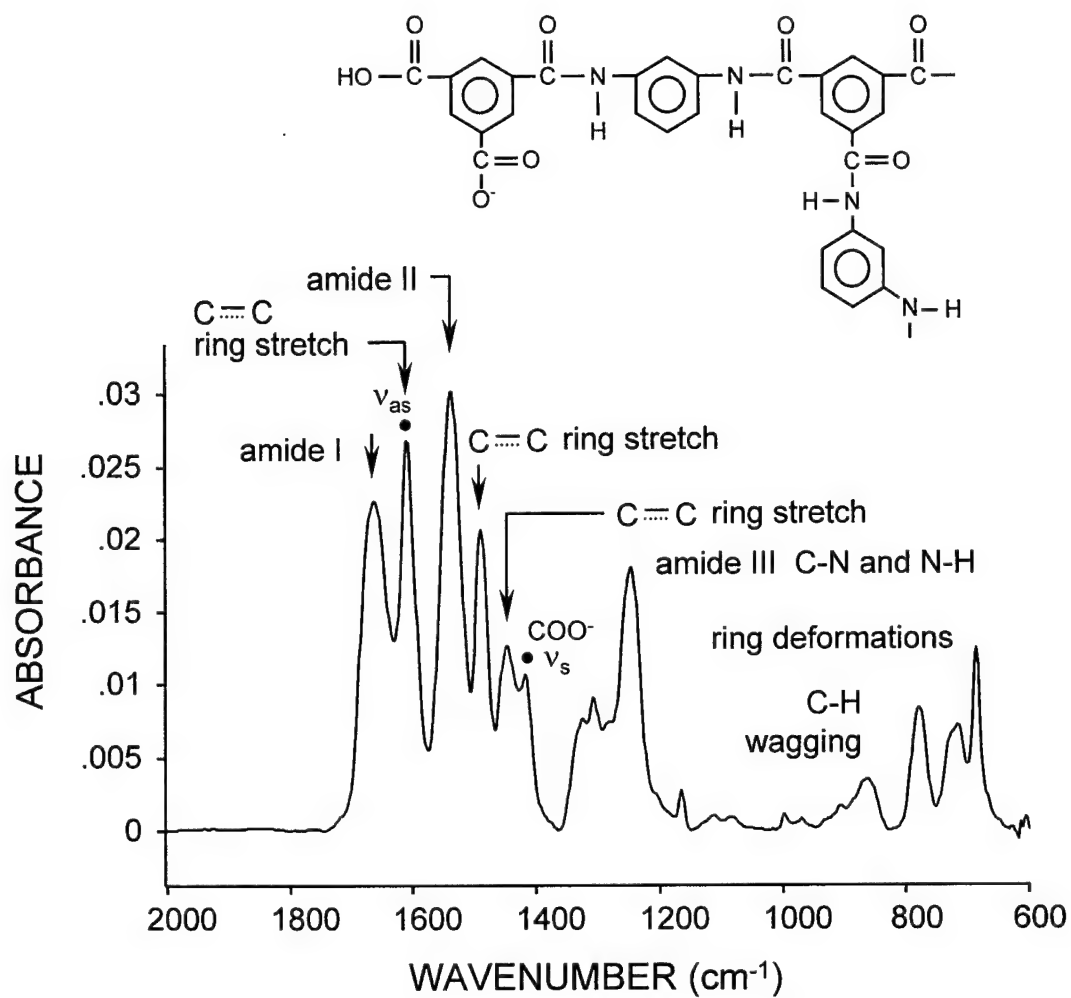
Figure 10.5 Assignments for some of the major mid-IR vibrational bands of PA.
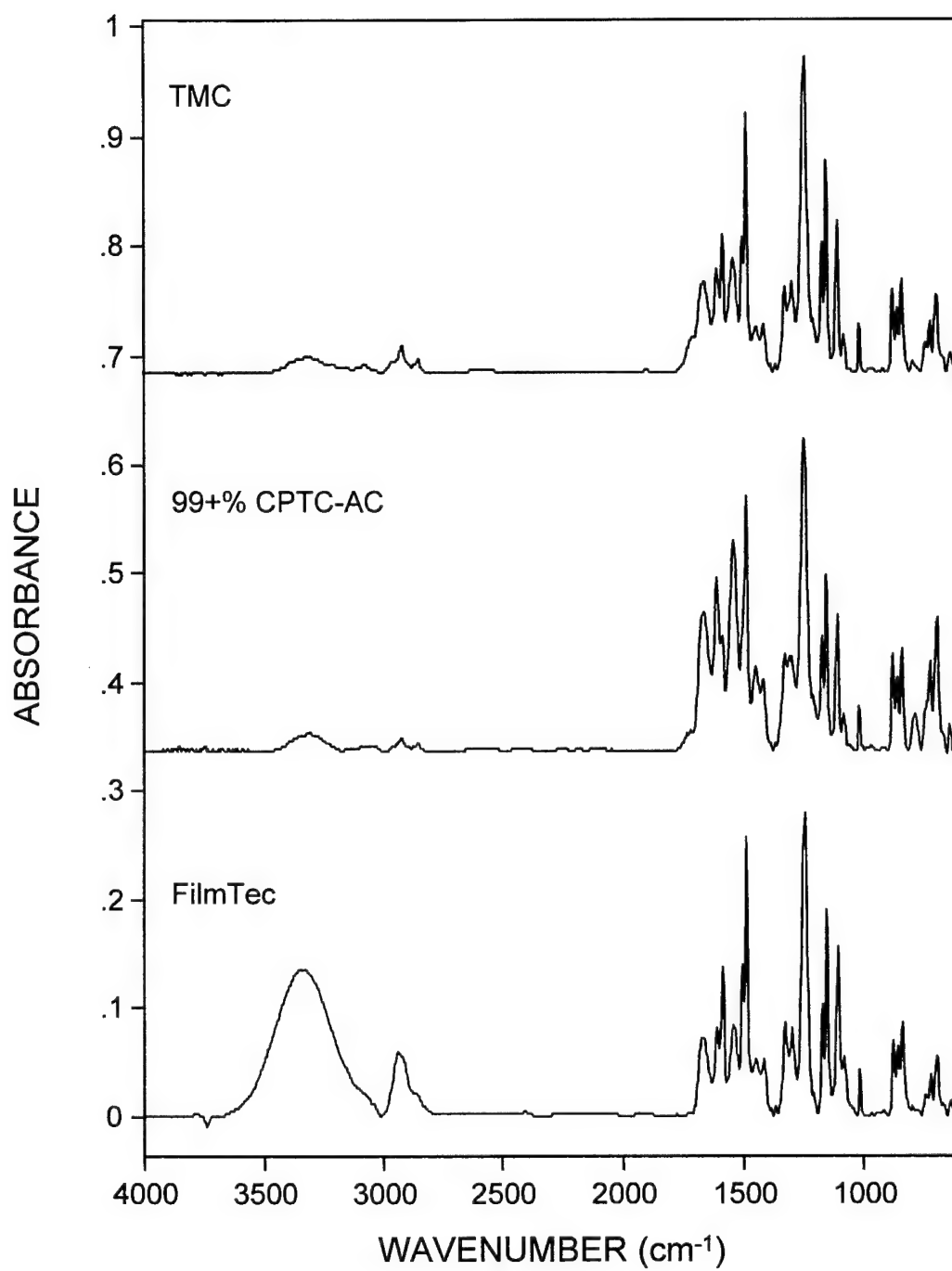
Figure 10.6   ATR/IR spectra of three different membranes between 4000 cm^{-1} and 600 cm^{-1}.
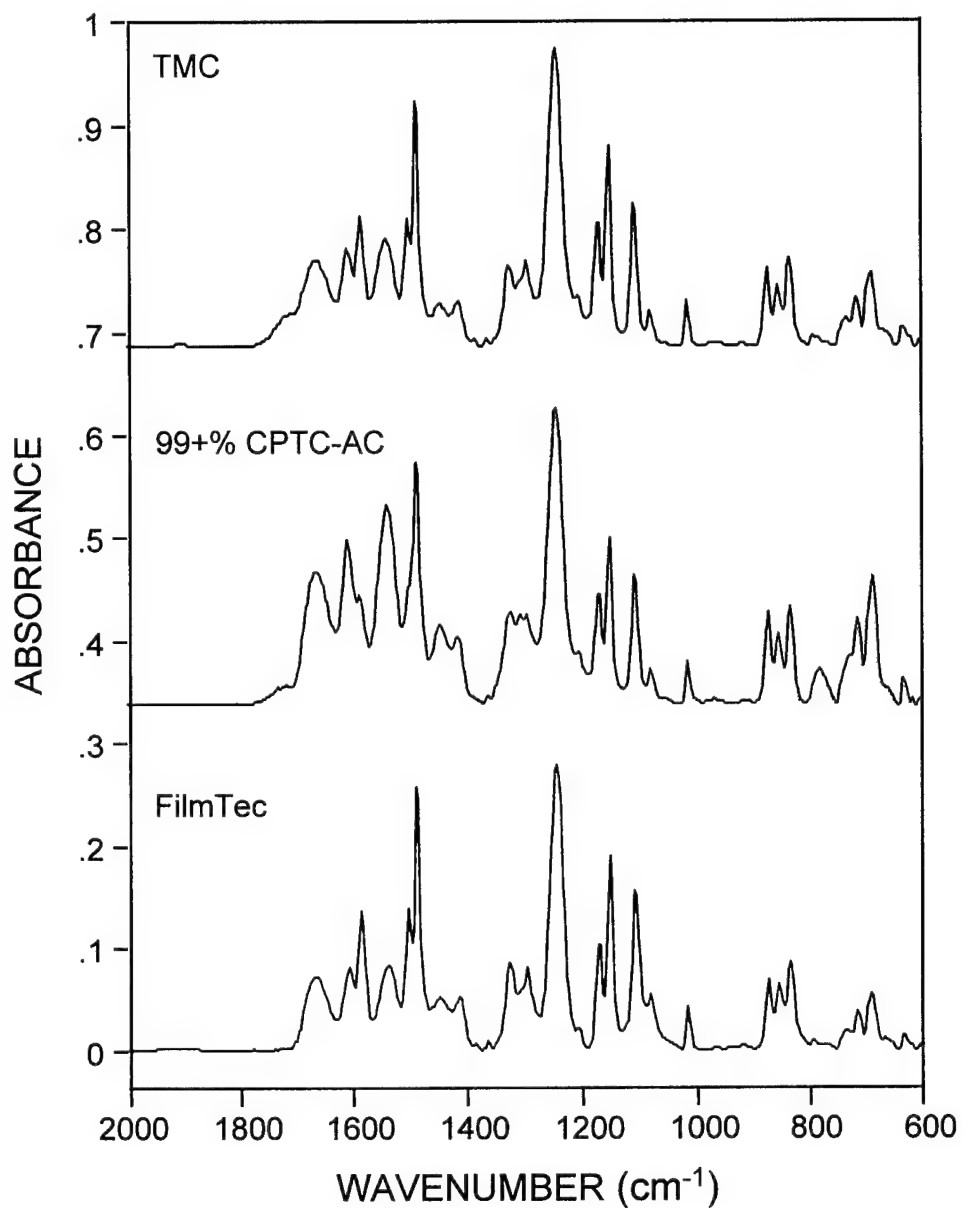
Figure 10.7   ATR/IR spectra of three different membranes between 2000 cm^{-1} and 600 cm^{-1}.

11.0 OPTIMIZATION OF TMC MEMBRANES

11.1 Removal of Unreacted MPD from Membrane During Processing

In the preparation of thin-film composite membranes, MPD is one of the monomers used in the interfacial polymerization to form the thin semipermeable desalination barrier. MPD, used in excess, thoroughly penetrates and saturates the porous PS supporting membrane during processing. After the interfacial reaction of MPD with TMC has occurred, the excess amine is very difficult to remove from the polymer matrix. To remove the excess amine the membrane is passed through a series of leaching baths before passing through a final solution of 3% glycerin in water prior to oven drying. Glycerin is added to the membrane to enhance re-wetting once the membrane has been dried. A flow diagram is shown in Section 9, Figure 9.13 for the processing of this membrane.

Once MPD has oxidized within the membrane, it becomes very insoluble in water and cannot be easily removed. Any residual amine left in the membrane slowly oxidizes, becomes very hydrophobic and discolors the membrane. As oxidation of the amine progresses within the membrane both before and after RO testing and during long-term element storage, the water flux of the membrane deteriorates significantly. This is a serious problem in the manufacture of membranes today.

Traces of MPD remain in most commercial membranes. The search for the optimal leaching process is ongoing. A large number of leaching solutions were evaluated in varying sequences at various times and temperatures. After each leaching process the membranes are examined in RO tests, both before and after exposure to ultraviolet light. If the membranes discolor after the leaching process and upon exposure to light, an inevitable loss in transport properties will occur.

An effective leaching process was developed based on removing the amine by first passing the membrane through an oxalic acid solution followed by subsequent rinses in deionized water for varying times and temperatures before oven drying. To optimize the leaching sequence a set of membranes, designated HR-17, HR-18 and HR-19, were prepared by the standard procedure using 2 wt-% MPD and 0.15 wt-% TMC. The membranes were nominally the same except for differences in the DI leach bath processes. These leaching processes are summarized in Figures 11.0 through 11.2 for membranes HR-17, HR-18 and HR-19, respectively.

The discoloration of membranes HR-17, HR-18 and HR-19 , after three days in air and unprotected from light, is shown in Figure 11.3. It is quite apparent that the rinse process for HR-19, described in Figure 11.2, is most effective.
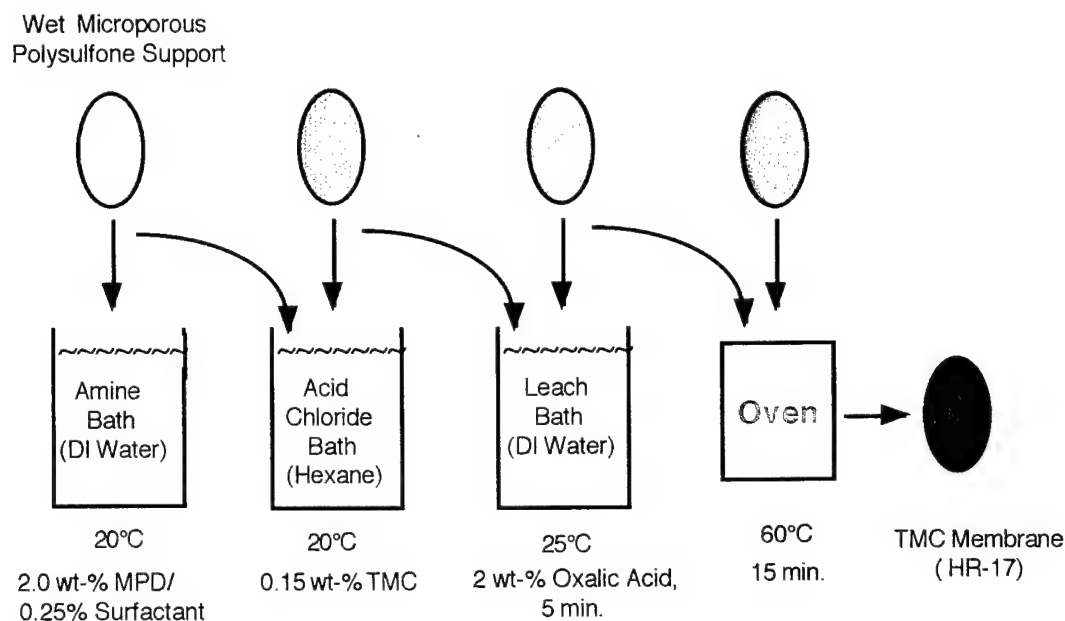
Figure 11.0   Process flow diagram for preparation of TMC membrane HR-17
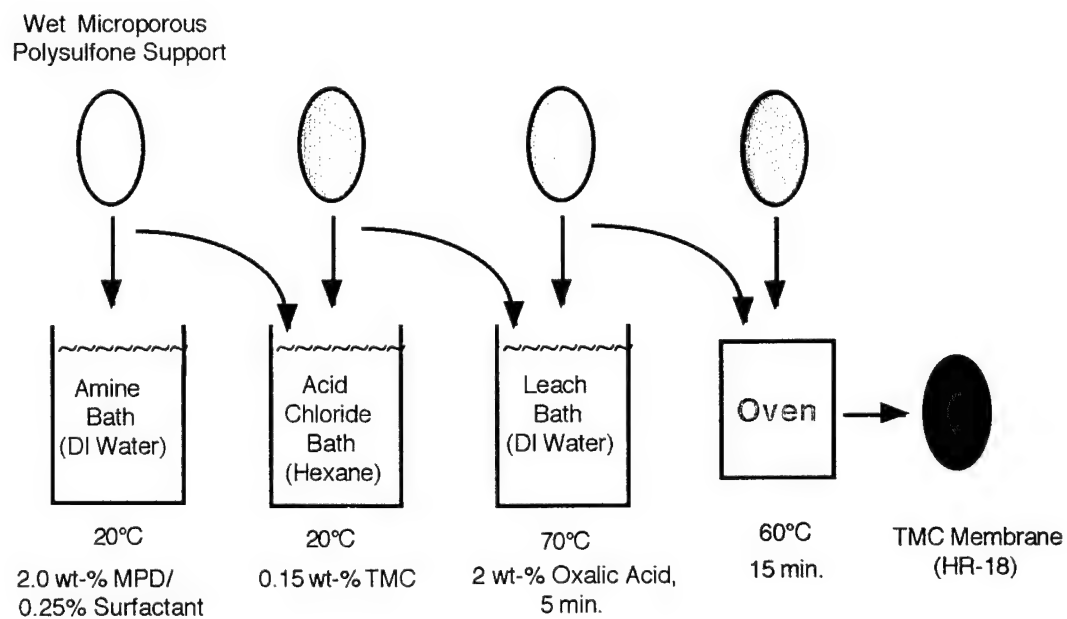
Figure 11.1   Process flow diagram for preparation of TMC membrane HR-18
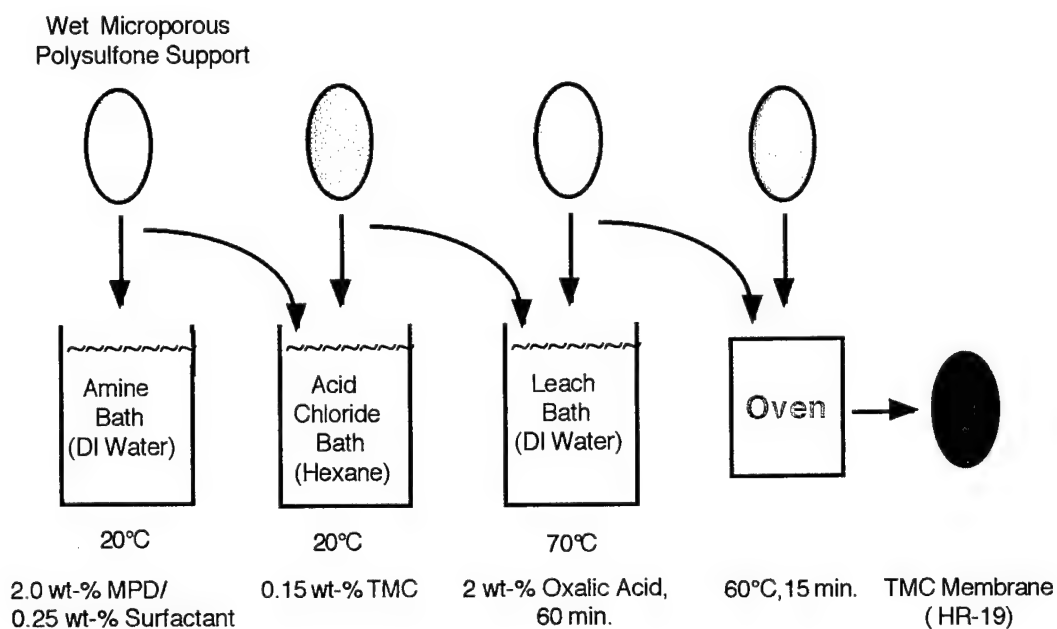
Figure 11.2 Process flow diagram for preparation of TMC membrane HR-19
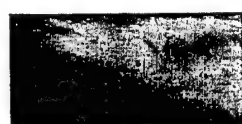
HR-17   **HR-18**   **HR-19**

Figure 11.3 Discoloration of membranes HR-17, HR-18 and HR-19 as a function of process extraction method. Membrane discoloration is indicative of residual monomers remaining in the membranes after the formation of the thin film by the interfacial polymerization process.
(See accompanying process diagrams)

120

Atomic force microscopy (AFM) was used to evaluate the surfaces of these membranes with varying degrees of leaching. It was observed repeatedly that the structure of the surface of the thin film changes with time if the extraction process is inadequate and if MPD remains in the membrane. Surface roughness, surface peak height and surface area all decrease. This is consistent with the lower water flux that is observed in RO.

Other factors that change the surface structure of the membrane containing traces of residual MPD are:

- Exposure to light, both ultraviolet and fluorescent (visible)
- Exposure of the membrane to air
- Exposure of the membrane to oxygen

AFMs were taken of the thin film surface of membranes HR-17, HR-18 and HR-19 that had been stored under nitrogen and in the dark for three days prior to imaging. A comparison of the root mean square roughness and the mean surface height for each membrane is shown in Figure 11.4. Surface statistics were averaged from six different sites. The difference in the surface of membrane HR-17 does appear to be significantly different than membranes HR-18 and HR-19. Thus, it would appear that the rinsing may not be totally adequate. Atomic force stylus profilometry for these membranes are shown in Figures 11.5 through 11.7, respectively.
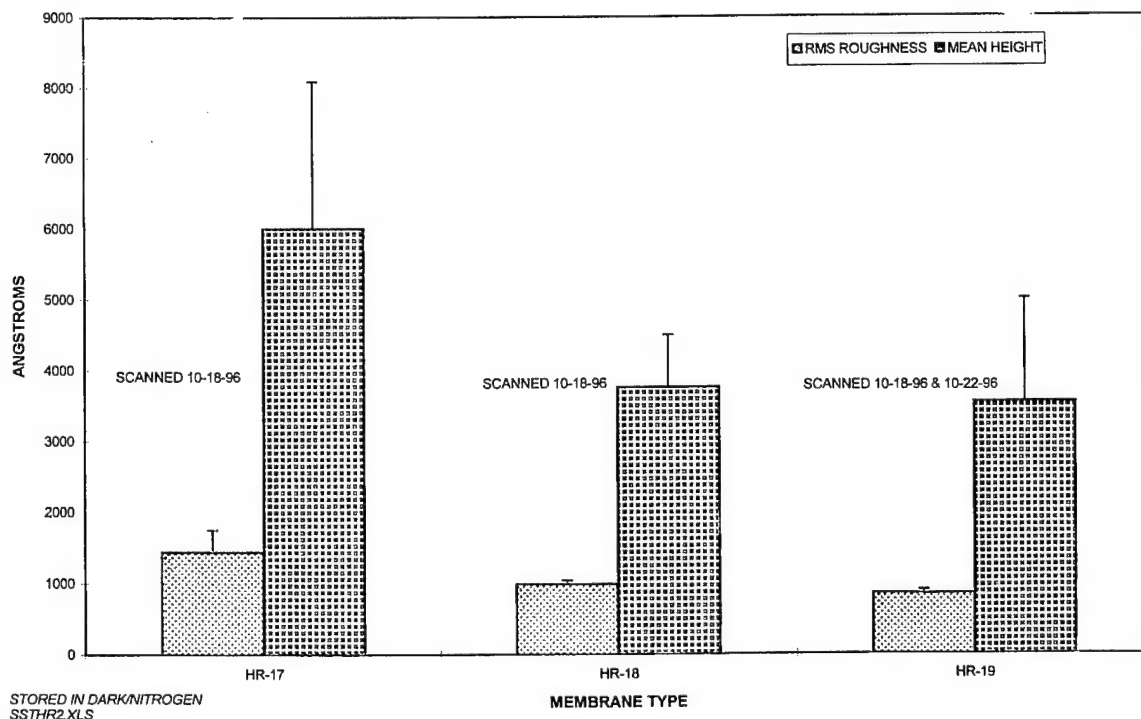
Figure 11.4   Comparison of the root mean square surface roughness (RMS) and the average surface peak heights of membranes HR-17, HR-18, and HR-19. The membranes were rinsed under different conditions and stored in the dark under nitrogen prior to examination by AFM.

121

μm
1.00
0.50
0.00

μm   8   6   μm   4   2   0
8   6   4   2   0

μm
1.0
0.8
0.6
0.4
0.2
0.0

0   2   4   6   8 μm

Histogram

(#)
4000
3000
2000
1000
0

0   0.2   0.4   0.6   0.8   1
Height (μ)

Selected Area

Bearing Ratio

(%)
80
60
40
20
0

0   0.2   0.4   0.6   0.8   1
Height (μ)

Area Statistics:

Median height :   4222 Å
Mean height :   3885 Å
Surface area : 170.71 μ²
Projected area : 99.11 μ²
Rms rough :   1189 Å
Ave rough :   931 Å

Figure 11.5   Atomic force stylus profilometry of membrane HR-17-Dry. Stylus contact
(IC-AFM) with membrane surface. AFMs showing the topography of a
selected membrane area and a summary of the surface area statistics for
the membrane after being rinsed in 2% oxalic acid at 25°C for 5 min and
subsequently dried in oven at 60°C for 15 min.

122

Area Statistics:

Median height : 4233 Å
Mean height : 4247 Å
Surface area : 179.70 µ²
Projected area : 100.00 µ²
Volume : 42.47 µ³
Rms rough : 1030 Å
Ave rough : 820 Å

Figure 11.6   Atomic force stylus profilometry of membrane HR-18-Dry. Stylus contact (IC-AFM) with membrane surface. AFMs showing the topography of a selected membrane area and a summary of the surface area statistics for the membrane after being rinsed in 2% oxalic acid at 70°C for 5 min and subsequently dried in oven at 60°C for 15 min.

123

Histogram

Selected Area

Bearing Ratio

Area Statistics:

Median height : 3258 Å
Mean height : 3014 Å
Surface area : 168.07 µ²
Projected area : 100.00 µ²
Volume : 30.14 µ²
Rms rough : 861 Å
Ave rough : 682 Å

Figure 11.7 Atomic force stylus profilometry of membrane HR-19-Dry. Stylus contact (IC-AFM) with membrane surface. AFMs showing the topography of a selected membrane area and a summary of the surface area statistics for the membrane after being rinsed in 2% oxalic acid at 70°C for 60 min and subsequently dried in oven at 60°C for 15 min.
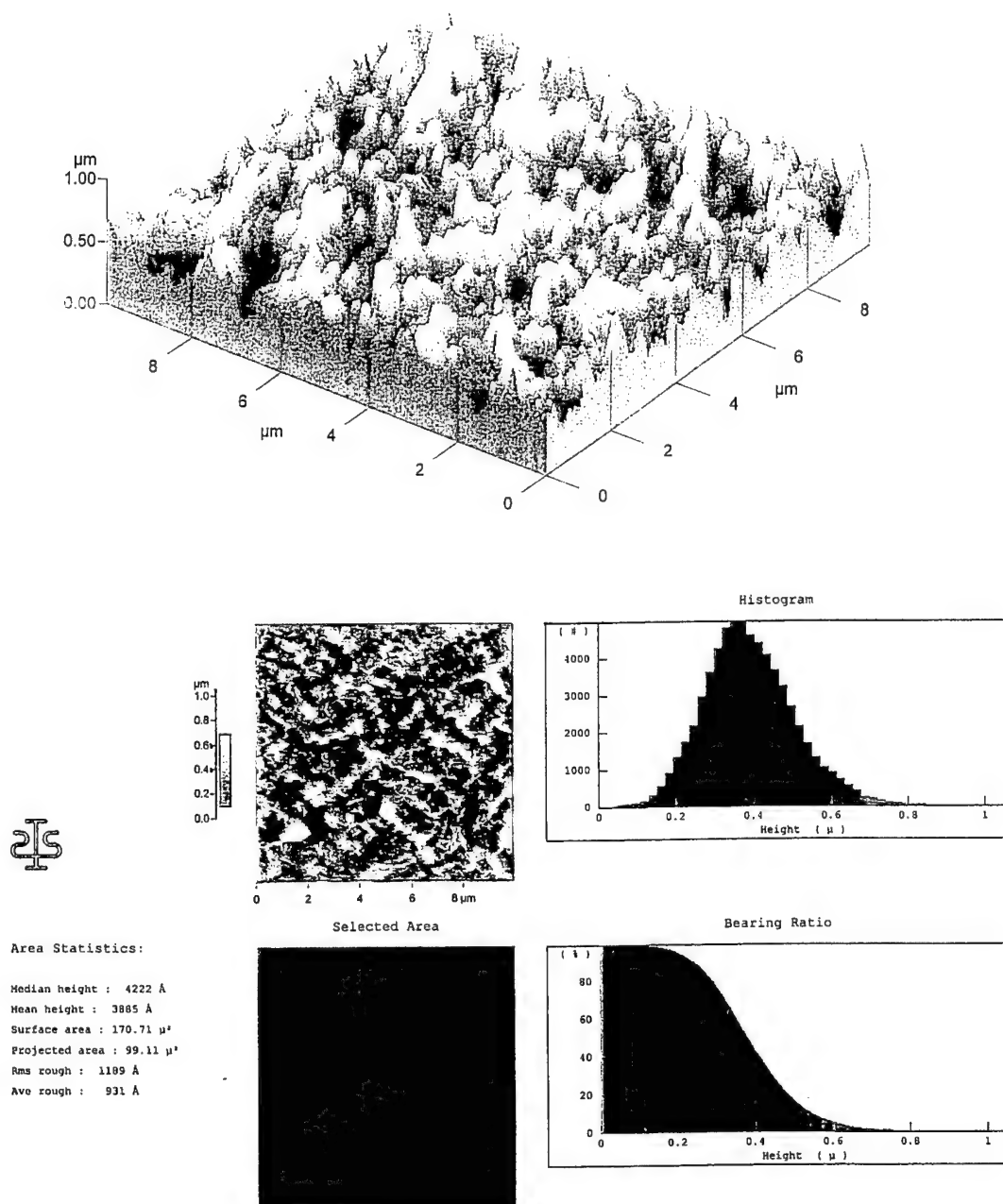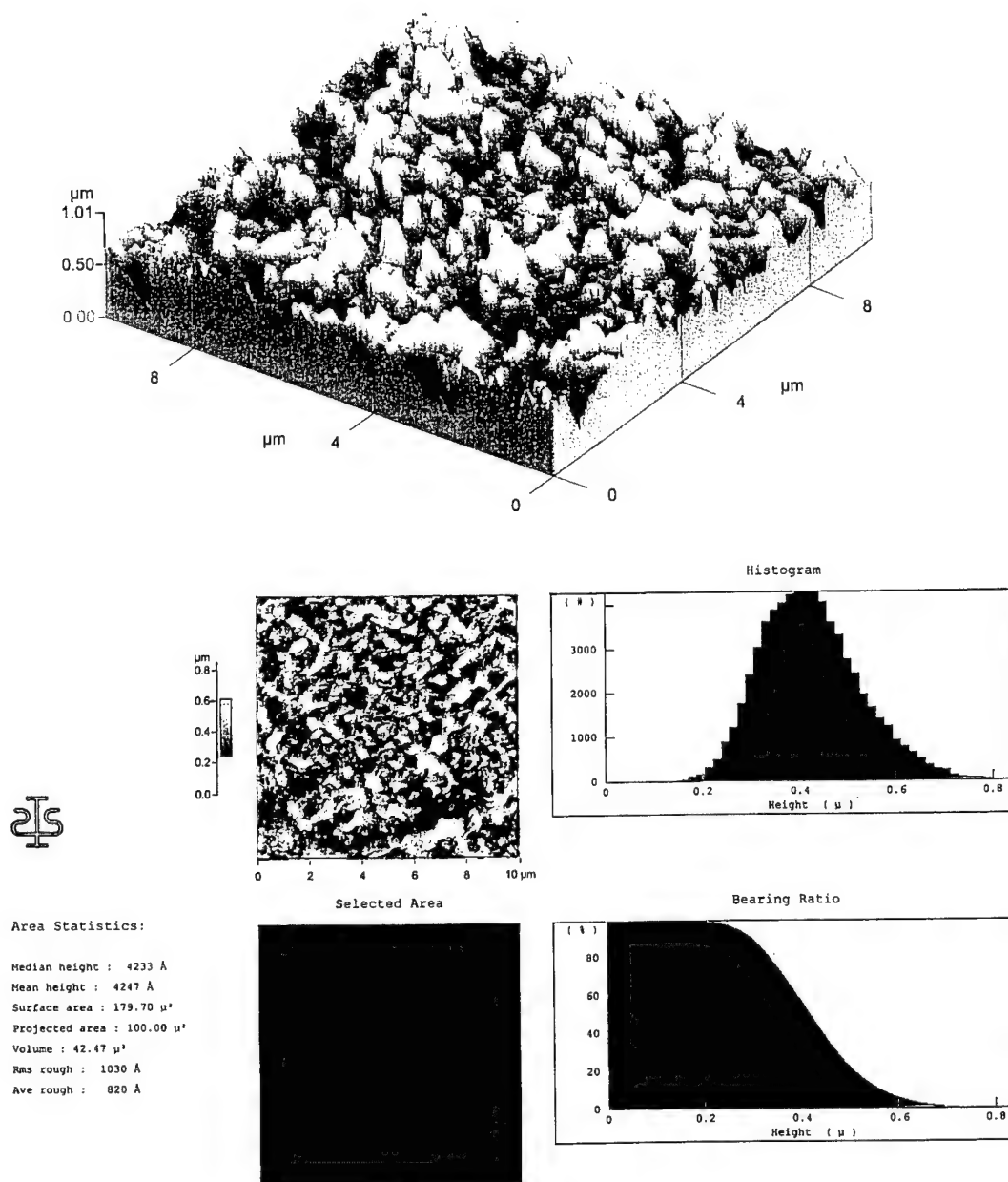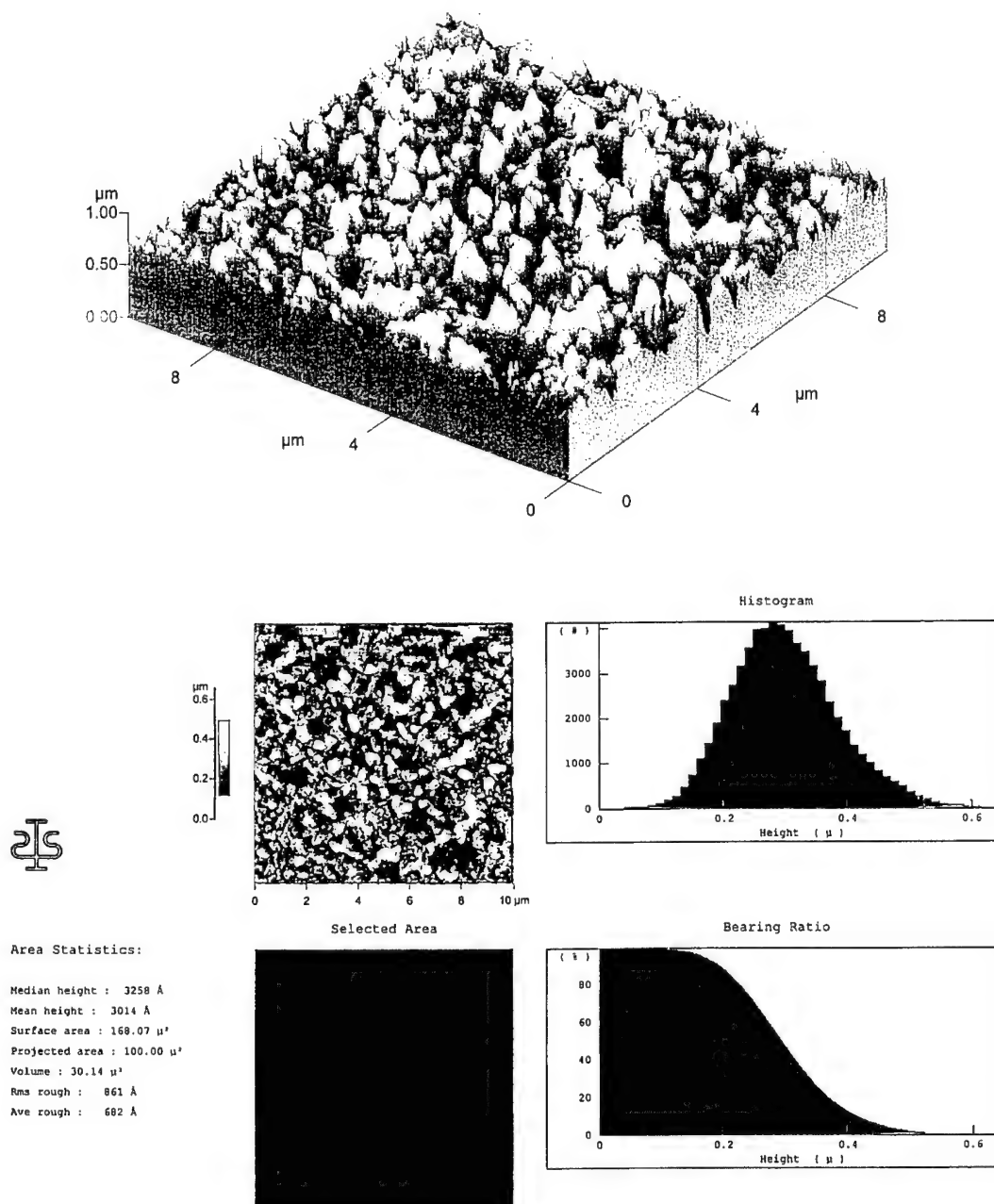
124

A second extraction study was conducted to further optimize the leaching step. In this study the oxalic acid concentration was increased to 3 wt-% and a deionized water rinse was added to remove the residual oxalic acid left in the membrane before glycerin treatment and oven drying. Membranes were made, designated HR-20 and HR-21, and extracted according to the process schematics shown in Figures 11.8 and 11.9. After passing through the aforementioned extraction processes, the membranes were sealed in polyethylene bags and stored in a dark environment. After ten days the membranes were examined by AFM. The membranes had discolored only slightly as shown in Figure 11.10.

Wet Microporous
Polysulfone Support

Amine Bath (DI Water)	Acid Chloride Bath (Hexane)	Leach Bath (DI Water)	(DI Water)	(DI Water)	
20°C	20°C	65°C	65°C	90°C	
2.0 wt-% MPD/ 0.25 wt-% Surfactant	0.15 wt-% TMC	3 wt-% Oxalic Acid, 8 min.	8 min.	8 min.	TMC Membrane (HR-20)
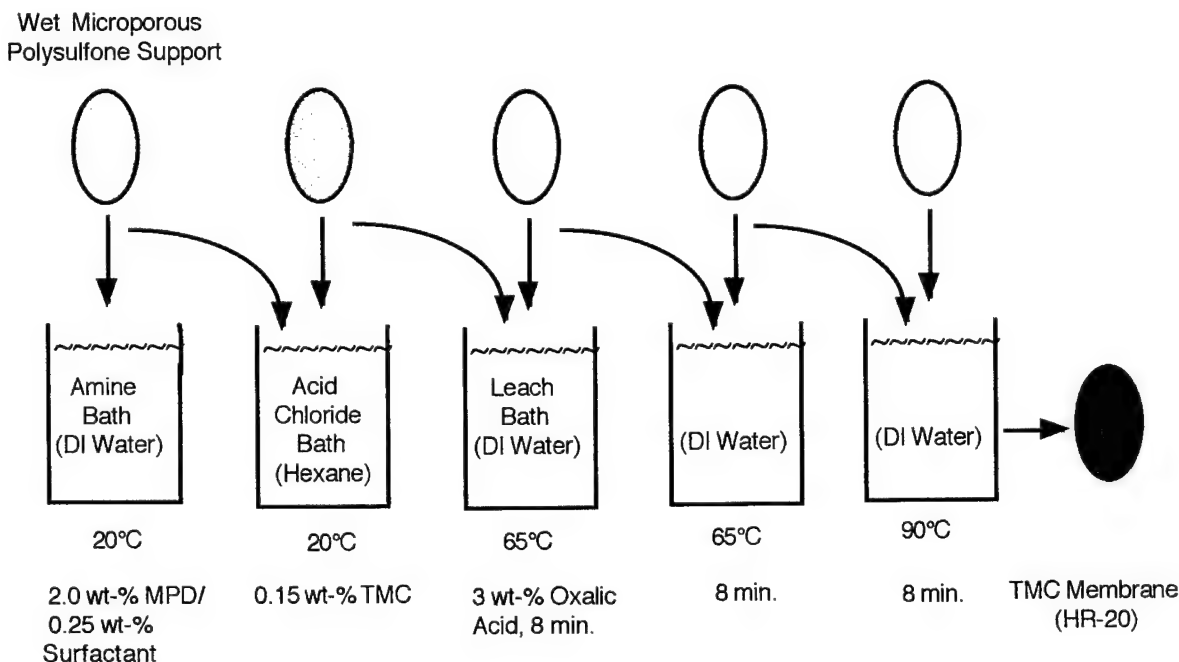
Figure 11.8   Process flow diagram for preparation of membrane HR-20

The AFMs for membranes HR-20 and HR-21 are shown in Figures 11.11 and 11.12, respectively. Infrared spectra were taken of the thin film surface of HR-20 and HR-21 ten days after processing and before being evaluated by AFM. ATR/IR analysis was determined for each membrane sample before and after rinsing with deionized water. The spectra for membranes HR-20 and HR-21 are shown in Figures 11.13 and 11.14 and Figures 11.15 and 11.16 respectively. All of the spectra appear to be nominally the same with the exception of membrane HR-21 before washing, (Figure 11.15). Before washing, the absorbance at 3300 cm^{-1} was 0.35; after washing the absorbance dropped to 0.025. This difference is believed to be due to the removal of glycerin from the membrane surface that was only used with membrane HR-21.

Figure 11.9 Process flow diagram for preparation of membrane HR-21

HR-20   **HR-21**

Figure 11.10 Discoloration of membranes HR-20 and HR-21 as a function of process
extraction method. Membrane discoloration is indicative of residual
monomers remaining in the membranes after the formation of the thin film
by the interfacial polymerization process. (See accompanying process
diagram)

Area Statistics:

Median height : 6956 Å
Mean height : 6835 Å
Surface area : 260.29 µ²
Projected area : 100.00 µ²
Volume : 68.35 µ³
Rms rough : 2021 Å
Ave rough : 1632 Å
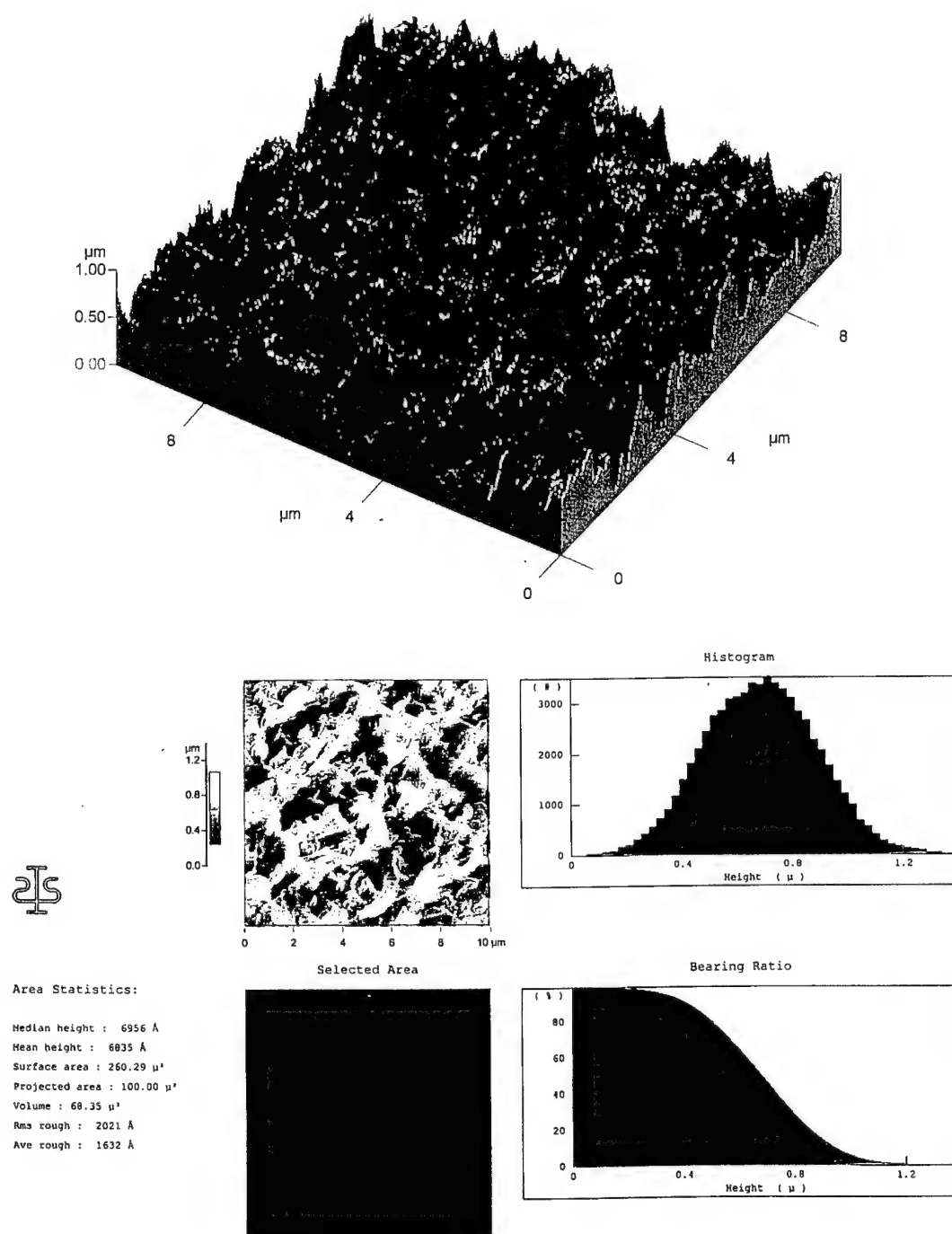
Figure 11.11 Atomic force stylus profilometry of membrane HR-20-Dry. Stylus
in partial contact (IC-AFM) with membrane surface. Top photo -
AFM showing three dimensional rendering of membrane surface.
Bottom photo - Monograph showing the topography of a selected
membrane area and a summary of the surface area statistics taken
four days after membrane processing.

127

Area Statistics:

Median height : 7001 Å
Mean height : 6609 Å
Surface area : 245.43 µ²
Projected area : 100.00 µ²
Volume : 66.09 µ³
Rms rough : 1854 Å
Ave rough : 1460 Å
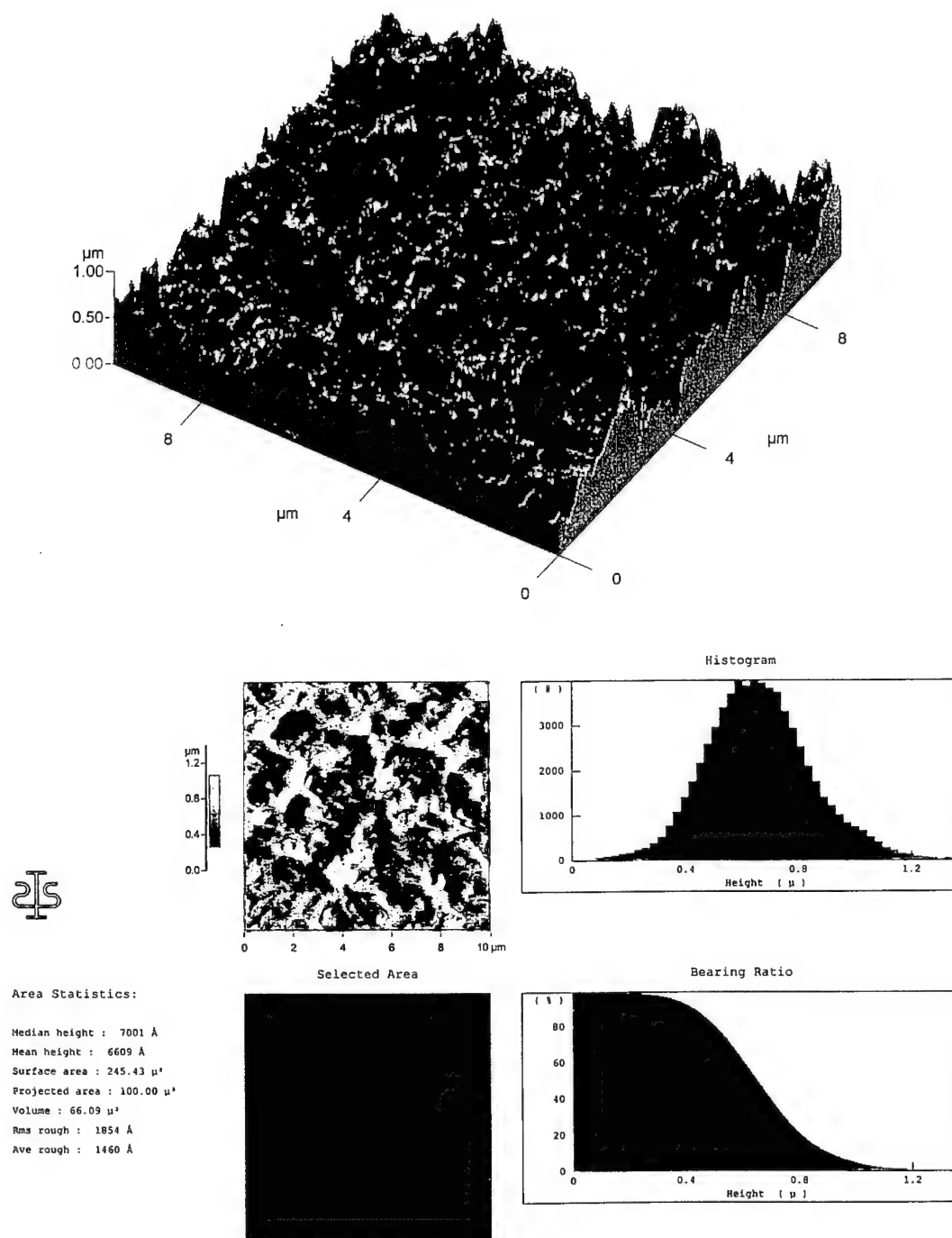
Figure 11.12 Atomic force stylus profilometry of membrane HR-21-Dry. Stylus in partial contact (IC-AFM) with membrane surface. Top photo - AFM showing three dimensional rendering of membrane surface. Bottom photo - Monograph showing the topography of a selected membrane area and a summary of the surface area statistics taken four days after membrane processing.
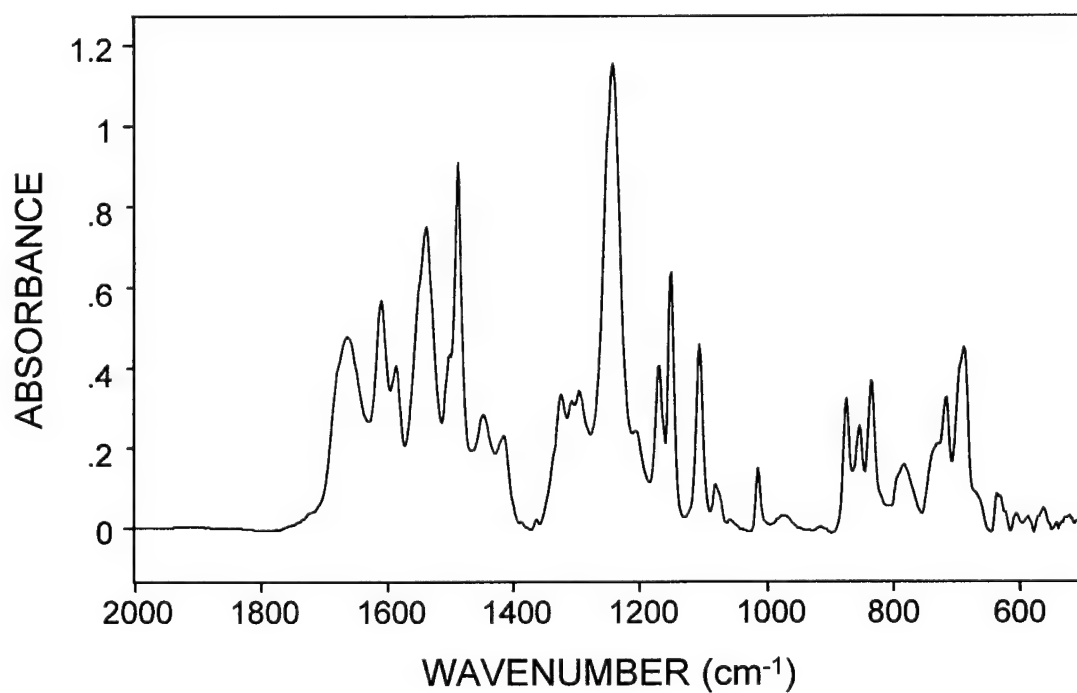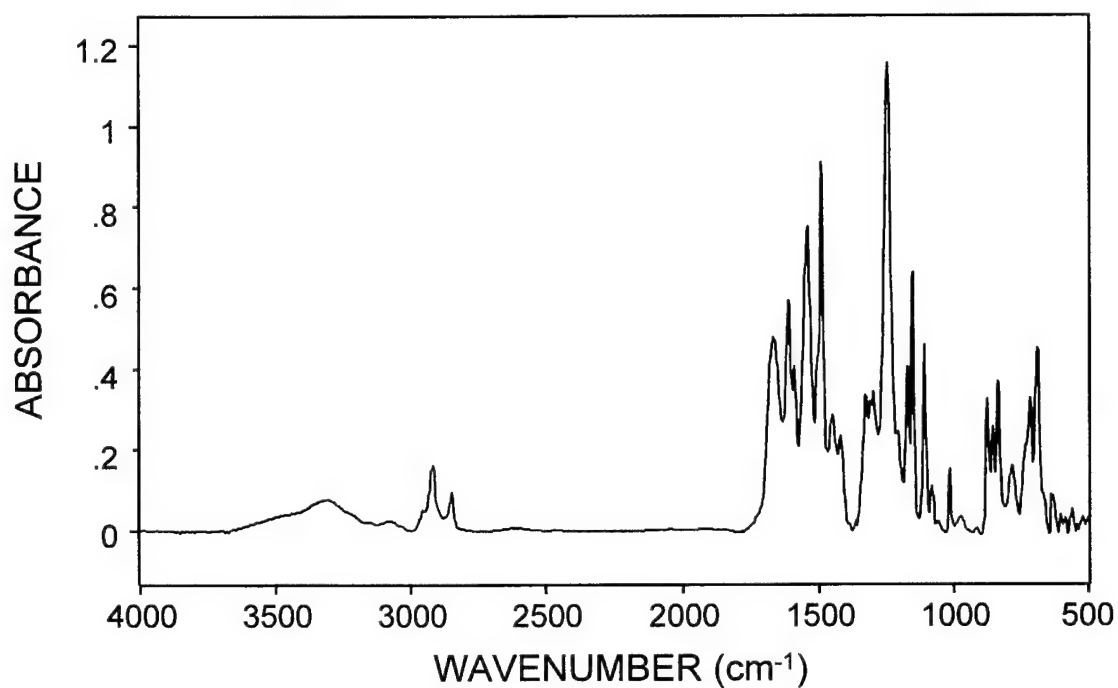
Figure 11.13 ATR/IR spectrum of thin-film PA membrane surface of HR-20 taken
10 days after processing. Membrane surface was not rinsed in deionized
water before evaluation.

Figure 11.14 ATR/IR spectrum of thin-film PA membrane surface of HR-20 taken 10 days after processing. Membrane surface was not rinsed in deionized water before evaluation.

Figure 11.15 ATR/IR spectrum of thin-film PA membrane surface of HR-21 taken 10 days after processing. Membrane surface was not rinsed in deionized water before evaluation.

131
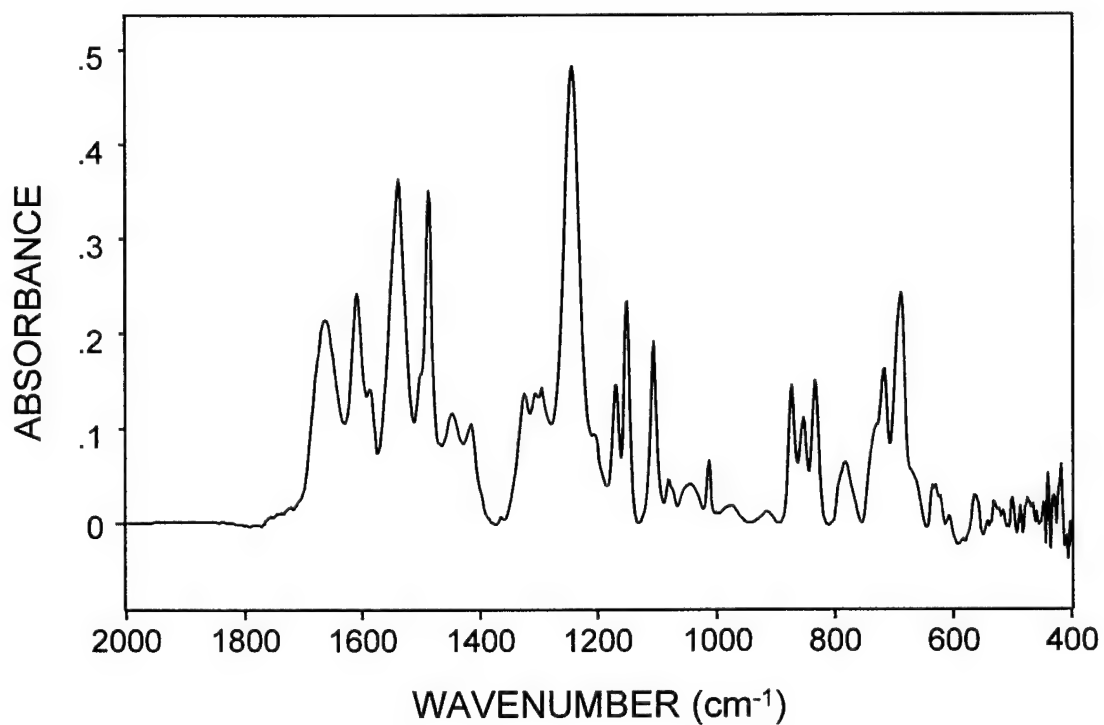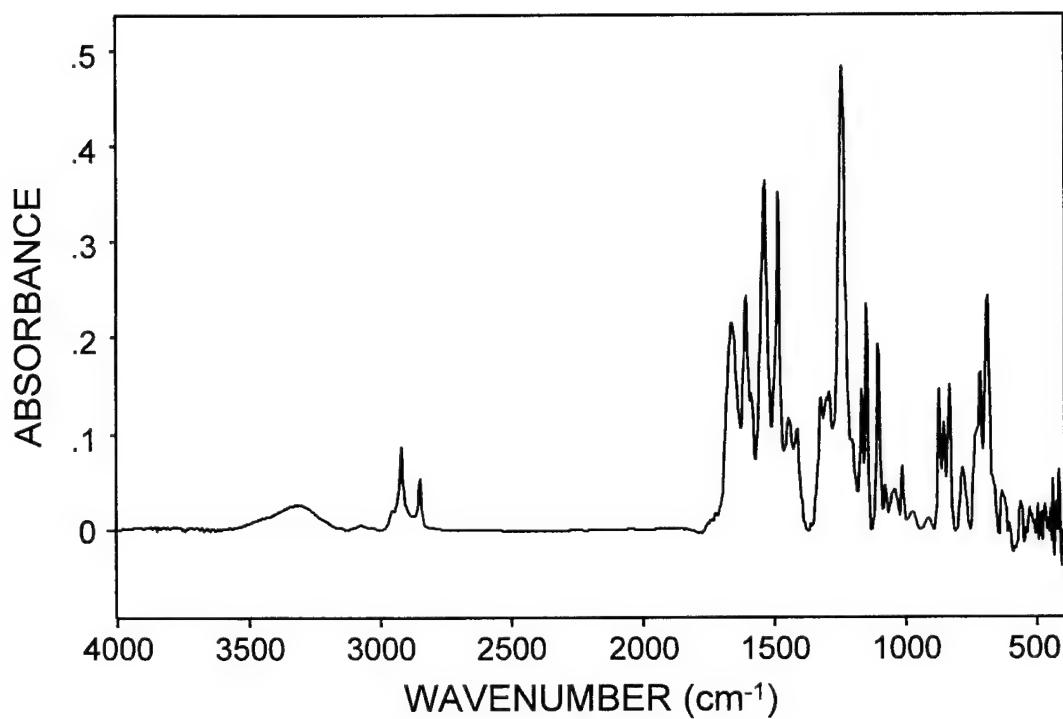
Figure 11.16 ATR/IR spectrum of thin-film PA membrane surface of HR-21 taken 10 days after processing. Membrane surface was rinsed in deionized water before evaluation.

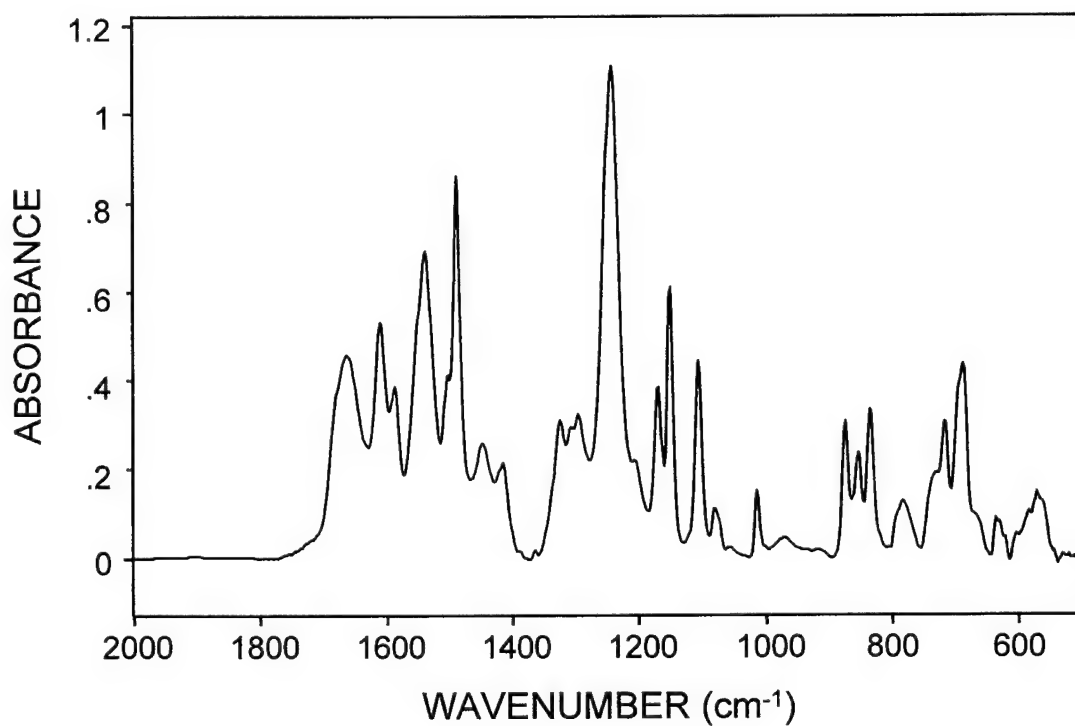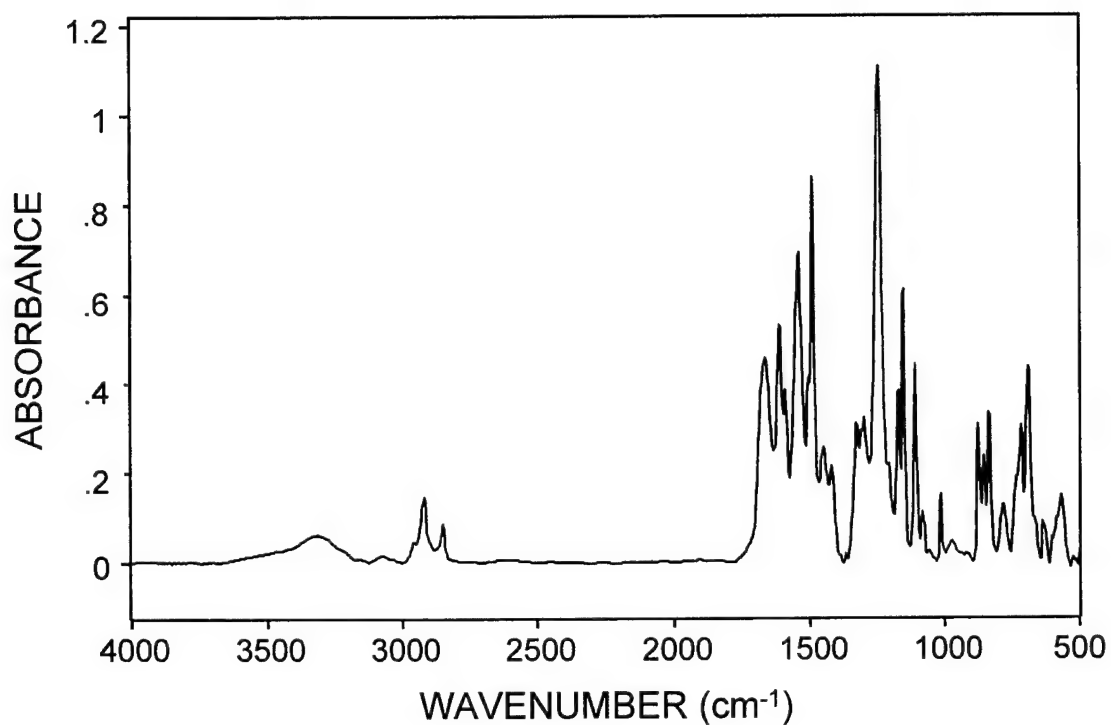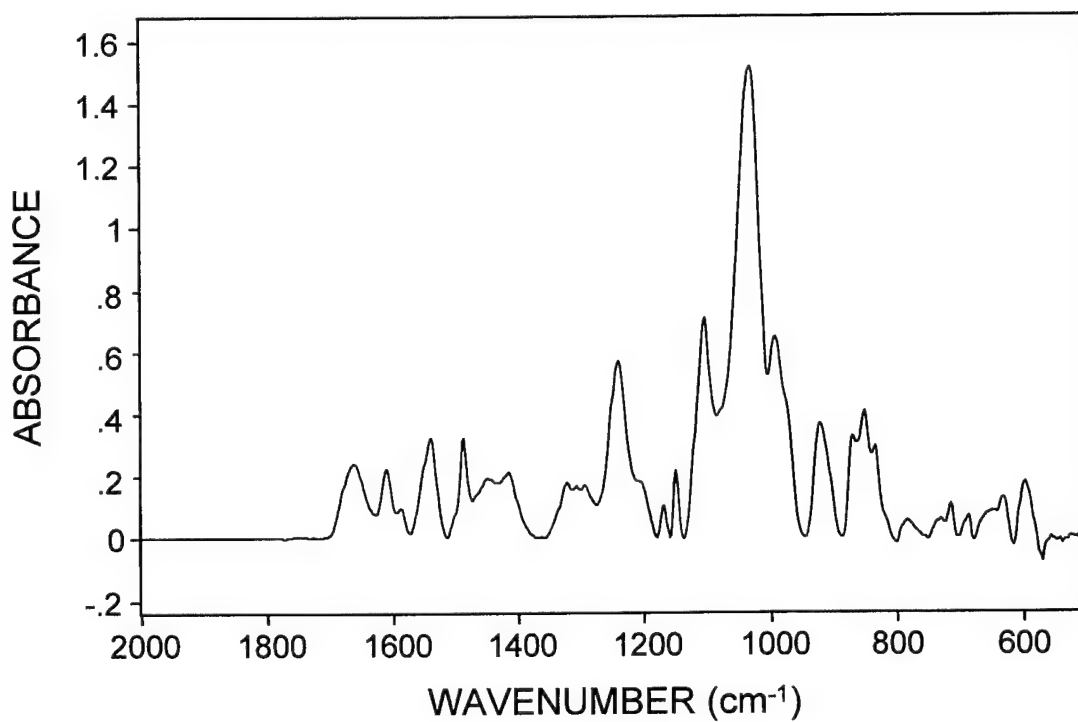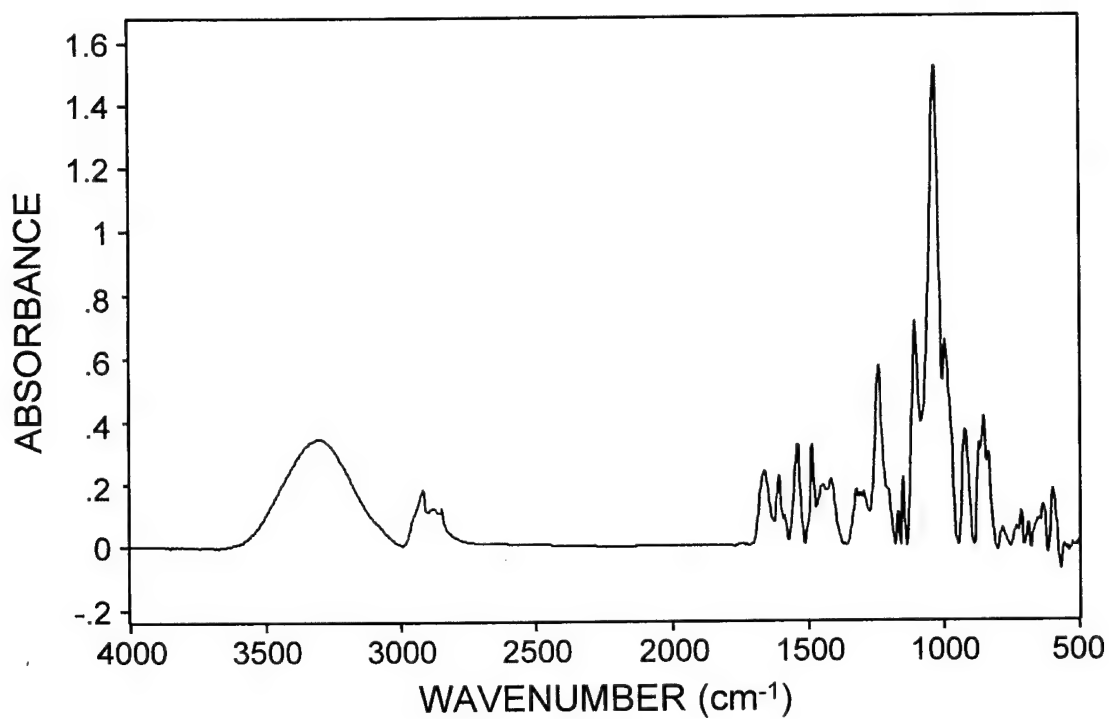A comparison of the root mean square surface roughness (RMS) and the average peak heights of the membranes are shown in Figure 11.17. The surface area statistics and the appearance of the surfaces of both membranes are nominally the same.

Bacterial attachment, (described in Section 11.4) was determined for the surfaces of both membrane HR-20 and HR-21; this data is also shown in Figure 11.17. Even though the surface chemistry and the surface statistics are nominally the same, the bacterial attachment level for membrane HR-20 was considerably greater. The reason for this difference is not certain.
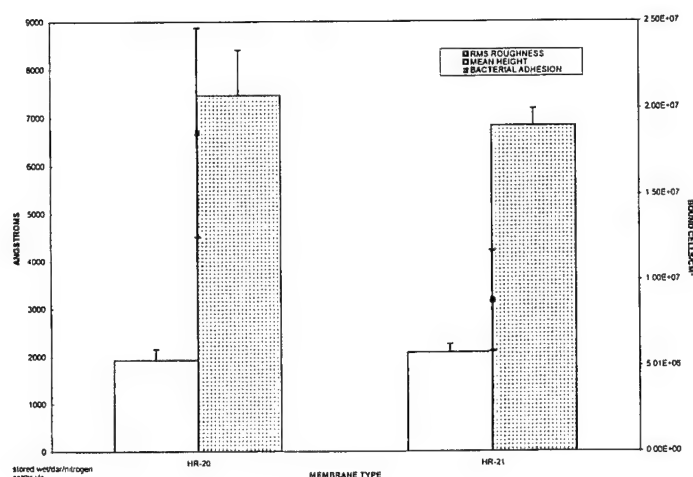
Figure 11.17 Comparison of the root mean square roughness, the average surface peak height and the number of bacterial cells attached on the surfaces of membranes HR-20 and HR-21.

11.2   Effect of Acid Chloride Solvent System on Membrane Surface Morphology

Initially, in the development of a composite membrane, screening experiments were conducted to determine if a selected amine dissolved in water will react with a selected acid chloride dissolved in a water immiscible hydrocarbon to form a durable thin film. If a film forms and the film has sufficient strength, the monomer pairs become candidates for further development. To conduct the experiment, the respective solutions of each monomer are prepared - an amine in water and the acid chloride in a hydrocarbon solution, generally hexane. Subsequently, the heavier aqueous amine solution is placed in a small beaker followed by the lighter acid chloride-hexane solution which is carefully poured onto the surface of the aqueous amine solution. Immediately upon contact of the two solutions, a thin film is formed at the water-hydrocarbon interface. The reactivity of the monomers, the rate of film formation and the strength of the resultant film can be rated.

133

Experiments of this type can be run with incrementally small changes in pH, monomer concentrations, solvent types, solvent additives, etc. to facilitate the identification and optimization of important process variables.

Figure 11.18 shows photographs of the formation of fully aromatic thin films by interfacial polymerization at the interface between a 2 wt-% aqueous solution of MPD containing 0.25 wt-% sodium lauryl sulfate and variable quantities of IPA and a 0.15 wt-% solution of TMC in hexane. IPA, which is also soluble in the organic phase, was added to the aqueous amine phase to vary and control the diffusive characteristics at the reaction interface, thereby changing the properties of the thin-film structure. Observations on the formation and physical properties of each of the films formed, experiments 2 through 6, are summarized in Table 11.0.

The observations regarding film formation and strength, reported in Table 11.0 are very similar to those observed for the *ctct*-CPTC-AC system. Figure 11.19 shows photographs of the formation of aromatic/aliphatic thin films by interfacial polymerization between a 2 wt-% aqueous solution of MPD containing 0.25 wt-% sodium lauryl sulfate and variable quantities of IPA and a 0.15 wt-% solution of *ctct*-CPTC-AC in hexane. Observations on the formation and physical properties of each of the films formed, experiments 2 through 6, are summarized in Table 11.1.

These screening experiments indicate that film formation and the resulting properties are similar when films are made from either the aromatic TMC or the aliphatic *ctct*-CPTC-AC. This technique is very useful for the initial screening of monomer pairs and was used routinely throughout this program.
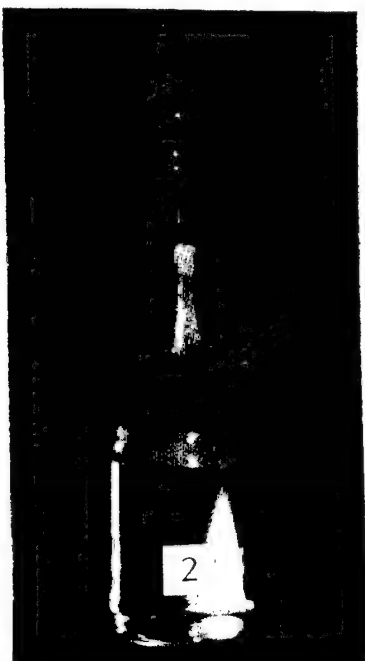
0 wt-% IPA in aqueous
amine phase
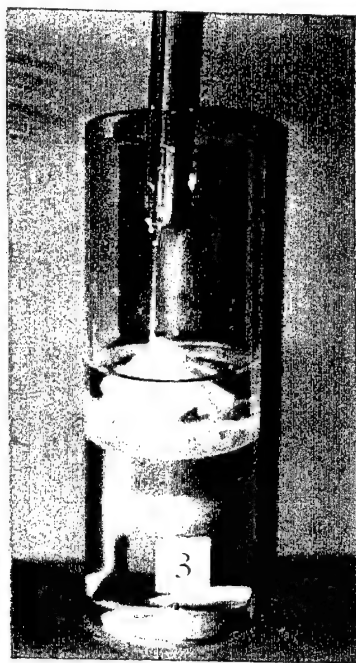
5 wt-% IPA in aqueous
amine phase

10 wt-% IPA in aqueous
amine phase
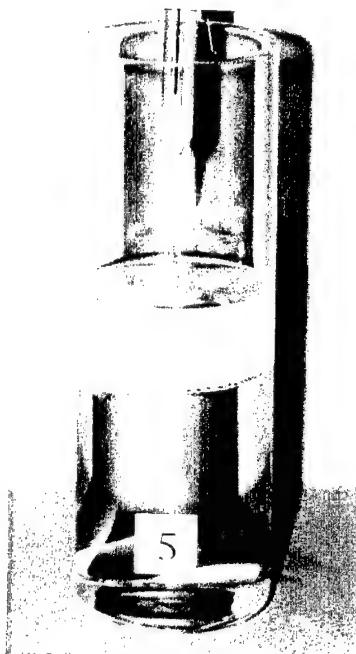
20 wt-% IPA in aqueous
amine phase
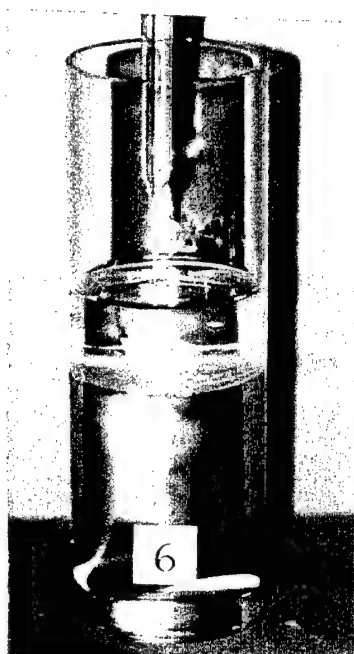
40 wt-% IPA in aqueous
amine phase
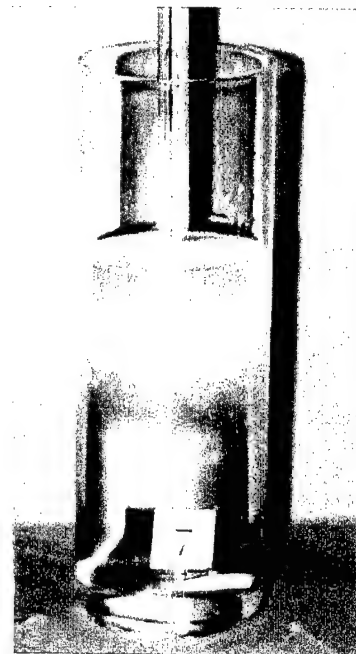
60 wt-% IPA in aqueous
amine phase

Figure 11.18   Formation of fully aromatic thin films by polymerization at the interface
between an aqueous solution of 2 wt-% MPD and a 0.15 wt-% solution of
TMC in hexane. The aqueous MPD solutions contain varying amounts of
IPA.

0 wt-% IPA in aqueous
amine phase
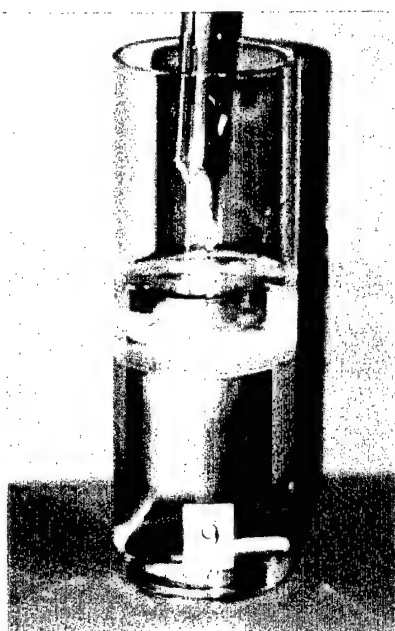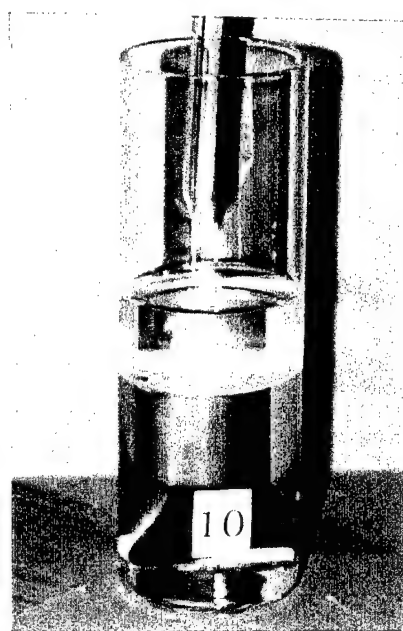
5 wt-% IPA in aqueous
amine phase

10 wt-% IPA in aqueous
amine phase
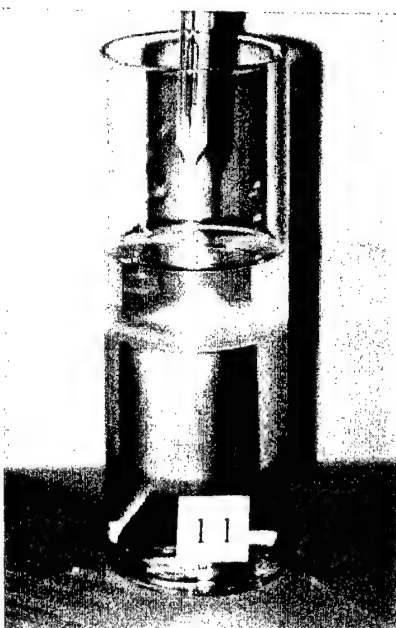
20 wt-% IPA in aqueous
amine phase
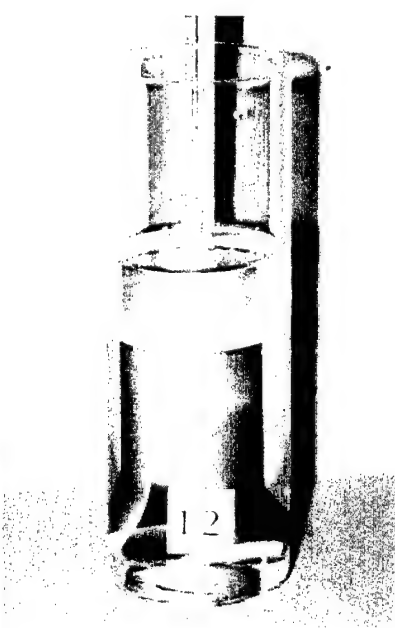
40 wt-% IPA in aqueous
amine phase
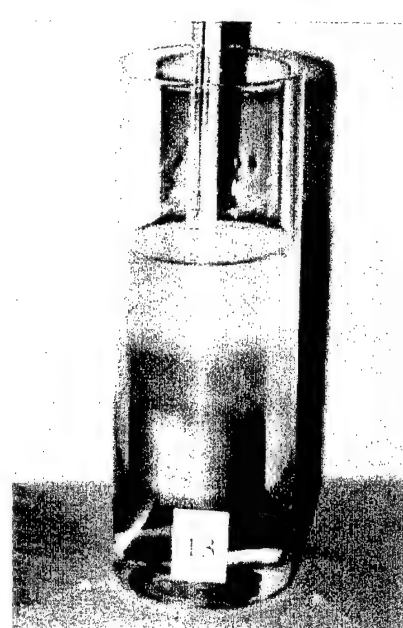
60 wt-% IPA in aqueous
amine phase

Figure 11.19   Formation of fully aromatic thin films by polymerization at the interface
between an aqueous solution of 2 wt-% MPD and a 0.15 wt-% solution of
ctct-CPTC in hexane. The aqueous MPD solutions contain varying
amounts of IPA..

Table 11.0

Properties of Thin Films Formed Interfacially from MPD and TMC

Experiment	Photo Reference Figure	Isopropanol Addition to Aqueous Phase	Observations Film Formation / Properties
1	2	0	Rapid film formation, weak but capable of withdrawal
2	3	5	Rapid film formation, weak, brittle but capable of withdrawal
3	4	10	Rapid film formation, weak, brittle but capable of withdrawal
4	5	20	Rapid film formation, weak brittle but capable of withdrawal
5	6	40	Film thick and brittle, film not capable of withdrawal
6	7	60	No film formed

Table 11.1

Properties of Thin Films Formed Interfacially from MPD and *ctct*-CPTC-AC

Experiment	Photo Reference Figure	Isopropanol Addition to Aqueous Phase	Observations Film Formation / Properties
1	2	0	Rapid film formation, weak but capable of withdrawal
2	3	5	Rapid film formation, weak, brittle but capable of withdrawal
3	4	10	Rapid film formation, weak brittle but capable of withdrawal
4	5	20	Rapid film formation, weak brittle but capable of withdrawal
5	6	40	Rapid film formation, film not capable of withdrawal
6	7	60	No film formed

11.3 A Comparison of Cross-linked and Linear Thin-Film Surface Structure Characteristics

One objective of this program was to improve the fouling characteristics of current membranes by reducing the surface roughness and by increasing the hydrophilic nature of the thin film. To reduce surface roughness it is first necessary to identify the reaction factors that are responsible. Surface roughness is determined during the interfacial polymerization at the amine (water phase)/acid chloride (hydrocarbon phase) interface during membrane formation. Several film forming variables were systematically studied and the surface roughness of each membrane determined by AFM. Several of the more important variables evaluated were:

- Determine the influence of cross-linking on the surface roughness of PA membranes prepared from di- and tri-functional amines and acid chlorides.

* Modify both the aqueous (amine) and hydrocarbon (acid chloride) phases to influence the diffusion of reactants at the interface after the initial monolayer has been formed. For example, the addition of varying amounts of alcohols and/or surfactants to the aqueous amine phase.

- Evaluate various organic solvents as carriers for the acid chlorides having varying levels of solubility in the aqueous amine phase.

A series of membranes were prepared by interfacially reacting MPD with an aromatic tri-acid chloride and a family of aromatic di-acid chlorides, namely the ortho, meta, and para isomers of benzenedicarboxylic acid chlorides. The interfacial reaction of MPD with TMC produces a highly cross-linked fully aromatic thin film while the diacid chlorides produce linear fully aromatic thin-films. A diagram of the membranes prepared for this study is shown in Figure 11.20. All membranes produced in this series, HR-1, HR-2, HR-3 and HR-4, were prepared using the same procedures, concentrations of reactants, etc. The process flow diagram for the preparation of the membranes is shown in Figure 11.21.

After the interfacial reaction is complete on the surface of the porous PS membrane support, the wet composite membrane is subsequently passed through a leaching step to remove the unreacted residual monomers. If the monomers are not totally removed, the membranes will discolor with time and the transport properties of the membrane will deteriorate, even while the membrane is stored in roll form.
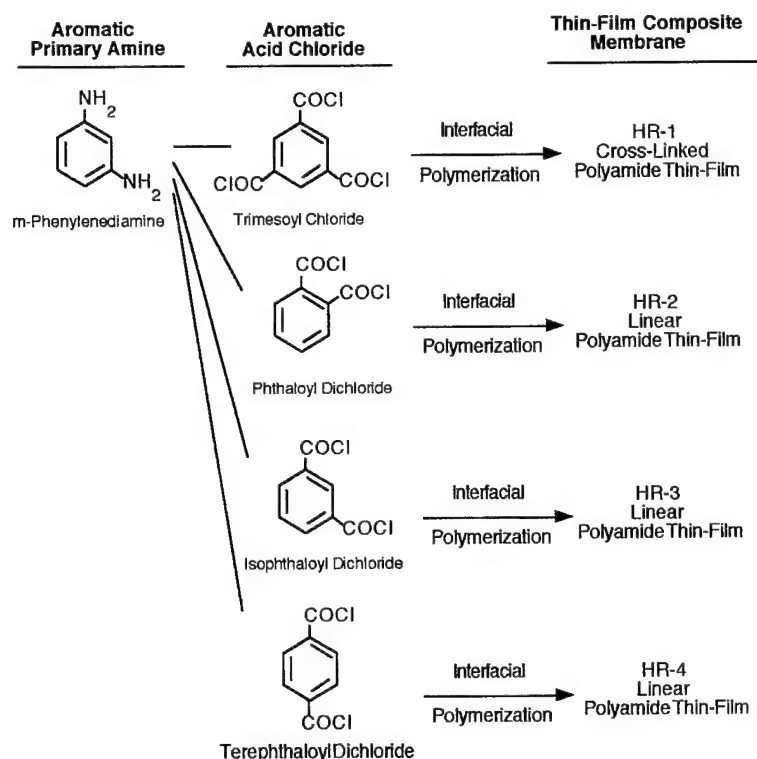
Figure 11.20 Interfacial formation of membranes using four different aromatic acid chlorides for the determination of membrane surface roughness and bacteria attachment.
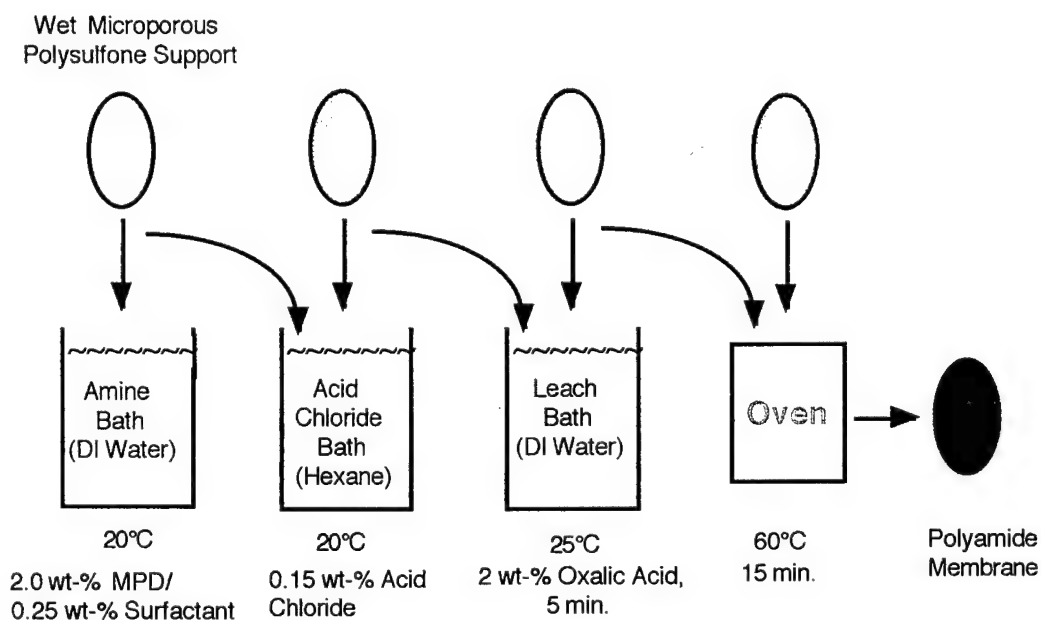
Figure 11.21 Process flow diagram for preparation of membranes HR-1, HR-2, HR-3, and HR-4.

139

Currently, membrane manufacturers have not optimized this step. The leaching process used in the preparation of this series of membranes was minimal. That is, the membranes were rinsed in DI water at 70°C for 5 min after which time they were dried in an air flow oven at 60°C for 15 min. This was done to determine if the structure of the thin film changed with time after the membranes were prepared.

The surface roughness and the surface area statistics were determined for all membranes. The AFMs for membranes HR-1, HR-2, HR-3 and HR-4 are shown in Figures 11.22, -23, -24 and -25, respectively. Membrane HR-1, a ROWPU type membrane having a cross-linked thin film, exhibited a rough membrane surface. Composite membranes HR-2, HR-3 and HR-4, having linear thin films, also exhibited a high degree of surface roughness. It can be concluded therefore that cross-linking *per-se* is not the major contributing factor in determining surface roughness.

It was also noted in other micrographs that the surface roughness decreased significantly with time after membrane preparation and after the membranes had discolored. Apparently, the reduction in transport properties of the membranes with time after processing is due to a change in surface morphology caused by the residual monomers. The importance of removing all traces of residual monomers from the composite membranes cannot be overemphasized. Efforts to develop the optimal extraction process, that is compatible with large scale-high speed processing, will be developed at a later date.

The RO performance of the membrane is presented in Table 11.2. It is apparent from the data that the transport properties of the linear PA membranes are poor. This is attributed, in part, to the poor physical properties of the membrane.

Table 11.2

RO Performance of HR-1, HR-2, HR-3, and HR-4 Membranes

Test conditions: 225 psi applied pressure, 2,000 mg/L sodium chloride feed, 25°C, pH = 7.0, 0.9 gal/min feed flow

Membrane Designation	Water Flux (gfd)	Salt Rejection (%)
HR-1	19.5	99.1
HR-2	v. high	v. low
HR-3	v. high	v. low
HR-4	30.3	24

Area Statistics:

Median height : 6527 Å
Mean height : 6283 Å
Surface area : 124.68 µ²
Projected area : 100.00 µ²
Volume : 62.83 µ³
Rms rough : 1161 Å
Ave rough : 865 Å

Figure 11.22 Atomic force stylus profilometry of membrane HR-1-Dry. Stylus contact (IC-AFM) with membrane surface. Top photo - AFM showing three dimensional rendering of membrane surface. Bottom photo - Micrograph showing the topography of a selected membrane area and a summary of the surface area statistics taken 15 days after membrane processing.

141

Histogram

(N)
4000

3000

2000

1000

0
0   0.2   0.4   0.6   0.8   1
Height   (µ)

µm
1.00

0.50

0.00

8

8

µm   4

4   µm

0   0

µm
1.0
0.8
0.6
0.4
0.2
0.0

0   2   4   6   8   10 µm

Selected Area

Bearing Ratio

(%)
80

60

40

20

0
0   0.2   0.4   0.6   0.8   1
Height   (µ)

Area Statistics:

Median height :   4971 Å
Mean height :   4754 Å
Surface area : 198.17 µ²
Projected area : 100.00 µ²
Volume : 47.54 µ³
Rms rough :   1262 Å
Ave rough :   990 Å

Figure 11.23 Atomic force stylus profilometry of membrane HR-2-Dry. Stylus contact (IC-AFM) with membrane surface. Top photo - AFM showing three dimensional rendering of membrane surface. Bottom photo - Micrograph showing the topography of a selected membrane area and a summary of the surface area statistics taken 15 days after membrane processing.

Area Statistics:

Median height :   6678 Å
Mean height :   6579 Å
Surface area : 118.90 µ²
Projected area : 100.00 µ²
Volume : 65.79 µ³
Rms rough :   1185 Å
Ave rough :   928 Å

Figure 11.24   Atomic force stylus profilometry of membrane HR-3-Dry. Stylus
contact (IC-AFM) with membrane surface. Top photo - AFM showing
three dimensional rendering of membrane surface. Bottom photo -
Micrograph showing the topography of a selected membrane area
and a summary of the surface area statistics taken 15 days after
membrane processing.

143

Area Statistics:

Median height : 9983 Å
Mean height : 9886 Å
Surface area : 124.32 μ²
Projected area : 100.00 μ²
Volume : 98.86 μ³
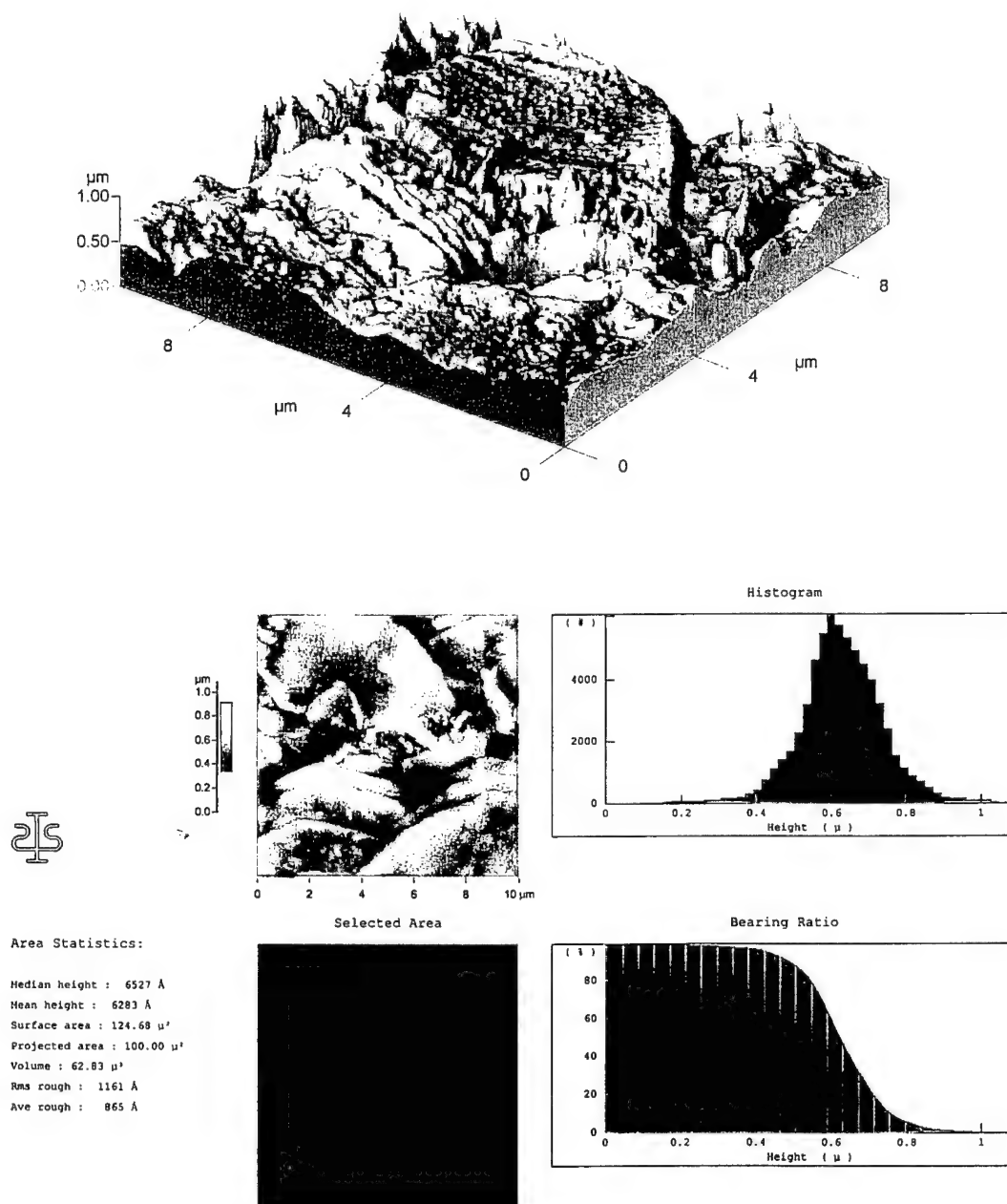Rms rough : 1570 Å
Ave rough : 1191 Å

Figure 11.25 Atomic force stylus profilometry of membrane HR-4-Dry. Stylus contact (IC-AFM) with membrane surface. Top photo - AFM showing three dimensional rendering of membrane surface. Bottom photo - Micrograph showing the topography of a selected membrane area and a summary of the surface area statistics taken 10 days after membrane processing.
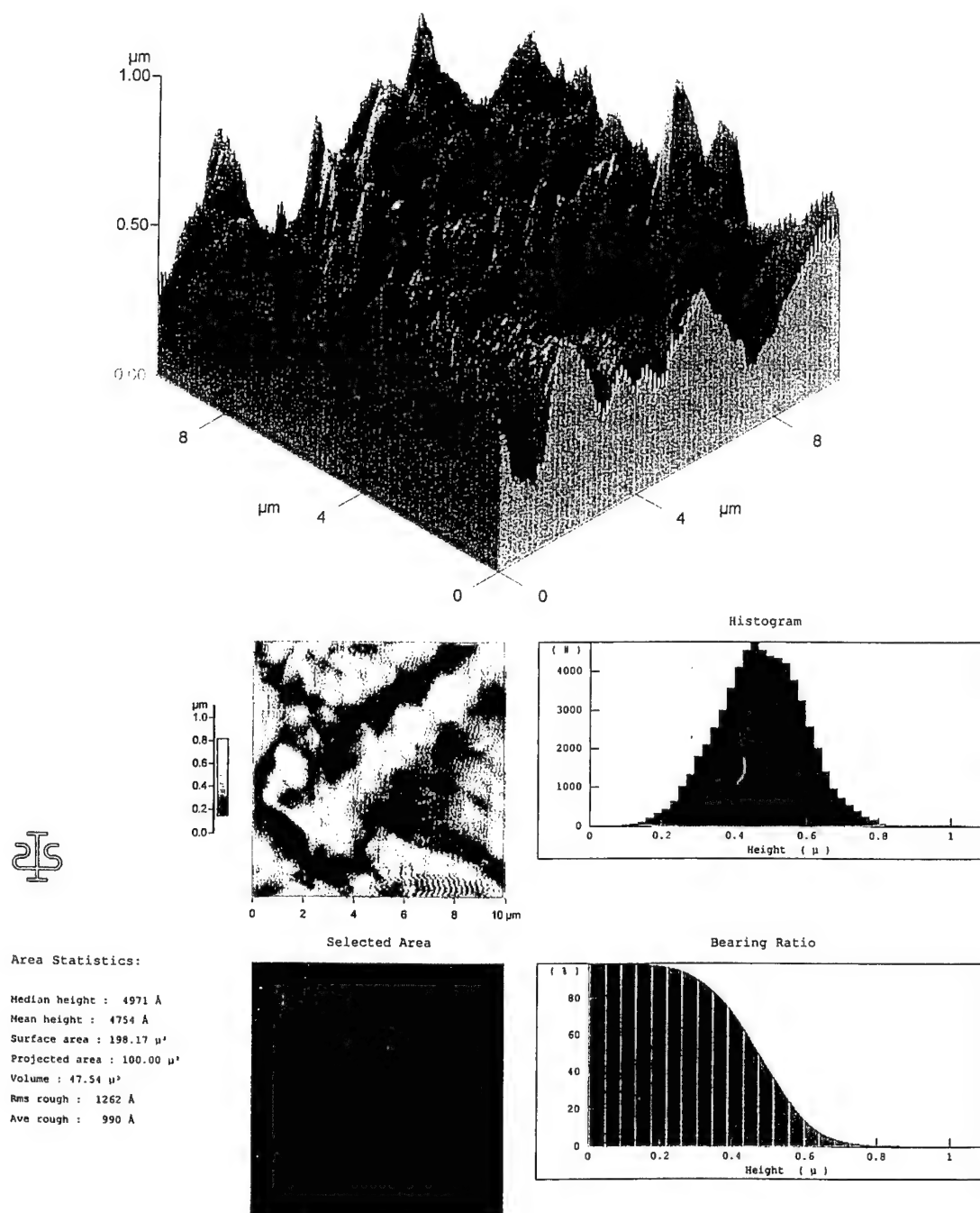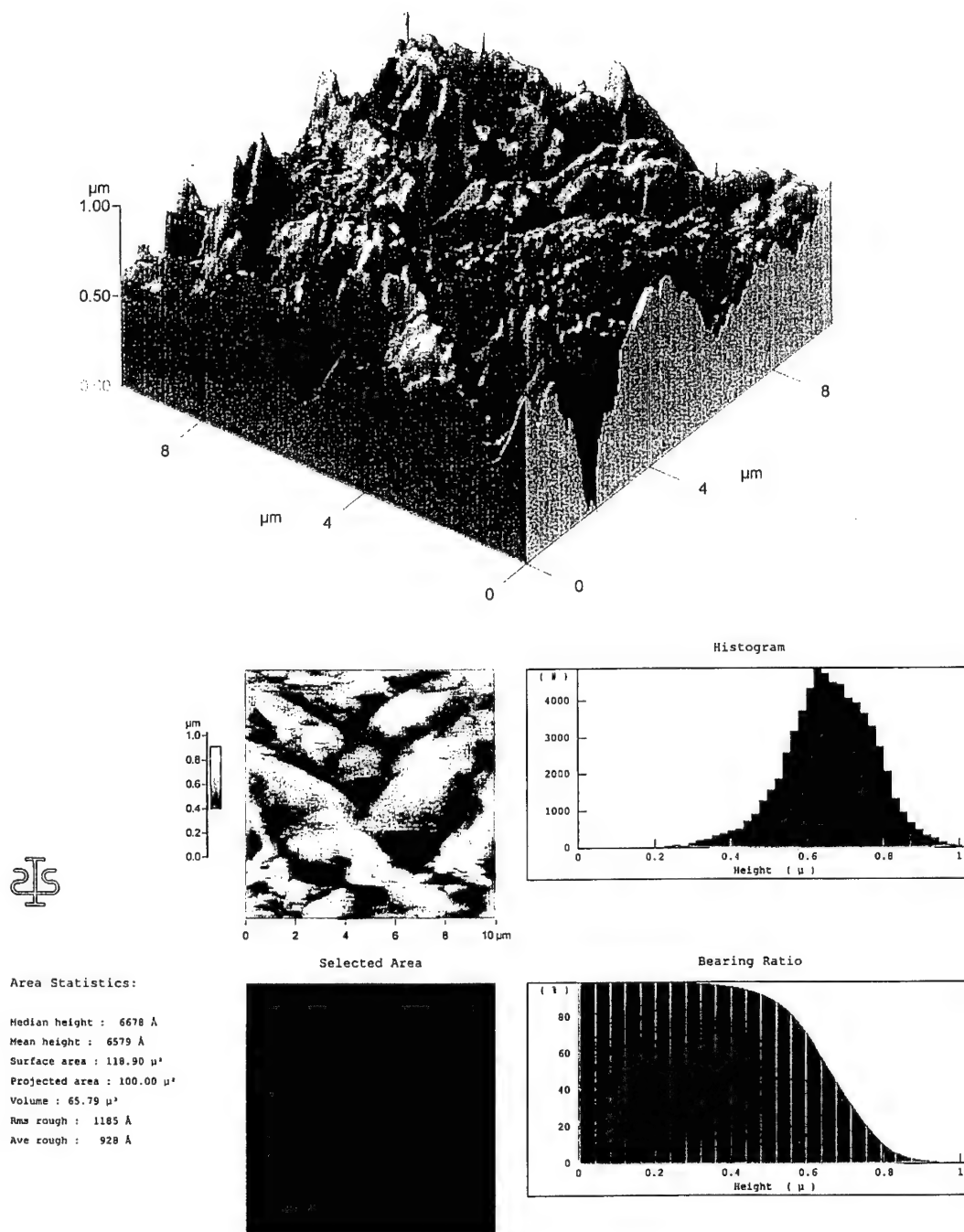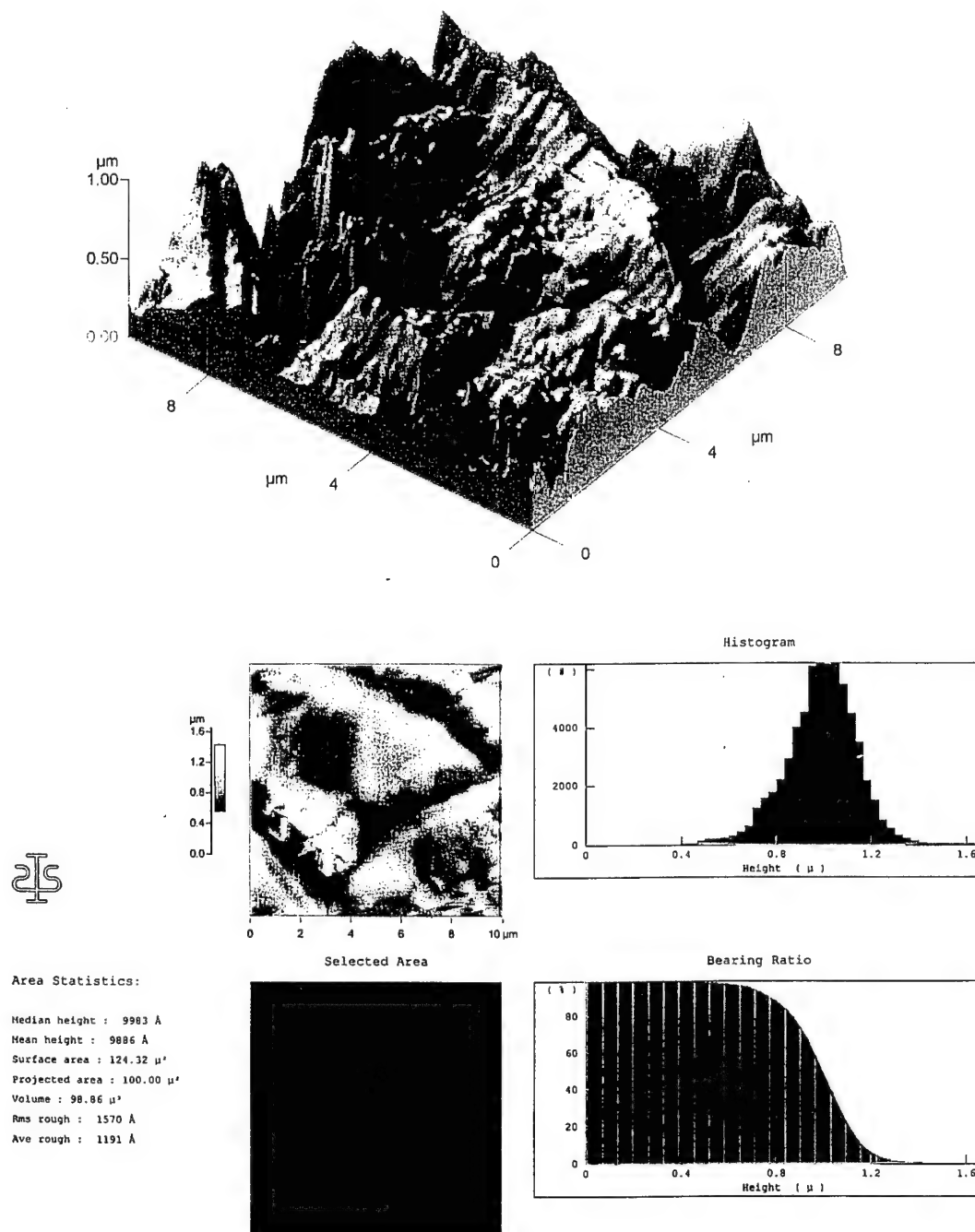
144

11.4 Membrane Fouling - Bacterial Attachment to Membrane Surfaces

The PA membranes exhibit greater biofouling than other types of RO membranes. Biofouling of new membranes can be predicted by a laboratory procedure that determines the number of bacteria that attach to a membrane surface. This procedure is very useful in the development of new composite membranes and is being used for that purpose during this program.[1]

The attachment behavior of Mycobacterium strain BT 12-100 to the experimental membranes was determined using a modification of the disk adhesion assay procedure described by Ridgway and Safarik.[7] Briefly, the mycobacteria were uniformly radiolabeled by growing cells for 48 hr in a mannitol+mineral salts (MS) medium containing 5 μCi/mL of (35)S-sulfate. Labeled cells were harvested by centrifugation and resuspended in MS medium lacking a carbon source (to limit growth during the adhesion assay). The cell attachment assay was carried out using screw-capped 16 x 125 mm plastic disposable test tubes ("reaction vessels") whose cap liners were replaced with a 1-in. diameter disk of the experimental polymer membrane. When the cap was placed on the tube, the active semipermeable surface of the membrane was facing toward the tube interior. The inward orientation of the membrane ensures that cell attachment to only that surface was measured. The bottom two thirds of the tube was cut off such that when the tube was placed in an inverted position, reagents could be readily added or withdrawn. Five mL of MS buffer (lacking mannitol) was placed in each tube at T=0. An adjustable aliquot of the washed radiolabeled cell suspension was added to initiate the adhesion assay. The specific conditions of the assay are summarized in Table 11.4.

Table 11.4

Summary of Bacterial Attachment Assay Parameters

Assay Parameter	Value or Description
Test organism	Mycobacterium strain BT12-100
Buffer system	MS buffer (no carbon source)
Buffer pH	7.0
Assay temperature	28°C
Agitation	Gyratory shaking at 200 rpm
Cell concentration at T=0	About 10^8/mL at T=0
Contact time	5 hr
Rinse protocol	Two consecutive 5 mL rinses with MS buffer
Label quantitation	Liquid scintillation counting

The above cell attachment assay method provided useful quantitative information concerning the inherent affinity of the fouling bacterium for the polymer membrane surface. Hydrodynamic influences, which could complicate the interpretation of the results, were purposely eliminated from the assay since the test membranes experience no applied pressures or fluxes during the assay.

The results of the bacterial attachment study to membranes HR-1, HR-2, HR-3 and HR-4, along with a summary of the surface roughness, are shown in Figure 11.26. For the most part, the surface roughness of the cross-linked HR-1 membrane was quite similar to that of the linear HR-2, HR-3 and HR-4 membranes.

Bacterial attachment for HR-1, HR-2 and HR-3 membranes were very similar. However, composite membrane HR-4, showed much greater bacterial attachment even though the surface roughness was the similar for all membranes. It is believed that the hydrophobic nature of the thin film formed from MPD and terephthaloyl dichloride is greater.

11.5 Mechanism for Controlling Membrane Surface Roughness

The surface structure of the TMC and CTPC film formed during membrane processing is very rough, having many high peaks and valleys. As a result, the membrane surface area is several times greater than that of a smooth membrane surface. It is commonly hypothesized that the high water flux exhibited by these composite membranes is due to the increase in surface area although there has been no morphological study to confirm this. The mechanism responsible for the formation of surface roughness has not been established. During this program it was shown that surface roughness is not due to:

- The hydrocarbon solvent used in the acid chloride phase during the interfacial polymerization and formation of the thin film. There is little, if any, difference in the surface roughness when the hydrocarbon is hexane, isopar or freon.

- Cross-linking of the polyamide thin-film structure. Non-cross-linked thin films formed interfacially between difunctional amines and difunctional acid chlorides also exhibited very rough surfaces when examined by AFM.

- Post-treatment processes following the interfacial formation of the thin film. It was shown by AFM, that the surface roughness is the same regardless if the membrane is dried immediately after the interfacial formation or if the membrane is subsequently washed in DI water and/or acid treated.
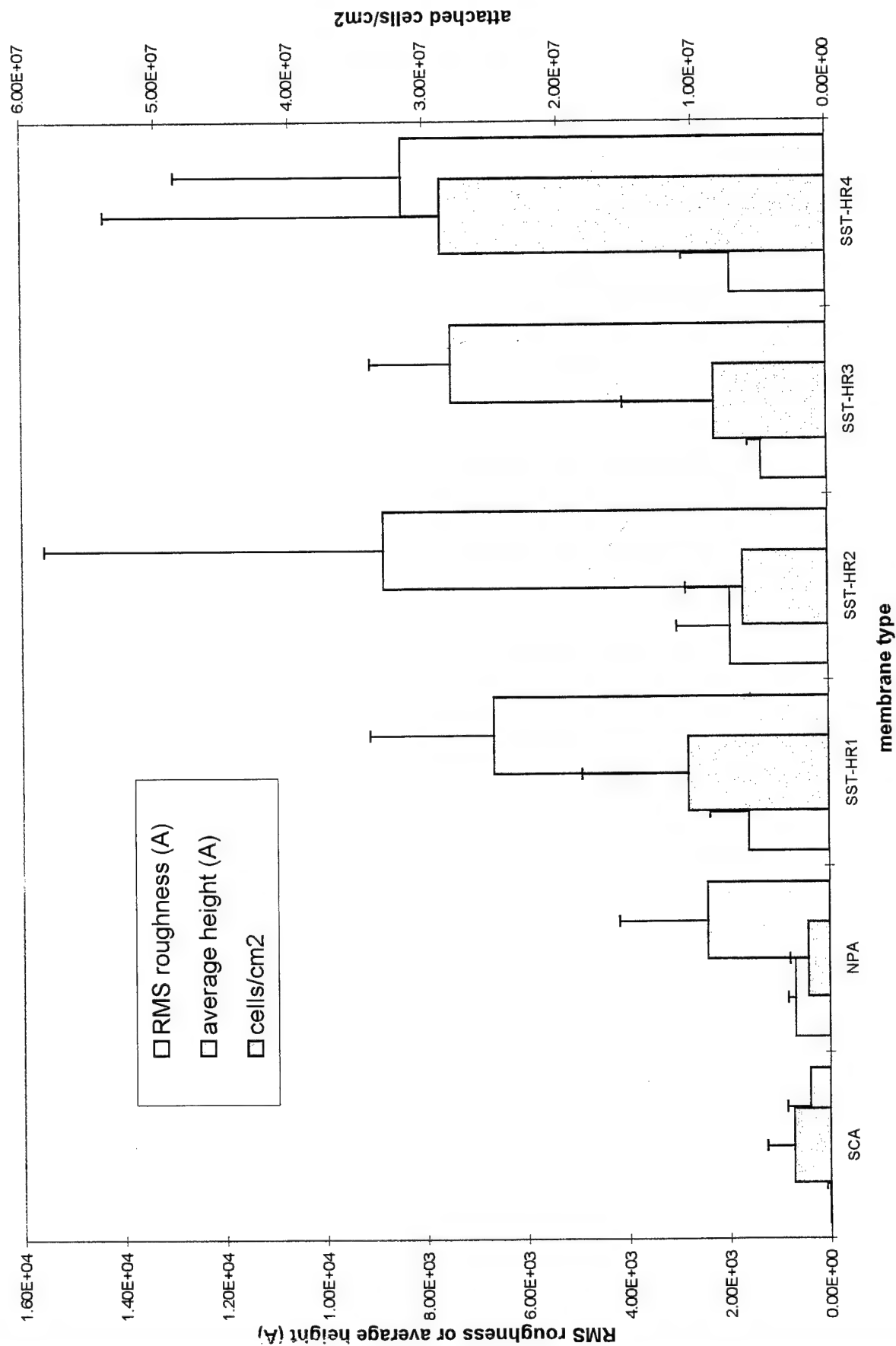
146

Figure 11.26   Comparison of the root mean square surface roughness (RMS), the average surface peak height and the number of bacterial cells attached on the surfaces of an asymmetric CA membrane (SCA) and composite membranes HR-1, HR-2, HR-3 and HR-4.

147

Some of the variables affecting the interfacial reaction between MPD and TMC in the formation of the membrane are:

1. Chemical reaction rates
2. Precipitation rate of PA polymer (solubility)
3. Impurities in reactants and solvents
4. **Transfer rate of MPD**
5. Partition potential of reactants
6. Concentration rations of phases
7. Mixing
8. Concentration level
9. Hydrolysis of TMC
10. Transfer rate of salts
11. Fluid and polymer solution viscosities
12. **Polarity of solvent**
13. Interfacial energy barriers

Many of the aforementioned variables are interrelated, and most are expected to have an influence on the surface morphology of the polymer that is formed during the interfacial formation. Initially it was decided to determine the influences of Items 4 and 12 on determining surface roughness of the thin barrier; that is, polarity of solvent and transfer rate of MPD. The polarity of the aqueous MPD phase was modified by incorporating varying amounts of isopropanol (IPA) in this phase during the interfacial formation of the PA barrier.

To increase the polarity of the aqueous MPD phase, varying amounts of IPA were added to the aqueous amine solution. Membranes were prepared by interfacially reacting the alcoholic amine solution with TMC in hexane. With this exception, the membranes were prepared using the standard methods of preparation and post treatment. Subsequently the membranes were evaluated in RO and the surfaces of the PA barrier were examined by AFM to determine surface roughness. A series of six membranes were prepared with MPD solutions containing 0, 5, 10, 20, 40, and 80 wt-% IPA, respectively. It was found that the RO performance of the membranes was not dramatically changed when up to 10 wt-% IPA was incorporated into the aqueous amine solution; however, when 40 wt-% and greater was added, the transport properties changed dramatically. The results are summarized in Table 11.5.

The surface analysis/morphology of each of the membranes described in Table 11.5 was determined by AFM. Dramatic structural changes were observed on the surfaces of the membranes as the IPA content of the MPD solution was increased. An overview of these changes can be seen in the presentations of the membrane surfaces as shown on the 30-μm and 10-μm square images in Figures 11.27 and 11.28, respectively.

148

The 3-D and region analysis of the surfaces are shown in Figures 11.29 through 11.40. It appears that smaller amounts of IPA reduce both the surface roughness and area. However, when the IPA was further increased, the surface roughness and area increases with a very significant change in structure. At higher IPA levels, raised hollow volcano-like structures developed that appear to be open in the center. Apparently, the open center of these structures penetrates the thin barrier film as the rejection properties of the membrane increase dramatically.

It can be concluded from this study that the surface structure of the film can be modified by altering the diffusion rates of the reactant/reactants, MPD and/or TMC, in the interfacial reaction zone. This approach for modifying the surface of the thin semipermeable barrier, to reduce membrane fouling, has great potential.

Table 11.5

RO Performance of Composite Membrane

Modification of Membrane Surface Morphology

Test Conditions: 225 psi applied pressure, 2,000 mg/L sodium chloride feed, 25°C, pH = 7.0, 0.9 gal/min feed flow

Membrane Identification	Polyamide Formation Monomers	Reverse Osmosis Performance	
		Water Flux (gfd)	Rejection, (%)
HR-26	2 wt-% MPD 0.15 wt-% TMC	38.6	98.8
HR-27	2 wt-% MPD 0.15 wt-% TMC 5 wt-% IPA	35.1	98.3
HR-28	2 wt-% MPD 0.15 wt-% TMC 10 wt-% IPA	46.4	96.9
HR-29	2 wt-% MPD 0.15 wt-% TMC 20 wt-% IPA	31.2	94.9
HR-30	2 wt-% MPD 0.15 wt-% TMC 40 wt-% IPA	72.7	10
HR-31	2 wt-% MPD 0.15 wt-% TMC 80 wt-% IPA	22.2	27.1

MPD = *m*-phenylenediamine
TMC = trimesoyl chloride
IPA= isopropanol
A value for polysulfone support membrane = 1737 x 10^{-5} g/cm^2-sec-atm

Membrane post treatment sequence:
(1) 2 wt-% oxalic acid, 30 min, 80°C
(2) 80*C, deionized water, 80°C,
(3) 3 wt-% glycerin, 15 min, 80°C
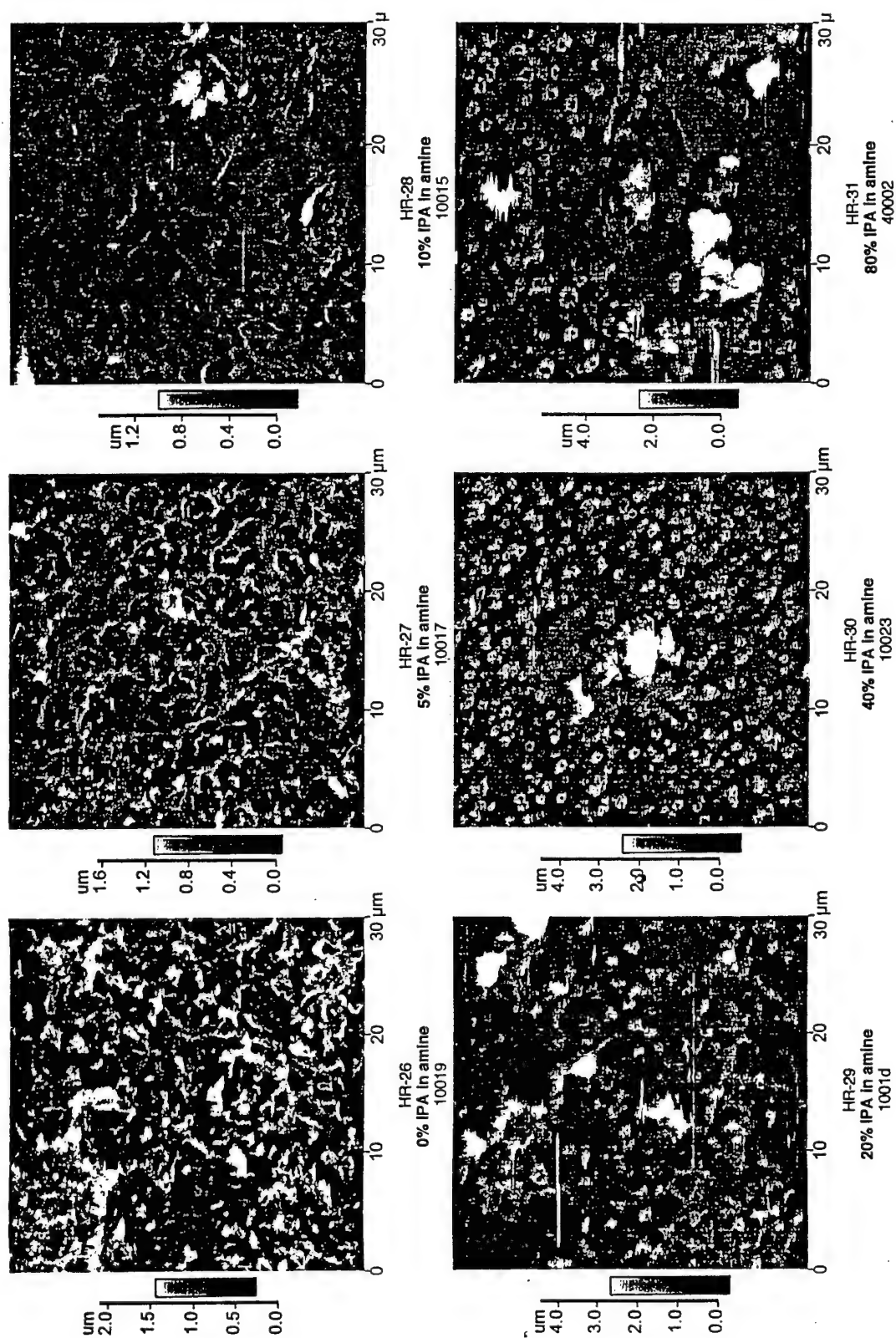
Figure 11.27 Atomic Force Micrographs: Changes in surface structure as a function of IPA concentration in the aqueous MPD reaction solution during interfacial polymerization and formation of membranes HR-26, HR-27, HR-28, HR-30 and HR-31.

151
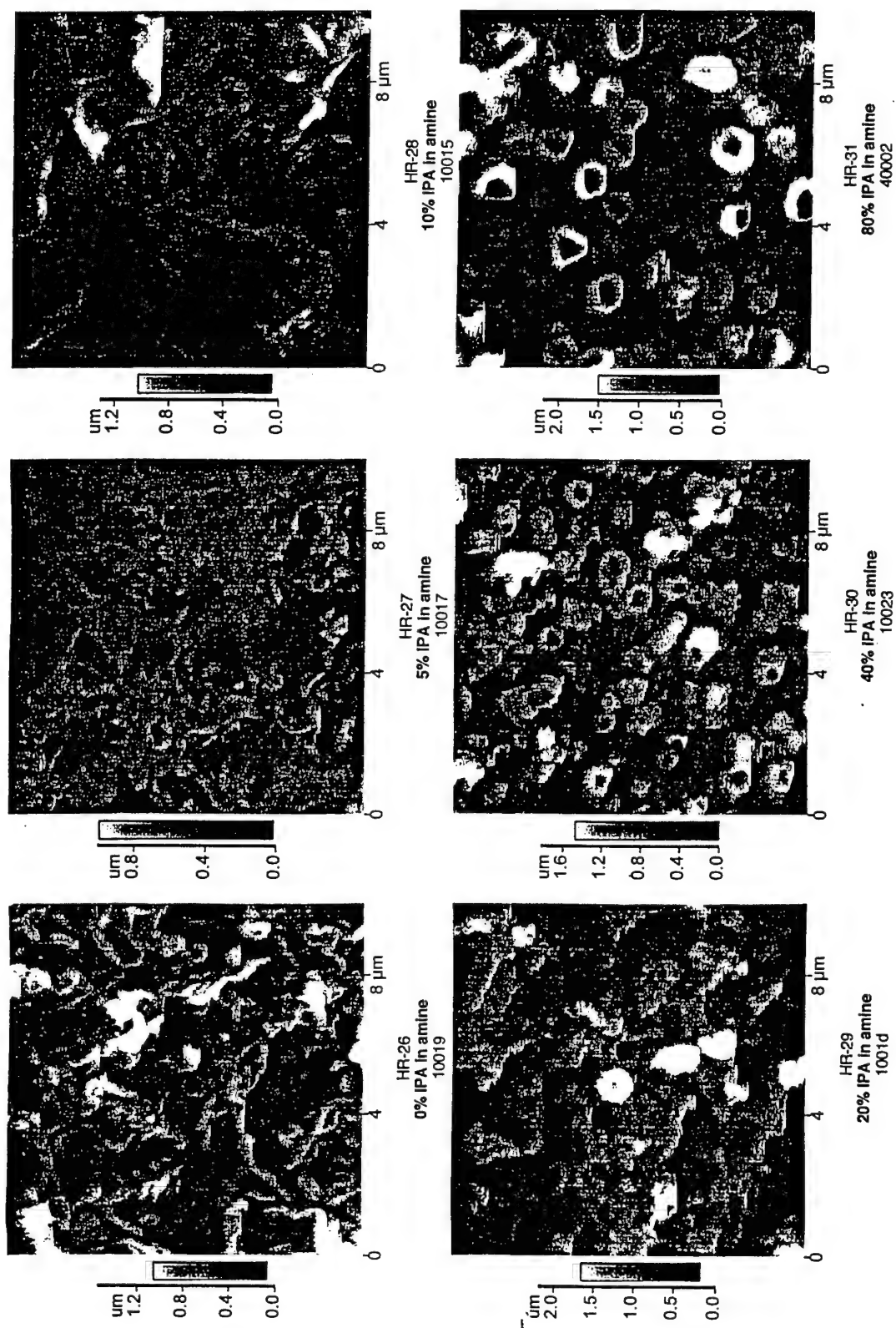
Figure 11.28   Atomic Force Micrographs: Changes in surface structure as a function of IPA concentration in the aqueous MPD reaction solution during interfacial polymerization and formation of membranes HR-26, HR-27, HR-28, HR-30 and HR-31.

152

Figure 11.29   3-D Analysis: Atomic force profilometry of HR-26 membrane. Stylus not in contact with membrane surface. Micrograph (10005) showing three dimensional rendering of membrane surface at 10 µm scale. Membrane area shown in bottom photo (10005) of Figure 11.30 scanned for 3-D analysis.

153

Figure 11.30   Region Analysis: Atomic force profilometry of HR-26 membrane. Stylus not in contact with membrane surface. Top Photo (10019) - Micrograph showing surface peak height histogram at 30 μm scale. Bottom photo (10005) - Micrograph showing surface peak height histogram at 10 μm scale. Three dimensional rendering of this area shown in Figure 11.29

154

Figure 11.31   3-D Analysis: Atomic force profilometry of HR-27 membrane.   Stylus not in contact with membrane surface.   Top micrograph shows three dimensional rendering of membrane surface at 10 μm scale. Membrane area shown in bottom photo of Figure 11.32 scanned for 3-D analysis.

Figure 11.32   Region Analysis: Atomic force profilometry of HR-27 membrane. Stylus not in contact with membrane surface. Top Photo - Micrograph showing surface peak height histogram at 30 μm scale. Bottom photo - Micrograph showing surface peak height histogram at 10 μm scale. Three dimensional rendering of this area shown in Figure 11.31.

156

Figure 11.33   3-D Analysis: Atomic force profilometry of HR-28 membrane. Stylus not in contact with membrane surface. Top micrograph (10013) showing three dimensional rendering of membrane surface at 10 μm scale. Membrane area shown in bottom photo (10013) of Figure 11.34 scanned for 3-D analysis.

157

Figure 11.34 Region Analysis: Atomic force profilometry of HR-28 membrane. Stylus not in contact with membrane surface. Top Photo (10015) - Micrograph showing surface peak height histogram at 30 μm scale. Bottom photo (10013) - Micrograph showing surface peak height histogram at 10 μm scale. Three dimensional rendering of this area shown in Figure 11.33
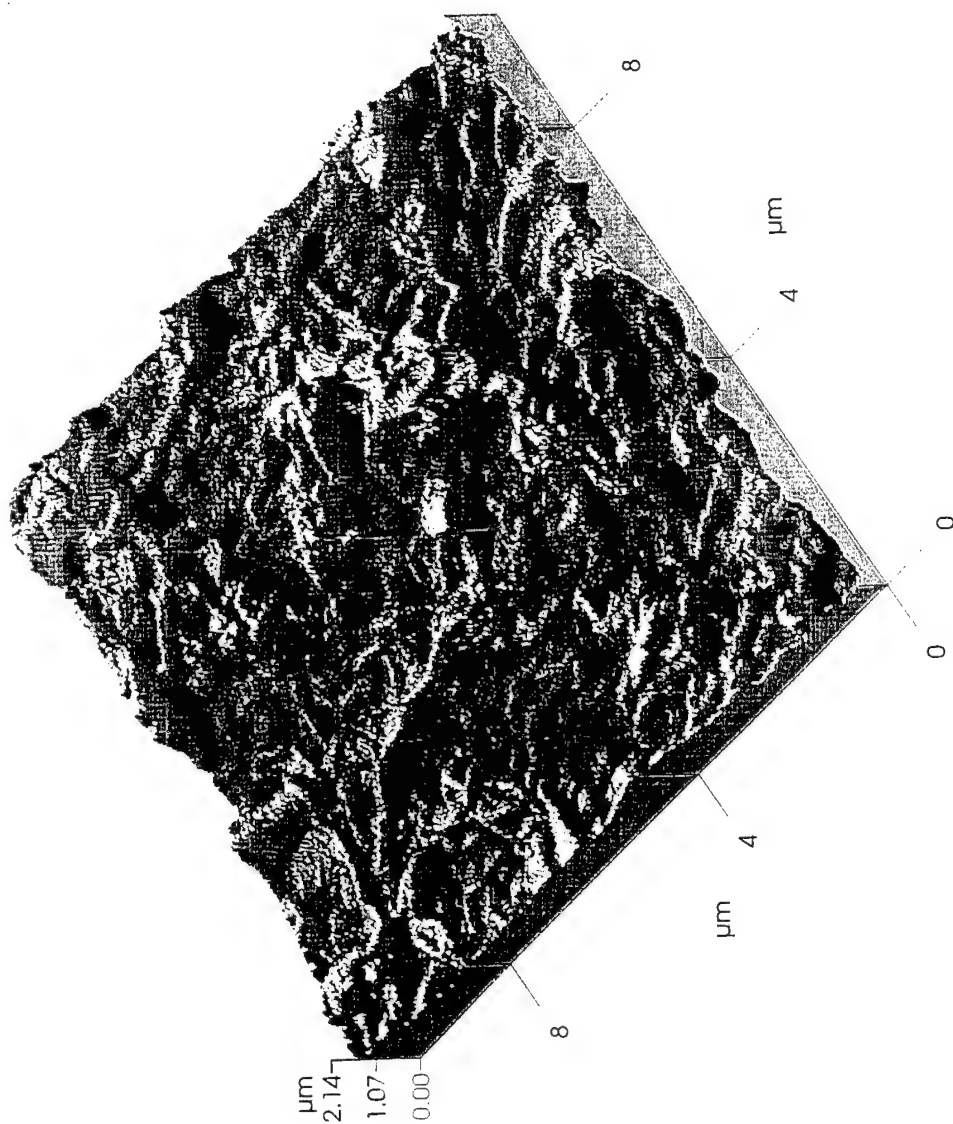
158
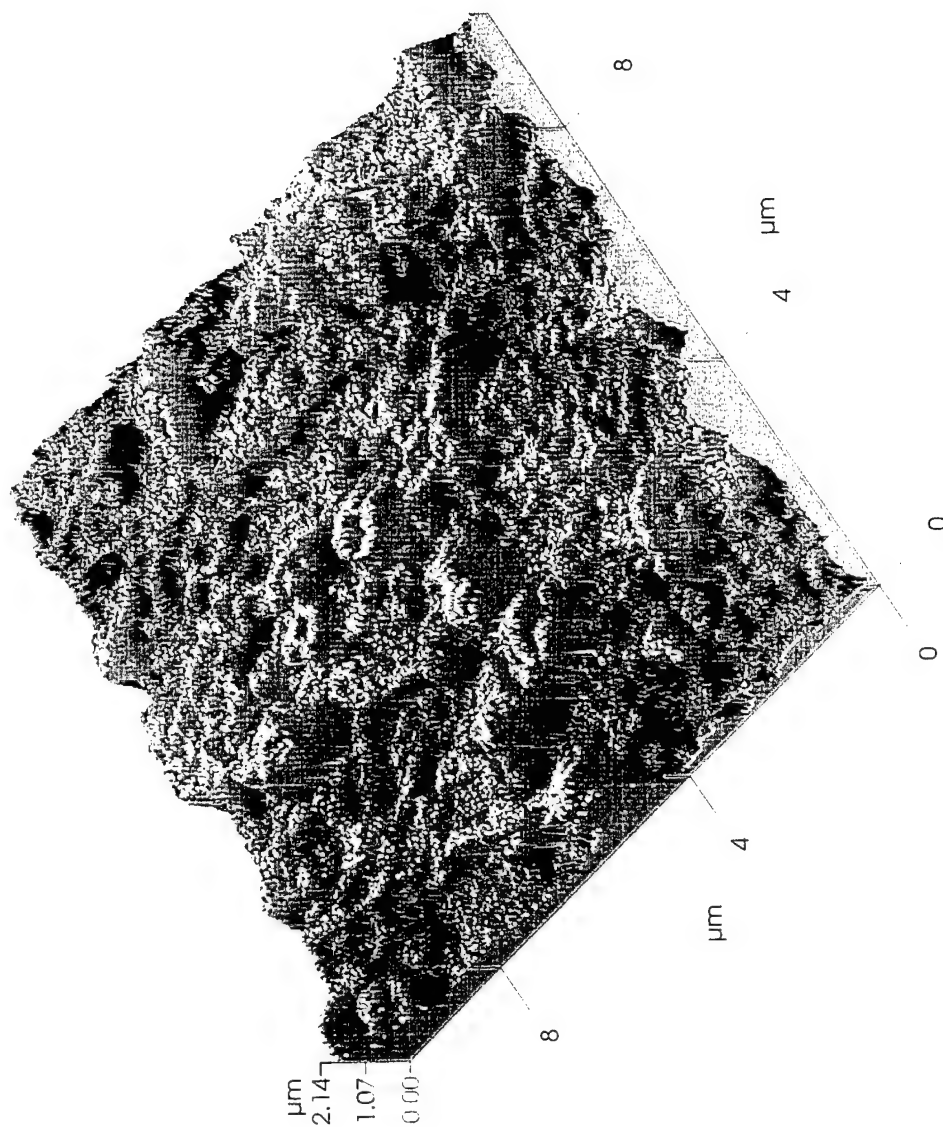
Figure 11.35   3-D Analysis: Atomic force profilometry of HR-29 membrane. Stylus not in contact with membrane surface. Micrograph (1001f) showing three dimensional rendering of membrane surface at 10 μm scale. Membrane area shown in bottom photo (1001f) of Figure 11.36 scanned for 3-D analysis.
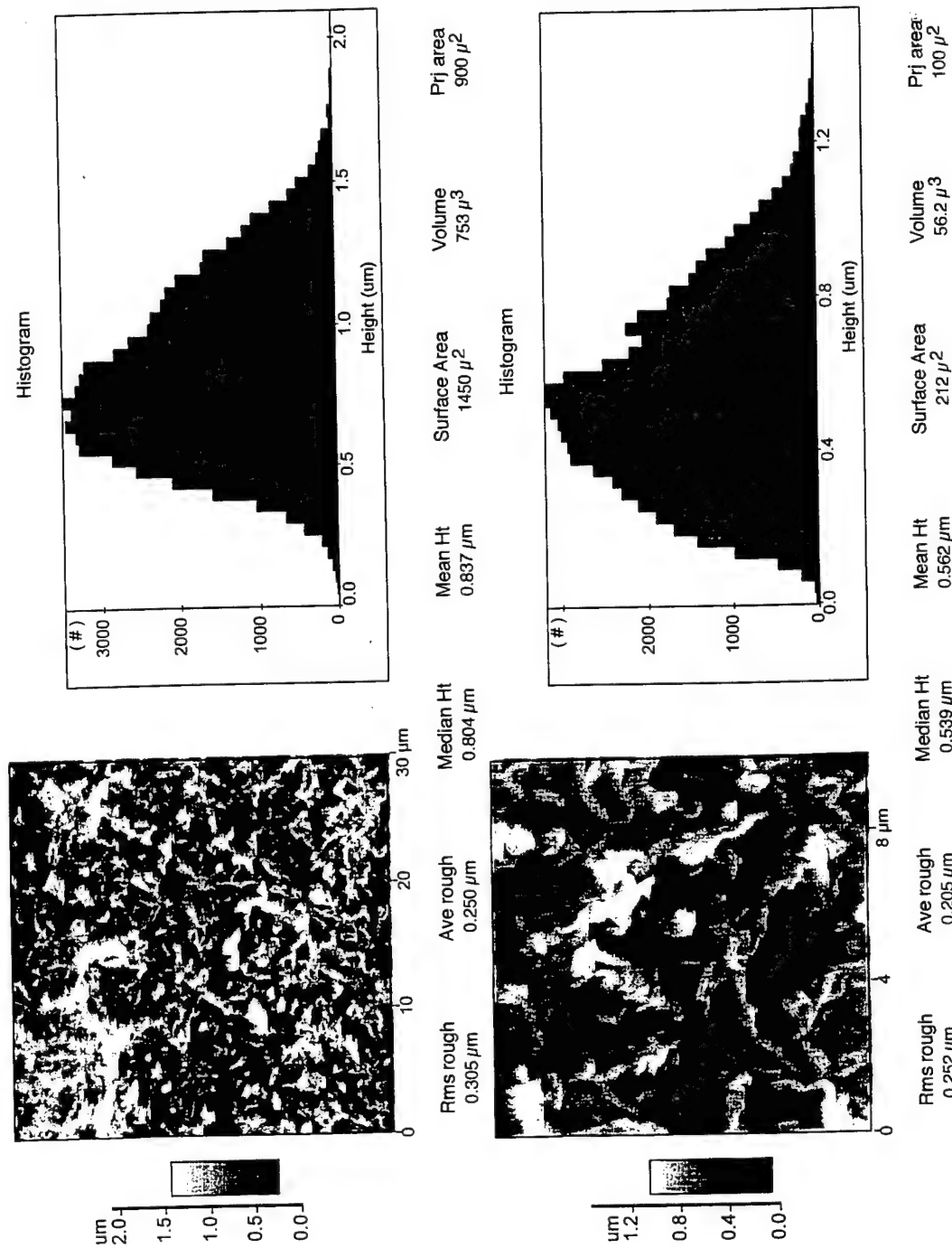
159
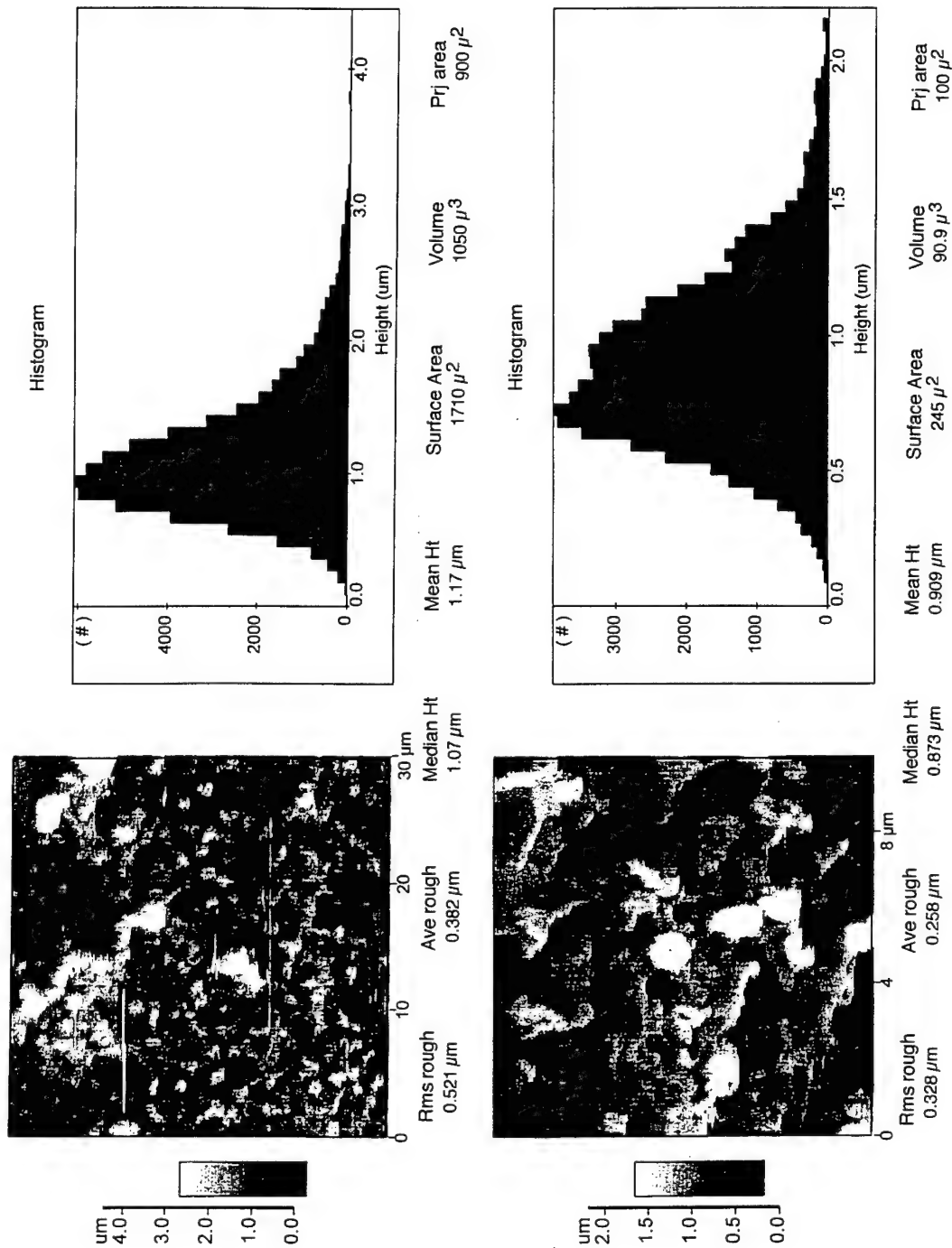
Figure 11.36   Region Analysis: Atomic force profilometry of HR-29 membrane. Stylus not in contact with membrane surface. Top Photo (1002D) - Micrograph showing surface peak height histogram at 30 μm scale. Bottom photo (1001f) - Micrograph showing surface peak height histogram at 10 μm scale. Three dimensional rendering of this area shown in Figure 11.35.
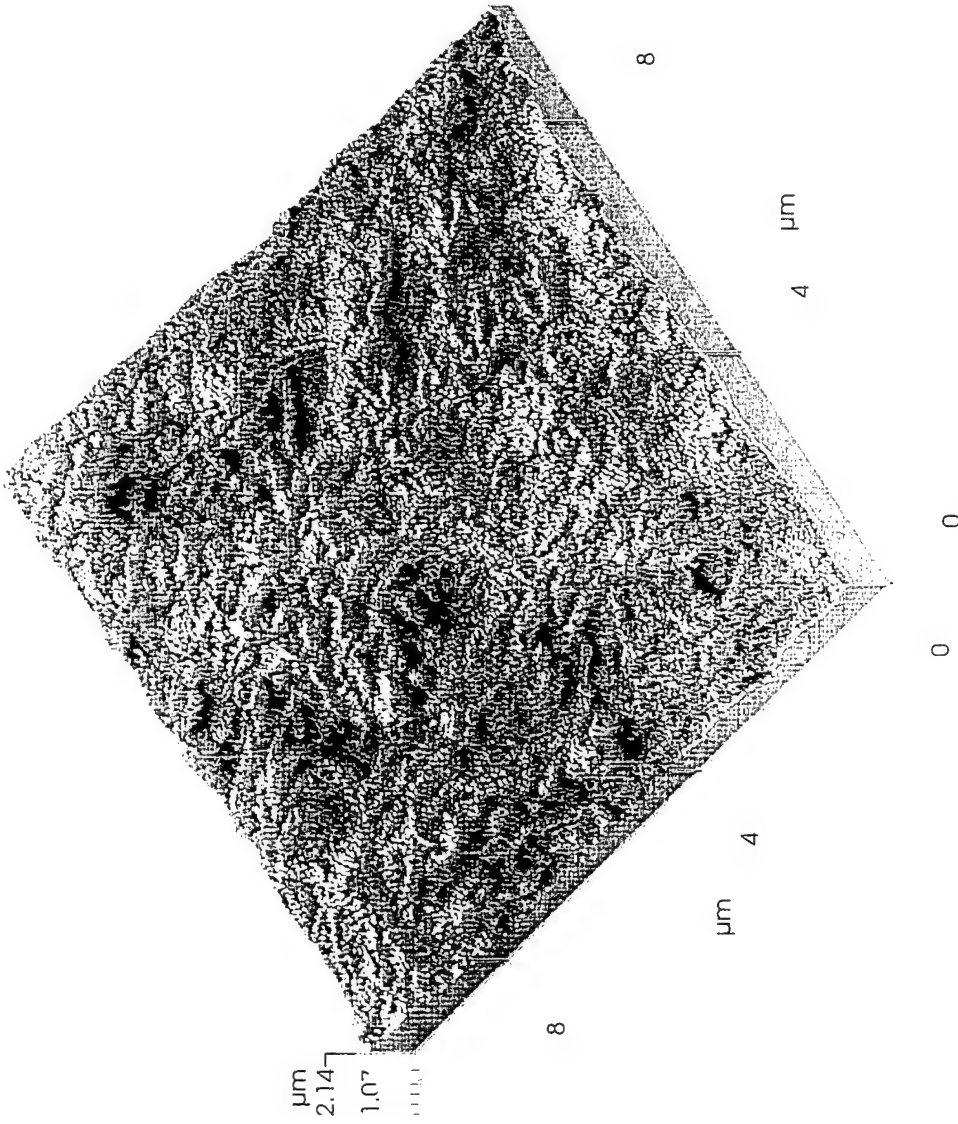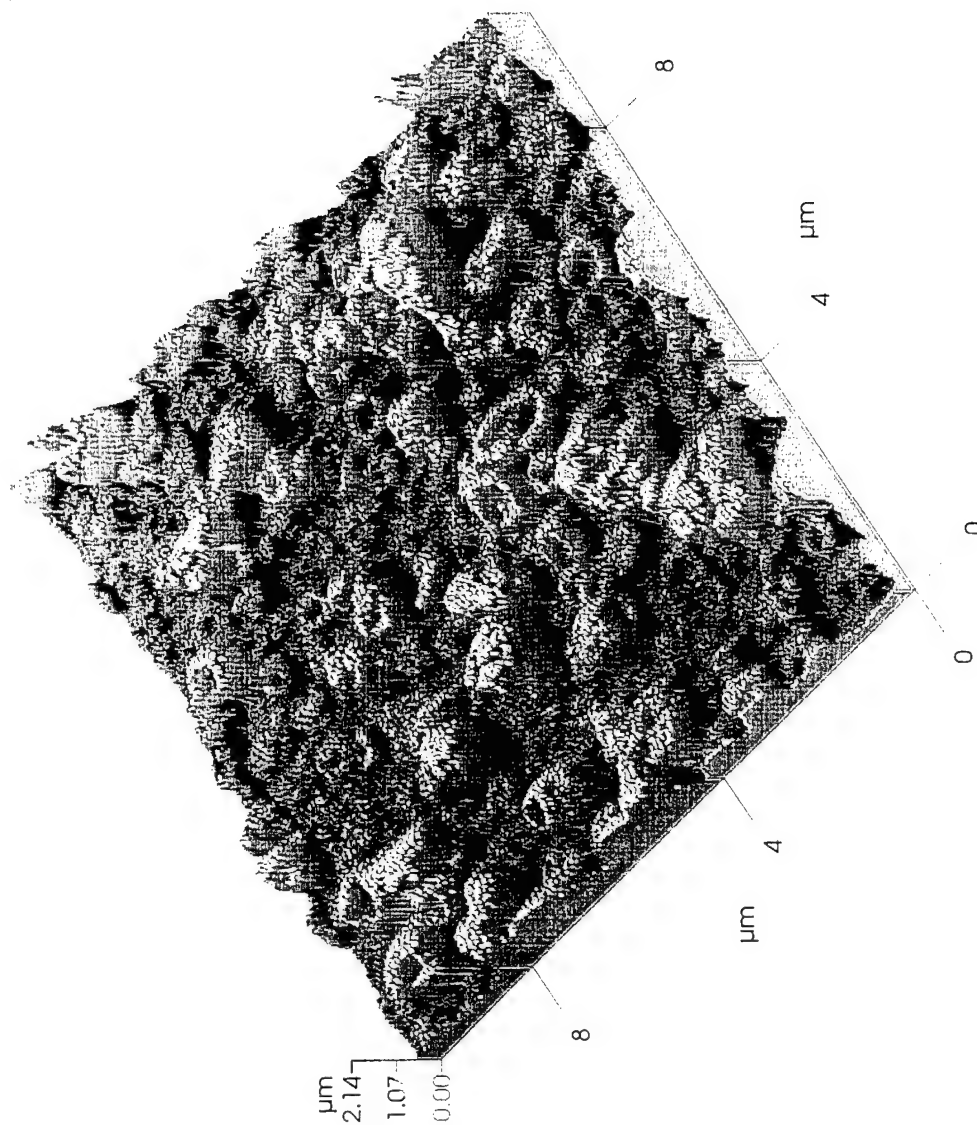
Figure 11.37   3-D Analysis: Atomic force profilometry of HR-30 membrane.   Stylus not in contact with membrane surface.   Micrograph (10025) showing three dimensional rendering of membrane surface at 10 μm scale.   Membrane area shown in bottom photo (10025) of Figure 11.38 scanned for 3-D analysis.
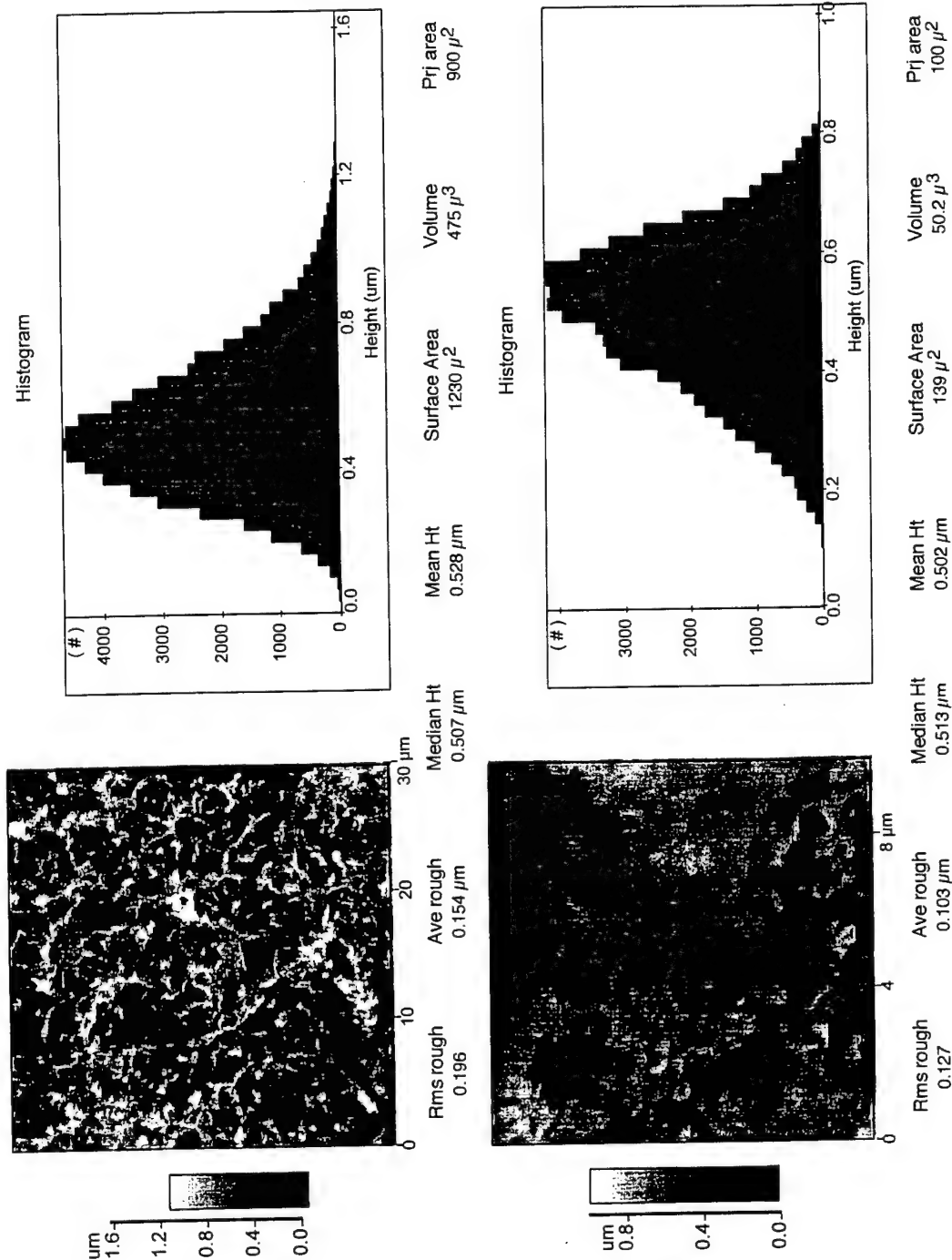
161
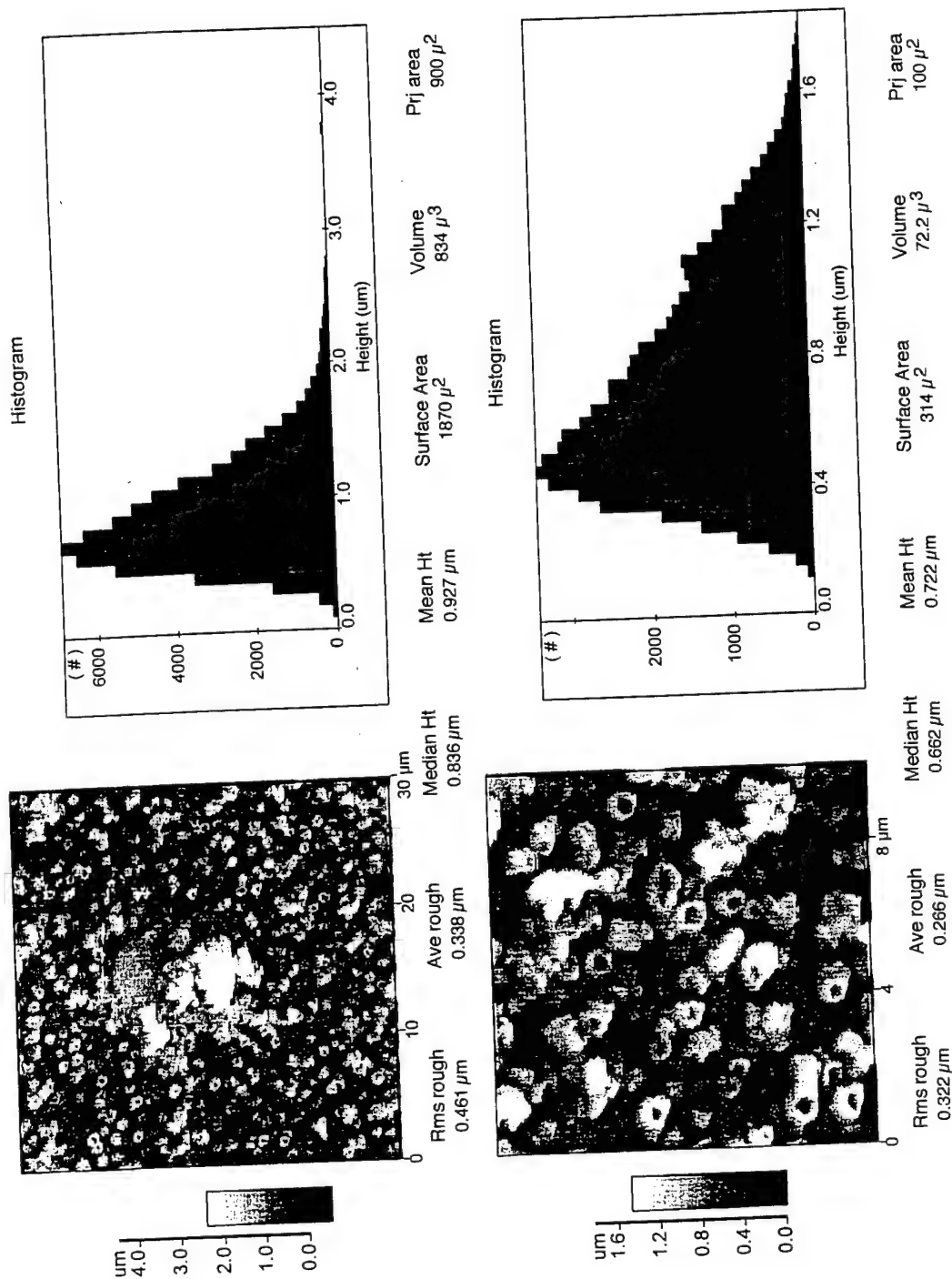
Figure 11.38   Region Analysis: Atomic force profilometry of HR-30 membrane.   Stylus not in contact with membrane surface.   Top Photo (10023) -   Micrograph showing surface peak height histogram at 30 µm scale.   Bottom photo (10025) - Micrograph showing surface peak height histogram at 10 µm scale.   Three dimensional rendering of this area shown in Figure 11.37.
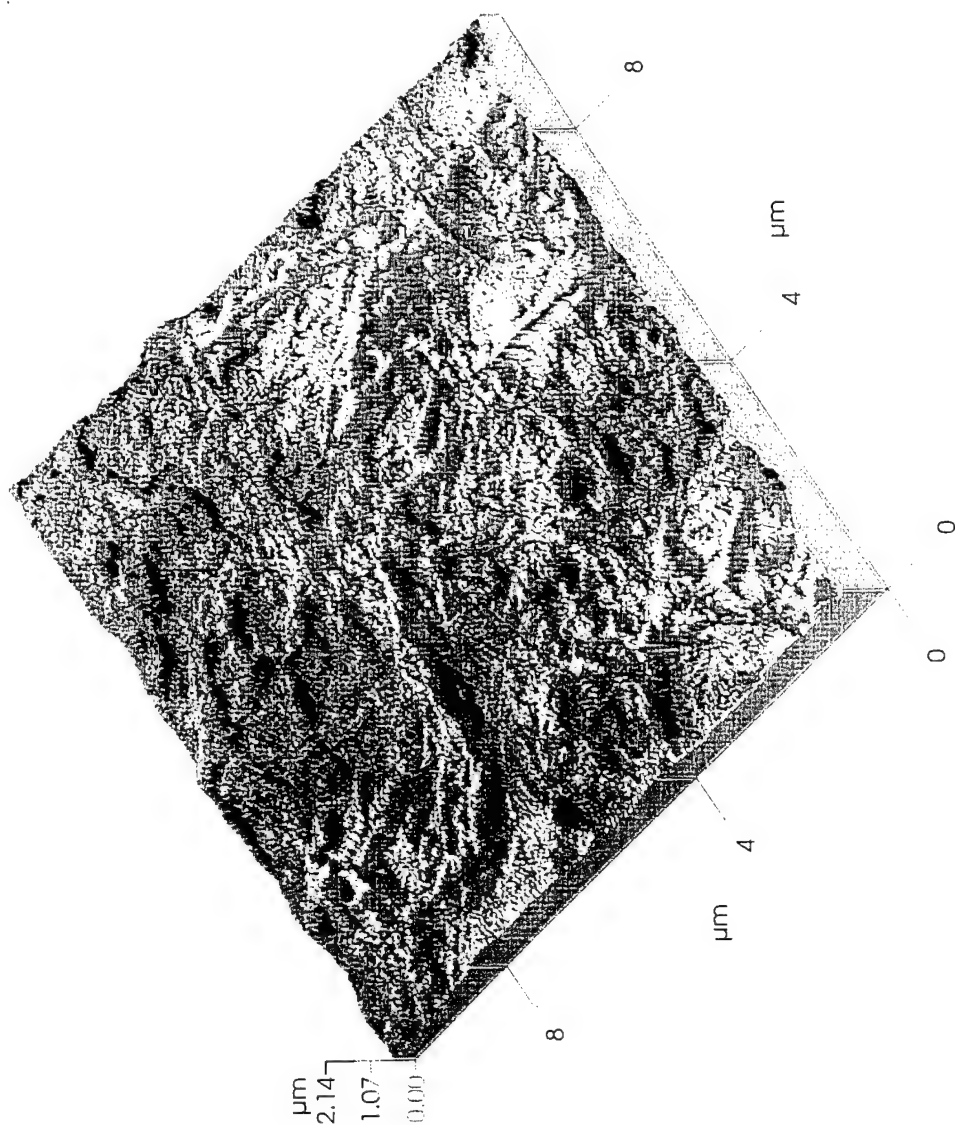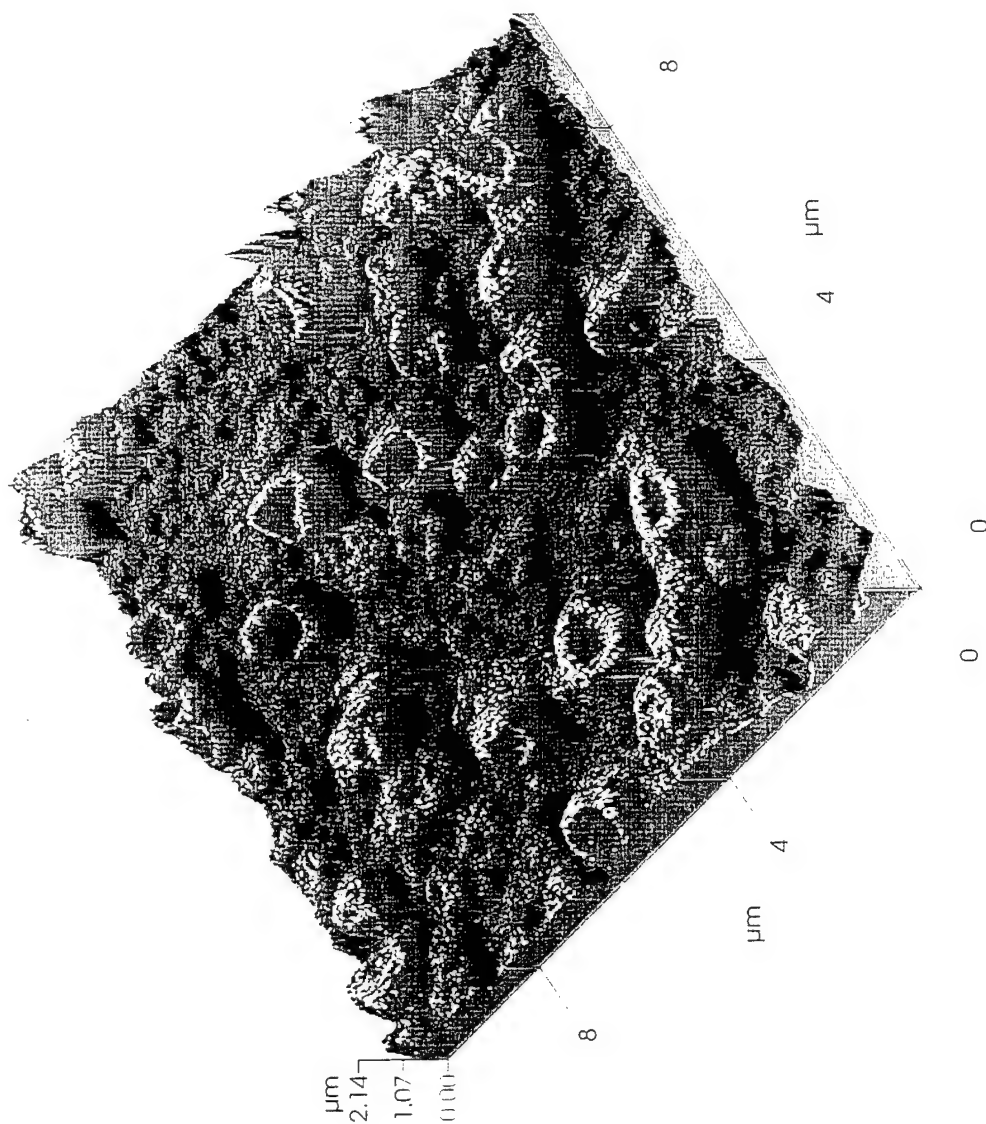
Figure 11.39   3-D Analysis: Atomic force profilometry of HR-31 membrane.   Stylus not in contact with membrane surface.   Micrograph (40006) showing three dimensional rendering of membrane surface at 10 μm scale.   Membrane area shown in bottom photo (40006) of Figure 11.40 scanned for 3-D analysis.
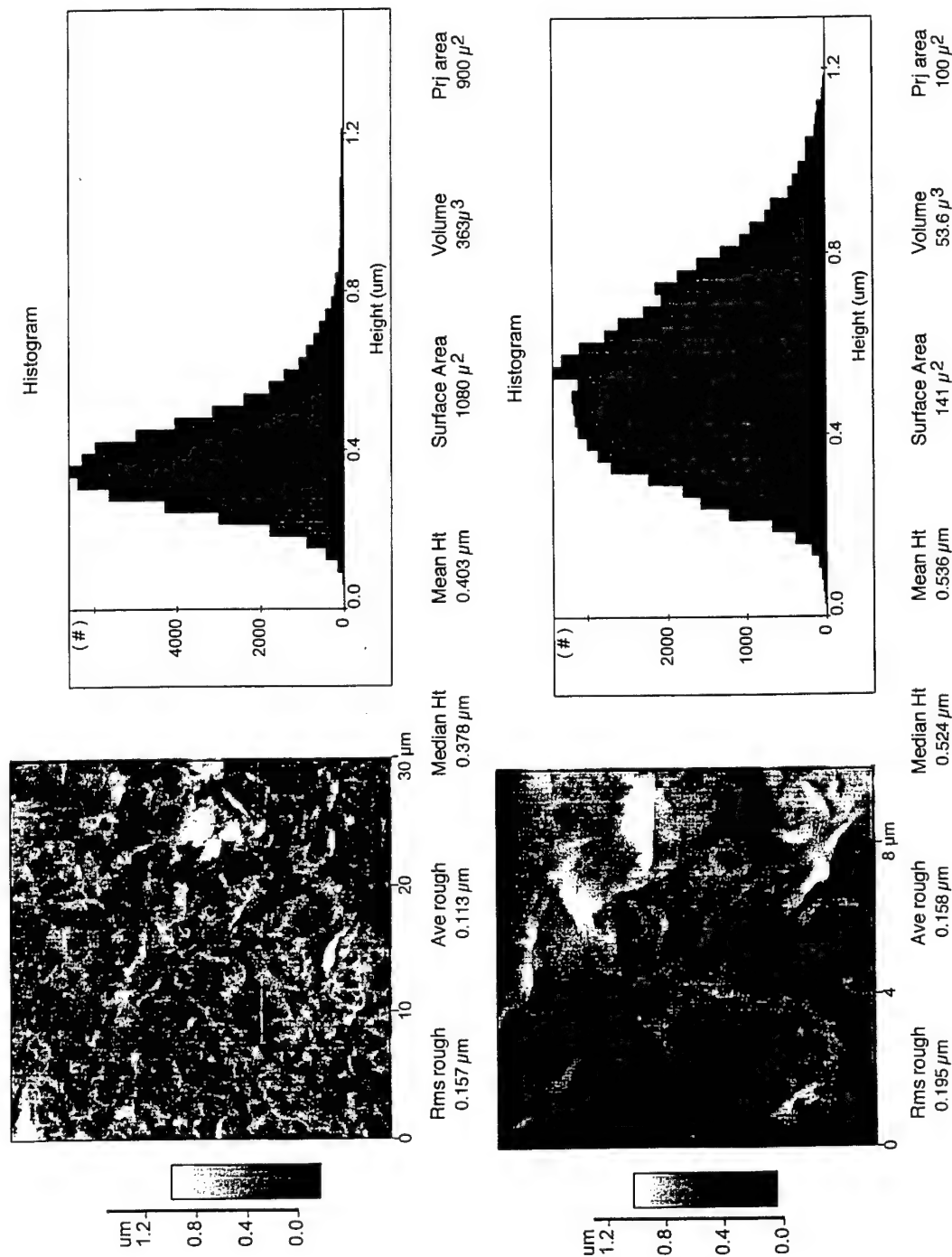
Figure 11.40   Region Analysis: Atomic force profilometry of HR-31 membrane. Stylus not in contact with membrane surface. Top Photo (40002) - Micrograph showing surface peak height histogram at 30 μm scale. Bottom photo (40006f) - Micrograph showing surface peak height histogram at 10 μm scale. Three dimensional rendering of this area shown in Figure 11.39.
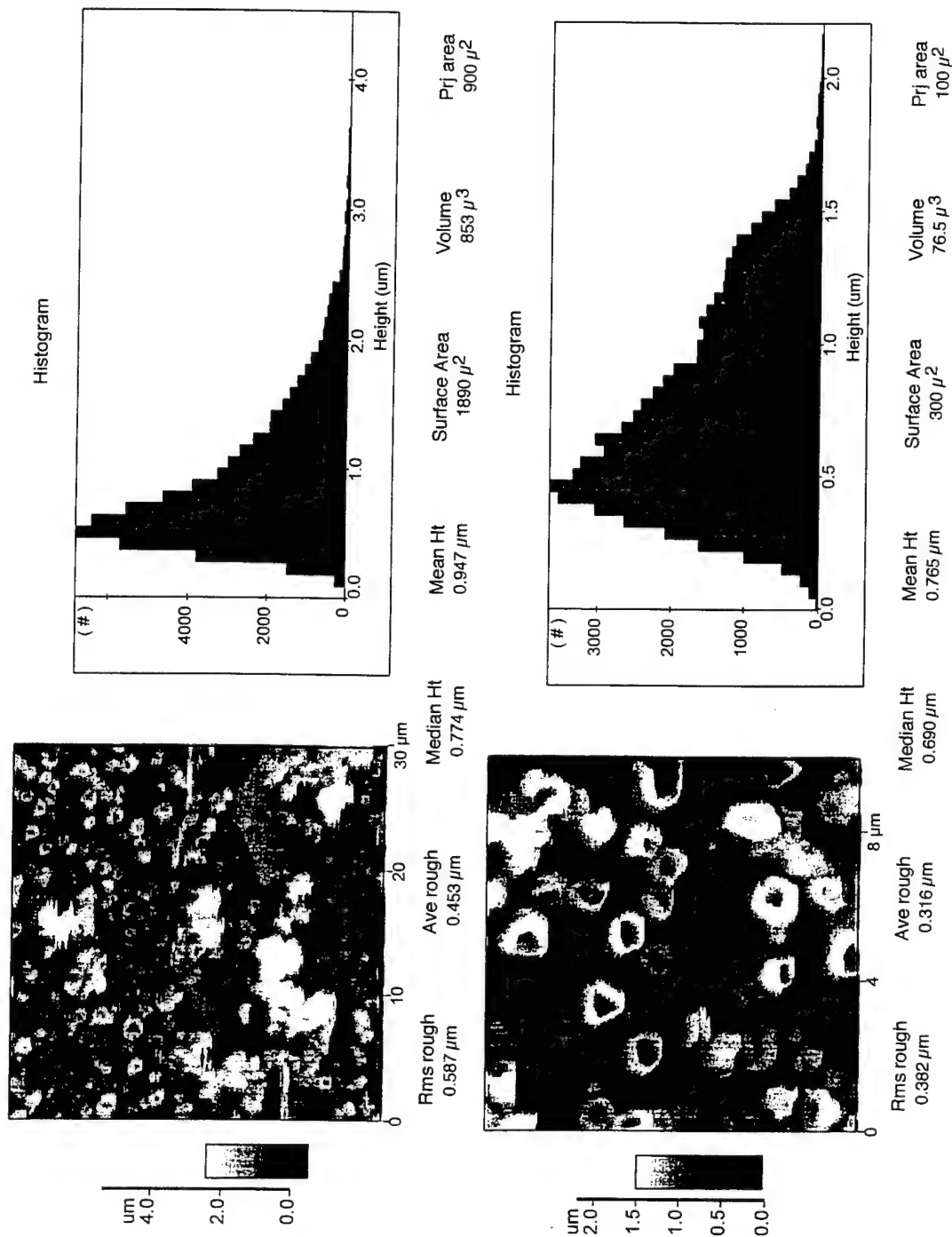
11.6 Effect of MPD Concentration on Relative Carboxylate Density and Relative PA Film Thickness

The effect of MPD concentration on relative carboxylate density, relative PA film thickness and membrane performance was investigated. Experimental CPTC and TMC (control) membranes were tested. The acid chloride concentration was held at 2.36 mM. Membranes made at MPD concentrations of 2.0, 3.0 and 4.0 wt-% were analyzed by ATR/IR spectrometry. Calculations of the relative carboxylate density and the relative film thickness are shown in Figures 11.41 and 11.42, respectively. The relative carboxylate charge density of the CPTC membrane decreased slightly when the MPD concentration was increased from 2.0 to 3.0 wt-% and from 3.0 to 4.0 wt-%. A decrease in this ratio indicates a decrease in free carboxylate groups relative to amide bonds. These results suggest that the MPD at 2.0 wt-% was a limiting factor in the reaction to form a polyamide bond. As the MPD concentration is increased, more amine groups are available to undergo reaction with acid chloride to form amide bonds, leaving less free acid chloride to be hydrolyzed to form carboxylate groups. Therefore, relative carboxylate charge density should decrease with increasing MPD concentration. The relative carboxylate density of the TMC membrane actually increased when the MPD concentration was increased from 2.0 to 3.0 wt-% (Figure 11.41). However, the carboxylate density did decrease when the MPD concentration was increased to 4.0 wt-%. Both CPTC and TMC membrane made with 4.0 wt-% MPD had a carboxylate density less than the FilmTec membrane.

The relative film thickness of the CPTC membrane increased with increasing MPD concentration (Figure 11.42). These results could be expected having seen the results of relative carboxylate density. If there are more amine groups available to react with acid chloride more amide bonds can form and a more extensive PA layer can form. The PA layer of the CPTC membrane increased in thickness with increasing MPD concentration. The amide II / 874 cm^{-1} intensity ratio of the TMC membrane actually dropped when the MPD concentration was increased to 3.0 wt-% but did increase when the MPD concentration was increase to 4.0 wt-%. CPTC and TMC membranes made at a concentration of 3.0 wt-% were similar in thickness to the FilmTec membrane.

A concentration of 2.36 mM acid chloride (CPTC or TMC) and 4.0 wt-% MPD was used throughout the remainder of the project as this was believed to produce the most consistent, reliable membrane.

Figure 11.41 Effect of MPD concentration on relative carboxylate density of CPTC (■) and TMC (□) membranes.
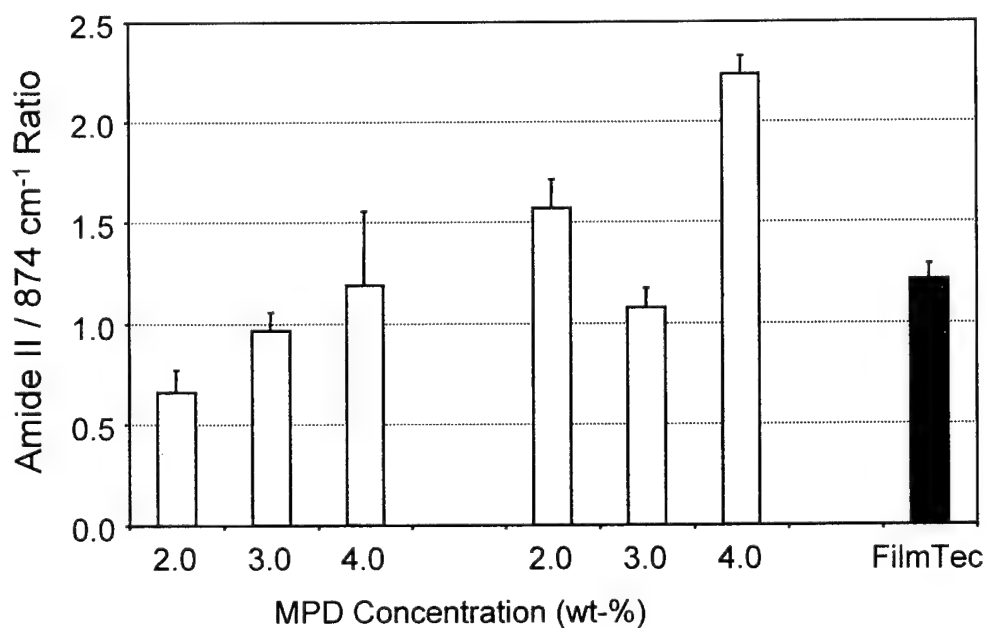
Figure 11.42 Effect of MPD concentration on relative polyamide film thickness of CPTC (□) and TMC (□) membranes.

11.7 Effect of TMC Concentration on Relative Carboxylate Density and Relative PA Film Thickness

The effect of TMC concentration on relative carboxylate density and relative film thickness was investigated. Membranes were made at TMC concentrations of 0.30, 0.59, 2.36 and 9.34 mM, while the MPD concentration was held at 2 wt-%. The typical TMC concentration used to manufacture membrane is 2.36 mM. In theory, the more complete the reaction between individual acid chloride and amine groups, the lower the carboxylate density should be, i.e., fewer free carboxylate groups relative to amide bonds.

Membranes were cut into small swatches, analyzed by ATR/IR spectrometry and the ratio of the symmetric carboxylate and amide II band intensity and relative PA film thickness was determined. The carboxylate density increased with increasing TMC concentration (Figure 11.43). This suggests that as the TMC concentration was increased, more of the acid chloride groups were left unreacted, leading to more free carboxylate groups, as the unreacted acid chloride is quickly hydrolyzed to form carboxylic acids. All membranes made for this study had a lower carboxylate density relative to the FilmTec PA membrane.

On average, the film thickness (0.30 mM TMC) was similar to the FilmTec membrane (Figure 11.44). However, the standard deviation for this measurement was quite high. This is probably a reflection of the non-uniform distribution of PA on the PS support. The other three films (0.59, 2.36 and 9.34 mM TMC) were thicker than the FilmTec and 0.3 mM TMC membranes. Variation in the TMC concentrations for this study did not significantly alter the relative carboxylate density. Therefore, a similar set of experiments with the CPTC acid chloride was not run.
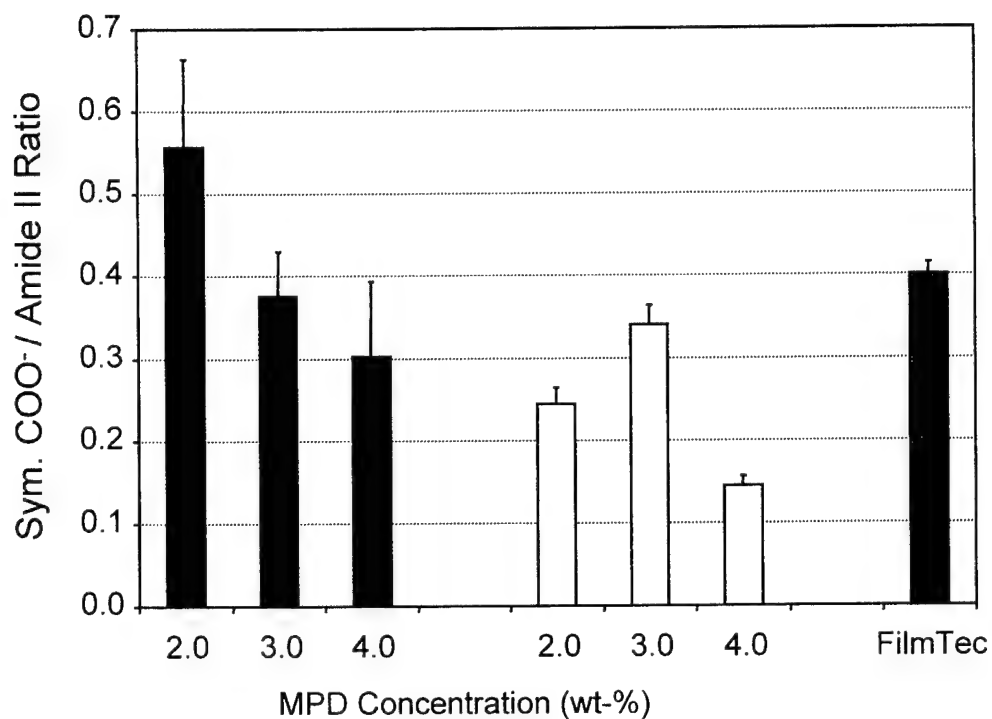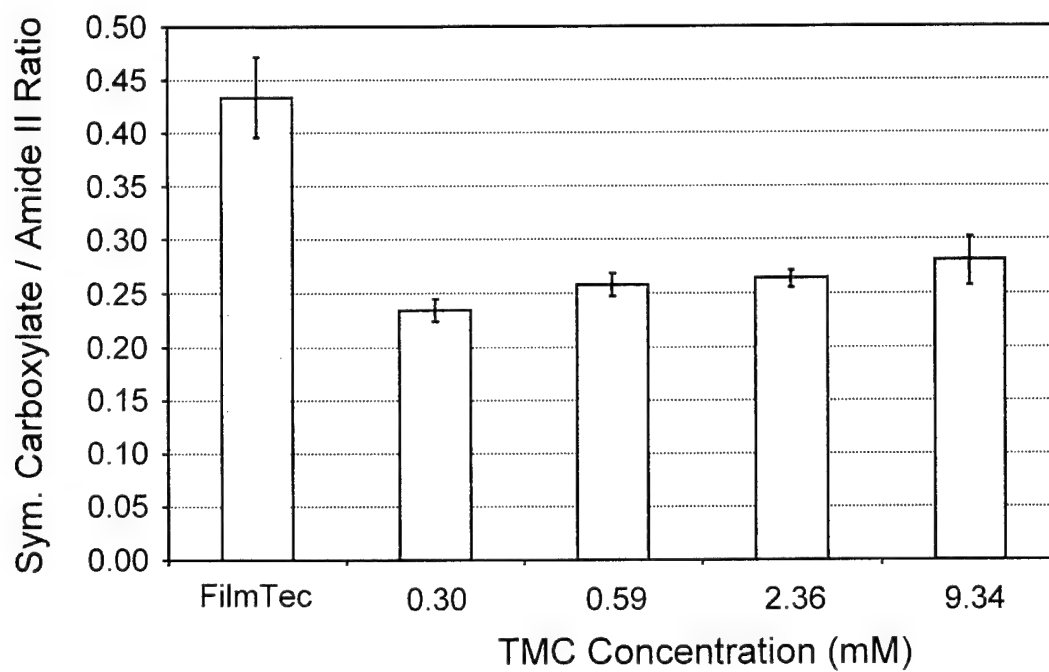
Figure 11.43 Effect of TMC concentration on the relative carboxylate density of polyamide membranes.
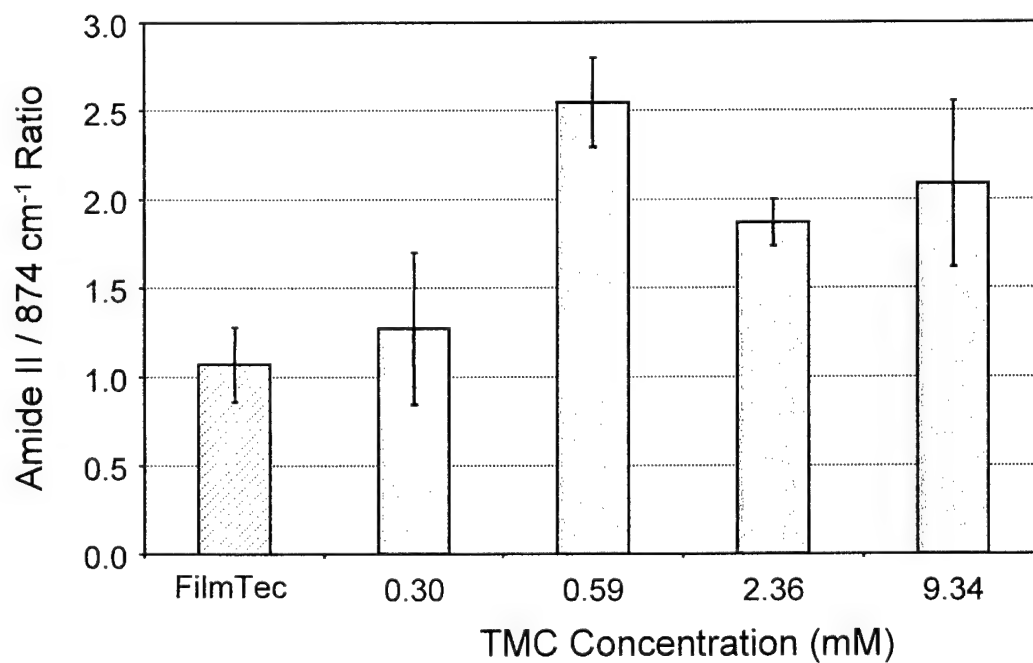

Figure 11.44 Effect of TMC concentration on the relative polyamide film thickness.

12.0 TRANSMISSION ELECTRON MICROSCOPY OF THE MEMBRANE DESALINATION BARRIER OF *ctct*-CPTC, *cccc*-CPTC, TMC AND FILMTEC MEMBRANES

In a previous study, TEM was used to determine the thickness and morphology of the desalination barrier of cellulose acetate RO membranes.[26] Efforts to elucidate the cross-sectional structure of the PA barrier of composite membranes using scanning electron microscopy (SEM) were not satisfactory. For these reasons, TEM was selected to determine the cross-sectional structure of the barrier of the CPTC membrane supported on the surface of a finely porous PS support membrane. The objective of this work was to determine the barrier structure, morphology, thickness, uniformity, integrity, physical bonding to the PS substrate and possible causes for membrane deterioration.

The chemical stability of the CPTC membrane to NaOCl is good. For example, when CPTC membranes are immersed in 15,000 mg/L NaOCl for 1 hr, the transport properties do not deteriorate. Also, continuous long-term field testing of CPTC membrane swatches with 1.5 mg/L NaOCl feed have operated for several thousand hours without deterioration. However, deterioration in membrane transport properties was observed in field tests after repeated shutdowns. Physical damage to the membrane appears to occur after shutdowns, either at the point of O-ring contact with the membrane, structural damage to the thin-film barrier itself or both. The TEM study was focused on providing insight into this phenomenon. The study compared structural similarities and differences between:

* PS porous support membrane
* *cccc*-CPTC, *ctct*-CPTC,TMC and FilmTec commercial membranes
* Membranes made by different formulations, preparative parameters and process methods
* Membrane structure before and after exposure to NaOCl/NaOBr
* *cccc*-CPTC and *ctct*-CPTC membranes before and after long-term field tests on chlorinated feed.

Specimens were prepared for the electron microscope according to the procedure described in Section 8.4. Specimen sections were taken on an RMC-MT-X ultramicrotome and viewed on a Philips CM 300 Transmission Electron Microscope located at the University of California at Riverside, CA. Personnel from SST assisted in the viewing and image selection.

A parallel but smaller TEM study was conducted at Texas Tech University in Lubbock, TX to confirm the methods and techniques used in this study. The TEM images were very similar to those presented in this study.

Magnifications of all TEM images throughout the study were standardized. Each membrane image in this report is presented at 1.0 μm (3,200X) and 0.30 μm (12,600X).

Although the micrographs showed the structure of the barrier in great detail, it was often difficult to draw definite conclusions. It was observed, however, that all PA membranes, *cccc*-CPTC, *ctct*-CPTC, TMC and FilmTec membranes have a similar cross-sectional structure. A predominant feature is the large hollow cellular (closed) structure that rests on a thin dense layer of PA. The hollow cells vary in shape, size and packing density and range from a single to multiple layers. These cellular structures appear as peaks on AFM images taken perpendicular to the barrier. It can be assumed, therefore, that the peaks are hollow.

12.1 PS Porous Membrane Support

The cross-section of a PS porous support membrane, upon which the film is formed, is shown in Figure 12.1. The grey areas of the micrograph are indicative of embedding resin while the dark areas are osmium stained PS. The interface between the grey (left) and dark (right) areas of the 1.0 μm micrograph shows the cross-section of the surface upon which the barrier is formed. The round grey areas within the darker PS matrix appear, with some degree of uncertainty, to be microvoids.

12.2 Commercial FilmTec Brackish and Seawater Membranes, TMC and CPTC Membranes

The FilmTec brackish and seawater membranes are composed of two distinctive layers, a cellular bubble-like layer supported on a dense PA layer which in turn contacts the PS membrane surface. The dense PA layer of the seawater membrane is much thicker than the same layer on the brackish water membrane. (See Figures 12.2 and 12.3.)

The structure of the barrier of TMC and CPTC membranes are not greatly different. There is some indication that the PA barrier of the CPTC membrane is delaminating from the PS support membrane. Previous studies have shown that the barrier of membranes prepared with aliphatic amines is not as well bonded to the surface of the PS substrate membrane. This may also be the case for the CPTC membrane since the acid chloride is aliphatic. (See Figures 12.4 and 12.5.)

12.3 CPTC Membranes Prepared with Freon and Hexane Solvents as the Acid Chloride Carrier

PA barriers are shown in Figures 12.6 and 12.7 for CPTC membranes made with hexane and Freon as the solvent carrier of the acid chloride. While there are some differences in thickness and structure they are not striking. The only process difference in barrier formation was the quantity of sodium lauryl sulfate surfactant in the aqueous MPD solution during formation. The membrane made with hexane contained 0.10 wt-% surfactant in the MPD solution while the membrane made with Freon contained 0.25 wt-% surfactant.

170
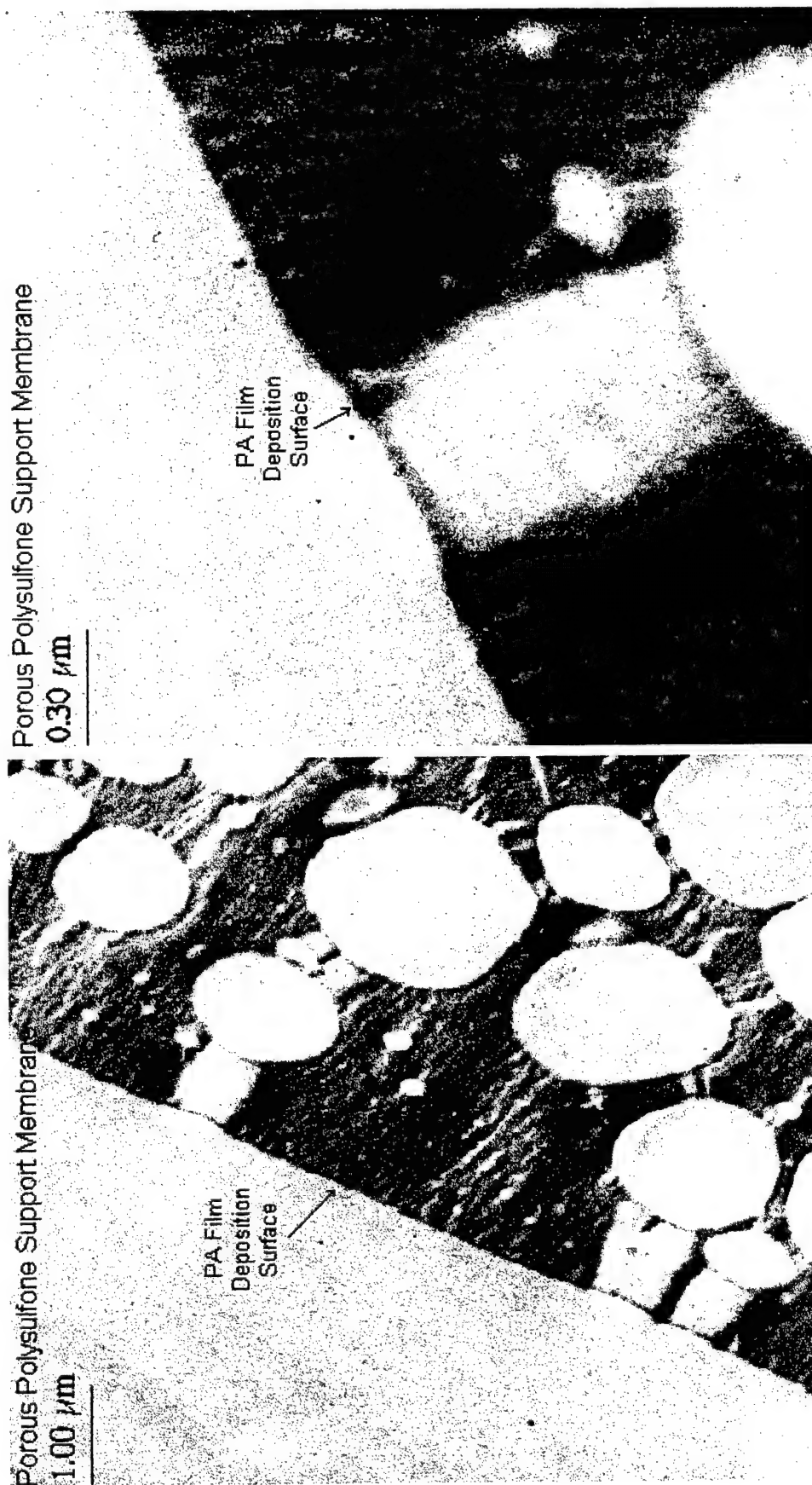
Figure 12.1 Transmission Electron Micrograph of the osmium stained cross-section of PS porous supporting membrane before PA film formation. PS membrane supplied by a major commercial RO membrane manufacturer.

171
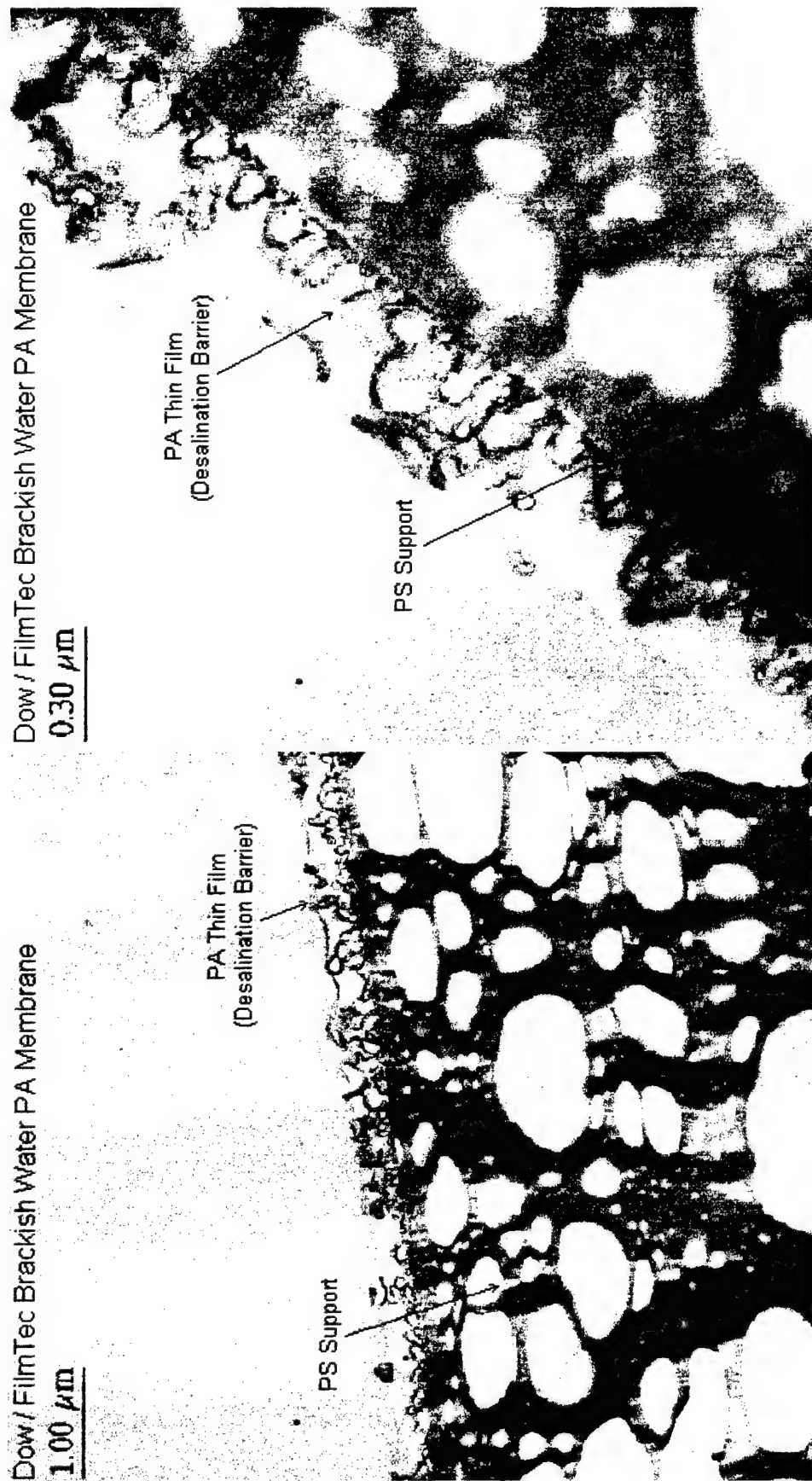
Figure 12.2 Transmission Electron Micrograph of the osmium stained cross-section of FilmTec brackish water PA membrane
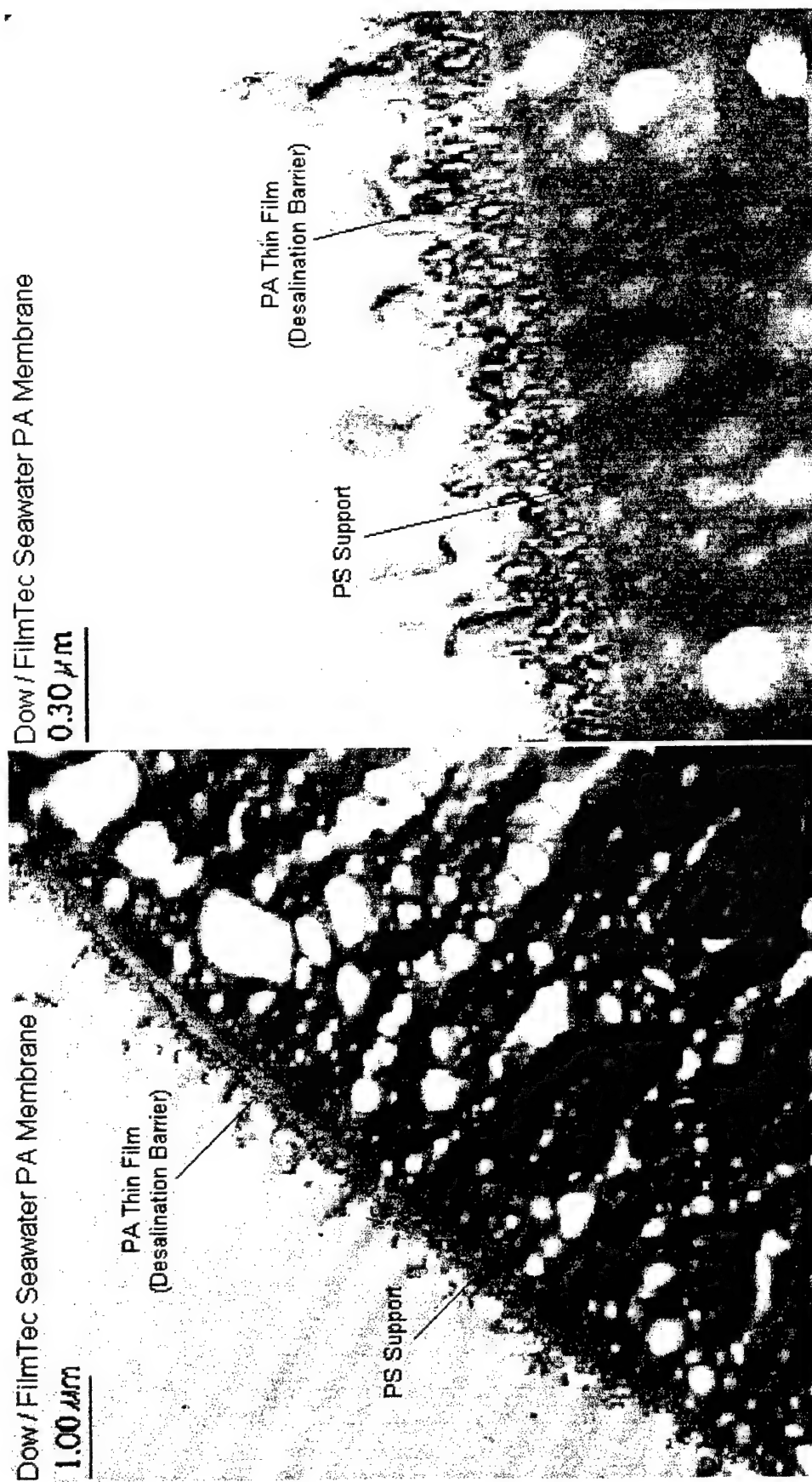
Figure 12.3 Transmission Electron Micrograph of the osmium stained cross-section of FilmTec seawater PA membrane

173

TMC-838 PA Membrane
1.00 μm

PA Thin Film
(Desalination Barrier)

PS Support

TMC-838 PA Membrane
0.30 μm

PA Thin Film
(Desalination Barrier)

PS Support
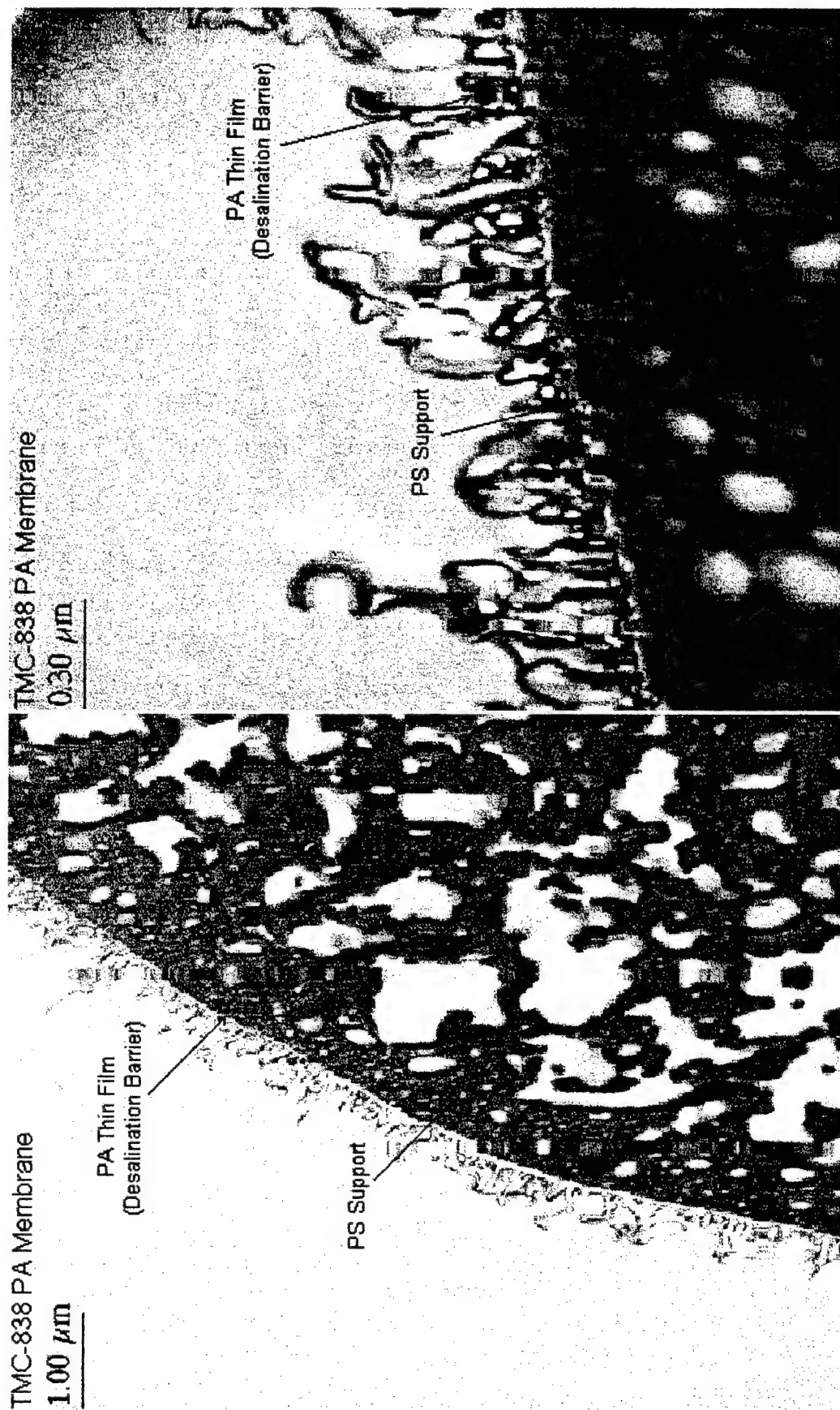
Figure 12.4 Transmission Electron Micrograph of the osmium stained cross-section of TMC-838 PA membrane

174
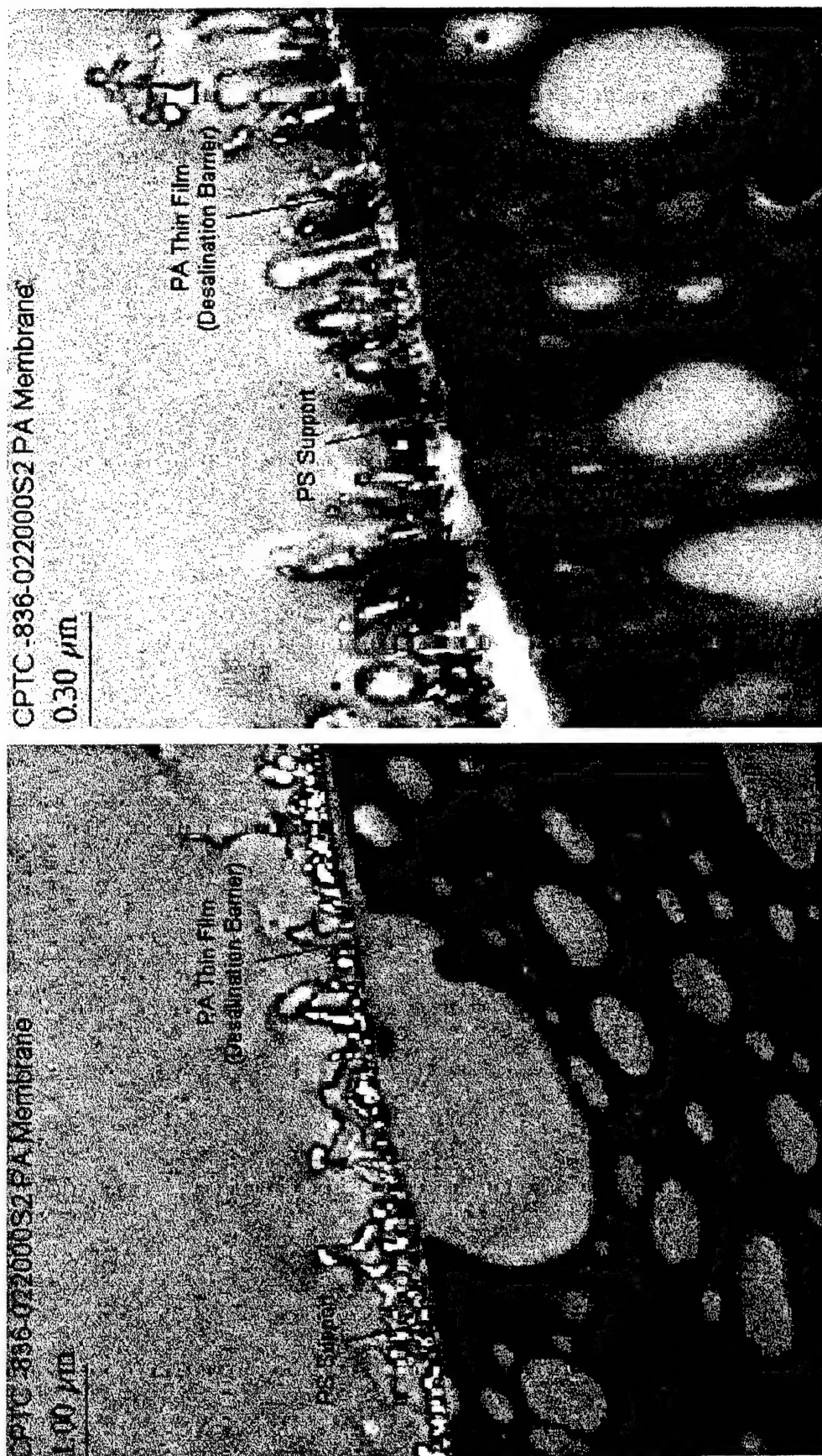
Figure 12.5 Transmission Electron Micrograph of the osmium stained cross-section of CPTC-836 PA membrane
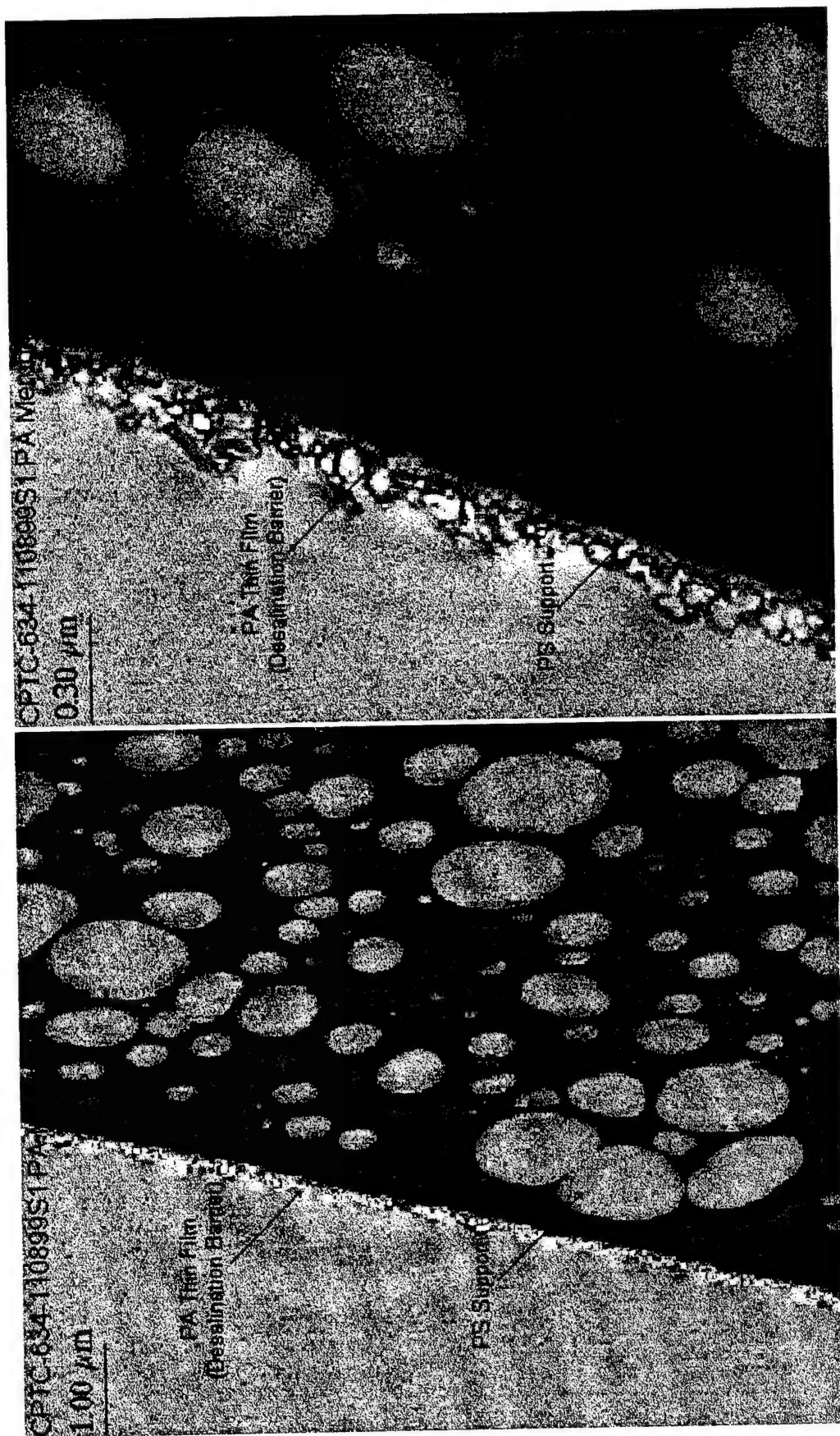
Figure 12.6 Transmission Electron Micrograph of the osmium stained cross-section of CPTC-634 PA membrane made with hexane as the solvent of the acid chloride

CPTC-333-061099S2 PA Membrane

0.30 μm

CPTC-333-061099S2 PA Membrane

1.00 μm

PA Thin Film
(Desalination Barrier)

PS Support

PA Thin Film
(Desalination Barrier)

PS Support
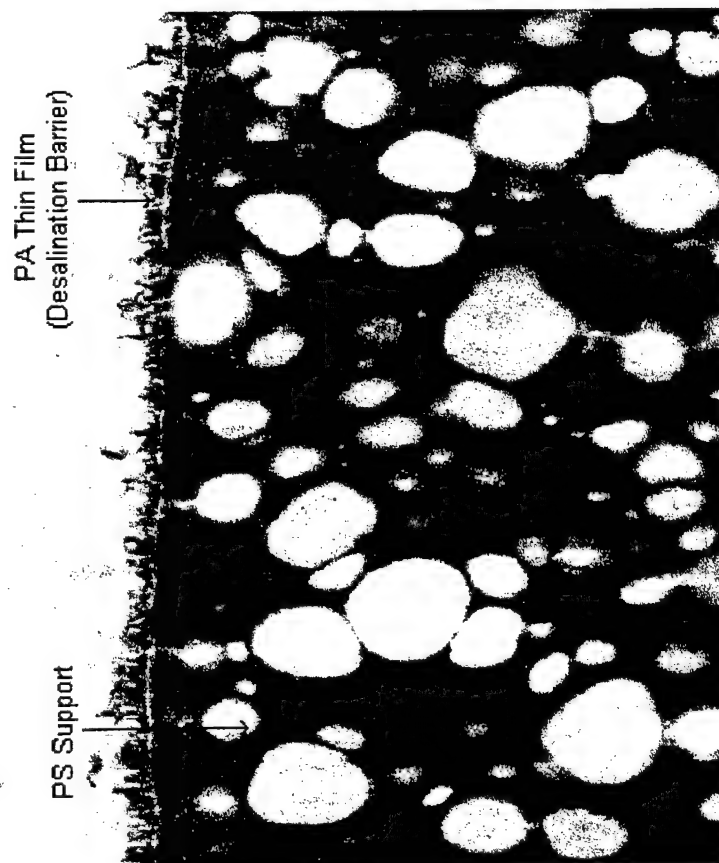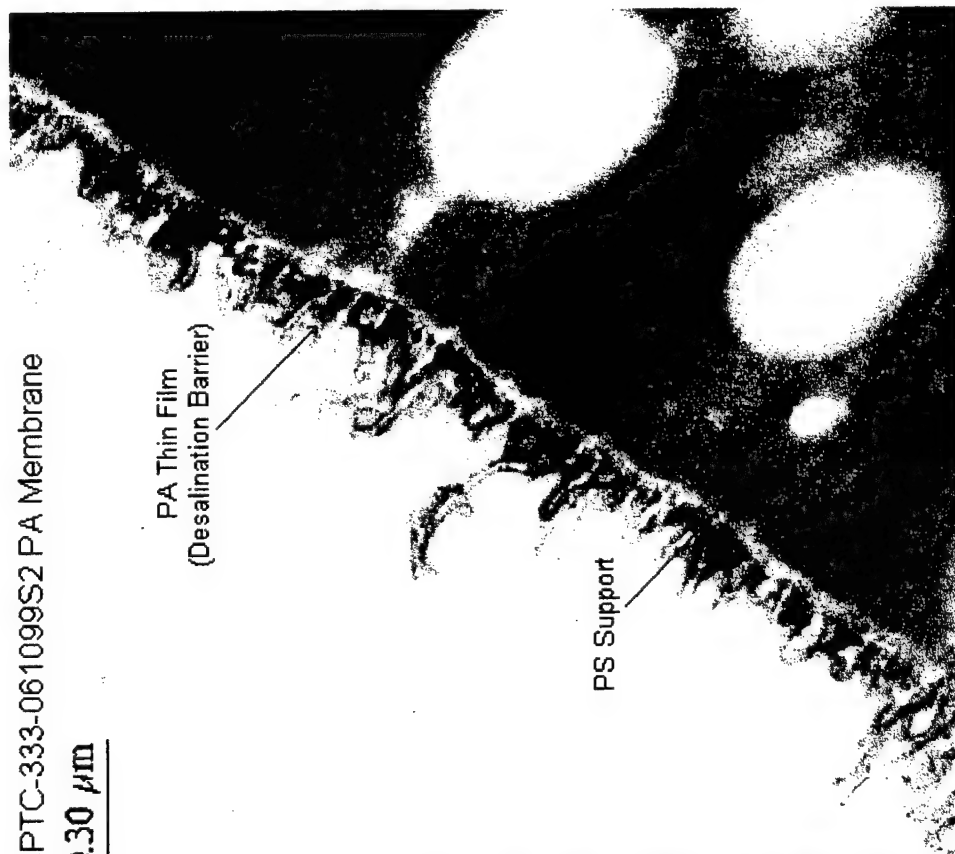
Figure 12.7   Transmission Electron Micrograph of the osmium stained cross-section of CPTC-333 PA membrane made
with Freon as the solvent of the acid chloride

177

12.4 Comparative Study of *ctct*-CPTC and *cccc*-CPTC Membranes

The thickness of the CPTC PA barrier shown in Figure 12.8 is considerably thinner than the *cccc*-CPTC PA barrier shown in Figure 12.9. The cellular formation of the PA barriers are quite different

.

12.5 Comparative Study of CPTC Membranes Prepared from 2-wt%, 3-wt% and 4-wt% MPD

CPTC membranes were prepared from aqueous MPD solutions of varying concentrations to determine what effect, if any, this parameter has on membrane structure. The standard concentration used in the preparation of commercial membranes is 2 wt-% MPD. Both the structure and thickness of the barriers of CPTC membranes prepared from aqueous solutions of 2, 3 and 4 wt-% MPD do not appear to be greatly different. In future studies, it would be of interest to determine the thickness and structure of barriers made with lower concentrations of MPD (see Figures 12.10, 12.11 and 12.12).

This study did not determine the effect of the acid chloride concentration on PA barrier structure. This would be of interest in future studies.

12.6 CPTC Membrane Made with Sodium Hydroxide (pH 12.5) Acid Acceptor in MPD Solution

Hydrochloric acid (HCl) is formed during the interfacial condensation reaction between CPTC with MPD. As HCl is formed it can react with an amine group of MPD to form the amine salt, thereby blocking that site for further reaction with an acid chloride. This could have a significant effect on the chemical structure of the PA and influence the physical structure and thickness of the barrier layer. The pH of the standard aqueous 2-wt% MPD solution is ~ 9.0. Sodium hydroxide was added to the MPD solution to raise the pH to 12.5, thereby acting as the acid acceptor. The TEM image shown in Figure 12.13 does show a change in the barrier structure; the cellular structure appears more elliptical in shape and the film appears to be well bonded to the PS substrate. The transport properties were unchanged.
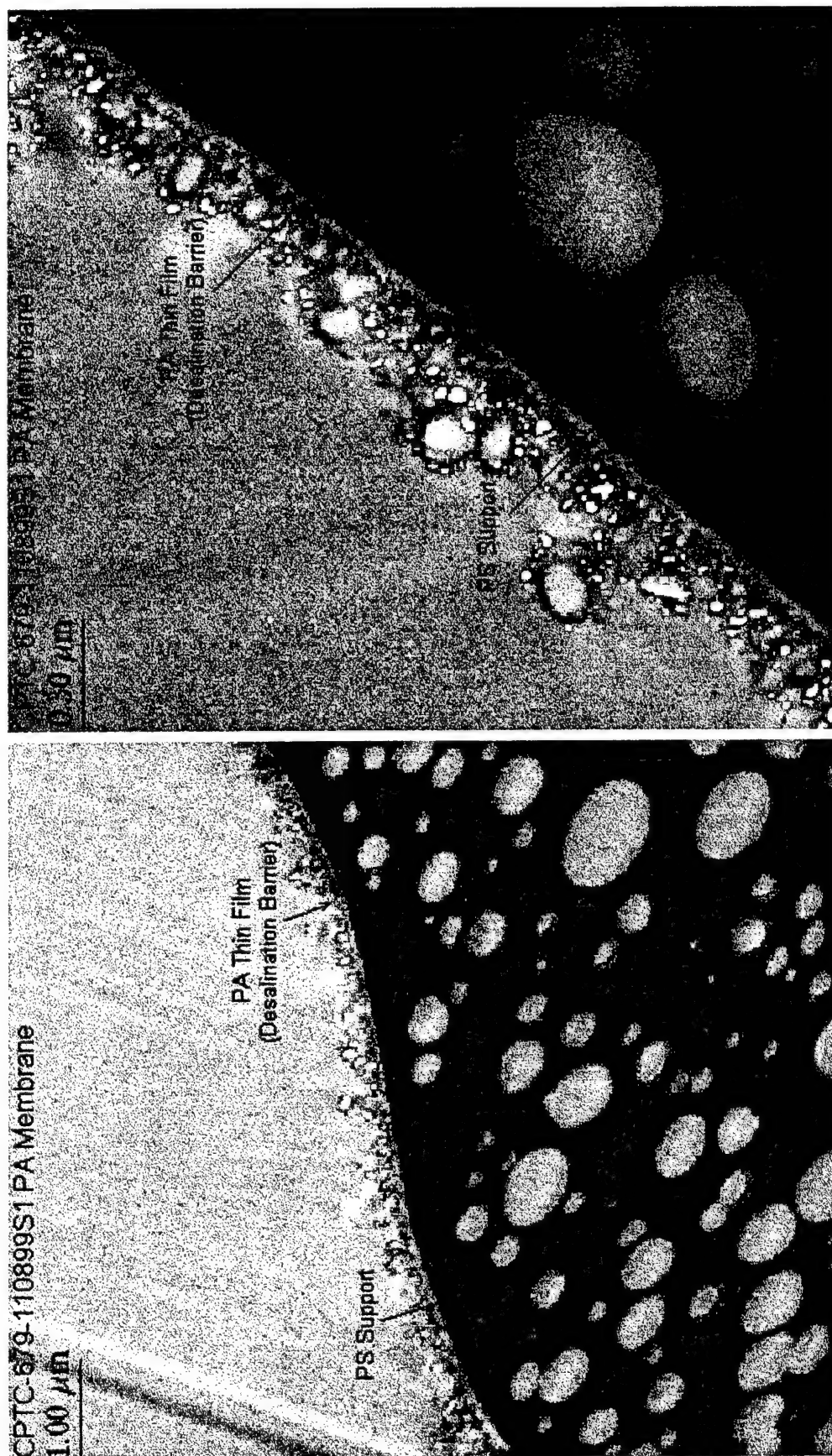
Figure 12.8 Transmission Electron Micrograph of the osmium stained cross-section of CPTC-679 PA membrane with polyvinyl alcohol protective coating on PA film surface

179
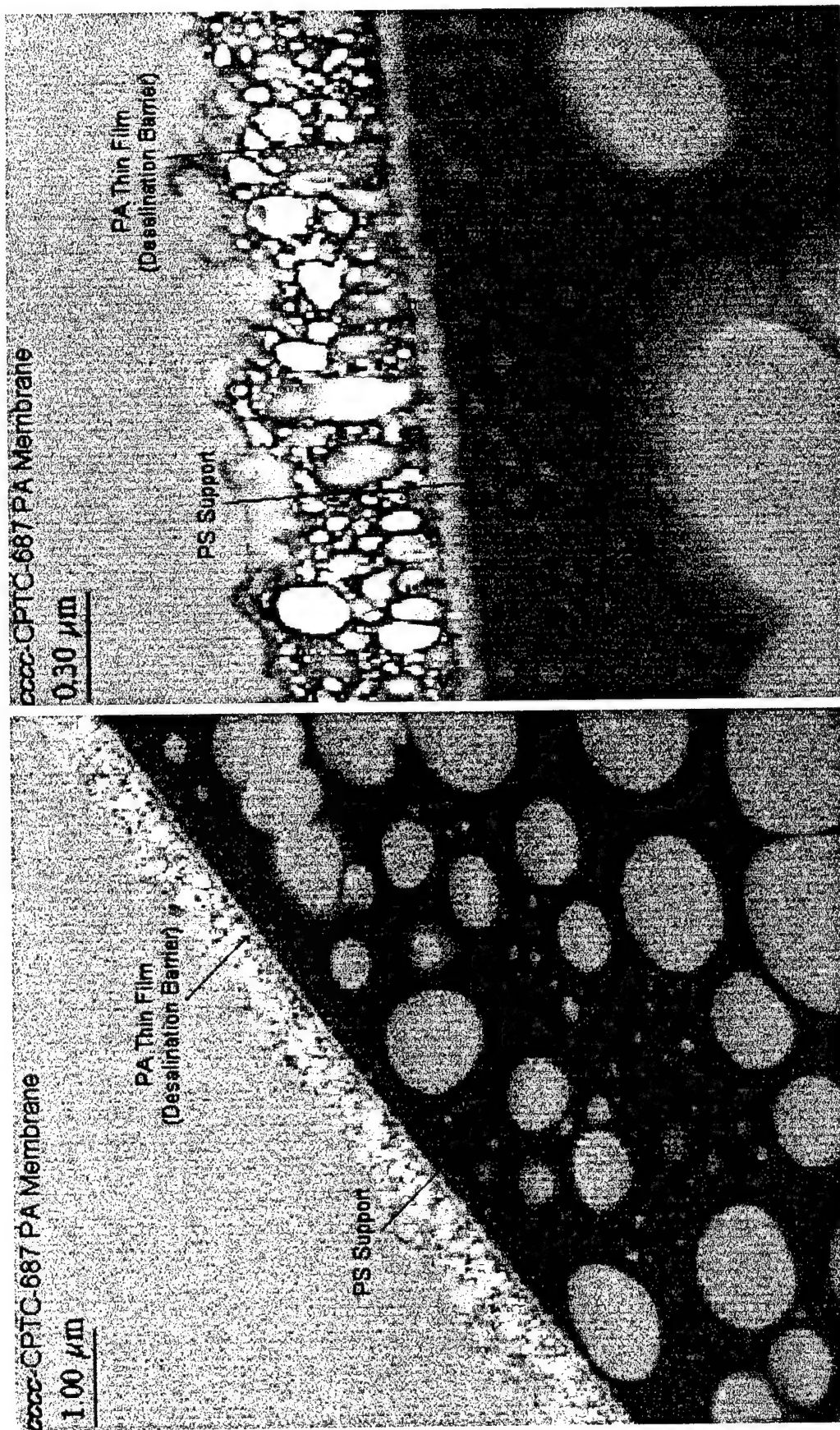
Figure 12.9 Transmission Electron Micrograph of the osmium stained cross-section of *cccc*-CPTC-687 PA membrane with polyvinyl alcohol protective coating on PA film surface

180

Figure 12.10 Transmission Electron Micrograph of the osmium stained cross-section of CPTC-634 PA membrane prepared with 2-wt% MPD

CPTC-633-110899S1 PA Membrane

1.00 μm

CPTC-633-110899S1 PA Membrane

0.30 μm

PA Thin Film
(Desalination Barrier)

PS Support

PA Thin Film
(Desalination Barrier)

PS Support

Figure 12.11 Transmission Electron Micrograph of the osmium stained cross-section of CPTC-633 PA membrane prepared with 3-wt% MPD

Figure 12.12 Transmission Electron Micrograph of the osmium stained cross-section of CPTC-632 PA membrane prepared with 4-wt% MPD

183

Figure 12.13 Transmission Electron Micrograph of the osmium stained cross-section of CPTC-832 PA membrane prepared with 2-wt% sodium hydroxide (pH 12.5) acid acceptor in MPD solution

12.7   Addition of Acetone to MPD Solution to Improve Adhesion of PA Barrier to PS Substrate

AFM micrographs of the cross-linked barrier formed during membrane processing show a very rough surface with many peaks and valleys. The membrane surface area is several times greater than that of a smooth membrane surface like cellulose acetate. It has been commonly hypothesized that the high water flux exhibited by these membranes is due to the increase in surface area. This TEM study has now shown that the peaks are hollow which would further explain high water flux. (See Figures 12.14 and 12.15) The mechanism responsible for the formation of surface roughness has not been established. (See Section 11.5)

Many of the variables described in Section 11.5 affecting the interfacial reaction between MPD, CPTC and TMC in the formation of the PA barrier are inter-related and most would be expected to have an influence on the surface morphology of the polymer that is formed during the interfacial formation. The influence of transfer rate of the amine MPD and the partition potential of the reactants was studied by incorporating IPA of varying concentrations in the aqueous MPD phase during the interfacial polymerization. IPA was selected because of its solubility in hexane, the hydrocarbon carrier for the acid chloride, TMC.   With this exception, the membranes were prepared using the standard methods of preparation and post treatment. A series of six TMC membranes were prepared with aqueous MPD solutions containing 0, 5, 10, 20, 40 and 80 wt-% IPA, respectively. It was found that the RO performance of the membranes was not changed appreciably when up to 10 wt-% IPA was incorporated into the MPD solution. When 40 wt-% and greater was added, the transport properties changed dramatically; that is, both water flux and salt transport increased. With concentrations up to 40 wt-% IPA, the water flux increased with little, if any, change in salt rejection. A surface analysis of each membrane was determined by AFM. Very noticeable structural changes were observed on the surfaces of the membranes as the isopropanol content in the aqueous MPD solution increased. As the concentration of isopropanol increased, the surface roughness and area increased with a very significant change is structural appearance. At the highest isopropanol levels, raised volcano-like structures with hollow openings appeared. At this point, both the water and salt passage was very high.

Other alcohols, phenol, surfactants and ketones were evaluated. Each affected the transport properties of the membrane by increasing surface roughness and area. These additives are believed to play a significant role in controlling the amine diffusion into the interface during polymerization.

In an effort to improve the adhesion of the PA barrier to the PS substrate as well as to enhance the transport properties, 4 wt-% acetone was added to the aqueous MPD solution during CPTC membrane preparation. Since PS is soluble in acetone it was hypothesized that a small amount of acetone may improve bonding of the barrier to the substrate. TEM micrographs of a CPTC membrane control and a CPTC membrane prepared with 4 wt-% were shown in Figures 12.14 and 12.15, respectively. Both membranes exhibited similar transport properties when tested in RO. The cross-
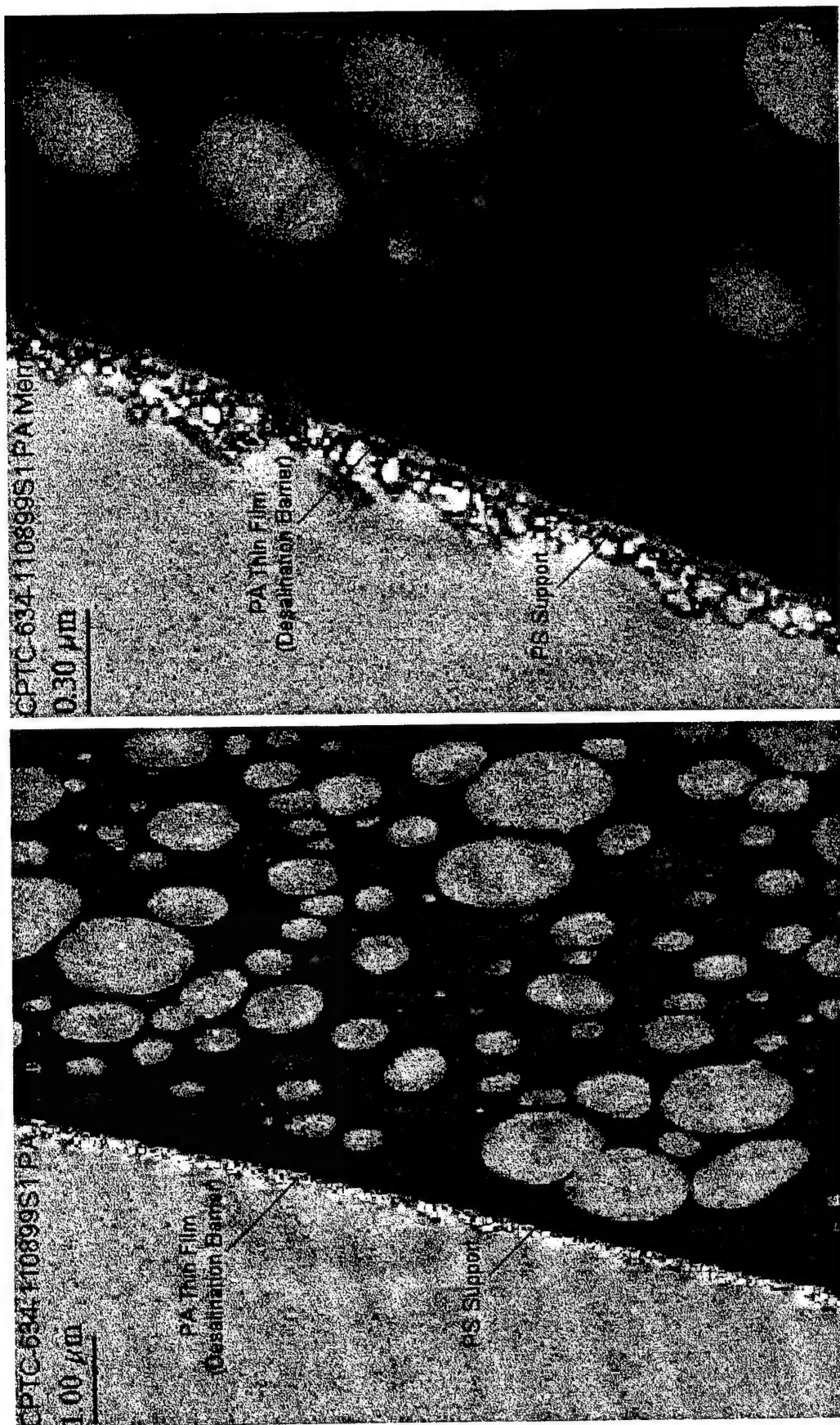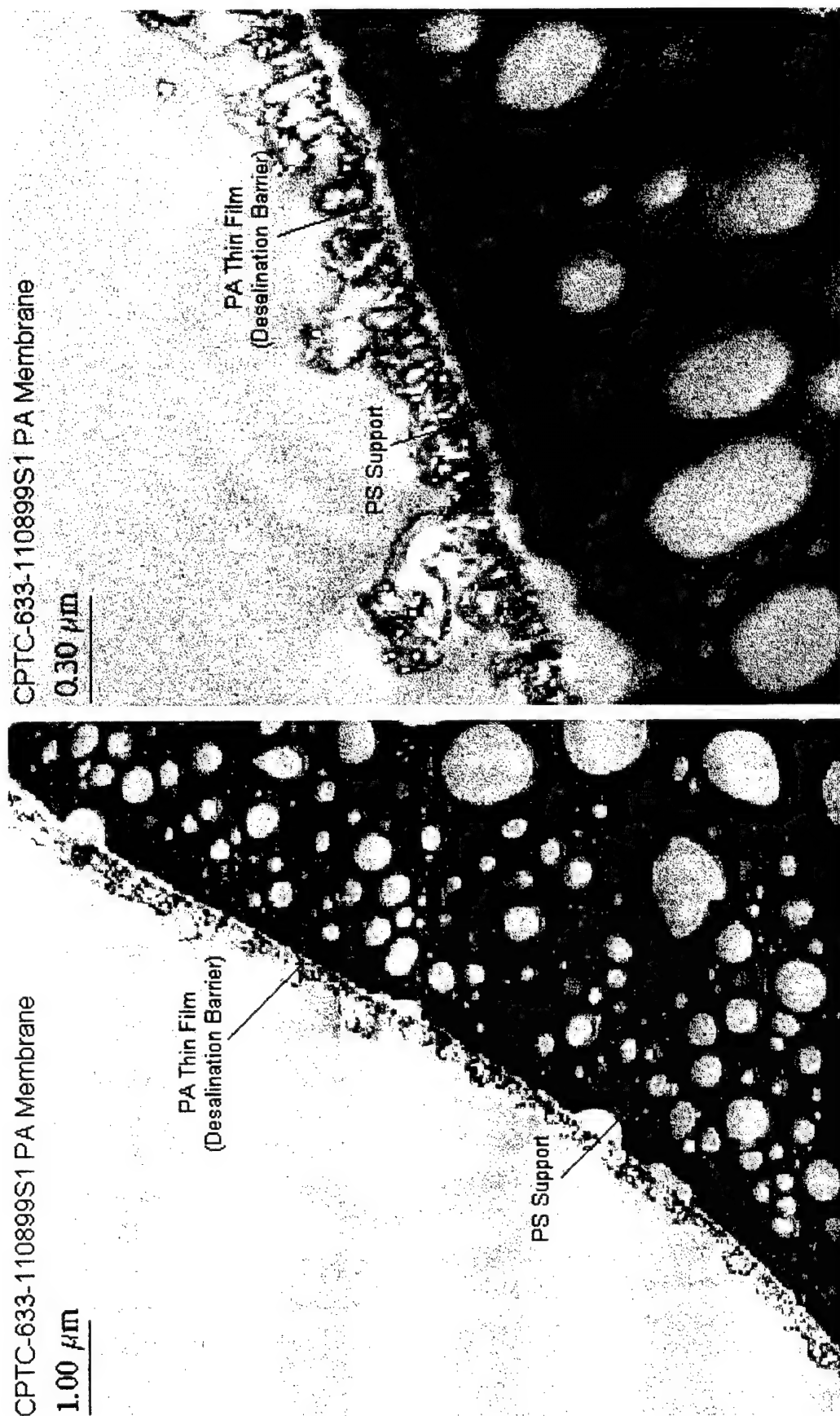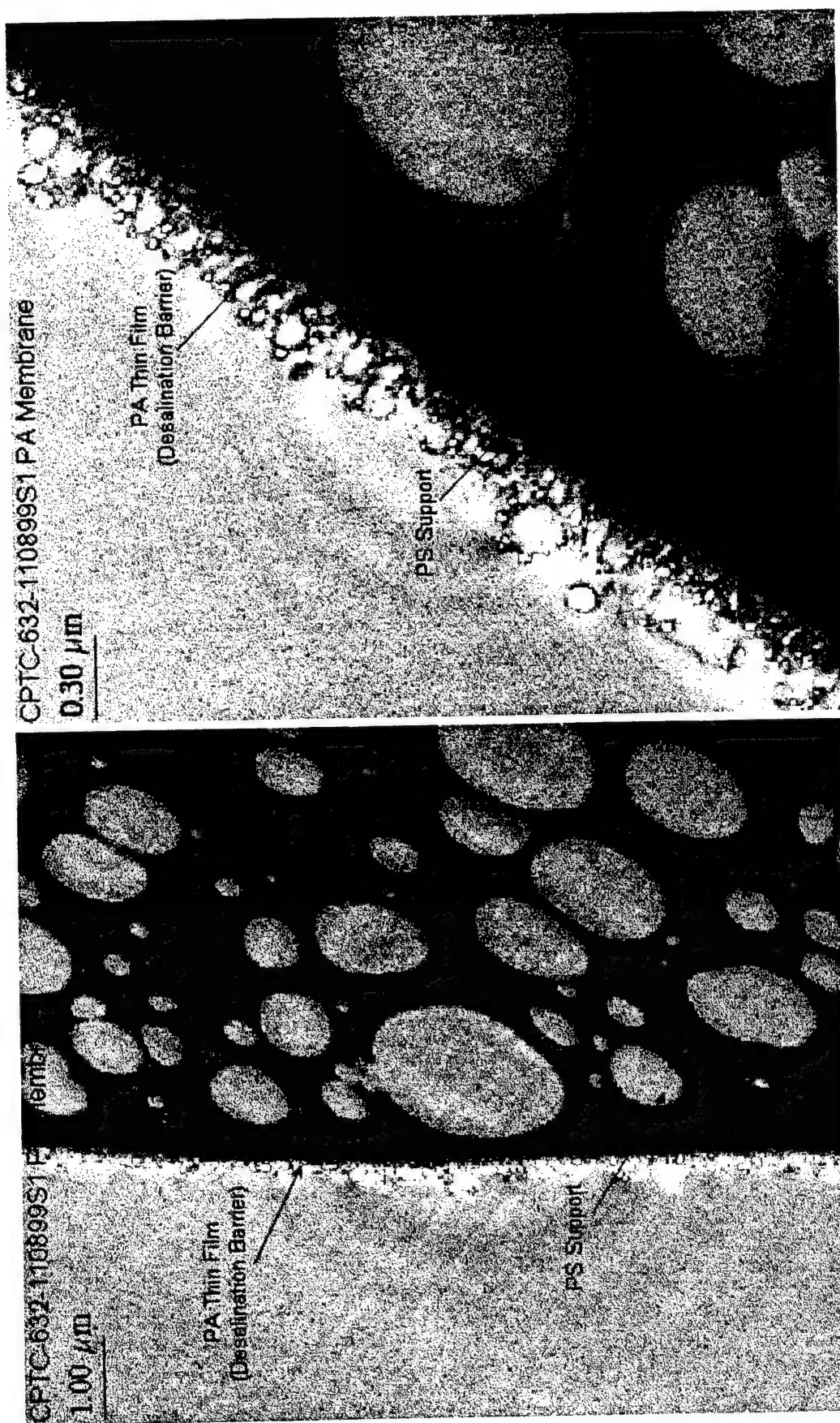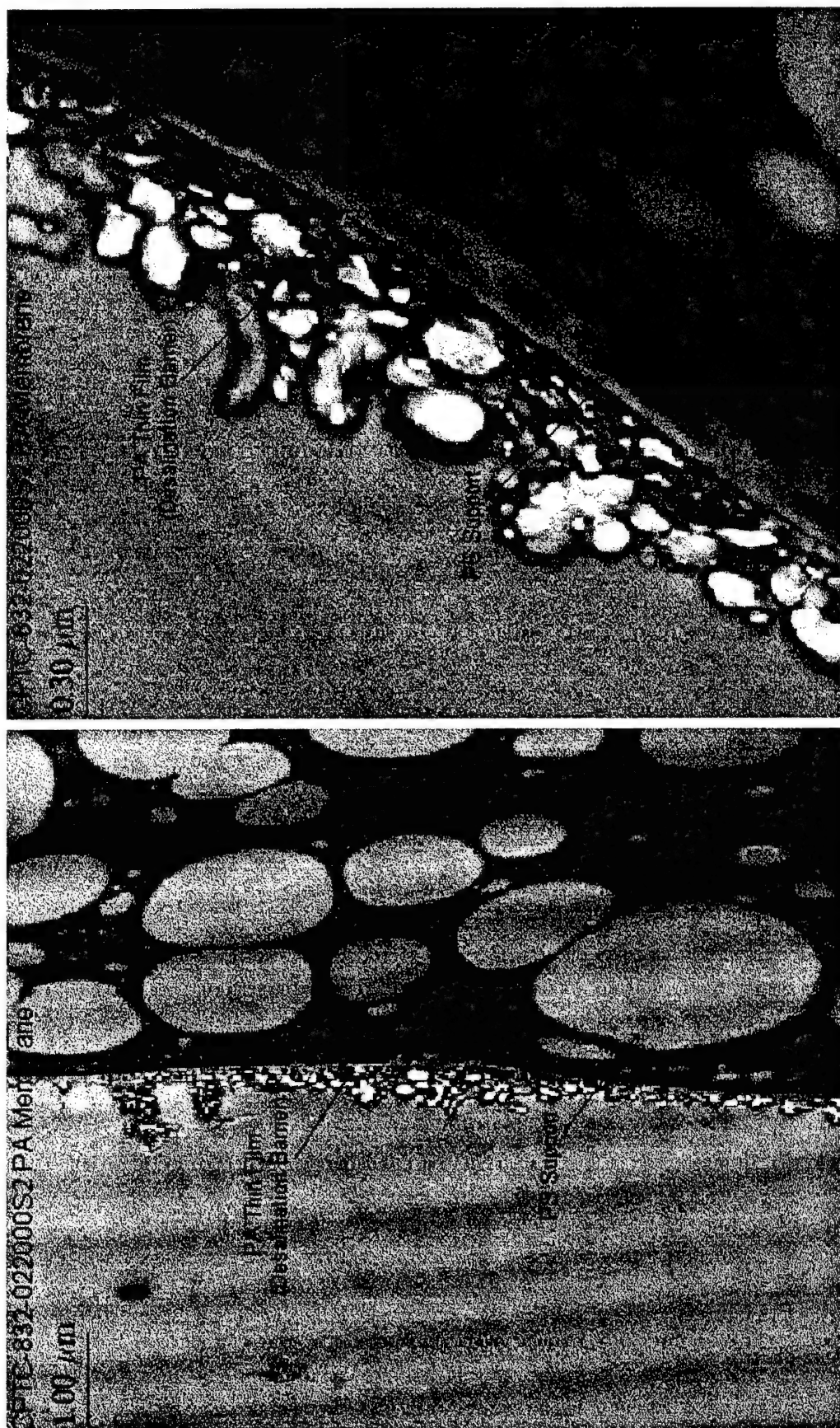
185

Figure 12.14 Transmission Electron Micrograph of the osmium stained cross-section of CPTC-632 PA membrane prepared without acetone in MPD solution

186

Figure 12.15   Transmission Electron Micrograph of the osmium stained cross-section of CPTC-696 PA membrane prepared with 4-wt% acetone in MPD solution

187

sectional structure also appeared to be similar. The membranes showed some loss in performance in long-term RO field testing after multiple shut-downs. An improvement in PA barrier adhesion was not apparent.

12.8 CPTC Membranes Processed Using Different Rinsing Conditions (Osmotic Gradient Differences)

Very small blisters are often observed on the PA barrier immediately after formation and after the membrane is immersed into the first rinse solution to remove unreacted MPD. The composition and concentration of the rinse solutions vary depending on the manufacturer. Usually, the solution is a hot (80°C) acid solution of fairly high osmotic pressure. Often, but not always, when the osmotic pressure of the rinse solution is substantially less than the osmotic pressure of the fluid MPD layer (~183 psi) directly beneath the barrier layer, water will rapidly flow from the rinse solution into the MPD layer and blistering is visually observed. After the final rinse, the barrier draws down on the PS substrate and an imperfection appears at the site of the blister. This phenomenon, `shown schematically in Figure 12.16, is to be avoided during membrane processing by avoiding osmotic shock across the barrier.

The blistering described was visible to the eye and was on a macroscale. The closed cellular structure of the barrier, as elucidated by TEM micrographs, may also be subject to rupture by this same osmotic mechanism. It was of interest to vary the processing conditions to induce both types of blistering to assess damage to the PA barrier. CPTC membranes were rinsed in DI water, 0.05, 0.12, 0.25 and 0.50 wt-% solutions of sodium chloride; the osmotic pressures were 0, 5.7, 13.7, 28.5, and 57 psi, respectively. Micrographs of membranes rinsed in these solutions are shown in Figures 12.17 through 12.22. None of the membranes show any evidence of osmotic blistering during rinsing. In future studies the osmotic pressure of the rinse solutions should be varied over a broader range of concentrations. The focus of this study may have been too narrow.
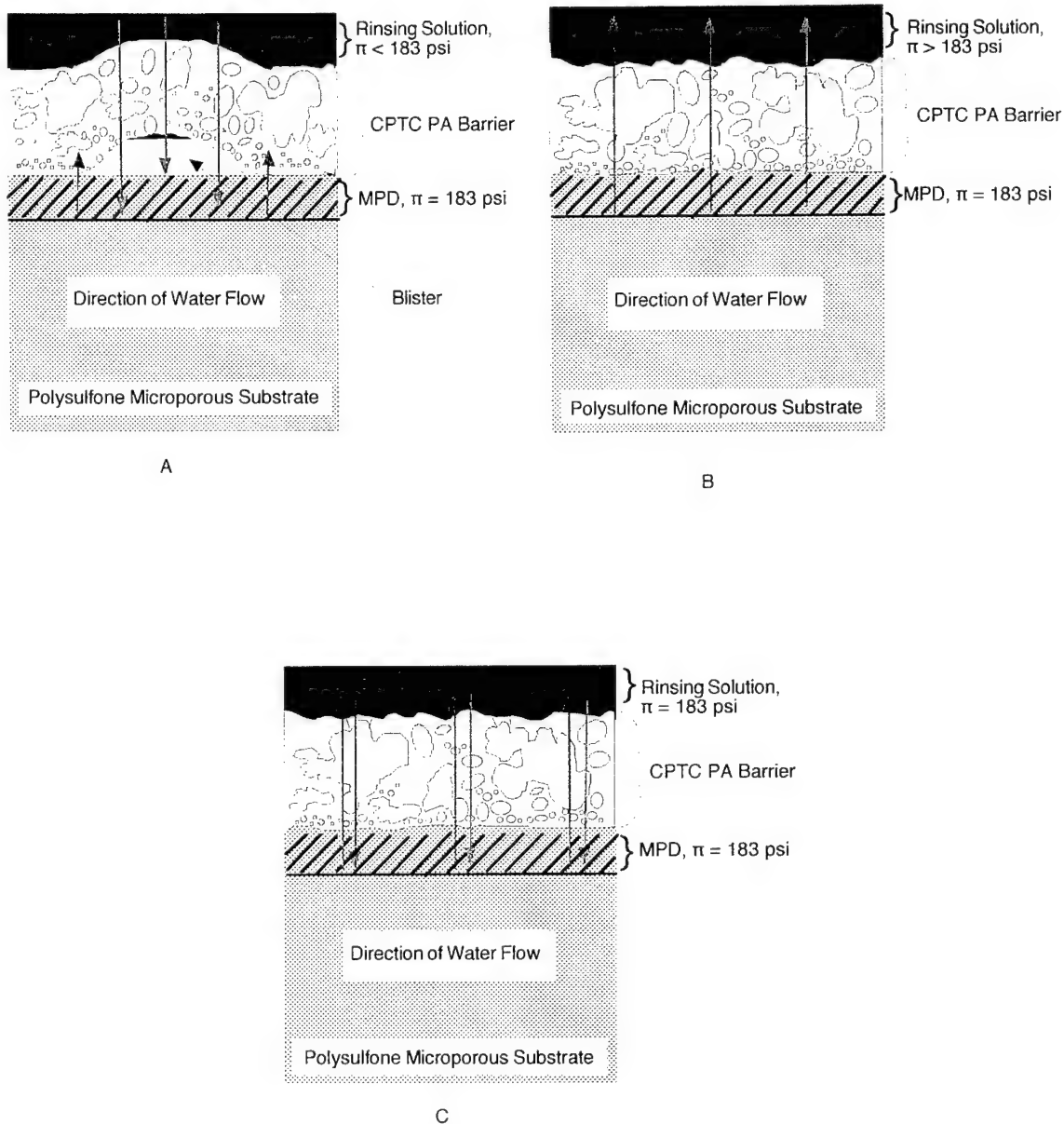
Figure 12.16   Drawing showing the potential for osmotic blistering of the PA barrier in the rinsing step during CPTC membrane processing. Blistering of the PA barrier is due to osmotic pressure differences between the rinse solution and the unreacted MPD between the PA barrier and the PS supporting membrane.
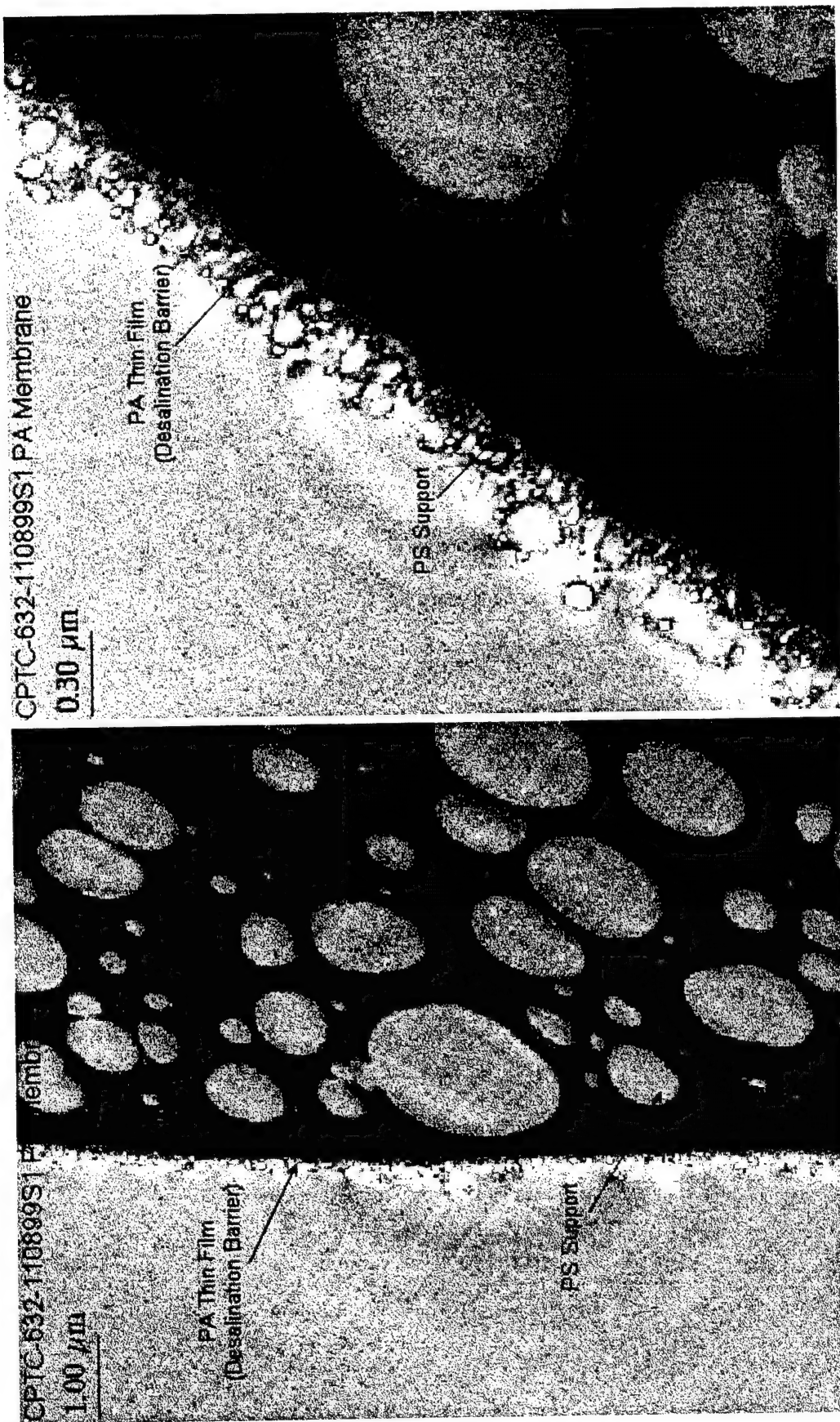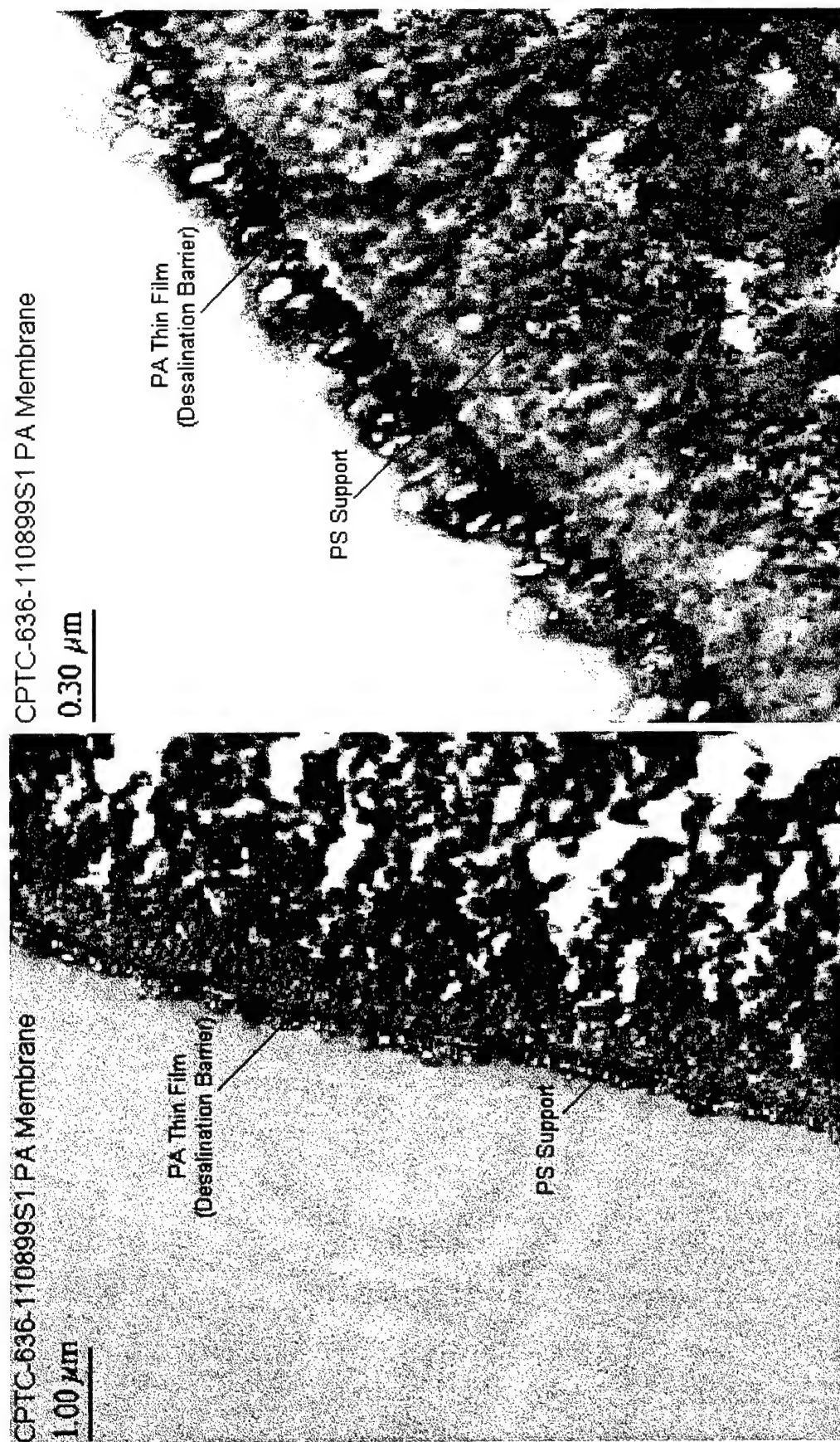
Figure 12.17 Transmission Electron Micrograph of the osmium stained cross-section of CPTC-636 PA membrane prepared without rinsing
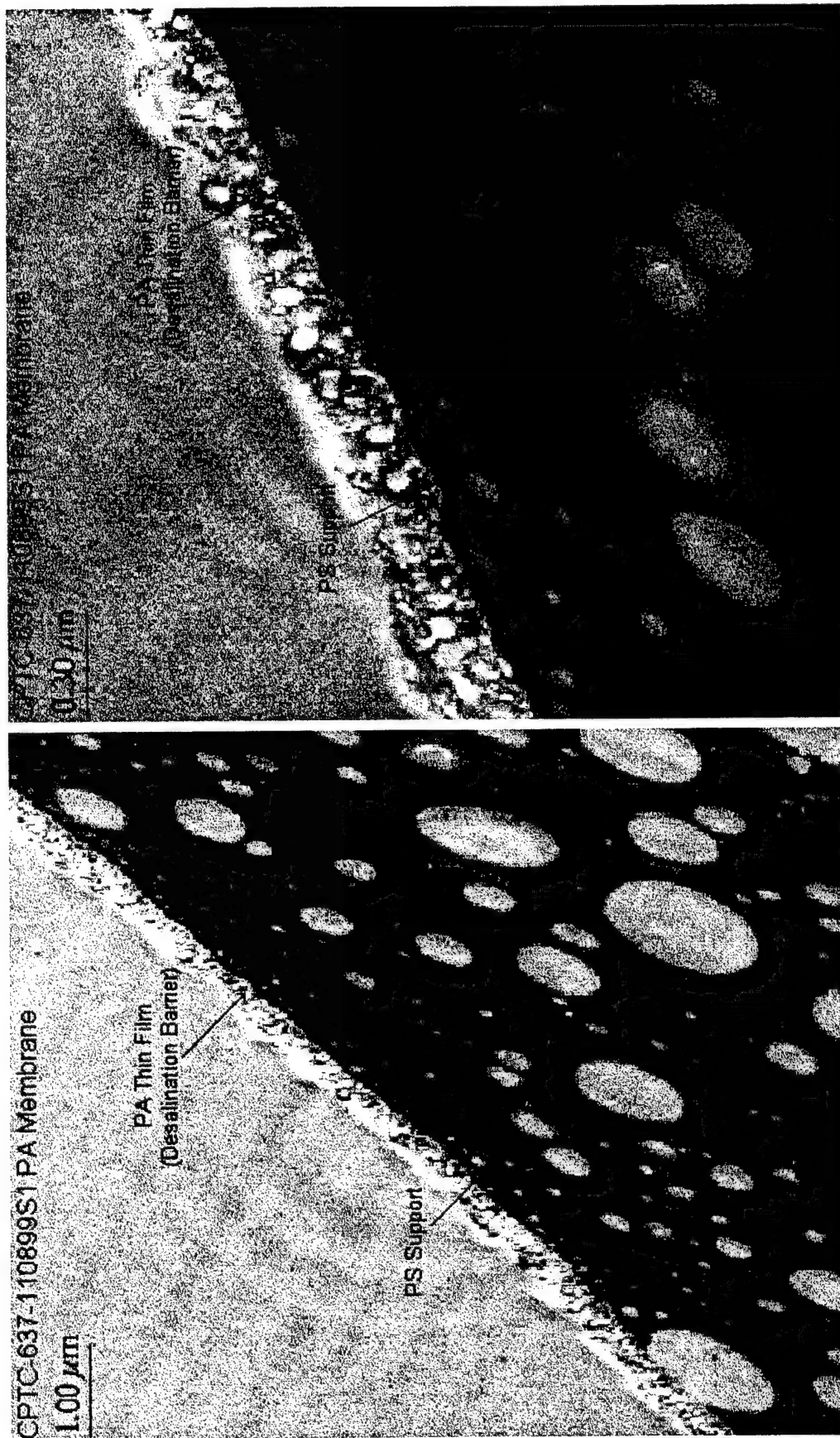
Figure 12.18 Transmission Electron Micrograph of the osmium stained cross-section of CPTC-637 PA membrane prepared with rinsing in deionized water for 30 minutes
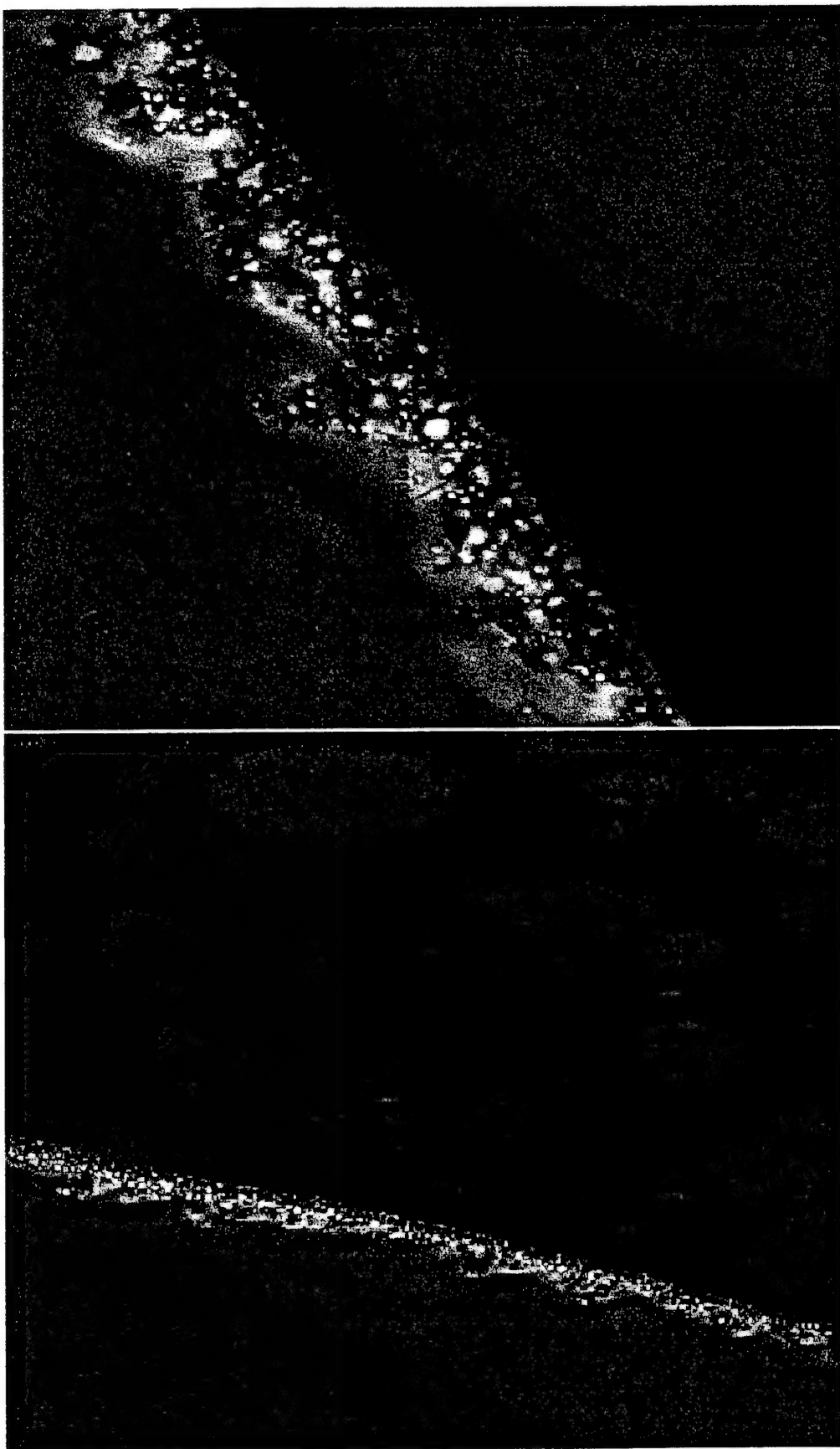
Figure 12.19 Transmission Electron Micrograph of the osmium stained cross-section of CPTC-638 PA membrane prepared with rinsing in 0.05-wt% sodium chloride solution for 30 minutes
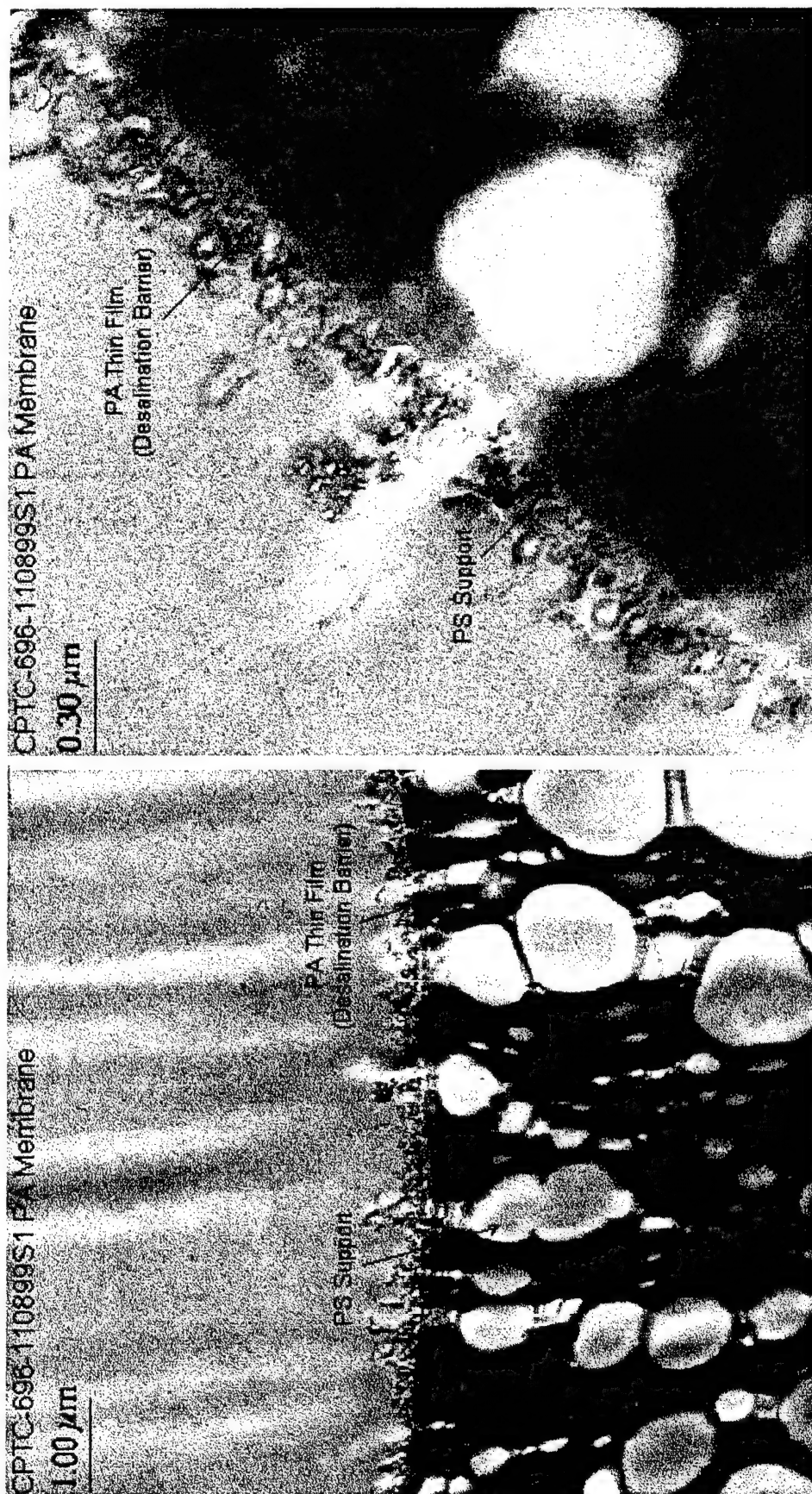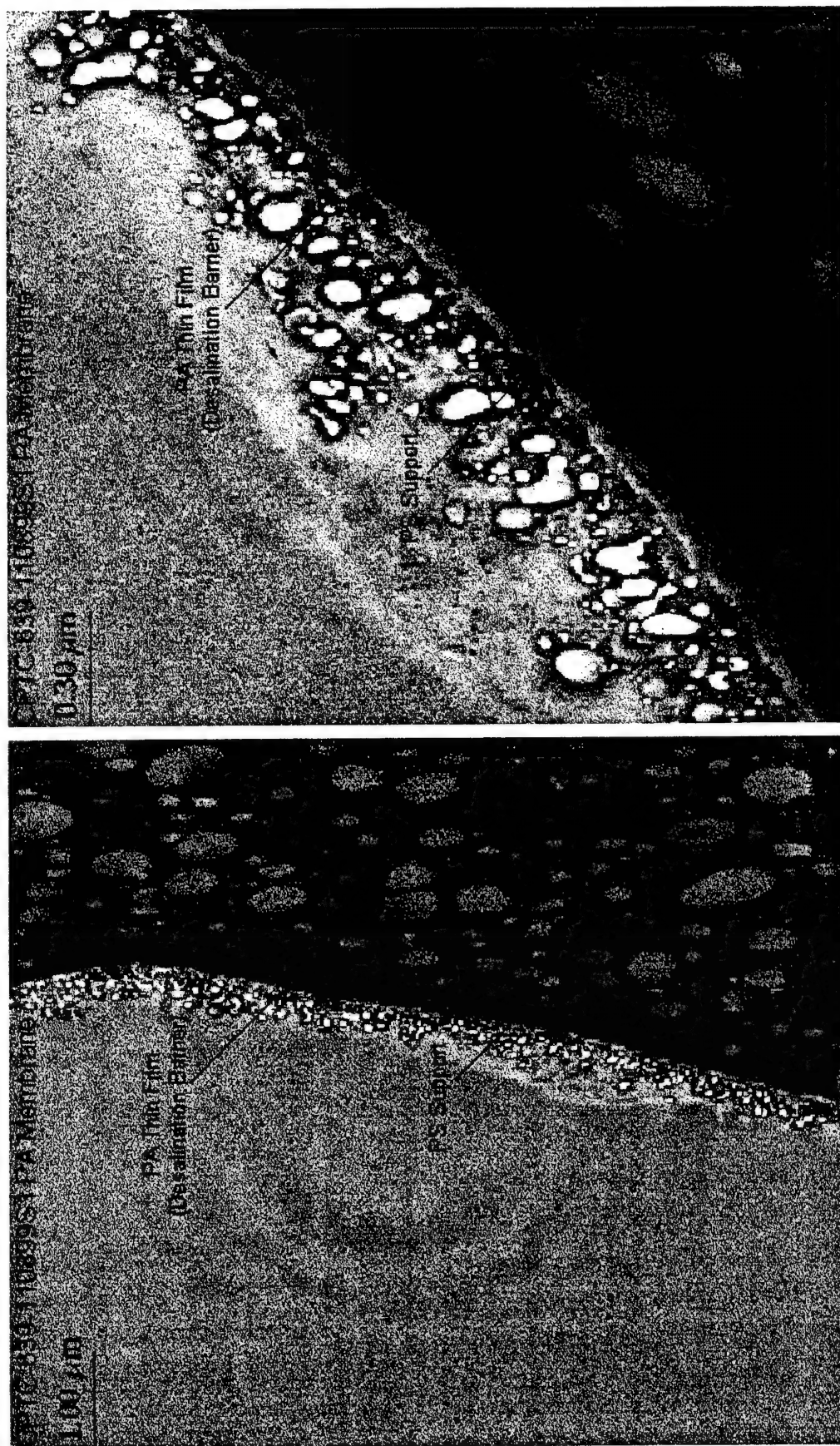
Figure 12.20   Transmission Electron Micrograph of the osmium stained cross-section of CPTC-639 PA membrane prepared with rinsing in 0.12-wt% sodium chloride solution for 30 minutes
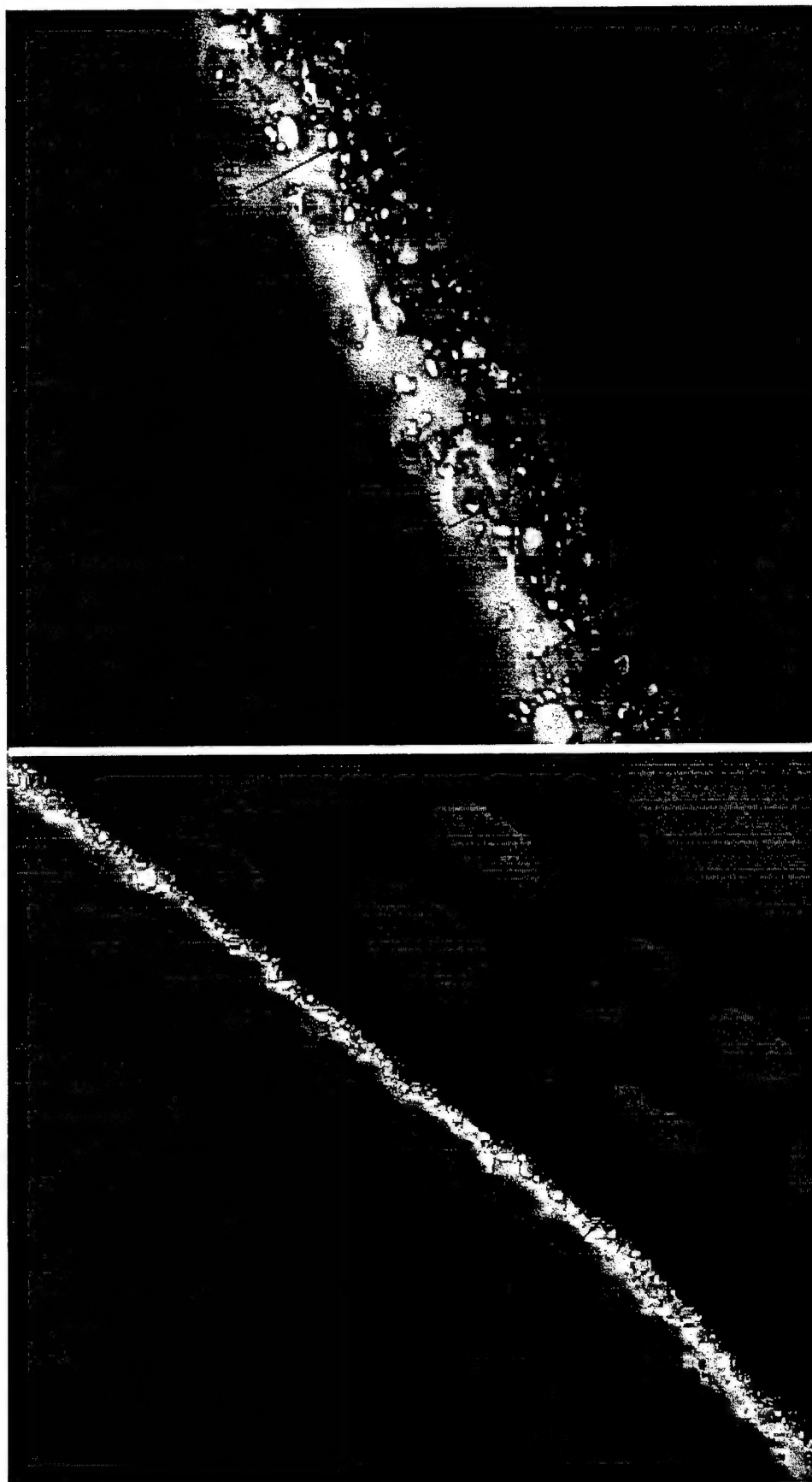
Figure 12.21   Transmission Electron Micrograph of the osmium stained cross-section of CPTC-640 PA membrane prepared with rinsing in 0.25-wt% sodium chloride solution for 30 minutes

194
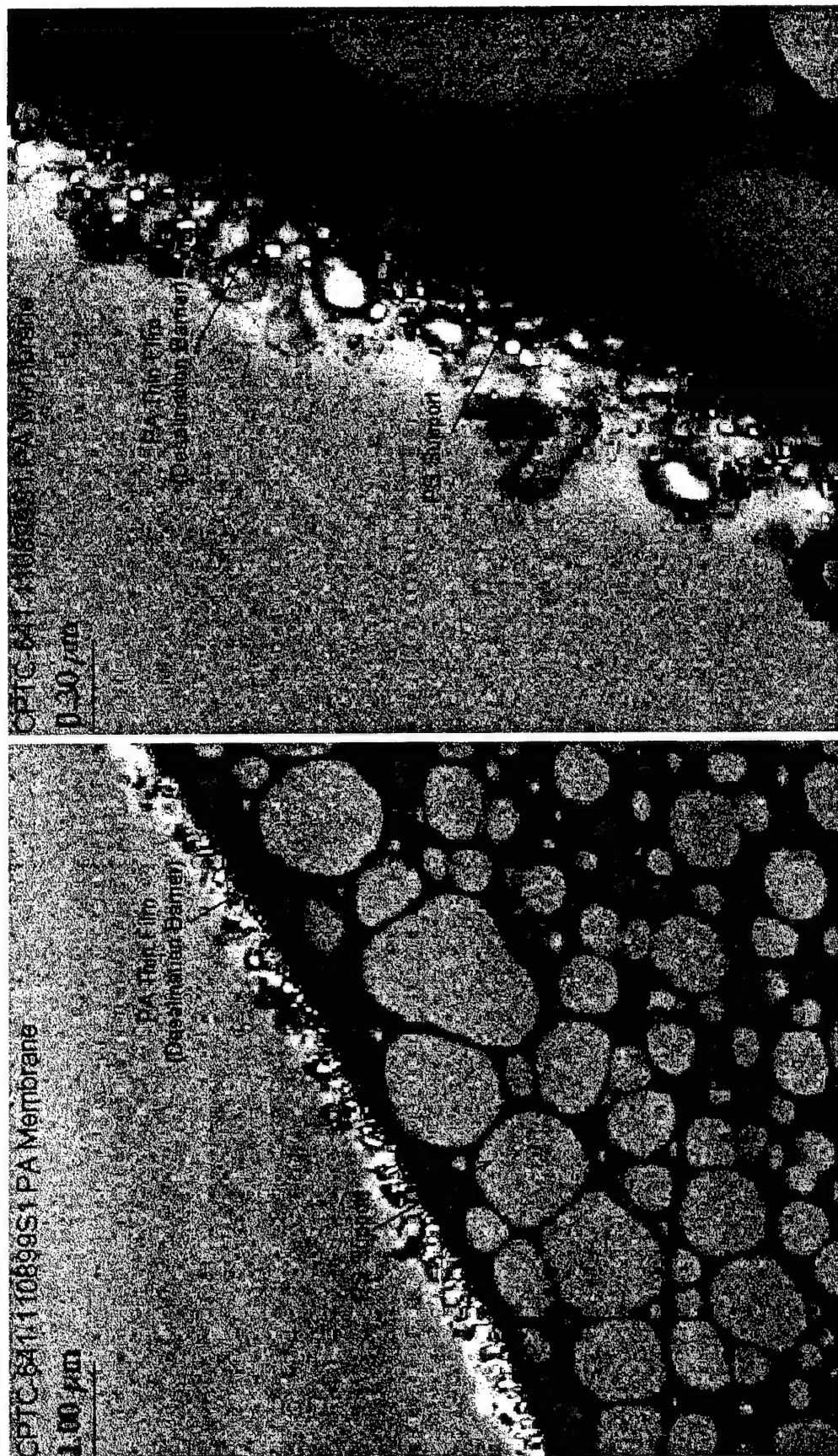
Figure 12.22 Transmission Electron Micrograph of the osmium stained cross-section of CPTC-641 PA membrane prepared with rinsing in 0.50-wt% sodium chloride solution for 30 minutes

12.9 Comparative Study of CPTC Membrane Before and After Exposure to Sodium Hypochlorite in the Absence and Presence of Bromide Ion in Short-Term Laboratory RO Tests

The cross-sectional structure of the PA barrier of CPTC membranes 905 and 898 were examined by TEM before and after the membranes were exposed to 3.5 mg/L sodium hypochlorite and after subsequent addition of 5.5 mg/L KBr. The RO tests are described in detail in Section 17.4; the performance data is presented in Figures 17.2 and 17.3. The PA surface of these membranes were also examined by EDX for C, O, Cl and Br. The results of these analyses are presented in Section 17.9, Table 17.4.

The electron micrographs are presented for CPTC 905 membrane in Figures 12.23, 12.24 and 12.25; the electron micrographs for CPTC membrane 898 are presented in Figures 12.26, 12.27 and 12.28. There are no striking differences in the barrier structure between new CPTC 905 membrane after the membrane was exposed to hypochlorous acid or after the membrane was exposed to hypobromous acid. Localized concentrations of osmium stain that are opaque to the electron beam (dark areas) appear in the PA barrier after chlorination (See Figure 12.24). However, the stain does not appear to penetrate the dense PA barrier beneath the cellular structure. This was not observed when the membrane was exposed to hypobromous acid. It is also important to note that the PA barrier was separated (delaminated) from the PS support membrane in several locations (See Figure 12.26). It is not certain if the separation is a result of osmotic blistering and/or poor adhesion to the PS support membrane. These characteristics were not observed for CPTC 898 membrane. (See Figures 12.27 and 12.28.)

12.10 Cross-Sectional Views of CPTC Membranes Before and After Short-Term RO Laboratory Tests with and without Sodium Hypochlorite. Osmium Stain Diffused into PA Barrier from Top Surface

Electron micrographs were taken of CPTC 836 membrane before and after exposure to 3.5 mg/L sodium hypochlorite in a short-term RO test. The membranes were stained with osmium prior to the electron microscope by diffusing the stain into the barrier from the top surface. Micrographs of the membrane before and after exposure to sodium hypochlorite, are shown in Figures 12.29 and 12.30. The membrane exposed to sodium hypochlorite shows very distinct areas where osmium has concentrated and has passed into the cellular formation of the barrier (see Figure 12.30). It appears as if some of the cellular structure of the barrier was ruptured by sodium hypochlorite. It is not clear, however, if the osmium has passed through and damaged the underlying dense PA film. The transport properties of the membrane were not deteriorated by the presence of sodium hypochlorite during the RO test.
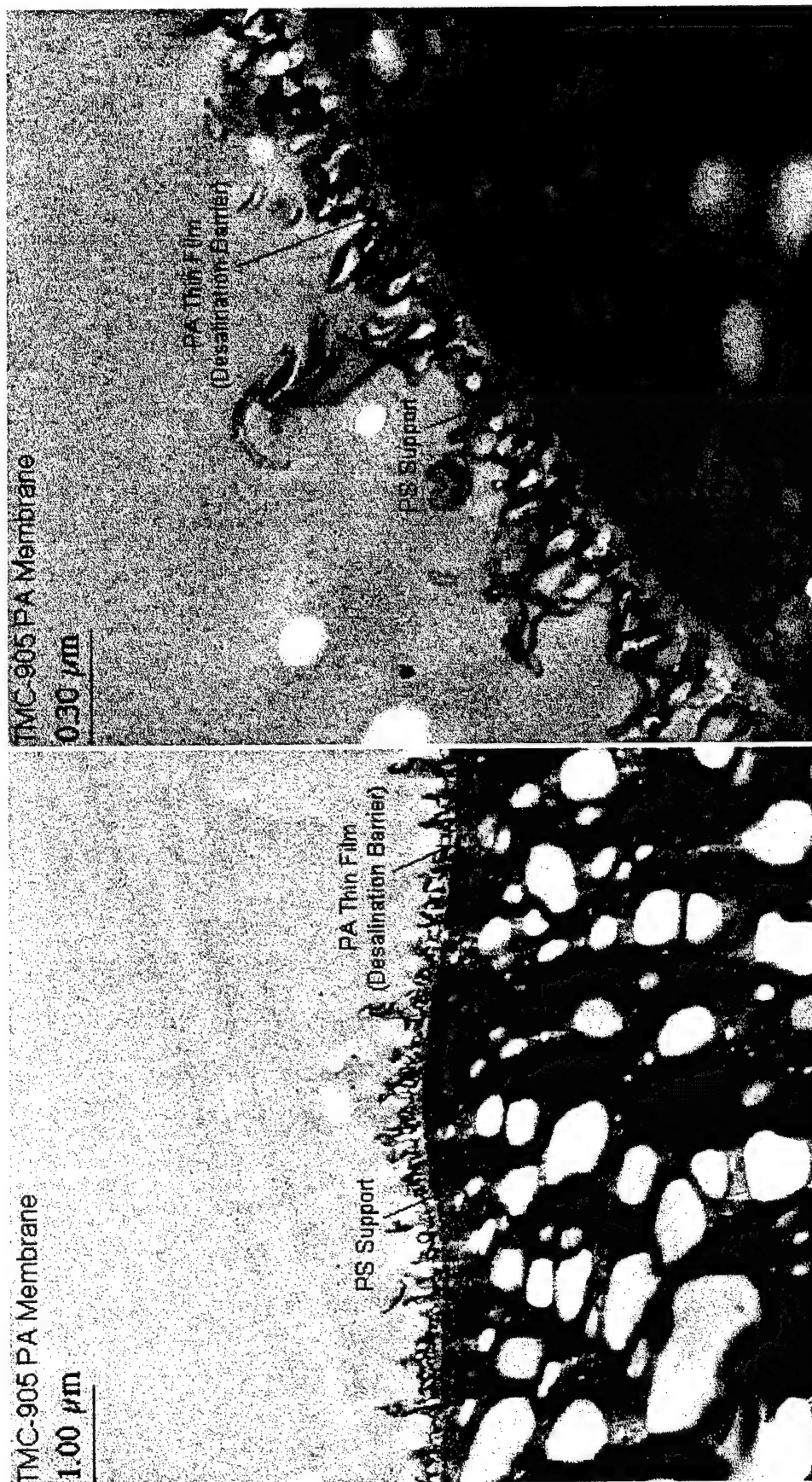
Figure 12.23 Transmission Electron Micrograph of the osmium stained cross-section of TMC-905 PA membrane (New)

Figure 12.24   Transmission Electron Micrograph of the osmium stained cross-section of TMC-905 PA membrane after exposure to sodium hypochlorite in RO

TMC-905 PA Membrane

1.00 μm

TMC-905 PA Membrane

0.30 μm

PA Thin Film
(Desalination Barrier)

PS Support

PA Thin Film
(Desalination Barrier)

PS Support

Figure 12.25   Transmission Electron Micrograph of the osmium stained cross-section of TMC-905 PA membrane after exposure to sodium hypochlorite in the presence of sodium bromide in RO

199

CPTC-898-022000S2 PA Membrane

0.30 μm

PA Thin Film
(Desalination Barrier)

PS Support

CPTC-898-022000S2 PA Membrane

1.00 μm

PA Thin Film
(Desalination Barrier)

PS Support

Figure 12.26   Transmission Electron Micrograph of the osmium stained cross-section of CPTC-898 PA membrane (New)

CPTC-898-022000S2 PA Membrane

1.00 μm

CPTC-898-022000S2 PA Membrane

0.30 μm

PA Thin Film
(Desalination Barrier)

PS Support

PA Thin Film
(Desalination Barrier)

PS Support

Figure 12.27   Transmission Electron Micrograph of the osmium stained cross-section of CPTC-898 PA membrane after exposure to sodium hypochlorite in RO

Figure 12.28   Transmission Electron Micrograph of the osmium stained cross-section of CPTC 898 PA membrane after exposure to sodium hypochlorite in the presence of sodium bromide in RO
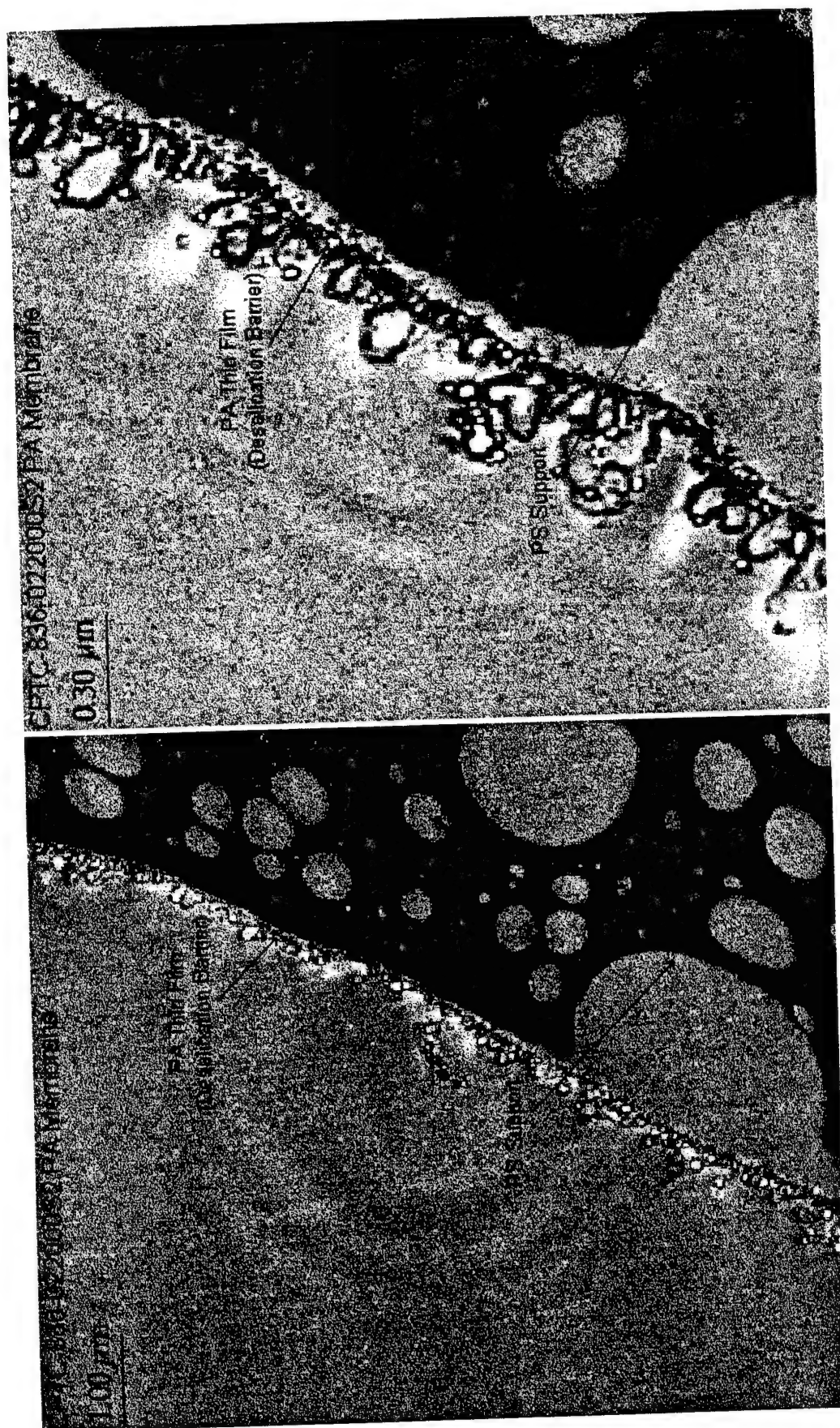
Figure 12.29 Transmission Electron Micrograph of the osmium stained cross-section of CPTC-836 PA membrane (New). Osmium stain diffused into PA barrier from top surface.
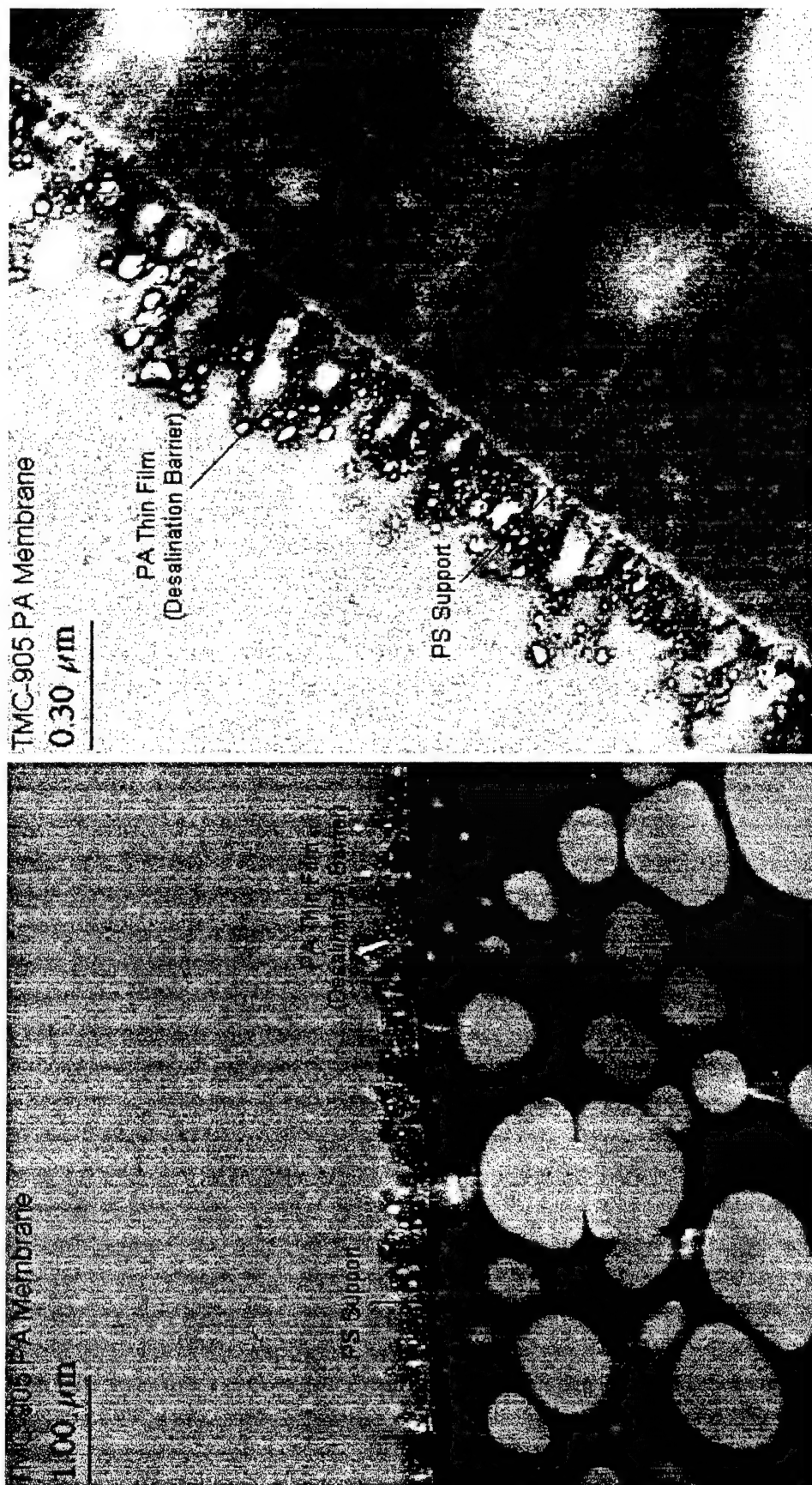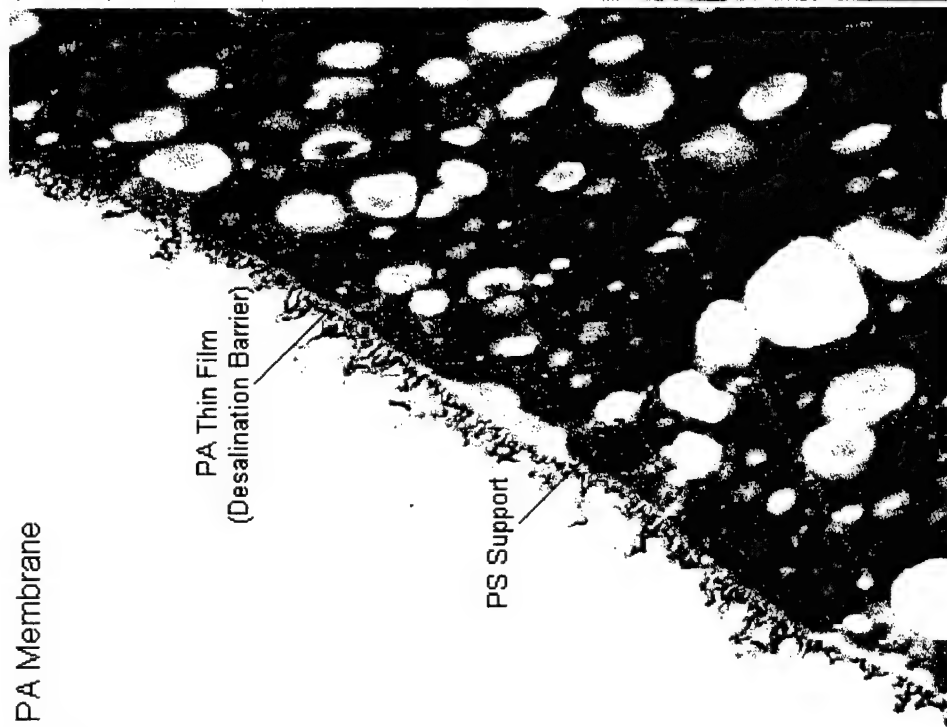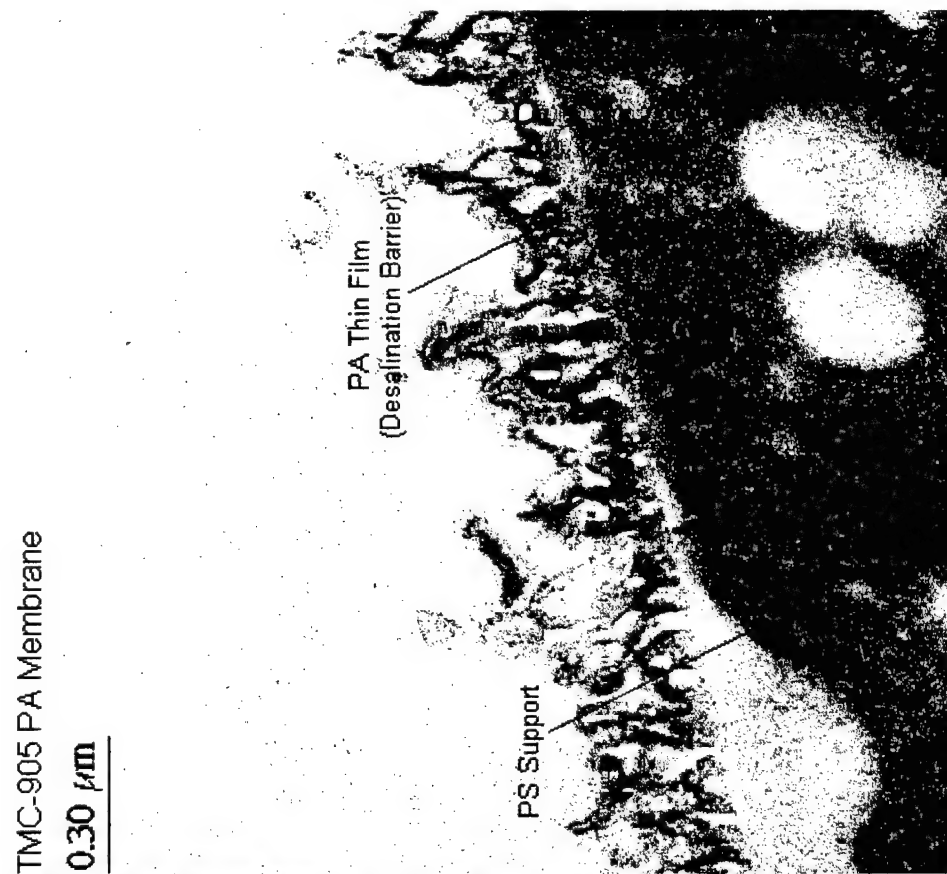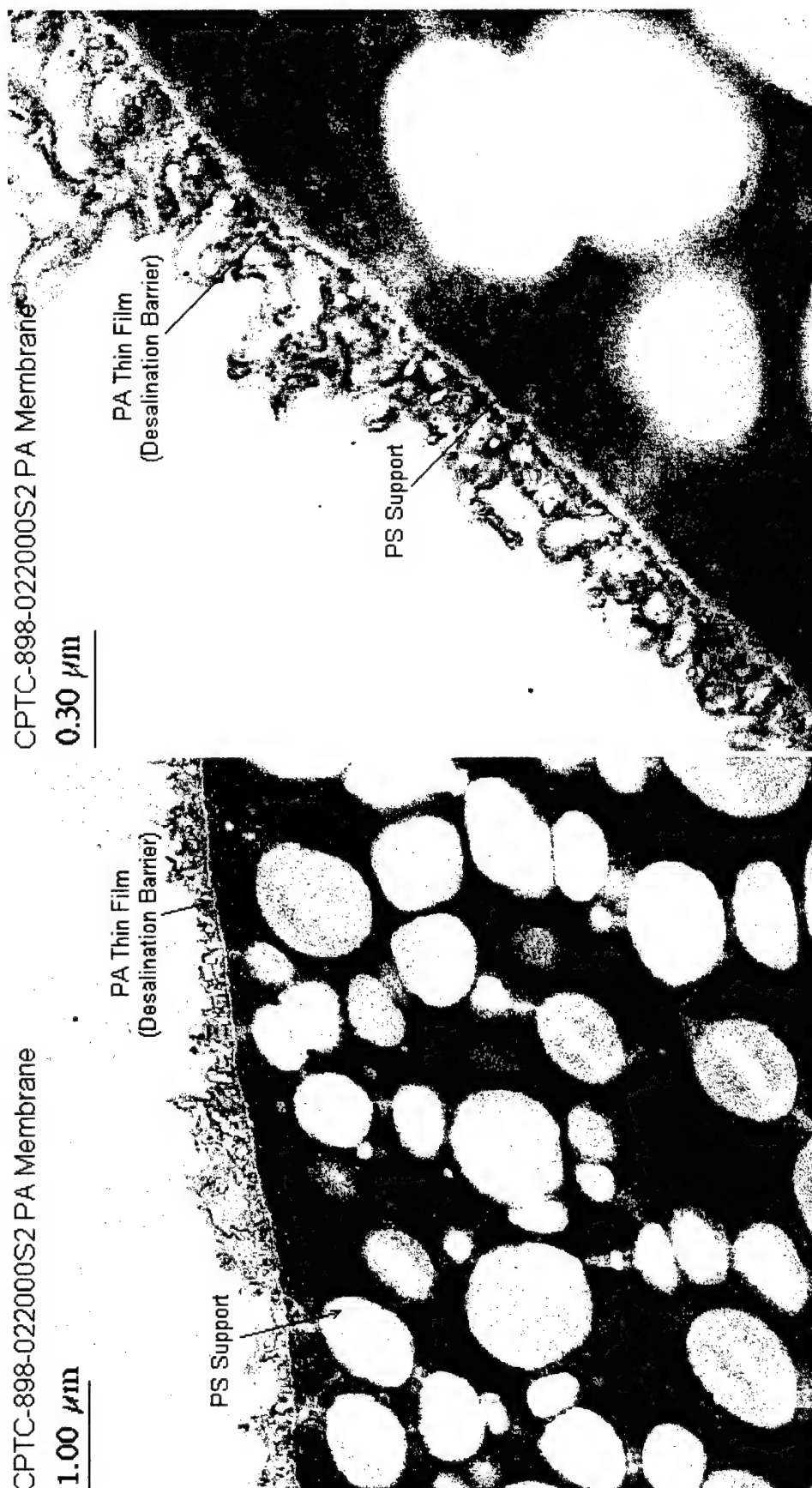
Figure 12.30   Transmission Electron Micrograph of the osmium stained cross-section of CPTC-836 PA membrane after exposure to sodium hypochlorite in RO. Osmium stain diffused into PA barrier from top surface.

12.11 CPTC Membrane Before and After Exposure to Sodium Hypochlorite in a Long-Term RO Test with Multiple Scheduled Shutdowns

Long-term RO field testing of CPTC membrane, as described in Sections 8.1.1 and 8.1.2, was conducted at the WQIC on brackish water and at NFESC on seawater. The results of those tests are summarized in Sections 21.0 and 22.0, respectively. All of the testing was conducted with membrane swatches using 1- x 3-in. test cells. The duration of these tests was shortened due to the number of shutdowns experienced at the field test sites. After shutdowns, significant increases in salt passage through the CPTC membranes were commonly observed; this was not observed with TMC membranes. The loss in performance of CPTC membranes after shutdown was believed to be physical rather than chemical. The PA barrier of the CPTC membrane could be compromised by osmotic blistering during membrane processing, poor adhesion to the PS substrate or to O-ring contact with the membrane when in a test cell. The latter would not be expected to be a problem if the membrane were incorporated into a spiral-wound element.

To verify the effect of RO shutdowns on CPTC and TMC membrane performance, a laboratory test was designed using the same test cells to simulate the conditions encountered in field testing. During the 200-day test the system was operated for 8-hr periods and depressurized approximately 100 times. After 90 days of operation, 3.5 mg/L of sodium hypochlorite was added daily. The performance, shown in Figure 12.31 clearly shows the effect of shutdowns on both water and salt passage through the CPTC membrane. As in the field tests, water and salt passage through the TMC membrane were not affected by shutdowns.

Electron micrographs were taken of the cross-section of the PA barriers of TMC 611 and CPTC 616 membranes after they had been subjected to sodium hypochlorite and after completion of the RO test. The osmium stain was introduced into the barrier by two different methods. In one case the membranes were totally immersed into the osmium solution and in the other case the osmium solution was contacted with only the desalination surface of the barrier. Micrographs of TMC membrane prepared by each method of staining are shown in Figures 12.32 and 12.33. Similarly, micrographs of CPTC membrane prepared by each method of staining are shown in Figures 12.34 and 12.35. There is no significant difference in appearance between any of the membranes due to the difference in staining methods. However, the barrier structure of the CPTC membrane appeared very different after approximately 100 shutdowns in RO. The cellular structure on the barrier has expanded, is much thicker and appeared somewhat fragmented. Delamination also appeared to be more prevalent.

Test Conditions: 2,000 mg/L NaCl feed, 225 psi applied pressure, 1.0 gal/min feed flow, pH 6.5, 25°C, 5.0 mg/L EDTA

Figure 12.31   Effect of programed shutdowns on the long-term RO performance of CPTC 616 and TMC 611 membranes. The RO system was run daily for 8 hr both with and without chlorine.   Approximately 100 depressurization cycles were conducted over a 200-day period.

TMC-611 PA Membrane
0.30 µm

PA Thin Film
(Desalination Barrier)

PS Support

TMC-611 PA Membrane
1.00 µm

PA Thin Film
(Desalination Barrier)

PS Support

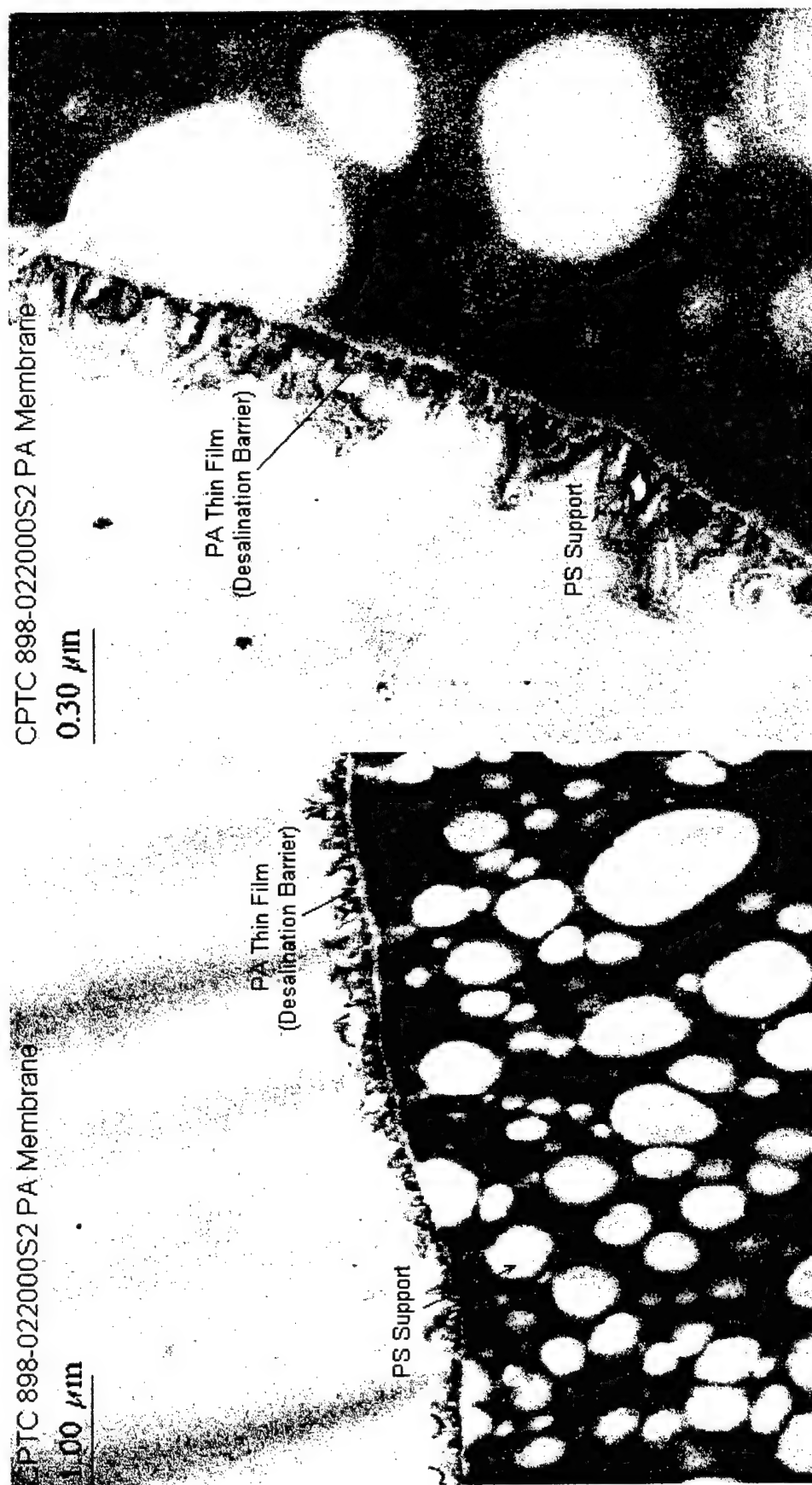Figure 12.32 Transmission Electron Micrograph of the osmium stained cross-section of TMC-611 PA membrane after exposure to sodium hypochlorite in RO shut down test (See Fig. 12.31)

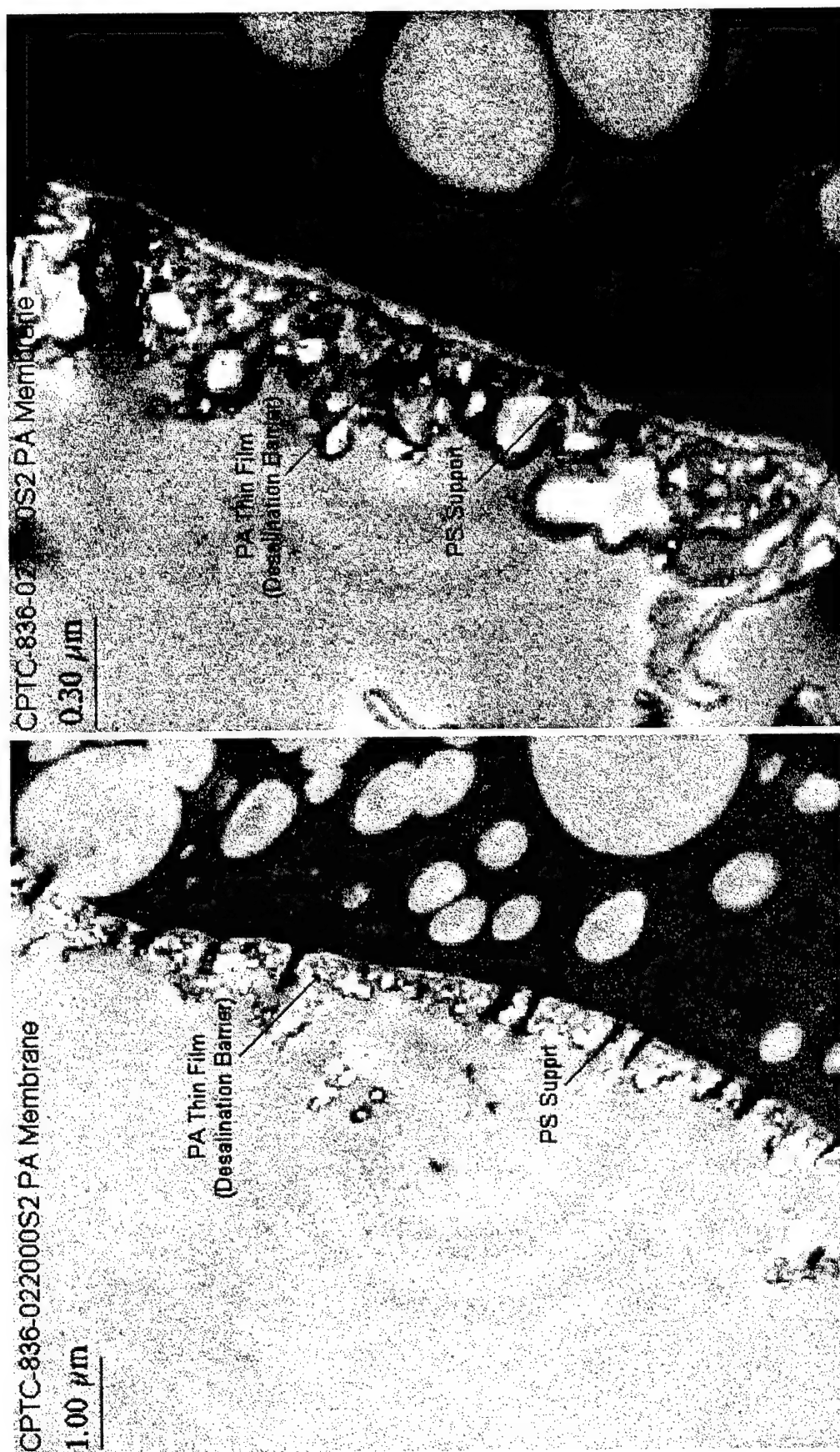Figure 12.33   Transmission Electron Micrograph of the osmium stained cross-section of TMC-611 PA membrane after exposure to sodium hypochlorite in RO shut down test (See Fig. 12.31). Osmium stain diffused into PA barrier from top surface.

208

CPTC-616-110899S1 PA Membrane
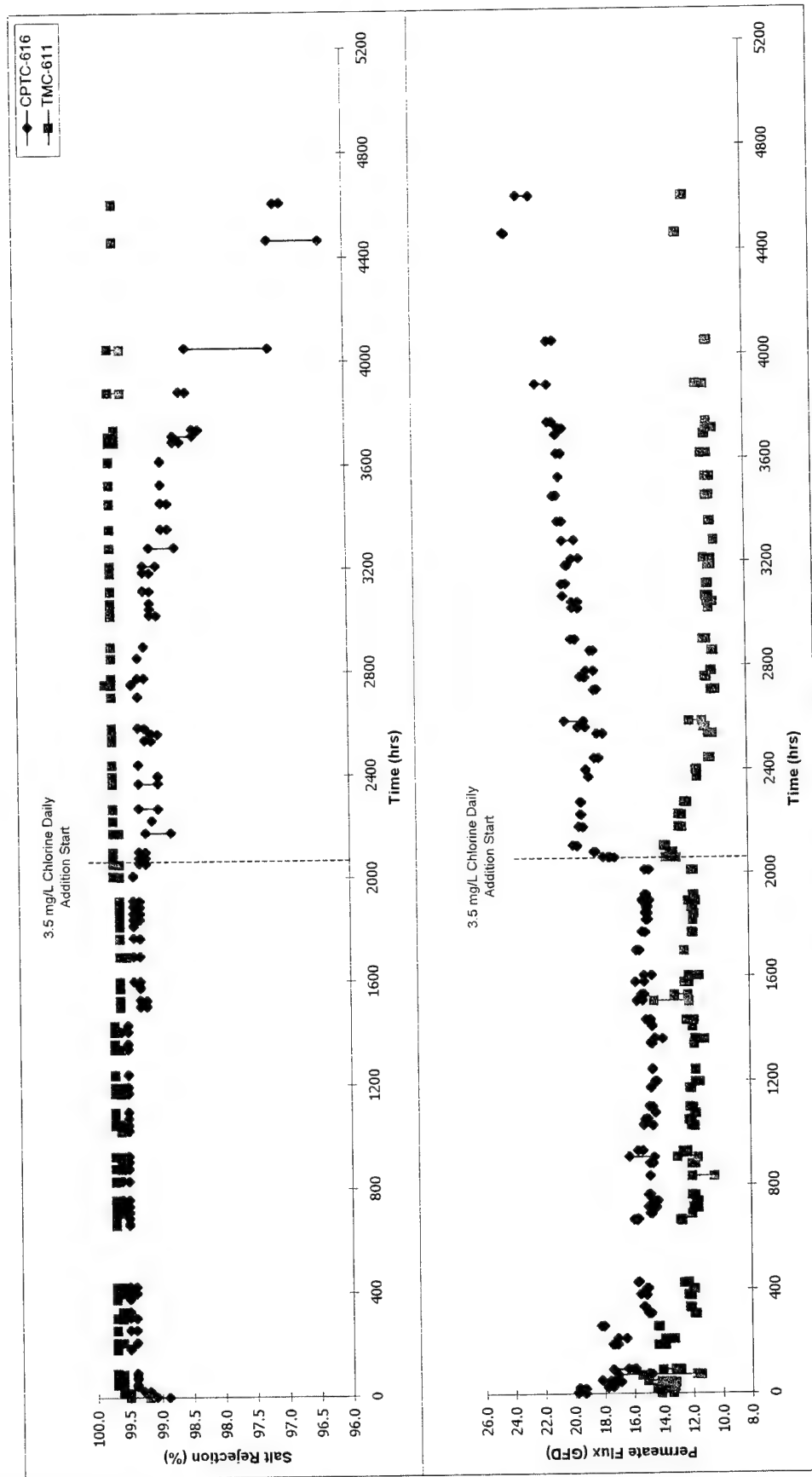1.00 μm

PA Thin Film
(Desalination Barrier)

PS Support

Figure 12.34   Transmission Electron Micrograph of the osmium stained cross-section of CPTC-616 PA membrane after exposure to sodium hypochlorite in RO shut down test (See Fig. 12.31).   Membrane totally immersed in osmium solution for staining.

Figure 12.35 Transmission Electron Micrograph of the osmium stained cross-section of CPTC-616 PA membrane after exposure to sodium hypochlorite in RO shut down test (See Fig. 12.31). Osmium stain diffused into PA barrier from top surface.

210

12.12 Comparative Study of ctct-CPTC and *cccc*-CPTC Membranes After Exposure to Sodium Hypochlorite in Long-Term RO Field Tests at WQIC in Yuma, AZ

The comparative performances of *ctct*-CPTC 677 and *cccc*-CPTC 686 membranes were determined in 1-hr laboratory RO tests and in long-term RO field tests at WQIC with 0.5 to 1.5 mg/L free chlorine in the feed. The structure of the PA barrier of each membrane was determined by TEM at the completion of the tests. In field tests, the *ctct*-CPTC membrane had lost performance after 1,000 hr while the *cccc*-CPTC membrane steadily lost performance from the beginning of the test. Cross-sections of the barrier of the CPTC 677 membranes are shown in Figures 12.36 and 12.37. The PA barrier structure of the membrane removed from the short-term RO test shows no significant changes. The presence of a thick fouling layer was the main feature observed on the membrane removed from the long-term RO test at WQIC. Both the cellular structure and the dense PA layer could be seen within the fouling layer. No physical signs of membrane deterioration were evident.

Cross sections of the barrier of *cccc*-CPTC 686 membranes are shown in Figures 12.38 and 12.39. The barrier of the membrane removed from the short-term RO test shows numerous areas where osmium stain has penetrated the cellular structure and in some areas the PA dense barrier. The latter could be indicative of membrane failure. A similar pattern was seen in the PA barrier of the membrane operated in the long-term field test at WQIC. A thick fouling layer was also evident on the latter membrane.

13.0 EFFECT OF MPD APPLICATION ON SURFACE ROUGHNESS

AFM analysis of membranes made at the start of the project revealed striations or contours on the polymer surface. Membranes with high surface area per unit volume are generally desirable. These membranes typically perform more efficiently, i.e., greater water flux per unit area. Therefore, the effect of MPD application on surface morphology or roughness was investigated. In the process of making a membrane, the MPD-treated PS surface was brushed to reduce concentration polarization on the surface and to assure uniform distribution and reaction of MPD with the acid chloride. Subsequently, the excess aqueous MPD solution was removed by "rubber nip roller" treatment just prior to passage of the membrane into the acid chloride solution. The striations observed earlier resulted from either the brushing or the rubber nip roller applicator or both.

13.1 Experimental Method

To investigate whether the brush treatment was a factor in the formation of these surface striations, three different brush types were utilized, a sponge brush, a fine brush and a "regular" brush. A non-brushed sample served as a control. MPD was applied to the surface of the PS membrane support, brushed accordingly and then rolled by the rubber nip roller. Acid chloride, TMC or CPTC (Lot No. 030399S1), dissolved in hexane was immediately applied to the roller-brushed MPD layer and then removed by rinsing.
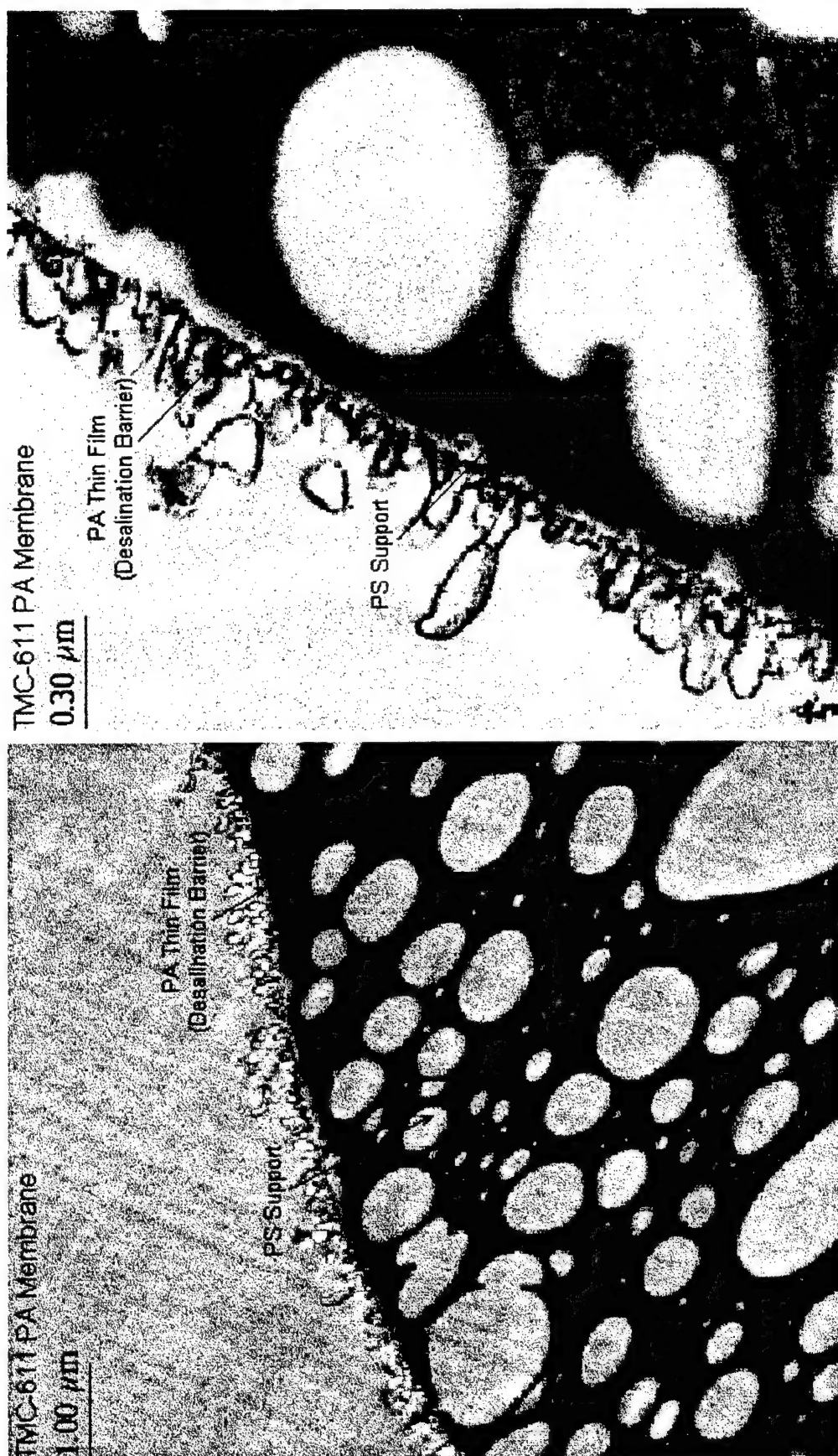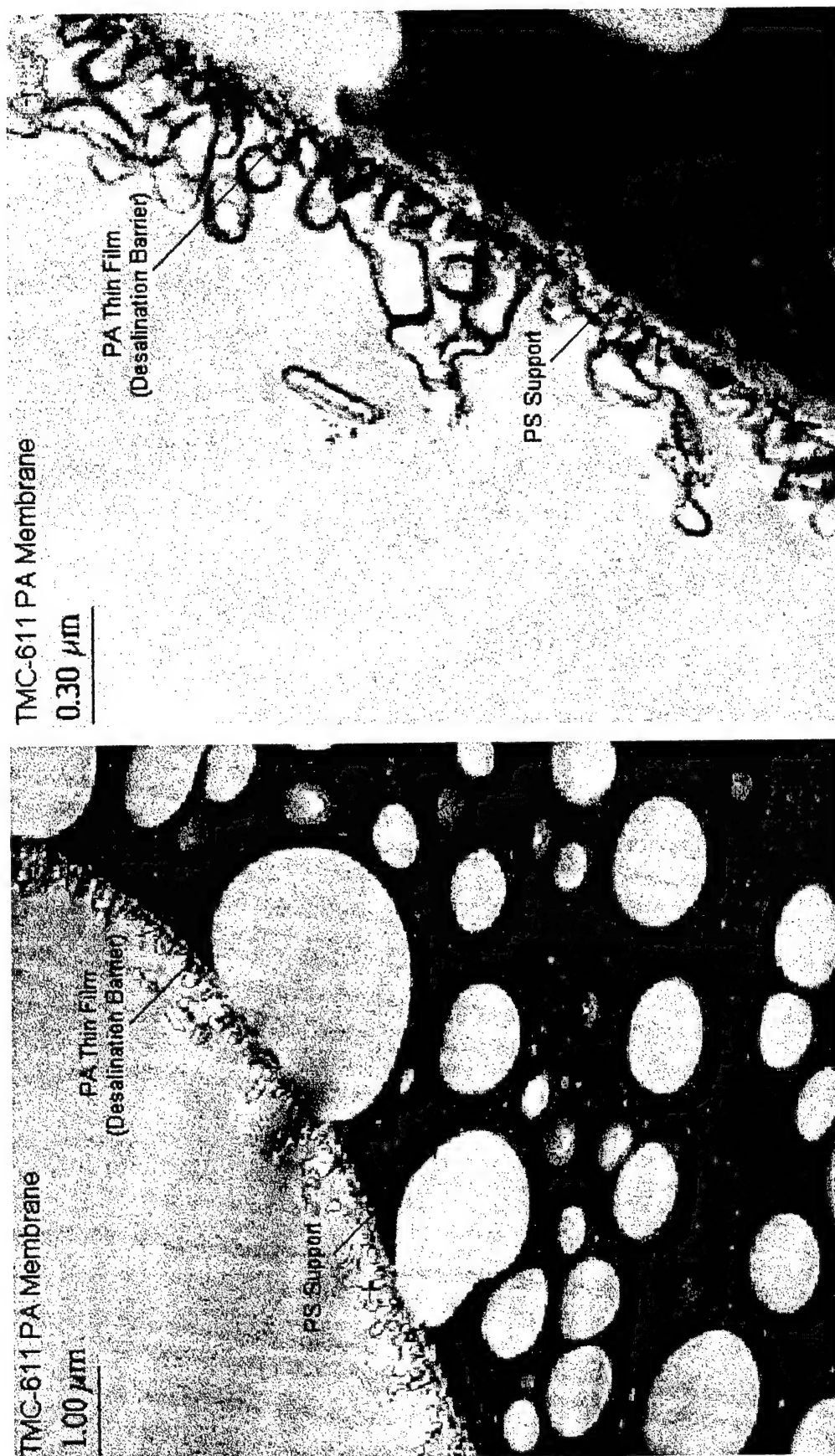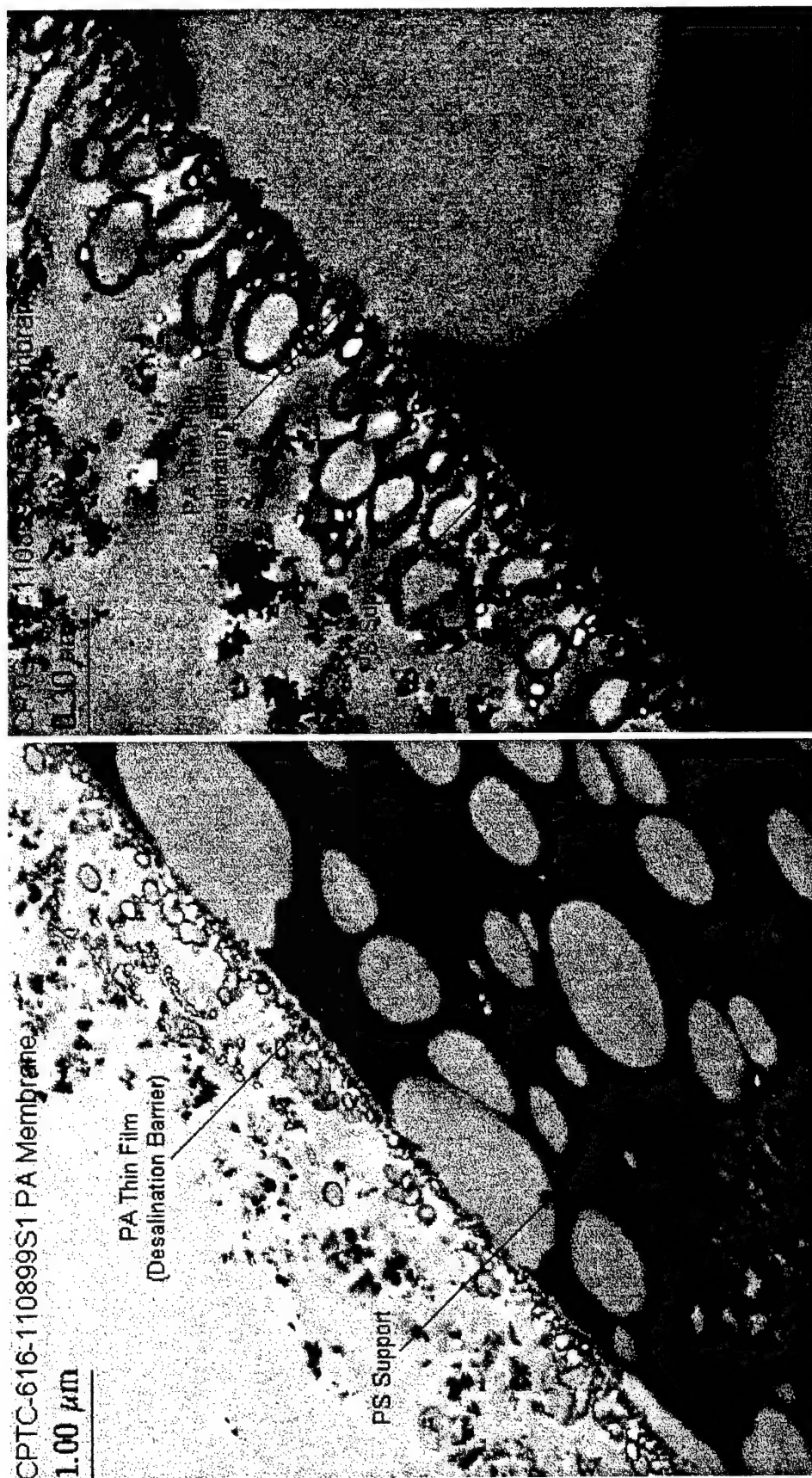
Figure 12.36 Transmission Electron Micrograph of the osmium stained cross-section of CPTC-677 PA membrane after exposure to sodium hypochlorite in short-term laboratory RO test. Membrane from same lot evaluated in RO testing at WQIC in Yuma, AZ (See Fig. 12.37).

CPTC-677-110899S1 PA Membrane

CPTC-677-110899S1 PA Membrane
0.30 µm

PA Thin Film
(Desalination Barrier)

PS Support

CPTC-677-110899S1 PA Membrane
1.00 µm

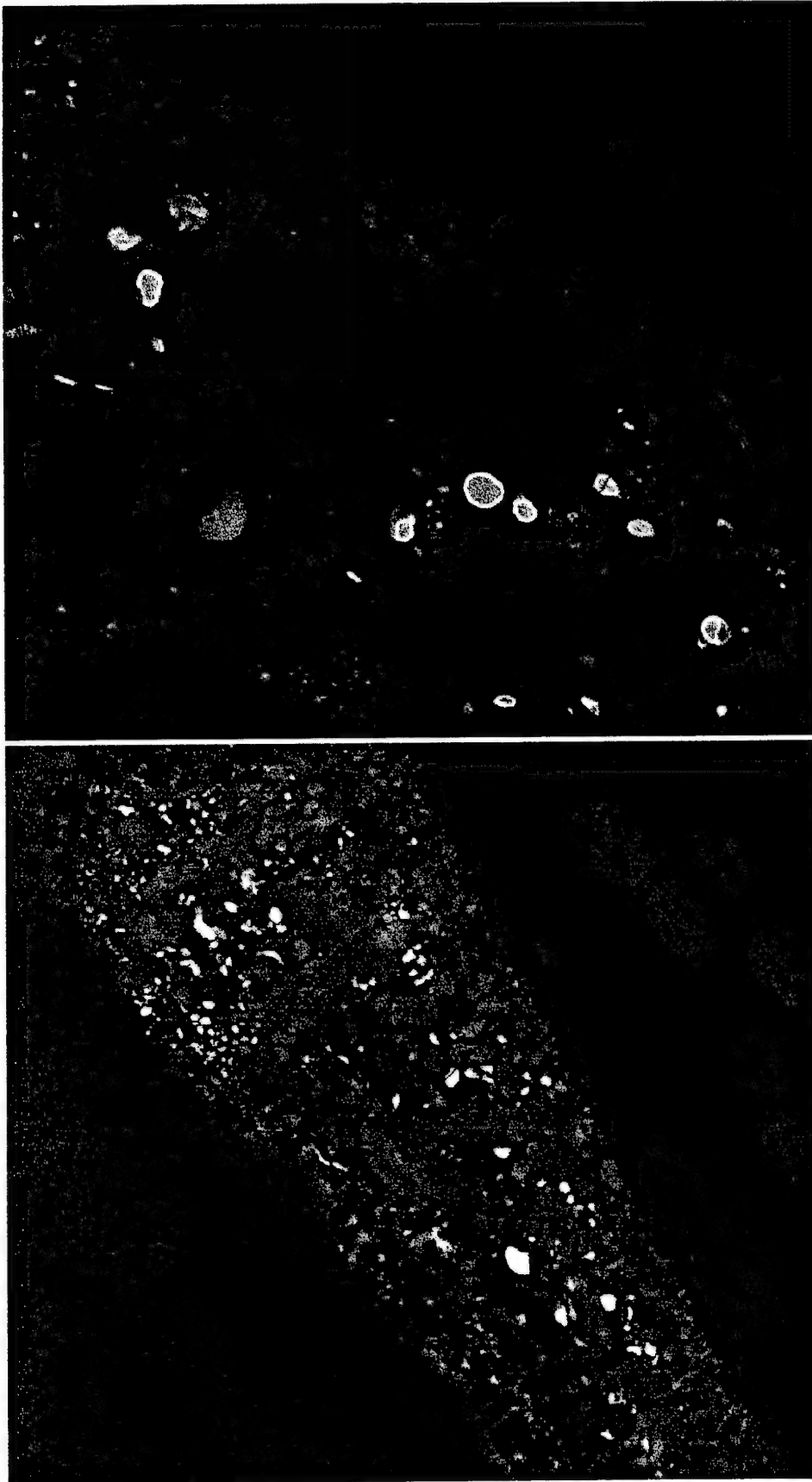PA Thin Film
(Desalination Barrier)

PS Support

Figure 12.37   Transmission Electron Micrograph of the osmium stained cross-section of CPTC-677 PA membrane after exposure to sodium hypochlorite in RO field testing at WQIC in Yuma, AZ.   See Figure 20.3 for RO performance data.

cccc-CPTC-686 PA Membrane

1.00 µm

PA Thin Film
(Desalination Barrier)

PS Support

Figure 12.38 Transmission Electron Micrograph of the osmium stained cross-section of cccc-CPTC-686 PA membrane after exposure to sodium hypochlorite in short-term laboratory RO test. Membrane from same lot evaluated in RO testing at WQIC in Yuma, AZ (See Fig. 12.39).

cccc-CPTC-686 PA Membrane
0.30 μm

PA Thin Film
(Desalination Barrier)

PS Support

cccc-CPTC-686 PA Membrane
1.00 μm

PA Thin Film
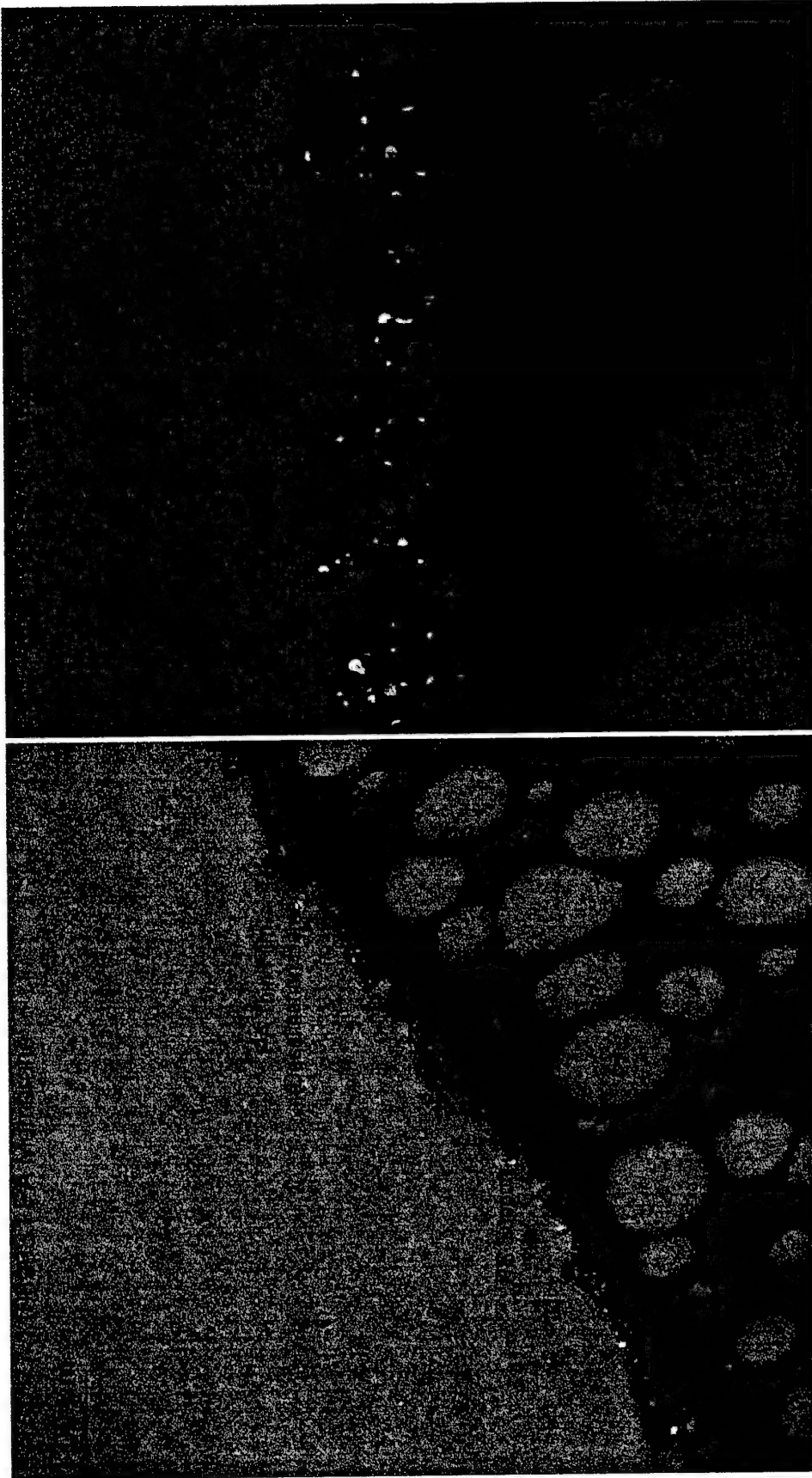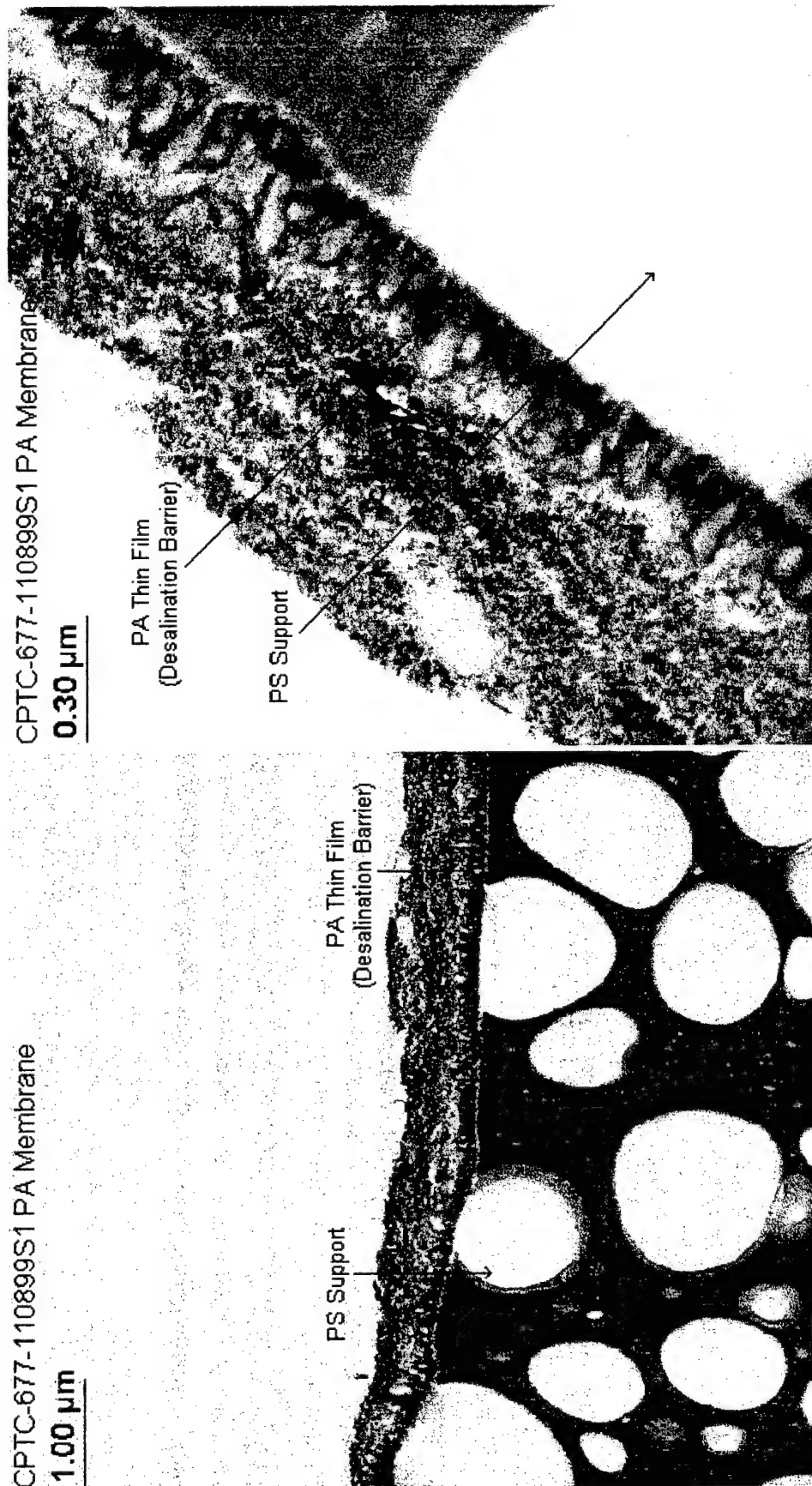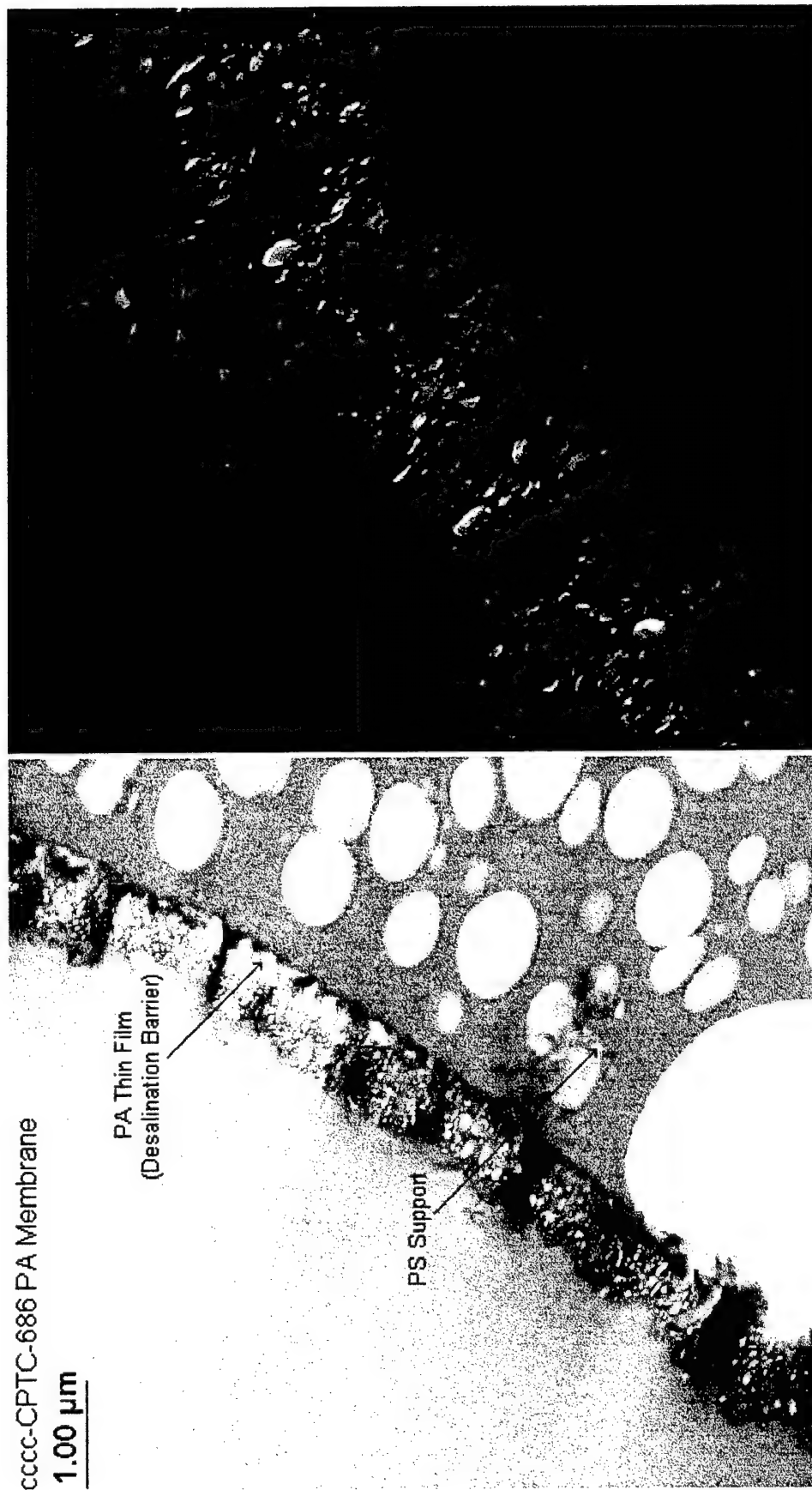(Desalination Barrier)

PS Support
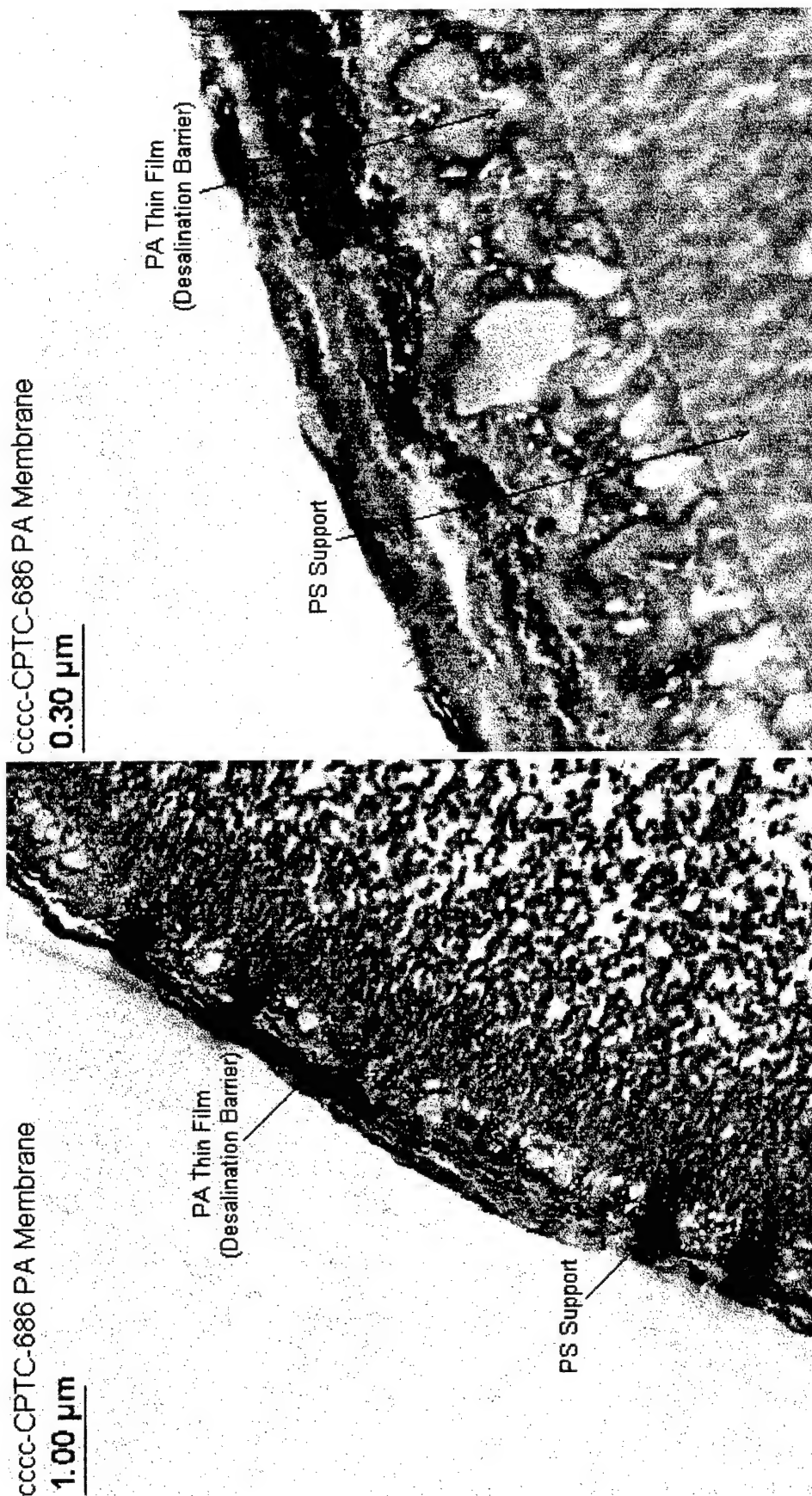
Figure 12.39   Transmission Electron Micrograph of the osmium stained cross-section of cccc-CPTC-686 PA membrane after exposure to sodium hypochlorite in RO field testing at WQIC in Yuma, AZ. See Figure 20.2 for RO performance data.

215

13.2 Results and Discussion

A series of four AFM images (10 µm) of membranes made with CPTC acid chloride applied with a fine brush, sponge brush, regular brush and no brush are shown in Figure 13.0. A similar series of AFM images from membranes made of TMC are also shown in Figure 13.1. Plots of the RMS roughness and mean height are displayed in Figure 13.2. Application of the sponge brush and regular brush techniques prior to acid chloride addition both produced membranes that were smoother than the fine brush and non-brushed membranes. Presumably, more MPD was removed from the PS support membrane by these brushes, leaving less to react with the acid chloride. This conclusion is supported by the fact that the non-brushed and fine brush MPD applications resulted in films that were significantly thicker than the sponge-brushed and non-brushed membranes Figure 13.3. The amide II / 874 cm^{-1} band intensity ratio for a FilmTec membrane is displayed for comparison in Figure 13.3. Similar trends in RMS roughness, mean height and relative thickness were observed for films made with TMC (Figure 13.2 and 13.3).

While distinct differences in surface morphology were observed, varying the standard procedures was not determined to be critical to the success of the project. However, in the future, issues related to altering surface morphology may be readdressed.

14.0 EFFECT OF FEEDWATER pH ON THE PERFORMANCE OF CPTC MEMBRANES

The purpose of these experiments was to determine the effect of pH on the performance, i.e., sodium ion (sodium chloride) rejection, of the CPTC membrane and determine the optimum pH range at which the membrane operates. As more studies were completed, it became apparent that the CPTC membrane performance improved with purity and that exposure to chlorine and sodium chloride resulted in an improvement in membrane performance over a broader pH range. The results of these studies are discussed below. In this Section, reference to sodium ion implies sodium chloride, as determined by ICP-MS measurements.

14.1 Experimental Method

Three membrane types were tested that included a FilmTec, TMC and CTPC. membrane samples were initially operated on a 2,000-mg/L sodium chloride feed, pH 4.5 at 225 psi applied pressure at 25°C. After 1 hr, flux and (conductivity) rejection were measured and then the feedwater was adjusted to pH 6.5. After 1 hr of operation, a second permeate sample was collected. The pH was adjusted to pH 9.0, and after 1 hr the flow and rejection were measured. The pH was then dropped back to 6.5, operated for 1 hr and flow and rejection remeasured. Finally, the pH was dropped back down to 4.5, the membrane operated for 1 hr and flux and rejection measured one last time. After each 1-hr operational period small (25-50 mL) samples of permeate were collected and shipped to OCWD for sodium ion analysis by ICP-MS.
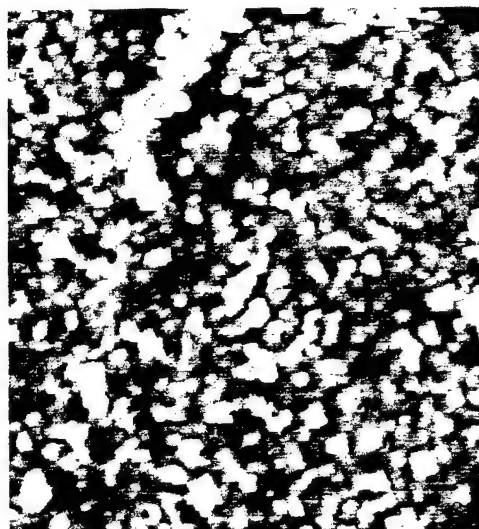
fine brush
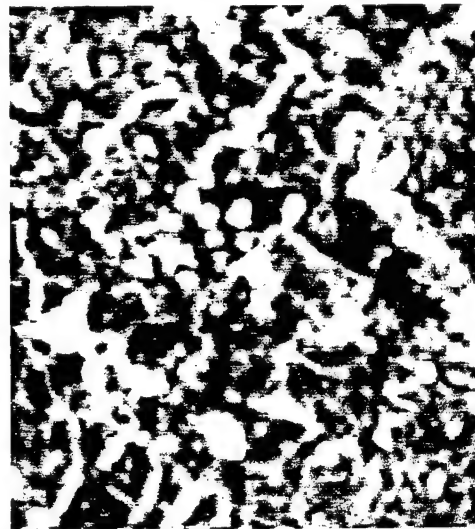
sponge brush

regular brush

no brush

Figure 13.0   Effect of MPD application on membrane surface topography. AFM images (10 μm) of membranes prepared from CPTC-AC Lot No. 030399S1) and MPD.

fine brush
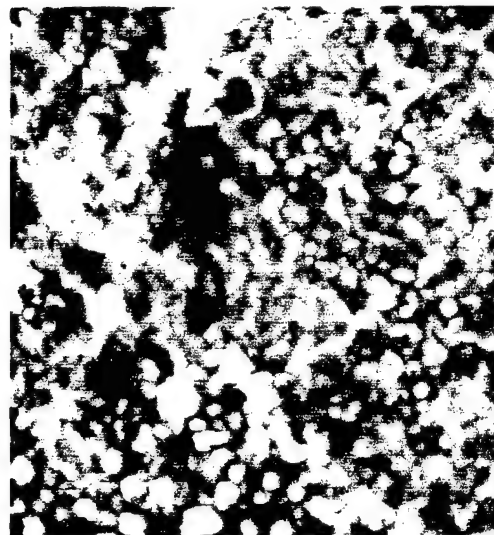
sponge brush
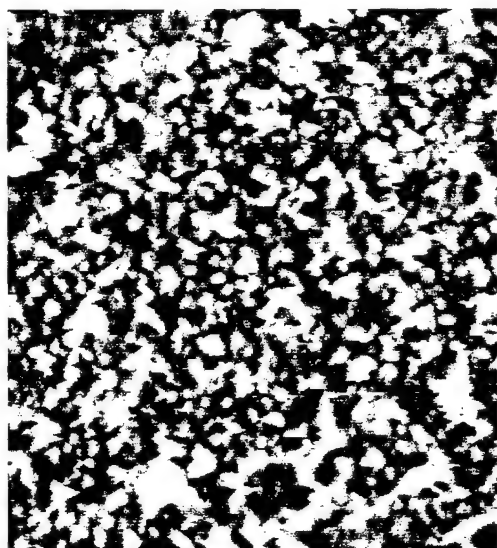
regular brush

no brush

Figure 13.1   Effect of MPD application on membrane surface topography. AFM images
(10 μm) of membranes prepared with TMC and MPD.
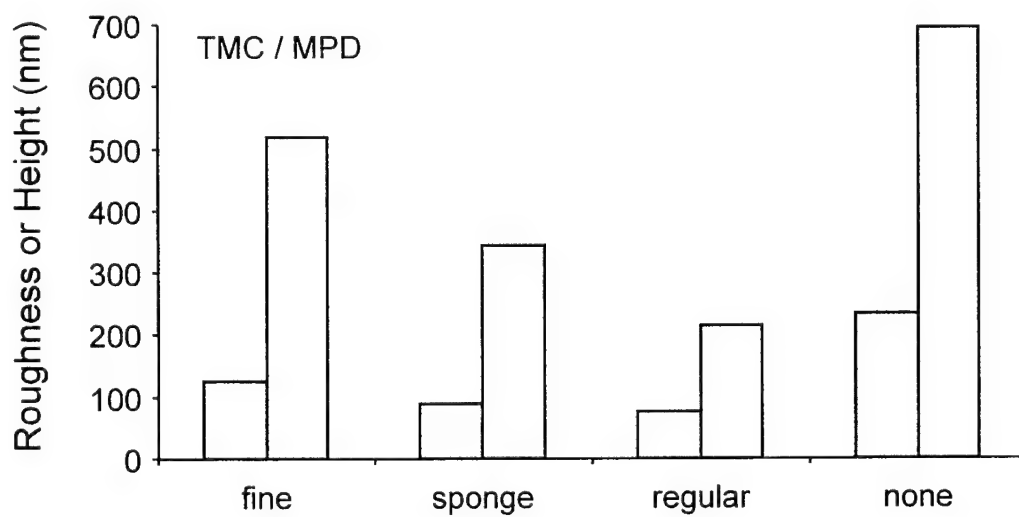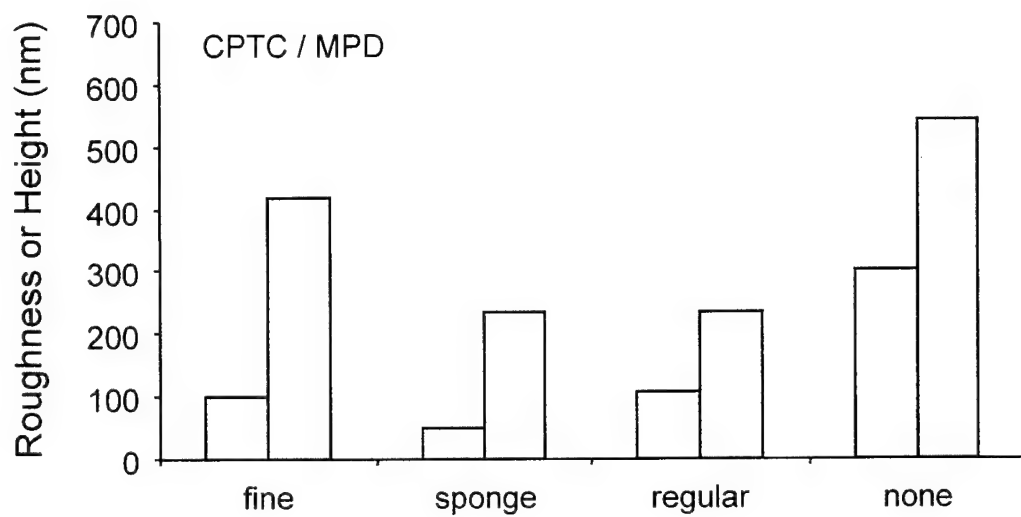
Figure 13.2   Effect of brush application on polyamide surface roughness, RMS roughness (□) and mean height (□).
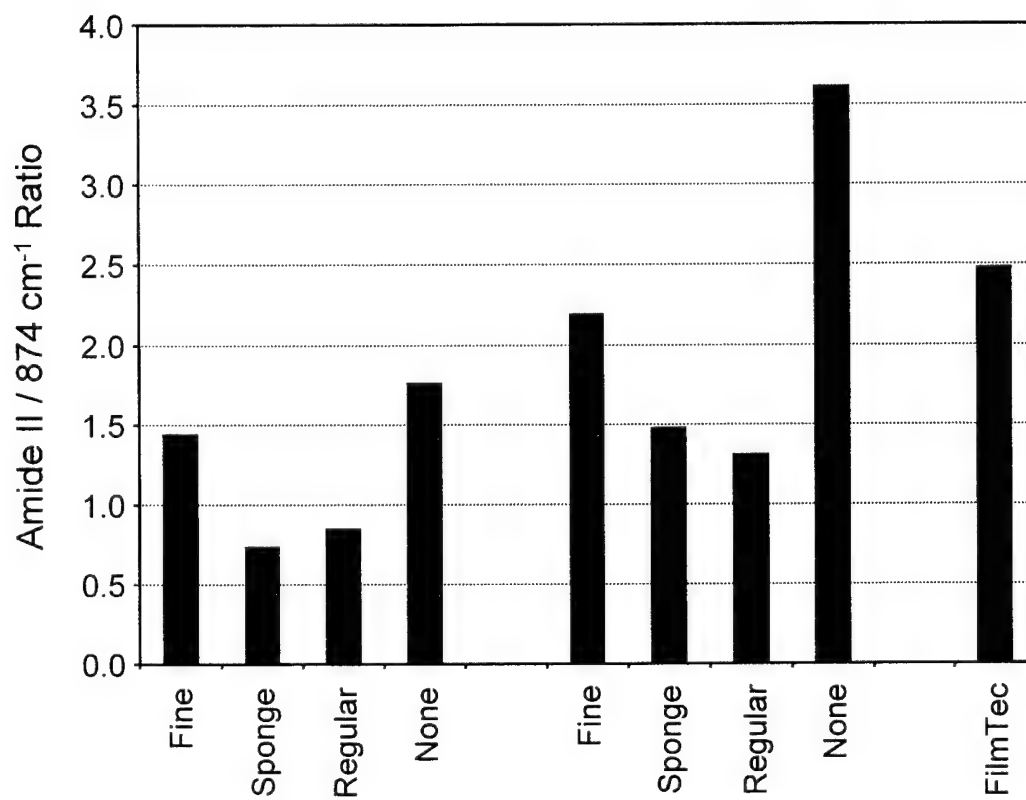
Figure 13.3 Effect of MPD application by brush type on relative polyamide film thickness
of CPTC / MPD (■), TMC / MPD (■) and FilmTec control membrane.

14.2   Results and Discussion

The first set of membranes to be tested were made from CPTC acid chloride (CPTC-AC Lot No. 061099S1). Membrane made from this lot did not perform well at low pH, i.e., 4.5 (Figure 14.0). A sodium ion rejection of only 94.5% was measured compared to 98.75% for the FilmTec and 98.2% for the TMC membranes. When the pH of the feedwater was increased to 6.5, the sodium ion rejection improved significantly, increasing from 94.5% to 98.9%. The sodium ion rejection of the FilmTec and TMC membrane also improved after the pH was increased to 6.5. The feedwater pH was increased a second time to 9.0. The rejection of the CPTC membrane (CPTC-AC Lot No. 061099S1) dropped slightly to 98.5%, but essentially was unchanged (Figure 14.0). The sodium ion rejection of the FilmTec membrane increased slightly, while the rejection of the TMC membrane dropped only slightly. The pH was dropped back to 6.5, and no major changes in sodium ion rejection were recorded for any of the membranes. The pH of the feedwater was adjusted one final time back down to 4.5. The rejection of the CPTC membrane dropped from 98.65% to 94.55% (Figure 14.0) and the TMC membrane from 99.2% to 97.3%. The sodium ion rejection of the FilmTec membrane dropped down to 98.75% near its value at the start of the experiment.

The experiment was repeated after a purer CPTC-AC (Lot No. 092099S2) was prepared and membranes made. Sodium ion rejection improved significantly, increasing from 94.5% (Trial No. 1) to 97.7% (Trial No. 2) rejection at pH 4.5 (Figure 14.1). While the sodium ion rejection improved at pH 4.5 from CPTC-AC Lot No. 061099S1 to Lot No. 092099S2, the overall trend in sodium ion rejection with change in feedwater pH remained the same. The sodium ion rejection of the CPTC membrane (CPTC-AC Lot No. 092099S2) increased to 99.55% when the pH was increased to 6.5, remained constant with changes in feedwater pH up to 9.0 and back down to 6.5. However, when the pH of the feedwater to the CPTC membrane was dropped back down to pH 4.5, sodium ion rejection dropped below the 97.7% starting point to 95.5%.

In Trial No. 2, the TMC membrane (Figure 14.1) demonstrated an overall improvement in sodium ion rejection over the same pH range, which suggests that the lot-to-lot improvement in rejection is associated with experimental error or membrane variation to some extent. The TMC membrane did not perform as well at pH 4.5 as compared to pH 6.5 and pH 9.5. The FilmTec membrane performed similarly. The sodium ion rejection actually improved after the pH was increased to 9.0 and dropped back down when the pH of the feed was reduced to 6.5 and then 4.5 (Figure 14.1). Again, the overall differences in sodium ion rejection from Trial No. 1 and Trial No. 2 are likely associated with experimental error associated with the measurement process and variations in the membrane swatches. However, the FilmTec membrane does appear to perform with greater consistency over the pH range of 4.5 to 9.0.

The performance of one final CPTC membrane (CPTC-AC Lot No. 022000S2) membrane was tested before the end of the project. Only feedwater at pH 4.5 and 9.0 were tested due to logistical and time constraints The CPTC membrane performed well with a sodium ion rejection greater than 99% initially at pH 4.5 and then pH 9.0 (Figure 14.2). When the feedwater pH was dropped back down to 4.5, sodium ion rejection
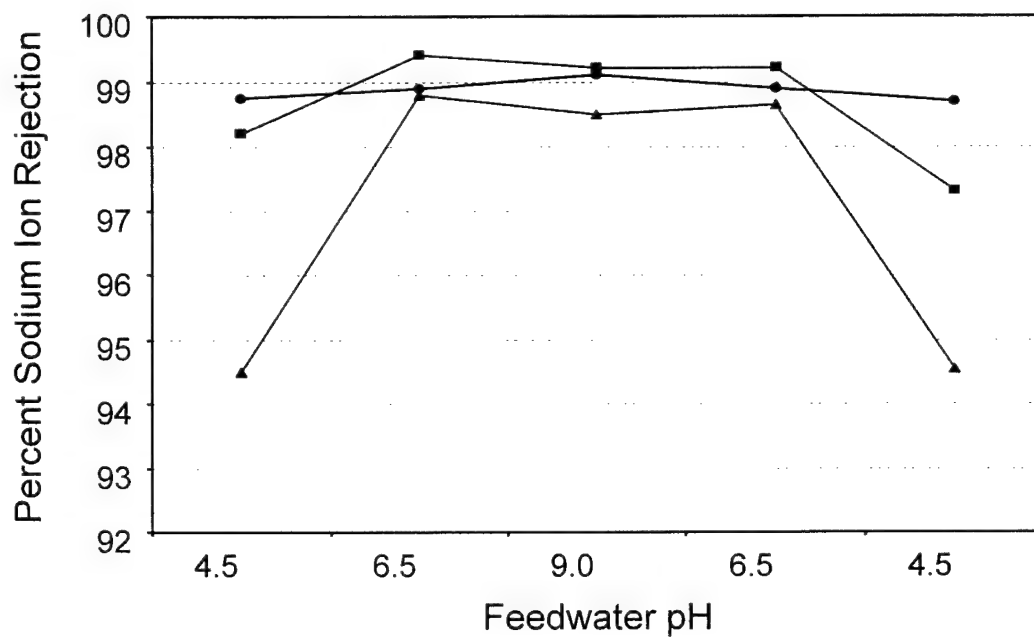
Figure 14.0   Effect of feedwater pH on sodium ion rejection of CPTC
(CPTC-AC Lot No. 061099S1), TMC and FilmTec membranes.
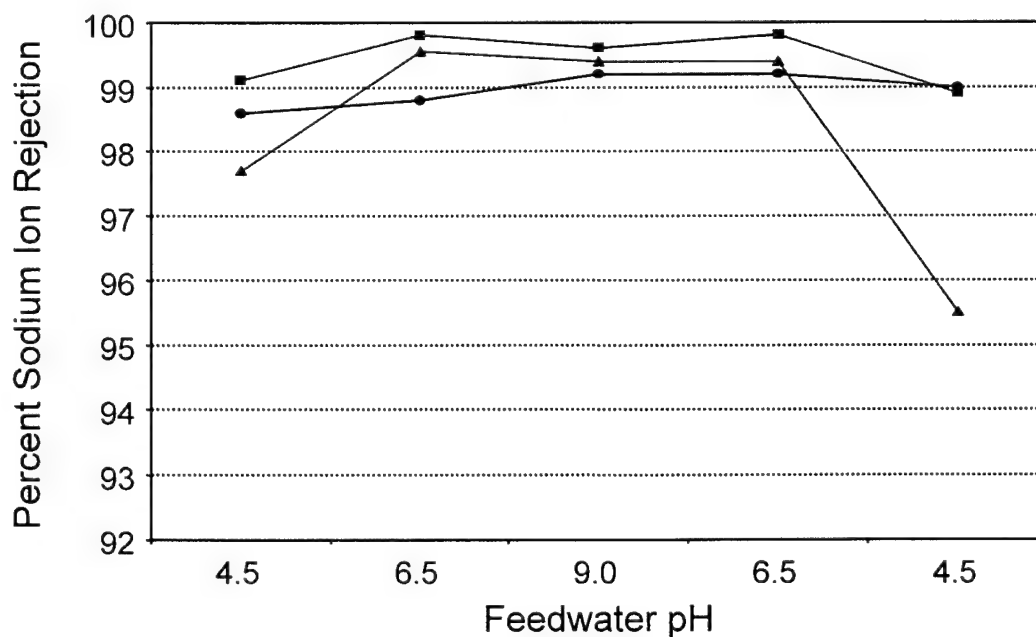
Figure 14.1   Effect of feedwater pH on sodium ion rejection of CPTC
(CPTC-AC Lot No. 092099S1), TMC and FilmTec membranes.
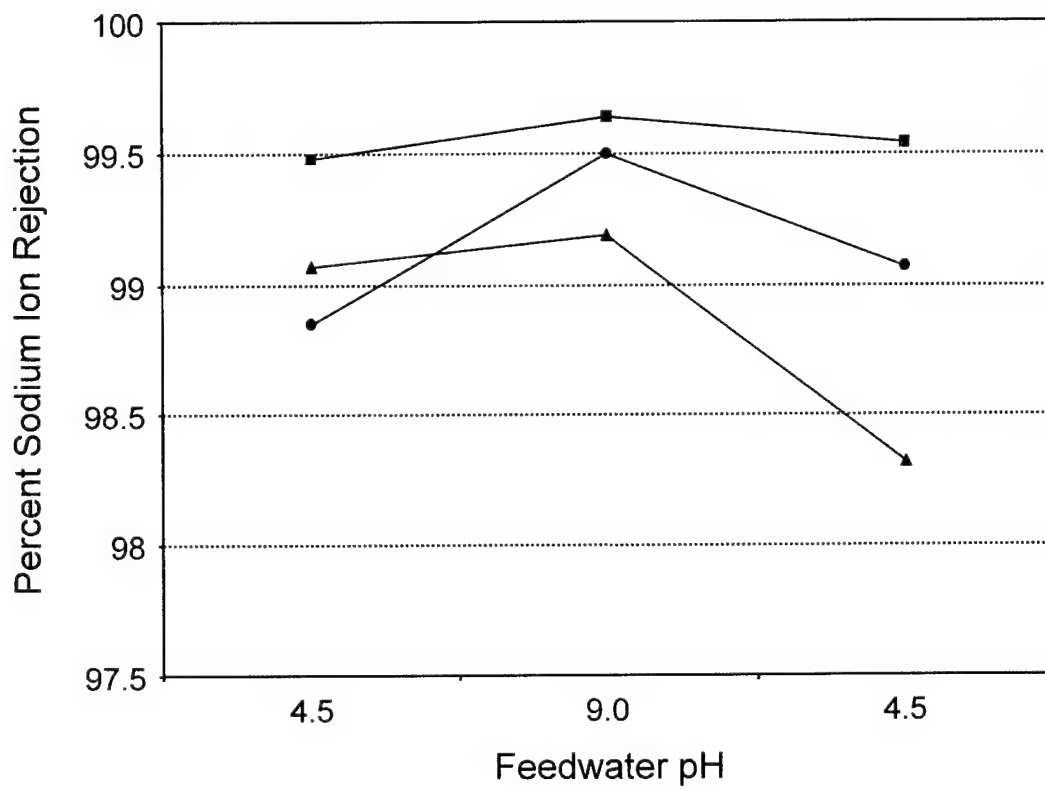
Figure 14.2 Effect of feedwater pH on sodium ion rejection of CPTC
(CPTC-AC Lot No. 022000S2) (▲), TMC (■) and FilmTec (●)membranes.

dropped to 98%. However, this reduction in sodium ion rejection was still small compared to the loss in rejection observed with membranes made from CPTC-AC Lot No. 061099S1 and No. 092099S2. Sodium ion rejection of both the TMC and FilmTec membranes remained above 99% when the pH of the feedwater was returned to 4.5.

The sensitivity to pH may be related to the extent of cross-linking or the number of free carboxylate groups. The FilmTec membrane is made continuously under well-defined, well-controlled conditions, which is believed to be the reason for the "tighter" performance of the membrane over the pH range between 4.5 and 9.0. Generally speaking the TMC and CPTC membrane appear to perform better when the feedwater pH is greater than 4.5. This pH effect is presumably related to the acid-base equilibrium of the free carboxylate groups.

15.0 EFFECT OF SODIUM CHLORIDE AND CHLORINE PRETREATMENT ON CPTC MEMBRANE PERFORMANCE AT VARIABLE FEEDWATER pH

In the process of testing the membranes to determine performance, i.e., sodium chloride rejection and chlorine resistance, it was discovered that chlorine pretreatment in the presence of sodium chloride led to a significant improvement in salt rejection, as measured by conductivity. Several controlled experiments were set up to accurately measure sodium ion rejection after exposure to a sodium chloride and chlorine feed.

15.1 Experimental Method

Three membrane types were tested that included FilmTec, TMC and CPTC (CTPC-AC Lot. No. 022000S2). Membrane samples (~1- x 3-in.) were initially operated on a 2,000 mg/L sodium chloride feed with 2.5 mg/L free chlorine at pH 4.5 under 225 psi applied pressure at 25°C. After 1 hr, flux and (conductivity) rejection were measured and then the feedwater was adjusted to pH 6.5. After 1 hr of operation, a second permeate sample was collected. The pH was adjusted to pH 9.0, and after 1 hr the flow and rejection were measured. The pH was then dropped back to 6.5, operated for 1 hr and flow and the rejection remeasured. Finally, the pH was dropped down to 4.5, the membrane operated for 1 hr and flux and rejection measured one last time. After each 1-hr operational period small (25-50 mL) samples of permeate were collected and shipped to OCWD for sodium ion analysis by ICP-MS.

15.2 Results and Discussion

Pretreatment with sodium chloride and chlorine resulted in improved sodium ion rejection for all three membranes independent of the pH of the feedwater. Rejection of the FilmTec improved to greater than 99.6%, TMC improved to greater than 99.8% and CPTC improved to greater than 99.7% (Figure 15.0). Membranes were also tested without pretreatment to validate this effect. Plots of this data are also included in Figure 15.0. The effect on membrane performance produced by the pretreatment was reproducible. A second set of membrane samples made from the same lot (CPTC-AC Lot No. 022000S2) of CPTC were treated with NaCl and chlorine and tested with a

2000 mg/L feedwater at pH 4.5 then 9.0 and back to 4.5. The second set of membranes also demonstrated significantly improved sodium ion rejection (≥99.7%) after the pretreatment (Figure 15.1)

16.0 EFFECT OF FEEDWATER pH ON MEMBRANE CHEMISTRY - RELATIVE CARBOXYLATE DENSITY

Early studies of the performance of the CPTC membrane at different feedwater pH indicated a narrow operating range. Membranes made from less pure CPTC acid chloride did not reject sodium ions well at pH 4.5 or 9.0 (see Section 14.0). When MPD reacts with acid chloride, amide bonds form. When more of the acid chloride groups react, i.e., when all three acid chloride groups react, cross-linking occurs within the membrane. More amide bonds form, leaving fewer free carboxylate groups. A ratio of the carboxylate and amide II band intensities provides an estimate of the relative carboxylate density or cross-link density between membrane samples. Results from this study provide some information on how chemical structure or acid-base equilibrium affects water flux and salt rejection of the membrane.

16.1 Experimental Method

ATR/IR spectra of membrane samples operated on feedwaters of various pH were analyzed to determine the effect pH has on polymer chemistry. Special attention was paid to the symmetric (1414 cm^{-1}) carboxylate band intensity of PA. The carboxylate is the primary acidic functional group of the membrane. To a much lesser extent, terminal tertiary amines (-NH$_2$) originating from incompletely reacted MPD can undergo protonation, but only at low pH, as this amine is a weak base (MPD: $K_b = 10 \times 10^{-10}$). Changes in chemistry were assessed by measurement of the relative carboxylate amide II band intensity ratio of the membrane samples.

Three types of membranes, CPTC, TMC and FilmTec, were operated on feedwater at pH 4.5, 7.0 and 9.0. After operation at the given pH, the membrane sample was removed from the pressure cell, sealed in a plastic bag and shipped to OCWD for analysis. Each membrane sample was dried, and ATR/IR spectra were collected. Band intensities were recorded near 1541 cm^{-1} (N-H bend, amide II) and 1414 cm^{-1} (symmetric COO$^-$ stretch). Corrections were made to the 1414 cm^{-1} to account for the contribution of asymmetric CH$_3$ bending vibration (1410 cm^{-1}) from the PS support. The 874 cm^{-1} ring deformation band of PS in the membrane spectrum was used as a normalization factor to account for differences in film thickness and determine the contribution of the CH$_3$ band of PS in the membrane spectrum. Reference spectra for each PS support membrane were collected and the 1414 cm^{-1} / 874 cm^{-1} (and 1416 cm^{-1} / 874 cm^{-1}) band intensity ratio were determined (see Table 9.2). This ratio was used to correct for the PS contribution to the 1414 cm^{-1} band intensity in the calculation of the carboxylate/amide II ratio of each membrane. The experiment was run twice, first with membranes made from CPTC-AC Lot No. 061099S1 then with membranes from CPTC-AC Lot No. 022000S2.
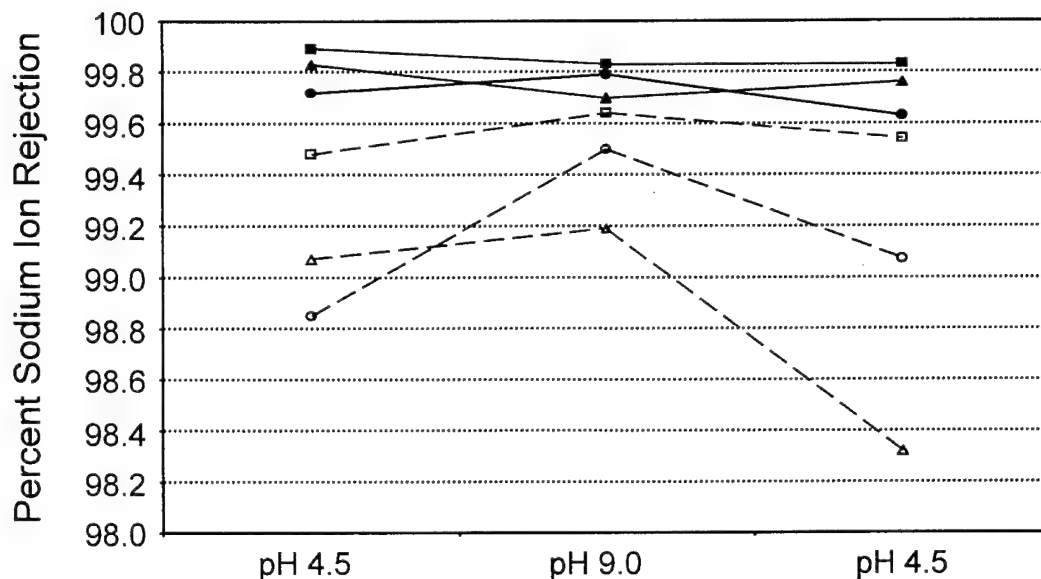
Figure 15.0   Effect of feedwater pH on sodium ion rejection of membranes pretreated
with sodium chloride and chlorine, CPTC (CPTC-AC Lot No. 022000S2)
(▲), TMC (■) and FilmTec (●) membranes and without any pretreatment
(dashed lines).
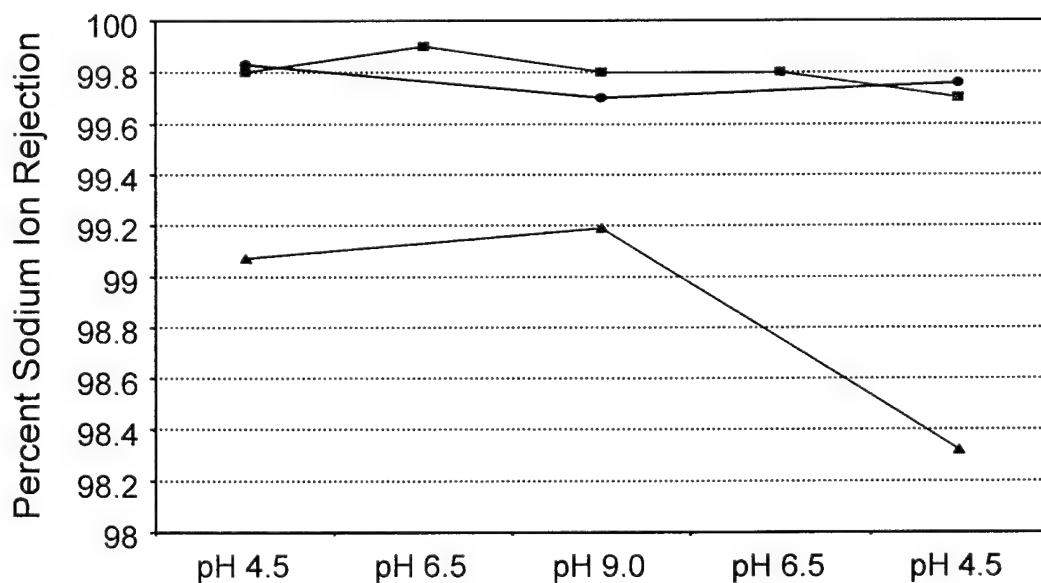
Figure 15.1   Effect of pH on sodium ion rejection of CTPC membranes
(CPTC-AC Lot No. 022000S2), no pretreatment/control (▲) and pretreated
with NaCl and chlorine, Trial No.1 (■) and Trial No. 2 (●).

16.2   Results and Discussion

The carboxylate/amide II intensity ratio of the TMC and FilmTec membranes did not change significantly when exposed to feedwaters at pH 4.5, 7.0 and 10 (or 9.0) (Figure 16.0). (Note that the pH was dropped from 10 to 9.0 in the second experiment to match the sodium ion rejection studies run at pH 4.5, 7.0 and 9.0 [see Section 15.0]). These results suggest that free carboxylate groups can undergo protonation and deprotonation when the pH of the feedwater is altered. This also suggests that there is more extensive cross-linking in these two membranes.

The COO⁻/amide II intensity ratio of the CPTC membrane made from CPTC-AC Lot No. 061099S2 was unchanged at pH 4.5 and 7.0. However, when the pH of the feedwater was increased a significant change in the ratio was measured. The ratio increased from 0.38 at pH 7.0 and 4.5 to 0.47 at pH 9. This suggests that there were a significant number of free carboxylate groups in the membrane made from CPTC-AC Lot No. 061099S1. These carboxylate groups are free to undergo protonation and deprotonation with change in pH. This also means that the membrane was not highly cross-linked or consists of more individual polymer chains, each with two terminal carboxylate groups.

The experiment was repeated using membranes from CPTC-AC Lot No. 022000S2. TMC and FilmTec COO⁻/amide II ratios were highly reproducible for the two pH studies, while the same ratio for membrane made from CPTC-AC Lot No. 061099S1 and No. 022000S2 were quite different. The difference in this intensity ratio indicates that the CPTC membrane made from CPTC-AC Lot No. 061099S1 has a greater negative charge density relative to membrane made from Lot No. 022000S2. This suggests that the membrane from Lot No. 022000S2 is more highly cross-linked than membrane made from Lot No. 061099S1. CPTC membrane from CPTC-AC Lot No. 061099S1 likely contains a greater mixture of the other isomers of the acid chloride. The presence of these isomers apparently leads to the formation of a polymer membrane with a greater number of unreacted acid chloride groups that are ultimately hydrolyzed to a carboxylic acid.

Comparison of the COO⁻/amide II ratios of the three membrane types reveals that the CPTC membrane (CPTC-AC Lot No. 061099S1) has the highest relative carboxylate density, i.e., has greater number of free carboxylate groups versus amide bonds. The TMC membrane has the lowest COO⁻/amide II ratio and possesses a higher level of cross-linking, with the FilmTec membrane falling between the CPTC and TMC membranes. Finally, membrane made from CPTC-AC Lot. No. 022000S2 had the lowest COO⁻/amide II ratio, indicating that it was the most highly cross-linked of the three membranes and possessed the lowest relative carboxylate density.

Figure 16.0   Effect of pH on carboxylate/amide II band intensity ratio of membranes
CTPC (CPTC-AC Lot No. 061099S1 (-•-), FilmTec (—▲— , -▲-),
TMC (—■— , -■-) and CPTC Lot No. 022000S2 (—•—). pH 10 dashed lines
and pH 9 solid lines.
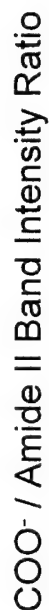
17.0 CHEMISTRY OF RO FEEDWATER CHLORINATION AND EFFECTS ON CPTC MEMBRANE TRANSPORT PROPERTIES

17.1 Chlorine Chemistry of RO Feedwater

17.1.1 Fundamental Concepts

Sodium hypochlorite is commonly utilized for chlorination of RO feed waters and is injected into the feed as a solution. Hypochlorites dissociate in water as follows:

$$NaOCl + H_2O \rightarrow HOCl + NaOH$$

The chemistry involving hypochlorous acid in freshwater systems is identical whether Cl_2 gas or a hypochlorite salt is used for chlorination. Once the hypochlorous solution is injected into the RO feed water, the HOCl molecule rapidly dissociates to (H^+) and hypochlorite ions (OCl^-) as follows:

$$HOCl \Leftrightarrow H^+ + OCl^-$$
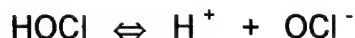
The mole fractions of Cl_2, HOCl and (OCl^-) in the feed water are dependent on the water chemistry. These are referred to as free residual chlorine. Chlorine can also bond with various ammonia and amines in water to form compounds referred to as combined residual chlorine. The free residual and combined residual chlorine together are referred to as total residual chlorine.

The germicidal efficiency of a free chlorine residual is directly related to the amount of undissociated hypochlorous acid (HOCl) present in solution. Hypochlorous acid is 100 times more effective that the hypochlorite ion (OCl^-) as a biocide.[25] The concentration of HOCl depends on the pH, temperature and ionic strength of the feed water, according to the following relationships:

pH. The available HOCl concentration in the RO feedwater will vary considerably with relatively small changes in pH as shown in Figure 17.0. The remaining free available chlorine is present as hypochlorite ion.

Temperature. The dissociation of HOCl varies with temperature of the feedwater in accordance with the dissociation constant, K. As the temperature increases, the dissociation of HOCl increases, thereby raising the concentration of the OCl^- ion.

Ionic Strength. The ionic strength is the charge-weighted sum of the concentrations of each ion in solution. Ionic strength is therefore directly related to the total composition and dissolved solids content of the RO feedwater. The ionic strength affects the dissociation of all ions in water, including HOCl.
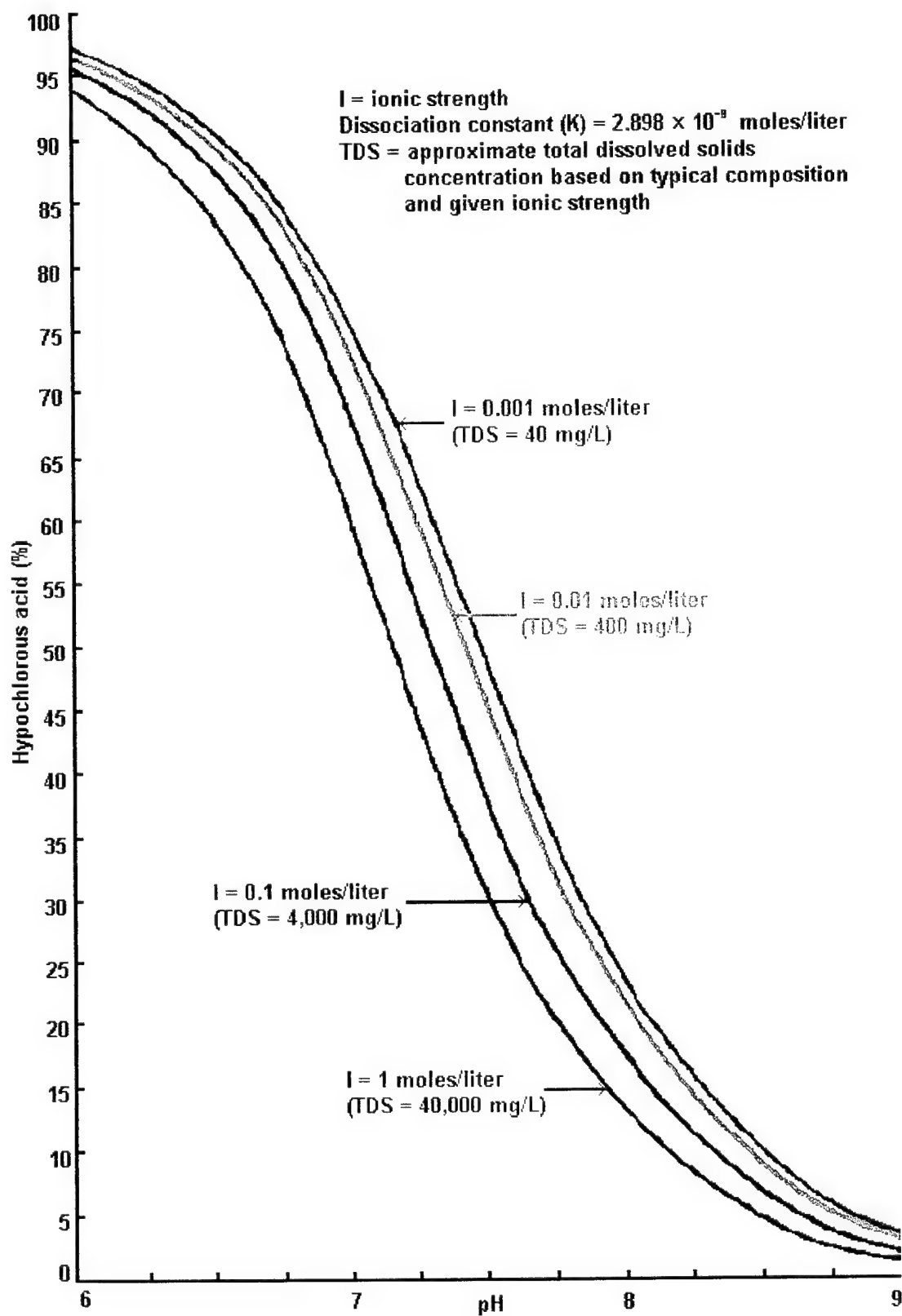
Figure 17.0   Effect of pH and ionic strength on the dissociation of hypochlorous acid at 25°C [25]

17.1.2 Chlorination in the Presence of Bromine or Bromide Ion.

The chemistry of seawater chlorination is more complex than that of brackish water due to the high concentration of dissolved salts. Average seawater contains total dissolved solids concentrations of 35,000 mg/L. The salinity due to the chloride ion alone is usually about 19,000 mg/L. However, the ion having the most effect upon chlorination is the bromide ion.

Bromide is commonly found in seawater at concentrations as high as 70 mg/L. When sodium hypochlorite is added to seawater, some of the bromide present is oxidized to form hypobromous acid and hypobromite ions. The formation of hypobromous acid (HOBr) in chlorinated seawater at pH 8 proceeds as follows:

$$Br^- \ + \ HOCl^- \ \rightarrow \ HOBr \ + \ Cl^-$$
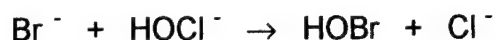
Hypobromous acid then dissociates to hypobromite ions (OBr $^-$) as follows:[25]

$$HOBr \ \Leftrightarrow \ OBr^- \ + \ H^+$$

The reaction rate for the formation of HOBr is rapid. The reaction proceeds to 99% completion within ten seconds in highly saline water. The amount of undissociated HOBr is much greater for any given pH than its chlorine counterpart HOCl. At pH 8, the undissociated HOBr is 83% while HOCl is only 28%.

17.1.3 Bromide Ion Concentration in Simulated RO Feedwaters

Two types of feedwaters were used to simulate brackish and seawater conditions. These feedwaters were used to test and measure the transport properties of CPTC, TMC and FilmTec membranes. To simulate seawater conditions, a 35,000 mg/L sodium chloride feed solution was used at an operating pressure of 800 psi; to simulate brackish water conditions a 2,000 mg/L sodium chloride feed solution is used at an operating pressure of 225 psi. All RO feed solutions are made with DI water. The feed solutions were chlorinated with a commercial grade sodium NaOCl solution. All commercial grades of NaCl and NaOCl contain bromide ion. The bromide ion contribution from each is as follows:

NaCl (Morton food grade)	=	156 mg/kg
NaOCl (Commercial Grade)	=	4,200 mg/L

Accordingly, the concentration of bromide ion in a simulated 2,000 mg/L brackish water RO feed is 0.31 mg/L; the concentration of bromide ion in a simulated 35,000 mg/L NaCl solution is 5.5 mg/L. When NaOCl is added to the feed, generally 3.5 mg/L, an additional 0.24 mg of bromide ion is added. Thus, the total bromide ion concentration in the RO feed solutions used throughout this study are shown in Table 17.0.

231

Table 17.0

Bromide Ion Concentrations in Seawater and Brackish Water Feeds

RO Feedwater	Bromide Ion Concentration (mg/L)
35,000 mg/L NaCl	5.5
35,000 mg/L NaCl + 3.5 mg/L NaOCl	5.7
2,000 mg/L NaCl	0.3
2,000 mg/L NaCl + 3.5 mg/L NaOCl	0.5

The first of several experiments designed to test membrane performance in the presence of free chlorine was run at pH 6.0 on brackish water and seawater feeds. These experiments were later expanded upon and the results are included in Sections below.

17.2 Effect of Free Chlorine on CPTC Membrane Performance at pH 6.0 When Operated on Brackish Water and Seawater

A comparison of 1-hr RO performance for CPTC membranes tested at pH 6.0, before and after the addition of 3.5 mg/L free chlorine on brackish and seawater feeds, is shown in Table 17.1 and Figure 17.1. The effect of the chlorine feed on all four membranes was similar and did not appear to vary with the composition of the feedwater. The salt rejection of all four membranes improved to near 99.5%, independent of their initial performance before chlorine addition. It did not seem to matter if the feed was brackish or seawater. The water flux of the three membranes exposed to brackish feed increased slightly, while the membrane exposed to seawater decreased (see Figure 17.1).

17.3 Comparative Performance of CPTC Membranes at pH 5.0, 7.0 and 9.0 Before and After Exposure to Hypochlorous/Hypobromous Acid in 35,000 and 2,000 mg/L RO Feeds

It soon became apparent that the transport properties of CPTC membranes changed when NaOCl is added to the RO feed containing bromide ions. When HOCl is present in sufficient quantity, bromide is converted to hypobromite (OBr^-), and when exposed to the membrane, the changes in transport properties are significant. The magnitude of change is believed to be strongly dependent on the concentration of bromide ion and, thus, the hypobromous acid concentration in the RO feed. The degree to which pH influences the HOBr effect on membrane transport properties was investigated below.

Table 17.1

Performance of CPTC Membranes Before and After NaOCl Addition to Feeds

Test Conditions: 225 psi applied pressure, 2,000 mg/L sodium chloride feed, pH 6.0, 25°C, 1 gal/min feed flow

800 psi applied pressure, 35,000 mg/L sodium chloride feed, pH 6.0, 25°C, 1 gal/min feed flow

Reverse Osmosis Performance After One Hour

Membrane Identification	Before Sodium Hypochlorite Addition to Feed		After Addition of 3.5 mg/L Free Chlorine to Feed	
	Water Flux (gfd)	Rejection (%)	Water Flux (gfd)	Rejection (%)
2,000 mg/L Sodium Chloride RO Feed				
CPTC-580*	15.9	98.3	22.9	99.27
CPTC-581*	15.6	98.9	21.3	99.38
CPTC-582*	14.8	96.6	20.3	99.30
35,000 mg/L Sodium Chloride RO Feed				
CPTC-573*	24.9	96.7	10.8	99.60

*   CPTC-AC Lot No. 100199

17.3.1   Seawater Feed

A comparison of the RO performances of CPTC and TMC membranes at pH 5.0, 7.0 and 9.0, before and after the addition of 3.5 mg/L free chlorine (NaOCl) to a 35,000 mg/L NaCl feed (5.7 mg/L bromide ion), are shown in Figures 17.2 and 17.3, respectively. With only one exception, a dramatic decrease in water flux and an increase in salt rejection of both CPTC and TMC membranes were observed immediately after NaOCl was added to the RO feed at pH 5.0, 7.0 and 9.0. Only the water flux of the CPTC membrane at pH 5.0 did not change after NaOCl was added to the seawater feed.
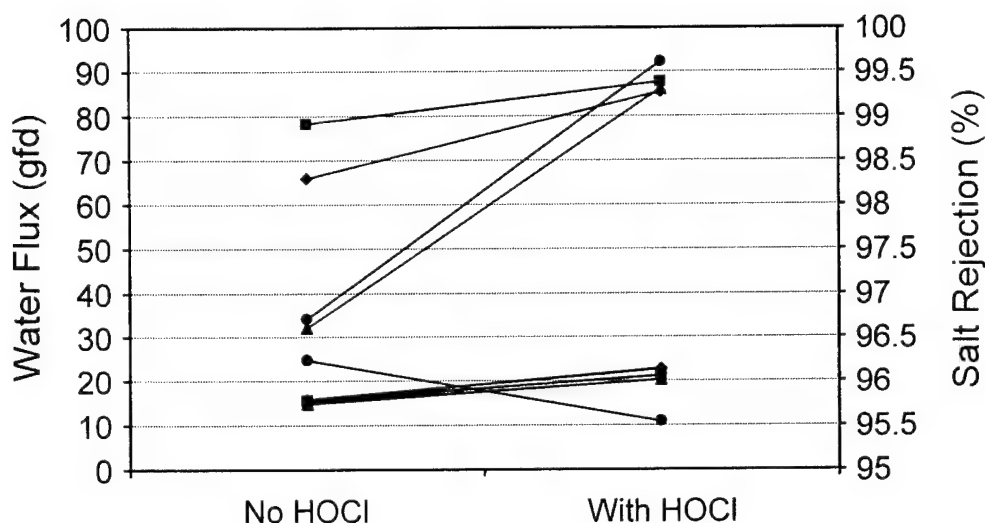
Figure 17.1   Performance of CPTC membranes before and after NaOCl addition to the feed at pH 6.0. Brackish water feed: CPTC-580 (◆), 581 (■), 582 (▲) and seawater feed: CPTC-573 (●).

While significant improvements to the salt rejection of the CPTC and TMC membranes were made upon exposure to NaOCl at pH 9.0, the rejection of these membranes were still lower than the rejection of the membranes tested at pH 5.0 and 7.0 (see Figures 17.2 and 17.3). The salt rejection of these membranes was improved by lowering the pH of the seawater feed to 5.0. Presumably, when the pH was adjusted to 5, the acid-base equilibrium was shifted toward HOBr formation, and the newly generated HOBr reacted with the CPTC membrane.

When the pH was dropped back to 9.0, the salt rejection remained high, i.e., the effect of enhanced performance was not reversed. This suggests that the membranes were chemically altered, most likely by hypobromous acid (HOBr). Bromine may have been incorporated into the PA structure, thereby altering the physical properties of the membrane. One observed drawback to the chlorine treatment is the loss in water flux. It is also of significance to note that the amount of "free chlorine" allowed to pass through the CPTC and TMC membranes was highly dependent on the pH of the solution. At pH 9.0 the passage was low for both CPTC and TMC membranes. At pH 5.0, the level of chlorine found in the permeate of the CPTC membrane was also low. Passage of chlorine (HOCl) is likely low because (1) there is not much free chlorine as it was converted to HOBr, and (2) there is not going to be much HOCl present at pH 9.0, as it exists primarily as OCl⁻ (>95%.).
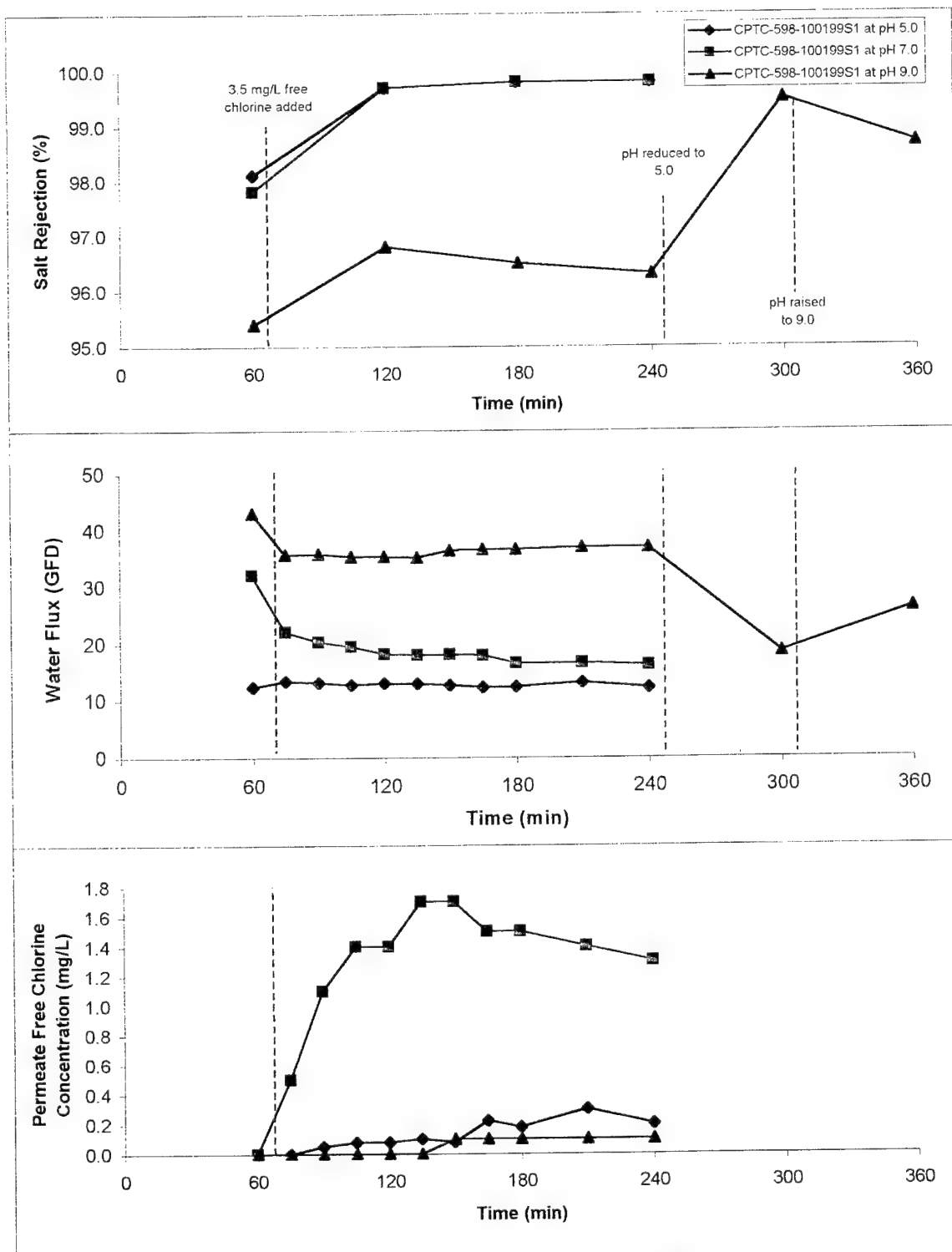
Test Conditions: 800 psi feed pressure, 35,000 mg/L NaCl feed, pH 5.0-9.0 and 1.0 gal/min feed flow

Figure 17.2   Performance of CPTC 598 membranes with 35,000 mg/L sodium chloride feed at pH 5.0, 7.0 and 9.0 before and after addition of 3.5 mg/L free chlorine (sodium hypochlorite)
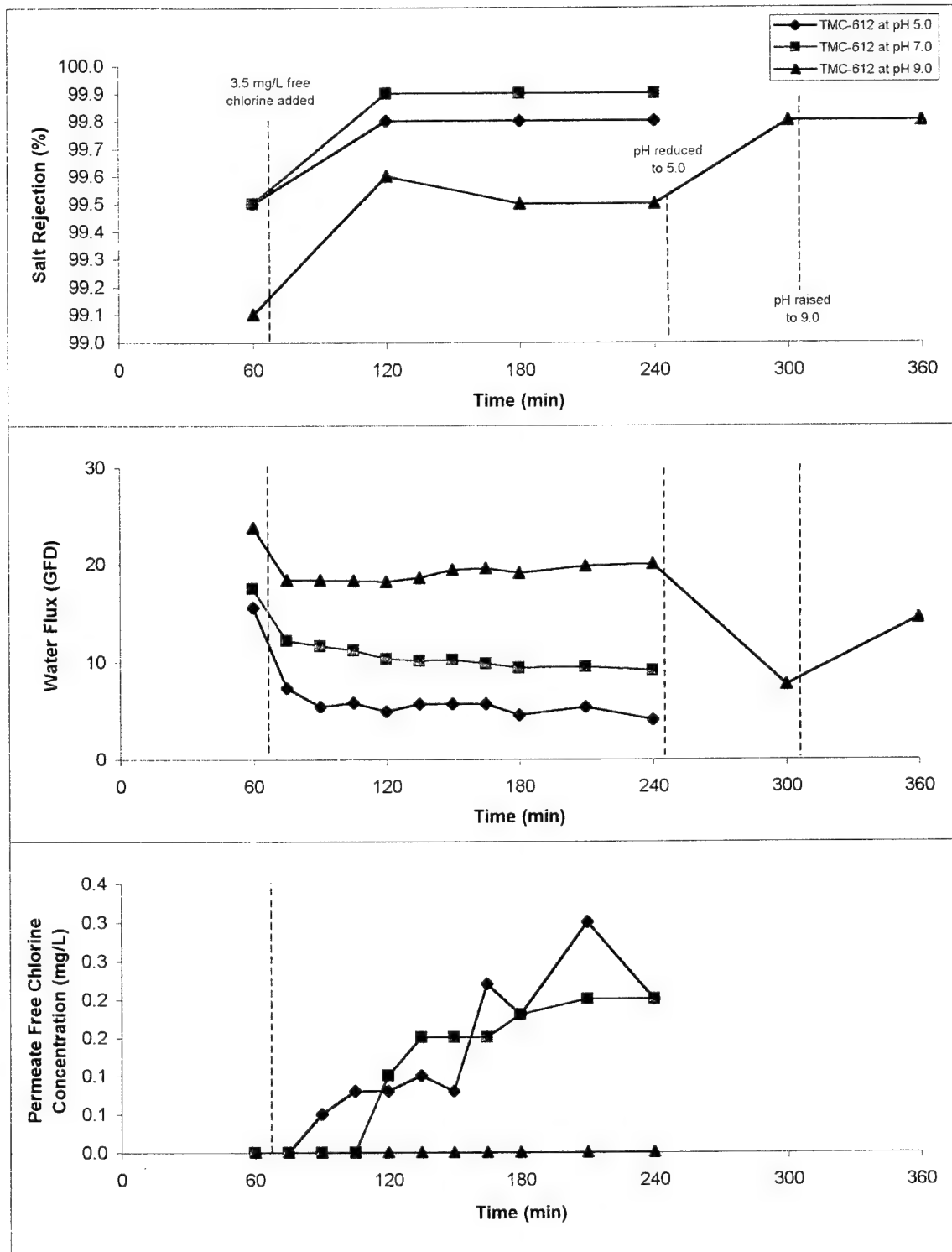
Test Conditions: 800 psi feed pressure, 35,000 mg/L NaCl feed, pH 5.0-9.0 and 1.0 gal/min feed flow

Figure 17.3   Performance of TMC 612 membranes with 35,000 mg/L sodium chloride feed at pH 5.0, 7.0 and 9.0 before and after addition of 3.5 mg/L free chlorine (sodium hypochlorite)

236

17.3.2 Brackish Water Feed

RO performance for CPTC membranes tested at pH 5.0, 7.0 and 9.0, before and after the addition of 3.5 mg/L free chlorine with a 2,000 mg/L NaCl feed is shown in Figure 17.4 (0.5 mg/L bromide ion) The transport properties of the membrane behaved differently under these conditions when the bromide ion concentration was lower. After the addition of 3.5 mg/L free chlorine to the feed at pH 5.0, the salt rejection increased from 97 to nearly 99%. The water flux initially increased slightly but essentially remained unchanged after the 3 hr experiment. Improvements in salt rejection were also observed for membranes exposed to the 3.5 mg/L chlorine at pH 7.0 and 9.0 over the 3-hr period. The membranes run at 7.0 and 9.0 already showed rejections of nearly 99% at the start of the experiment. The water flux of these membranes increased slightly after the initial exposure. However, at pH 7.0, the water flux of the CPTC membrane eventually dropped after 3 hr of exposure to the chlorine feed, while at pH 5.0 and 9.0 the flux essentially remained unchanged. The change in flux upon exposure to the 3.5 mg/L chlorine brackish feed was quite different than the effect of the seawater feed, where the water flux dropped rapidly.

A significant amount of free chlorine began to appear in the permeate at pH 7.0 and 9.0 approximately 15 min after the initial exposure to 3. 5 mg/L chlorine in the feed. A very small amount (<0.5 mg/L) of free chlorine was detected in the permeate of the CPTC membrane operated at pH 5.0 (see Figure 17.4).

The rate and degree to which membrane properties are altered appears to be dependent on the concentration of hypobromous acid in the feed. However, it is not known what effect CPTC-AC lot purity has on these experiments. Membranes made from CPTC-AC Lot No. 1000199 were used for the seawater feed as compared to membranes made from CPTC-AC Lot No. 110899 for the brackish feed. The response of CPTC and TMC transport properties to free chlorine in the presence of bromide ions was very similar. Most natural waters contain some bromide ions, particularly seawater. If RO membranes are operated on natural waters, a similar response is expected over the same pH range of 5.0 to 9.0.

17.4 Effects of Hypochlorous/Hypobromous Acid in a Deionized Water Feed on the Transport Properties of CPTC and TMC Membranes

The question arose as to whether ionic strength affects the way hypobromous acid reacts with the CPTC and TMC membranes to produce the performance enhancing effects, i.e., does HOBr have the same effect on membranes in the absence of the 35,000 mg/L sodium chloride feed? An experiment was carried out to determine the importance of the high ionic strength in the reaction of HOBr with the polymer membranes.
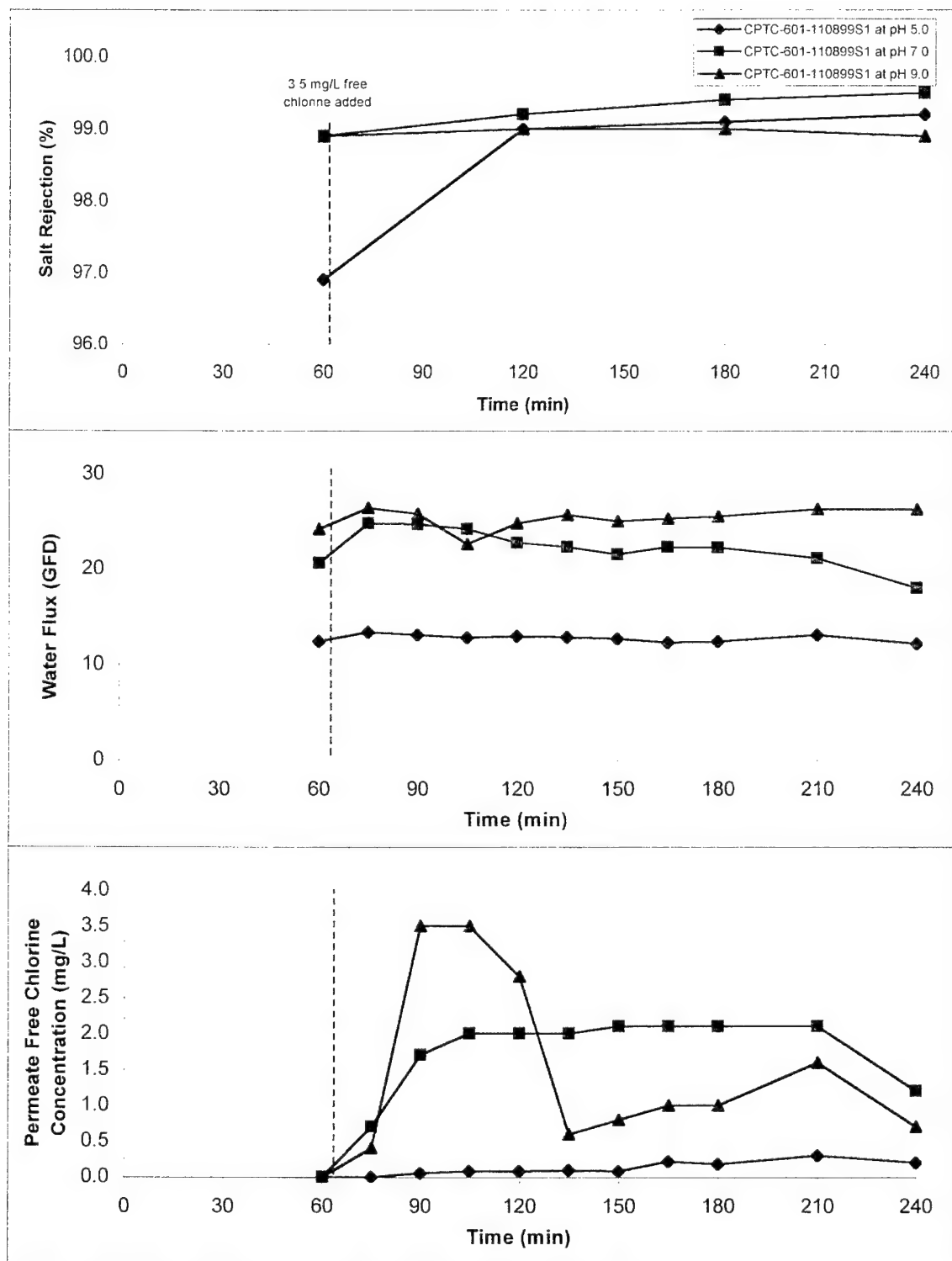
Test Conditions: 225 psi feed pressure, 2,000 mg/L NaCl feed, pH 5.0-9.0 and 1.0 gal/min feed flow

Figure 17.4 Performance of CPTC membranes with 2,000 mg/L sodium chloride feed at pH 5.0, 7.0 and 9.0 before and after addition of 3.5 mg/L free chlorine (sodium hypochlorite)

17.4.1 Experimental Method

Six test cells containing one sample each of TMC membranes were operated in RO tests for 2 hr on a 35,000 mg/L NaCl feed at 800 psi applied pressure, pH 6.5 and 25°C to obtain baseline transport properties. After the data collection, two of the test cells were isolated from the system with 800 psi pressure still applied to the membranes.

Feed to the remaining four cells was replaced with DI water while maintaining the applied pressure (see schematic diagram in Figure 17.5). Free chlorine was added to the feed while maintaining pH 6.5. The membranes were operated for 1 hr and then two more cells were isolated while maintaining pressure.

The two remaining cells were then operated on a seawater feed containing 10 mg/L NaBr and 3.5 mg/L free chlorine at a pH of 6.5. After 1 hr of operation and following data collection, all six test cells were flushed with DI water under 800 psi pressure, and the feed was readjusted to 35,000 mg/L NaCl at pH 6.5. The system was returned to the original test conditions and operated for 1 hr. Transport properties were measured from all six samples and compared to the initial test readings.
The test was repeated using CPTC membranes.

17.4.2 Results and Discussion

Data from this experiment is displayed in Table 17.2 and in Figures 17.6 and 17.7.

* Free chlorine (3.5 mg/L) in DI water at pH 6.5 placed in the feed has little, if any, effect on the transport properties of the CPTC membrane. Hypochlorous acid does not appear to react with the membrane under these conditions.

* When 5.5 mg/L bromide ion is added to the DI water feed containing 3.5 mg/L free chlorine, the transport properties of CPTC and TMC membranes are significantly affected. Dramatic decreases in both water and salt transport through the membrane are observed.

* Hypobromous acid has a profound effect on the transport properties of CPTC and TMC membranes.

* The concentration of NaCl, i.e., ionic strength in the feed does not influence the effect of hypobromous acid on the transport properties of CPTC and TMC membranes.

It was further demonstrated that the transport properties of CPTC and TMC membranes can be modified by simply immersing the membranes in an aqueous solution containing NaOCl and bromide ion or hypobromous acid. This process has potential for tailoring membrane properties either during membrane manufacturing and/or as a post-treatment step.
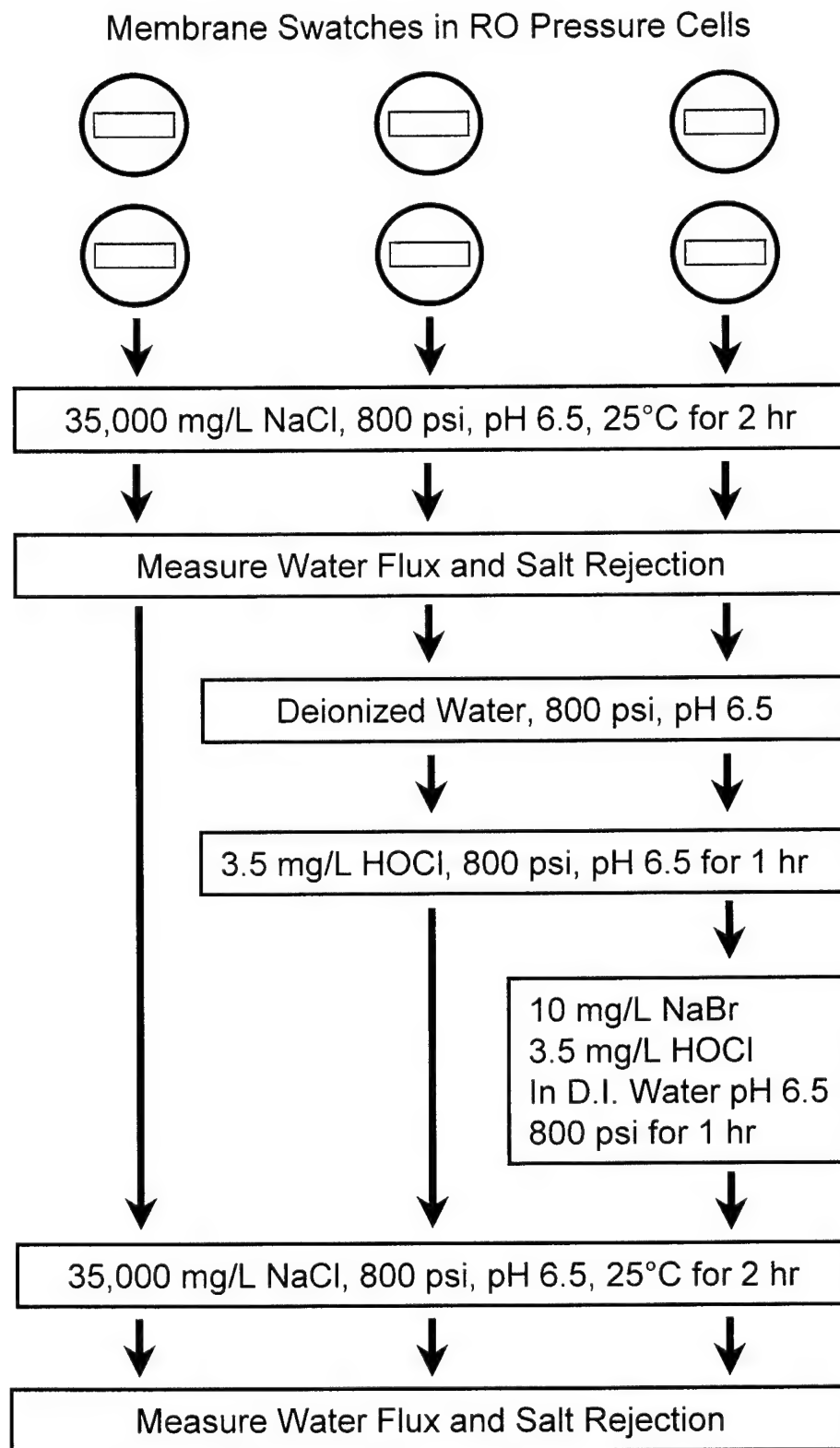
Figure 17.5   Schematic diagram of the experimental set up.

Table 17.2

RO Performance of TMC and CPTC Membranes Before and After NaOCl Addition to Feeds

Test Conditions: 800 psi applied pressure, 35,000 mg/L sodium chloride feed, pH 6.0, 25°C, 1 gal/min feed flow

Membrane	RO Performance After 2 Hours		Membrane Exposure between Operation Hours 2 and 3*	Membrane Exposure between Operating Hours 3 and 4*	RO Performance After 5 hours	
	Water Flux (gfd)	Rejection (%)			Water Flux (gfd)	Rejection (%)
RO Performance of TMC Membranes Before and After NaOCl Addition to Feeds						
TMC 905 EDX 1-1	18.2	99.5	-	-	-	-
TMC 905 EDX 2-1	18.0	99.5	-	-	-	-
TMC 905 EDX 3-1	16.9	99.5	3.5 mg/L free chlorine in DI water	-	18.9	99.7
TMC 905 EDX 4-1	16.9	99.5	3.5 mg/L free chlorine in DI water	-	18.9	99.7
TMC 905 EDX 5-1	19.8	99.5	3.5 mg/L free chlorine in DI water	3.5 mg/L free chorine in DI water 5.5 mg/L Potassium Bromide	14.6	99.9
TMC 905 EDX 6-1	19.8	99.5	3.5 mg/L free chlorine in DI water	3.5 mg/L free chorine in DI water 5.5 mg/L Potassium Bromide	14.6	99.9
RO Performance of CPTC Membranes Before and After NaOCl Addition to Feeds						
CPTC 898 EDX 1-1	16.2	98.7	-	-	-	-
CPTC 898 EDX 2-1	15.0	98.7	-	-	-	-
CPTC 898 EDX 3-1	13.3	98.7	3.5 mg/L free chlorine in DI water	-	14.1	98.7
CPTC 898 EDX 4-1	13.3	98.7	3.5 mg/L free chlorine in DI water	-	14.1	98.7
CPTC 898 EDX 5-1	16.2	98.7	3.5 mg/L free chlorine in DI water	3.5 mg/L free chorine in DI water 5.5 mg/L Potassium Bromide	14.7	99.7
CPTC 898 EDX 6-1	16.2	98.7	3.5 mg/L free chlorine in DI water	3.5 mg/L free chorine in DI water 5.5 mg/L Potassium Bromide	14.6	99.7

* RO feed was changed while system remained under 800 psi applied pressure.

241
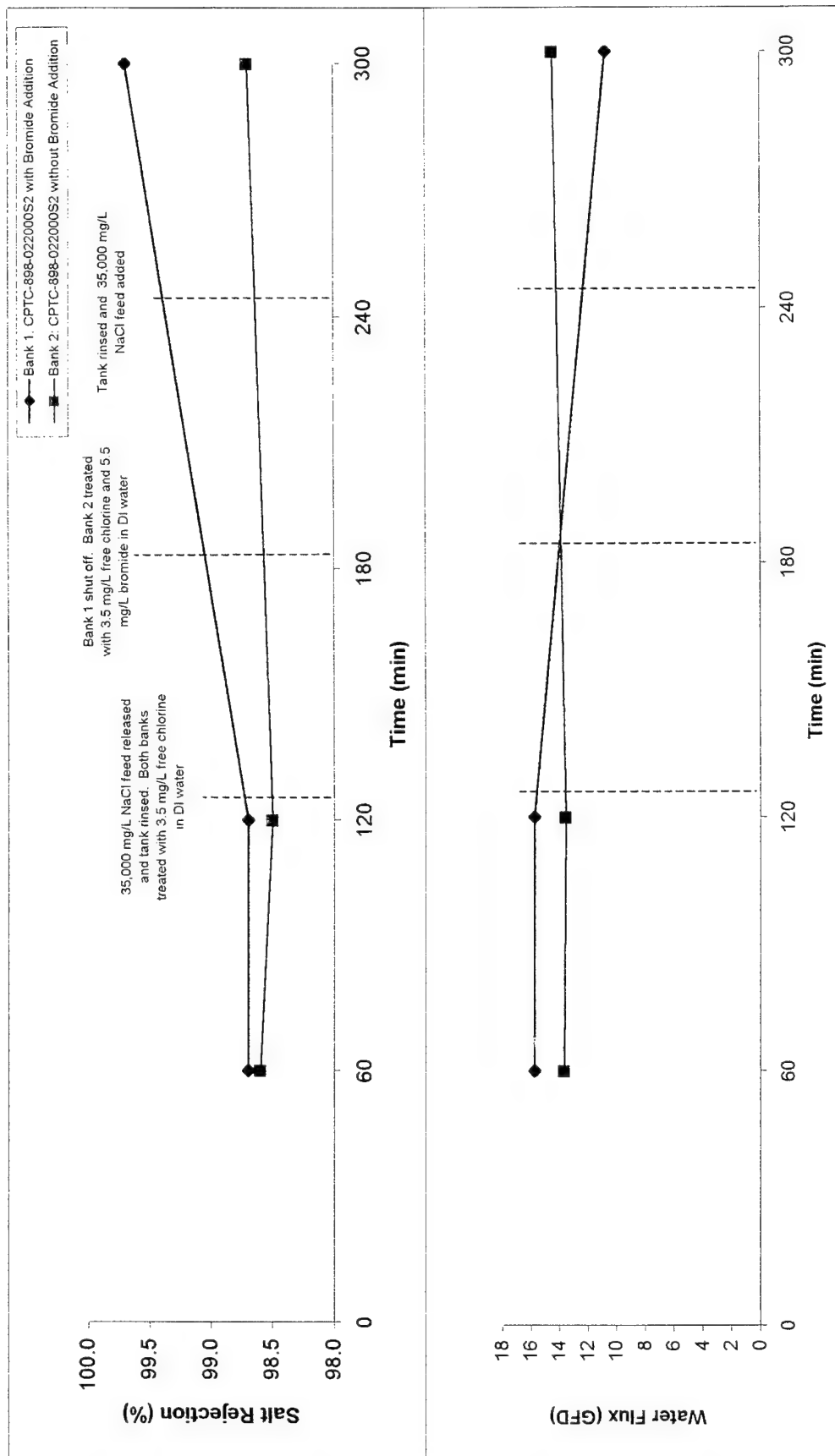
Figure 17.6   Performance of CPTC 898 membranes with 35,000 mg/L sodium chlcride feed before and after membranes had been treated as follows:
Treatment 1: (Membrane Bank 2) 3.5 mg/L free chlorine in DI water and with 5.5 mg/L bromide ion
Treatment 2: (Membrane Bank 1) 3.5 mg/L free chlorine in DI water
The 35,000 mg/L feed was removed and replaced with DI water while remainig pressurized during treatment of membranes in Banks 1 and 2

242

Figure 17.7 Performance of TMC 905 membranes with 35,000 mg/L sodium chloride feed before and after membranes had been treated as follows:
Treatment 1: (Membrane Bank 2) 3.5 mg/L free chlorine in DI water and with 5.5 mg/L bromide ion
Treatment 2: (Membrane Bank 1) 3.5 mg/L free chlorine in DI water
The 35,000 mg/L feed was removed and replaced with DI water while remainig pressurized during treatment of membranes in Banks 1 and 2
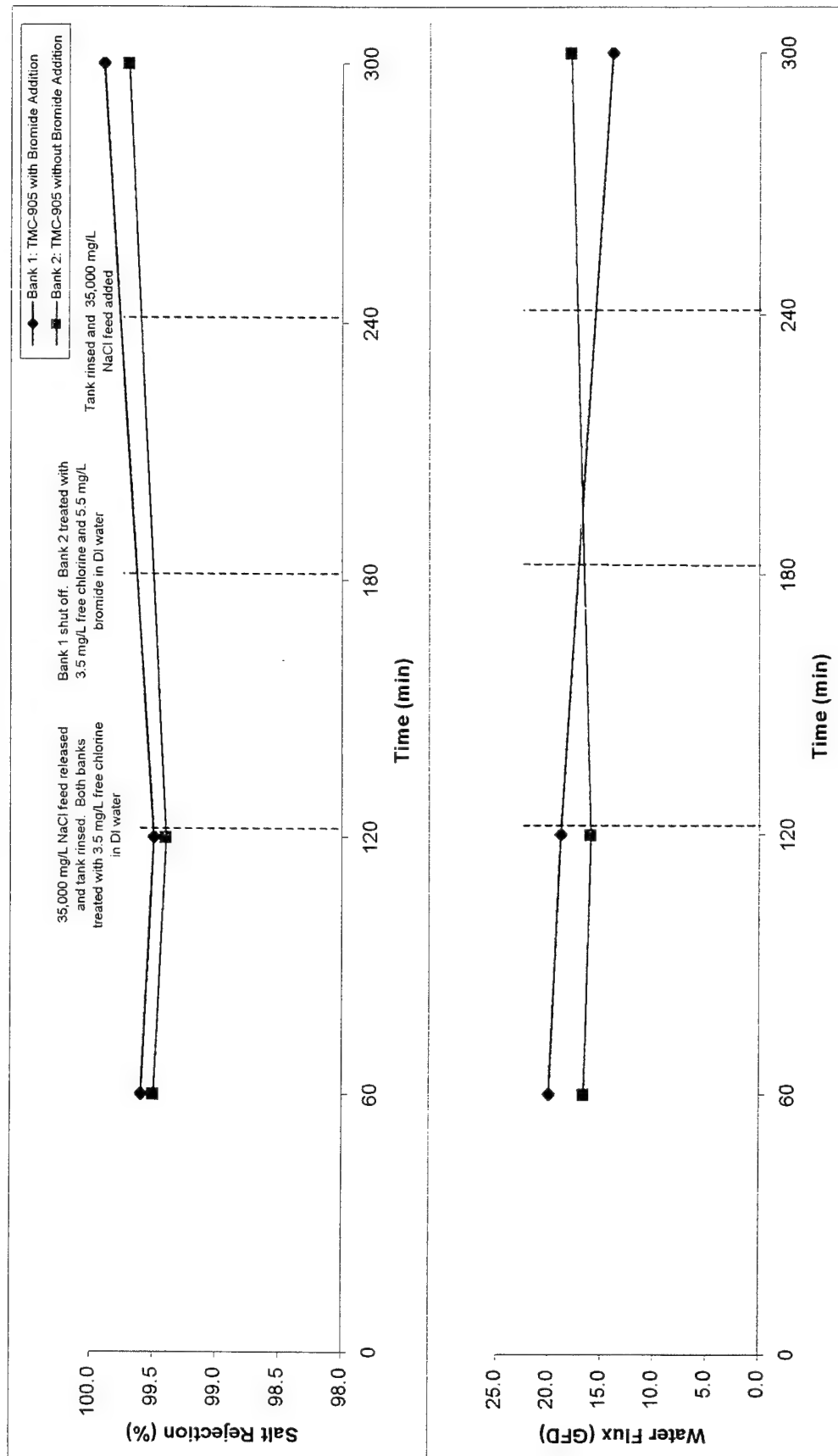
243

17.5 Comparative Effects of Hypobromous Acid on the Transport Properties of *ctct*-CPTC, *cccc*-CPTC, TMC and FilmTec Membranes.

The effects of hypobromous acid on the transport properties of *ctct*-CPTC, *cccc*-CPTC, TMC and FilmTec commercial membrane were determined in tests conducted at 800 psi applied pressure, 35,000 mg/L NaCl feed pH 6.5, 25°C. NaOCl was added to the feed to establish and maintain the targeted free chlorine concentrations of 0.5, 1.3 and 3.5 mg/L. The transport properties of the membranes were determined 1 hr after the test was initiated, after which time NaOCl was added to the feed to attain the desired level of free chlorine. One hour after the addition of free chlorine to the feed, the transport properties were again measured to compare with the previous determinations before the addition of free chlorine. Water flux and salt rejection for these membranes are shown in Table 17.3 and Figures 17.8 through 17.11, respectively. Several important observations were noted.

*   All of the membranes, with the exception of the FilmTec commercial membrane, exhibited dramatic changes in transport properties after exposure to hypobromous acid in the RO testing. The FilmTec membranes were removed from a previously wet-tested spiral-wound element and may have been previously exposed to hypobromous acid.

*   The decrease in water flux exhibited by the *ctct*-CPTC, *cccc*-CPTC, and TMC membranes showed little dependence on the level of free chlorine. The concentration of bromide ion in the 35,000 mg/L NaCl feed is sufficient to convert all of the free chlorine, which ranged from 0.5 to 3.5 mg/L, to hypobromous acid.

17.6 Performance of CPTC Membranes after Immersion in High Concentrations of Hypochlorous/Hypobromous Acid

The transport properties of CPTC membranes respond to low (3.5 mg/L) and high (30,000 mg/L) concentrations of sodium hypochlorite and sodium hypobromite in a similar manner (see Figures 17.12 and 17.13). Salt rejection increases dramatically within minutes after the membrane is contacted with the oxidant. This is generally associated with a decrease in water flux. After initial exposure to sodium hypochlorite, CPTC membranes have operated for thousands of hours in long-term RO field tests on chlorinated feeds without degradation.

The RO performance is shown in Figure 17.12 for CPTC membranes that had been immersed in 15,000 mg/L (1.5 wt-%) sodium hypochlorite for 1 hr at pH 6.0 and a set that had been immersed in 30,000 mg/L (3.0-wt%). A second series of CPTC membranes were immersed in like concentrations of sodium hypobromite at pH 6.0 for the same periods of time. At pH 6.0 the predominant species are hypochlorous and hypobromous acids. Membrane immersion in 30,000 mg/L oxidant is equivalent to 6.8 yr of membrane exposure at 0.5 mg/L, the concentration of free chlorine that could be found in RO pretreated feedwater.

Table 17.3

RO Performance of cccc-CPTC, ctct-CPTC, TMC and FilmTec Membranes Before and After Exposure to Hypobromous Acid

Reverse Osmosis Test Conditions: 800 psi applied pressure, 35,000 mg/L sodium chloride feed, 25°C, pH 6.5, 1.1 gal/min feed flow

Reverse Osmosis Performance

Membrane	Free Chlorine in Feed (mg/L)	No Sodium Hypochlorite in Feed			After adding Sodium Hypochlorite to Feed		
		Water Flux (gfd)	NaCl Passage (mg/L)	Salt Rejection (%)	Water Flux (gfd)	NaCl Passage (mg/L)	Salt Rejection (%)
CPTC Membrane							
CPTC 615 - 1	0	26.9	1120	96.8	-	-	-
	0.5	-	-	-	12.4	140	99.6
CPTC 615 - 2	0	26.3	840	97.6	-	-	-
	1.3	-	-	-	12.5	70	99.8
CPTC 615 - 3	0	29.8	980	97.2	-	-	-
	3.5	-	-	-	13.8	105	99.7
cccc-CPTC Membrane							
CPTC 686 - 1	0	14.4	1400	96.0	-	-	-
	3.5	-	-	-	7.5	210	99.4
CPTC 687 - 2	0	13.4	910	97.4	-	-	-
	1.3	-	-	-	8.4	175	99.5
CPTC 518 - 3	0	17.7	490	98.6	-	-	-
	3.5	-	-	-	7.5	140	99.4
TMC Membrane							
TMC - 1	0	21.8	245	99.3	-	-	-
	0.5	-	-	-	9.2	35	99.9
TMC - 2	0	20.6	280	99.2	-	-	-
	1.3	-	-	-	8.7	70	99.8
TMC - 3	0	21.9	315	99.1	-	-	-
	3.5	-	-	-	8.1	35	99.9
Commercial FilmTec Membrane							
FilmTec TMC - 1	0	12.9	280	99.2	-	-	-
	0.5	-	-	-	7.4	245	99.3
FilmTec TMC - 2	0	12.9	315	99.1	-	-	-
	1.3	-	-	-	8.5	315	99.1
FilmTec TMC - 3	0	13.0	280	99.2	-	-	-
	3.5	-	-	-	6.0	175	99.5
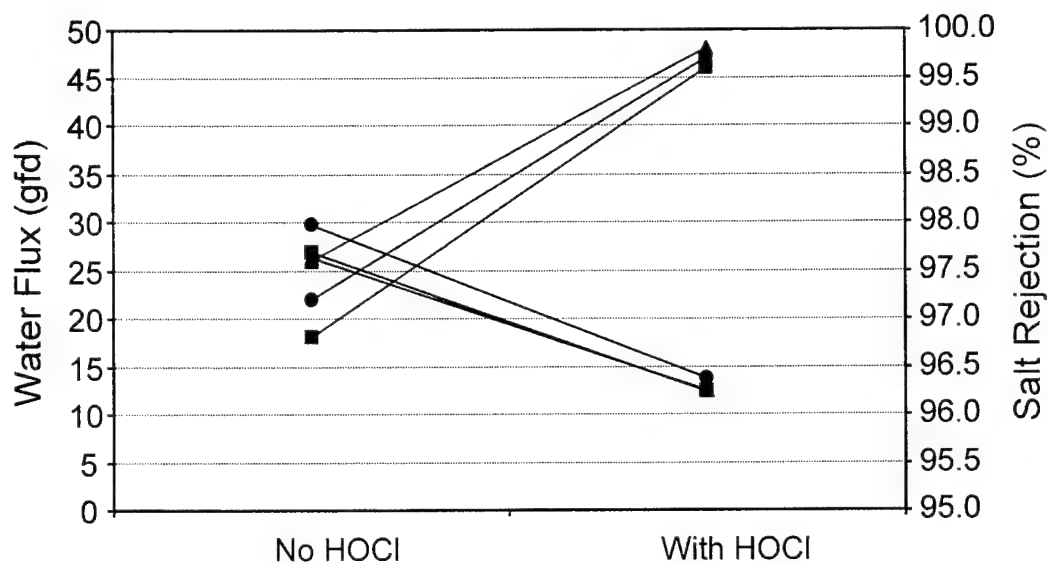
Figure 17.8   RO performance of CPTC membranes before and after NaOCl addition
to the feed at 0.5 (—■—), 1.3 (—▲—) and 3.5 (—●—) mg/L.
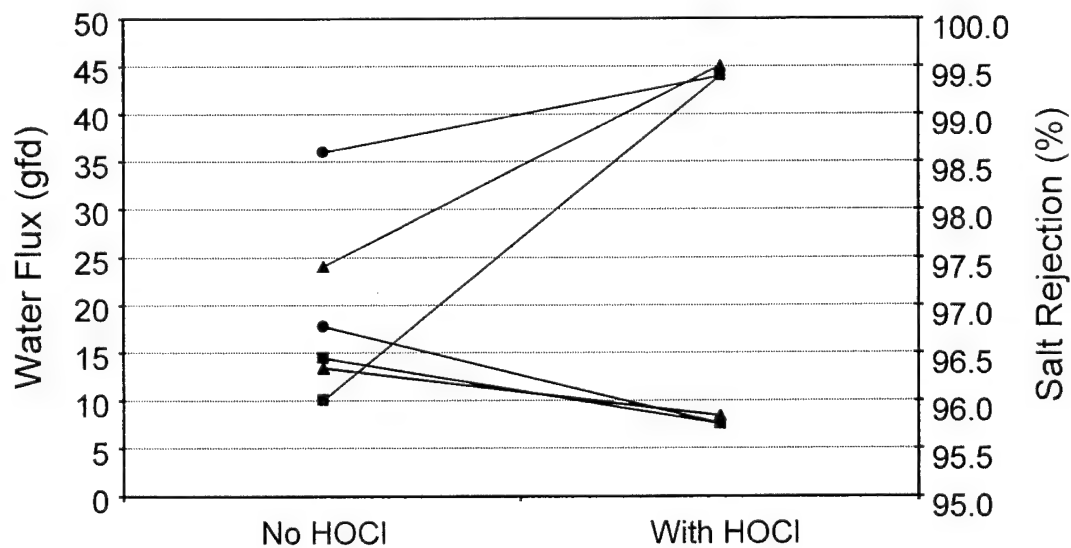
Figure 17.9   RO performance of *cccc*-CPTC membranes before and after NaOCl
addition to the feed at 0.5 (—■—), 1.3 (—▲—) and 3.5 (—●—) mg/L.
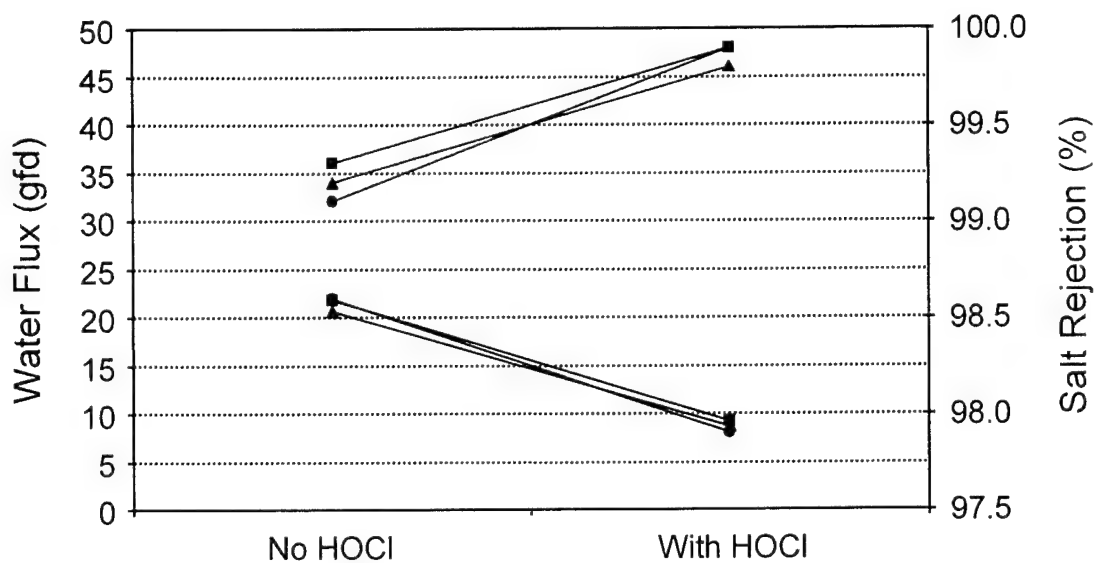
Figure 17.10 RO performance of TMC membranes before and after NaOCl addition to the feed at 0.5 (—■—), 1.3 (—▲—) and 3.5 (—●—) mg/L.
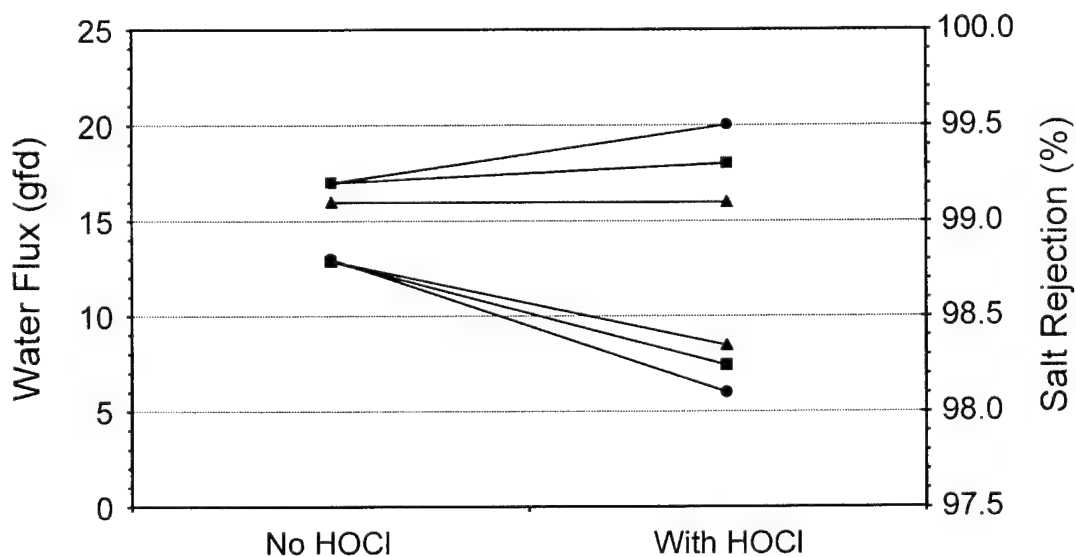
Figure 17.11 RO performance of FilmTec membranes before and after NaOCl addition to the feed at 0.5 (—■—), 1.3 (—▲—) and 3.5 (—●—) mg/L.
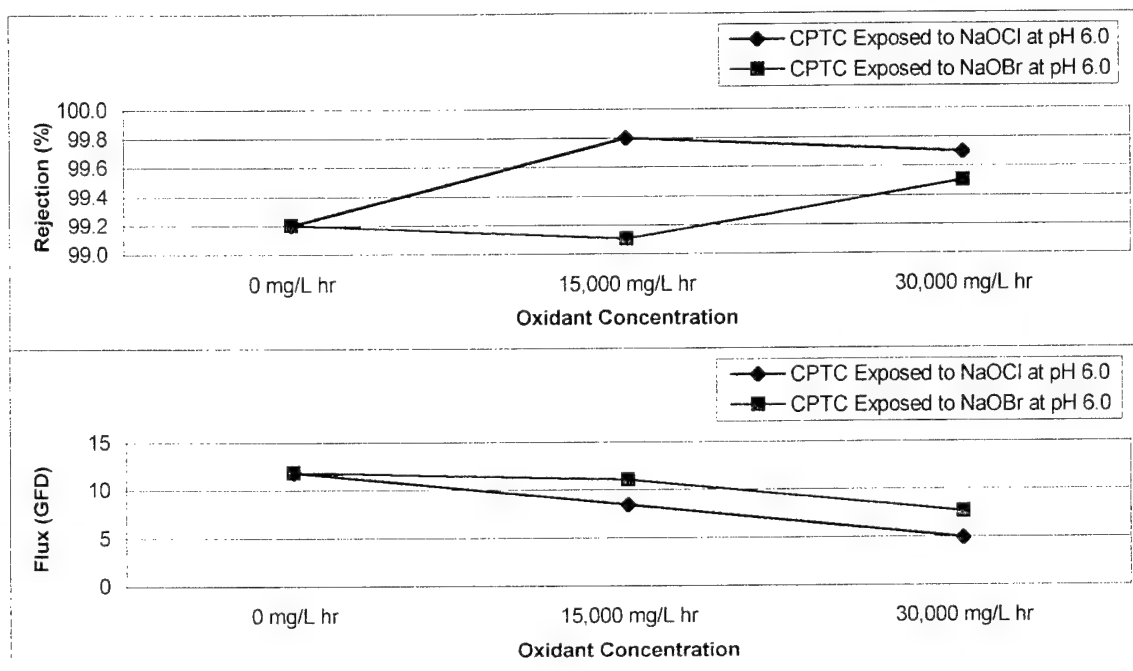
Test Conditions: 2,000 mg/L NaCl feed, 225 psi applied pressure, 1.0 gal/min feed flow, pH 6.0, 25°C

Figure 17.12   RO performance of CPTC 935 membranes after immersion in high concentrations of NaOCl and NaOBr at pH 6.0 for one or more hours.
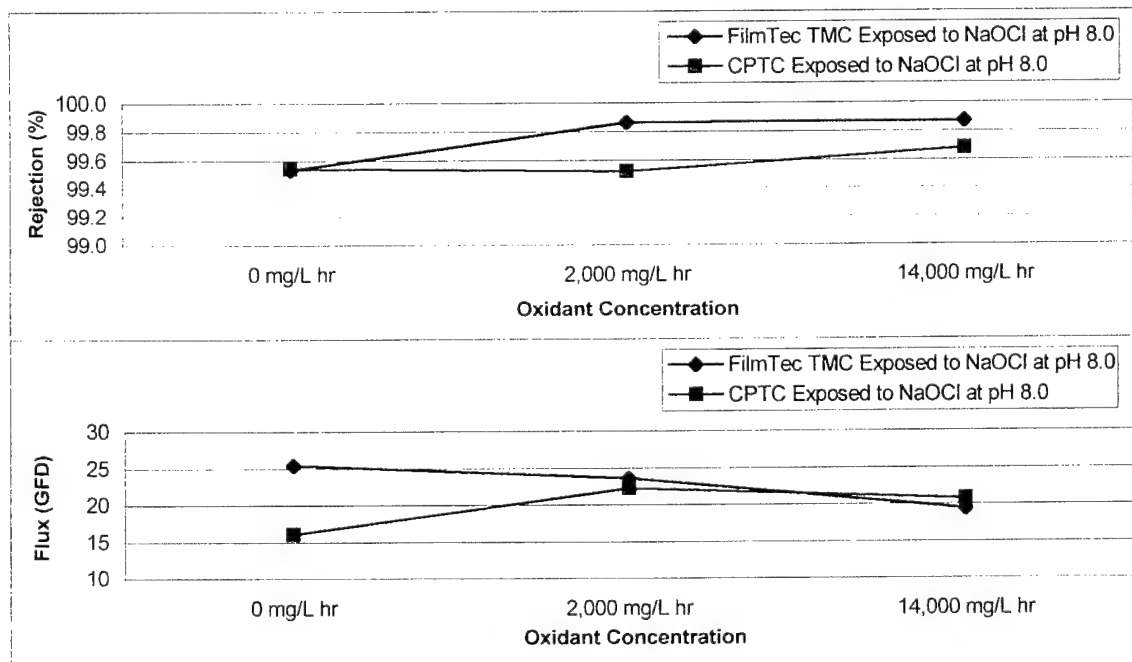
Test Conditions: 2,000 mg/L NaCl feed, 225 psi applied pressure, 1.0 gal/min feed flow, pH 7.5, 25°C

Figure 17.13   RO performance of CPTC and FilmTec TMC membranes after immersion in high concentrations of NaOCl at pH 8.0 for one or more hours.

248

In a parallel experiment, CPTC and a FilmTec membrane were contacted with 2,000 mg/L sodium hypochlorite at pH 8.0 for 1 hr and the transport properties were determined in RO tests. Subsequently, the membranes were exposed to an additional 8,000 mg/L sodium hypochlorite for 1.5 hr and again evaluated in RO. At pH 8.0, the oxidant is present primarily as chlorite ion. The performance of these membranes is shown in Figure 17.13. The total membrane contact time with sodium hypochlorite was 14,000 mg/L-hr or the equivalent of 3.2 years of membrane exposure to 0.5 mg/L.

CPTC membranes have demonstrated the ability to withstand high concentrations of oxidants without degradative effects. The CPTC membranes appear chemically stable to both hypochlorous acid (HOCl) and hypochlorite ion (OCl⁻) under these extreme conditions.

17.7 Effect of Hypochlorous/Hypobromous Acid Pretreatment on CPTC Membrane Surface Morphology and Chemical Structure

17.7.1 Experimental Method

CPTC and TMC membranes were tested to determine the effect chlorine and combined chlorine/bromine treatment has on surface morphology and chemical structure. A CPTC membrane made from CPTC-AC Lot No. 022000S2 membrane was cut into eight small samples. These samples were run in RO test cells for 1 hr at 800 psi on a synthetic seawater feed (35,000 mg/L NaCl). Flux and rejection were measured and then the samples were thoroughly rinsed with DI water. Two sampless were set aside and served as controls. The reservoir tank was thoroughly rinsed clean of NaCl and then the remaining six samples were tested on a feed of 3.5 mg/L NaOCl in DI water. After 1 hr, flow to three of the test cells was shut off. The tank was cleaned and filled with 3.5 mg/L NaOCl and 10 mg/L NaBr in DI water. The three remaining test cells were operated for 1 hr at 800 psi and then all six samples were rinsed with DI water. The tank was cleaned again, the test cells operated on seawater feed at 800 psi for 1 hr, and then flux and rejection were measured. The membrane samples were rinsed in DI water, removed and analyzed by ATR/IR, AFM, TEM and EDX. An additional set of TMC samples was treated identically.

17.7.2 AFM Analysis

AFM images (10 μm) of the control TMC and CPTC membranes and membranes exposed to NaOCl and combined NaOCl/NaBr are displayed in Figure 17.14. All six images look similar. RMS roughness and mean height calculations are displayed in Figure 17.15. At this level of resolution, all six membranes appear similar. The chlorine and bromine treatment did not appear to have a significant affect on the surface morphology.

249

CPTC

TMC

No treatment

NaOCl

NaOCl + NaBr
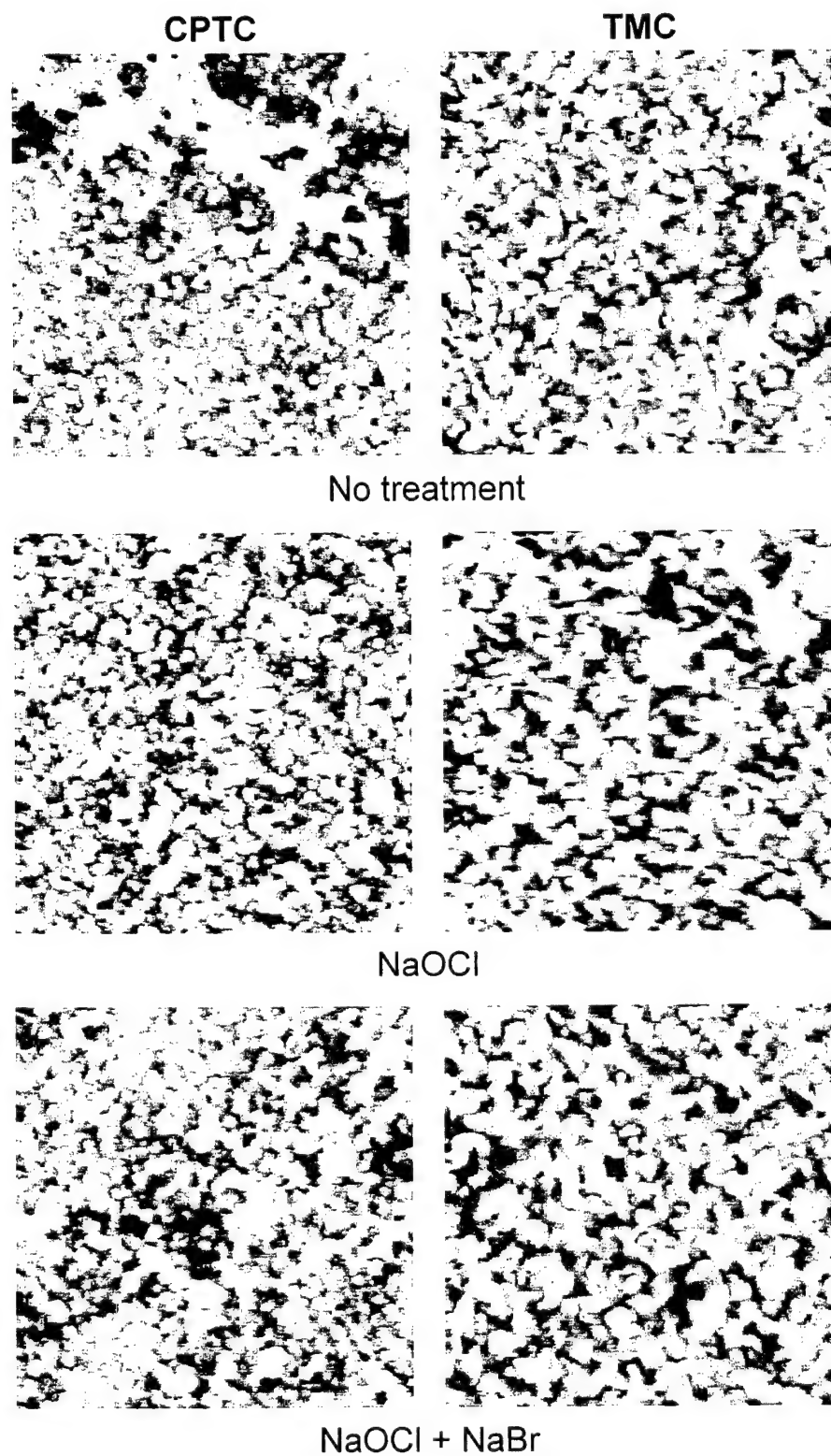
Figure 17.14 AFM images (10 μm) of CPTC (right) and TMC (left) membranes exposed to chlorine (HOCl) and chlorine plus bromine (NaOBr)in DI water RO feed.
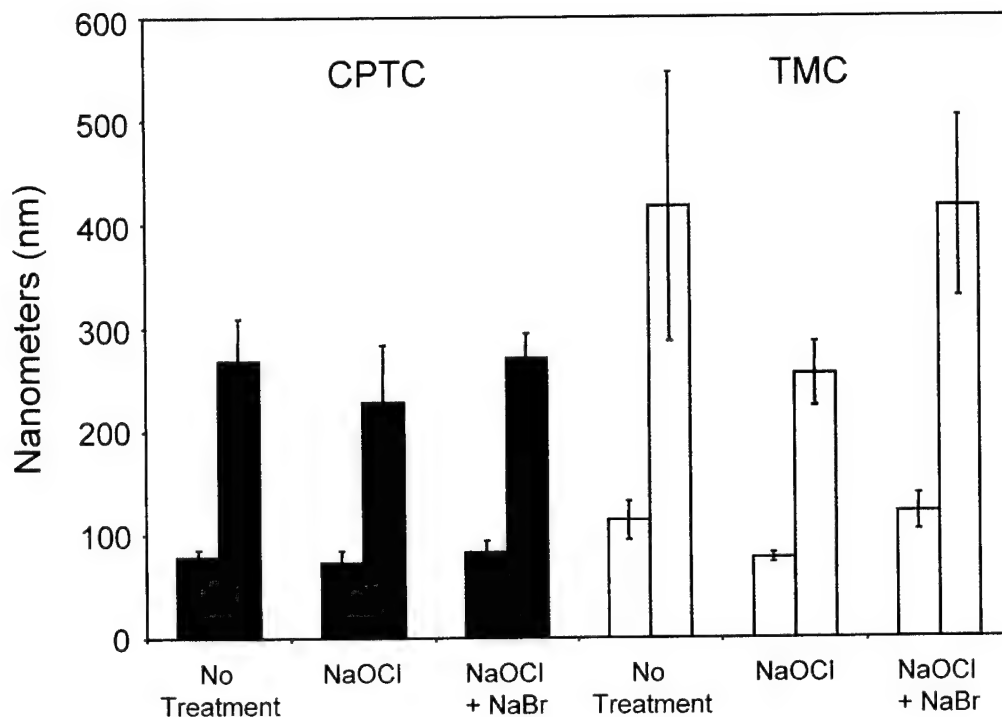
Figure 17.15 RMS roughness (■ □) and mean height (■ □) surface elevations of membranes exposed to NaOCl and NaBr.

17.7.3 EDX and TEM Analysis

Energy dispersive X-ray analysis (EDX) was conducted on the surface of both CPTC and TMC membranes to determine if bromine is incorporated into the structure after exposure to hypochlorous and hypobromous acid.

The following protocol was used to prepare the membrane specimens following membrane exposure to hypochlorous acid and hypobromous acid in RO. The membranes were thoroughly rinsed in distilled water with one membrane from each set having a final rinse of pH 6.0 and one membrane from each set having a final rinse of pH 8.0.

The specimens were then dehydrated in a graded ethanol series of 30-, 50-, 70-, and 90-wt% for 10 min each followed by three 10-min changes of 100 wt-% ethanol. Subsequently, the specimens were placed in 1/3 Spurr resin and 2/3 ethanol for 2 hr, then 2/3 Spurr - 1/3 ethanol for 2 hr and finally two changes of 100 wt % Spurr for 2 hr each. The resin impregnated specimens were placed in flat embedding molds in fresh resin and polymerized overnight at 70°C. Sections were taken on an RMC-MT-X ultramicrotome and viewed on a Philips CM 300 Transmission Electron Microscope located at the University of California at Riverside.

The elemental analyses by EDX of CPTC and TMC membrane surfaces, presented as elemental weight and element atomic weight percentages, are presented in Table 17.4. The following observations were made upon examination of the data:

- Elemental bromine was not detected on any of the CPTC and TMC membrane samples that had not been exposed to hypobromous acid.

- Elemental bromine was detected in increased percentages on all CPTC and TMC membrane samples exposed to NaOCl in the presence of NaBr (hypobromous acid). The percentage of elemental bromine detected on CPTC membranes was greater than for TMC membranes.

- The data suggests that hypobromous acid has brominated the PA structure making it an integral part of the membrane chemistry. Bromination is greater for CPTC than for TMC membranes.

- Both CPTC and TMC membranes can be brominated in RO at low hypobromous acid concentrations (< 3.5 mg/L free bromine) in DI water at pH 6.5.

- Elemental chlorine was detected on all CPTC and TMC membrane samples regardless of pre-treatment. A baseline level of 3.2 elemental weight percent was observed.

- The elemental weight percent of chlorine detected on CPTC membranes that had been exposed to hypochlorous acid are above baseline levels. It would appear that some chlorination of the membrane has occurred. Chlorination of TMC membranes is not as pronounced.

In summary, there is strong evidence that CPTC and TMC membranes are brominated very quickly by hypobromous acid at very low concentrations. Although the data is not as conclusive, chlorination of CPTC and TMC membranes by hypochlorous acid appears likely. The location of bromination on the CPTC membrane will be discussed in the following section.

The TEM analysis of CPTC 898 and TMC 905 membranes are presented in Section 12.9, Figures 12.23 through 12.28.

17.7.4 ATR/IR Analysis

ATR/IR spectra of TMC and CPTC membranes that were exposed to NaOCl and combined NaOCl/NaBr are displayed in Figures 17.16 and 17.17. Distinct changes in the IR spectra of the TMC and CPTC membranes were observed after exposure to the two test solutions, indicating changes in the polymer chemistry. These changes are (1) loss of the aromatic C=C stretching vibrations at 1608, 1489 and 1446 cm^{-1}, (2) loss of the ~1541 cm^{-1} amide II N-H bending band and a shift to lower frequency and (3) the loss of the C-H ring deformation band near 780 cm^{-1} (see Figures 17.18 through 17.21). Loss of the C=C and C-H ring vibrations is presumably associated with Cl or Br addition to the

Table 17.4

Elemental EDX Analyses of CPTC and TMC Membrane Surfaces Before and After Exposure to NaOCl and NaOCl / KBr in RO

Membrane Designation	Sample	Membrane History And Exposure	Final Membrane Rinse, pH	Element Weight %				Element Atomic %			
				C	O	Cl	Br	C	O	Cl	Br
CPTC Membrane											
CPTC 898	1-1	35,000 mg/L NaCl in RO	6.0	90.1	6.5	3.4	nd	93.7	5.1	1.2	nd
CPTC 898	1-2	35,000 mg/L NaCl in RO	6.0	89.4	8.4	2.3	nd	92.6	6.6	0.8	nd
CPTC 898	2-1	35,000 mg/L NaCl in RO	8.0	90.1	7.0	3.0	nd	93.5	5.5	1.0	nd
CPTC 898	2-2	35,000 mg/L NaCl in RO	8.0	87.8	8.4	3.8	nd	92.0	6.6	1.4	nd
CPTC 898	3-1	NaOCl in RO	6.0	80.6	5.4	14.0	nd	90.2	4.5	5.3	nd
CPTC 898	3-2	NaOCl in RO	6.0	82.8	5.4	11.8	nd	91.2	4.4	4.4	nd
CPTC 898	4-1	NaOCl in RO	8.0	91.6	3.9	4.5	nd	95.3	3.1	1.6	nd
CPTC 898	4-2	NaOCl in RO	8.0	87.5	5.1	7.4	nd	93.3	4.0	2.7	nd
CPTC 898	5-1	NaOCl/KBr in RO	6.0	76.3	4.1	4.4	14.1	91.6	3.7	1.8	2.6
CPTC 898	5-2	NaOCl/KBr in RO	6.0	83.7	3.8	3.3	8.9	93.9	3.2	1.3	1.5
CPTC 898	6-1	NaOCl/KBr in RO	8.0	79.2	4.8	5.0	11.0	91.8	4.2	2.0	2.0
CPTC 898	6-2	NaOCl/KBr in RO	8.0	87.1	3.4	3.0	6.5	95.0	2.8	1.1	1.1
TMC Membrane											
TMC 905	7-1	New membrane	6.0	90.8	6.1	3.1	nd	94.1	4.8	1.1	nd
TMC 905	7-2	New membrane	6.0	90.3	6.6	3.2	nd	93.8	5.1	1.1	nd
TMC 905	8-1	New membrane	8.0	90.0	6.4	3.7	nd	93.7	5.0	1.3	nd
TMC 905	8-2	New membrane	8.0	90.7	6.5	2.8	nd	94.0	5.0	1.0	nd

253

Table 17.4 (cont)

Membrane Designation	Sample	Membrane History And Exposure	Final Membrane Rinse, pH	Element Weight % C	O	Cl	Br	Element Atomic % C	O	Cl	Br
TMC 905	9-1	NaOCl in RO	6.0	90.6	6.0	3.4	nd	94.1	4.7	1.2	nd
TMC 905	9-2	NaOCl in RO	6.0	89.2	6.0	4.8	nd	93.6	4.7	1.7	nd
TMC 905	10-1	NaOCl in RO	8.0	88.5	5.7	5.8	nd	93.4	4.5	2.1	nd
TMC 905	10-2	NaOCl in RO	8.0	83.5	7.2	9.3	nd	90.8	5.8	3.4	nd
TMC 905	11-1	NaOCl/KBr in RO	6.0	86.4	5.4	1.8	6.4	93.9	4.4	0.7	1.0
TMC 905	11-2	NaOCl/KBr in RO	6.0	86.4	5.0	2.6	6.0	93.9	4.1	1.0	1.0
TMC 905	12-1	NaOCl/KBr in RO	8.0	86.4	5.5	1.8	6.3	93.8	4.5	0.6	1.1
TMC 905	12-2	NaOCl/KBr in RO	8.0	80.1	7.5	3.3	9.1	90.8	6.3	1.3	1.6

nd = non detectable

Test conditions: 800 psi applied pressure, 35,000 mg/L sodium chloride feed, pH 6.5, 25°C, 1 gal/min feed flow.

Testing sequence:

(1) Hour 2: Membrane water flux and salt passage recorded.
(2) Hour 2.1: Without depressurizing, the 35,000 mg/L feed was replaced with deionized water containing 3.5 mg/L free chlorine.
(3) Hour 3.1: 10 mg/L sodium bromide was added to the feed.
(4) Hour 4: Without depressurizing, the deionized feed water containing free chlorine and sodium bromide was removed from the system and replaced with 35,000 mg/L sodium chloride.
(5 Hour 5: Membrane water flux and salt passage recorded.

The RO system was equipped with three parallel banks of cells that were isolated at different times

Membrane samples 1-1,1-2,2-1, 7-1,7-2,8-1 and 8-2 were removed from the system after sequence (1)
Membrane samples 3-1,3-2,4-1,4-2,9-1,9-2,10-1 and 10-2 were removed from the system at after sequence (2)
Membrane samples 5-1,5-2,6-1,6-2,11-1,11-2,12-1 and 12-2 were removed from the system after sequence (5)

All membrane were repeatedly soaked and rinsed in distilled water prior to EDX analysis. The final rinse was adjusted for pH 6 or 8.

254
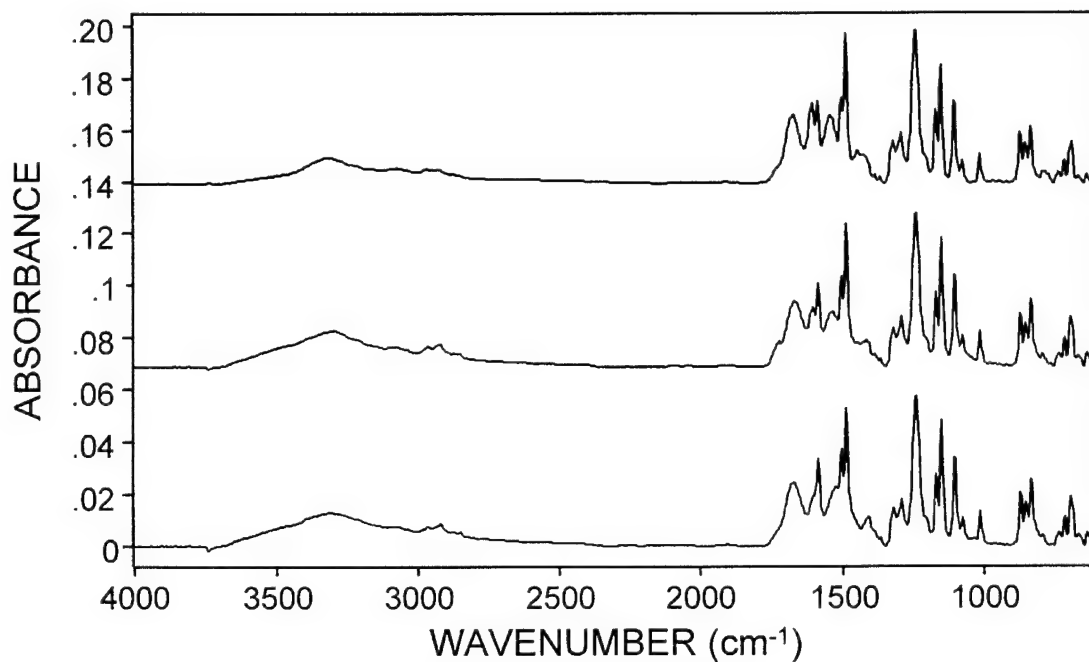
Figure 17.16 ATR/IR spectra of CPTC membranes, untreated (top), NaOCl-treated (middle) and NaOCl/NaBr-treated (bottom).
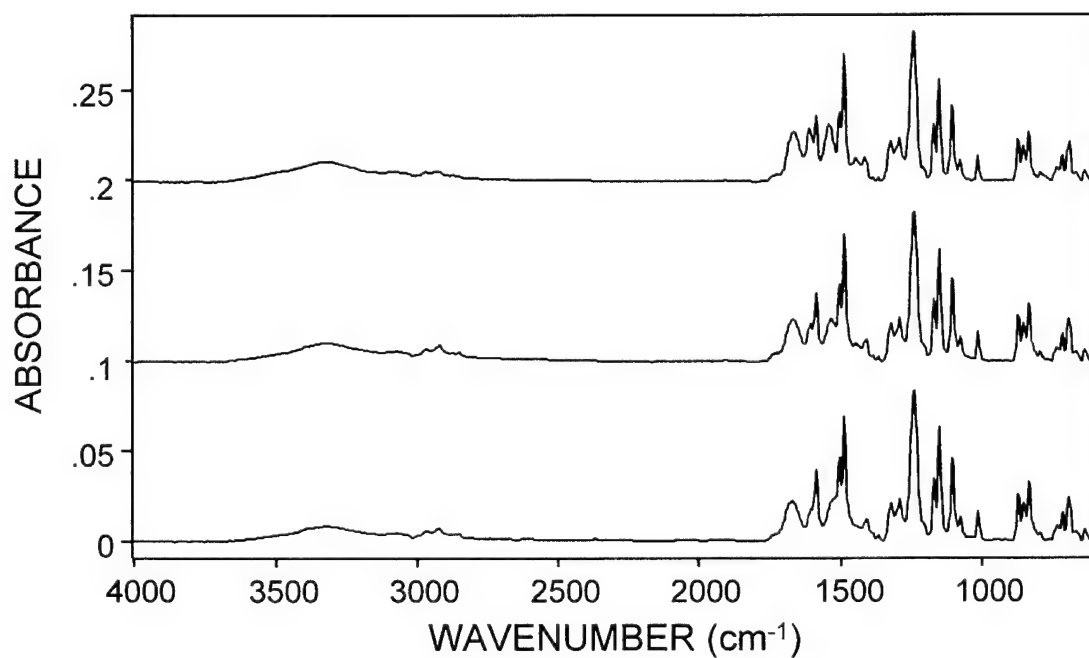
Figure 17.17 ATR/IR spectra of TMC membranes, untreated (top), NaOCl-treated (middle) and NaOCl/NaBr-treated (bottom).

Figure 17.18 ATR/IR spectra of TMC membrane (top) and NaOCl-treated membrane (bottom), revealing loss of C=C ring stretch and C-H deformation bands and loss and shift of N-H bend to lower wavenumber.

Figure 17.19 ATR/IR spectra of CPTC membrane (top) and NaOCl-treated membrane (bottom), revealing loss of C=C ring stretch and C-H deformation bands and loss and shift of N-H bend to lower wavenumber.

Figure 17.20 ATR/IR spectra of TMC membrane (top) and NaOCl/NaBr-treated
membrane (bottom), revealing loss of C=C ring stretch and C-H
deformation bands and loss and shift of N-H bend to lower wavenumber.

Figure 17.21 ATR/IR spectra of CPTC membrane (top) and NaOCl/NaBr-treated
membrane (bottom), revealing loss of C=C ring stretch and C-H
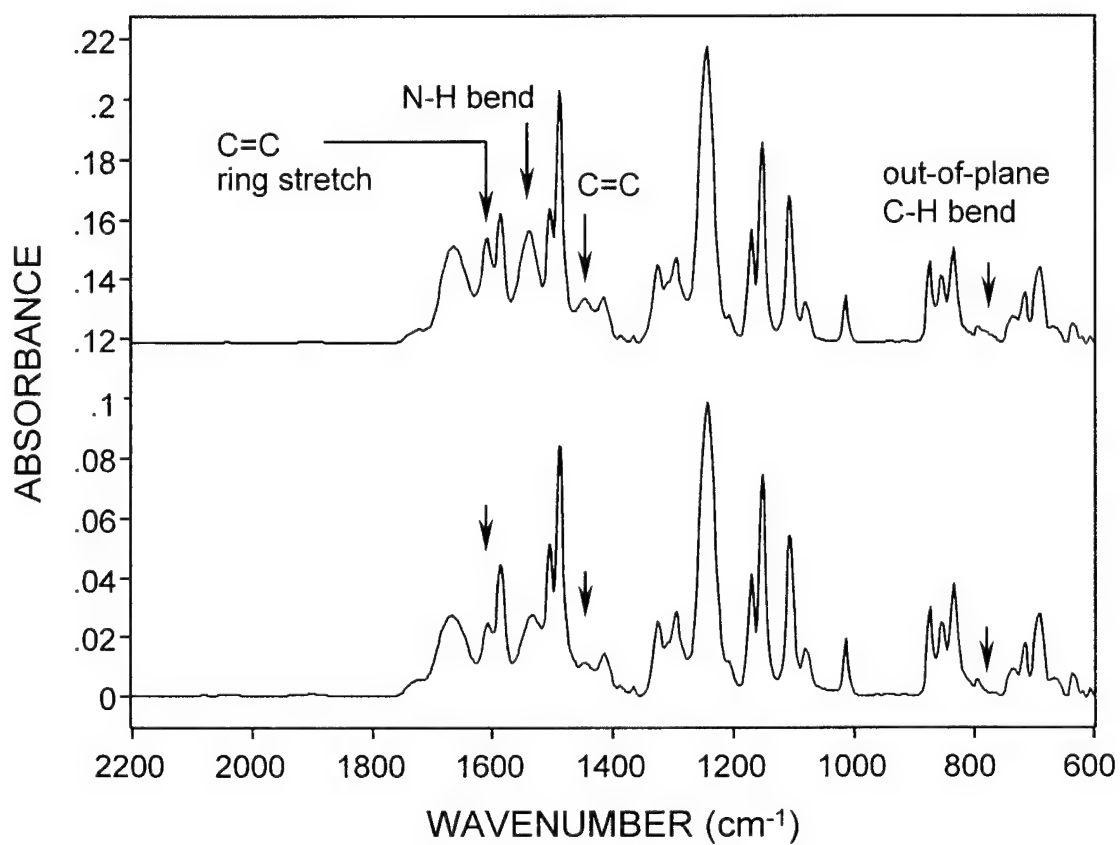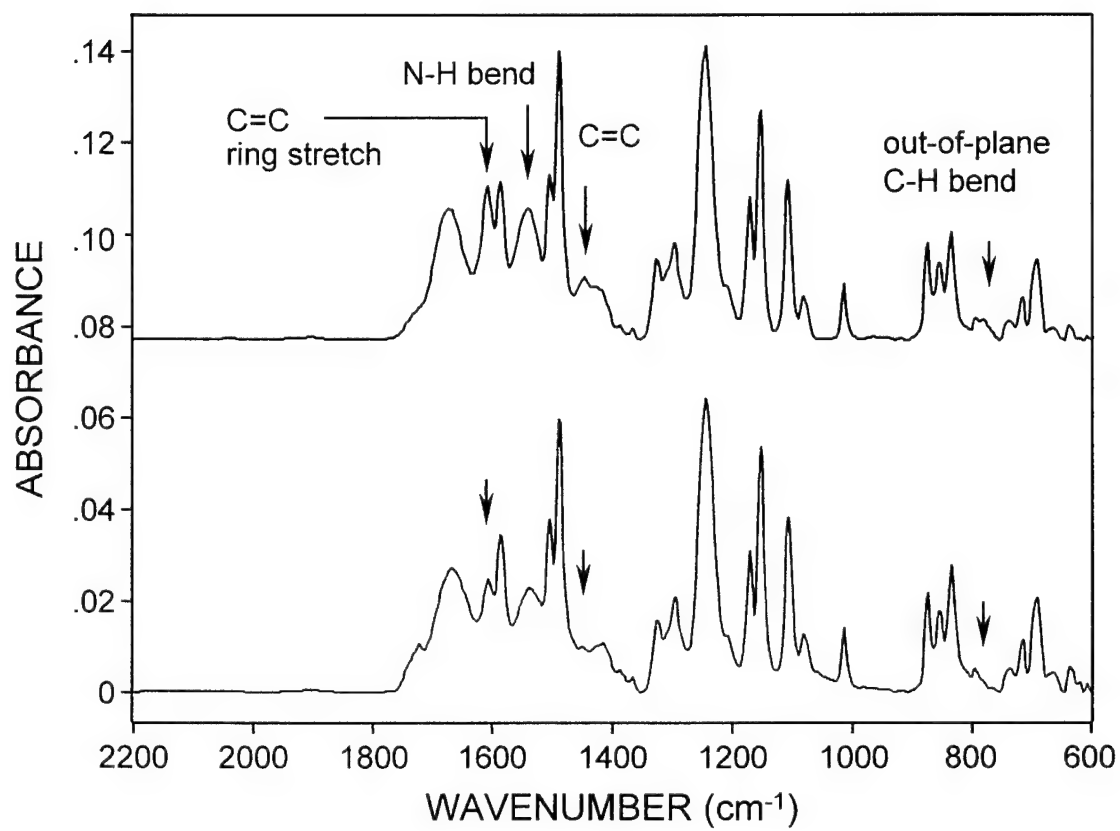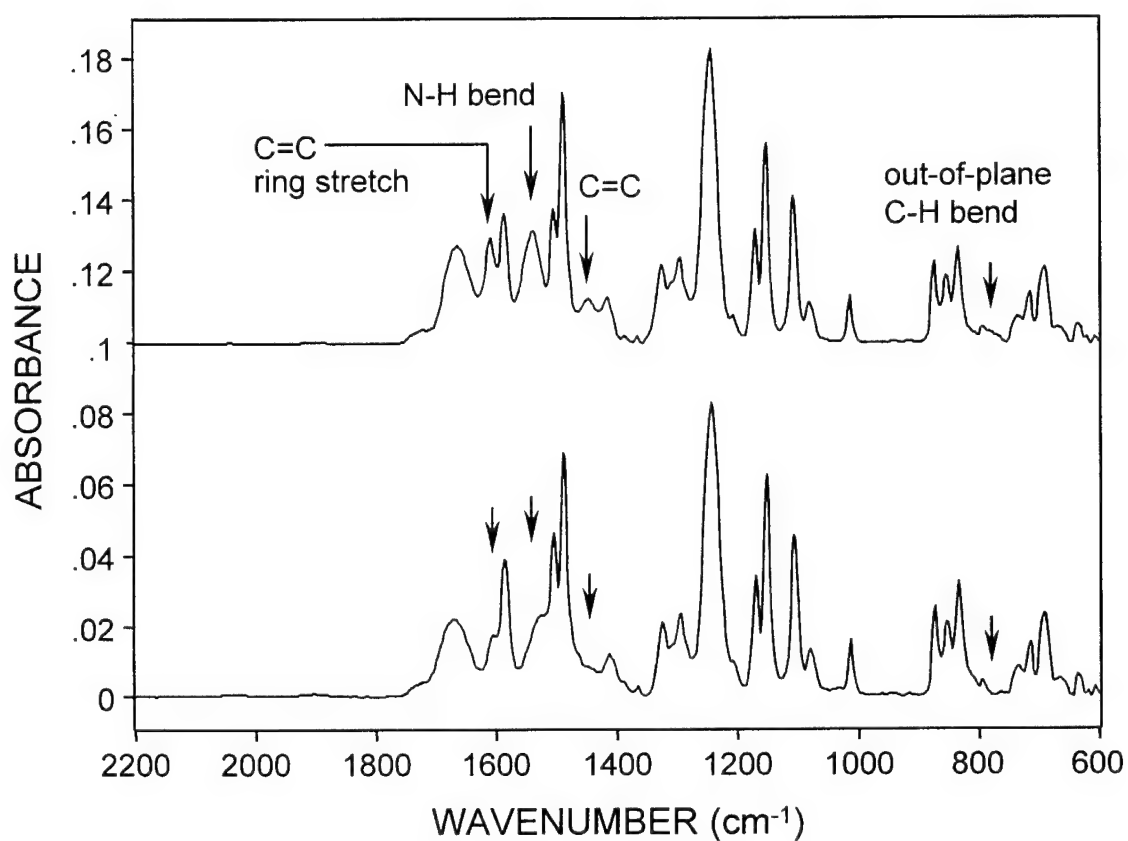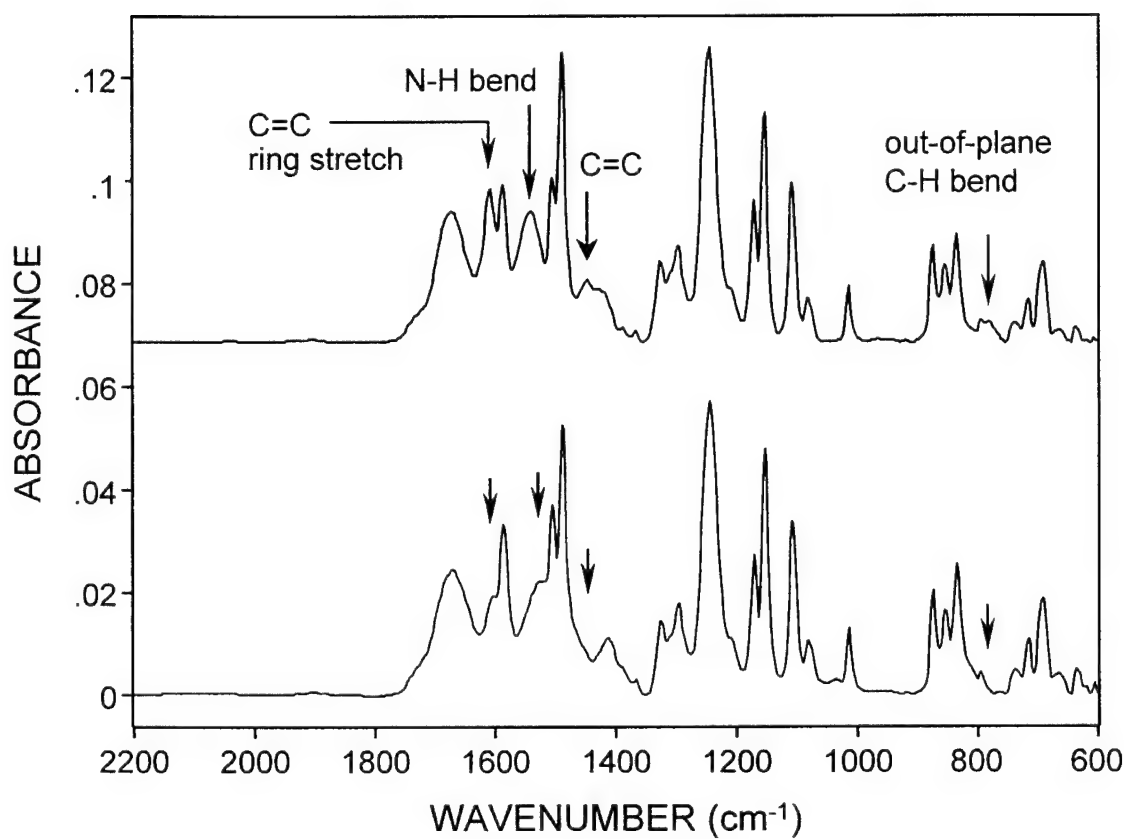deformation bands and loss and shift of N-H bend to lower wavenumber.

MPD ring as opposed to the tricarboxylate benzene ring (Figure 17.22). Results from previous chlorination studies indicate addition to the MPD ring.[23,24] Amine groups are strong ortho-, para- directors, and carboxylic acids are ring deactivators which further supports the conclusion of addition to the MPD ring. Addition to the cyclopentane ring is highly unlikely.

The drop and shift of the amide II band intensity of the TMC and CPTC membranes is most evident in the spectra of membranes exposed to the NaOCl/NaOBr solution (Figures 17.19 and 17.21). Loss of the amide II intensity indicates loss of the N-H, possibly through N-chlorination or N-bromination. However, both adducts are not supposed to be very stable. The shift in amide II band intensity suggests interaction with a nearby chemical group or something on the adjoining benzene ring. For example, hydrogen bonding often leads to band broadening and a frequency shift to lower wavenumber. It is difficult to say exactly what caused the amide II band to shift to lower wavenumber, possibly a change in secondary structure of the polymer chain and interaction of the (N-H) hydrogen with the chlorine or bromine substituents on the aromatic ring.

Finally, on the high wavenumber end of the spectrum, two bands at 3310 cm^{-1} and 3155 cm^{-1} appear to drop slightly after exposure to NaOCl/NaBr, suggesting the loss of the N-H stretch of the secondary amide. A band appears near 3394 cm^{-1} that has yet to be identified.

18.0 EFFECT OF CHLORINE AND HYPOBROMOUS ACID ON PA CHEMISTRY - KBr DISK TRANSMISSION SPECTROMETRY OF PA EXPOSED TO CHLORINE

In an effort to gain a better understanding as to how chlorine affects the PA chemistry, TMC and CPTC membranes were exposed to chlorine and sodium chloride and the PA film was stripped from the membrane surface and analyzed by IR transmission spectrometry by KBr disk.

18.1 Experimental Method

Sheets (7- x 10-in) of TMC and CPTC membranes were exposed to 1000 mg/L sodium hypochlorite and 35,000 mg/L sodium chloride for 2 hr. The sheets were transferred to a 500-mL distilled water bath and soaked for 1 hr. The PA layer was recovered from the RO membrane by first peeling the PA plus PS layers from the polyester backing material. The polymer layers were placed in a 15-mL glass vial with a Teflon-lined cap. NMP was added and the vial was shaken periodically until the PS layer dissolved. The PS was removed with a Pasteur pipette. The NMP addition was repeated four more times. The remaining PA material was transferred to a "shark skin" filter paper (Schleicher & Schuell Filter Paper, Order No. 16990). The PA material was washed with NMP until no milky suspension formed when the filtrate contacts the water below. This means that the PA film is free from contamination by PS. The PA was rinsed with water to remove NMP and acetone to remove the water. The filter paper with the PA were placed in an oven and dried at 80°C for 1 hr.
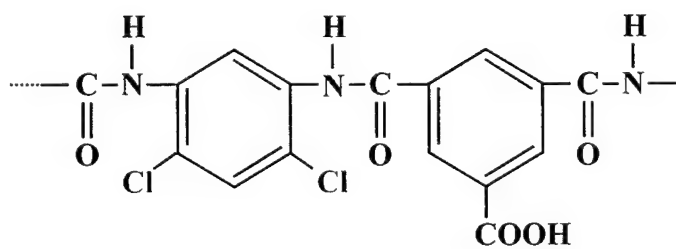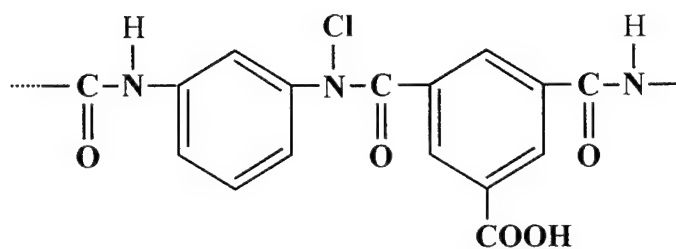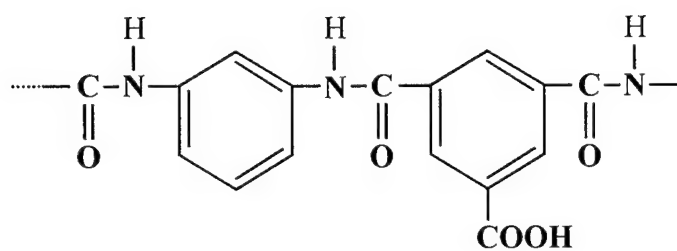
Figure 17.22   Chemical structure of PA (top), reversible N-chlorination (middle) and irreversible chlorination of aromatic ring (bottom)

KBr was ground into a fine powder with a mortar and pestle and then dried at 138°C prior to use. The PA from above was also ground into a fine powder. A small amount of PA was mixed with ~50 mg of KBr and then pressed into a disk ~0.45 mm thick. Spectra (128 scans) were collected on a Magna 550 spectrometer (ThermoNicolet Instrumentation Corporation, Madison, WI) at 4-cm^{-1} resolution. The single-beam spectra were ratioed against a KBr disk background spectrum and converted to absorbance utilizing GRAMS/32 software (Galactic Industries, Salem, NH). A Fourier smoothing function was applied to the absorbance spectra to eliminate the interference fringes generated from the pathlength differences, i.e., thickness, of the Kbr disks. Spectra were baseline corrected to zero absorbance.

18.2 Results and Discussion

ATR/IR spectra of the TMC and CPTC PA samples are displayed in Figures 18.0 and 18.1 between 4000 and 400 cm^{-1}. The fingerprint region of the TMC and CPTC control and chlorinated spectra are shown in Figures 18.2 and 18.3 between 2000 and 400 cm^{-1}. After exposure to chlorine, the following changes were observed in the IR spectra of the TMC PA sample.

* The amide I C=O stretch near 1662 cm^{-1} shifted to a higher wavenumber.
* The amide II N-H bend near 1542 cm^{-1} shifted to a lower wavenumber.
* Vibrational bands associated with the ring stretch (1611, 1492 and 1499 cm^{-1}) all dropped significantly in intensity.
* Vibrational bands near 1320 cm^{-1} and 1251 cm^{-1} associated with the C-N-H bend/C-N stretch dropped in intensity.
* The out-of-plane C-H bend near 780 cm^{-1} from the MPD ring dropped in intensity.
* The C=C out-of-plane bend near 686 cm^{-1} from the MPD ring dropped in intensity

Similar changes in the spectrum of the CPTC were observed.

* The C=O stretch at 1669 cm^{-1} shifted to a higher wavenumber.
* The N-H bend at 1546 cm^{-1} shifted to a lower wavenumber.
* Vibrational bands associated with the ring stretch (1620, 1492 and 1447 cm^{-1}) all dropped in intensity.
* Vibrational bands at 1307 cm^{-1} and 1232 cm^{-1} associated with the C-N-H bend/C-N stretch dropped in intensity.
* The out-of-plane C-H bend at 780 cm^{-1} from the MPD ring dropped in intensity.
* The C=C out-of-plane deformation at 688 cm^{-1} from the MPD ring dropped in intensity.

The changes in the C=C ring vibrations must be associated with the MPD ring since CPTC acid is a nonaromatic five carbon ring. Bands at 867, 778, 683 and 594 cm^{-1} appear in both the TMC and CPTC transmission spectra. Therefore, they must be associated with the MPD ring and not the TMC ring or the CPTC ring.

The shift of the carbonyl band to a higher wavenumber and the drop of the N-H band to a lower wavenumber may indicate loss of hydrogen bonding (C=O H-N) between adjacent polymer chains. If the N-H proton of the amide bond is replaced by chlorine, the hydrogen bonding that occurs between (and within) PA chains will be broken. The remaining amide bonds are left in a different environment since they are no longer hydrogen bonded, and thus the frequency of the two vibrational bands (C=O stretch and N-H bend) shifts. Loss of the C-N-H bend/C-N stretch near 1320 cm^{-1} and 1230 cm^{-1} provides further indication that chlorine has attacked the amide nitrogen.

If the MPD ring is chlorinated, a loss or change in the number and location of the out-of-plane C-H deformation and the C=C out-of-plane bend of the ring could be expected. The number and location of the substituents on the benzene ring affect these two vibrational bands. If there is chlorine addition to the ring (aryl-Cl), vibrational bands should appear between 1078 cm^{-1} and 1074 cm^{-1}. Some new bands do appear in this region of the spectrum of the CPTC that was exposed to chlorine. However, these bands do not appear in the spectrum of the TMC PA that was exposed to chlorine.

18.3   Summary and Conclusions

The chemistry of the PA component of these RO membranes was significantly altered after exposure to chlorine and presumably HOBr. A significant amount of HOBr is generated in the presence of a 35,000 mg/L NaCl and 1000 mg/L HOCl feed (see Section 17.1.3). Major changes in the ATR/IR spectra were noted that indicate damage or change in the polymer structure. Chlorine (or bromine) appears to attack both the amide (-C=O-N-H) bond and the MPD ring. The amide I carbonyl band shifted to a higher wavenumber and the amide II N-H band shifted to a lower wavenumber after exposure to chlorinated feedwater. If chlorine displaces the N-H (amide) proton, hydrogen bonding between polymer chains will be disrupted. This may be the cause of the frequency shifts of the amide I and amide II bands. Generally, hydrogen bonding leads to (1) a reduction in the NH$_2$ or (N-H) stretching frequencies, (2) an increase in the NH$_2$ bending frequencies, (3) a broadening of the spectral band and (4) increase in the IR intensity.

The exact opposite was observed after the PA was exposed to chlorine/bromine, which supports the conclusion that hydrogen bonding was disrupted. The drop in the C=C stretching bands could be a result of chlorination of the MPD ring, as addition of chlorine to the benzene ring would certainly affect these ring vibrations. While the finer detail of the TMC and CPTC PA membrane spectra is not visible below 1000 cm^{-1}, the KBr disk spectra of PA material reveal distinct changes in the C=C out-of-plane bend and C-H deformation bands. These spectral changes support the theory that both the amide bond and the MPD ring are affected by exposure to free chlorine or HOBr. However, what really is lacking is the presence of a definitive C-Cl (Cl-Br) or N-Cl (N-Br) vibrational band in the spectra of either membrane that would allow one to conclude that the PA has been chlorinated or brominated.

Figure 18.0   Mid-IR KBr disk transmission spectra of TMC (top) and HOCl-treated TMC (bottom) removed from membrane sheets.

264

Figure 18.1   Mid-IR KBr disk transmission spectra of CPTC (top) and HOCl-treated CPTC (bottom) removed from membrane sheets.
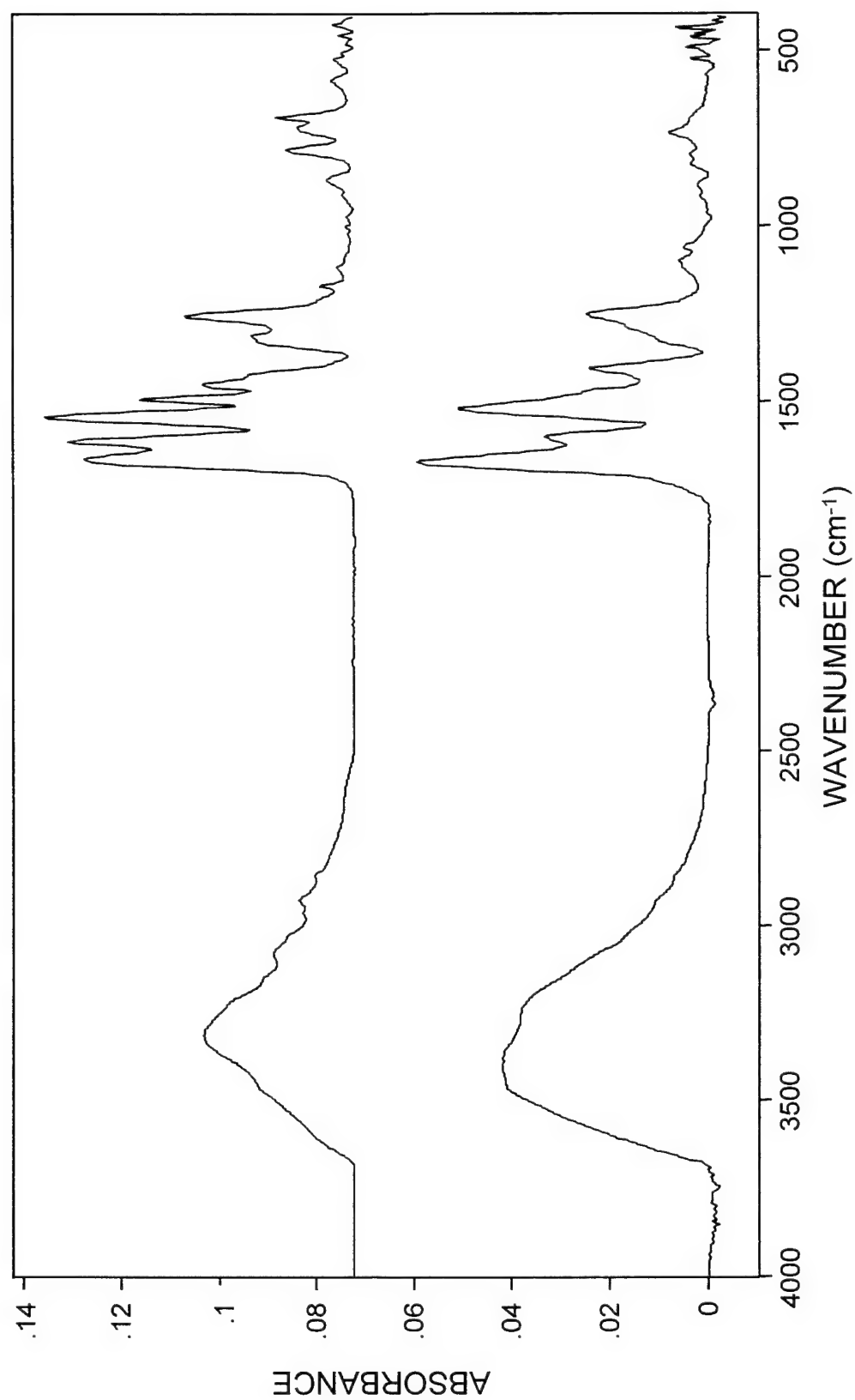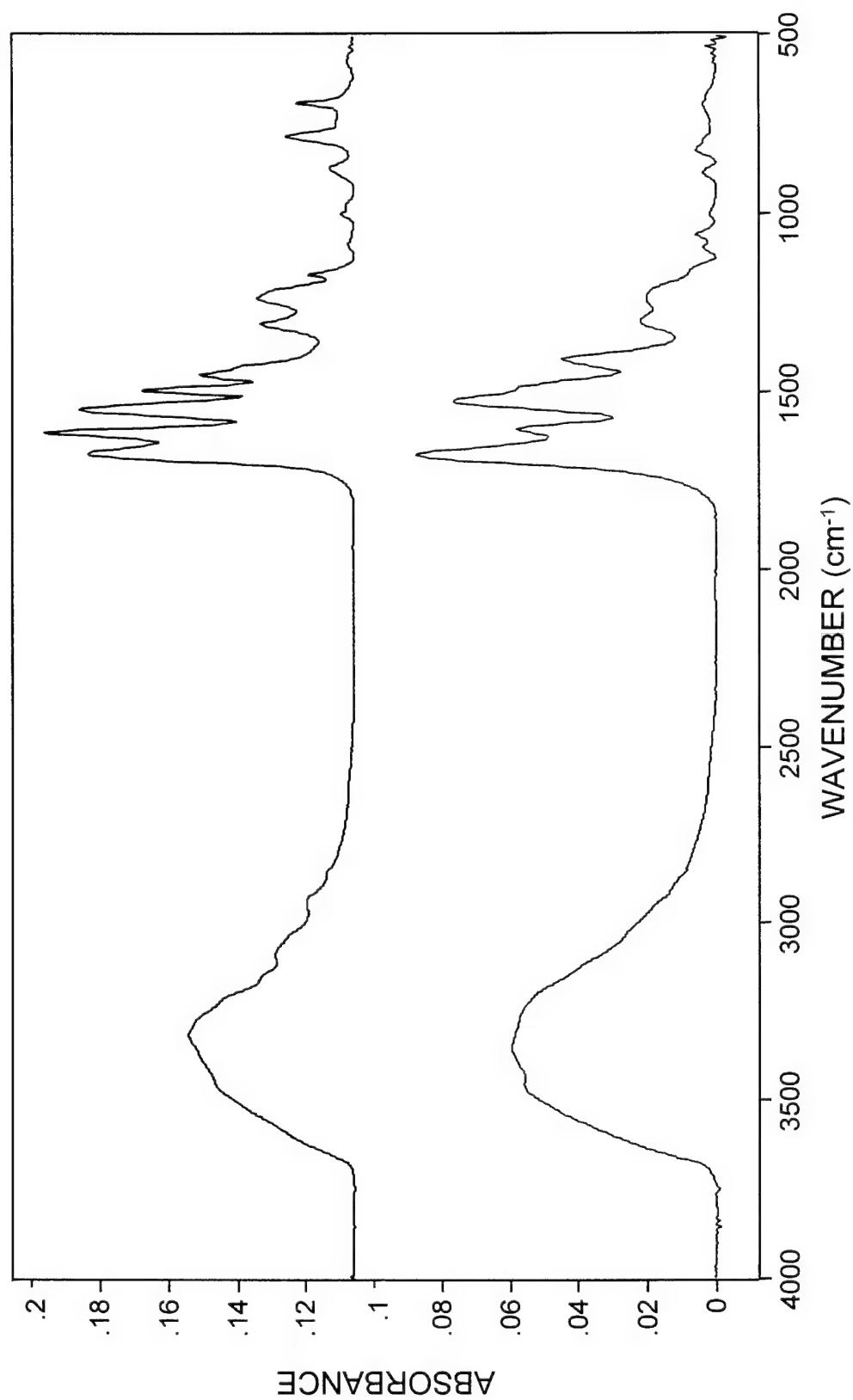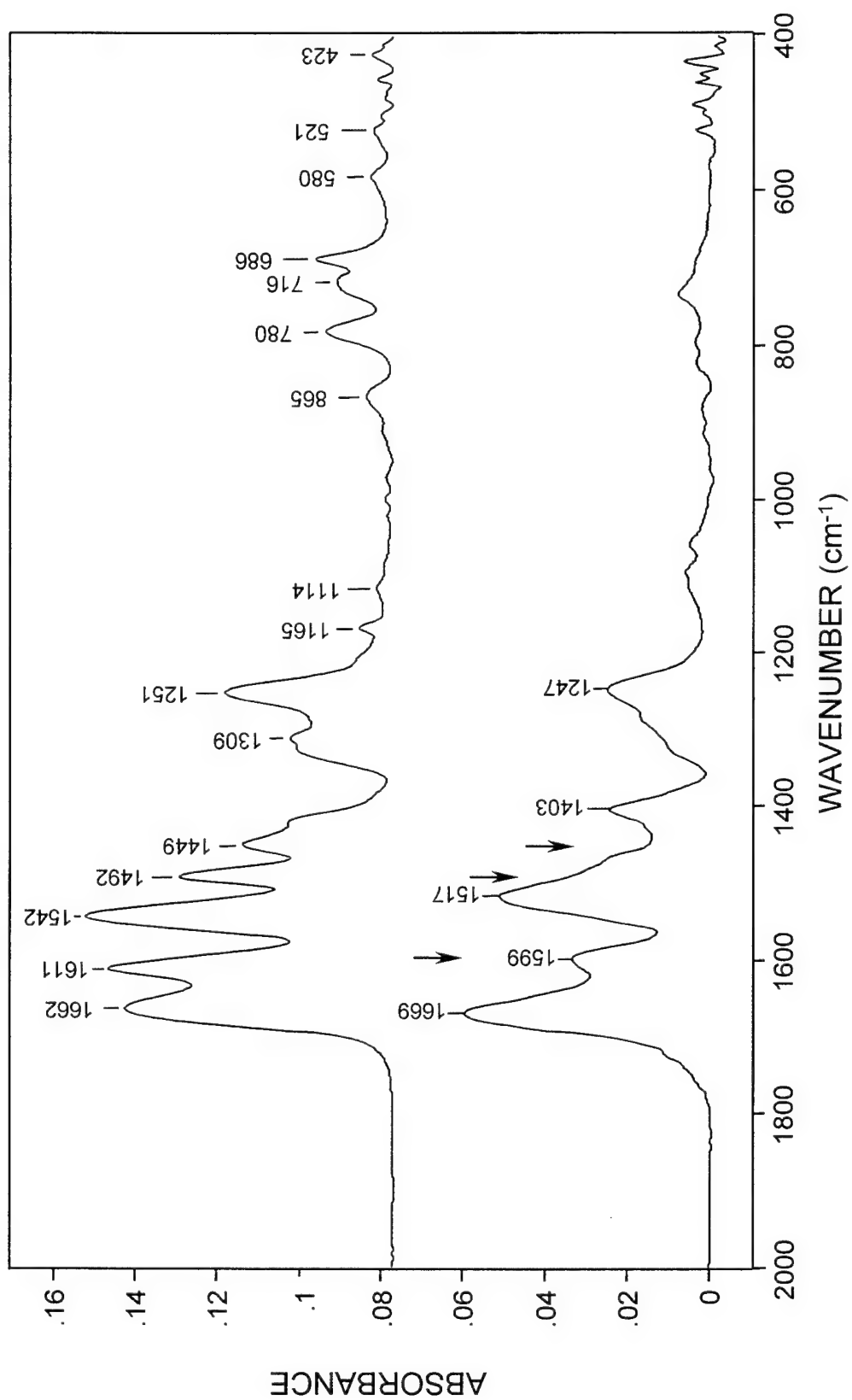
Figure 18.2 Mid-IR KBr disk transmission spectra of TMC (top) and HOCl-treated TMC (bottom) removed from membrane sheets.
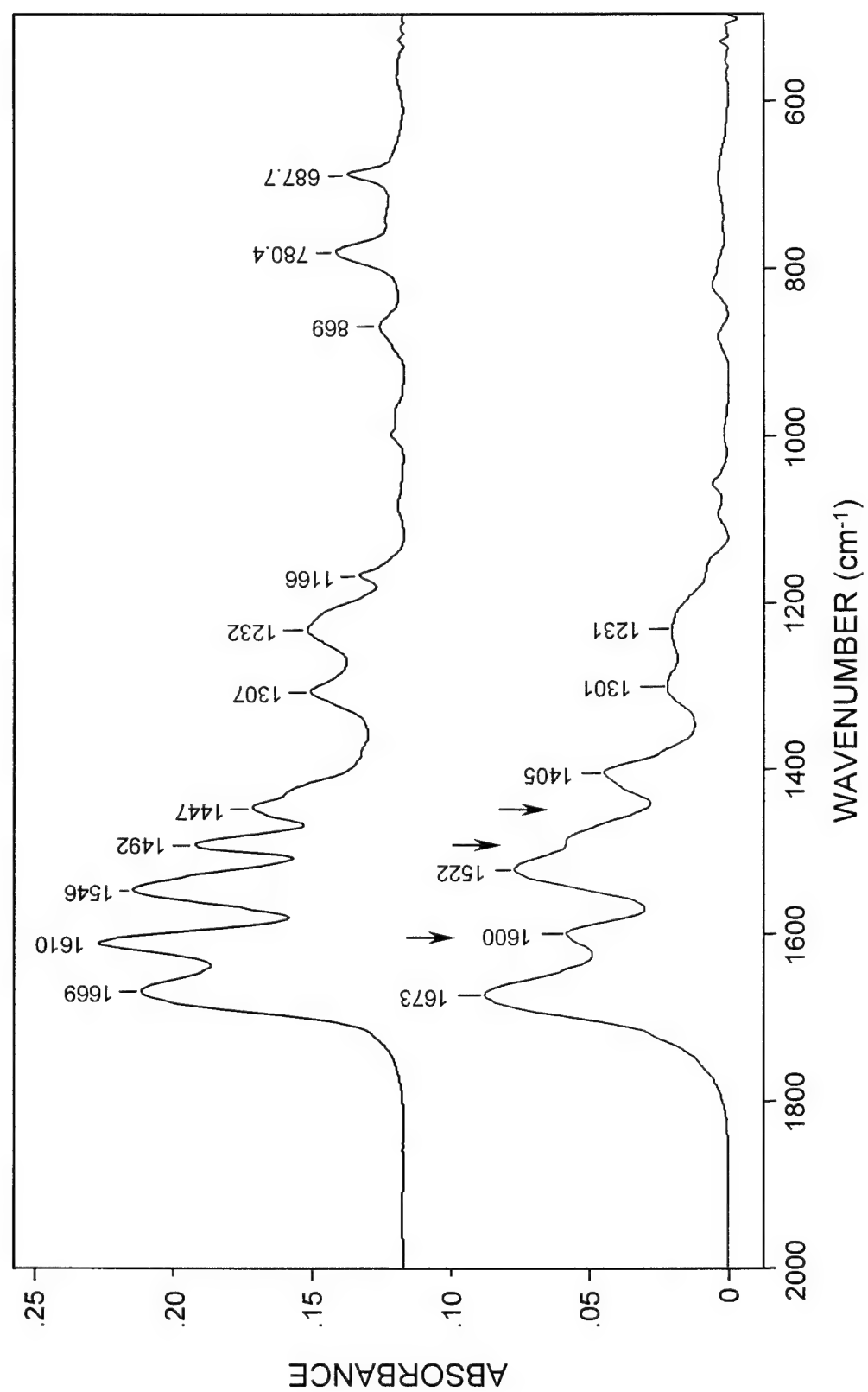
Figure 18.3 Mid-IR KBr disk transmission spectra of CPTC (top) and HOCl-treated CPTC (bottom) removed from membrane sheets.

267

19.0 CHARACTERIZATION OF THE SURFACE PROPERTIES OF CPTC MEMBRANES

Numerous measurements of the characterization of the CPTC membranes were made throughout the two-year program, including hydrophobicity by air bubble contact angle, membrane surface charge and biofouling potential. Data from these experiments are presented below. Data from membranes made from each CPTC-AC Lot of CPTC will be analyzed and discussed in the following section.

19.1 Membrane Surface Hydrophobicity as Determined by Captive Bubble Contact Angle

19.1.1 Solvent Effects on Surface Hydrophobicity

A series of CPTC and TMC membranes was prepared with different solvents (Freon and hexane), and membrane surface hydrophobicity was measured. Membrane CPTC-199 was made from CPTC-AC Lot No. 030399S1 and TMC-201 from TMC. Both membranes were made using a Freon solvent system. Membranes were made from other more purified batches of CPTC included CPTC-281 from CPTC-AC Lot No. 041099S1, and CPTC-315 and CPTC-331 from CPTC-AC Lot No. 061099S1. CPTC-AC Lot No. 06099S1 is more highly purified than CPTC-AC Lot No. 041099S1. Membrane TMC-286 served as the control. These four membranes were made with a hexane solvent system. The contact angles for these membranes are shown in Figure 19.0. It appears that the solvent system has some effect on surface hydrophobicity. CPTC-199, -281 and TMC-201 membranes made with the Freon solvent had contact angles that were lower than the other membranes made with the hexane solvent. These results indicate that the membranes made with the Freon solvent are less hydrophobic (or more hydrophilic) than membranes made with a hexane-based solvent system. Very little difference in contact angle was measured between the membranes made from different lots of CPTC and the TMC control using the hexane solvent system.

19.1.2 Effect of MPD Application on Membrane Hydrophobicity

TMC membranes were made at concentrations varying from 0.03, 0.59, 2.36 and 9.34 mM. The MPD concentration was held at 2.0 wt-% (185 mM). The concentration of TMC used to prepare commercial membranes is typically 2.36 mM. The air bubble contact angle measurements are displayed in Figure 19.1. Membranes made at a TMC concentration of 0.59 mM had the lowest contact angle. Therefore, they can be considered to be the least hydrophobic (or most hydrophilic). Membranes made at a TMC concentration of 2.36 mM were slightly more hydrophobic followed by 9.34 mM TMC membranes and the 0.30 mM TMC membrane. Overall, these differences in contact angle do not appear to be significant.

19.1.3 Effect of TMC Concentration on Membrane Hydrophobicity

Membranes made for the MPD application study in Section 13.0 were analyzed by contact angle to determine surface hydrophobicity. Contact angle measurements for the

four CPTC membranes (CPTC-AC Lot No. 030399S1) and the TMC controls are shown in Figure 19.2. There was no real trend with respect to surface hydrophobicity among the brushed samples and between the CPTC acid and TMC membranes.
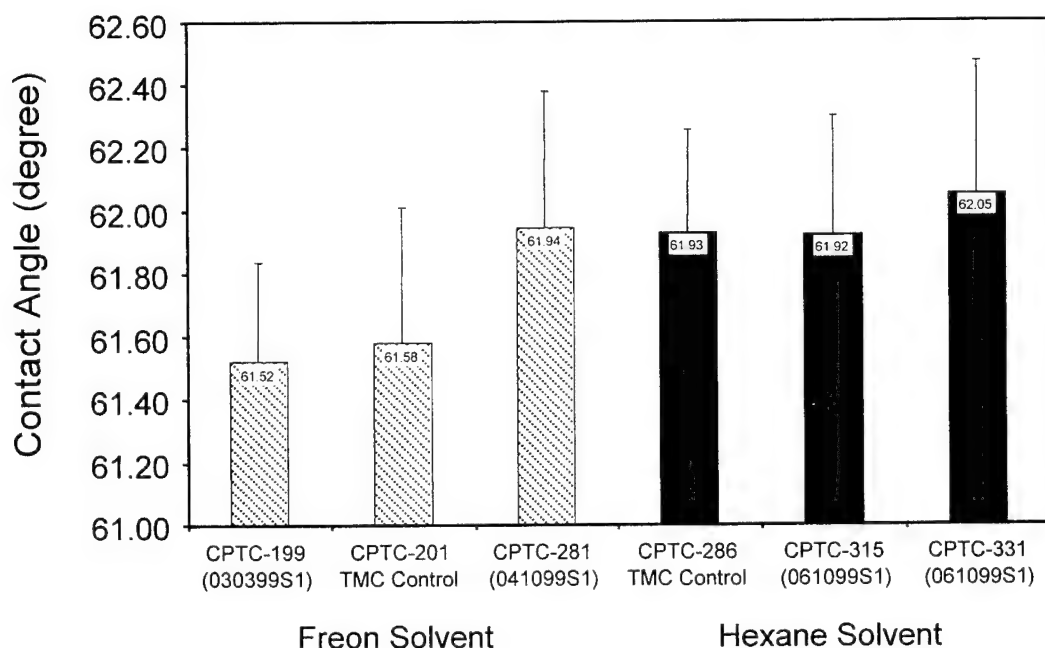

Figure 19.0 CPTC and TMC membrane surface hydrophobicity as determined by captive air bubble contact angle. (CPTC Lot number in parenthesis.)
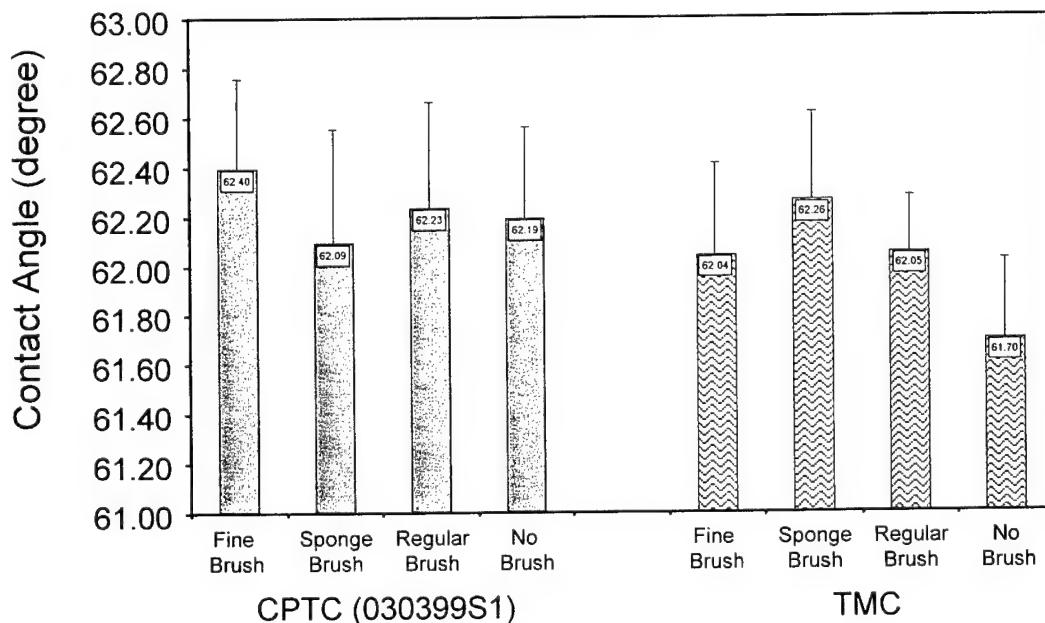

Figure 19.1 Effect of MPD application on CPTC and TMC membrane surface hydrophobicity as determined by captive air bubble contact angle.
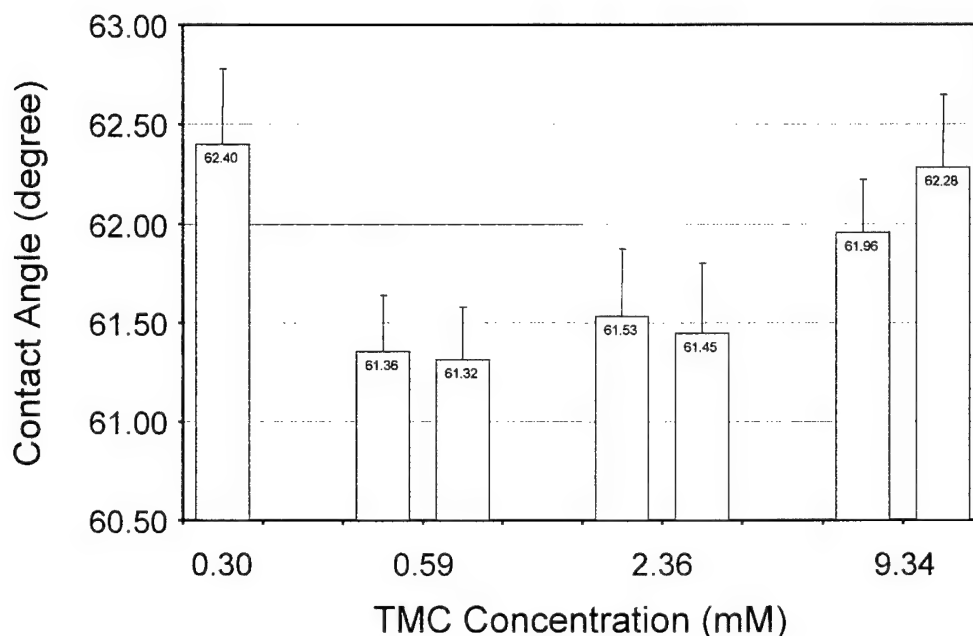
Figure 19.2 Effect of TMC concentration on TMC membrane surface hydrophobicity
as determined by captive air bubble contact angle.

19.1.4 Surface Hydrophobicity of CPTC Membrane from CPTC-AC Lot No. 102600

Captive air bubble contact angle measurements on membrane made from
CPTC-AC Lot No. 102600 are displayed in Figure 19.3. Three different membrane
preparations were analyzed. All had similar measures of contact angle.

19.1.5 Effect of Long-Term Storage on Membrane Hydrophobicity

Captive air bubble contact angle measurements on membranes made from 99+%
CPTC-AC Lot No. 021599S1 and CPTC-AC Lot No. 021799S1 were monitored over a
3-month period. The three included one made from CPTC-AC Lot No. 021799S1 and
two others made from CPTC-AC Lot No. 021599S1. The CPTC acid chloride from
CPTC-AC Lot No. 021799S1 was purified only by selective extraction. The acid chloride
from CPTC-AC Lot No. 021599S1 was purified by SE and processed by FF to remove
phosphorous. The effect of long-term contact with water on the surface hydrophobicity
was investigated. Air bubble contact angle measurements were made on all three
membranes. The membranes were then stored in DI water at 4°C until the next
measurement was made. Plots of the initial contact angle and measurements after
1- and 3-months storage in water are displayed in Figure 19.4. The contact angle
dropped with time, indicating a decrease in the membrane's surface hydrophobicity, or
that the membranes became more hydrophilic. These results suggest that the
membranes become more hydrated with time as none of these membranes were
operated in RO prior to analysis. All membranes were in a dry state prior to the initial
analysis by captive bubble contact angle.

270

Figure 19.3 Captive air bubble contact angle measurements of three CPTC membrane samples (CPTC-AC Lot No. 102600) as compared to the three reference materials, glass, FilmTec, cellulose acetate and PMMA.
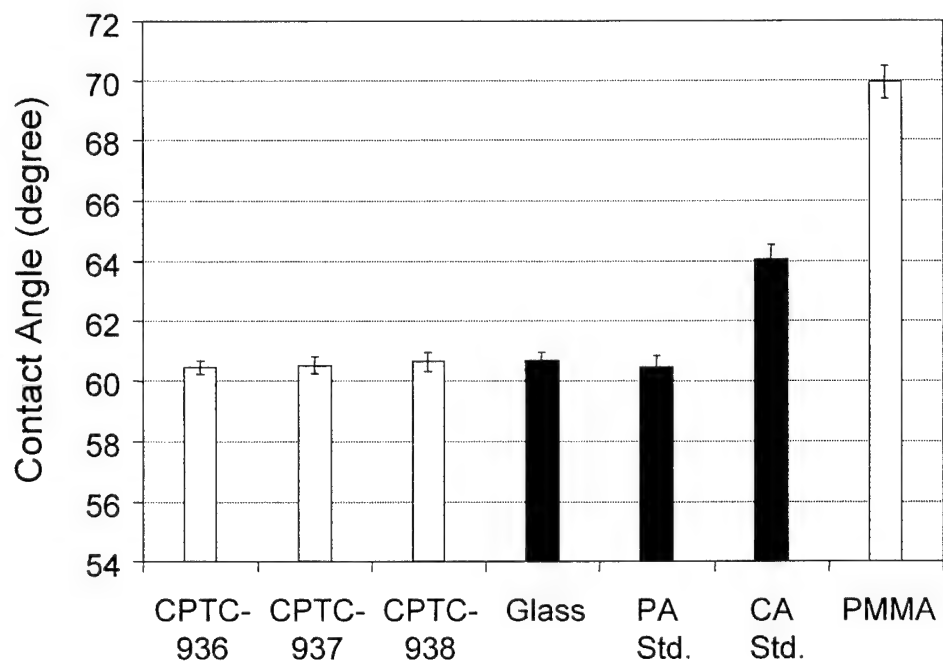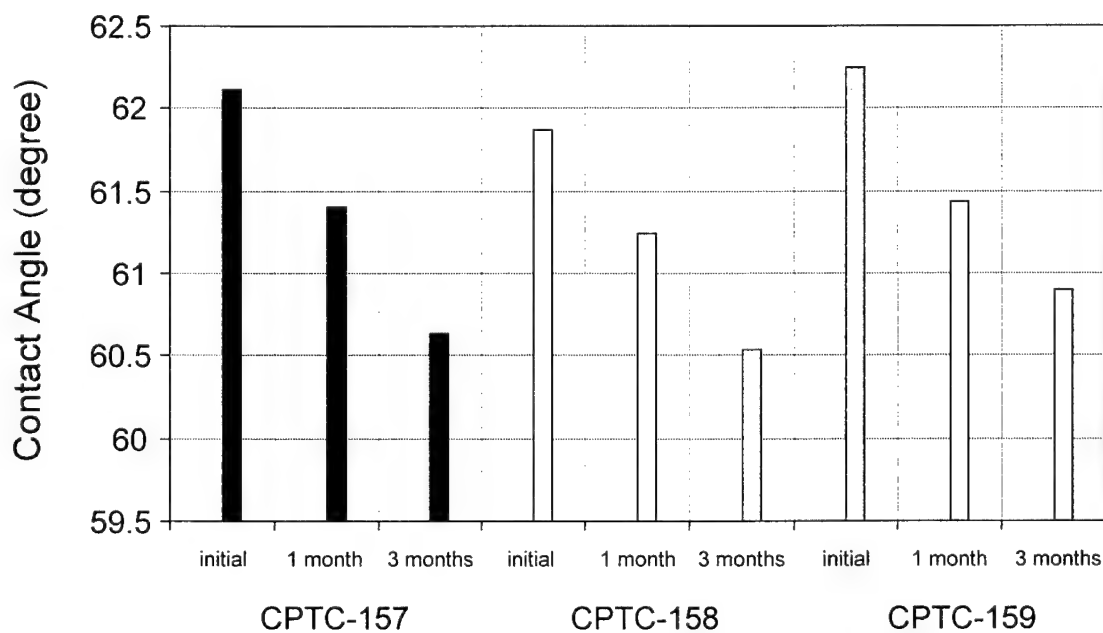

Figure 19.4 Effect of long-term storage on membrane surface hydrophobicity as determined by captive air bubble contact angle.

19.2 Membrane Surface Charge - UCB

Membranes made from each Lot of CPTC-AC were analyzed to determine negative surface charge by the UCB assay. CPTC membranes made from CPTC-AC Lot Nos. 041299, 061099, 110899 and 102600 were tested as they were made available during the study. FilmTec, CA and TMC membranes served as controls. In some cases, both new and old FilmTec membranes were tested. FilmTec recently changed the manufacturing process of their membrane to make it less fouling. Later the old FilmTec membrane was dropped from the study because the supply on hand had become unreliable due to perceived deterioration.

Results from the UCB studies are shown in Figures 19.5 through 19.9. Experimental conditions related to the preparation of the uranyl acetate solution varied slightly from experiment to experiment throughout the study. Therefore the magnitude of UCB was not always the same for the controls (FilmTec and CA) membranes. However the relative degree of binding (or negative charge) did remain the same for the membranes from experiment to experiment. The data from all five experiments was normalized based on cation binding to the CA membrane. DPM counts from each test membrane were divided by the counts of the CA control membrane in each experiment. The results from this normalization process are shown in Figure 19.10.

Analysis of the control membranes revealed that the new FilmTec membrane is more negatively charged than the CA membrane. All five plots show greater UCB at the surface of the new membrane over the CA membrane. The old FilmTec membrane had the lowest negative charge of the three control membranes. CPTC membrane made from CPTC-AC Lot No. 041299 had the lowest relative surface charge of the five membranes of different lot purities (Figure 19.6) CPTC membrane made from CPTC-AC Lot No. 061099 had the highest negative surface charge. Membrane made from CPTC-AC Lot No. 092099 and 110899 had a surface charge similar to the new FilmTec membrane. Membrane made from the last and purest batch of CPTC-AC had a surface charge more negative than the new FilmTec membrane.

19.3 Membrane Biofouling Potential - MBP

Only three of the CPTC membranes made from CPTC-AC Lot. Nos. 041299, 061099 and 102600 were tested to determine their biological fouling potential. All three CPTC membranes fouled to a greater extent than the FilmTec membrane, which is considered the industry standard (Figures 19.11, 19.12 and 19.13). CPTC membrane made from CPTC-AC Lot No. 061099 fouled more heavily with *Flavobacterium* PA-6, the hydrophylic bacterium, than with *Mycobacterium* BT12-100, the hydrophobic bacterium. Otherwise, all the membranes, including the controls, fouled more heavily with *Mycobacterium* BT12-100 than with *Flavobacterium* PA-6.

272
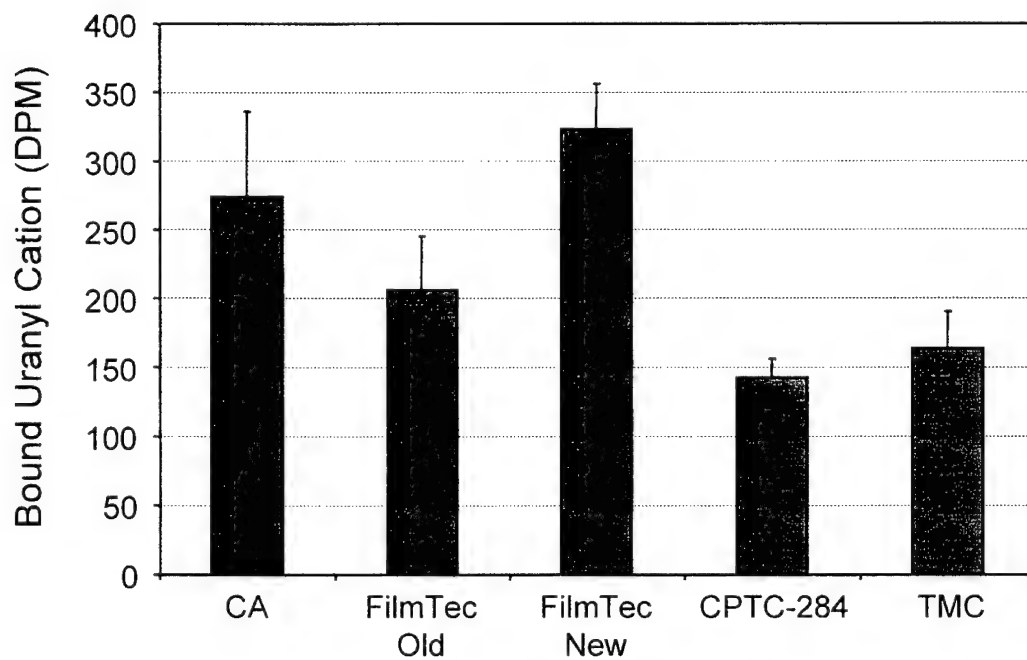
Figure 19.5 Uranyl acetate binding to CPTC membrane CPTC-AC Lot No. 041299.
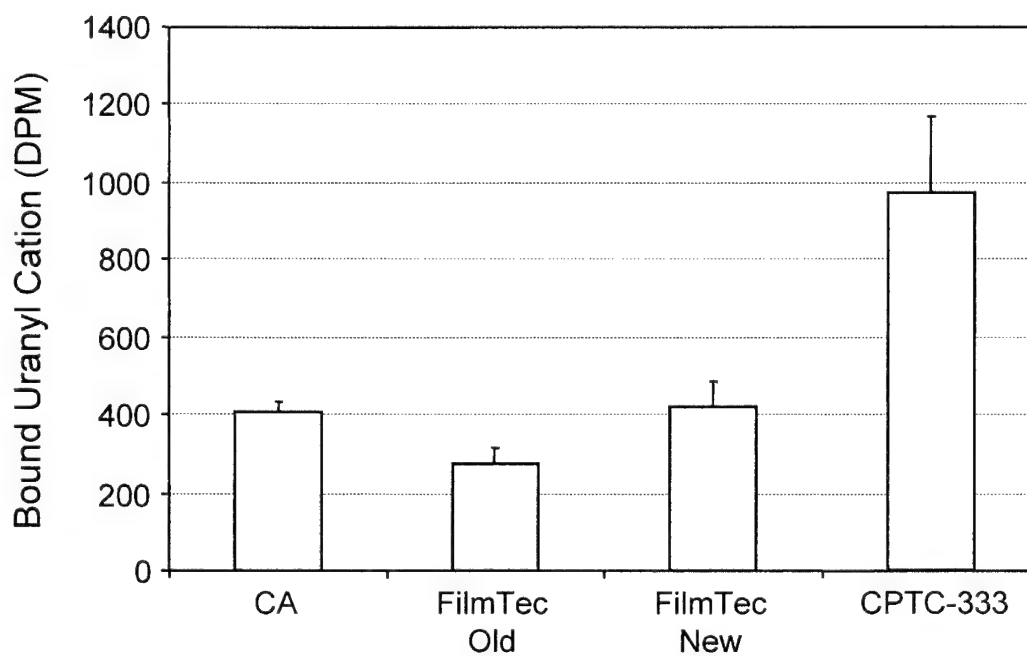
Figure 19.6 Uranyl acetate binding to CPTC membrane CPTC-AC Lot No. 061099.
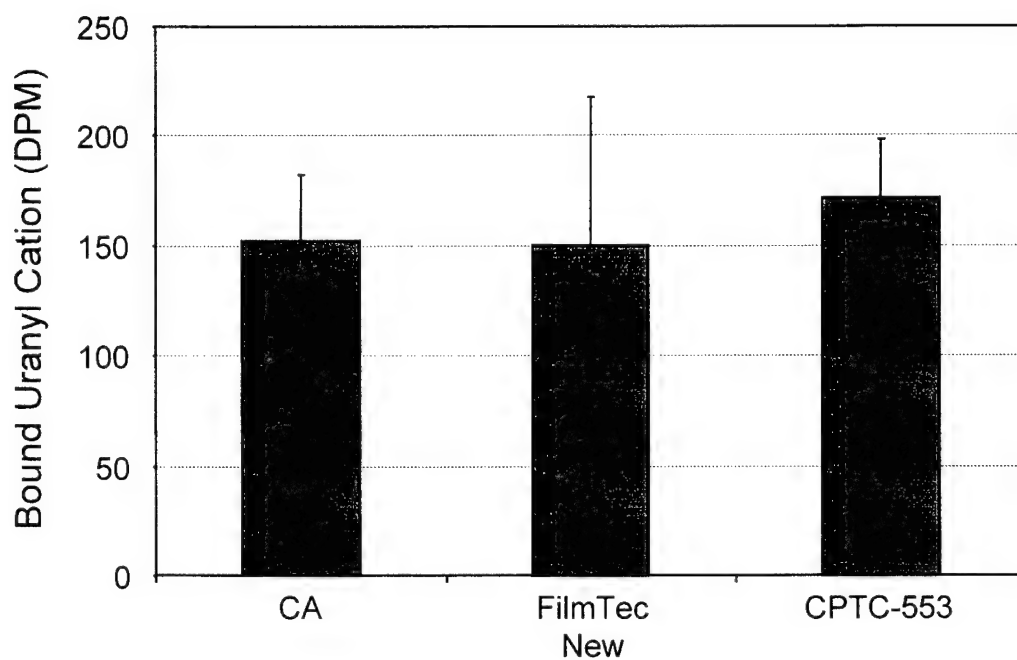
Figure 19.7   Uranyl acetate binding to CPTC membrane prepared from CPTC-AC
Lot No. 092099.
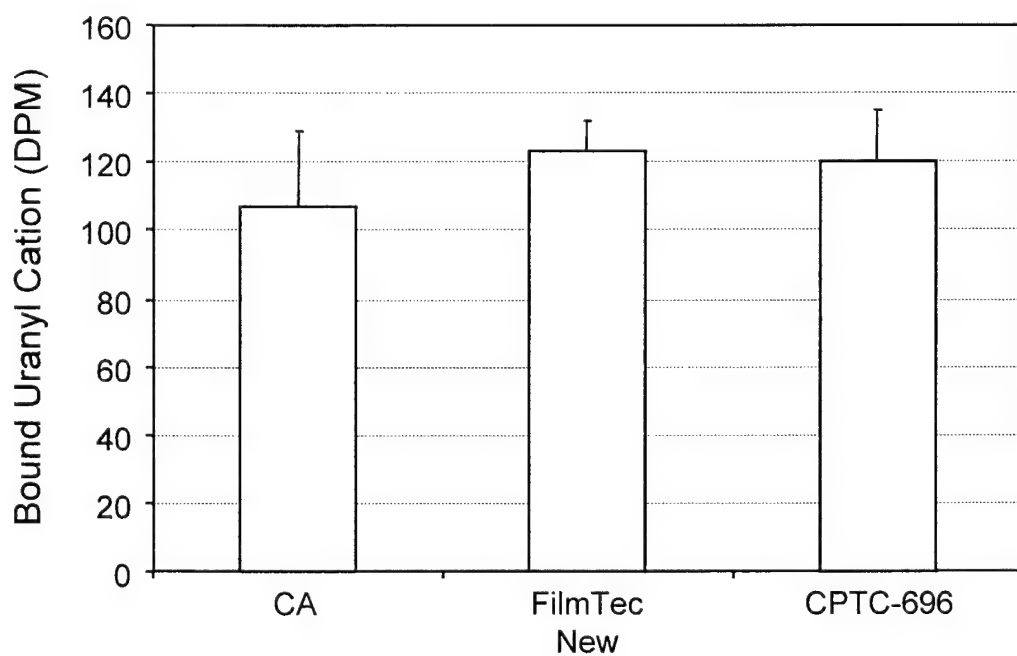
Figure 19.8   Uranyl acetate binding to CPTC membrane prepared from CPTC-AC
Lot No. 110899.
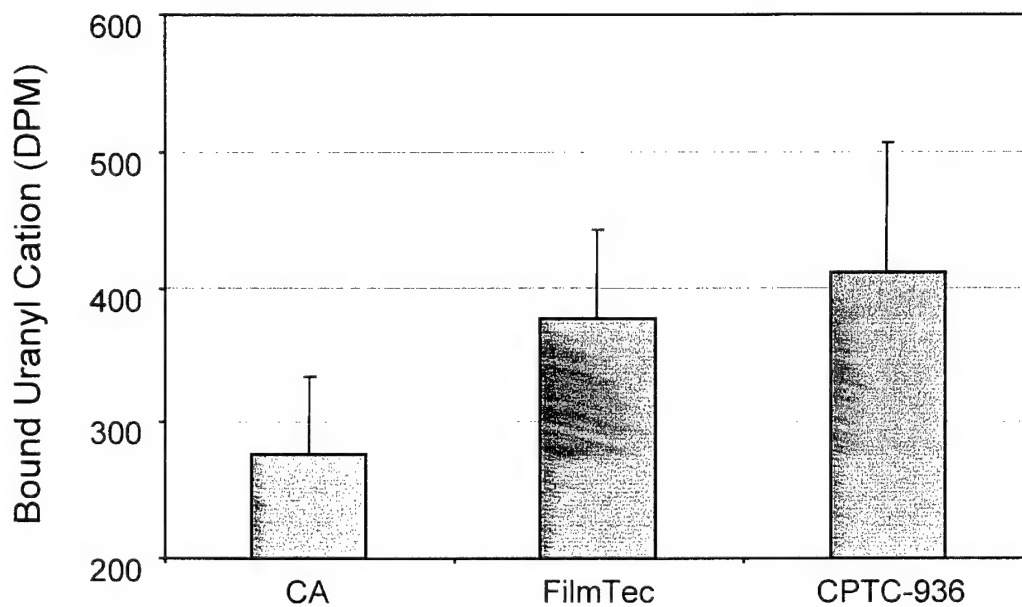
Figure 19.9   Uranyl acetate binding to CPTC membrane prepared from CPTC-AC Lot No. 102600.
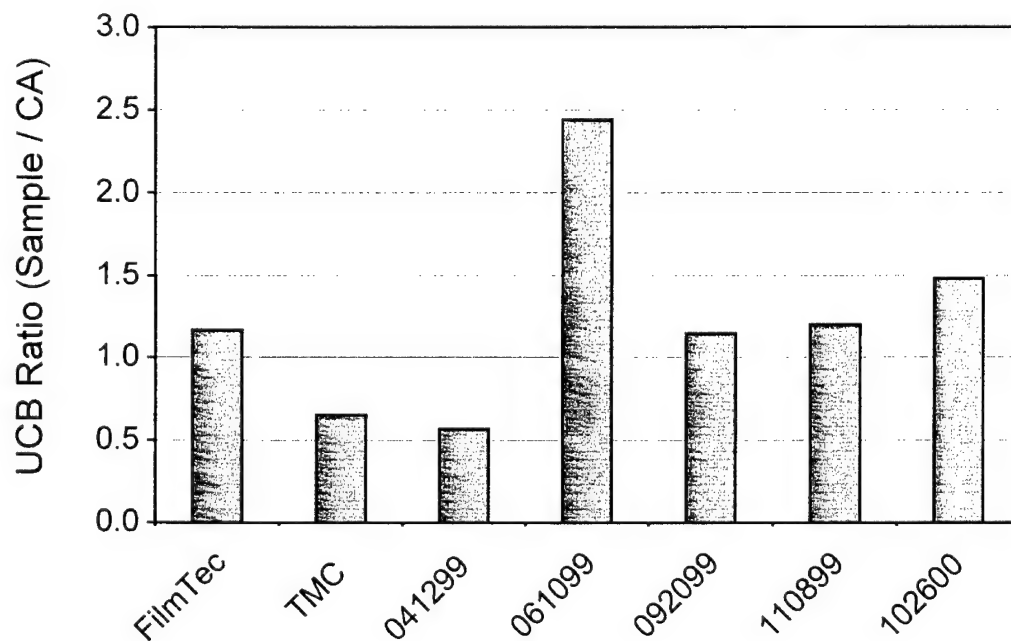
Figure 19.10 Normalized uranyl cation binding data based on uranyl acetate binding to the standard cellulose acetate membrane. CPTC Lot No. displayed at bottom of plot.
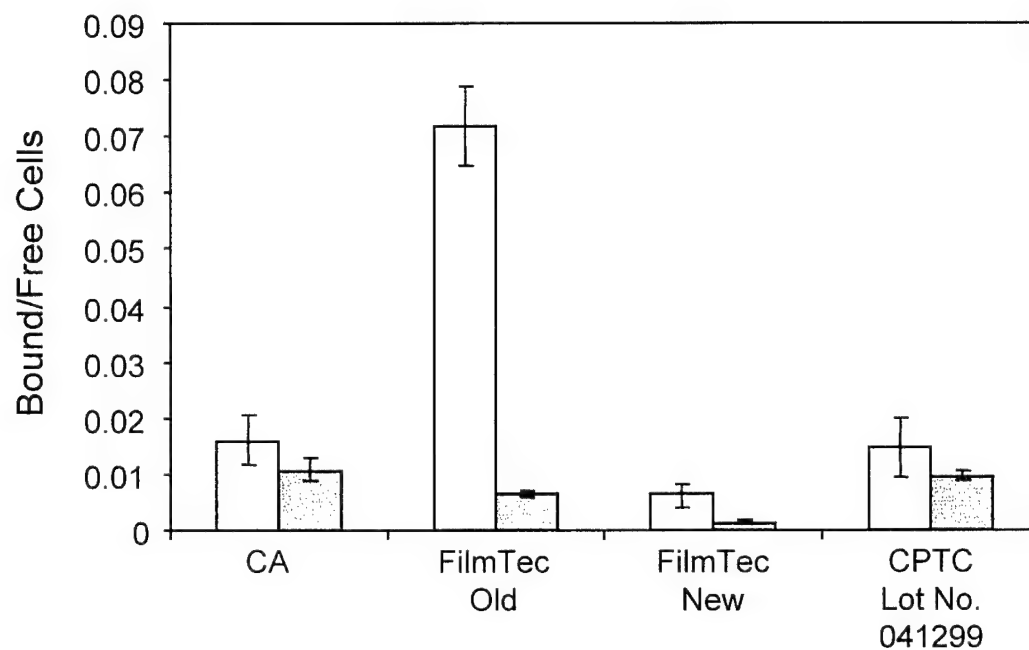
Figure 19.11 Bacterial adhesion on the surface of RO membranes, *Mycobacterium* BT12-100 (□) and *Flavobacterium* PA-6 (▩).
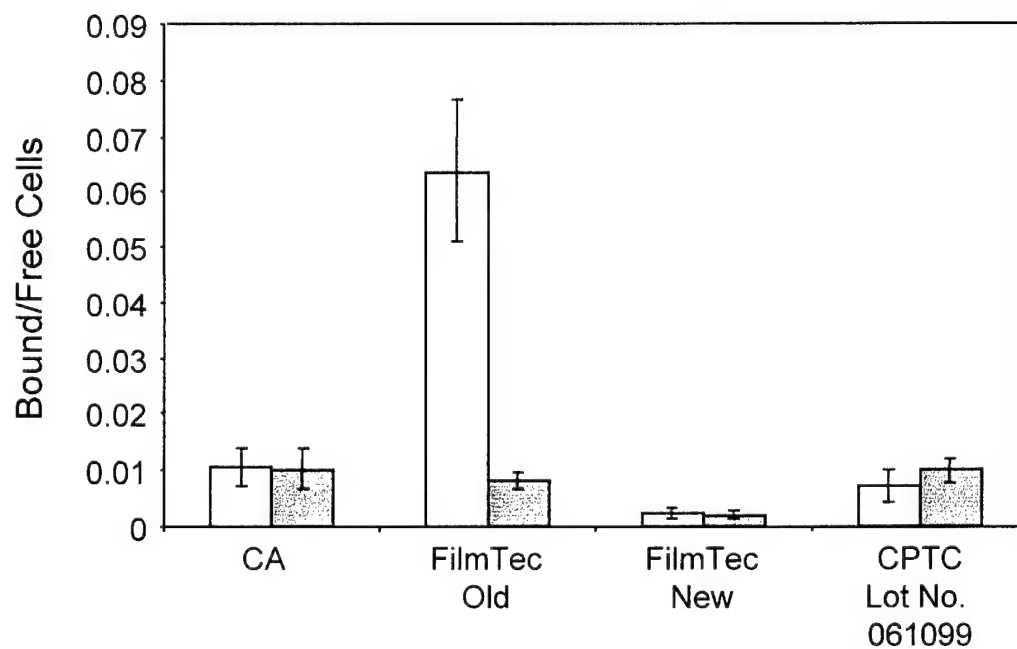
Figure 19.12 Bacterial adhesion on the surface of RO membranes, *Mycobacterium* BT12-100 (□) and *Flavobacterium* PA-6 (▩).
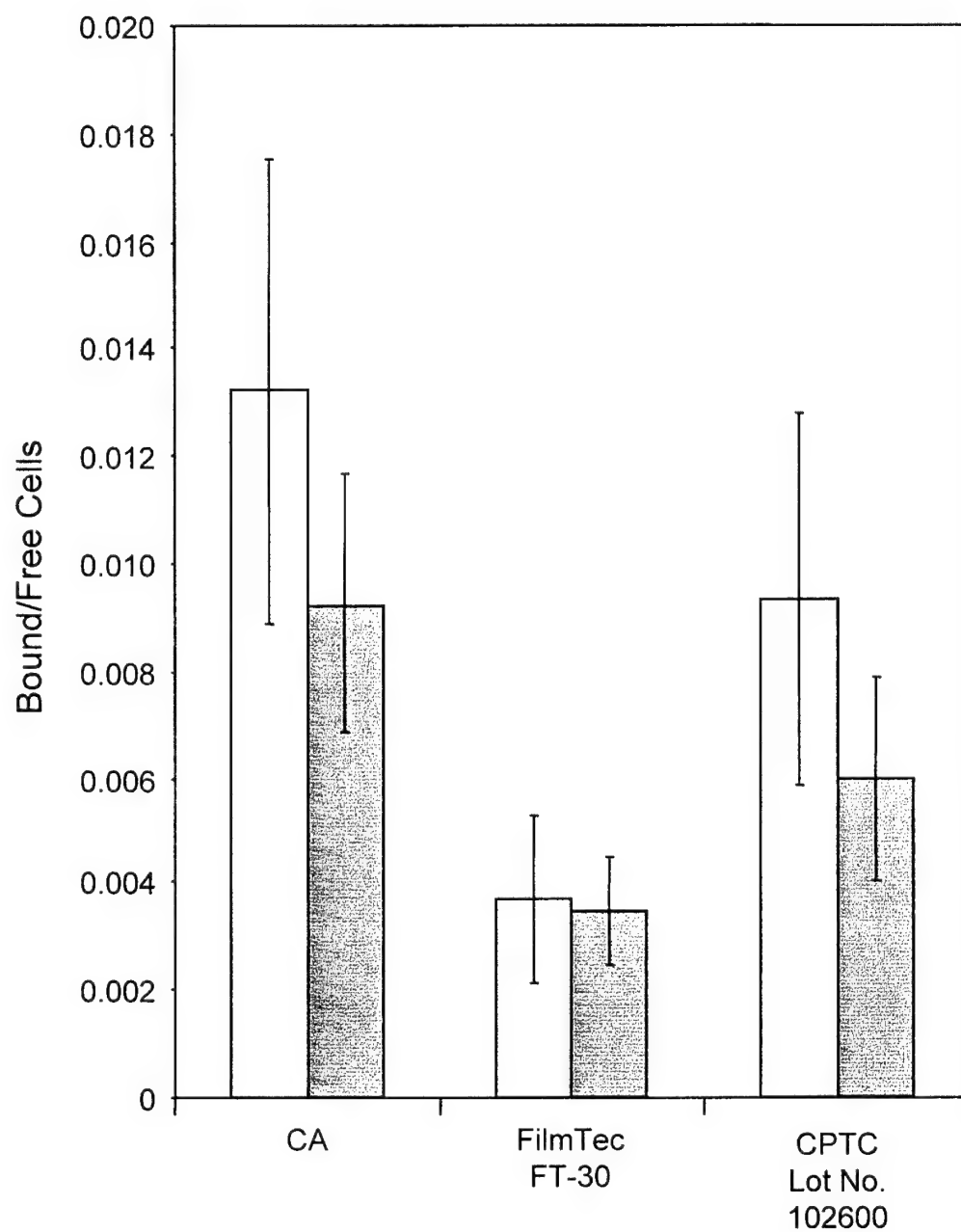
Figure 19.13 Bacterial adhesion on the surface of RO membranes, *Mycobacterium* BT12-100 (□) and *Flavobacterium* PA-6 (▦).

20.0 ^{15}N-LABELED MPD MECHANISM STUDY OF MEMBRANE CHLORINATION

An understanding of the mechanism of oxidative damage to membranes by the addition of chlorine to water supplies may lead to advances on how to build superior oxidation-resistant membranes. Mechanism studies have to be anchored properly in the applied world less they continue ad infinitum. To arrive at an understanding of what is occurring during oxidation, the approach was to use a stable isotope of nitrogen, ^{15}N, on the amine molecule and cast a membrane that would then be isotopically enriched. By using this stable isotope, solid state NMR signals can be greatly enhanced on the membrane, producing data on the nitrogen environment where, it seems likely, much of the chemistry is taking place.

20.1 Synthesis of ^{15}N-Labeled MPD

The procedure adopted for this synthesis was based on the methods cited in the literature.[19,20] Due to the high cost of the ^{15}N-labeled precursors, the literature procedures were first evaluated by carrying out each step of the synthesis using non-labeled compounds for product yield and purity. If necessary, the procedures were then modified to achieve maximum yield and purity. The synthesis of the labeled MPD involves two steps starting with ^{15}N-labeled nitrobenzene. First the labeled nitrobenzene was nitrated to produce the 1,3-dinitrobenzene and then the nitro groups were reduced to amino groups to produce the labeled MPD.

20.1.1 Synthesis of ^{15}N-Labeled 1,3-Dinitrobenzene

This step in the synthesis was relatively simple and did not pose a problem. A 100 mL round bottom flask equipped with a reflux condenser and a stirrer was charged with 14 mL of concentrated sulfuric acid and cooled in an ice bath. To this was slowly added 10 mL of fuming nitric acid while stirring. The mixture was taken off the ice bath and 10 g of ^{15}N-labeled nitrobenzene was added in small portions over a period of 15 min. The stirred reaction mixture was then heated and maintained at 100°C for 30 min. The reaction mixture was allowed to cool to room temperature and then poured into a beaker containing 400 mL of crushed ice and stirred to yield a yellow solid. The solids were isolated by vacuum filtration and washed with water until the filtrate was colorless. The crude product (12.5 g) was air dried and recrystallized from methanol to yield 10.5 g of 1,3-dinitrobenzene (77% yield). The purity of the product was confirmed by ^{1}H and ^{13}C NMR and final melting point.

20.1.2 Synthesis of ^{15}N-Labeled MPD

This second step of the synthesis was not as straight forward as described in the literature. Various reduction methods including titanium tetrachloride,[21] zinc hydrochloric acid, sodium borohydride with palladium on carbon and catalytic hydrogenation were tried. Although these methods yielded the expected reduction product, the purity and yields were far from acceptable. All these reactions produced blackish or deeply colored oil and did not yield to traditional purification methods. Among the procedures

278

investigated, the catalytic hydrogenation method was found to be the most acceptable and was used in the reduction of the dinitrobenzene prepared above.

A Parr hydrogenation bottle was charged with 50 mL of methanol and purged with nitrogen and then 50 mg of 10% palladium on carbon was added. During purging of the suspension, 10.5 g of the ^{15}N-labeled 1,3-dinitrobenzene was added in small portions. The mixture was then placed in a Parr hydrogenation apparatus and hydrogenated at 40 psi overnight (or until no noticeable hydrogen uptake). The reaction mixture was then filtered through a bed of Celite to remove the catalyst and then rotary evaporated. The resulting oil was dissolved in 100 mL of methanol and boiled with activated carbon for about 1 hr and filtered through a bed of Celite. The filtrate was stripped off the solvent at reduced pressure and stored in the freezer to crystallize.

20.2 Membrane Preparation and RO Performance

A direct osmosis (DO) cell (see Figure 20.0) was constructed in Denver and shipped to SST. The osmotic driving force is the difference in concentration between the sodium chloride solution on one side and fresh water on the other. This cell made it possible to test a large enough membrane samples (6 in. diameter) so that at the end of the test the PA film could be "floated" off by dissolving the PS backing with sufficient sample for solid state NMR analysis.

Two ^{15}N-labeled PA membranes were made with different acid chlorides. TMC and CPTC acid chloride were also included in the testing. Each of these membranes was divided into two, one a control in which only sodium chloride solution was used, the other a test in which chlorine was added to the sodium chloride solution side.

20.3 Chlorination of Membranes

Because the sodium chloride (even ACS grade) contains trace concentrations of bromide ions, the chlorine added will produce bromine species. Rather than attempt to remove bromine from the experiment, which would not be an easy task, and knowing that the "real world" application of chlorine to seawater and other water supplies will result in bromine species, the decision was to continue and study the fate of both chlorine and bromine on the desalting membranes (see Section 17.0).

20.4 Summary

Solid state NMR data collection on the synthesized membranes for the isotopes ^{15}N, ^{13}C, ^{79}Br are underway. The interpretation of this data will result in valuable information that will make possible a more complete understanding of the mechanism(s) of membrane chlorination.
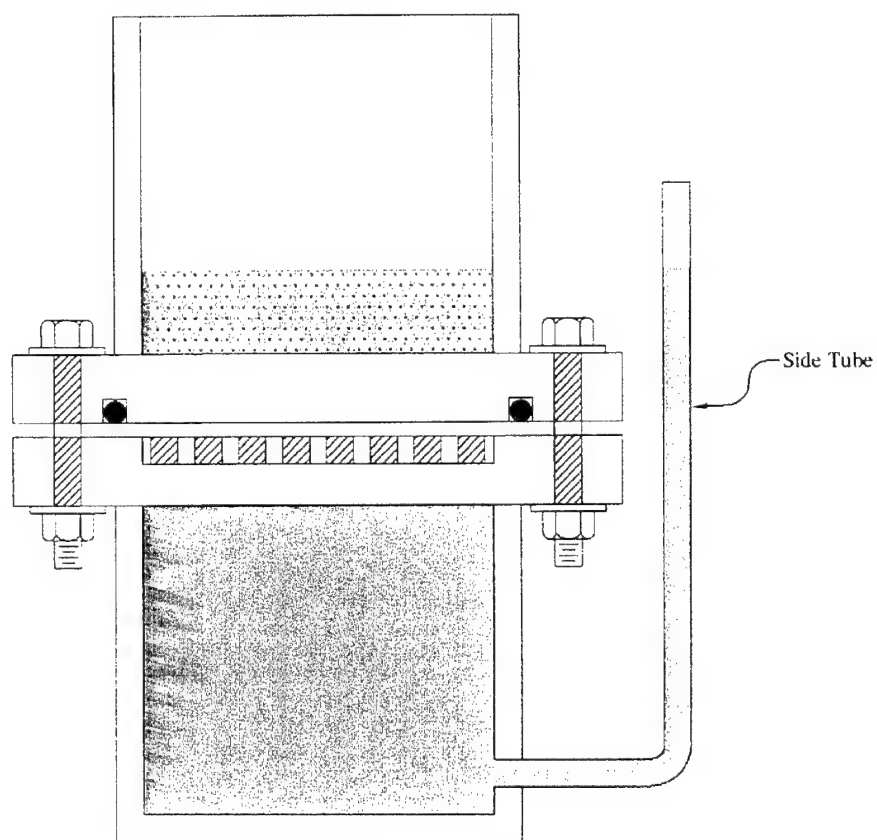
Side Tube

Figure 20.0   Diffusion cell for chlorination studies

21.0 LONG-TERM FIELD TESTING OF MEMBRANES AT THE WATER QUALITY IMPROVEMENT CENTER, YUMA, AZ ON CHLORINATED BRACKISH WATER FEEDS

Field testing of CPTC membranes at the WQIC was initiated early in the program with two test cell units (TCUs), each operating on a different feedwater. Initially, each TCU operated with three PVC test cells connected in series, with a membrane area of 19.4 cm^2/cell. After several months, the test cells were upgraded, and the number of cells was increased to nine in each TCU. TCU-1 operated on a clearwell feed with a feed conductivity of ~3,800 µS/cm and TCU-2 operated on a potable water feed with a feed conductivity ranging from ~350 - 1,000 µS/cm. In addition, an acid injection-pH control system was installed so that both systems could be pH controlled. A 5-mg/L EDTA concentration was maintained in the feedstream to prevent iron fouling.

Each of the TCU operates with three test cell sets, such that each set can be isolated to allow membrane replacement without shutting down the entire train. TCU-1 operates in a single-pass mode with a reservoir located ahead of the test cell train to allow switching to a recirculation mode if a shutdown is planned. TCU-2 operates in a similar fashion except in a partial recycle mode, where fresh feedwater is added as the overflow goes to drain.

Shutdowns were more frequent than anticipated at WQIC. Both test cell units were shut down for three months to accommodate a research group from Los Alamos National Laboratory who had established a CRADA with WQIC, thereby establishing precedence over SST. To avoid further interruptions, SST established a CRADA with WQIC. This CRADA assured future testing through December 31, 2000, although it later was extended through July 2001.

21.1 Water Sources

Operating on two WQIC water sources made it possible to evaluate the effects of different pH, varying chlorine levels and different feed compositions. The approximate compositions of the two waters were:

Test Unit	Water Source	TDS (mg/L)	pH	Cl_2 (mg/L)
TCU-1	PSI Clearwell	3,000	4.0	1.5
TCU-2	Potable water	350	8.0-8.5	0.5

21.2 Operating Pressures

Operating pressures were adjusted to maintain approximately equal and constant product water flow for each of the membrane samples. The product flow for each cell is approximately 1.0 mL/min or 18 gfd.

21.3 Membrane Locations

The initial and present test cell locations are shown in bold type.

Test Unit	Water Source	Test Cell Designation			Date Installed
TCU-1	PSI Clearwell	**1**	**2**	**3**	December 98
		4	**5**	**6**	April 99
		7	**8**	**9**	August 99
TCU-2	Potable water	**1**	**2**	**3**	December 98
		4	**5**	**6**	April 99
		7	**8**	**9**	August 99

21.4 Data Collecting and Reporting

The frequency of the manual data collection is 3 times per 24-hr shift. The raw data is telefaxed to SST daily where it is entered into an Excel spreadsheet, standardized, evaluated and plotted. Data collection includes: Pressure (kPa), Temperature (°C), pH, Free Chlorine (mg/L), Conductivity (µS/cm) and Permeate Flow (g/min).

21.5 Test Results

21.5.1 CPTC Membranes

At the time TCU-1 was shut down to accommodate the Los Alamos Research Laboratory testing, a successful long-term test was in progress. The system was operating with CPTC membranes prepared from CPTC-AC Lot. Nos. 021599 SE-FF and 021799 SE which were both determined to have an isomeric purity of approximately 98%. Also included in the test were control membranes made with TMC. Prior to shut-down, the membranes had accumulated 1760 hr (73 days) of continuous testing on the clearwell feed containing 1.5 mg/L free chlorine at a feed pH of 4.0 - 4.24. The performance of all the membranes, shown in Figure 21.0, showed no signs of deterioration.

When the membranes were placed back on line, after three months off line in the test cells, the performance of the CPTC membranes showed an abrupt loss in rejection. The TMC control, was not affected significantly, except an increase in flux was observed. Nevertheless, the performance of the CPTC membranes was very encouraging. Due to the abrupt loss of performance after shutdown, it appeared to be due to physical damage rather than chemical deterioration. In a parallel program it was shown by ATR/IR that the thin film of the CPTC membranes is somewhat thinner than that of the TMC control. In addition, the test system was operating at a low pH where the performance is less than optimal. In subsequent studies, both the thickness of the barrier film and the pH of the feed were increased to enhance membrane longevity.
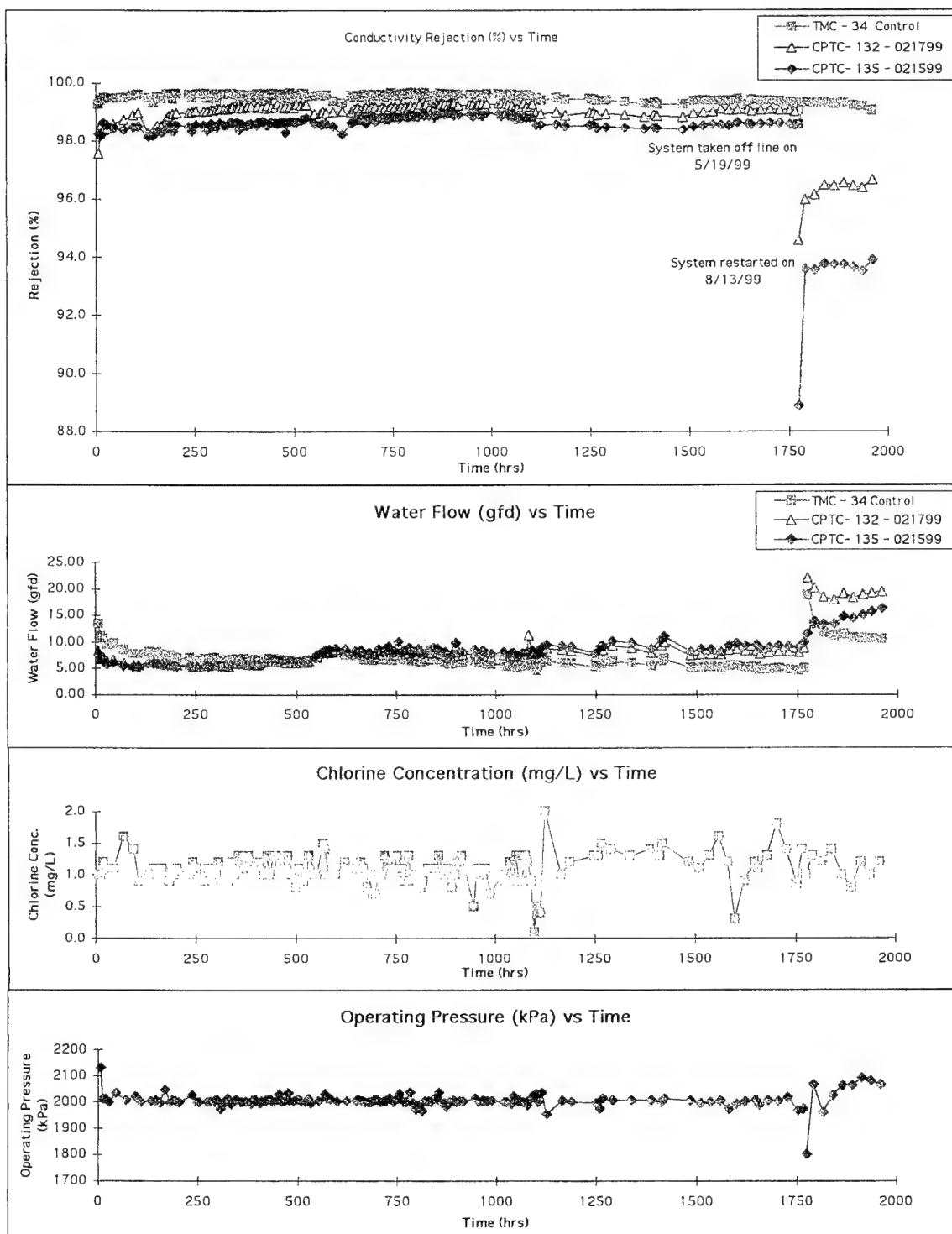
Figure 21.0   Performance of CPTC membranes in TCU-1 at WQIC.   Test Conditions:
Cells 1, 2, 3, clearwell feed, pH 4.0 - 4.25, 25°C.   (3/12/99 - 8/23/99).
System off line from 5/19/99 to 8/13/99.

283

The purity of CPTC-AC used to prepare these membranes was only 98%. The purity of the TMC used to prepare the control membranes, after double distillation, was ~99.9%. The synthesis of CPTC-AC ultimately progressed to the point where 99.9+% purity was obtained. However, variations between synthetic lots, as shown by membrane performance, still exist even at the higher CPTC-AC purity level. The need for very high purity CPTC-AC was apparent.

21.5.2 *cccc*-CPTC Acid Chloride Based Membranes

As with the *ctct*-CPTC-AC isomer described in Section 7.0, the *cccc*-CPTC-AC isomer was isolated from the mixture and purified to ~98% purity. The membranes prepared from the *cccc*-CPTC-AC (ITM-All Cis) were evaluated in two separate tests at WQIC. The performance of the SST-137 membranes, tested in TCU-2 with a 350 TDS feed, pH 8.0 - 8.5., 0.5 mg/L chlorine and 25°C, is shown in Figure 21.1. Figure 21.2 shows the performance of pre-chlorinated *cccc*-CPTC membranes tested in TCU-1 with a 3,800 TDS feed, pH 6.2-6.5, 1 mg/L chlorine and 25°C. It is quite apparent that the oxidation resistance of the *cccc*-CPTC SST 137 membrane is very much less than for the TMC -34 control membrane. After only 75 hr of operation, the salt passage increased to an unacceptable level. Furthermore, membranes made from the *cccc*-CPTC-AC are much more susceptible to chlorine damage at 0.5 mg/L chlorine than the *ctct*-CPTC-AC membranes (shown in Figure 21.0) and operated at 1.5 mg/L chlorine.

The need for isomeric purity of *ctct*-CPTC-AC becomes very apparent when the performance of the *cccc*-CPTC membranes are compared with the *ctct*-CPTC membranes. Even traces of other isomers in the *ctct*-CPTC-AC would be expected to be detrimental to long-term chlorine resistance. For this reason, the emphasis was focused on membranes prepared from 99.9% isomeric purity.
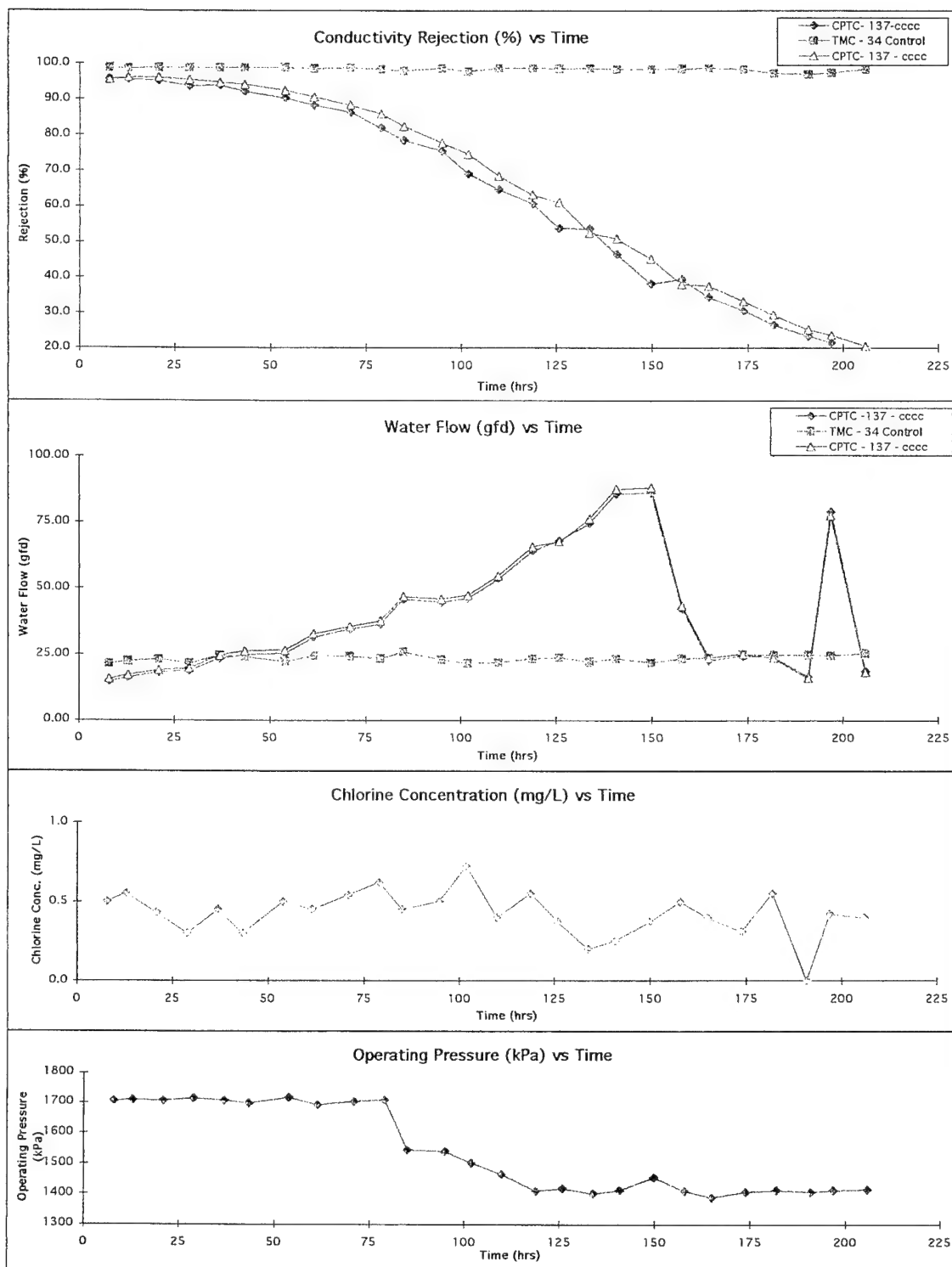
284

Figure 21.1 Performance of *cccc*-CPTC membranes in TCU-2 at WQIC. Test conditions: Cells 1, 2, 3, potable water feed, pH 8.0 - 8.5, 25°C. (3/12/99 through 3/18/99).
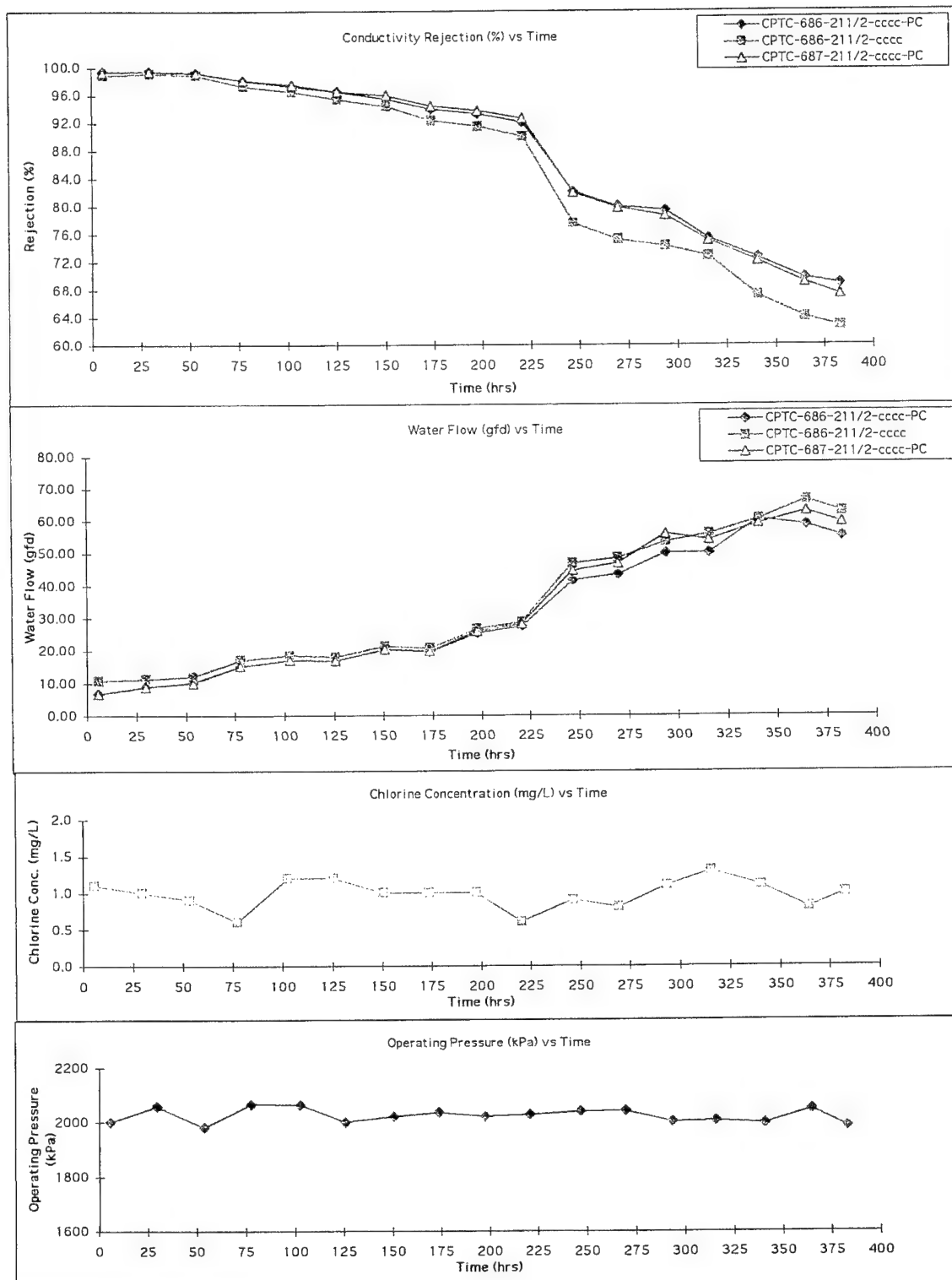
285

Figure 21.2 Performance of *cccc*-CPTC membranes in TCU-1 at WQIC. Test
conditions: Cells 1, 2, 3, clearwell feed, pH 6.2-6.5, 25°C.
(2/16 -3/3/99)

286

21.5.3 Test Cell Limitations - Recommendations

Long-term testing of membrane samples in the 1- x 3-in test cells at WQIC proved difficult due to the frequent shutdowns that occurred. An increase in salt transport was typically observed after shutdown. Subsequent dyeing of the membranes indicated that the membranes were physically damaged at the O-ring/membrane interface. The area of O-ring contact with the membrane is quite large relative to the area of the membrane surface in the test cells. Thus, damage to the membrane can be quite significant.

Figure 21.3 shows the effect of two shutdowns of CPTC membranes and a TMC control membrane after 70 and 226 hr of operation on a clearwell feed at pH 6.5. The first shutdown (after 70 hr) showed no effect on membrane performance, with the rejection of all three membrane samples remaining above 99.5%. After the second shutdown, the salt passage suddenly increased by a factor of two for the CPTC membranes and continued to increase steadily during the 1295-hr run. Although not reported on the raw data sheets received from the WQIC, it is strongly suspected that another shutdown occurred at 1020 hr, resulting in a sharp decrease in rejection, accompanied by a sharp increase in flux.

Figure 21.4 shows an interesting effect of the randomness that can occur during an unexpected shutdown. After nearly 1300 hr into this run, operating on a clearwell feed with no shutdowns, essentially no significant change in rejection was noted in the two identical CPTC membrane samples, remaining above 99.4%. During a period of unusually heavy rains in Yuma, flooding occurred in the clearwell channel, and the system shut down during this period. Upon restart, a significant loss in rejection had taken place in the CPTC samples, accompanied by a large increase in flux. Rejections of these samples decreased to 97.8 and 96.1%. The TMC membrane sample remained unaffected, except for a slight flux increase.

Over the next 1500 hr, the membrane performance remained essentially unchanged, with the exception of the lower rejecting CPTC membrane sample. This indicates that the O-ring damage was more severe for this sample than for the other CPTC sample.

Future tests should be conducted in an O-ring free environment, if reliable data is to be obtained. It is recommended that new membranes be incorporated into small 2.5- x 14-in. spiral elements for future chlorine resistance testing. In the spiral configuration, there is no contact on the surface of the membrane as all seals are made on the back side of the membrane.
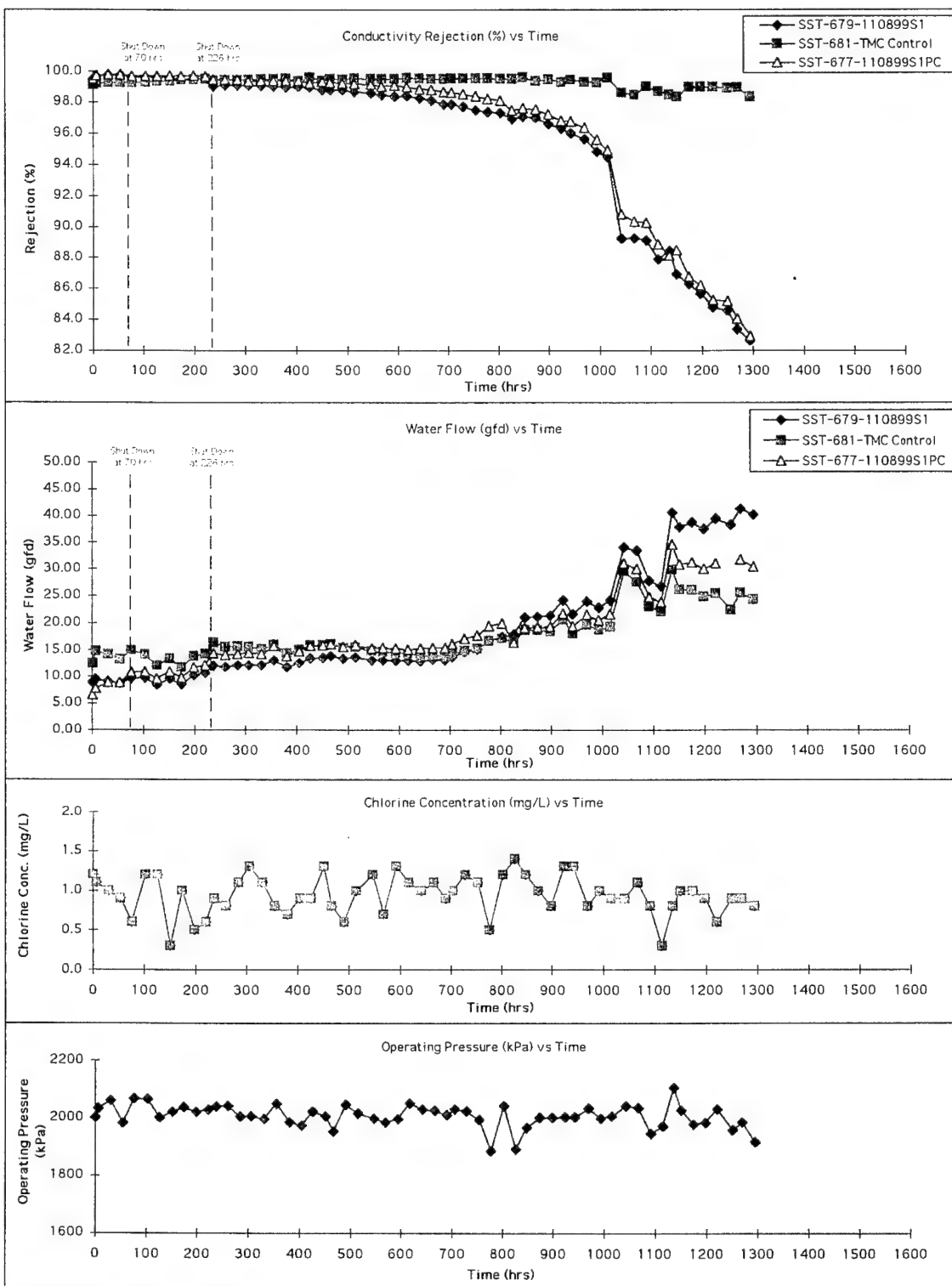
Figure 21.3 Performance of CPTC membranes in TCU-1 at WQIC. Test conditions:
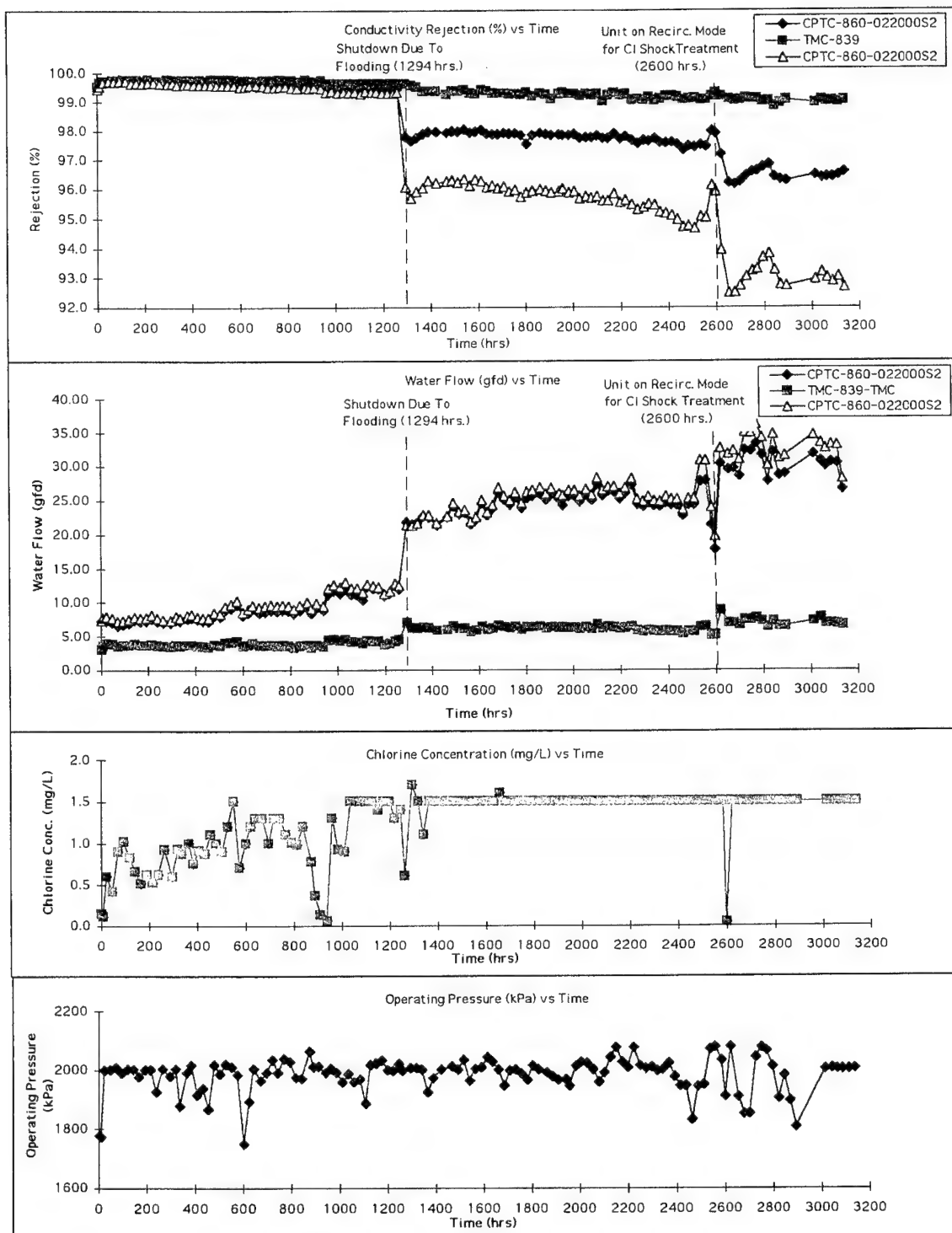Cells 1, 2, 3, clearwell feed, pH 6.5, 25°C (2/16 - 4/12/99)

288

Figure 21.4   Performance of CPTC membranes in TCU-1 at WQIC.   Test conditions:
Cells 1, 2, 3, clearwell feed, pH 6.5, 25°C (8/30/00 - 1/03/01)

289

21.6   ATR/IR Analysis of Membranes Operated at WQIC

Membrane samples operated a the Yuma Test Facility were analyzed by ATR/IR spectrometry to determine the chemical changes that resulted from operation on the brackish and potable feedwaters. A photograph of the 15 membrane samples are shown in Figure 21.5. Each membrane is identified in Table 12.0 below. Membrane samples from test cell units (TCU) 7,8 and 9 were not shipped to OCWD for analysis.

Table 21.0

RO Membranes Operated on Brackish and Potable Feedwates at WQIC

Test Cell Unit	Membrane Identification	Feedwater
TCU-1	CPTC-860-022000S2	Clearwell
TCU-2	TMC-839	Clearwell
TCU-3	CPTC-860-022000S2	Clearwell
TCU-4	CPTC-975-022000S2	Clearwell
TCU-5	FilmTec Brackish	Clearwell
TCU-6	CPTC-882-022000S2	Clearwell
TCU-11	CPTC-882-022000S2	Potable
TCU-12	FilmTec Brackish	Potable
TCU-13	CPTC-875-022000S2	Potable
TCU-14	CPTC-9007000823-0220002	Potable
TCU-15	TMC-906-7000823	Potable
TCU-16	CPTC-903-7000823-022000S2	Potable
TCU-17	CPTC-882-022000S2	Potable
TCU-18	TMC-839	Potable
TCU-19	CPTC-875-022000S2	Potable

21.6.1   Clearwell Feedwater

Nine membrane swatches were operated on the clearwell feed. Six were analyzed by ATR-IR spectrometry. IR spectra of the samples from the first six test cells are displayed in Figures 21.6 through 21.8 between 4000 cm^{-1} and 600 cm^{-1} 2000 cm^{-1} and 600 cm^{-1}. These membranes fouled at varyong levels. TMC-839 (Figure 21.6, middle spectrum) and CPTC-875-022000S2 (Figure 21.7, top spectrum) appeared to be fouled to the least extent. Membrane CPTC-860-022000S2) Figure 21.6, bottom spectrum) appeared to be the most heavily fouled of the six membranes operated on the clearwell feed. The fouling component, which has yet to be not identified, contributes heavily to the O-H stretching region near 3300 cm^{-1}. Neither IR spectra of the TMC or CPTC membrane contain a significant amount of O-H stretch. The other possibility is that the membrane chemistry itself has changed and an O-H group was formed. It is entirely

290

TCU1   TCU2   TCU3   TCU4   TCU5   TCU6

TCU11   TCU13   TCU15   TCU17   TCU19
    TCU12   TCU14   TCU16   TCU18
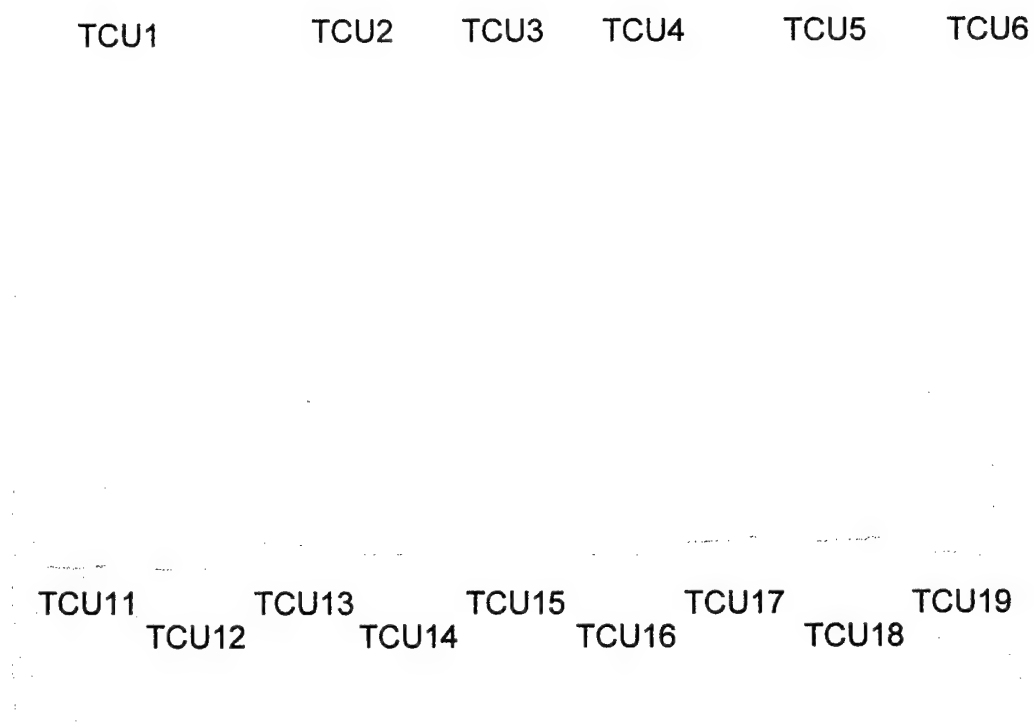
Figure 21.5   Samples of RO membrane operated on clearwell (top) and potable (bottom) feed waters at WQIC, Yuma, AZ.
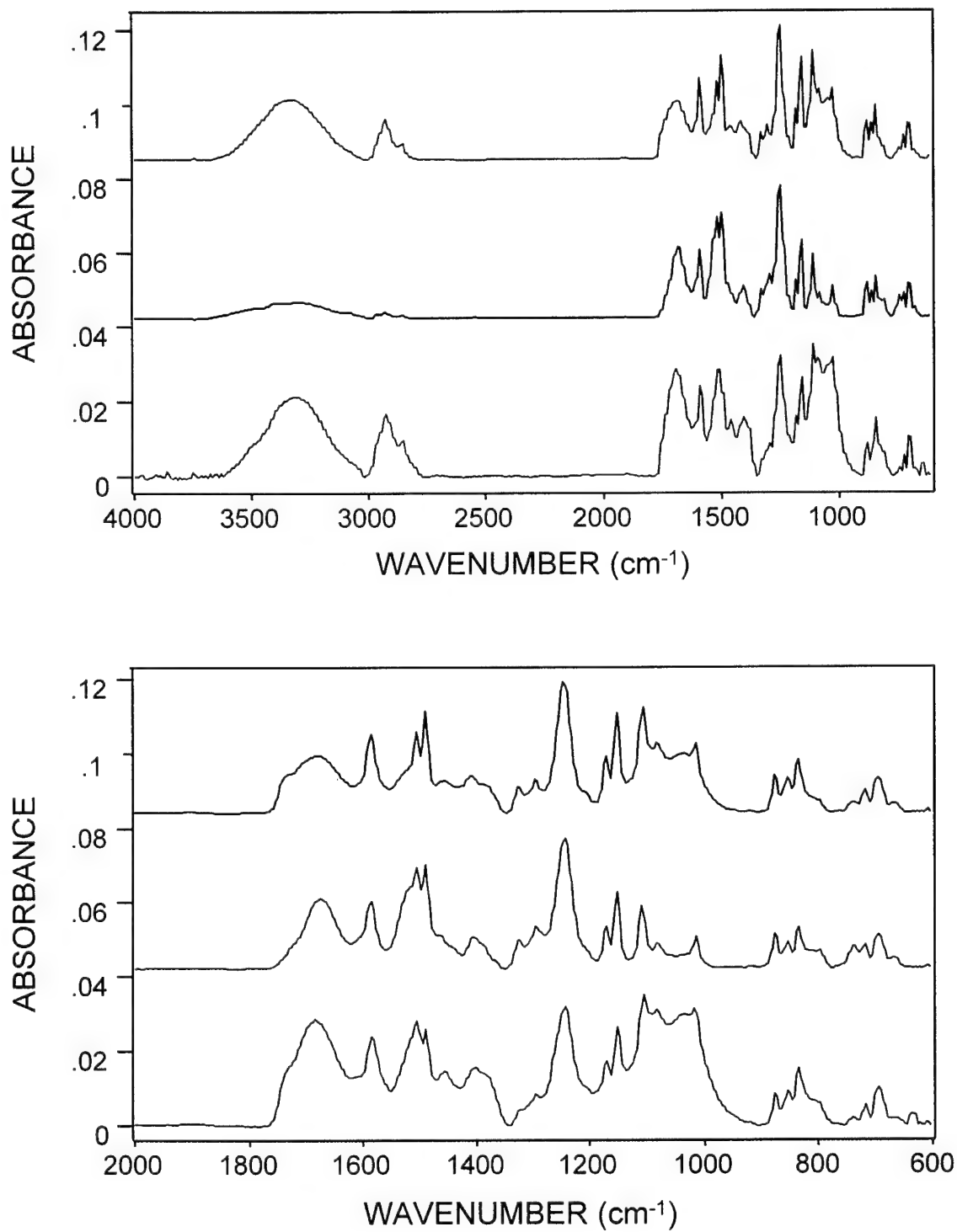
Figure 21.6 ATR-IR spectra of fouled CPTC-860-022000S2 (blue and green) and
TMC-839 (red) membranes operated on a clearwell feed at WQIC,
Yuma, AZ.

Figure 21.7   ATR-IR spectra of fouled CPTC-875-022000S2 (red), FilmTec (green) and CPTC-882-022000S2 (blue) membranes operated on a clearwell feed at WQIC, Yuma, AZ.
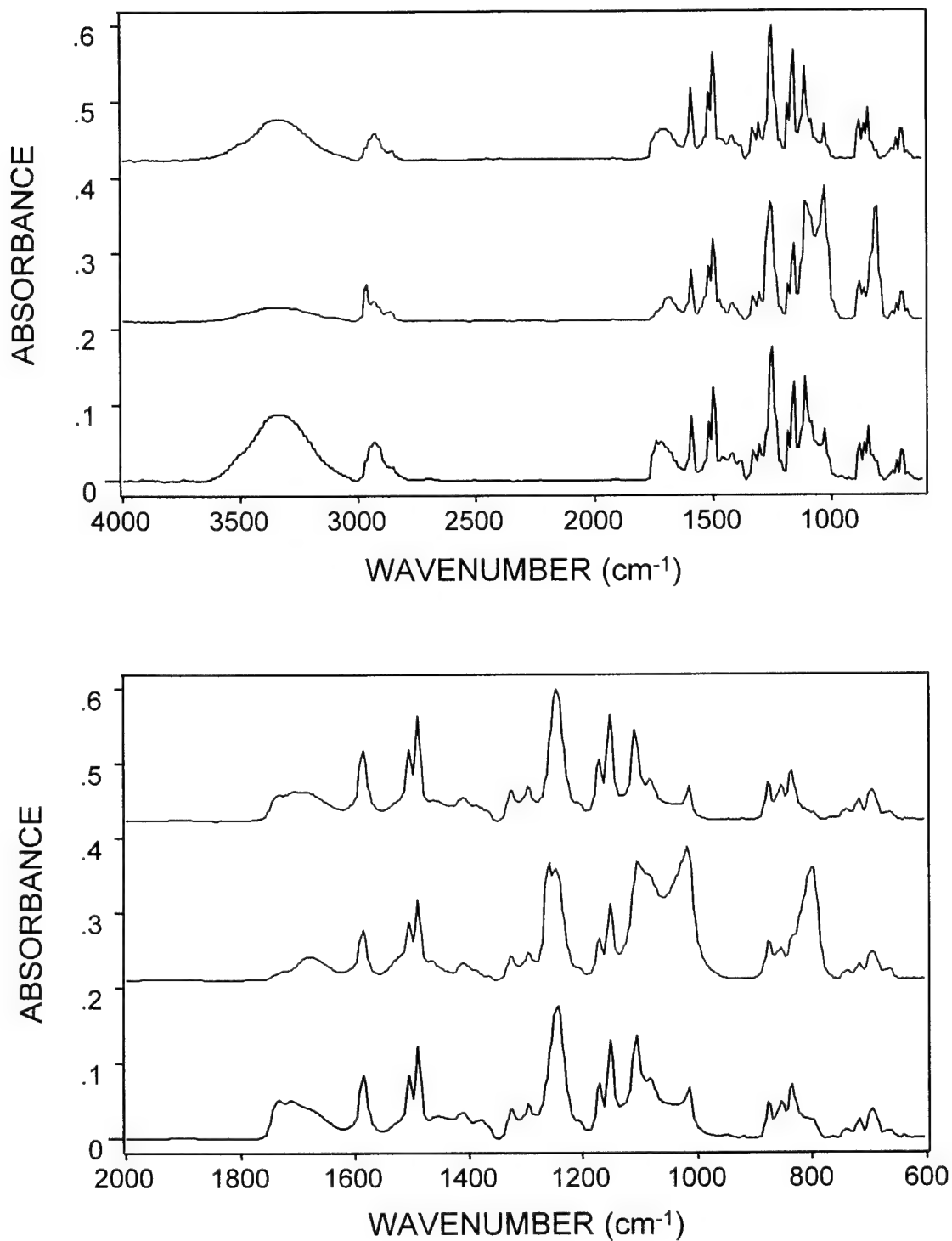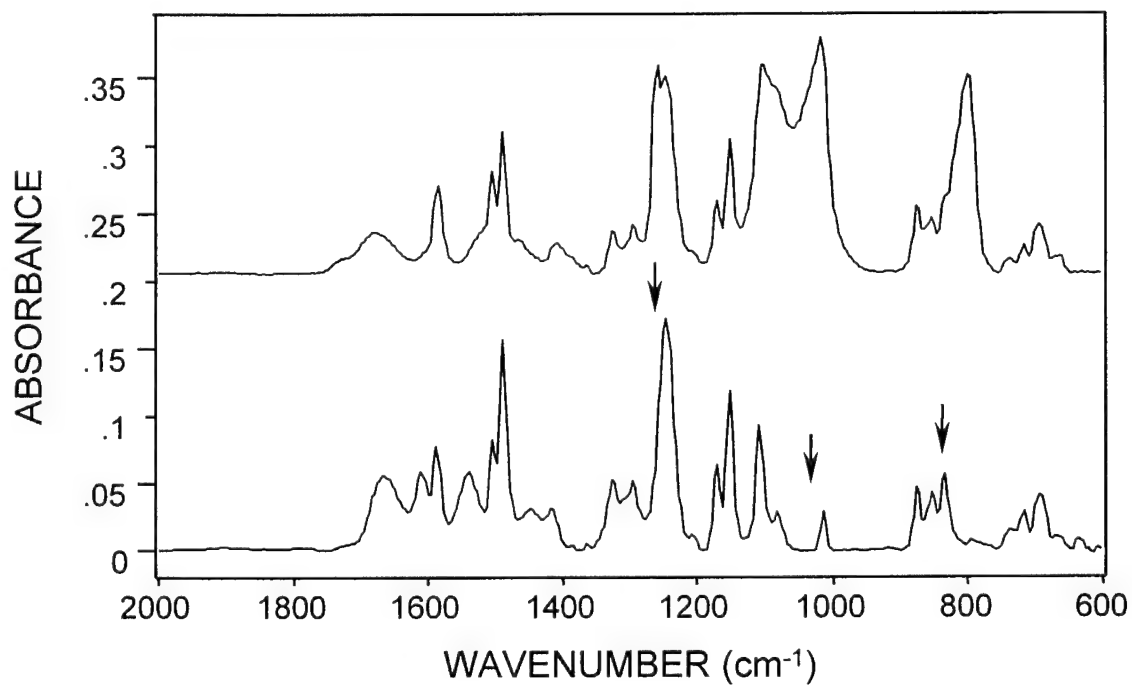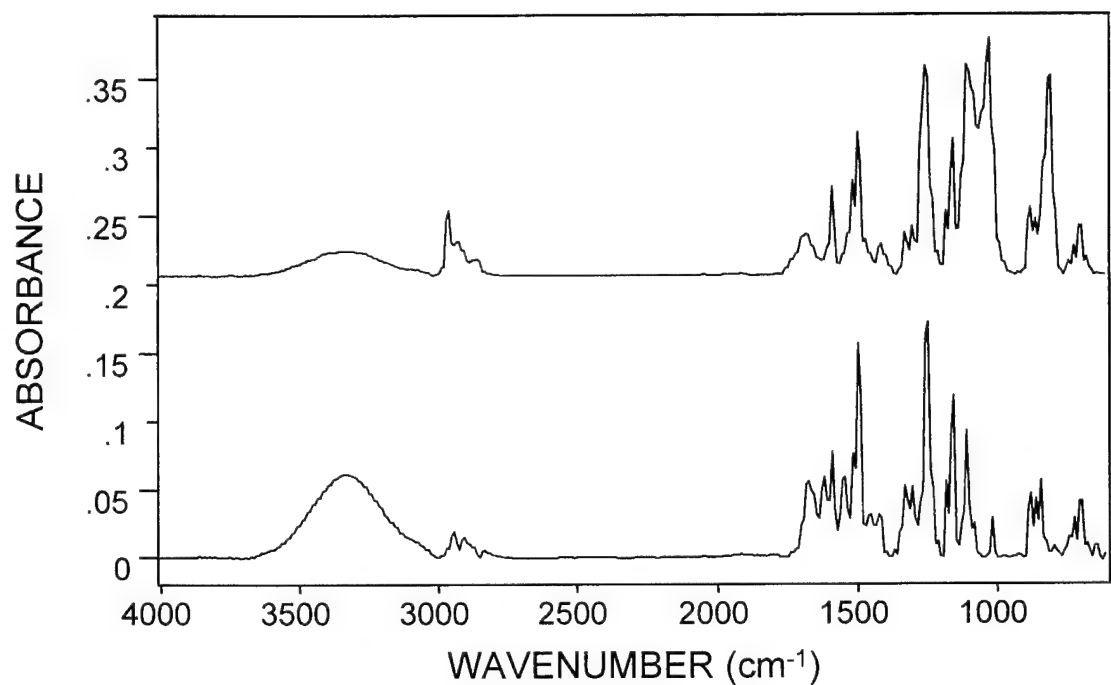
Figure 21.8 ATR-IR spectra of fouled FilmTec (green) operated on a clearwell feed at WQIC, Yuma, AZ and unused FilmTec control membrane (purple).

possible that carboxylate groups on the membrane were protonated to the acid (-COOH) form, thereby contributing to the O-H region of the spectrum (see discussion below).

Another unique fouling agent appears in the spectrum of the FilmTec membrane. An intense sharp band visible near 800 cm^{-1} (Figure 21.8). This band is also present to a much lesser extent in other membrane spectra (see Figure 21.6 and 21.7). The 800 cm^{-1} band is also accompanied by intense bands near 1259 cm^{-1} and 1030 cm^{-1}. The location of these bands is marked on the FilmTec spectrum in Figure 21.8. The identity of this fouling material is not known.

All six membranes operated on the clearwell feed appear to have been chemically altered. These spectral changes are attributed to changes in the polymeer chemistry and are identical to those observed when TMC, FilmTec and CPTC membranes were exposed to free chlorine and hypobromous acid (see Section 17.7). Most notable is the visible loss of the C=C ring stretching bands at 1610 cm^{-1}, 1489 cm^{-1} and 1448 cm^{-1}, combined with the loss and shift of the amide ii band at 1541 cm^{-1} to a lower wavenumber. This loss and shift in band intensity suggest chlorination or bromination of the *m*-phenylene ring.

The O-H stretching bands in many of the Yuma-tested membrane spectra are enhanced relative to the unfouled membrane controls. The IR spectra of the new (or unused) TMC and CPTC membrane spectra made during this study do not have strong O-H stretching band intensities. "Strong" in this case would imply an intensity greater than the amide I (1666 cm^{-1}) band of the PA component of the membrane. This enhancement of the O-H stretching band could be related to the fouling layer or possibly related to a change in the polymer chemistry itself. The 1610 cm^{-1} band is associated with the asymmetric stretching band of carboxylate. Therefore, the loss of the 1610 cm^{-1} band could be attributed to the loss of carboxylate and the formation of the protonated carboxylic acid. A greater contribution to the 1725 cm^{-1} carbonyl region is also visible in the fouled membrane spectra. It is difficult to tell if the symmetric stretching carboxylate band actually shifts to a lower wavenumber or just disappears with the appearance of a new band at slightly lower frequency. If the carboxylate does in fact become protonated to form the carboxylic acid, the O-H and carbonyl C=O stretching bands should increase in intensity, and the asymmetric and symmetric carboxylate stretch should decrease in intensity. This does appear to happen, however, these spectral changes all could be related to the adsorption of an organic foulant at the membrane surface.

Finally, one last spectroscopic change in the IR spectrum of the FilmTec membrane was observed that was not previously seen. The IR spectrum of the membrane operated on the clearwell feed had a significantly reduced O-H stretching band intensity. The one unique characteristic feature of the FulmTec membrane is the presence of a strong O-H stretching band. Neither the TMC nor the CPTC membrane possesses this strong O-H stretching band. This loss of the O-H stretching band was not observed during previous studies when the FilmTec membranes were exposed to free chlorine and hypobromous acid.

21.6.2 Potable Feedwater

Nine membrane swatches operated on potable water feed at the Yuma Test Facility were analyzed by ATR/IR spectrometry. Two TMC, one FilmTec and six CPTC membranes were tested. The IR spectra are displayed in Figures 21.9 through 21.11 between 4000 cm^{-1} and 600 cm^{-1} and between 2000 cm^{-1} and 600 cm^{-1}. There was no visible pattern of fouling among the nine membranes, i.e., one type of membrane did not foul more than any of the others. As with the membranes operated on the clearwell feed, a few of the CPTC membranes picked up a strong O-H stretching band (see Figure 21.9). Three of the membranes accumulated material that lead to the appearance of the intense 1030 cm^{-1} and 800 cm^{-1} bands seen in the spectra of the FilmTec membrane operated on the clearwell feed. Three membranes, a FilmTec and two of the CPTC membranes, appeared to be the most heavily fouled (Figures 21.9 and 21.11).

Independent of the level of fouling on each membrane, the same gross spectroscopic changes were observed on both the clearwell and potable feed operated membranes. The amide II band near 1541 cm^{-1} shifted to a lower wavenumber and dropped slightly in intensity and the C=C ring stretching bands virtually disappeared. All nine membranes also appeared to pick up more carbonyl intensity near 1730 cm^{-1}.

In conclusion, there is no apparent trend in the IR data that leads one to conclude that one membrane type fouls more than the other. While some of the membranes accumulated an unusual foulant that has yet to be identified, there was no correlation to the type of feedwater they were operated on and the type of fouling observed. All fifteen membranes did however, go through similar spectroscopic changes, the loss of C=C ring stretching band and the shift of the amide II band to a lower wavenumber with a slight reduction in intensity.

22.0 LONG-TERM FIELD TESTING OF MEMBRANES AT THE ORANGE COUNTY WATER DISTRICT ON A CHLORINATED MUNICIPAL WASTEWATER FEED

22.1 Long-Term RO Test Results at the Orange County Water District

On April 1, 1999, OCWD began evaluating the performance of CPTC membranes prepared from CPTC-AC Lot Nos. 021599 SE-FF and 021799 SE (see Table 10.0 in Section 10.0). The estimated isomeric purity of these samples was approximately 98%. Sample CPTC-AC Lot No. 021599 passed through falling-film distillation and was free of phosphorous. A FilmTec commercial control and a TMC control membrane were evaluated simultaneously for comparative purposes. Codes for the membranes evaluated are as follows:

TMC	= Control membrane made with trimesoyl acid chloride
CPTC-132	= Membrane made with *ctct*-CPTC (CPTC-AC Lot No. 021799S1)
CPTC-135	= Membrane made with *ctct*-CPTC (CPTC-AC Lot No. 021599S1)

Figure 21.9   ATR-IR spectra of fouled CPTC-882-022000S2 (green), FilmTec (red) and CPTC-875-022000S2 (blue) membranes operated on potable water feed at WQIC, Yuma, AZ.

Figure 21.10 ATR-IR spectra of fouled CPTC-900-022000S2 (red), TMC-906 (green) and CPTC-903-022000S2 (blue) membranes operated on a potable water feed at WQIC, Yuma, AZ.
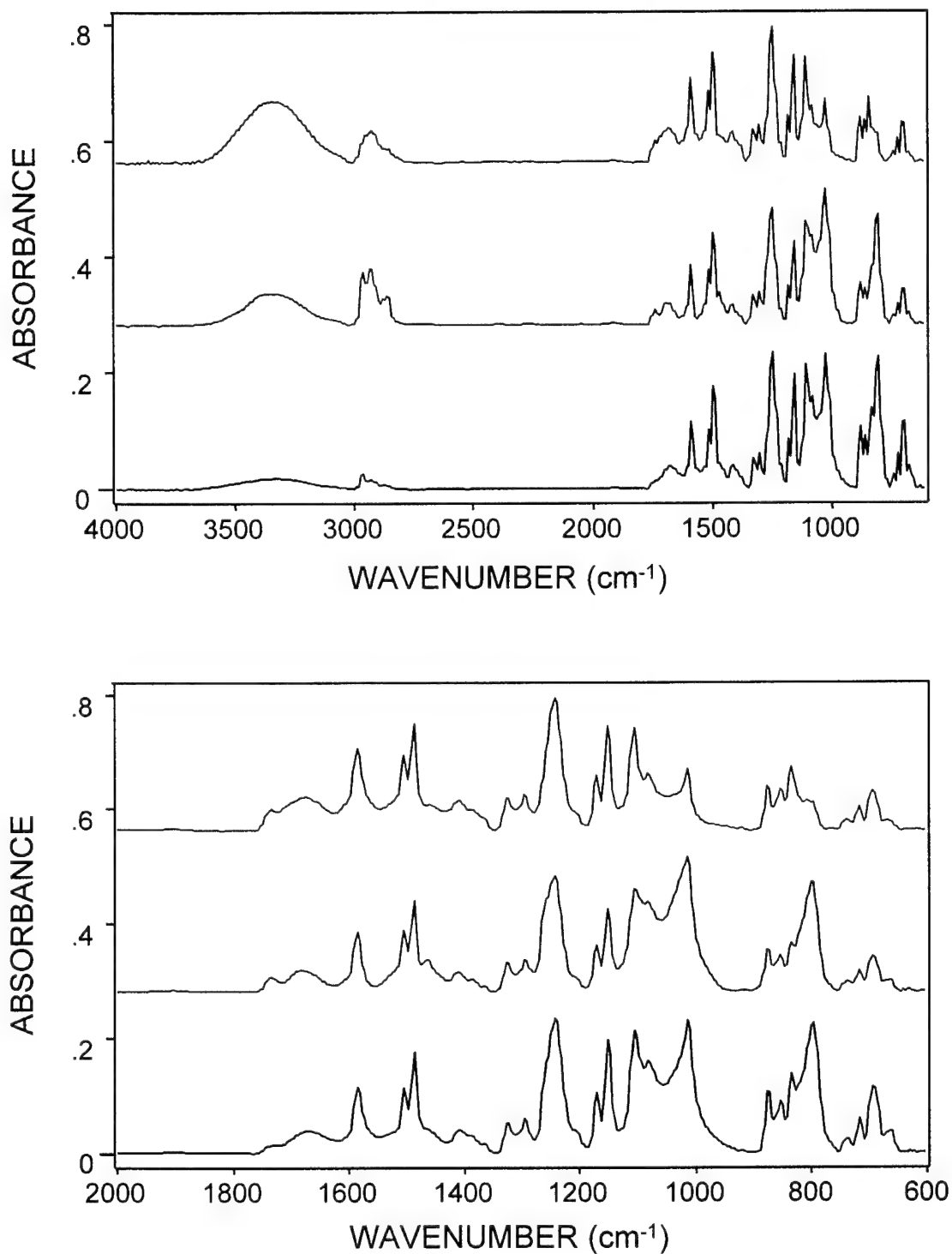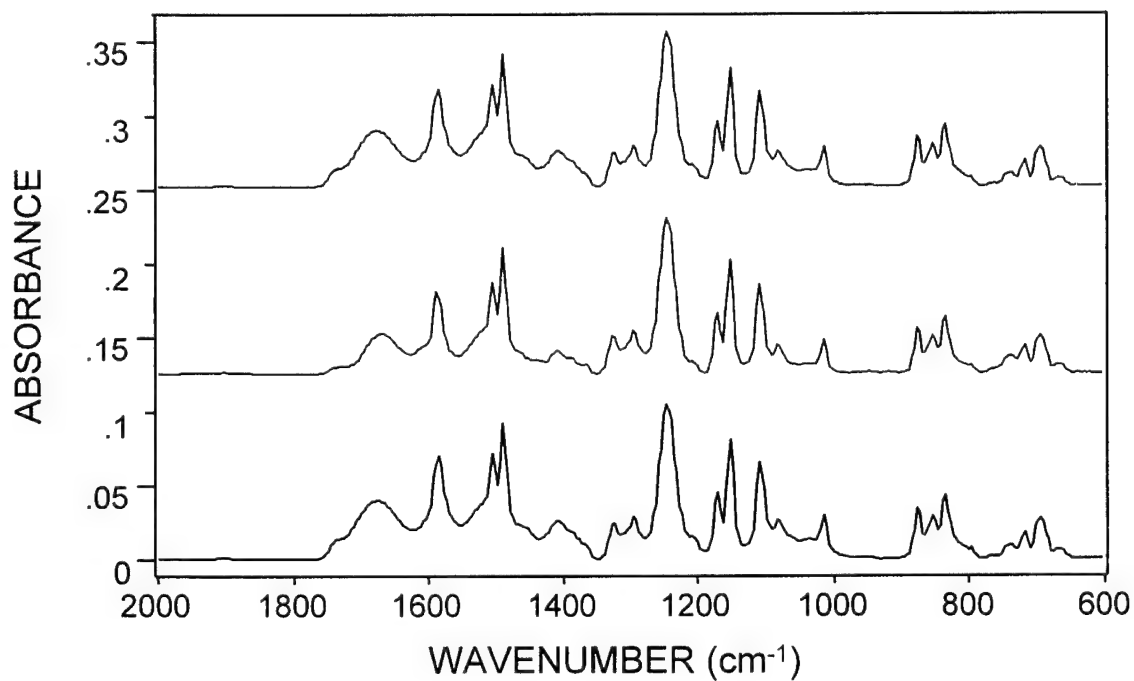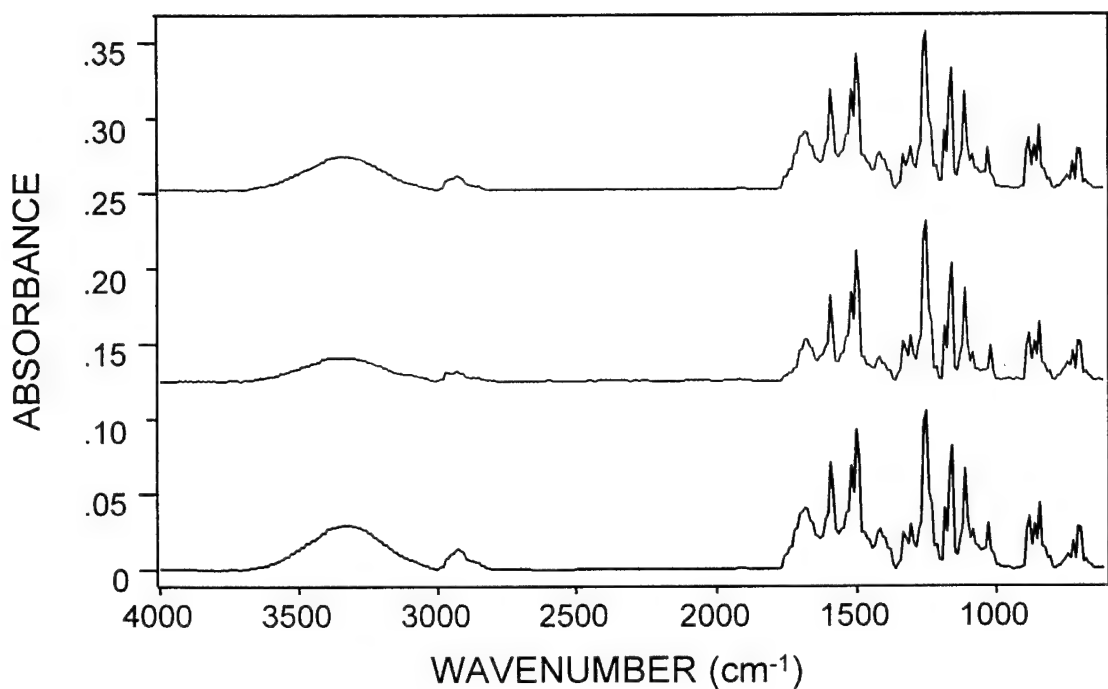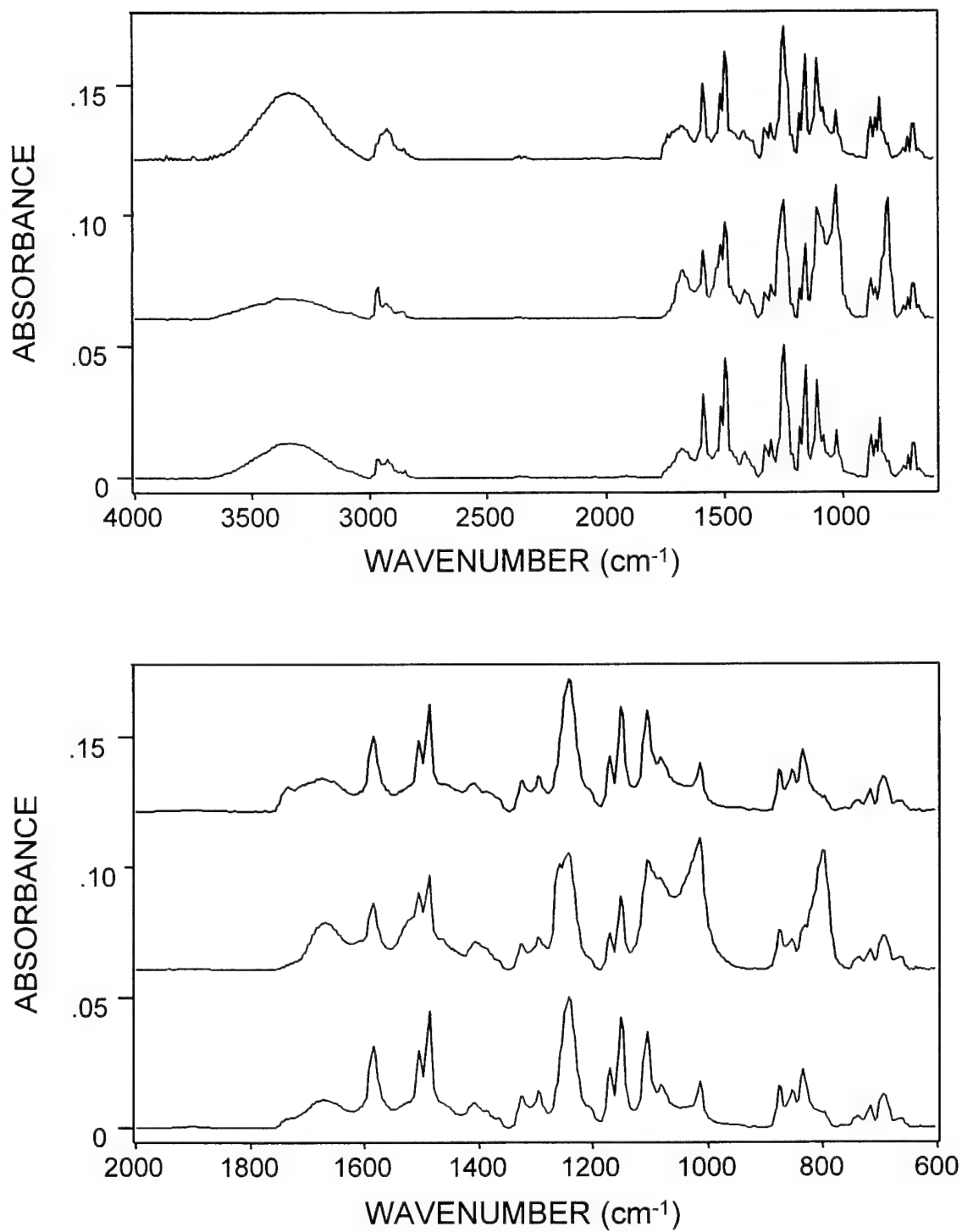
Figure 21.11 ATR-IR spectra of fouled CPTC-882-022000S2 (blue), TMC-839 (red) and CPTC-875-022000S2 (green) membranes operated on a potable water feed at WQIC, Yuma, AZ.

The membranes were fed with conventionally pretreated secondary effluent from Water Factory 21 at OCWD. The pretreatment process includes chemical clarification, multimedia filtration, antiscalent, sulfuric acid and approximately 5 mg/L chlorine addition before water was passed through the RO system. The wastewater feed is high in nitrogenous materials. Thus, chlorine combined with these materials to form chloramines; the combined chlorine contacting the membrane ranges from 2 to 5 mg/L.

Membranes were evaluated in 1 x 3 in. flat sheet test cells operated at 225 psi applied pressure at a flow rate of 0.9 gal/min. Operating conditions are such that there have been only two supervised shutdowns throughout the entire 5,000 hr run (April 30, 1999 for 48 hr and May 4, 1999 for 24 hr). Permeate flow and conductivity measurements were taken daily (Monday - Friday). Data was normalized to 25°C using FilmTec temperature correction factor tables. Feedwater pH and total residual chlorine (TRC) concentrations were monitored on a regular basis. pH measurements were taken on a daily basis while TRC values were taken via an on-line meter every 15 sec and the daily averages plotted. A more thorough ion rejection analysis was carried out after 1,000 hr of operation. The water flux, conductivity rejection, chlorine concentration of the feed and feedwater pH are given in Figure 22.0 a-d. The ion rejection analysis of the permeate after 1,000 hr (114 days) is given in Table 22.0.

As expected with a municipal wastewater feed, considerable fouling occurred on all of the membranes; the membranes were not cleaned during the run. In spite of the high fouling feed, membrane CPTC-132 (CPTC-AC Lot No. 021799S1 SE) clearly outperformed the other membranes, including the controls; it also exhibits the highest conductivity rejection. The membranes appear to be very stable with 4-5 mg/L combined chlorine in the form of chloramine; this performance was encouraging. A second test was run under the same conditions using different membrane samples. Results of this test are shown in Figure 22.1 a-e.
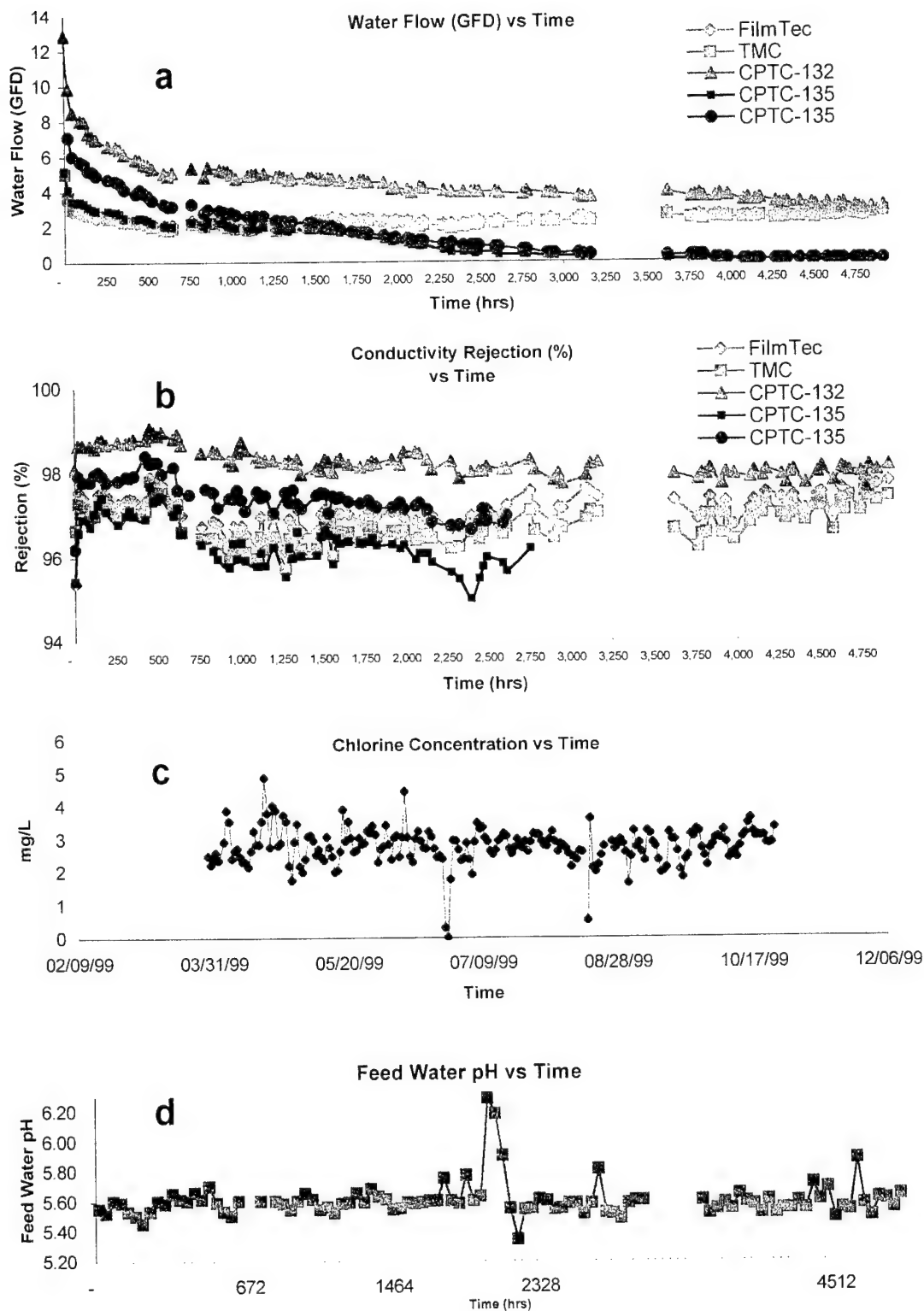
Figure 22.0 Performance of CPTC membranes and controls at OCWD. Permeate flow and conductivity measurements are shown in panels (a) and (b). respectively. Feed water parameters are shown in panels (c and (d).

301

Table 22.0

Ion Rejection Data for Membranes after 1000 Hr Operation at OCWD on a Municipal Wastewater Feed

Test Conditions: Municipal Wastewater Feed, 225 psi applied pressure, 1 gal/min feed flow rate, 2-4 mg/L chlorine (total residual chlorine)

Membrane	Na	K	Mg	Ca	Totl. hd.	B	Cl	SO_4	Br	NO_2-N	NO_3-N	PO_4-P
FlimTec	96.3	95.6	bdl	99.8	99.5+	bdl	98.4	99.4	bdl	bdl	73.9	bdl
TMC	95.8	95.6	bdl	99.8	99.5+	bdl	98.4	99.5	bdl	bdl	73.9	bdl
CPTC 132 - 021799	99.3	96.5	bdl	99.6	99.5	bdl	96.5	99.5	bdl	bdl	bdl	bdl
CPTC 135 - 021599	95.9	95.6	bdl	99.8	99.5+	bdl	96.2	99.5	bdl	bdl	69.6	bdl
CPTC 135 - 021599	98.1	96.3	bdl	99.8	99.5+	bdl	98.4	99.5	bdl	bdl	bdl	bdl
Feed (mg/L)	183	13.5	0.6	80.5	203	0.24	202	385	<0.2	<0.4	0.46	<0.1

Ion Rejection (%)

bdl = below detection limits
ICP = Inductively Coupled Plasma for Na, K, Mg, Ca, B (Total detection limit = 0.1 mg/L)
Total hardness (Total detection limit = 1.0 mg/L)
IC = Ion Chromatography for Cl, $S0_4$, Br, NO_2-N, NO_3-N, and $P0_4$-P (Total detection limit = 0.5,0.5,0.5,0.2,0.4,0.1,and 0.1)
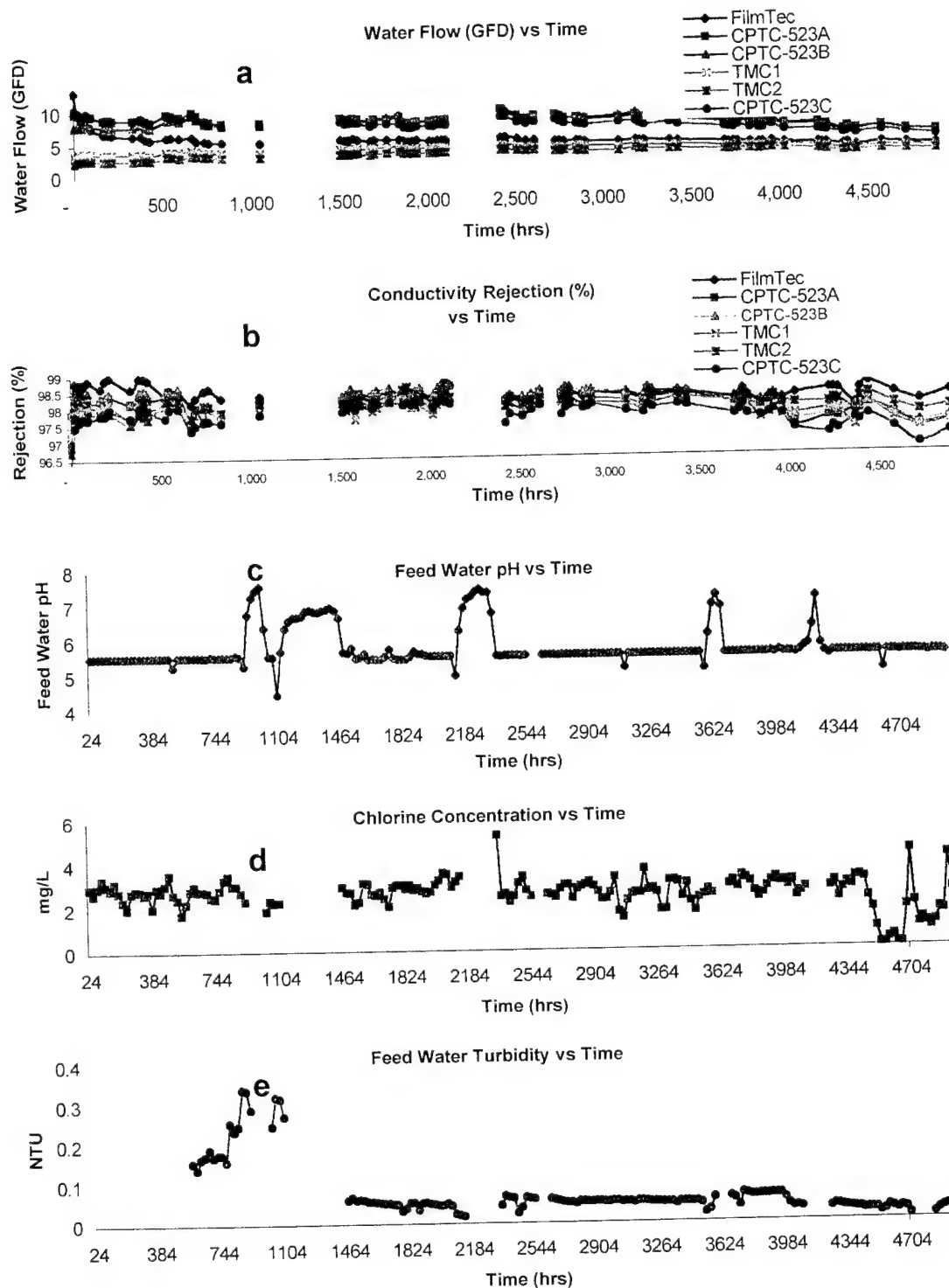
Figure 22.1   Performance of CPTC membranes and controls at OCWD.   Permeate
flow and conductivity measurements are shown in panels (a) and (b).
respectively.   Feed water parameters are shown in panels (c, d, and e).

303

A third set of CPTC membranes, along with a Koch Membrane Systems membrane, was tested on the same feed as the membranes described above and under the same test conditions. The performance of these membranes is shown in Figure 22.2.

As expected the flux was greater for the Koch ULP membrane, however the rejection was considerably lower than that of the CPTC membranes. At the end of the run, all membranes had approached the same level of flux. No iron foulant was found on the membrane samples at termination of the 2,800-hr test.

Large swings in the feedwater quality were observed, related to the presence of N-nitrosodimethylamine in the feed. Upon occasion, it was necessary to use treated deep well water, as opposed to secondary municipal effluent, because of high levels of NDMA. This explains the low levels of chlorine and turbidity between 1,200 - 2,200 hr of operation. This also explains the increase in flux during this time when operating on deep well water. The concentration of salts in this feed were approximately 600 mg/L as compared to 1,500 mg/L in the secondary wastewater. At approximately 2,200 hr the plant returned to normal operations.

23.0 LONG-TERM FIELD TESTING OF MEMBRANES AT THE NAVAL FACILITY ENGINEERING SERVICE CENTER AT PORT HUENEME, CA ON CHLORINATED SEAWATER

During the past year, membrane testing on seawater at the Naval Facility Engineering Service Center (NFESC) in Port Hueneme, CA was delayed for several months due to other commitments of naval personnel. Consequently, membrane testing did not get underway until June 17, 1999, with the installation of three (6.614 in^2) membrane disks in the test cells. Testing was carried out using a 1500-gal seawater reservoir connected to a three-cell system which had been constructed for this operation. All components were constructed from Type 316 stainless steel.

Initially, for several days, the system shut down at random times before all problems were apparently eliminated. Chlorine injection into the feed reservoir at about 0.5 mg/L began after 127 hr of normal operation. The test continued for another 220 hr before the system was shut down to replace these initial membranes, which had begun to deteriorate in performance after only 225 hr of operation. One of the problems associated with membrane testing on seawater, especially in a closed loop operation, was the presence of iron in the feedwater, which rapidly catalyzes membrane deterioration. Although small amounts of iron are inevitable, even in a stainless steel system, this amount would be sufficient to eventually lead to deterioration in membrane performance with time.
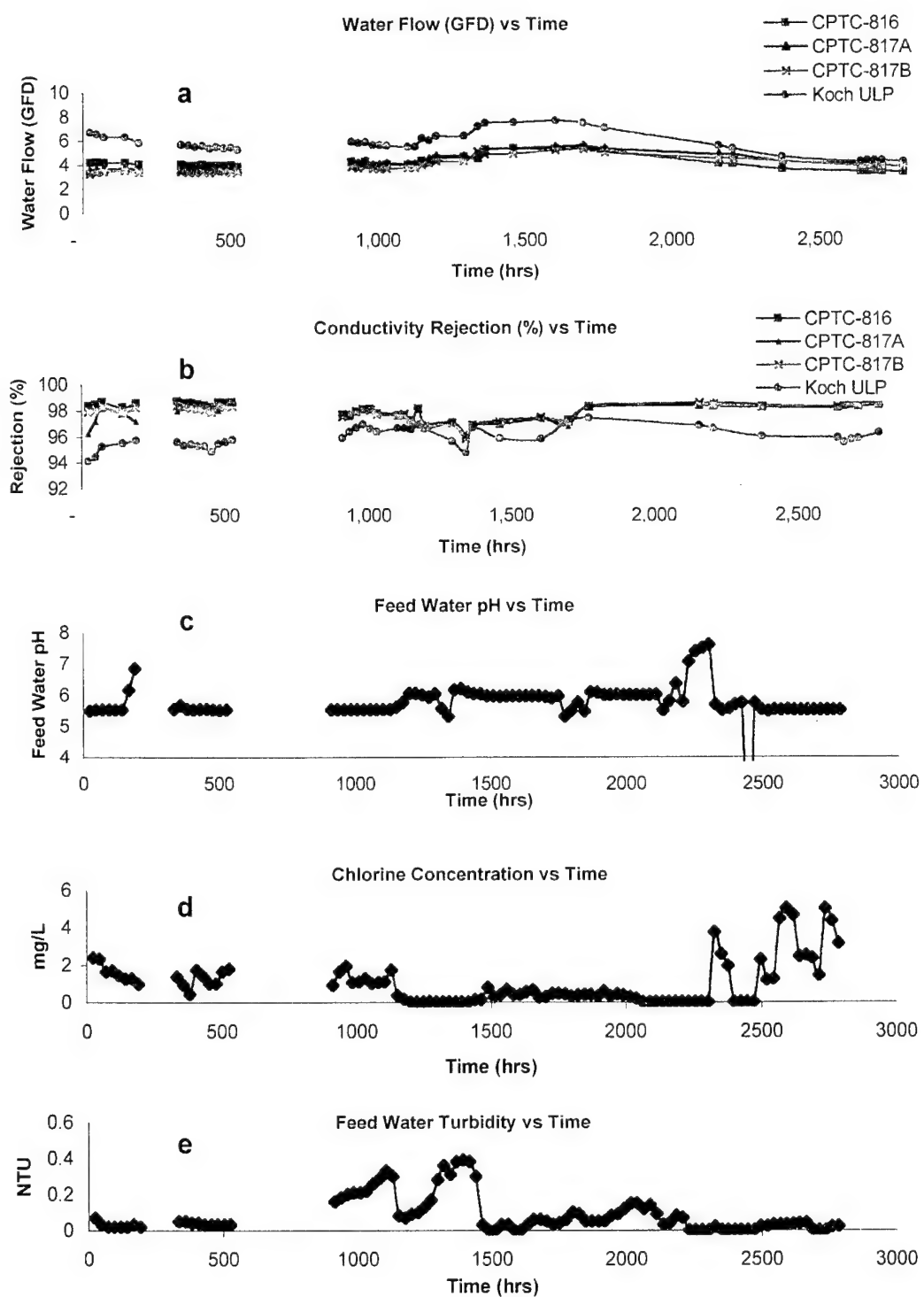
Figure 22.2 Performance of CPTC membranes and Koch ULP membranes at OCWD. Permeate flow and conductivity measurements are shown in panels (a) and (b). respectively. Feed water parameters are shown in panels (c, d, and e).

305

Prior to restarting the system with a new set of membranes, 5 mg/L of EDTA was added to the seawater reservoir to complex any iron before the addition of chlorine was resumed. New membrane disks, consisting of CPTC, TMC and a seawater FilmTec control membrane, were loaded into the test cells on September 14, 1999. The system was placed in operation for nine days at pH 8.0, the normal pH level of seawater. After 218 net operating hours, the pH of the seawater was lowered to ~5.5. Chlorine addition began on September 28 at 339 net operating hours. As noted in Figure 23.0, control of the chlorine concentration level was extremely difficult during the test.

Immediately after the addition of chlorine to the system, the flux of all three membranes declined sharply and the rejections rose above 99++%, due to the presence of a high concentration of bromine and the subsequent formation of hypobromous acid. The performance of the membranes remained essentially constant from 380-hr of operation to 1032 hours. At that time, it became apparent that the pump was beginning to fail and the system had to be shut down on October 28. The membranes were flushed at low pressure with tap water and sealed off pending repair of the pump.

Pump repairs were completed in late November and the system was restarted on November 23, 1999. It was apparent that the membrane samples had been severely damaged during the shutdown period, although some recovery in performance was evident over the next 150 hr. Ultimately the test system had to be shut down permanently, since the test facility was scheduled to be moved to another location during December and January. New membrane samples were installed for the next test.

At the time of shutdown (1032 hr of uninterrupted operation), it was noted that both the CPTC membrane performance (99.38% rejection, 11.7 gfd) and the TMC membrane (99.82% rejection, 6.24 gfd) were superior to the FilmTec membrane (98.82% rejection, 4.67 gfd) in the presence of chlorine.

Completion of the movement of the Seawater Test Facility was completed in late February 2000. The membrane test system continued to operate in a closed loop mode, except the 1500-gal feed reservoir (previously located outdoors) was replaced with a 500-gal feed reservoir located inside of the building. It was anticipated that this would provide a more steady level of chlorine in the feed and control of the feed pH would be easier. In addition, the seawater feed was passed through a Xenon ultrafiltration system before entering the reservoir. Thus, fouling of the membranes should be minimized. A 5 mg/L EDTA concentration was maintained to prevent iron fouling resultin from the stainless steel components in the test system.

The second seawater test run using CPTC membranes that had been prechlorinated following preparation was started on March 7 and terminated 16 days later after three shutdowns during the first 185 hr of operation. It is interesting to note that little effect on membrane performance occurred during the first two shutdowns, before the addition of chlorine to the system. However, a sharp increase in salt passage and product flux was observed after chlorine addition. This effect is shown in Figure 23.1.

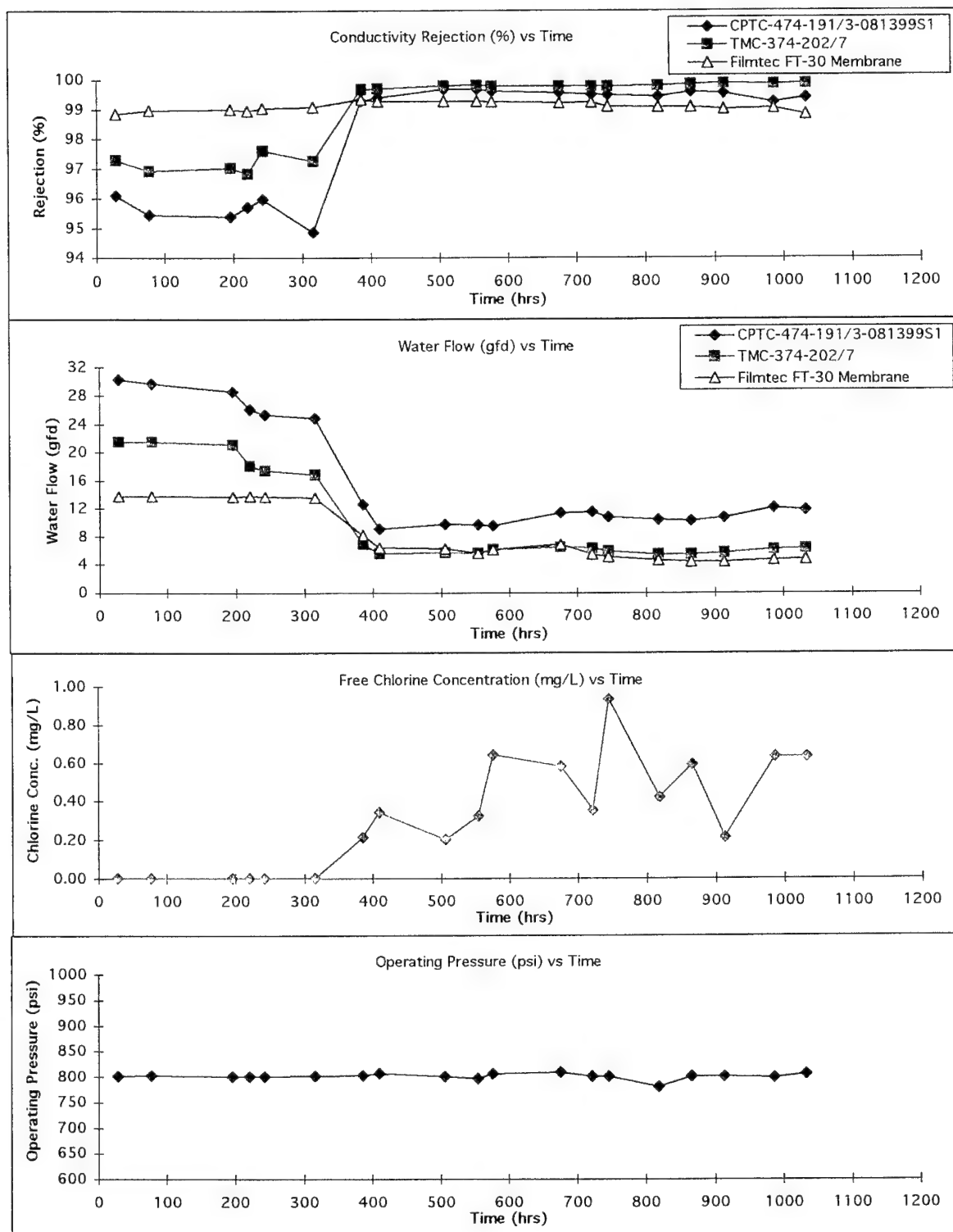Figure 23.0   Performance of CPTC membrane 474-191/3 (CPTC-AC Lot No. 081399S1), TMC 374-202/7 and FilmTec membranes operating on a seawater feed at 800 psi, 25°C, 1.0 gpm feed flow, pH 5.0 - 5.6.
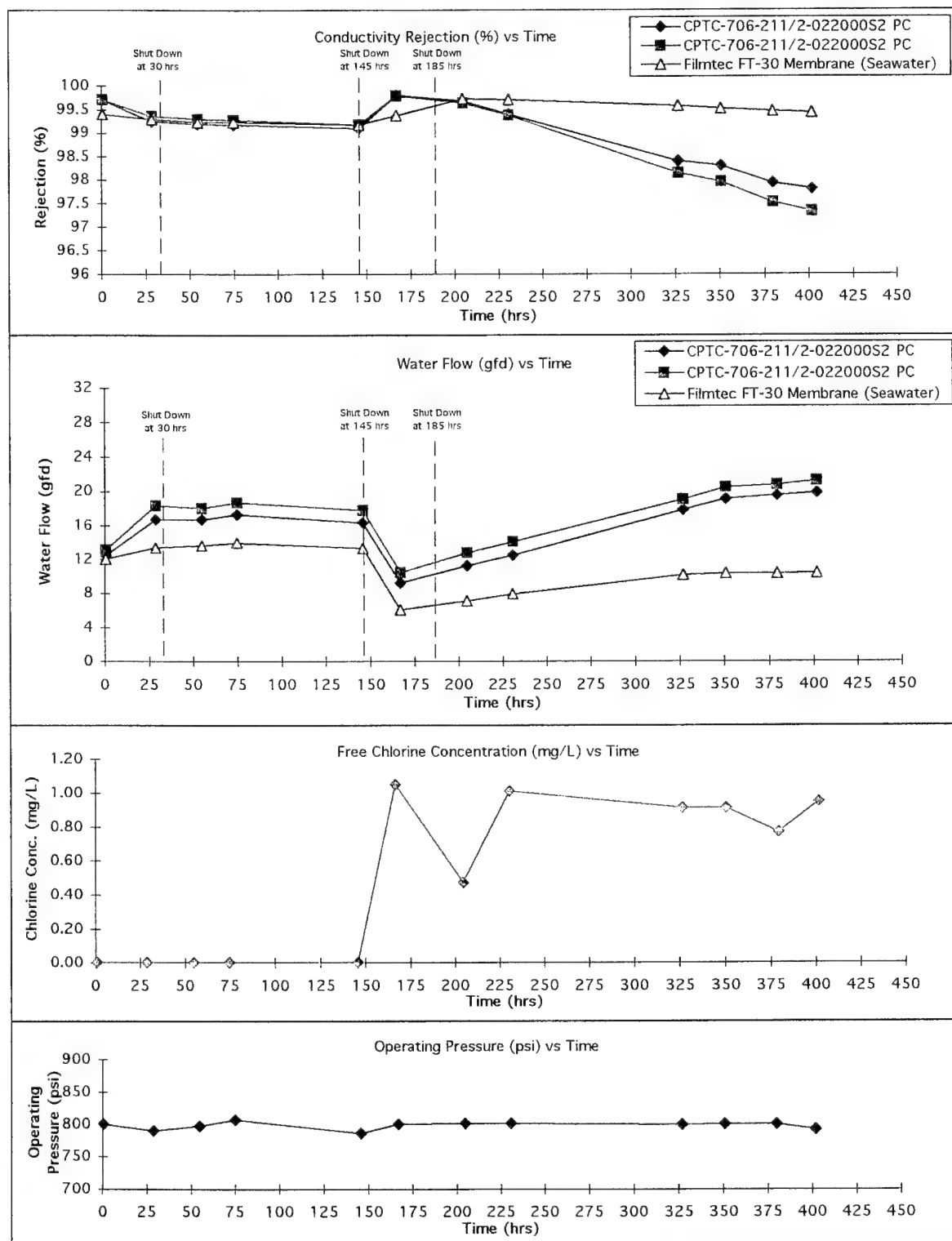
Figure 23.1 Performance of prechlorinated CPTC membranes 706-211/2 (CPTC-AC Lot No. 0022000S2) and a FilmTec control membrane operating on a seawater feed at 800 psi, 25°C, 1.0 gpm feed flow, pH 6.4 - 6.7.

308

Five additional seawater test runs were conducted using CPTC membranes and one control membrane, either FilmTec or TMC seawater membranes. Test Run 3 used two pre-chlorinated CPTC membrane samples and a FilmTec membrane. Startup of the system was with an initial chlorinated seawater (0.3 wt-% free chlorine) feed. Salt rejections of the CPTC membranes were in excess of 99.6% and the FilmTec control membrane showed a rejection of 99.4% rejection. The seawater pH was 6.2 - 6.6 at 800 psi. At approximately 125 hr of operation, the system shut down. Upon restart, the CPTC rejections had dropped to 99.1% with a flux increase from 5 - 8 gfd to 10 - 13 gfd. The FilmTec membrane rejection was unchanged, although the flux increased from 6.5 to 8.8 gfd. Further deterioration of membrane performance was observed during the next 160 hours and the system was shut down. Fluxes of the CPTC samples had increased to 16.5 - 20 gfd, and the FilmTec membrane flux had increased to 12 gfd.

Test runs 4 through 7 all failed after 300 to 500-hr operation, although there were no shutdowns during any of these runs. Following Run 4, during which the seawater temperature rose to ~34°C, a chiller was installed to maintain feed temperatures of ~25°C during the tests. In all of these tests, rejections increased from about 97% to ~99.6% upon the addition of chlorine to the seawater, with a subsequent decline in flux of about 50%.

Test run 7 (shown in Figure 23.2) initially showed the greatest promise for a successful long-term test, but after about 600 hr of operation, the CPTC membrane samples had deteriorated to below 99.6% rejection, from a high of 99.9%. During this period, the flux increased from ~6 to 10 gfd. These membranes were prepared from the highest purity CPTC-AC (99.9%) available and the TMC control membrane rejection remained above 99.8% for over 1000 hr.

Although attempts were made to maintain the pH of the seawater feed at ~6.5, throughout the series of tests, this proved to be very difficult to do. During the collection of permeate flow, and for conductivity measurements, the pH was observed to decrease during this period. Furthermore, a direct correlation was observed between rejection and feed pH with lower conductivities occurring at pH 6.3 - 6.6. At feed pH levels in the 4 - 4.5 range permeate conductivities are higher, as well as when the pH is above 7.

Each morning, before collecting flow measurements and conductivities, the pH was observed to be below 5 and the chlorine had all dissipated. Sodium hypochlorite bleach was added to raise the chlorine level to about 1 mg/L free chlorine and the pH was readjusted to ~6.5. Once again the pH would slowly decrease each day. It is puzzling that there seemingly is no buffering action from the seawater, which is contrary to previous observations. It was suspected that the seawater from the Xenon ultrafiltration system used as the seawater feed may have softened the seawater by removal of calcium, magnesium and carbonate such that its buffering capacity was essentially eliminated.

A chemical analysis of the filtrate from the Xenon system was made on September 27, 2000. The analysis showed no change in the mineral content from the original raw seawater analyzed at the same time.
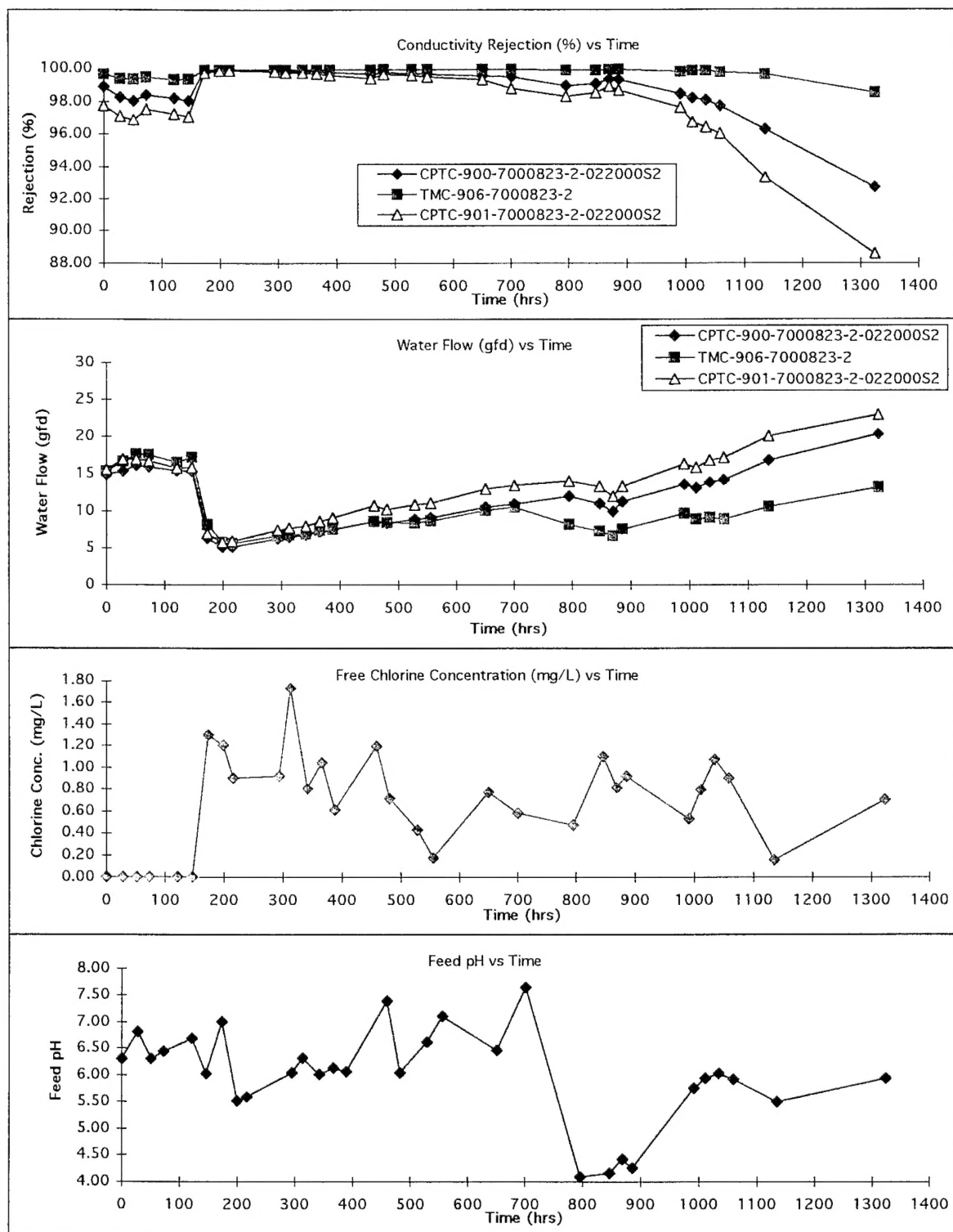
Figure 23.2   Performance of CPTC membranes 900-7000823-2 (CPTC-AC Lot No.
022000S2) and a TMC control membrane operating on a seawater feed
at 800 psi, 25°C, 1.0 gpm feed flow, pH 4.1 - 7.5.

310

A second test was conducted in early January 2001, whereby two 1-L beakers of raw seawater (pH 8.19) were collected. Five mg/L of EDTA was added to one of the beakers and both were neutralized to pH 5.7 with sulfuric acid. The beakers were covered with Parafilm and pH measurements were taken each day for eight days. Results of these tests indicate that each day the pH of both solutions increased noticeably. The Parafilm cover was removed long enough only to obtain the pH measurement, then tightly sealed again. A plot of the pH data shows a smooth curve for both solutions, increasing from 5.7 to 7.6 over the eight day period. The logical explanation for this behavior is the slow release of CO_2 from the acidified seawater which would be trapped below the Parafilm cover. As the cover was removed, the CO_2 would escape into the air. Following covering the beakers after the measurement apparently allowed more CO_2 to be released from the seawater as a new HCO_3 - CO_2 equilibrium was established above the seawater and the cover.

This occurrence does not explain the decrease in pH of the seawater each day during RO testing, where the 500-gal reservoir was open to the atmosphere continuously with agitation. Discussions with several chemists and engineers that regularly work with seawater in RO tests did not reveal any logical explanation for this behavior.

The most plausible explanation of why CPTC membrane performance during the initial test remained very good, shown in Figure 23.0, in which the feed reservoir was the 1,500-gal tank located outside the old test site, was the condition of the tank itself. This tank had been located under the sun for many years. Under these conditions, the condition of the polypropylene tank may have become stabilized due to leachables (binders) from the plastic, even though the pH of the tank had never been below normal seawater pH of about 8 until this recent test. Coupled with the larger volume of the seawater feed, residual chlorine would remain longer in the feed and, consequently, the pH of the seawater was somewhat easier to control.

Moving of the test facility to a new location, in which a smaller 500-gal tank was located inside the facility, any leachable materials from the polypropylene tank might occur slowly. This could explain why the pH became harder to control on a daily basis as the chlorine dissipated. In the absence of shutdowns, CPTC membrane shows a lower perrformance at low pH levels.

24.0 REFERENCES

1. J. E. Cadotte, R. J. Peterson, R. E. Larson and E.E. Erickson, Desalination, **32**, 25-31 (1980)

2. K, Ikeda et. al., *Novel Reverse Osmosis Composite Membranes,* Proceedings of the IDA and WPRC World Conference on Desalination and Water Treatment, November 3-6, 1993, Yokohama, Japan, Vol. 1, pp. 93-100

3. R. Singh, *Characteristics of a Chlorine-Resistant Reverse Osmosis Membrane,* Desalination, **95** (1994) 27-37

4. J. Glater, Seung-Hong and M. Elimelech, *The Search for a Chlorine Resistant Reverse Osmosis Membrane,* Desalination, **95**, 325-345 (1994)

5. Elimelech, X. Zhu, A. E. Childress, and S. Hong, *Role of Membrane Surface Morphology in Colloidal Fouling of Cellulose Acetate and Composite Aromatic Polyamide Reverse Osmosis Membranes,* Journal of Membrane Science, **127**, 101-109 (1997)

6. H. F. Ridgway et. al., *Analysis of Bacterial Adhesion and Biofouling Membrane Separations Processes,* An Interim Progress Report to AWWA Research Foundation, Biotechnology Research Department, Orange County Water District, Fountain Valley, CA, March 1997

7. H. F. Ridgway and J. Safarik, *Biofouling of Reverse Osmosis Membranes,* in Biofouling and Biocorrosion in Industrial Water Systems, 81-111, H. C. Flemming and G.G. Geesey (eds.), Springer-Verlah, New York (1991)

8. H. F. Ridgway and H. C. Flemming, *Membrane Biofouling,* pp 6.1-6.62, In: Water Treatment Membrane Processes, J. Mallevialle, P. E. Odendaal, and M. R. Weisner (Eds.), McGraw-Hill Publishers, New York, 1996

9. S. A. Sundet, S. D. Arthur, D. Campos, T. J. Eckman and R. G. Brown, Desalination, **64**, 259-269 (1987)

10. Arthur et al., U. S. Patent 4,749,488 (1988)

11. H. F. Ridgway, *Molecular Modeling of Organics Adsorption to Synthetic Polymer Membranes,* Proc. International Membrane Science and Technology Conference, 12-14 November 1996, Sydney, Australia

12. R. M. Prokop, O. I. del Rio, N. Niyakan and A. W. Neuman. *Interfacial Tension from the Height and Diameter of Sessile Drops and Captive Bubbles with an Arbitrary Contact Angle,* Can. J.Chem. Engineering **74**, (1996)

13. M. Rosenberg, R. J. Doyle, *Microbial Cell Surface Hydrophobicity: History, Measurement and Significance*, (Ed.) Microbial Cell Surface Hydrophobicity, 1-38, American Society for Microbiology, Washington, D. C.

14. J. Farrar, S. M. Neale and G. R. Williamson, *A Gravimetric Estimation of the Carboxylic Acid Group in Cellulose*, Nature, **168**, 566

15. H. F. Ridgway, *Microbial Adhesion and Biofouling of Reverse Osmosis Membranes*, In Parekh, B. (Ed), Reverse Osmosis Technology: Application for High-Purity Water Production, Marcel Dekker, Inc., New York and Base

16. G. Leslie, Orange County Water District, private communication

17. P. W. Morgan, *Condensation Polymers: By Interfacial and Solution Methods,* Intersciences Publishers, New York (1965)

18. Aldrich Chemical Co., Handbook of Fine Chemicals and Laboratory Equipment, 2000-2001

19 Neilson et al., J. Chem. Soc., **371** (1962)

20. T. Peltier, Compt. Rend., **259**, 400 (1964)

21. Gaylord, *Reduction with Complex Metal Hydrides,* Interscience Publ., Inc., New York, p. 776 (1956)

22. M. J. Kotelyanskii, N. J. Wagner and M. E. Paulaitis, *Atomistic Simulation of Water and Salt Transport in the Reverse Osmosis Membrane FT-30,* J. Membrane Science, **139**, 1-16 (1998)

23. T. Kawaguchi and H. Tamura, *Chlorine-Resistant Membrane for Reverse Osmosis. I. Correllation Between Chemical Structures and Chlorine-Resistance of Polyamides*, J. Applied Polymer Sci, **29**, 3359-3367 (1984)

24. M. M. Jayarani et. al, *Synthesis of Model Diamide, Diester and Esteramide Adducts and Studies on their Chlorine Tolerance*, Desalination **130**, 1-16 (2000)

25. *Dechlorination Technology Manual*, Electric Power Research Institute, EPRI CS-3748 (1984)

26. R. L. Riley, J. O. Gardner and U. Merten, Science, **143**, 801 (1964)

27. R. L. Riley, *Development of Improved Membranes for ROWPU Spiral-Wound Elements*, SBIR Phase I Final Report to the U. S. Army Research Office, Contract No. DAAG55-97-C-0016, Separation Systems Technology, Inc, July 8, 1997.